High-precision infrared spectroscopy of tritiated water vapour isotopologues and tritium hydride

Zur Erlangung des akademischen Grades eines
Doktors der Naturwissenschaften (Dr. rer. nat)
von der KIT-Fakultät für Physik
des Karlsruher Instituts für Technologie (KIT)
genehmigte
Dissertation
von
M.sc.

Valentin Baptiste Hermann

aus Sarrebourg (F)

Referent: Prof. Dr. Johannes Orphal
                   Bereich IV- Natürliche und gebaute Umwelt
                   Karlsruher Institut für Technologie

Korreferentin: Prof. Dr. Kathrin Valerius
                   Institut für Astroteilchenphysik
                   Karlsruher Institut für Technologie

Tag der mündlichen Prüfung: 22.11.2024

Declaration of Authorship

Herewith I affirm that I wrote the current thesis on my own and without the usage of any other sources or tools than the cited ones and that this thesis has not been handed neither in this nor in equal form at any other official commission.

Erklärung der Selbstständigkeit

Hiermit versichere ich, die vorliegende Arbeit selbstständig angefertigt zu haben und keine Hilfsmittel jenseits der kenntlich gemachten verwendet zu haben. Weiterhin habe ich weder diese noch eine äquivalente Version dieser Arbeit bei einer anderen Prüfungskommission vorgelegt.

Karlsruhe, den 14. Oktober 2024

Valentin Baptiste Hermann

Contents

List of Figures

List of Tables

1 Introduction

Tritium (^{3}H = T), the radioactive isotope of hydrogen, is essential in diverse fields including nuclear fusion, neutrino mass determination, and molecular spectroscopy. Its unique nuclear and chemical properties enable critical advancements in these areas, despite its small natural abundance on Earth (around $3.8\,\mathrm{kg}$ [Oms19]). However, accurate measurements of tritium isotopologues are essential to fully exploit its potential, particularly for improving theoretical models and ensuring safety in applications like nuclear fusion. This work contributes to these efforts by focussing on high-precision infrared measurements of tritiated water and tritium hydride.

In nuclear fusion, among all potential fuels, the deuterium-tritium reaction requires the lowest energy to give the highest cross section. Therefore, the realisation of a deuterium-tritium fusion reactor is the principal goal of the present fusion research [Tan18]. In neutrino physics, from high-accurate electron spectroscopy of the tritium β-decay, upper boundaries for the mass of the electron neutrino ν_e are derived. Here, the decay properties of tritium, a short half-life of 4500 days [Luc00] and low decay energy of $E_{\beta(^3H)} = 18.6\,\mathrm{keV}$, make it an ideal candidate [Lok22; Ake22].

In molecular spectroscopy, the larger mass of tritium relative to ^{1}H = H and ^{2}H = D ($\mathrm{m(H) : m(D) : m(T)} = 1 : 2 : 3$) enables fundamental tests of quantum mechanical effects, particularly mass-dependent adiabatic and non-adiabatic contributions [Zob96; Pol13; Lai20]. Simple hydrogen-containing molecules, like molecular hydrogen and water, provide ideal systems for these investigations.

The focus of this work is the precise determination of ro-vibrational transitions in (i) tritiated water (HT^{16}O, DT^{16}O, and T$_2^{16}$O) and (ii) tritium hydride (HT). These measurements are crucial not only for improvement of theoretical quantum mechanical models, but also for monitoring tritiated water vapour, a highly radiotoxic byproduct in fusion research [Wat87; Kal93; Vel08].

Tritiated water Due to its nature as an asymmetric-top rotor, water is particularly sensitive to exchange of isotopes, making it ideal for testing mass-dependent contributions in theoretical models. In addition to extensive studies of the stable isotopologues, only few experimental studies on tritiated species were performed prior to this work, as reported in Chapter 3.1. However, these studies cover only limited spectral ranges, which does not allow for a substantial test or improvement of theoretical calculations.

Beyond its role in testing quantum dynamics, accurate measurements of tritiated water isotopologues are critical for practical reasons. Tritiated water vapour, a byproduct of fusion

processes, is highly radiotoxic and therefore poses significant safety concerns [Wat87; Kal93; Vel08]. Trace-concentration monitoring of this vapour requires high-resolution spectral data, which this work aims to provide. These measurements are crucial not only for the improvement of theoretical models but also for ensuring the safety and effectiveness of tritium-handling protocols in fusion research.

This work uses FTIR spectra obtained from the optical cell developed by Johannes Müller et al. [Mül19]. The cell complies with tritium-related requirements, including a limitation of the activity by European law to $1\,\mathrm{GBq}$. The samples were prepared in the TLK and then transported to a measurement container of the Institute of Meteorology (IMK-ASF) where the high-resolution FTIR spectrometer is located. Therefore, measurements have not been performed within a licensed laboratory and are restricted to a single amount of tritium (T2) of $1183\,\mathrm{Pa\,mL}$.

To better access the lines of the DTO and T_2O species, a modified version of this cell is developed, which, among other improvements, allowed to increase the activity to $10\,\mathrm{GBq}$. The acquisition of spectra with this cell was performed under the licence of a KIT department.

The assignment of spectra obtained from both samples is based on predictions from variational calculations available in the SPECTRA database [Mik05]. Since the accuracy of these calculations is over an order of magnitude less than the width of the measured lines, visual assignment becomes mandatory. This visual assignment at the same time requires careful validation of the obtained data sets. This was performed using a cross-check of spectra from both samples and by comparing the rotational spacings with independent microwave measurements.

In this work, a data set of in total 4589 lines is obtained from the HTO, DTO, and T_2O species. This data set allows a systematic comparison with the theoretical predictions, determining and potentially unveiling the sources of the limited accuracy.

Tritium hydride   Tritium hydride (HT), a heteronuclear species of molecular hydrogen, offers distinct advantages for high-precision spectroscopy. The centres of gravity and of charge do not coincide for HT. This leads to a small dipole moment, enabling precise ro-vibrational absorption measurements. Unlike HD, the hyperfine structure of HT is simpler, as tritium is a fermion ($I_T = 1/2$) compared to bosonic deuterium ($I_D = 1$), resulting in fewer spectral components and a single isolated hyperfine component [Jóź21].

In this work, the three strongest transitions of the first vibrational overtone ($\nu = 0 \to 2$) are targeted using the sub-Doppler resolution technique NICE-OHMS in a collaborative project of LaserLaB at Vrije Universiteit Amsterdam (VU), and the Tritium Laboratory Karlsruhe (TLK) at Karlsruhe Institute of Technology (KIT). NICE-OHMS (Noise-Immune Cavity Enhanced Optical Heterodyne Molecular Spectroscopy) offers ultra-high resolution and sensitivity [Axn14], making it ideal for precise measurements of tritium isotopologues. Previously used for HD isotopologues [Coz18a; Dio19], its ability to measure sub-Doppler

transitions makes it well-suited for extending these measurements to the radioactive isotopologue HT and therefore to test quantum mechanical predictions and improve the accuracy of experimental data.

For this purpose, a dedicated cavity was constructed to perform laser spectroscopic measurements at variable pressures, and with very low residual background pressure. These measurements were performed at VU where precision spectroscopy infrastructure in the form of a frequency comb and an atomic caesium clock is available. Thus, measurements are performed outside of a licensed tritium laboratory and therefore need to use less than 1 GBq activity.

A key component of the experimental setup is the non-evaporable metal getter (NEG) (*SAES* St171) that allows provisioning of HT samples at different and well-controlled pressures in a closed setup through its ability to reversibly absorb hydrogen when heated.

The ability to trap and release hydrogen was tested prior to the spectroscopy campaign in a sorption study at TLK. The range of parameters (amount of gas, volume, and pressure range) is chosen to fulfill requirements of the targeted NICE-OHMS measurement campaign or those of comparable future experiments. The results for gases H_2, D_2, T_2 and a H_2:HT:T_2 mixture (with H:T=1:1) are presented and compared to discuss a potential isotope effect. As sorption properties for this getter material are temperature dependent, an in situ temperature read-out is developed. The optical setup was tested, and a proof-of-principle for gas provision was performed using HD, which provided the highly-accurate transition of the $\nu = 0 \rightarrow 2$ P(3) line ($J = 3 \rightarrow 2$).

The experiences of the getter system for NICE-OHMS on HT and the spectroscopic results of at sub-Doppler precision are presented and discussed. This includes the first determination of the HT transitions frequencies of the R(0) ($J = 0 \rightarrow 1$), R(1) ($J = 1 \rightarrow 2$) and P(1) ($J = 1 \rightarrow 0$) of the first vibrational overtone ($\nu = 0 \rightarrow 2$) with a relative accuracy of 10^{-10}.

Outline of this work The theoretical overview of molecular energy levels and infrared transitions for HT and tritiated water is given in Chapter 2. Chapter 3.1 and Chapter 3.2 review the current state of knowledge on infrared spectroscopy of tritiated water and precision measurements of molecular hydrogen, respectively. The methodologies employed, Fourier-Transform Infrared Spectroscopy (FTIR) and Noise-Immune Cavity Enhanced Optical Heterodyne Molecular Spectroscopy (NICE-OHMS), are described in Chapters 4.1 and 4.2. The experimental results for tritiated water isotopologues are presented in Chapter 5, while the collaborative NICE-OHMS project on HT is discussed in Chapter 6. Finally, concluding remarks and future directions are presented in Chapter 7.

2 Quantum mechanical description of molecular IR spectroscopy

In this chapter, a basic derivation of the quantum mechanical description of (i) the energy levels of the HT and tritiated water molecules and (ii) the IR transitions in these molecules is provided. For further information, the author suggests the following literature that is taken as a reference for this chapter [Dem08; Bro03; Pap97; Sch07].

2.1 Molecular energy levels

The introduction of energy levels in quantum mechanics lectures starts with a particle in a potential well. By solving the time-independent Schrödinger equation,

$$\mathcal{H}(\mathbf{x})|\Psi(\mathbf{x})\rangle = E|\Psi(\mathbf{x})\rangle, \tag{2.1}$$

using the boundary conditions one derives that energy is defined as discrete values, eigenvalues E of the Hamiltonian $\mathcal{H}(\mathbf{x})$. This Hamiltonian

$$\mathcal{H}(\mathbf{x}) = -\frac{\hbar^2}{2m}\nabla^2(\mathbf{x}) + V(\mathbf{x}), \tag{2.2}$$

describes particle motion and the potential $V(\mathbf{x})$ of the well.
The simplified picture of a particle in a potential well can be extended to the molecular case by including the motion for all particles N, nuclei and electrons, of this many-body-problem. The Coulomb interaction between each of these particles keeps the particles as (stable), molecular system together,

$$\mathcal{H}(\mathbf{x}) = -\sum_i^N \frac{\hbar^2}{2m_i}\nabla_i^2(\mathbf{x}) + \sum_{i,j>i}^N \frac{e^2}{4\pi}\frac{Z_i Z_j}{|\mathbf{x}_i - \mathbf{x}_j|} \tag{2.3}$$

This expression can be reformulated as

$$\mathcal{H}(\mathbf{x}, \mathbf{X}) = T_e(\mathbf{x}) + T_n(\mathbf{X}) + V_{ee}(\mathbf{x}) + V_{nn}(\mathbf{X}) + V_{en}(\mathbf{x}, \mathbf{X}) \tag{2.4}$$

by separating the kinetic (T, first term in Equation 2.3) and interaction (V, second term in Equation 2.3) terms for electrons (e) and nuclei (n) and adding a mixing interaction term V_{en}.

Since all particles interact with each other, the solution of the Schrödinger is a complex problem. One solution ansatz is a variational approach, which is already used for systems with few particles reaching the limits of current computation techniques. For the simplest molecule, molecular hydrogen (two nuclei, two electrons), this approach is used with accuracy of few MHz [Puc19b; Puc19a].

To obtain solutions for more complex systems, a common approach is to use the Born-Oppenheimer approximation. For this approximation, the independent motions of nuclei and electrons is assumed. This can be justified by the large difference in the mass of nuclei and electrons that leads to a large difference in the time scales of their motion. So, nuclei are treated as static for the electrons, and electrons are treated as charge density for the nuclei.

Mathematically, this so called is made by treating the wave functions of atomic nuclei $\Psi_n(\mathbf{X})$ and electrons in a molecule $\Psi_e(\mathbf{x}, \mathbf{X})$ separately

$$\Psi(\mathbf{x}, \mathbf{X}) = \Psi_e(\mathbf{x}, \mathbf{X})\Psi_n(\mathbf{X}). \tag{2.5}$$

The separation of the wave function allows for the separation of the total Hamiltonian $\mathcal{H}(\mathbf{x}, \mathbf{X})$ in an electronic Hamiltonian

$$\mathcal{H}_e(\mathbf{x}, \mathbf{X}) = T_e(\mathbf{x}) + V_{ee}(\mathbf{x}) + V_{en}(\mathbf{x}, \mathbf{X}) \tag{2.6}$$

and a pure nuclear Hamiltonian

$$\mathcal{H}_n(\mathbf{X}) = T_n(\mathbf{X}) + V_{nn}(\mathbf{X}), \tag{2.7}$$

where the interaction of electron and nuclei is treated for static nuclei coordinates $\mathbf{X}$. Solving the Schrödinger equation, one obtains the following result

$$(\mathcal{H}_e(\mathbf{x}, \mathbf{X}) + \mathcal{H}_n(\mathbf{X})) |\Psi_e(\mathbf{x}, \mathbf{X})\Psi_n(\mathbf{X})\rangle = E_e|\Psi_e(\mathbf{x}, \mathbf{X})\rangle + E_n(\mathbf{X})|\Psi_n(\mathbf{X})\rangle. \tag{2.8}$$

For further considerations, the Hamiltonian is reduced to an effective nuclear Hamiltonian using

$$\tilde{\mathcal{H}}_n(\mathbf{X}) = T_n(\mathbf{X}) + V_{nn}(\mathbf{X}) + E_e(\mathbf{X}) = T_n(\mathbf{X}) + V_{\text{eff}}(\mathbf{X}). \tag{2.9}$$

The nuclear Hamiltonian is base for the description of molecular properties like rotation and vibration.

2.1.1 Introduction to molecular rotation and vibration

Starting from this general description the examples of HT and the tritiated water isotopologues are presented in Sections 2.1.2, and 2.1.3, respectively.

Rotation of molecules

To derive a general description of the rotation of a molecule, the assumption of a rigid rotor is a suitable approach. The rigid rotor model assumes that the bond lengths in the molecule are fixed and only rotational motion is considered.
Using that assumption the kinetic energy is given by

$$\hat{T} = \frac{1}{2} \sum_{i=1}^{3} \frac{\hat{J}_i^2}{I_i} \tag{2.10}$$

$$= \frac{1}{2} \left(\frac{\hat{J}_A^2}{I_A} + \frac{\hat{J}_B^2}{I_B} + \frac{\hat{J}_C^2}{I_C} \right), \tag{2.11}$$

where I_i are the principal moments of inertia and $\hat{J}_i$ are the components of the angular momentum operator around the principal axes $i = A, B, C$.
Depending on the principal moments of inertia molecules are classified in different rotors:

  (i) Spherical top molecules: $I_A = I_B = I_C$

  (ii) Linear molecules: $I_A = I_B$, $I_C = 0$; valid for HT.

  (iii) Symmetric top molecules: $I_A = I_B > I_C$ for prolate symmetric top and $I_A = I_B < I_C$ for oblate symmetric top molecules

  (iv) Asymmetric top molecules: $I_A \neq I_B \neq I_C$; valid for tritiated water isotopologues.

Depending on the classification of the molecule, its description and parameterisation can be specified. Depending on the type of rotor, different expansions from the rigid rotor energy (Equation 2.10) are used to take into account non-rigidity, distortion of the molecule with increasing rotation, $\hat{J}$. In the following, such an expansion of the rigid model is performed for the HT molecule and the tritiated water isotopologues.

Derivation of vibrational modes

Mathematically, vibrations come into play when the nuclear motion in the vicinity of the equilibrium position $\mathbf{X}_0$ is considered. By Taylor-expansion of the effective potential V_{eff} around this equilibrium position with small displacements $\Delta\mathbf{X}_i = (\mathbf{X}_0 - \mathbf{X}_i)$ the following expression is obtained.

$$V_{\text{eff}}(\mathbf{X}) \approx V_{\text{eff}}(\mathbf{X}_0) + \frac{1}{2} \sum_{i,j} \left. \frac{\partial^2 V_{\text{eff}}}{\partial\mathbf{X}_i \partial\mathbf{X}_j} \right|_{\mathbf{X}=\mathbf{X}_0} \Delta\mathbf{X}_i \Delta\mathbf{X}_j. \tag{2.12}$$

The second term represents a quadratic potential around the equilibrium geometry, leading to the harmonic approximation. The quadratic form is characteristic of simple harmonic oscillators.

After transformation to normalised coordinates using

$$\mathbf{Q}_k = \sum_i L_{ki} \Delta \mathbf{X}_i, \tag{2.13}$$

where L_{ki} are the elements of the transformation matrix, Equation 2.9 transforms to

$$H_{\text{vib}} = \sum_k \left(-\frac{\hbar^2}{2} \frac{\partial^2}{\partial \mathbf{Q}_k^2} + \frac{1}{2} \omega_k^2 \mathbf{Q}_k^2 \right). \tag{2.14}$$

Here, ω_k are the vibrational frequencies corresponding to the normal modes. Each term in the vibrational Hamiltonian resembles the Hamiltonian of a quantum harmonic oscillator. The solutions to this Hamiltonian are well-known:

$$E_{\text{vib},k} = \left(\nu_k + \frac{1}{2} \right) \hbar \omega_k \tag{2.15}$$

where ν_k is the vibrational quantum number for the k-th normal mode, taking values $\nu_k = 0, 1, 2, \ldots, 3N - 6$ for a N-atomic molecule.

Note that the harmonic approximation is only valid for small displacements and does not take into account the dissociation energy D_e. For higher modes $\nu_k > 2$ and mixing of modes, anharmonic contributions should be taken into account.

In the anharmonic case, the spacing of the energy levels decreases as ν increases, reflecting the nature of real molecular vibrations.

2.1.2 Molecular energy levels of HT

Tritium hydride (HT) is a diatomic molecule consisting of protium (^{1}H) and the radioactive hydrogen isotope tritium (^{3}H). For the determination of the ro-vibrational transitions in HT in Section 6 essential information about (i) rotation, (ii) vibration, and (iii) the hyperfine structure of this molecule are presented.

The simplified Hamiltonian for HT is given by

$$\hat{H}_{\text{HT}} = \hat{H}_{\text{rot}} + \hat{H}_{\text{vib}} + \hat{H}_{\text{HF}} + \hat{H}_{\text{e}} \tag{2.16}$$

forming the base for the quantum mechanical understanding of HT.
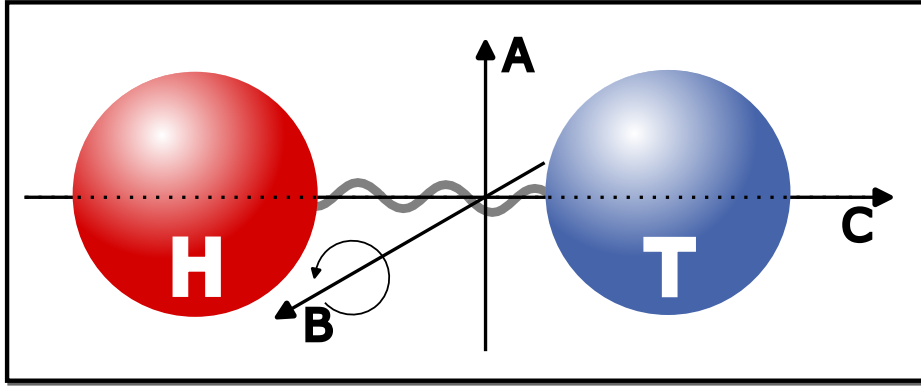
Figure 2.1: Illustration of the rotation and vibration in HT. The rotational axis A, B and C with the centre of mass as origin of ordinates. Rotation is only possible for the A and B axis. Only vibrational mode is a stretching vibration along the C axis.

Rotation

In Figure 2.1 the HT molecule and its rotational axis (A, B and C) intersecting in the centre of mass are illustrated. As a diatomic molecule, the moments of inertia for the x and y axes are the same $I_A = I_B$, while the one for the C axis vanishes $I_C = 0$. The moment of inertia about an axis perpendicular to the bond axis (C) is $I = \mu a^2$, where a is the equilibrium bond length and μ is the reduced mass.

The rotational Hamiltonian for the HT molecule starting from Equation 2.10 can be written as

$$\hat{H}_{\mathrm{rot}} = \frac{\hat{J}^2}{2I} \tag{2.17}$$

where $\hat{J}^2$ is the square of the total angular momentum operator.
The corresponding Schrödinger equation

$$\hat{H}_{\mathrm{rot}}|\Psi(\theta, \phi)\rangle = E_{\mathrm{rot}}|\Psi(\theta, \phi)\rangle, \tag{2.18}$$

where $|\Psi(\theta, \phi)\rangle$ are the rotational wavefunctions in spherical coordinates using the angles θ and ϕ, is solved by the following rotational energy eigenvalues

$$E_{\mathrm{rot},J} = \frac{\hbar^2 J(J+1)}{2I}. \tag{2.19}$$

In order to account for the non-rigidity of molecules, one can evolve the Hamiltonian by including contributions with higher orders of $\hat{J}^2$ that reflect the linear ($\sim (\hat{J}^2)^2$) or nonlinear ($\sim (\hat{J}^2)^{x>2}$)) stretching of the molecule during rotation.
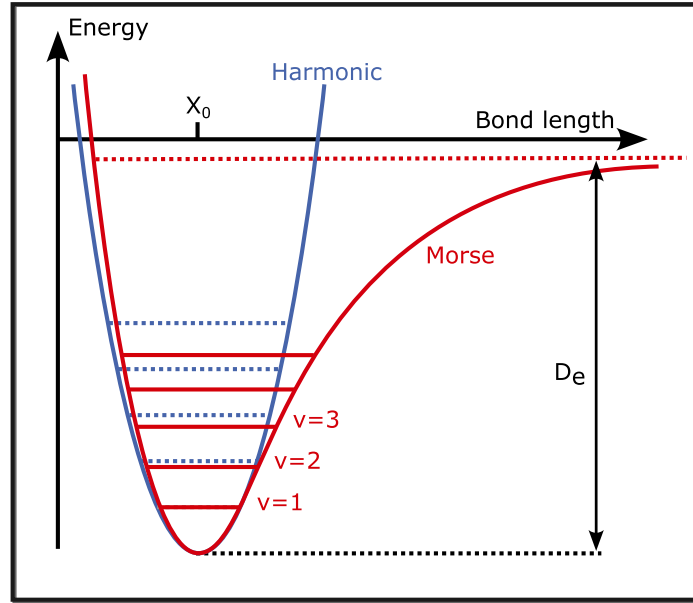
Figure 2.2: Comparison of the harmonic and Morse potential. The equilibrium position X_0 is same for both potentials. The spacing between vibrational states (ν) are same for the harmonic case (blue) and decreasing for increasing excitation for the Morse potential (red). In addition, the Morse potential takes into account the dissociation energy D_e as upper boundary.

Vibration

As visible in Figure 2.1, the only possible vibration for HT is a stretching vibration along the C axis. In the previous section, the description of the vibrational motion using the harmonic oscillator approach was derived (cf. Equation 2.15). However, this approach is only valid for small displacements. For a diatomic molecule, like HT, the Morse potential [Mor29] is a suitable ansatz which is defined as

$$V_{\text{Morse}}(\mathbf{X}) = D_e \left(1 - e^{-a(\mathbf{X}-\mathbf{X}_0)}\right)^2, \tag{2.20}$$

where the dissociation energy D_e is implemented as upper boundary and parameter a is controlling the width of the potential well, the distance between the nuclei. Solutions for this potential are

$$E_{\text{vib},\nu} = \left(\nu + \frac{1}{2}\right)\hbar\omega_e - \left(\nu + \frac{1}{2}\right)^2 \frac{\hbar\omega_e x_e}{2}, \tag{2.21}$$

where x_e is the anharmonicity constant. These energy levels show that the spacing between them decreases as ν increases, reflecting the anharmonic nature of real molecular vibrations. In Figure 2.2, the Harmonic and Morse potential are sketched with indicated vibration levels, the equilibrium bond length of the nuclei X_0 and the dissociation energy D_e.

Molecular hyperfine structure

When calculating energy levels on a very precise level (order of hundreds of kHz or $<$ 10^{-10} eV), more corrections to the BO solution than the adiabatic, non-adiabatic, relativistic and QED contributions are needed. On this scale, the hyperfine coupling, is relevant and leads to a splitting of the energy levels.

The hyperfine coupling in the HT molecule results from interaction of nuclear spin I of the molecule's nuclei and the molecule rotation. For HT there are two different interactions: (i) nuclear spin-rotation interaction $\hat{H}_{\text{IJ}}$ and (ii) the nuclear spin-spin dipole coupling $\hat{H}_{\text{II}}$,[1]

$$\hat{H}_{\text{HF}} = \hat{H}_{\text{IJ}} + \hat{H}_{\text{II}}. \tag{2.22}$$

These magnetic dipole terms were first derived for diatomic molecules by Frosch and Foley [Fro52] and recently computed for the HT molecule by Jóźwiak et al. [Jóź21].

To solve the terms, the rotational angular momentum of the molecule J, is coupled with one of the nuclear spins I_1, forming the intermediate angular momentum F_1, which is then subsequently coupled with the nuclear spin of the other nucleus, I_2. The resulting total angular momentum and its projection on the B axis were denoted by F and m_F, respectively. The coupled basis vector is therefore given by $|\nu, ((J'I_1)F_1I_2), F, m_F\rangle$.

The eigenvectors of the hyperfine Hamiltonian, diagonalised with respect to total angular momentum, are denoted in [Jóź21] as $|\nu, J, F, (\pm)\rangle$ where the labels $(\pm)$ mark the eigenstates for given J and F that are higher (+) or lower energy (-).

The relation between the eigenvectors is given by

$$|\nu, J, F, (\pm)\rangle = \sum_{F_1=|F-I_2|}^{F+I_2} \sum_{J'=|F_1-I_1|}^{F_1+I_1} a_{J'F_1}^{\nu JF(\pm)} |\nu, ((J'I_1)F_1I_2), F, m_F\rangle, \tag{2.23}$$

where $a_{J'F_1}^{\nu JF(\pm)}$ is the coupling factor. A coupling between different rotational states $J \neq J'$ is according to Jóźwiak et al. 9-11 orders of magnitude suppressed meaning that only $J = J'$ is considered.

In Figure 2.3, an energy level diagram is provided that shows how the rotational levels split when considering the hyperfine structure. As an example, the R(0) transition ($J = 0 \to 1$) is indicated, which when the hyperfine components are considered, splits into 7 transitions.

Notation and currently leading computations

The term with a complete set of quantum numbers for an energy state of the HT molecule describing its rotation, vibration and the molecular hyperfine state is:

$$|\nu, J, F, (\pm)\rangle. \tag{2.24}$$

---

[1]Note, that the, here missing, electric quadrupole interaction is only relevant when the nuclei spins are $I \geq 1$.
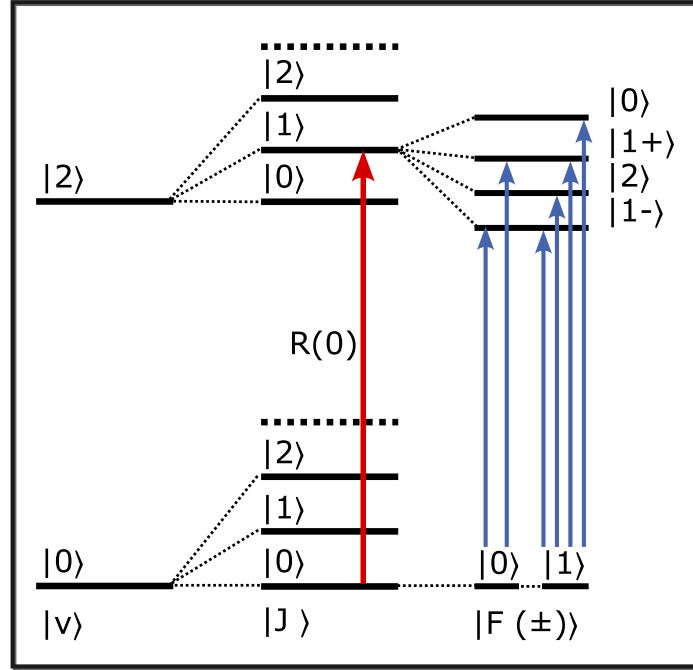
Figure 2.3: Energy level diagram for selected levels in HT. The energy levels of vibrational (ν) ground state and the first overtone are shown for rotational quanta $J < 3$. For the rotational level of the R(0) line ($J = 0 \rightarrow 1$) the hyperfine components are indicated. When considering (or resolving) those hyperfine components the pure ro-vibrational transition (red) splits into 7 lines (blue).

The quantum numbers for the vibration is ν, for the rotation (angular momentum of the molecule) J and the total angular momentum plus the denotation whether higher or lower energy level are given by F and ($\pm$).

The energy levels of HT which are base for assignment of the transition energies are computed using two different approaches. Pachucki et al. use a direct non-adiabatic variational approach (DNA) that does not use the Born-Oppenheimer approximation [Pac22]. The solution accounts for all the non-adiabatic effects and yields directly the non-relativistic energy of a rovibrational level. The results from this non-relativistic approach are refined using computations of relativistic and quantum electrodynamical (QED) corrections.

The other method is the Non-Adiabatic Perturbation Theory (NAPT) [Pac08] which is based on the perturbative separation of electronic and nuclear movements. The expansion uses the ratio of electron mass m_e and the reduced nuclear mass μ_n. The solutions of NAPT are refined using non-relativistic quantum electrodynamics (NRQED) [Kom19a]. The principal assumption in NRQED is that the total energy can be expanded in powers of the fine-structure constant α

$$E(\alpha) = \alpha^2 m E^{(2)} + \alpha^4 m (E^{(4)} + E^{FS}) + \alpha^5 m E^{(5)} + \alpha^6 m E^{(6)} + ... \qquad (2.25)$$

where E^{FS} is the finite nuclear size correction. The expansion terms are interpreted as the non-relativistic energy $E^{(2)}$, the relativistic correction $E^{(4)}$, the leading QED correction $E^{(5)}$, and the higher-order QED corrections $E^{(i)}$ $i \geq 6$. The energy levels obtained from these calculations and the Fortran source code are available on the H2SPECTRE website[2]. Note that accurate measurement of transitions in HT, as performed in this work, will challenge QED corrections. Transitions between these energy levels are further discussed in Section2.2.

2.1.3 Molecular energy levels of tritiated water isotopologues

Tritiated water isotopologues, such as HTO (hydrogen tritium oxide), DTO (deuterium tritium oxide) and T_2O (tritium oxide), are different species of the water molecule in which one or more hydrogen atoms are replaced with tritium. These isotopologues maintain the bent molecular structure characteristic of water and belong to the C_{2v} point group. These molecules are the subject of this work that determine differences in molecular energy levels. Note that in this work only the species containing ^{16}O were studied.
This chapter provides a comprehensive derivation of the molecular energy levels of tritiated water isotopologues, focussing on their rotational and vibrational structures.

Rotation and the Watson A-reduced Hamiltonian

As presented in the illustration in Figure 2.4, tritiated water isotopologues rotate around the rotational axes A, B and C. Due to the asymmetry of the molecules the moment of inertia for rotation around these axes are all different, which, according to the introduction section to molecular rotation (cf. Section 2.1.1), classifies tritiated water as an asymmetric rotor.

The Hamiltonian for rigid-rotor from Equation 2.10 does only apply for small $\hat{J}$ and is therefore an incomplete model when describing the rotational states of tritiated water. In 1967, James K. G. Watson [Wat67] derived a reduced Hamiltonian to describe asymmetric top molecules the <u>A-reduced Watson Hamiltonian</u>[3]. His model consists of terms depending on the powers of the rotational quantum numbers $\hat{J}^2$ and $\hat{J}_z^2$, which is the component around the main rotation axis, and of off-diagonal elements using $\Delta \hat{J}_{xy} = \left(\hat{J}_x^2 - \hat{J}_y^2 \right)$.

The terms can be subdivided in combined power of $\hat{J}^2$, $\hat{J}_z^2$ and $\Delta \hat{J}_{xy}$:

$$H_{\mathrm{red}}^A = H^{(2)} + H^{(4)} + H^{(6)} + H^{(8)} + H^{(10)}. \tag{2.26}$$

---

[2]H2SPECTRE https://qcg.home.amu.edu.pl/H2Spectre.html
[3]The A indicates the reduced Hamiltonian for the asymmetric tops.
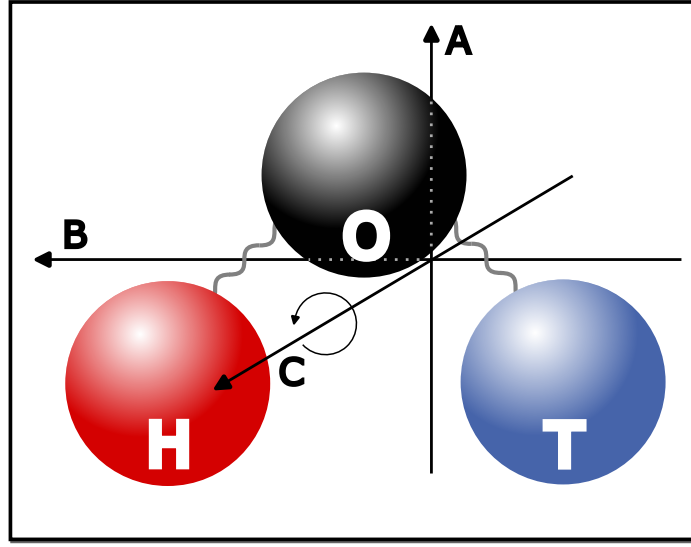
Figure 2.4: Illustration of the rotation tritiated water on the example of HTO. The rotational axes A, B, and C intersect the centre of mass as the origin of the ordinates. Rotation for all three axes occurs with different moments of inertia.

The superscript represents the combined power of the rotational quantum numbers. The second order term is given by

$$
\begin{aligned}
H^{(2)} = & \left[\frac{1}{2}(A+B)\hat{J}^2 + \left(C - \frac{1}{2}(A+B) \right) \hat{J}_z^2 \right] \\
& + \left[\Delta \hat{J}_{xy} \left(\frac{1}{4}(A-B) \right) + \left(\frac{1}{4}(A-B) \right) \Delta \hat{J}_{xy} \right].
\end{aligned}
$$

(2.27)

Here, the only parameters are A, B and C, the effective principal rotational constants. The quartic order is given by

$$
\begin{aligned}
H^{(4)} = & \left[-\Delta_J (\hat{J}^2)^2 - \Delta_{JK} \hat{J}^2 \hat{J}_z^2 - \Delta_K \hat{J}_z^4 \right] \\
& + \left[\Delta \hat{J}_{xy} \left(-\delta_J \hat{J}^2 - \delta_K \hat{J}_z^2 \right) + \left(-\delta_J \hat{J}^2 - \delta_K \hat{J}_z^2 \right) \Delta \hat{J}_{xy} \right],
\end{aligned}
$$

(2.28)

with Δ_J, Δ_{JK}, Δ_K, δ_J and δ_K as quartic distortion parameters. The sextic distortion terms have been presented later by Watson in [Wat68] with

$$
\begin{aligned}
H^{(6)} = & \left[+ H_J \left(\hat{J}^2 \right)^3 + H_{JK} \left(\hat{J}^2 \right)^2 \hat{J}_z^2 + H_{KJ} \hat{J}^2 \hat{J}_z^4 + H_K \hat{J}_z^6 \right] \\
& + \left[\Delta \hat{J}_{xy} \left(h_J \left(\hat{J}^2 \right)^2 + h_{JK} \hat{J}^2 \hat{J}_z^2 + h_K \hat{J}_z^4 \right) \right. \\
& \left. + \left(h_J \left(\hat{J}^2 \right)^2 + h_{JK} \hat{J}^2 \hat{J}_z^2 + h_K \hat{J}_z^4 \right) \Delta \hat{J}_{xy} \right],
\end{aligned}
\tag{2.29}
$$

and the corresponding sextic distortion parameters H_J, H_{JK}, H_{KJ}, H_K, h_J, h_{JK} and h_K. Analogous parameters for the octic (using L_i, l_i),

$$
\begin{aligned}
H^{(8)} = & \left[L_J \left(\hat{J}^2 \right)^4 + L_{JJK} \left(\hat{J}^2 \right)^3 \hat{J}_z^2 + L_{JK} \left(\hat{J}^2 \right)^2 \hat{J}_z^4 + L_{KKJ} \hat{J}^2 \hat{J}_z^6 + L_K \hat{J}_z^8 \right] \\
& + \left[\Delta \hat{J}_{xy} \left(l_J \hat{J}^6 + l_{JK} \hat{J}^4 \hat{J}_z^6 + l_{KJ} \hat{J}^2 \hat{J}_z^4 + l_K \hat{J}_z^6 \right) \right. \\
& \left. + \left(l_J \hat{J}^6 + l_{JK} \hat{J}^4 \hat{J}_z^6 + l_{KJ} \hat{J}^2 \hat{J}_z^4 + l_K \hat{J}_z^6 \right) \Delta \hat{J}_{xy} \right],
\end{aligned}
\tag{2.30}
$$

and dectic order (using parameters P_i, p_i)

$$
\begin{aligned}
H^{(10)} = & \left[P_{JJK} \left(\hat{J}^2 \right)^5 + P_{JJK} \left(\hat{J}^2 \right)^4 \hat{J}_z^2 + P_{JK} \left(\hat{J}^2 \right)^3 \hat{J}_z^4 \right. \\
& \left. + P_{KJ} \left(\hat{J}^2 \right)^2 \hat{J}_z^6 + P_{KKJ} \hat{J}^2 \hat{J}_z^8 + P_K \hat{J}_z^{10} \right] \\
& + \left[\Delta \hat{J}_{xy} \left(p_J \hat{J}^8 + p_{JJK} \hat{J}^6 \hat{J}_z^2 + p_{JK} \hat{J}^4 \hat{J}_z^4 + p_{KKJ} \hat{J}^2 \hat{J}_z^6 + p_K \hat{J}_z^8 \right) \right. \\
& \left. + \left(p_J \hat{J}^8 + p_{JJK} \hat{J}^6 \hat{J}_z^2 + p_{JK} \hat{J}^4 \hat{J}_z^4 + p_{KKJ} \hat{J}^2 \hat{J}_z^6 + p_K \hat{J}_z^8 \right) \Delta \hat{J}_{xy} \right],
\end{aligned}
\tag{2.31}
$$

are used in some cases. This model can be used to describe the experimental data obtained from a molecule. By determining the lower and upper vibrational state (except for data of pure rotational transitions), the data can be represented by two (one) sets of parameters. At the same time, a good agreement of the complete data set with the fit can validate the assignment.

For water, Messer et al. [Mes84] and J.W.C. Johns [Joh85] demonstrated early that the
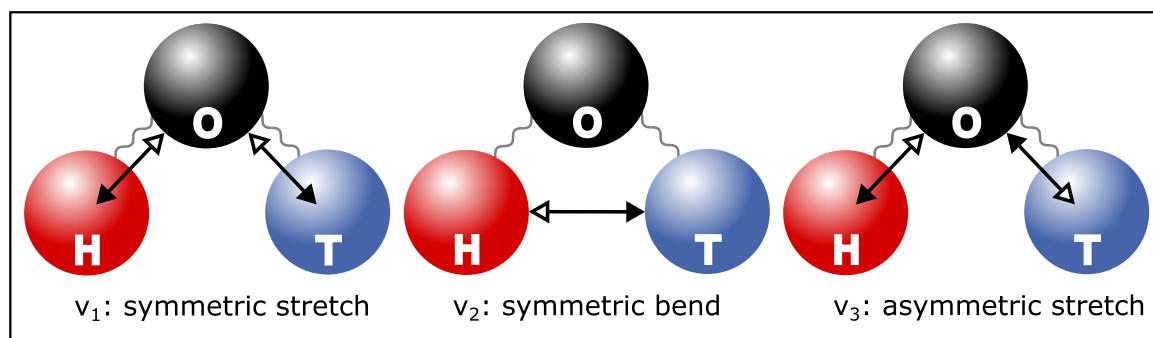
Figure 2.5: Illustration of the vibrational modes in tritiated water on the example of HTO. Three independent modes occur in (tritiated) water. Arrows indicate movement of the nuclei. When several arrows, white / black directed motions ocure synchronously.

fits converge slowly using this model, demanding high-order parameters (up to the 12th order). A discussion of different calculations is presented in [Wat06]. For the tritiated water species, similar behaviour is expected.

It should be noted that the conventional notation of rotational states: For water, the angular momentum is provided using J, K_A, K_C, corresponding to the general notation J, J_z, J_y.

Vibrational modes

Water species possess three independent vibrational modes. As illustrated in Figure 2.5, these modes can be understood as

- **Symmetric stretch (ν_1)**: a vibration of the two hydrogen-oxygen bonds in the same direction;
- **Symmetric bend (ν_2)**: a bending of the molecule by changing the angle between the two hydrogen-oxygen bonds;
- **Asymmetric stretch (ν_3)**: a vibration of the two hydrogen-oxygen bonds with opposite atomic motions.

While the stretch vibration modes are of the same order of magnitude, the bending mode requires about factor two less energy. The vibrational energy levels for the tritiated water species are shown in Figure 2.6. They have been extracted from the predictions of the SPECTRA database [Mik05]. From the comparison of the energy of same vibrational modes from different species the strong influence of the mass in the vibrational energies become evident. It should be noted that for transitions between vibrational states the rotational states need to be included. This leads to hundreds of measurable lines for each vibrational excitation that cover over hundreds of wavenumbers.
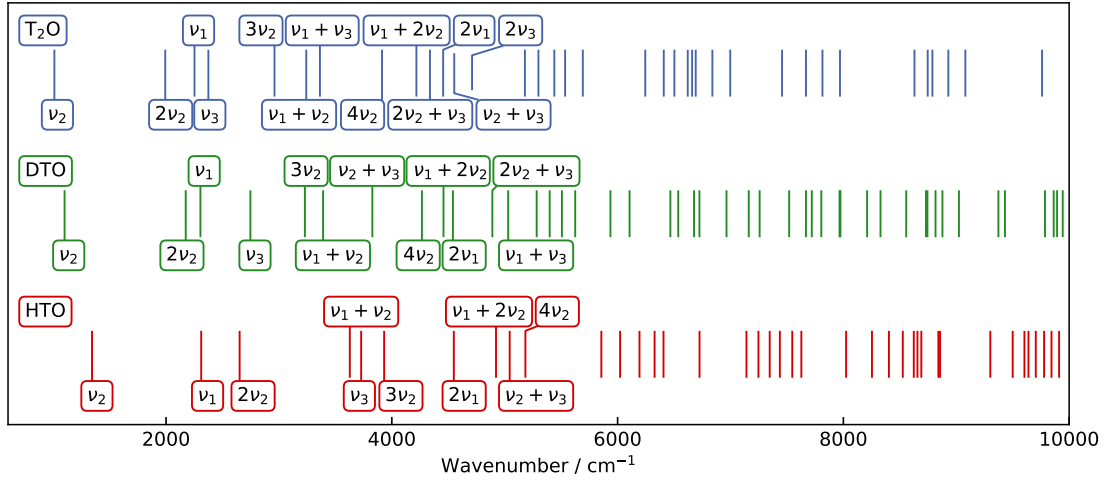
Figure 2.6: Vibrational energy levels for the tritiated water species. The vibrational energies were extracted from predictions in the SPECTRA database [Mik05]. The lowest states are labeled with the vibrational quanta ν_1, ν_2 and ν_3.

In summary, for the tritiated water species a state is named using

$$|\nu_1, \nu_2, \nu_3, J, K_A, K_C\rangle, \qquad (2.32)$$

including the 3 vibrational modes and the 3 rotational quantum numbers.

2.2 IR transitions between energy levels

This work makes use of the ability of infrared light (IR) to interact with the molecules of interest, HT and the tritiated water species. The range of IR light used extends from $\lambda^{-1} = 2000 - 10\,000\,\mathrm{cm}^{-1}$, or $\lambda = 5 - 1\,\mu\mathrm{m}$, corresponding to mid-infrared (MIR) and near-infrared (NIR) light. Its energy E_γ, defined by

$$E_\gamma = \frac{h \cdot c}{\lambda}, \qquad (2.33)$$

with Planck's constant h and c the speed of light in a vacuum, is sufficient to transition the investigated molecules from the ground states to a vibrationally excited energy states.
In this section, a brief derivation of the quantum-mechanical description of these transitions is derived, including the molecule-specific conditions. Then, an overview of the underlying effects on spectra, measurement of transition energies, is provided.

2.2.1 Quantum mechanical description of IR transitions

When a photon is interacting with a molecule, the molecule's system $\hat{H}_0$ is perturbed by the interaction with the photon, $\hat{H}'$:

$$\hat{H} = \hat{H}_0 + \hat{H}'(t)$$
$$\text{with}$$
$$\hat{H}'(t) = -\hat{\mu} \cdot \mathbf{E}_\gamma(t)$$

(2.34)

Here, $\hat{\mu}$ is the dipole moment operator, a molecule specific quantity which determines the coupling strength of the electric field of the photon $\mathbf{E}_\gamma(t)$ to the molecule. For a monochromatic plane wave, $\mathbf{E}_\gamma(t)$ can be expressed as

$$\mathbf{E}_\gamma(t) = \mathbf{E}_0 \cdot e^{-i\omega t} + \mathbf{E}_0^* \cdot e^{-i\omega t},$$

(2.35)

where $\omega = \dfrac{2\pi c}{\lambda}$ implies the photon's wavelength.

For a transition from an initial state $|i\rangle$ to a final state $|f\rangle$ one needs to evaluate the transition probability $P_{i \to f}(t)$,

$$
\begin{aligned}
P_{i \to f}(t) &= \left| \frac{1}{i\hbar} \int_0^t \mathrm{d}t' \langle f|\hat{H}'(t')|i\rangle \right|^2 \\
&\approx \frac{1}{\hbar^2} \left| \langle f|\hat{\mu}|i\rangle \int_0^t \mathbf{E}_0 \cdot e^{-i(\omega_{fi}-\omega)t'}\mathrm{d}t' \right|^2 \\
&= \frac{1}{\hbar^2} \left| \langle f|\hat{\mu}|i\rangle \frac{e^{-i(\omega_{fi}-\omega)t} - 1}{i(\omega_{fi}-\omega)} \right|^2 \\
&= \frac{1}{\hbar^2} |\langle f|\hat{\mu}|i\rangle|^2 \left[\frac{\sin\left((\omega_{fi}-\omega)/2 \cdot t\right)}{(\omega_{fi}-\omega)/2} \right]^2 \\
&\overset{t\to\infty}{=} t \cdot \frac{2\pi}{\hbar} |\langle f|\hat{\mu}|i\rangle|^2 \cdot \delta(\omega_{fi}-\omega),
\end{aligned}
$$

(2.36)

where for simplification in second step only the real part of the wave function is considered. It is evident from the delta function that for a significant transition amplitude the frequency must match the energy gap between the initial state E_i and the final state E_f,

$$\hbar\omega_{fi} = E_i - E_f.$$

(2.37)

An other condition for transition is given by the matrix element $|\langle f|\hat{\mu}|i\rangle|^2$, which must not vanish. This leads to a set of requirements on the changes of quantum numbers within a transitions. The selection rule for the total angular momentum for absorption transitions is given by

$$\Delta J = -1, 1.$$

(2.38)

For the vibrational quantum number changes are given by

$$\Delta\nu = 0, \pm 1, \pm 2, ... \tag{2.39}$$

For IR absorption of the investigated molecules in this work, only transitions with change of vibrational state are measured.

2.2.2 Line intensity

The line intensity recorded in the experiment depends on the light source intensity I_0, the interaction path length z, and the absorbance function $\alpha(\omega)$

$$I = I_0 e^{-\alpha(\omega)z}. \tag{2.40}$$

This absorbance function is related to a transition probability $P_{i\to f}$ in an interaction path length z and the density of molecules in the lower state N_i

$$\alpha(\omega) \propto |\langle f|\hat{\mu}|i\rangle|^2 \cdot N_i = \sigma_{fi} N_i. \tag{2.41}$$

The relation resulting from inserting Equation 2.41 in Equation 2.40

$$I = I_0 e^{-\sigma_{fi} N_i z} \tag{2.42}$$

is known as **Beer-Lambert law**.

2.2.3 Line shape and broadening effects

Spectral lines in discrete absorption spectra are never strictly monochromatic. Even with ideal spectrometers, one would observe a spectral distribution $I(\nu)$.
This so-called observed line shape is characterised by (i) its position, which should correspond to the transition frequency ω_{fi} derived in the previous chapter, and (ii) its profile, including a finite line width. The line width or FWHM (full-width at half-maximum) describes the spectral width of the profile with $I(\nu) > \frac{1}{2}I_0$. Both the line profile and the line width are dependent on effects causing such broadening. In the following, the broadening effects relevant for this work are explained.

2.2.3.1 Natural linewidth and Lorentzian profile

The intensity I of a plane wave passing in the z-direction through an absorbing sample decreases along the absorption path. The spectral absorbance feature $\alpha(\omega)$, introduced in the previous section, is given by

$$I = I_0 e^{-\alpha(\omega)z} = I_0 e^{-\sigma_{ij} N_i z}, \tag{2.43}$$
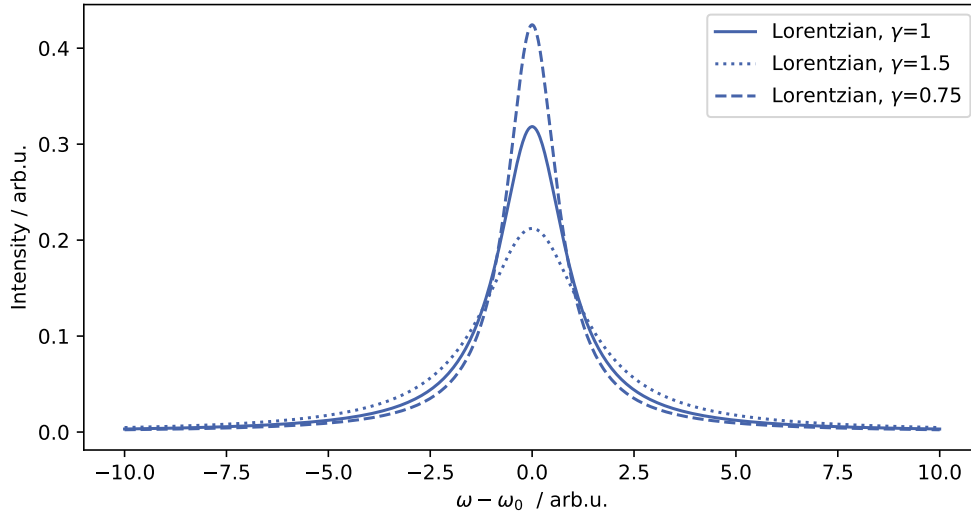
Figure 2.7: Lorentzian profile for three different width γ.

with the absorption cross-section σ_{ij} and the density of particle in the initial state N_i. The absorption profile $\alpha(\omega)$, which will be observed in the recorded spectrum, can be obtained from *Kramers–Kronig* dispersion relations (derived in Chapter 3.1.3 in [Dem10]) for frequencies in the vicinity of a molecular transition frequency ω_0 where $|\omega_0 - \omega| \ll \omega_0$.

$$\alpha(\omega) = \frac{Ne^2}{4\epsilon_0 mc} \frac{\gamma}{(\omega_0^2 - \omega^2) + (\gamma/2)^2}, \tag{2.44}$$

with the number of molecules N, the molecule mass m and the natural line width γ. The natural linewidth is related to the lifetime of the excited state. Effects shortening the lifetime of the excited state are broadening the natural line width, fulfilling Heisenberg's uncertainty principle. Namely, there are three aspects to highlight:

- Dipole moment: A large dipole moment results in a short lifetime of the excited state leading to a broader natural line width.

- Energy gap: The lifetime is antiproportional to the cube of the transition energy (ω_0^3).

- Selection rules: Specific excited states in molecules can have long lifetimes as a result of selection rules. These forbidden transitions have extremely reduced probabilities but are therefore much narrower.

The line profile in $\alpha(\omega)$,

$$L(\omega) = \frac{1}{\pi} \frac{\gamma}{(\omega_0 - \omega)^2 + (\gamma/2)^2}, \tag{2.45}$$

is known as **Lorentzian** profile as displayed in Figure 2.7.

2.2.3.2 Doppler broadening and Gaussian profile

Lorentzian line profile with natural linewidth can only be observed under certain conditions since other broadening effects usually dominate. One of the major contributions to the spectral linewidth in gases at low pressures is the Doppler broadening, which is due to the thermal motion of the absorbing molecules.

Thermal motion of a molecule changes the absorption frequency ω_a according to the relative projection of its velocity $\mathbf{v}$ to the wave vector $\mathbf{k}$ of the incident light

$$\omega_a = \omega_0 + \mathbf{v} \cdot \mathbf{k} = \omega_0 \left(1 - \frac{v_k}{c} \right). \tag{2.46}$$

This means a higher frequency ω_a is needed when the molecule is moving with propagation of the probing light, and lower when it is counter-propagating.

Considering a gas in thermal equilibrium, the velocity of the molecule follows the Maxwell-Boltzmann distribution velocity distribution. At the temperature T, the number of molecules $N_i = \int ni(v_k) \mathrm{d}v_k$ in the level E_i per unit volume with a velocity component between v_k and $v_k + \mathrm{d}v_k$ is given by

$$ni(v_k) \mathrm{d}v_k = \frac{N_i}{v_p \sqrt{\pi}} e^{(v_k/v_p)^2} \mathrm{d}v_k. \tag{2.47}$$

Here, $v_p = \sqrt{(2k_\mathrm{B}T/m)}$ is the most probable velocity of the molecules with mass m, k is the Boltzmann constant.

From Equation 2.46 one can derive $\mathrm{d}v_k = (c/\omega)\mathrm{d}\omega$ and insert it in Equation 2.47

$$n_i(\omega) \mathrm{d}\omega = \frac{N_i c}{\omega v_p \sqrt{\pi}} \exp \left[-\left(\frac{c(\omega - \omega_0)}{\omega_o v_p} \right)^2 \right] \mathrm{d}\omega \tag{2.48}$$

As the absorbed radiant power $P(\omega)\mathrm{d}\omega$ is proportional to the density of molecules $n_i(\omega)\mathrm{d}\omega$ absorbing in the interval $\mathrm{d}\omega$, the intensity profile of a Doppler-broadened spectral line can be written as

$$I(\omega) = I_0 \exp \left[-\left(\frac{c(\omega - \omega_0)}{\omega_o v_p} \right)^2 \right]. \tag{2.49}$$

This line shape follows a **Gaussian** profile as presented in Figure 2.8 with a Doppler width of $\sigma = \frac{\omega_0}{c} v_p = \frac{\omega_0}{c} \sqrt{2k_\mathrm{B}T/m}$. This implies that the Doppler-width is depending on the square root of the temperature. Also, it depends on the mass with $\sqrt{\frac{1}{m}}$ therefore the effect is more dominant for light molecules. For the application in this work, the FWHM width is used instead of the derived root-mean square. This is given by $\sigma_\mathrm{FWHM} = \frac{\omega_0}{c} \sqrt{8k_\mathrm{B}T \ln 2/m}$.
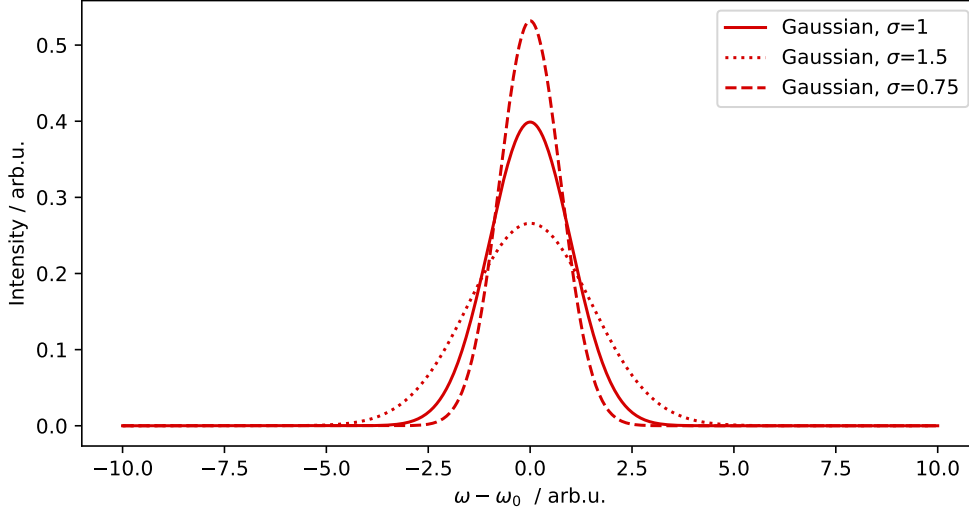
Figure 2.8: Gaussian profile for three different widths σ.

2.2.3.3 Collisional broadening and collisional shift

When a molecule i in the energy state E_i encouters another molecule j in the energy state E_j, the energy state of i is shifted by the interaction with molecule j. This shift can be positive as well as negative and leads in an absorbing gas to an additional broadening and a shift of the transition frequency. Often, this effect is named **pressure broadening and pressure shift**, but this collisional interaction depends on the electronic structure of the interacting molecules and therefore depends on the composition of the gas.

When measuring a gas mixture of many species as e.g. in atmospheric observations, one approach is to calculate the influence to a molecule for each relevant interaction partner (species), like here [Gam19] for H_2O in H_2. This requires extensive calculations and has not been performed for tritiated species yet. Also, a machine learning approach [Gue24] is not yet available for the tritiated water species measured in this work.

A phenomenological description of this broadening is obtained by using a modified Lorentzian

$$I(\omega) \propto \frac{1}{(\omega_0 - \omega - \Delta\omega)^2 + (\gamma_{\text{eff}}/2)^2}, \tag{2.50}$$

where $\Delta\omega = N_j \cdot \bar{v} \cdot \sigma_{s,j}$ is the collisional shift and $\gamma_{\text{eff}} = \gamma + N_j \cdot \bar{v} \cdot \sigma_{b,j}$ the collisional broadening.

Those parameters depend on the density of the interaction partner j, the mean velocity of the probed species $\bar{v}$, and the collisional cross sections $\sigma_{s,j}$ for the shift and $\sigma_{b,j}$ for the broadening. As these are not available for tritiated species, the broadening is taken into account by introducing a fit parameter. The collisional shift can be measured when
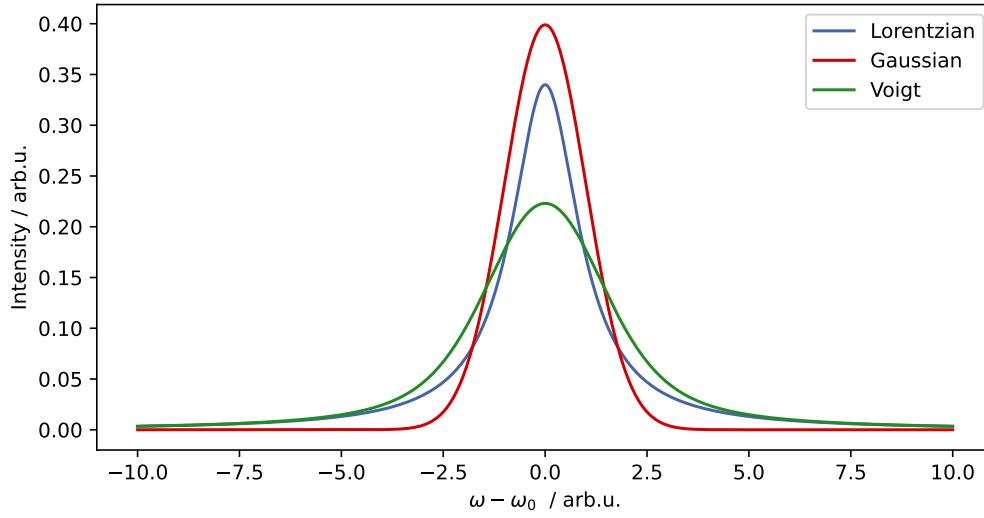
Figure 2.9: Voigt profile in comparison with a Gaussian and a Lorentzian of comparable width. The Voigt profile is the convolution of both, Lorentzian and Gaussian. The width of all three curves is set to unity for better comparison.

performing several measurements with same composition but different pressures and extrapolating to pressure $p = 0$.

2.2.3.4 The Voigt profile

The previous section introduces the natural line width, the Doppler broadening, and the collision-induced broadening and shift. In most experiments, all these contributions jointly affect the observed line.

The resulting line shape exhibits features of Lorentzian as well as of Gaussian. In fact, this line shape is a convolution of Gaussian-like broadening contributions and Lorentzian-like contributions. This convolution

$$
\begin{aligned}
V(\omega; \sigma, \gamma) &= \int_{-\infty}^{\infty} G(\omega'; \sigma) L(\omega - \omega'; \gamma) \mathrm{d}\omega' \\
&\propto \frac{\gamma \sigma}{\omega_0} \int_{0}^{\infty} \frac{\exp\left[-(\sigma(\omega_0 - \omega')/(\omega_0))^2\right]}{(\omega_0 - \omega')^2 + (\gamma/2)^2} \mathrm{d}\omega'
\end{aligned}
\tag{2.51}
$$

is known as **Voigt profile** which takes into account both widths, the Gaussian width σ and the Lorentzian width γ. As an example in Figure 2.9, a Gaussian and a Lorentzian width comparable width are convoluted to a Voigt profile.

This model serves as a good base for fitting spectral lines with collisional and Doppler broadening and is therefore used for the determination of the tritiated water lines in this work.

3 Current research and objectives in spectroscopy of water and molecular hydrogen with tritium

This chapter presents a summary of work in the field of (i) spectroscopy of tritiated water, including a brief overview of research performed on non-tritiated species, and (ii) precision measurements of molecular hydrogen, with a particular focus on ro-vibrational studies. From the current state of research, the objectives of this work are derived.

3.1 Spectroscopy of tritiated water

The interest in water spectroscopy originates, in part, from the fact that water spectra are essential to a wide range of scientific and engineering applications, such as combustion, atmospheric sciences, and astronomy. In many cases, accurate knowledge of water lines is necessary to subtract their influence and reveal the lines of interest [Ber02]. As a result, an extensive database for water isotopologues has been developed, with resources such as HITRAN [Gor22] and GEISA [Jac16] serving as key references.

For the most common water isotopologue, $H_2^{16}O$, existing spectroscopic databases contain more than 300,000 experimental ro-vibrational lines and 20,000 empirical energy levels. In particular, Jean-Marie Flaud has made significant contributions to the collection of these spectroscopic data, providing thousands of measured line positions, intensities, and collision parameters for various water isotopologues [Fla72; Cam73; Fla73; Fla75].

From the pioneering work of Flaud et al. [Fla76], which introduced the conversion of measured transitions into empirical energy values, Furtenbacher et al. derived the MARVEL (Measured Active Rotational-Vibrational Energy Levels) protocol [Fur07; Fur12]. This method allows for the validation and refinement of experimental data while also facilitating predictions of yet unmeasured lines.

In the past decade, advancements in precision spectroscopy have enabled the determination of transition energies in water isotopologues with kilohertz precision [Kas18; Che18a] ($3\,\mathrm{kHz} \approx 1 \cdot 10^{-7}\,\mathrm{cm}^{-1}$). Techniques such as NICE-OHMS have also allowed for precise measurements of transitions in $H_2^{17}O$ [Mel21], $H_2^{18}O$ [Dio21], and $HD^{16}O$ and $HD^{18}O$ [Dio22] isotopologues.

Despite the advancements for the more common isotopologues, studies on water isotopologues with very low abundances on Earth and in the universe remain scarce. The Tomsk-Grenoble group has emerged as a key contributor in the data acquisition of stable water isotopologues HD^XO and D_2^XO, specifically with $^{16-18}O$ oxygen [Mik24].

Tritiated water, however, is due to its very low abundance of $10^{-17} - 10^{-18}$ [Age02] not considered relevant for the fields of combustion, atmospheric sciences, or astronomy. Therefore, only limited data were acquired prior to this work.

The first tritiated water measurements were performed by Staats et al. [Sta56] in 1956 where they determined the vibrational fundamental energies of HTO, DTO and T_2O with uncertainties of $\pm 5\,\mathrm{cm}^{-1}$. In 1972, Fayt and Steenbeckeliers measured the fundamental ν_1 and ν_3 bands of HTO [Fay72], while Carpenter et al. measured the ν_2 of T_2O [Car72], achieving an accuracy of $0.03\,\mathrm{cm}^{-1}$. These IR measurements were followed by microwave measurements of HTO, DTO and T_2O by Bellet et al. [Bel72] and by Helminger and De Lucia [De 73; Hel74].

For the HTO species, Cope et al. reanalyzed the ν_1 band in 1988 [Cop88]. Ulenikov et al. measured the ν_2 [Ule91] in 1991. In 2012, Tine et al. performed a reanalysis of the ν_3 band before, in 2019, Reinking et al. presented the $2\nu_2$ band using the first spectrum obtained from a custom-built optical cell [Mül19]. More spectra have been obtained from this cell, which are the object of this work.

Besides FTIR measurements, the HTO species was also been subject to laser spectroscopy: (i) in 1987, Cherrier and Reid presented a detection setup of tritiated water vapour using tuneable diode lasers [Che87], (ii) in 2015, Bray et al. introduced a method using cavity ring down spectroscopy [Bra15], (iii) in 2013, Down et al. presented a high-resolution analysis of the $2\nu_3$ band [Dow13], recorded by Kobayashi et al. [Kob11].

An overview plot of the spectral regions of previous HTO measurements is presented in Figure 3.1.

For the T_2O species, Fry et al. studied the ν_2 [Fry84] and Cope et al. investigated the ν_3 [Cop86]. The $T_2^{18}O$ species was studied by Kanesaka et al. [Kan84] in 1984. In contrast, there is a lack of IR data for the DTO species, with only pure rotational microwave measurements available.

In summary, while a limited number of studies cover the fundamental bands and some higher bands for HTO, T_2O and DTO have few or no data available. This lack of experimental data presents a significant challenge, particularly as any detection of tritiated water species for monitoring in and around fusion facilities or for future tasks in atmospheric observation and astronomy relies heavily on variational predictions made by Mikhailenko et al.[Mik05] (available in the SPECTRA database[1]). These calculations were based on the Potential-Energy-Surface (PES) of Partridge and Schwenke from 2000, derived from data on non-tritiated water species. Although the precision of these calculations was investigated for the HDO species, revealing a root mean square deviation of $0.25\,\mathrm{cm}^{-1}$[Par97;

---

[1]http://spectra.iao.ru/
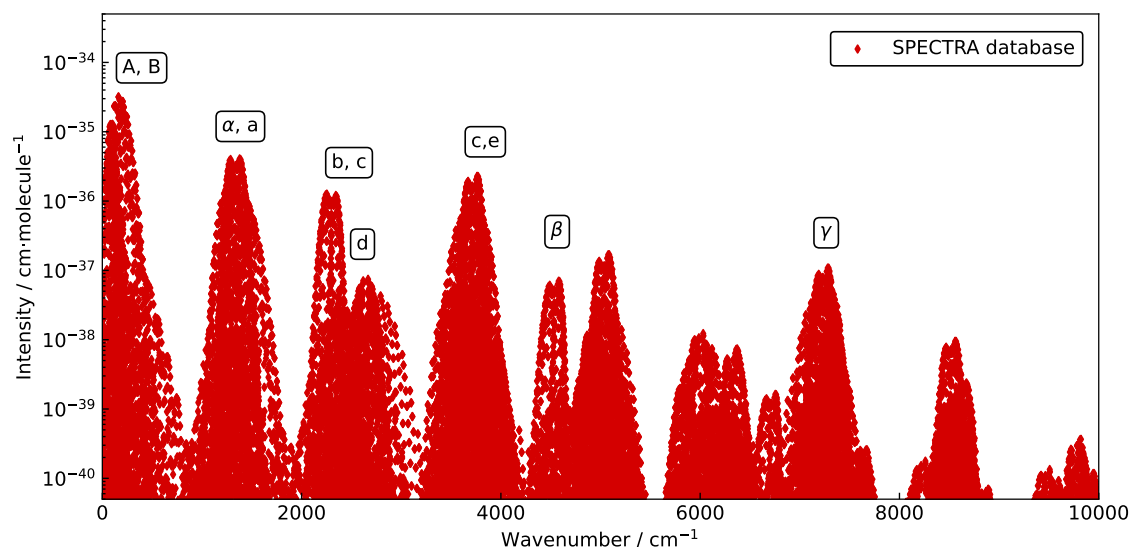
Figure 3.1: Overview of the experimental work on HTO. Line positions and intensities are taken from the SPECTRA variational calculation database (http://spectra.iao.ru/). Microwave measurements: A) Bellet et al. [Bel72], B) Helminger et al. [Hel74]. FTIR measurements: a) Ulenikov et al. [Ule91], b) Cope et al. [Cop88], c) Fayt and Steenbeckeliers [Fay72], d) Reinking et al. [Rei19], e) Tine et al. [Tin12]. Laser spectroscopy: α) Cherrier and Reid [Che87], β) Bray et al. [Bra15], and γ) Down, Kobayashi et al. [Kob11; Dow13].

Sch00], such a study for tritiated species had not been performed prior to this work. However, previous observations using only a small number of lines indicate a similar level of accuracy [Bra15; Dow13].

Unfortunately, this level of accuracy is incompatible with the stringent requirements of detection methods for tritiated water.

Objectives of this work: One of the main objectives of this work is to acquire high-accuracy data for the tritiated species HTO, DTO, and T_2O, addressing the gaps identified in the benchmark. This will be achieved in part by analysing the measured spectra of the tritiated water cell of Johannes Müller [Mül19]. In addition, an improved sample will need to be developed and measured to enhance data acquisition for the DTO and T_2O species. Accurate line positions require calibration of the spectra and extensive validation, as the predicted line positions currently deviate more than the width of the measured lines.

The resulting data will provide the scientific community with valuable information for (i) detecting tritiated water species and (ii) improving the PES of water or predicted line positions.

3.2 Precision measurements on molecular hydrogen

The hydrogen molecule is the smallest neutral molecular entity, making it an ideal benchmark system for precision tests of quantum chemical calculations. A comparison of high-precision spectroscopic measurements of transitions in these systems against their theoretical predictions validates the theory of quantum electrodynamics (QED) in molecules. Molecular hydrogen and its isotopologues serve as test objects for QED due to their simplicity and well-defined theoretical framework, making them ideal candidates for high-precision tests of fundamental physics. In the recent decade, rapid progress was made in precision investigations of the quantum level structure of this system.

On the theory side, non-relativistic QED calculations, using an expansion series in the fine structure constant α with separate treatment of the Born-Oppenheimer (BO) Hamiltonian with adiabatic, non-adiabatic, relativistic, and QED corrections, was developed into the framework of non-adiabatic perturbation theory (NAPT) [Cza18; Kom19b]. The resulting code for computing the level energies in molecular hydrogen [Kom19a] is publicly accessible.

In parallel, pre-BO methods, which use a direct variational approach for the 4-particle system, have led to the most accurate binding energies for molecular hydrogen [Sim13; Wan18; Puc19a; Puc19b]. While NAPT relies on adiabatic treatment with successive corrections, pre-BO approaches bypass this approximation, enabling very accurate results, especially for vibrational transitions in tritium-bearing isotopologues [Pac22].

On the experimental side, measurements for benchmark quantities such as the dissociation and ionisation energies of H_2 [Che18b], D_2 [Hus22], and HD [Höl23] have now reached accuracies at the 1 MHz level, in agreement with theoretical predictions. These experiments provide essential cross-checks for the validity of QED corrections in molecular systems.

A complementary alternative to electronic excitation is the study of vibrational splittings in the electronic ground state of molecular hydrogen. These splittings involve lower-energy transitions, which reduces the impact of relativistic and QED effects, offering a complementary benchmark for testing molecular theory. The weak dipole moment in the HD isotopologue, a heteronuclear species, allows dipole-allowed vibrational transitions, which were first measured by Herzberg in 1950 [Her50].

More recently, high-precision measurements using Doppler-broadened absorption spectroscopy [Kas11; Fas18; Kas22] and saturation spectroscopy [Tao18; Coz18b] have reached accuracies in the kilohertz regime. However, the full potential of extremely narrow Lamb dips remains unexploited due to asymmetries in the observed lineshapes, attributed to underlying unresolved hyperfine structures [Dio19], as well as other phenomena such as standing waves in intracavity experiments [Lv22; Jóź22].

The HT isotopologue, containing tritium, is similarly accessible via dipole transitions. If the experimental challenges associated with handling radioactive gas can be overcome, tritium-containing hydrogen molecules (HT, DT, and T_2) provide a valuable extension for

testing QED in small molecules. One of the primary challenges for such experiments in laser laboratories across the European Union, where precision spectroscopy infrastructure is available, is the strict tritium activity limit of $1\,\text{GBq}$, corresponding to $1183\,\text{Pa}\,\text{mL}$ for T_2. A recent collaboration between LaserLaB at Vrije Universiteit Amsterdam (VU) and the Tritium Laboratory Karlsruhe (TLK) has made progress by performing Coherent Anti-Stokes Raman Scattering (CARS) measurements on small samples of T_2 [Tri18], DT [Lai19], and HT [Lai20]. These measurements achieved frequency accuracies of $10\,\text{MHz}$ for the fundamental vibrational excitation ($\nu = 0 \rightarrow 1$). Benchmark studies on tritium isotopologues prior to this were limited to spontaneous Raman [Vei87] and intracavity laser absorption measurements [Chu87].

Additionally, rovibrational transitions in HT exhibit a simplified hyperfine structure compared to that of HD. With fewer hyperfine components due to $I_T = 1/2$ compared to $I_D = 1$, HT's transitions offer a single isolated hyperfine component that is more easily resolved in high-resolution saturated absorption experiments [Jóź21].

Objectives of this work: The other main objectives of this work is the construction of a saturation spectroscopy experiment to measure rovibrational lines in HT. This will add a precise benchmark for previously unmeasured transitions. Additionally, the advantageous hyperfine structure of HT offers an opportunity to investigate the asymmetric lineshape observed in HD. In this context, the NICE-OHMS technique (cf. Section 4.2) will be employed, using an optical setup similar to the HD experiments performed at VU [Coz18b; Dio19].

Although the optical setup can be adapted for the spectral range of the first vibrational overtone transitions ($\nu = 0 \rightarrow 2$), specific tritium requirements must be addressed for the cavity and sample provision system, such as safe gas confinement, material compatibility, and maintaining different pressures with limited tritium quantity. The results of this work will not only provide new QED benchmarks but also contribute to refining theoretical models, and offer insights into handling tritium-specific challenges in precision spectroscopy experiments.

4 IR spectroscopy techniques

In this work, two infrared spectroscopy techniques are utilised: (i) Fourier-Transform Infrared Spectroscopy, and (ii) the Noise-Immune Cavity Enhanced Optical Heterodyne Molecular Spectroscopy. In the following, both techniques are briefly introduced.

4.1 Fourier-Transform Infrared (FTIR) Spectroscopy

This chapter is based on [Her10], Chapter 15.3.2 and [Has00].

The Fourier-Transform Infrared (FTIR) spectrometer, presented in Figure 4.1, is based on the principle of a Michelson interferometer. A beam (here, continuous IR light) is split in two beams using a beam splitter. One beam is reflected by a mirror, passes the beam splitter, and arrives at the detector. The second beam is reflected by a moveable mirror, where the position s is known precisely at any time. The reflected beam passes through the beam splitter and arrives at the same detector. The superposition of both beam is recorded. Depending on the path difference between both beams, displacement $\delta = 2s/c$, the interferogram $I(\delta)$ resulting from both beams is given by

$$I(\delta) = \mathrm{Re} \left(\int_{-\infty}^{\infty} (1 + e^{\mathrm{i}\omega\delta}) \tilde{I}(\omega) \mathrm{d}\omega \right), \tag{4.1}$$

with $\tilde{I}(\omega)$ as the spectral intensity from the IR light source.
When a sample (or any IR active gas in the beam line) is introduced, absorption features are being imprinted on the spectral intensity $\tilde{I}(\omega) \rightarrow \tilde{S}(\omega)$.
The spectrum $\tilde{S}(\omega)$ is the subject of interest and needs to be reconstructed from the interferogram introduced in Equation 4.1

$$\mathrm{Re} \left(\int_{-\infty}^{\infty} e^{\mathrm{i}\omega\delta} \tilde{S}(\omega) \mathrm{d}\omega \right) = \tilde{I}(\delta) - I_0. \tag{4.2}$$

A Fourier transformation of the interferogram is, therefore, proportional to the spectrum $\tilde{S}$

$$\tilde{S}(\omega) \propto \mathrm{Re} \left(\int_{-\infty}^{\infty} e^{-\mathrm{i}\omega\delta} \tilde{I}(\delta) \mathrm{d}\delta \right). \tag{4.3}$$

This Fourier transformation is usually performed by the software of the recording spectrometer using a Fast Fourier Transform (FFT) algorithm [Coo65] and provides the spectrum $\tilde{S}$ as an 2D array. The step size of this array, containing intensity and wavenumber, is defined by the spectral resolution which is presented below.
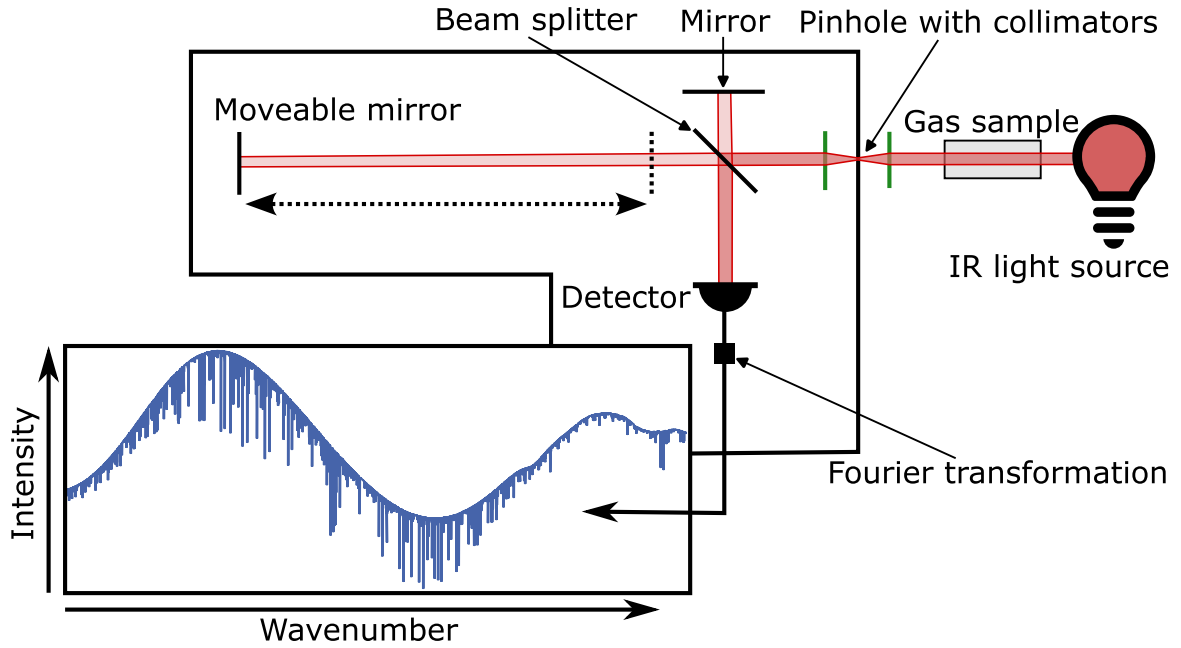
Figure 4.1: Principle of an FTIR spectrometer. The FTIR spectrometer is based on a Michelson interfero-
meter with a moveable mirror. The intensity recorded at the detector as function of the position of
the moveable mirror is Fourier-transformed to a spectrum containing the absorption features of the
gas in the beamline.

Spectral resolution

The spectral resolution is mainly determined by the geometry of the spectrometer, more
precisely by the maximum displacement δ achievable by the spectrometer.
In the following example the resolution for a Lorentzian signal is derived. The signal $\tilde{I}(\omega)$
and its Fourier transformation $\tilde{I}(\delta)$ is given by

$$
\tilde{I}(\omega) = \frac{(\gamma/2)^2}{(\omega - \omega_0)^2 + (\gamma/2)^2}
$$
$$
I(\delta) \propto e^{-\frac{\gamma}{2}\delta}.
$$

(4.4)

Now, when this signal $I(\delta)$, measured by an FTIR spectrometer, is Fourier transformed,

$$
\tilde{S}(\omega) \propto \int_0^{t_1} e^{-\mathrm{i}\omega\delta} I(\delta)\mathrm{d}\delta
$$
$$
\propto \int_0^{t_1} e^{-\mathrm{i}\omega\delta} e^{-\frac{\gamma}{2}\delta}\mathrm{d}\delta,
$$

(4.5)

the finite movement distance of the mirror s_{max} is limiting the integral to $t_1 = s_{\mathrm{max}}/c$. In
Figure 4.2, the resulting signal for two different s_{max} are presented and compared with the
Lorentzian which would be obtained for $s_{\mathrm{max}} \to \infty$. The relative proportions of the FTIR
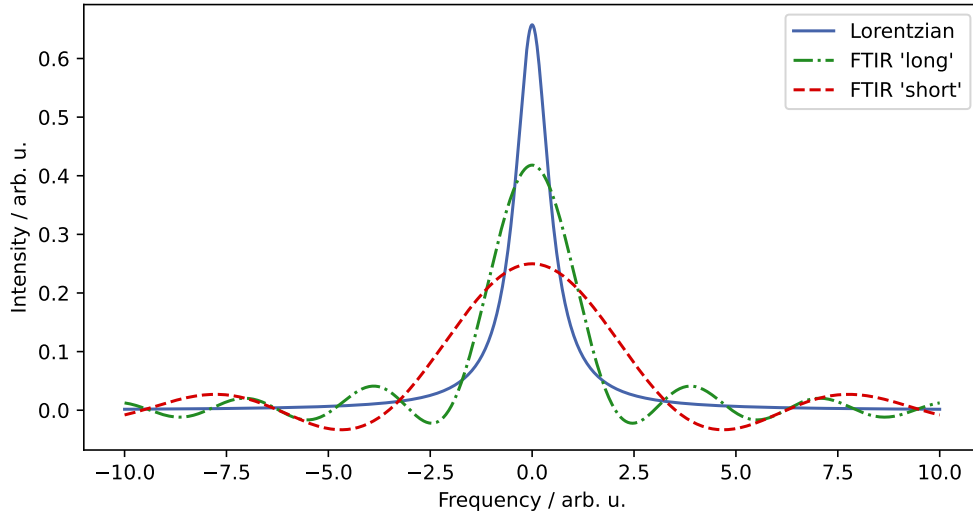
Figure 4.2: Typical signal of an FTIR spectrometer. A Lorentzian signal is compared to two simulated FTIR spectrometer measurements. The finite beam path difference achievable by the moveable mirror affects the resolution of the Lorentzian signal. The FTIR 'short' has a significant lower resolution than the FTIR 'long' with double the mirror movement distance ($s_{\text{max,FTIR 'short'}} = {}^1/_2\, s_{\text{max,FTIR 'long'}}$).

simulations with label 'long' and 'short' are $s_{\text{max,FTIR 'short'}} = {}^1/_2\, s_{\text{max,FTIR 'long'}}$.
Resulting from that limited integration, the line width is broadened depending on the available optical displacement.
To find a formulation of the optical resolution of an FTIR spectrometer, one can compare two neighbouring spectral lines at $s = s_{\text{max}}$

$$
\begin{aligned}
n \cdot \lambda_1 &= 2\, s_{\text{max}} \\
(n+1) \cdot \lambda_2 &= 2\, s_{\text{max}}.
\end{aligned}
\tag{4.6}
$$

These neighbouring lines remain distinguishable when

$$
\lambda_1 - \lambda_2 > \frac{1}{2\, s_{\text{max}}},
\tag{4.7}
$$

which equivalently delivers the optical resolution of an FTIR spectrometer.
The spectral resolution is also limited in the frequency range. As the Fourier transformation is performed iteratively for a mirror step size of Δx, the upper wavenumber ν_{max} is limited with

$$
\nu_{\text{max}} = \frac{1}{2\Delta x}.
\tag{4.8}
$$

Signals higher than this so-called Nyquist frequency are folded in the frequency range $\nu = [0, \nu_{\text{max}}]$, impeding unambiguous assignment.

In summary, FTIR spectroscopy measures wide spectral ranges in short acquisition time but with high resolution. Therefore, it is suitable for atmospheric observation or astronomy, where the composition of gases needs to be extracted within short recording times.

In this work, the advantages of this techniques are used to measure two samples containing a mixture tritiated water species in vapour. In several hours of recording, a wide spectral range was measured. From these spectra, a large number of lines from all three tritiated water species could be assigned, and due to its high resolution, with high accuracy.

4.2 Noise-Immune Cavity Enhanced Optical Heterodyne Molecular Spectroscopy (NICE-OHMS)

This chapter is based on [Axn14; Fol08; Fol09].

With the Noise-Immune Cavity Enhanced Optical Heterodyne Molecular Spectroscopy, dubbed as NICE-OHMS, a sensitive IR spectroscopy technique has been developed that can overcome the Doppler limitation. This technique combines advantages of the Cavity Enhanced Absorption Spectroscopy (CEAS) and the Frequency Modulation Spectroscopy (FM) techniques and is sketched in this chapter. For further information, the author recommends [Axn14].

First, frequency modulation and enhancement by cavity are introduced. Then, the combination of both techniques, NICE-OHMS, is explained. Further improvement of the used NICE-OHMS setup is obtained by saturation spectroscopy and wavelength modulation, which are described subsequently. An expected line shape of a measurement with sub-Doppler resolution is derived. Then, the absolute frequency calibration using a frequency comb is presented. Finally, a summary of the advantages of NICE-OHMS with regard to the HT measurements is provided.

Frequency modulation

The Frequency modulation spectroscopy (FM) was introduced by Bjorklund in 1980 [Bjo80] in order to enhance the sensitivity and selectivity of spectroscopic measurements. It is a technique using the change in dispersion that occurs during absorption. This change of dispersion influences the phase of the light which can be measured with much higher sensitivity than measurements probing the change in transmittance.

For FM, a laser with frequency f_c is modulated at frequency f_m with amplitude β[1]. The electrical field is therefore given by

$$E_{\mathrm{FM}}(f_c, t) = \frac{E_0}{2} \cdot e^{\mathrm{i}[2\pi f_c t + \beta \sin(2\pi f_m t)]} \tag{4.9}$$

---

[1]Note, this can be technically implemented using an optical modulator (EOM or AOM)
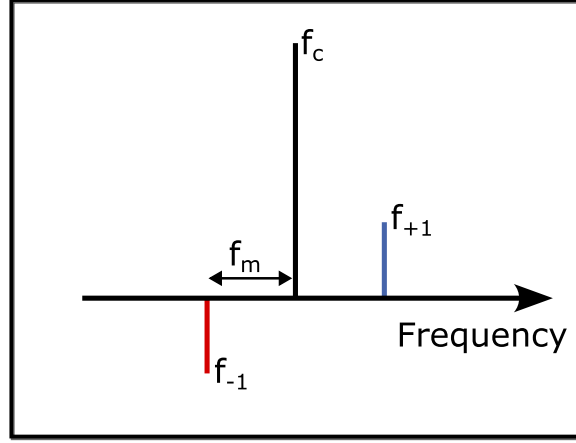
Figure 4.3: Illustration of the carrier and sideband frequencies in FM. The carrier frequency is denoted with f_c, the sidebands, separated by the modulation frequency f_m, as $f_{\pm 1}$. Both sidebands are phase-shifted indicated by the opposing orientation in the illustration. Usually, most of the power is assigned to the carrier frequency as indicated here by the length of the bars.

in propagation direction of the laser light.

The field can be expressed in terms of Bessel functions $J_i(\beta)$

$$
\begin{aligned}
E_{\mathrm{FM}}(f_c, t) &= \frac{E_0}{2} \cdot e^{\mathrm{i}2\pi f_c t} \cdot \sum_{j=-\infty}^{\infty} J_j(\beta) e^{\mathrm{i}2\pi j f_m t} \\
&= \frac{E_0}{2} \cdot e^{\mathrm{i}2\pi f_c t} \cdot \left[J_0(\beta) + J_1(\beta) e^{\mathrm{i}2\pi f_m t} - J_{-1}(\beta) e^{-\mathrm{i}2\pi f_m t} \right],
\end{aligned}
\tag{4.10}
$$

where for the application in this work only first harmonics ($\pm j \leq 1$) are considered. As $J_{-1}(\beta) = -J_1(\beta)$ this shows, that the optical beam will consist of a carrier wave at frequency f_c and two side bands at $f_{\pm 1} = f_c \pm f_m$. The side bands are out of phase. An illustration of the frequencies is presented in Figure 4.3.

When the carrier with intensity S stimulates a transition (at transition frequency f_0) in a gas of N_i particles, the interaction induces a dispersion change notable as a phase shift in the side bands. To extract this signal, a demodulation of the transmitted signal is performed at modulation frequency f_m. Mathematically, this can be expressed starting with the transmitted electric field E_{T},

$$
E_{\mathrm{T}}(f_c, t) = \frac{E_0}{2} \cdot e^{\mathrm{i}2\pi f_c t} \cdot \left[T_0(f_c) J_0(\beta) + T_1(f_c) J_1(\beta) e^{\mathrm{i}2\pi f_m t} + T_{-1}(f_c) J_1(\beta) e^{-\mathrm{i}2\pi f_m t} \right],
\tag{4.11}
$$

where $T_j(f_c) = \exp(-\delta_j(f_c) - \mathrm{i}\phi_j(f_c))$ is the complex transmission function of the analyte. $\delta_j(f_c)$ and $\phi_j(f_c)$ are the dispersion and absorption at frequency $f_j = f_c + j \cdot f_m$ with $j = 0, \pm 1$.

The intensity of a frequency-modulated field transmitted through a sample contains a term

oscillating at the modulation frequency. For low absorption this term can be written as

$$
\begin{aligned}
S_{\mathrm{T}}(f_d, t) =\, & 2S_0 J_0(\beta) J_1(\beta) \\
& \left[(\phi_{-1}(f_d) - 2\phi_0(f_d) + \phi_1(f_d)) \cos(2\pi f_m t) \right. \\
& \left. + (\delta_{-1}(f_d) - \delta_1(f_d)) \sin(2\pi f_m t)\right],
\end{aligned}
\tag{4.12}
$$

where $f_d = f_0 - f_c$ is introduced as relative frequency to the transition frequency f_0 of the analyte. S_0 is the intensity in absence of the sample gas. From this term, the FM signal S_{T} is obtained by demodulation of the detector signal at the modulation frequency at a given detection phase θ_{FM}:

$$
\begin{aligned}
S_{\mathrm{T}}(f_d, \theta_{\mathrm{FM}}) =\, & 2S_0 J_0(\beta) J_1(\beta) \\
& \left[(\phi_{-1}(f_d) - 2\phi_0(f_d) + \phi_1(f_d)) \cos(\theta_{\mathrm{FM}}) \right. \\
& \left. + (\delta_{-1}(f_d) - \delta_1(f_d)) \sin(\theta_{\mathrm{FM}})\right]
\end{aligned}
\tag{4.13}
$$

The signal consists of the dispersion and the absorption components, which are phase-shifted by $90°$. By phase demodulation, typically with a phase-sensitive or lock-in amplifier, either signal component can be selected. The phase setting in NICE-OHMS is usually performed by maximising the signal in the dispersion channel on a known transition, in this work from residual water vapour in the system.

Cavity enhancement

Fabry-Perot cavities are useful to increase the length of the optical interaction length without altering the amount of gas or the spatial parameters of the experimental setup. These cavities consist of high-reflective mirrors which reflect the incoupled light several times before it eventually gets transmitted through one of the mirrors. An illustration is provided in Figure 4.4. However, this enhancement of the interaction path length is only valid for light that fulfils the resonance conditions

$$
f = n \cdot \mathrm{FSR} = n \cdot \frac{c}{2\mathrm{L}}.
\tag{4.14}
$$

Hence, the frequency of the laser (f) must match to the cavity length (L), known as the free spectral range (FSR), or a nth overtone of it. c is the speed of light.
These cavity modes have a spectral width which is mainly determined by the reflectivity of the mirrors R,

$$
\Delta f = \frac{c \cdot (1 - R)}{2\mathrm{L}\pi\sqrt{R}}.
\tag{4.15}
$$

Usually the quantity of the Finesse (F) is used

$$
F = \frac{\mathrm{FSR}}{\Delta f} = \frac{\pi\sqrt{R}}{(1 - R)},
\tag{4.16}
$$
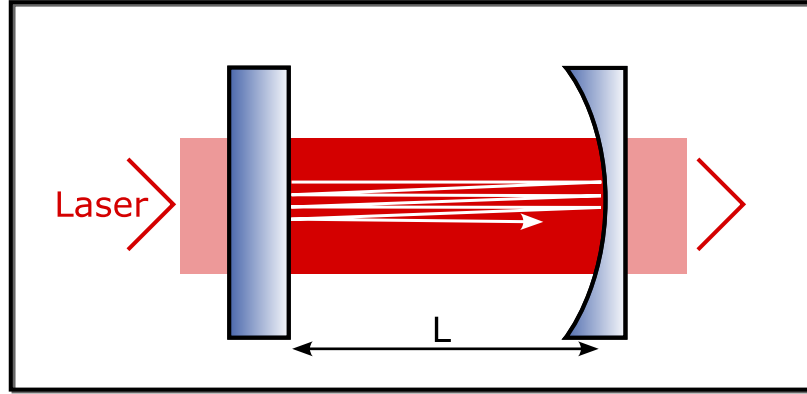
Figure 4.4: Illustration of a hemispherical cavity. The hemispherical Fabry-Perot cavity of length *L* consists of a concave and a plane mirror. The incoupled light is reflected multiple times before eventually being transmitted through one of the mirrors. This type of cavity is used in the NICE-OHMS setup.

which can be calculated or measured when scanning the cavity modes.

To use the enhancement of the (effective) interaction path length and, therefore, reach high sensitivity all over the spectral scanning range, the resonance conditions must be maintained at any frequency.

An approach to ensure resonance conditions during scanning or to react to minor disturbances of the system has been developed by Drever and Hall [Dre83] (refining Pound's stabiliser [Pou46]). The locking technique known as **Pound-Drever-Hall** (PDH) utilises frequency modulation with the light reflected by the cavity itself to lock the laser to the cavity mode. For this locking, the laser is modulated at a frequency f_{PDH} which is smaller than the FSR but greater than the width of the cavity fringe (Δf). The two sidebands produced from the modulation with the PDH frequency, similar as in the FM, create an error signal when hitting the entrance mirror of the cavity. When the carrier frequency is on top of a cavity fringe the two opposite-phase sidebands annihilate, when they are off they produce a signal that is used to correct the laser frequency via PID controller. To obtain this feedback signal, a demodulation of the recorded back reflection with the PDH frequency f_{PDH} is needed.

The scanning over the frequency range is then, with PDH locking active, preformed by slowly changing the length of the cavity, usually by using a piezoelectric module at one of the mirrors.

It should be noted, that the extended interaction path length also leads to an amplification of the light power in the cavity. This becomes clear when considering the cavity in this work. A hemispherical cavity, as illustrated in Figure 4.4, is used, where the curvature of the concave mirror ($2\,\mathrm{m}$) much larger than the cavity length ($37\,\mathrm{cm}$). The mirrors have a reflectivity of $R = 99.996\,\%$ leading to a Finesse given by $F \approx 80000$. This leads to an enhancement of the interaction path length of $L = 37\,\mathrm{cm}$ (length of cavity) to an (average)

interaction path length of

$$L_{\text{eff}} = L \cdot F \approx 30\,\text{km}. \tag{4.17}$$

This leads to a massive increase in the photon density, which could influence the physics of the measured gas. Such an effect could be, as suggested by Letokhov and Chebotayev [Let77], that molecules flying along the beam would be trapped or slowed down by the strong standing waves of the light. In case of this cavity with a maximum power of $P_{\text{in}} = 26\,\text{mW}$ and the efficiency of the incoupling light of $\eta = 60\%$, this adds up to

$$P_{\text{eff}} = P_{\text{in}} \cdot \eta \cdot \frac{F}{\pi} \approx 400\,\text{W}. \tag{4.18}$$

Therefore, it is feasible to present an effective intracavity power with the results to correctly acknowledge possible power dependent effects.

Frequency modulation in the cavity

The combination of FM and cavity enhancement is an ultra-sensitive technique known as Noise-Immune Cavity Enhanced Optical Heterodyne Molecular Spectroscopy (NICE-OHMS). It is basically conventional FM where the carrier and the sidebands are amplified by cavity enhancement.

Recapitulating the condition of cavity enhancement, it is clear that both frequencies, the carrier f_c and the sidebands $f_c \pm f_m$, must match the FSR.

While the carrier can be locked to the cavity resonance via the Pound-Drever-Hall technique, for the sidebands, an analogous technique must be devised. The DeVoe-Brewer [DeV84] involves locking the modulation frequency f_m applied to the optical modulator to the FSR, precisely one FSR, here $f_m \approx 405\,\text{MHz}$. Consequently, with the carrier locked to the FSR, the sidebands are also intrinsic.

The three beams in the cavity, separated in frequency by one FSR, counter-propagate and interact with each other, producing an FM signal. Nine beam combinations are possible at five different frequency detunings $\Delta f = f_d - f_c = 0,\ \pm^1\!/_2\text{FSR},\ \pm\text{FSR}$, visualised in Figure 4.5.

As a typical Doppler-broadened profile is larger than the FSR, spectroscopy on a selection of molecules with velocity $\mathbf{v}$

$$\mathbf{k} \cdot \mathbf{v} = \pm^1\!/_2\text{FSR},\ \pm\text{FSR} \tag{4.19}$$

can be performed (cf. Figure 4.5). The change between different detunings requires many adjustments and additional measurement time.

For this reason, in the context of this work only the carrier-carrier interaction (with a detuning frequency $f_d = f_c$) is used (corresponding to c in Figure 4.5). The power is therefore optimised for the carrier to reach high sensitivity and allow saturation spectroscopy. The sidebands are fed with sufficient power to obtain a decent FM signal.
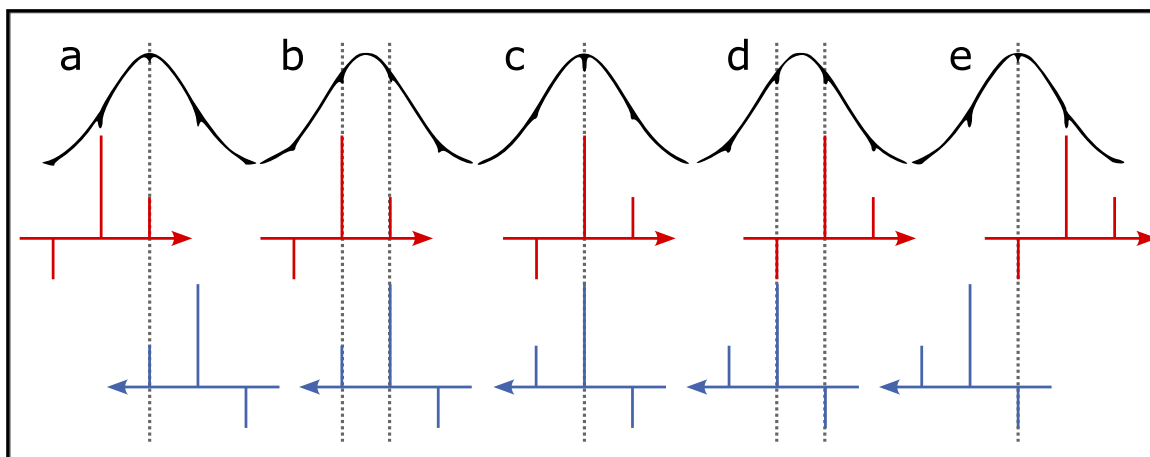
Figure 4.5: Illustration of spectral hole burning in a probing gas with a Gaussian velocity distribution at different detunings. A Doppler-broadened absorbance profile is affected by spectral hole burning (top row) from two counter-propagating FM triplets, (red and blue). The five panels correspond to the five detunings of the carrier from the centre of the transition at which various components of two counter-propagating FM triplets interact with a common velocity groups. In this work only configuration c is used.

Saturation spectroscopy

By providing sufficient power to the probing beam (here carrier) the saturation spectroscopy technique is enabled. This technique utilises the two counter-propagating beams to create a feature much narrower as the Doppler profile. One of the beams acts as a pump beam, interacting with the molecules and inducing a change in the population distribution between the two probed levels. This phenomenon is known as 'hole burning' [Ben62]. When the second beam interacts with the molecules (of the same velocity), the reduced population in the ground state results as a decrease in the absorption signal. The selection of molecules that are subject to the effect is limited to molecules with velocity (in beam propagation) $\mathbf{k}\cdot\mathbf{v} = 0,\ \pm 1/2\text{FSR},\ \pm\text{FSR}$ (cf. Equation 4.19)[2]. The hole burning is visualised in Figure 4.5 for the five detunings. In the context of this work, only the carrier-carrier interaction power was sufficient to create this feature, known as the Lamb dip.

Because this feature occurs on a velocity-selected part of the gas, there is no Doppler-broadening. Lamb-dips are only subject to natural and collisional broadening and therefore up to three orders of magnitude narrower than the Doppler profile.

---

[2]Note, that for velocities $\mathbf{v} \neq 0$ the Doppler-shift needs to bridge the frequency gap between the counter-propagating beams.
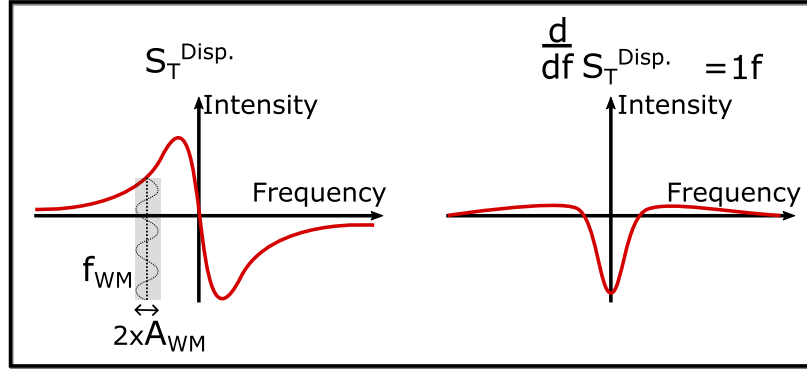
Figure 4.6: Illustration of a typical NICE-OHMS signal and its first derivative obtained from wavelength modulation. A typical signal for the dispersion $S_T^{disp.}$ is sketched on the left, with modulation by the dither (frequency f_{WM} and amplitude A_{WM}) is indicated. From the demodulation with the dither frequency the first derivative $1f$ is obtained, presented on the right.

Wavelength modulation and derivation of the NICE-OHMS signal

Wavelength modulation is an additional modulation employed in the NICE-OHMS of this work to further enhance sensitivity and reduce background noise. In the setup of this work, the modulation is applied using a low frequency of $f_{WM} = 395\,\mathrm{Hz}$ on the piezo that drives the mirror, in the following denoted as dithering. The resulting composite signal is subsequently demodulated with an optimised phase, producing the derivative of the NICE-OHMS signal. In Figure 4.6 an illustration of a typical signal for the dispersion phase and its first derivative obtained from the demodulation with the applied dither, frequency f_{WM} and amplitude A_{WM}.

This technical derivation of the signal suppresses background noise drifts and has been proven to enhance the performance of NICE-OHMS in various publications [3].

Note that this modulation reduces the resolution of the experiment. This is because the amplitude of the dithering results in averaging of the signal. This can be compared to a derivation of a function using finite derivation steps, where in this case the derivation step size is given by twice the dither amplitude. However, reducing the amplitude reduces the noise-reduction which is why a balance must be found. Because of its influence on the line shape, the dither amplitude is a measurement property that needs to be optimised and denoted beside the experiment (converted into a frequency). For this work, the peak-to-peak amplitude is given by $f_{dith} = 100\,\mathrm{kHz}$.

The demodulation of the signal can be performed multiple times to obtain higher-order derivations and reveal substructures [Mel21]. In this work, only the first derivation, denoted $1f$, is used. The function that describes this signal is derived in [Fol09].

---

[3] A good summary of NICE-OHMS measurements using this technique is given in the PhD thesis of Meissa L. Diouf [Dio23] and Frank M.J. Cozijn [Coz24b]

For the absorption and dispersion, it is given by

$$f_{1f}^{\text{abs}}(\omega) = \frac{8A\Gamma^2(\omega - \omega_0)^2}{\left[\Gamma^2 + 4(\omega - \omega_0)^2\right]^2} \tag{4.20}$$

and

$$f_{1f}^{\text{disp}}(\omega) = \frac{4A\left[\Gamma^2 - 4(\omega - \omega_0)^2\right]}{\left[\Gamma^2 + 4(\omega - \omega_0)^2\right]^2}, \tag{4.21}$$

where ω_0 is the line position, A the line intensity and Γ the line width. When the demodulating phase is optimised for the dispersion, the $1f$ of the Lamb-dip is Lorentzian-like.

Frequency calibration

Mandatory requirement for any precision laser spectroscopy is absolute frequency calibration. The most common approach and here employed in this work for NICE-OHMS is the Frequency Comb (FC) in combination with a precise (atomic) clock.

The FC is a cavity mode-locked laser that emits short light pulses, usually in a femtosecond repetition rate. This short pulse duration allows a laser frequency spectrum to span over a wide range, usually covering the range from the infrared to the ultraviolet. The FC generates equally spaced frequencies where the distance between the frequencies is given by $f_{\text{rep}} = \frac{1}{T_{\text{rep}}}$ depending on the repetition rate T_{rep}.

The repetition rate T_{rep} is the crucial part of the FC as slight changes will change the frequency. While in short term atomic clocks deviate more than in FC in long term, the precision remains unmatched. For this reason, the repetition rate is long-term compared to that of an atomic clock.

To compare a laser in matching frequency range, the laser light (or a fraction of it) is mixed with the light of the FC. This combination results in a beatnote frequency f_{beat}, which is the difference between the laser frequency f_c and the closest mode N of the FC, $f_{\text{FC,N}} = N \times f_{\text{rep}}$.

In a real experiment, the FC has a frequency offset f_0 also influencing the beatnote signal

$$f_{\text{beat}} = f_0 + N \times f_{\text{rep}} - f_c. \tag{4.22}$$

This offset is an unknown value between 0 and $\pm f_{\text{rep}}$ and would limit the absolute precision of the frequency for the used setup in this work to $500\,\text{MHz}$ if not determined.

By comparing the doubled frequency of a defined mode N with the frequency of the doubled mode $2N$ the offset can be determined,

$$2 \times f_{\text{FC,N}} - f_{\text{FC,2N}} = 2 \times (f_0 + N \times f_{\text{rep}}) - f_0 + 2N \times f_{\text{rep}} = f_0, \tag{4.23}$$

and the absolute frequency of f_c can be determined on a kHz level.

In summary, NICE-OHMS is a combination of multiple techniques: With Frequency Modulation Spectroscopy (FM), the dispersion is measured, which offers high sensitivity by the low-noise phase detection principle. Further sensitivity is obtained from the Cavity Enhanced Absorption Spectroscopy (CEAS), which, by maintaining resonance conditions of a Fabry-Perot cavity for the scanning frequency, enhances the interaction path length. By optical heterodyne detection of the laser frequency, which is performed by creating a beatnote with a frequency comb, the absolute frequency is obtained with high accuracy.

For this work, NICE-OHMS is performed in saturation, creating a Lamb dip feature which is up to three orders of magnitude narrower than the Doppler profile. This allows for a much higher accuracy of the assignment. Further modification of the technique is implemented by applying a wavelength modulation. This low-frequency modulation is used to technically create the derivation of the signal and therefore suppress low-frequency noise.

In combination, this technique is ideal for measuring small amounts of HT with high accuracy. The high sensitivity and high intracavity power are sufficient not only to measure such weak dipole molecules, but also to saturate them, as previously shown for HD [Coz18b; Dio19; Dio20].

5 Determination of ro-vibrational transitions of tritiated water isotopologues using FTIR Spectroscopy

5.1 Overview

FTIR spectroscopy is a powerful tool to acquire highly accurate spectroscopic data of gas samples. For the acquisition of the presented data, a Bruker IFS 125HR FTIR spectrometer is used with a resolution up to $0.019\,\mathrm{cm}^{-1}$. The spectrometer is designated for remote-sensing of atmospheric trace gases (see [Kie16a; Wun17]) and located outside of the tritium handling licensed laboratory in a shipping container at the Campus North of KIT. Tritium handling, especially outside of a licensed laboratory like the TLK, is subject to conditions set by European law. To nonetheless successfully perform accurate measurements of ro-vibrational transitions in tritiated water species, requirements regarding tritium handling and spectroscopy need to be fulfilled. The concept of these measurements can be subdivided in three major steps as illustrated in Figure 5.1:

(i) **Production of the sample:** To obtain highly accurate spectra from tritiated water vapour, an optical cell design was developed for two tritiated water samples. The design complies with the technical challenges of safe tritium confinement and restriction to total activities up to $1\,\mathrm{GBq}$, respectively $10\,\mathrm{GBq}$ for the second sample. The geometry of the optical cell has been chosen to gain the optimum signal-to-noise ratio (SNR) from the small amount of gas available. For the generation of the tritiated water species, an in situ oxidation reactor inside the optical cell is used, which converts the filled tritium (mixture) to water species by the usage of a redox reaction with copper oxide. In addition, various measures are implemented to achieve a high sample purity. In order to optimise the design and preparation, for the second sample, several improvements are implemented, including an increase of the total activity. A detailed description of this section can be found in Section 5.2.2.1.

(ii) **Acquisition of the spectra:** For the acquisition of the spectra, the tritiated water samples are placed in an experimental setup consisting of an infrared source and a FTIR spectrometer. Filters are used to grant access to high-resolution spectra of several $100\,\mathrm{cm}^{-1}$ that span the range of 1800 to $10\,000\,\mathrm{cm}^{-1}$. A description of the acquisition and an overview of the measured spectra can be found in Section 5.3.
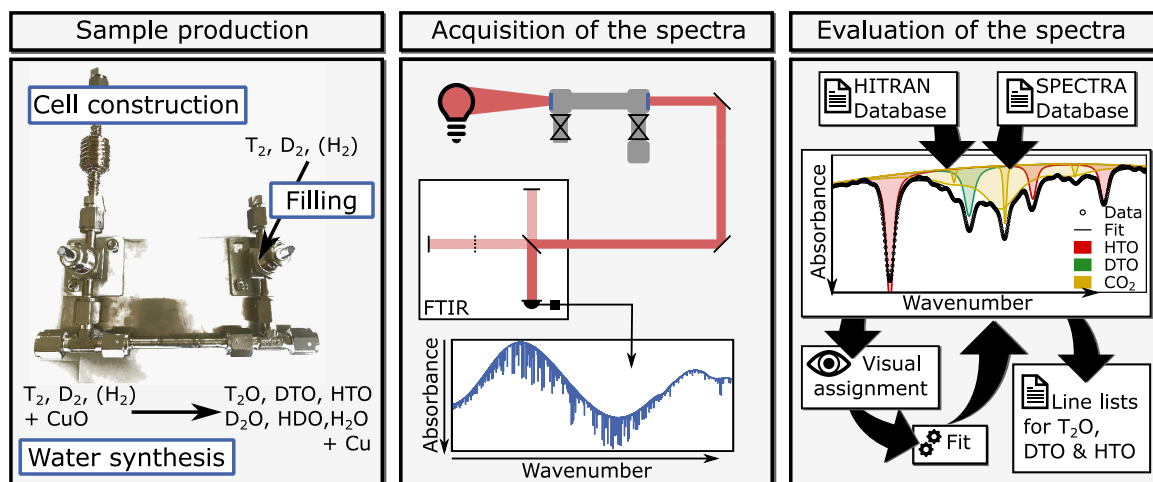
Figure 5.1: Concept of measurement of tritiated water using FTIR Spectroscopy. The concept can be subdivided in (i) production of the sample, (ii) acquisition of the spectra and (iii) evaluation of the spectra.

(iii) **Evaluation of the spectra:** The obtained spectra contain spectroscopic signatures of all (infrared-active) molecules from the samples. For the evaluation of the spectra, a procedure is developed to identify and assign transitions of molecule species that have been measured before and of those that have not prior to this work, namely transitions from the tritiated water species HTO, DTO and T_2O. In Section 5.4 the evaluation procedure is described in detail. A general analysis of the spectra is presented giving estimations for the composition of the two samples. In order to obtain an accurate reference of the measured transitions, a wavenumber axis calibration is performed. A Monte Carlo study of the assignment procedure is part of this section for validation of the assignment uncertainties.

Resulting from these measurements, spectroscopic data of in total 4589 lines of 13 vibrational bands of $HT^{16}O$, $DT^{16}O$ and $T_2^{16}O$ were obtained for the first time. These data are presented in Section 5.5. For the validation of the data in Section 5.6, two methods are presented, one based on a cross-check of datasets obtained from both samples, the other on a comparison with highly accurate microwave measurements using Watson Hamiltonian. In Section 5.7, spectroscopic constants of the Watson Hamiltonian are provided for the vibrational state of 5 different bands. For the other vibrational bands, the breakdown of the fit is observed which is discussed using statistical analysis. A comparison of the obtained data sets with the SPECTRA database, ab initio predictions that are used for the assignment of the tritiated water species, is presented in Section 5.8. The precision of these predictions is determined, and rotational quantum number dependencies are found and discussed.

5.2 Production of tritiated water vapour samples in compatible optical cells

In this section, first the requirements to the optical sample and the resulting concept are presented. Then, the construction of the cell and production of the tritiated water sample is described. For a second sample, improvements to cell and preparation are discussed and presented in the last part of this section.

5.2.1 Requirements and concept of an optical tritiated water cell

Optical cells for the spectroscopy of tritium-containing gas mixtures (e.g., for laser-Raman systems [Tay01]) have been successfully developed and used by the TLK for more than 20 years. Fulfilling TLK regulations on tritium-containing components [Tri16], these cells are used for gas analyses, calibration standards [Nie21a], or high-precision measurements [Lai20]. However, for high-resolution spectroscopy of tritiated water, a novel design needs to be developed, as the technological challenge of merging the following requirements must be faced:

- **Limited activity:** The total activity outside of licensed laboratories is restricted by European law [Eur14] to $1\,\mathrm{GBq}$. For the high-activity sample containing $10\,\mathrm{GBq}$, measurements were performed under the licence of the KIT department *Sicherheit und Umwelt* (SUM). This licence allows for the handling of activities up to $10\,\mathrm{GBq}$. Given the tritium half-life of 4500 days [Luc00], the legal amount of tritium (T_2) is given by $11.83\,\mathrm{mbar\,mL}$ ($1\,\mathrm{GBq}$), respectively $118.3\,\mathrm{mbar\,mL}$ for the $10\,\mathrm{GBq}$ activity sample. For spectroscopy, achieving a decent SNR with these small amounts of gas gives rise to technical challenges.

- **Tritiated water production:** For controlled gas transfers, usually defined volumes and calibrated pressure sensors are used. This quantification of gas amounts before, during, and after transfers is based on the assumption that the majority of the substance is gaseous. This is especially important when a certain limit must not be exceeded, as given with the limitation of the activity. In vacuum systems, water vapour forms thin films on the walls of vacuum components which are negligible for the used accountancy methods. Therefore, oxidation must be performed inside or in close proximity to the optical cell. A high conversion rate and transfer rate to the cell are favourable for remaining below the restricted amount of tritium.

- **Tritium-compatible materials:** Safe confinement of tritium can only be achieved by the right choice of materials. A list of suitable materials can be found in the Tritium Manual [Pen24]. Two aspects must be kept in mind when choosing from these materials: (i) As heating and cooling may be needed for water synthesis, the assortment of different materials should be tested for compatibility of their thermal expansion. Mismatches can cause leaks and the release of tritium from

its confinement. (ii) Due to its beta decay, tritium exhibits radiochemical activity, producing molecular, ionic, and radical species. These highly reactive components can initiate secondary reactions with other species present [Sou86]. In particular, it is crucial to avoid halogen-containing components as their radiation-induced decomposition will lead to the formation of halogen hydrides/tritrides (e.g., TF, TCl, etc.); species that can destroy the integrity of systems. Impurities inside the optical cell can not only lead to non-assignable signatures of all kinds of tritiated species in the spectra but also reduce the available quantity of tritium. To successfully face the challenge of a decent SNR despite limitation of the total activity and ensure high sample purity, a high conversion rate to the target species is mandatory. Therefore, the formation of such impurities should be suppressed.

The optical cell allowing the preparation and measurement of the tritiated water sample was developed and constructed in the Master's thesis of Johannes Müller [Mül18] and is published in [Mül19].

A sketch of the cell is shown in Figure 5.2. The optical cell consists of two ¼" VCR tees connected by a steel tubing. Inside, a 201 mm long aluminium pipe is installed. A valve connected to one of the tees allows connection from the tritium infrastructure. Another valve is used to separate the cell into two segments: the tritium oxidation unit filled with copper oxide powder and the light-guiding segment. A porous frit keeps the powder inside the oxidation unit. A copper cold finger can be connected to the light-guiding pipe during oxidation. The sapphire windows at each end of the light pipe are sealed with two copper gaskets pressed with two VCR face caps. In terms of the requirements of the cell, the setup can be subdivided into three main aspects: (i) the light-guiding pipe, (ii) the tritium oxidation unit, and (iii) the tritium confinement in general. In the following, these aspects are introduced in detail.

Light-guiding pipe   Core of the optical cell is a 201 mm long and 4 mm inner diameter wide aluminium pipe housed in a stainless steel tubing with two ¼" VCR tees. The inner surface of the pipe is polished using abrasive pastes to ensure high reflectivity. This design is based on the hollow waveguide / light-guiding pipe principle [Mal83; Yan84a; Yan84b; Gur88; Yin89]. The IR light is coupled in from one side of the pipe. The light propagates by reflection on the polished inner surface of the hollow aluminium waveguide through the pipe and exits on the other side. During this propagation, the infrared light is interacting with sample gas collecting absorption features from individual infrared active species in the sample. The geometry of the optical part of the cell is chosen to increase the product of interaction path length l and the particle density n which is following to Lambert-Beer-Law

$$I = I_0 e^{-\sigma n l}, \tag{5.1}$$

desirable to achieve high absorption in the intensity I using an initial intensity I_0. A longer or thinner pipe could on the one hand further increase the path length or the particle
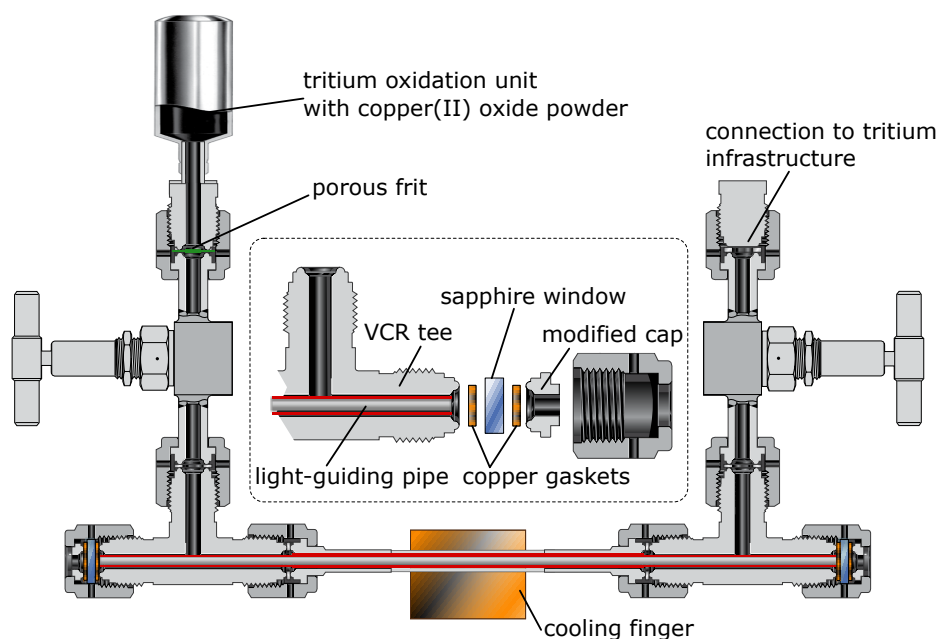
Figure 5.2: Custom-built optical cell and sealing of windows. The optical cell can be divided in a light-guiding segment containing a 201 mm long aluminium pipe (red) and an oxidation unit (top left part). Adapted from [Mül19]

density but on the other hand raise problems with coupling in the light. It is estimated by Müller et al. [Mül19], that the chosen geometry is a balance between increasing absorption properties and maintaining a high IR in-coupling efficiency.

Tritium oxidation unit   One requirement to the cell is a water synthesis reactor in close proximity to the cell. This is because accurate tritium accounting is complicated with tritiated water vapour as a water layer forms on the inner surfaces during transfer. The method of choice is a tritium oxidation unit connected with a valve to the light-guiding pipe segment of the optical cell. A steel cylinder filled with $\sim 30\,\mathrm{g}$ copper(II) oxide is used. The oxide powder is secured with a porous frit to retain the material in the unit.

The concept of oxidation is based on the method used by Kobayashi et al. [Kob11]. The copper oxide serves as oxygen reservoir for the redox reaction process

$$T_2 + Cu(II)O \longrightarrow T_2O + Cu.$$

At room temperature, the reaction rate is close to zero, but can be exponentially increased, according to the Arrhenius law, by external heating. This is implemented with heater wires around the cylinder.

In addition, a copper cold finger is temporarily installed around the light-guiding tube segment during the oxidation process. The cold finger is coupled to a liquid nitrogen bath and cools down the light-pipe to temperatures close to the boiling point of nitrogen. This

causes the tritiated water to freeze in the light-guiding pipe, leading to a (partial) pressure gradient of the water. Hence, the oxidation product is cryo-pumped into the light-guiding pipe segment. The procedure of sample production is described in detail in section 5.2.2.

This approach has several advantages: (i) Filling of the optical cell can be done using pure T_2 (or any desired hydrogen mixture) instead of the tritiated water vapour. As mentioned above, this is favourable for reasons of tritium accountancy. (ii) The oxidation of the tritium is very efficient, especially in combination with the cryo pump. By removing the tritiated water during the process from the oxidation segment, the backward reaction is highly suppressed. By this method, all tritium is converted into water. The only leftovers, the reduced copper and remaining copper oxide, both non-gaseous materials, are retained in the oxidation segment by the porous frit. This allows conversion close to 100% of the small amount of tritium available.

Here, it should be noted that it is expected that tritiated water will decompose to hydrogen and oxygen due to the presence of ions formed by tritium beta decay. Kobayashi et al. report, that this may amount to 5-10% hydrogen/oxygen gas with regard to the water molecules [Kob11]

$$T_2O \rightleftharpoons T_2 + \frac{1}{2}O_2.$$
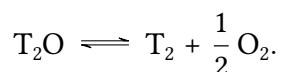
(iii) For this method no oxygen in gaseous form is used. The handling of oxygen gas, in general, but especially with hydrogen, is a delicate procedure that requires additional safety measures. By using bonded oxygen in the form of copper oxide, these can be avoided.

Tritium confinement   The confinement of tritium is based on the regulations set by the TLK [Tri16]. These regulations are implemented for high activities to comply with tritium's physical, radioactive, and radiochemical attributes. In a spectroscopy these strict rules are not needed, but serve as a guideline to ensure high sample purity. In general, as primary confinement, stainless steel components with metal face sealing connections (VCRs) are used. For spectroscopy, an optically transparent light access in the infrared is required. Sapphire windows, which have high transmission in the infrared, are widely tolerated for containing tritium.

The challenge arises at the metal-sapphire transition, at which sealing is required. Standard rubber O-ring sealings cannot be used since they do not meet the leak-tightness requirements. This problem is solved by direct metal-sapphire compression, a method inspired by [Joh86]. Two metal-sapphire face sealings are produced by compressing a ¼" VCR tee, the sapphire window with copper gaskets on each side, and a modified ¼" cap plug (see Figure 5.2). The compression is applied by a ¼" VCR nut and a specific torque of $25\,\mathrm{N\,m}$ that has been determined to seal but not break the sapphire. This assembly has been tested for tightness (leak rate $< 1 \cdot 10^{-9}\,\mathrm{mbar\,L\,s^{-1}}$) and sufficient temperature resilience (up to $300\,°\mathrm{C}$) such that acceptance could be granted for tritium operation. A detailed description of this study can be found in [Mül18].

5.2.2 Production of the tritiated water sample with $1\,\mathrm{GBq}$ activity

The production of this sample was performed by Johannes Müller prior to this work. In his master's thesis [Mül18], detailed descriptions of the development of the cell, the preparation of the sample, the acquisition of the sample, and the assignment of the $2\nu_1$ band of HTO are given. The concept of the cell and the first results have been published in [Mül19]. This section is based on these works.

This section is subdivided into (i) the construction procedure with all modifications made to the components, (ii) the preparation and filling of the cell with tritium, and (iii) the oxidation procedure where the tritiated water is produced.

5.2.2.1 Construction of the cell

The cell has been constructed according to the sketch in Figure 5.2. While most components can be utilized as produced from the supplier, some necessitate alteration. In the following, a list of components is presented, modifications to these components are described when made. All parts, as far as not described differently, are produced from 306 stainless steel. VCR components are from the manufacturer *Swagelok*.

- **aluminium lightpipe:** The lightpipe is made from $6/3\,\mathrm{mm}$ (outer/inner diameter) aluminium tubing of $201\,\mathrm{mm}$ length. It is further machined down to $5.5\,\mathrm{mm}$ (outer diameter) at its extremities to establish the necessary clearance for gas flow between the lightpipe and the union tees. The reflective quality of the lightpipe is enhanced by reducing the roughness of the inner surface through lapping with up to $5\,\mathrm{\mu m}$ abrasive paste.

- **2× Sapphire window:** The windows, with a 30 arcmin wedge and a thickness of $3\,\mathrm{mm}$, are crafted from sapphire material. The supplier, *Thorlabs*, specifies a nearly constant transmission larger than $> 85\%$ across the spectral range spanning from 2000 to $10\,000\,\mathrm{cm}^{-1}$. The choice of sapphire over materials like fused silica is driven by its high transparency to infrared radiation and impressive hardness rating of 9.0 Mohs. These properties make sapphire an ideal choice, especially when employed as a component within a compression seal system.

- **2× VCR tee:** The VCR tees need to accommodate the aluminium lightpipe and allow gas flow into the pipe. Therefore, the bore diameter of the VCR tees are enlarged to $6.3\,\mathrm{mm}$ along the opposing connections of the tee.

- **2× VCR cap plug:** The cap plugs, that are necessary to apply the right counter pressure to the copper gaskets and the window, are milled down from a ¼" VCR connection piece. It should be paid attention that the face sealing surface and the back side of the produced caps are sufficient parallel such that the pressure on the window is applied equally. The copper gaskets can correct slight misalignment due to

their softness but need already by design to correct for the wedged sapphire windows. Visually noticeable misalignment should be avoided.

- **Custom-built VCR tube:** This component consists of a $30\,mm$ segment of $8/6\,mm$ (outer/ inner diameter) stainless steel tubing, onto which two ¼" VCR connection pieces are welded at both ends.

- **Oxidation cylinder and copper oxide:** For the oxidation unit, a $10\,mL$ sample cylinder is employed, which is enveloped by a coaxial heating element (*ISOMIL*) and thermally insulated using glass wool for efficient temperature control. This cylinder is then loaded with approximately $30\,g$ of copper oxide using analysis-grade copper oxide wire by *Sigma-Aldrich*, broken into $3\,mm$ pieces. It consists of both copper oxides, the CuO and Cu_2O. The sample cylinder is sealed at one end with a cap, the other is connected to the gas cell using a porous frit with $60\,\mu m$ pore size. This gasket serves as a barrier to prevent any copper oxide dust from entering the valve and the gas cell.

- **2× VCR metal bellow valves:** The valves implemented in the optical cell are used to allow access to vacuum and tritium infrastructure and to separate the optical section from the oxidation unit. In combination with tritium often only two stem tip materials for bellow valves are considered: polyimide and stainless steel. Using stainless steel harbors the risk that tip and seat cold-weld when closing with too much torque. Re-opening can then cause deformation of the tip and disable tight closing. Polyimide on the other side will produce tritiated hydrocarbons in combination with tritium. For the cell, bellow valves with stainless steel tips have been used out of consideration of the sample purity. However, a seat-leak has been observed probably originating from the described process. Observations and consequences are briefly described in Section 5.2.2.2.

- **2× VCR nuts:** The VCR nuts are used to seal both sides of the lightpipe. By applying a torque of $25\,N\,m$, the sandwich of copper gaskets and sapphire window are compressed. The force is applied by the modified cap plug and the VCR face seal of the tee piece.

- **VCR gaskets:** All VCR connections are sealed with stainless steel gaskets. In total, four copper VCR gaskets are used to form the metal-sapphire sealing of the windows and a filter gasket with a $60\,\mu m$ pore size is installed to retain the cupric oxide in place.

- **Cold finger:** The cold finger is an about $20\,cm$ long copper rod with a cylindrical recess. By compression to the middle of the optical segment and the use of heat conductive paste, thermal connection is established during the oxidation process (cf. Figure 5.2). For cooling, the rod is immersed in a liquid nitrogen bath.

To ensure correct assembly and tightness of all connections a leak test is performed showing an integral leak rate below the detection limit of $1 \cdot 10^{-10}\,\mathrm{mbar\,L\,s^{-1}}$. The leak detector is connected to the valve that is designated for connection to vacuum or tritium infrastructure

(cf. right valve in Figure 5.2). The faulty valve seat, described in Section 5.2.2.2, was not be detected at this stage. To avoid loosening of the connections or any stress applied to the thin tube construction, the assembly is mounted on a steel plate of $4\,\text{mm}$ thickness.

For tritium filling, the light-guiding section of the cell is filled with the amount equivalent to $1\,\text{GBq}$ activity. This is performed by filling up the volume to a defined pressure, but can only be realised if the volume is accurately determined. For that reason, the volume was measured with the apparatus of Köllö et al. [Köl11]. The volume of the light-guiding section is found to be:

$$\text{Volume}_{\text{opt.section}} = (5.64 \pm 0.10)\,\text{cm}^3.$$

The volume of the oxidation unit was determined with $(14.11 \pm 0.18)\,\text{cm}^3$ in the empty state and $(8.49 \pm 0.16)\,\text{cm}^3$ once filled with cupric oxide.

5.2.2.2 Preparation procedures and filling of the cell

During assembly, all components, including the cupric oxide inserted into the oxidation segment, were exposed to ambient air. The natural humidity of the air during assembly forms a thin layer of water throughout the cell, including the inner surfaces that will later be in contact with the tritium. In addition, copper oxide tends to absorb moisture from the ambient air, leading to the formation of copper(II) hydroxide, $Cu(OH)_2$.

Both processes lead to a reservoir of protium of unknown capacity within the cell. This reservoir must be avoided to achieve a decent partial pressure of the T_2O water species in the beamline and, therefore, a valuable signal-to-noise ratio. Otherwise, isotope exchange reactions will lead to a conversion of the tritium to the HTO species.

Copper(II) hydroxide decomposes above $100\,°\text{C}$. To effectively eliminate all water content from the oxidation unit and the interior of the cell, several preparation procedures are included. First, the gas cell is placed in an oven and connected to a turbomolecular pump. With ambient air still present, the heating of the oxidation unit is set to $350\,°\text{C}$ for 30 minutes to react with any organic residues in the system, particularly with oxygen.

In addition, copper oxide wire pieces also consist of copper(I) oxide (Cu_2O) which can convert to copper(II) oxide in the presence of water. In summary, the following reactions transpire as the system is heated, gradually driving out any remaining water through the combination of heat and vacuum.

$$Cu_2O + 4\,H_2O + O_2 \longrightarrow 4\,Cu(OH)_2$$
$$Cu(OH)_2 \longrightarrow CuO + H_2O$$
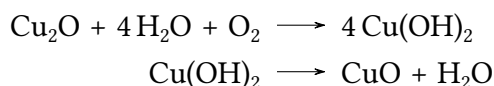
Then, after the initial 30-minute treatment, the turbomolecular pump is activated to create a vacuum within both the gas cell and the oxidation unit. The heating process in the oxidation unit continues for a total of 3 hours. The valve connecting the oxidation unit and the gas cell is then securely closed.

The next step involves setting the oven to $180\,°C$ for a duration of 6 hours, all the while the turbomolecular pump maintains a vacuum of approximately $1 \cdot 10^{-5}\,\text{mbar}$. After this period, the oven is turned off, the pump is disconnected, and a leak detector is connected to gauge the integral leak rate, which must be less than $1 \cdot 10^{-10}\,\text{mbar}\,\text{L}\,\text{s}^{-1}$. Throughout the heating process, the oven is continually flushed with dry nitrogen to prevent oxidation of the copper gaskets which is essential to maintain a reliable seal within the system.

The gas cell, now pristine and hermetically sealed, is transferred into the Tritium Laboratory for the tritium gas filling process. The TTS-f glovebox (now TRIHYDE [Nie21b]) contains the required access to tritium and pressure sensors to quantify the amount and uses a Laser-Raman system to measure the composition of the gas before filling. After connection to the TTS-f glovebox and opening of the valve, the TTS-f pressure sensor detected a slight pressure increase, even though the cell's valves were closed in evacuated state during the preparation procedure with the turbo molecular pump. **This indicates a leak in the seat of the valve of the 1 GBq activity sample.** During the time between bakeout and transfer to the TTS-f, the evacuated cell inadvertently drew in ambient air and therefore atmospheric moisture.

It is important to note that this issue does not pose any safety risk. As depicted on the right of the cell's blueprint in Figure 5.2, the valve is sealed after the filling process with a VCR end plug, which also limits the total amount of gas drawn in. The calculations in [Mül18] show that the impact of the additional gas is on a tolerable scale.

A gas amount of $9.81\,\text{mbar}\,\text{mL}$ (with a measured composition of $96.8\%\,\text{T}_2$, $2.2\%\,\text{D}_2$, and $0.9\%\,\text{H}_2$) was introduced into the cell. This accounts for only 82% of the maximum activity allowed to leave the laboratory. Given the step-like response of the pressure sensor and low accuracy in this pressure region, the next lower pressure was selected to avoid overshooting the target value. It should be noted that after a potential overshooting, evacuating and retrying is not possible. The ambient moisture could potentially trap tritium inside. A restart with a new cell would be necessary.

Upon sealing and capping the outer valve, the cell is extracted from the TTS-f glovebox and subjected to a first exterior decontamination to make it safe for handling during the oxidation phase. The filled cell is depicted in Figure 6.1.

5.2.2.3 Oxidation of tritium to tritiated water

For the oxidation process, the cell is placed in a fume hood located within the TLK facility. Fume hoods, generally used for open contamination treatment, are connected to tritium monitoring infrastructure. Although tritium is safely contained within the cell, this safety measure is taken because simultaneous heating and cooling of the cell can lead to breaking of the cell or loosening of connections. Such an event would be detected by tritium monitoring in the fume hood and require immediate termination of the oxidation process.
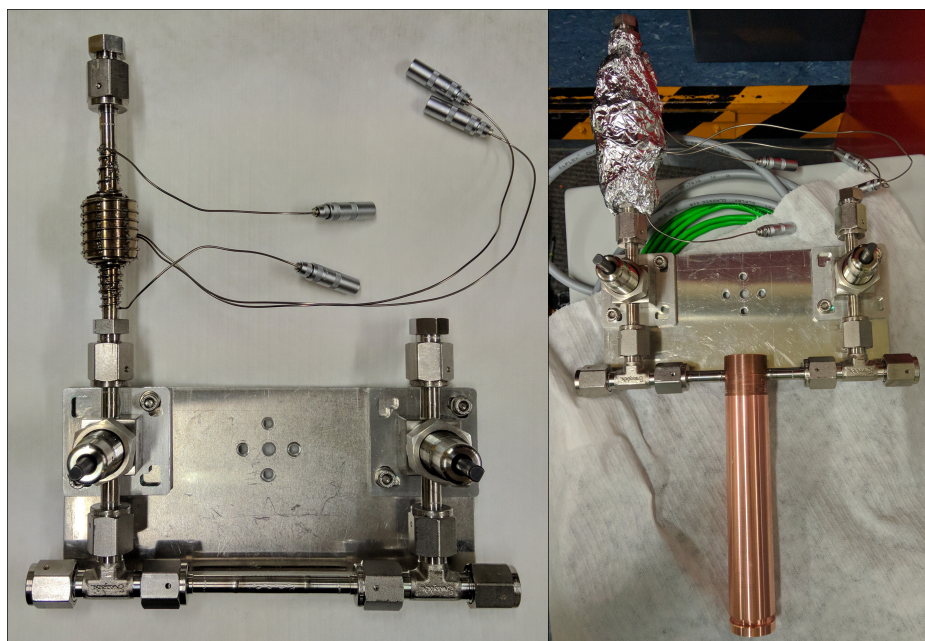
Figure 5.3: Photographs of the assembled cell. Left: Photograph of the assembled cell without any removable attachments. Right: Photograph of the assembled cell with the thermal insulation of the oxidation unit and the copper cold finger attached to the light-guiding segment.

In the fume hood, the copper cooling finger is attached to the middle section of the cell using thermal paste for good contact, and the oxidation unit is wrapped in glass wool and aluminium foil for thermal insulation. A picture of the cell with insulation and cooling finger can be found in Figure 5.3. Subsequently, the cooling finger is immersed in a Dewar vessel and the entire assembly is securely attached using a laboratory stand. Liquid nitrogen is poured into the Dewar and the oxidation unit is gradually heated to $350\,°C$. At this point, the valve connecting the gas cell to the oxidation unit is opened. The heating and cooling process is maintained for a duration of 2.5 hours with periodic replenishment of liquid nitrogen.

During this phase, specific chemical reactions take place. If not already decomposed, these reactions occur as outlined in the previous Section 5.2.2.2.

$$Cu_2O + T_2 \longrightarrow T_2O + 2\,Cu$$
$$CuO + T_2 \longrightarrow T_2O + Cu$$
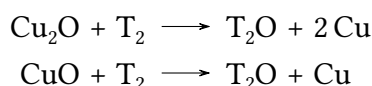
As soon as all the tritium is oxidised, the valve between the oxidation unit and optical segment is closed, the heating is turned off, and the cooling finger is detached. The surface contamination is checked to be below the detection limit. Surfaces that do not meet the requirement are subsequently decontaminated. The gas cell is now prepared for measurement.

At this point, it is important to note that due to valve seat leakage (see 5.2.2.2) some moisture has infiltrated the cell. This leads to isotopic exchange reactions driven by tritium's self-radiolysis [Pen24]:

$$T_2 \longrightarrow 2\,T\cdot$$
$$H_2O + 2\,T \rightleftharpoons HTO + HT$$
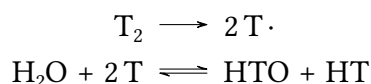
This process reduces the quantity of T_2O and introduces an undetermined amount of HTO into the cell.

The same processes do occur with deuterium, which could remain on inner surfaces from a proof-of-principle experiment performed before. This note will be relevant when explaining the presence of deuterated molecules in the spectra.

5.2.3 Implemented improvements and production of the sample with $10\,GBq$ activity

The production of this sample has been performed in collaboration with Alina Erygina. In her bachelor's thesis [Ery21], detailed descriptions of the development of the cell, the preparation of the sample, the acquisition of the sample, and comparison of the spectra with previous measurements are presented. The general concept of the cell is based on the $1\,GBq$ activity sample [Mül19]. This section is based on these works.

In addition to the obvious issue of the valve seat leak encountered during the preparation of the $1\,GBq$ activity sample, the analysis of the acquired spectra has revealed various deficiencies of the sample. When creating a new sample, some of these have been effectively addressed through alterations in the design, cell preparation, and tritium filling and oxidation processes. Since these deficiencies are only discernible through spectrum analysis, certain results from the subsequent analysis sections will be foreshadowed in this chapter. References to the relevant analysis sections will be provided as necessary.

In the following, an overview of the attributes of a sample is presented that can enhance the scientific result. Then, the implemented improvements are presented that can be subdivided in three categories: (i) Increasing the total activity to $10\,GBq$ and the associated legal requirements, (ii) changes in the design of the cell, (iii) the introduction of a reference cell and (iv) different proceedings in the preparation of the sample. At the end of this section, a summary of the changes is given.

5.2.3.1 Overview of attributes for enhancement in a new tritiated water sample

The central objective of the spectroscopy of tritiated water species is to measure a significant number of highly accurate transitions of all tritiated species. Thus, changes in design and preparation should enhance the following attributes of the cell in order to increase both the quantity and quality of spectral lines:

1. **Number of particles of a tritiated species in the beam path:** According to the law of Lambert-Beer (see. Equation 5.1), increasing the number of particles of a species in the beamline will enhance absorption. This enhancement will be noticeable as higher signal of all lines of a species and therefore elevate numerous lines from the noise level, enabling their evaluation.

   This can be achieved by increasing the filled amount if possible or by suppressing chemical reactions that reduce the amount. An example of a potential reaction is the radiochemical reaction of tritium with hydrocarbons, which leads to tritiated methane [Sch64; Tan65].

$$C_mH_n + T\cdot \longrightarrow C_{m-1}H_{n-3} + CH_3T$$
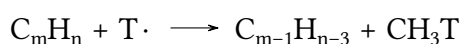
2. **Transmittance for infrared light:** Notable factors here are the IR-transmittance of the windows and losses during reflections inside the cell.

3. **Sample purity:** The sample purity contributes to the quality and quantity of lines in different ways:
   As mentioned in the first point of this section, they can be partners for chemical reactions that are not desired binding the tritium and reducing the amount of tritiated water in the beam path.
   In addition, IR-active impurities will leave a footprint in the spectra. When these lines have energies similar to the desired tritiated water lines, their line shapes overlap. This will impair the accuracy of the assignment or, when the line of the impurity is dominating, even impede the assignment of the weaker one.
   An other important point is the high abundance of protium (^{1}H). In regular steel components when not thermally treated and, from atmospheric moisture, in water films on the surfaces of components, protium is present. When not addressed, the abundance of protium can strongly shift the equilibrium reaction in favour of HTO. This effect was reported by Kobayashi et al. [Kob11].

4. **Sample pressure:** The absolute pressure in the cell leads to broadening of the lines. Broadened lines are more likely to overlap with others. However, it is important to note that reducing the amount of tritiated species or employing a longer cell conflict with points 1 and 2.

5.2.3.2 Increase of total activity to 10 GBq

As mentioned previously, a sample measurement must be performed outside of the TLK. Thus, the activity of the sample is limited by the European radiation law to $1\,\text{GBq}$ [Eur14]. However, exceptions from that limit can be made with a temporary radiation licence for the shipping container housing the FTIR-spectrometer and with the cell being transported by a licensed institution.

The TLK and the spectrometer are located on Campus North at KIT, a former Nuclear Research Centre. Due to several nuclear research groups on campus, there is a KIT institution with a licence to transport a tritium sample above $1\,\text{GBq}$, SUM (*Sicherheit und Umwelt*), but below $10\,\text{GBq}$ and a licence and equipment for the commissioning and decommissioning of a temporary radiation protection area.

Thanks to the support of SUM which the author explicitly wants to acknowledge, a sample with $10\,\text{GBq}$ activity could be transported to the shipping container with the spectrometer. This container has been temporarily designated as a radiation protection area for the duration of the experiment and FTIR measurements could be performed. After measurements were taken, the cell was transferred back to the TLK and an assessment of contamination within the container was carried out. Once the container has been verified to be free of any contamination, it is reopened for regular operational use.

Increasing the activity by a factor of 10 should benefit the signal of tritiated species on average of all three species by the same factor. If for the new sample, the absolute amount of protium and deuterium is comparable, the signal enhancement is estimated to be strongest for the T_2O species.

5.2.3.3 Design improvements

For the design, two aspects have been considered to be improved: (i) the oxidation unit and (ii) the light guide pipe.

Oxidation unit

The oxidation unit of the $1\,\text{GBq}$ sample has a volume of $(14.1 \pm 0.2)\,\text{cm}^3$ and contains $\sim 30\,\text{g}$ copper oxide. For a sample containing a total activity of $10\,\text{GBq}$, the amount of tritium is defined by the activity limit and tritium's half-life of $t_{1/2} = (4500 \pm 8)$ days [Luc00] and given with

$$n = \frac{A \cdot t_{1/2}}{\ln 2} = 5.6 \cdot 10^{17} \text{atoms.} \tag{5.2}$$

Thus, for a complete oxidation of tritium, the equivalent number of oxygen atoms is needed. As copper oxide may be present in both forms, CuO and Cu_2O, the one with fewer oxygen,

Cu_2O, will be assumed as conservative approach. The necessary amount is then given with

$$5.6 \cdot 10^{17} \cdot m_{Cu_2O} = 1.3 \, \text{mg}. \qquad (5.3)$$

This means that the amount of copper oxide used in the 1 GBq sample is more than three orders of magnitude higher than necessary. As mentioned in Section 5.2.2.2, the copper oxide forms copper hydroxide in the presence of water, e.g., in ambient air. Although procedures have been included to reduce this hydroxide, it cannot be completely removed. Using an abundance of material is therefore a significant source of protium and affects the sample purity.

For the 1 GBq sample, copper oxide wire pieces were used. The surface-to-volume ratio of this material was not optimally chosen for the intended purpose. Reaction products can migrate into the bulk and either be released during oxidation or are permanently trapped there. This would affect either the sample purity or reduce the amount of available tritium. The modification implemented reduces the total amount of copper oxide to 1 g. Instead of wire pieces, copper oxide powder is used with a grain size between 350 and 550 μm. This is the smallest grain size fitting to the available filter gasket installed to retain the material in the oxidation unit.

In addition, the oxidation unit is reduced in volume. A butt-welded VCR connection piece with a volume of $(2.9 \pm 0.1) \, \text{cm}^3$ is used.

Light-guiding pipe

For the 1 GBq sample, a 201 mm long aluminium pipe is used. With an inner diameter of 4 mm, it is designed to increase the length of the interaction path and the particle density of the tritiated species in the beam path to favour absorption.

A disadvantage and also a reason why it is not designed any longer and thinner is the loss due to reflections on the inner surface. Although a polishing of the inner surface is implemented, losses multiply with every additional reflection involved.

For the spectral range accessible with the Bruker IFS 125HR spectrometer, $1800 - 10\,000$ cm^{-1}, aluminium has an overall high reflectivity. However, other materials are more suitable, especially for transitions of higher energy. As increased total activity might enable access to these transitions, this argument gains in value. A comparison of the reflectivity of aluminium (Al) [Rak95], silver (Ag), and gold (Au) [Bab15] is presented in Figure 5.4.

Although the increase of reflected signal is on the order of one percent point, it is a significant factor when the angle of incidence is as high as it is in the case of a hollow light-pipe. Aluminium and all other metallic materials have a significant loss in reflectivity of light polarised perpendicular to the surface (parallel to the plane of incidence), P-polarised. For the unpolarised light used, which can be interpreted as half P-polarised and half S-polarised, this effect is noticeable with half the power.
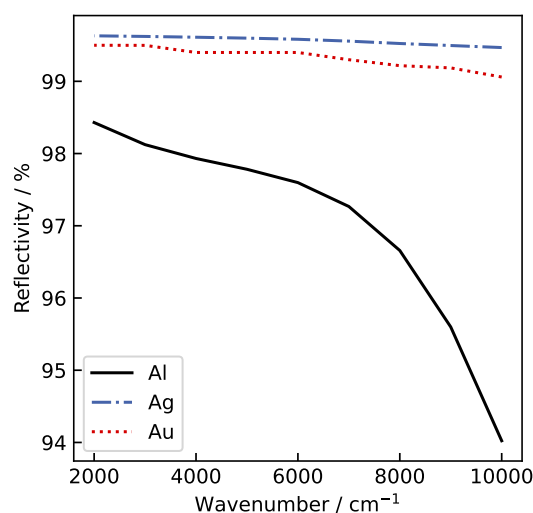
Figure 5.4: Comparison of the reflectivity of potential light-pipe materials. The compared materials are aluminium (Al), silver (Ag), and gold (Au) for the spectral range accessible via the FTIR spectrometer. The values correspond to reflection at normal incidence. Data are taken from [Rak95; Bab15].

In Figure 5.5, a demonstration of this effect is presented. For the angle of incidence between normal and parallel to the metallic surface, the reflectivity of aluminium for $S-$, $P-$ and unpolarised light at wavelength of $2\,\mu\mathrm{m}$ ($=5000\,\mathrm{cm}^{-1}$) is calculated by solving the Fresnel equations. Using the complex refractive indices of the materials aluminium, silver and gold, one notices that for shallow angles the changes in refractive index, order of one percent for normal incidence, will add up to $5 - 8\%$ per reflection. These losses will multiply for the number of reflections, which occur, extracted from geometrical calculations, up to 4 times.

For that reason, the light-guiding pipe for the new sample was produced from a silver pipe. The length, inner and outer diameter were the same as for the aluminium variant of the $1\,\mathrm{GBq}$ sample, and the inner surface was polished using different abrasive pastes.

Although the parameters of the first cell have been used, the volume of the optical part, the volume between the two hand valves, was reduced from $(5.64 \pm 0.10)\,\mathrm{cm}^3$ to $(4.32 \pm 0.14)\,\mathrm{cm}^3$. This change in volume is probably result of a reduction of the volume between the light-pipe and its steel containment. This change in volume is increasing the particle density in the light-pipe and is therefore benefiting the SNR.
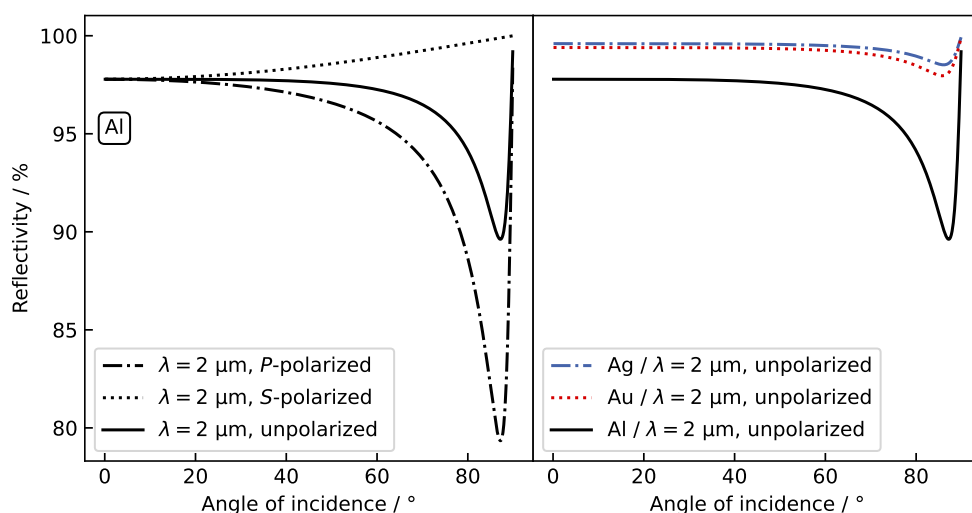
Figure 5.5: Influence of the angle of incidence on the reflectivity. Left: Demonstration of the influence of the angle of incidence on the reflectivity for $S-$, $P-$ and unpolarised light for the example of aluminium and light with a wavelength of $2\,\mu m$ (=5000 cm^{-1}). Right: Comparison of the reflectivity of aluminium (Al), silver (Ag), and gold (Au) for different angle of incidence. Calculations made with data from [Rak95; Bab15].

5.2.3.4 Implementation of a reference cell

The implementation of a reference cell is not a change that enhances the sample itself. However, its implementation is expected to enhance the quality of the spectral data.

All optical elements involved in the acquisition of the spectra, the source, mirrors, spectrometer, and the cell itself, have wavelength-dependent refractive and transmittive indices. Thus, the signal varies over the spectral range. The acquired line intensities could therefore be inconsistent. This effect can be corrected by using the signal baseline. However, dividing the spectra by reference spectra is the common approach.

There is another effect, which produces wavelength-dependent signal losses in the spectra not originating from the sample itself: As the IR beam propagates through the ambient air of the laboratory, absorption features of species in the air, mainly from water, are collected in the spectra. These up to tens of wavenumbers broad lines can mix with lines of tritiated water species and will impair the accuracy or impede the assignment. Correction of this effect is intended by employing a reference cell, possibly obtaining reference spectra with same absorption features from the ambient air.

The reference cell is an identical replica of the $10\,\mathrm{GBq}$ cell without the oxidation unit. After the identical cleaning procedure, it is filled with $1.3\,\mathrm{bar}$ nitrogen such that outgasing is suppressed or that at least potential absorption features are significantly pressure-broadened.

5.2.3.5 Improved sample preparation and production of the 10 GBq sample

The general proceeding of the sample preparation is based on the 1 GBq sample procedure (see section 5.2.2.2). For the oxidation unit of the new cell, a bake-out is performed at 300 °C for 30 minutes with ambient air present in the cell. During this bake-out, the copper hydroxide is expected to be reduced to copper oxide and water vapour. The water is then removed by evacuation for 3 hours with a turbomolecular pump with the heating of the oxidation unit still ongoing. After turning off the heating, the optical segment is evacuated for additional 15 hours, then a bake-out of the total cell is performed. The cell is backed out for additional 8 hours in a nitrogen-purged oven at 160 °C. The nitrogen atmosphere is essential to prevent the copper gaskets from oxidising. Validation of the integrity of the cell is given by performing a leak test.

Subsequently, the cell is then transferred into the glove-box of the *TRIHYDE* [Nie21b] infrastructure of the TLK where it is connected to a sample port. Here, a procedure is introduced that is deviating from the preparation of the 1 GBq sample. The cell is filled with 100 mbar deuterium for a duration of 48 hours. This procedure is implemented to reduce the amount of protium in the walls by replacing it with deuterium. By reducing the abundance of protium and introducing deuterium as an additional isotope, it is expected to get access to spectral data for the three tritiated isotopologues, HTO, DTO and T_2O.

After evacuating the cell for 12 hours, the optical part of the cell is filled with a tritium-deuterium mixture of 3:1 ratio. It has been decided to use a mixture with deuterium to get access to DTO transitions. The loading pressure of (34.40 ± 0.07) mbar takes into account all uncertainties (e.g. vessel volumes, pressure sensors, etc.) that meet the strict limit of 10 GBq activity.

After loading, the cell is disconnected and transferred out of the *TRIHYDE* glove-box. After ensuring no surface contamination is present, the cell is placed in a fume hood for oxidation procedure. Real-time activity monitoring guarantees the safety of the operator during the oxidation process.

In the fume hood, the copper cooling finger is attached to the optical segment. Thermal paste is used for good contact. The oxidation unit is wrapped in mineral wool and aluminium foil for thermal insulation. The cooling finger is immersed into a Dewar vessel and the entire assembly is secured using a laboratory stand. Liquid nitrogen is poured into the Dewar and the oxidation unit is gradually heated to 225 °C. To start the oxidation process, the valve connecting the gas cell to the oxidation unit is opened. The oxidation conditions are maintained for a duration of 4 hours with periodic refilling of liquid nitrogen.

The temperature used to heat the oxidation unit was reduced from 350 °C to 225 °C compared to the 1 GBq sample. This measure reduces the diffusion of tritium [Aus72; Sug85] into the walls but, with a total duration of 4 hours, it still meets the requirements for complete oxidation [Kim03].

During the oxidation process the gas mixture is oxidised

$$CuO + T_2 \longrightarrow T_2O + Cu$$
$$CuO + D_2 \longrightarrow D_2O + Cu$$
$$CuO + DT \longrightarrow DTO + Cu$$
$$CuO + H_2 (walls) \longrightarrow H_2O + Cu)$$
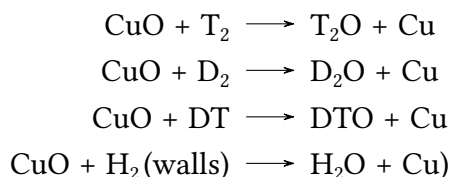
and permanent isotope exchange reactions take place.

$$T_2O + D_2O \rightleftharpoons 2\,DTO$$
$$(DTO + H_2O \rightleftharpoons HTO + HDO)$$
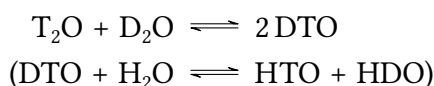
Note that the loaded gas is self-equilibrating producing amounts of DT, enhanced by the radiolysis from the tritium decay.

After the oxidation process, the valve between the oxidation unit and the optical segment is closed, the heating is turned off, and the cooling finger and insulation of the oxidation segment are removed. Wipe tests ensure that the surface is free from contamination. The gas cell is now prepared and handed over to *SUM* for transport to the container with the spectrometer.

5.2.3.6 Summary of implemented improvements for the 10 GBq sample

In Table 5.1, an overview of all the changes implemented and their expected effects is given. The changes are subdivided into categories that represent their implementation within the sample production and measurement timeline, respectively.

Optimisation of the oxidation unit by reducing the amount of copper oxide and changing from wire to powder form is estimated to improve the purity of the sample. Unavoidable impurities in the material are reduced to a minimum. The reduction of the abundance of protium in the material is particularly important [Kob11] as it shifts the chemical equilibrium to the protium-containing species, HTO.

For this reason, during cell preparation, a 48 hour purging with deuterium is implemented. Another effect of the deuterium purging, but mostly by using a tritium-deuterium mixture for filling, is to enable the formation of DTO. Like HTO and T_2O, DTO is an important benchmark molecule for molecular theory, and therefore the determination of ro-vibrational transitions with high accuracy is desirable. For the sample $1\,\text{GBq}$, deuterium was not introduced into the sample because only a small amount of tritium was available. By securing the support of *SUM*, a KIT institution with a licence for radiation handling outside the TLK, a sample with ten times activity, $10\,\text{GBq}$, can be measured. This enhancement will have a high impact on the number of lines, as the increased number of molecules will allow lower line intensity to be measured. This enables the measurement of transitions of higher energies, especially for of T_2O, containing two tritium atoms per molecule.

Table 5.1: Summary of all implemented changes of the $10\,\mathrm{GBq}$ sample and their expected effects.

Category	Improvement measure	Expected effect
Design	CuO powder instead of wire pieces	Enhanced sample purity; Reduction of species with protium
	Reduction of CuO material	Enhanced sample purity; Reduction of species with protium
	Light-pipe out of silver	Reduction of signal losses
Preparation	Purging cell with deuterium	Reduction of species with protium; Access to DTO lines
Filling	Increase of activity from $1\,\mathrm{GBq}$ to $10\,\mathrm{GBq}$	Enhanced SNR for tritiated species
	Mixture tritium-deuterium (3:1)	Access to DTO lines
Measurement	Reference cell	Correction for line mixing with atmospheric lines

A duplicate of the cell filled with $1.3\,\mathrm{bar}$ nitrogen is implemented as a reference cell. Immediately before or after the measurement with the tritiated water sample a measurement with this reference cell will be performed to better account for the wavelength-dependent transmission properties of the cell and, more importantly, to correct the spectra for lines from atmospheric absorption. This is expected to improve the fit accuracy of the line positions of tritiated species mixing with atmospheric water.

5.3 Acquisition of the spectra from tritiated water vapour samples

In this section, the acquisition of the spectra from both samples is presented. Both measurements were performed at the same location using the same setup and spectrometer. First, the experimental setup will be described. However, the measurement properties are different for the samples and are therefore presented separately.

5.3.1 Experimental setup

For the acquisition of the spectra, the samples are transported to a shipping container on the Campus North of KIT. In this container a *Bruker* IFS 125HR high-resolution FTIR spectrometer is used for atmospheric trace gas observation [Gis11; Has13; Kie16b].

Usually, measurements are performed using a solar tracker on the roof of the shipping container guiding sunlight with absorption features of the atmosphere to the spectrometer. As atmospheric absorption in tritiated water spectra is hampering the assignment, a temporary tabletop construction with a Globar light source is set up. The setup requirement is fast construction and deconstruction such that interruption of the regular operation is kept to a minimum. This is realised by placing the cell on a height-adjustable lab jack and guiding the light of an IR source with mirrors through the cell into the spectrometer, a configuration that is set up within a few minutes.

In Figure 5.6, a sketch of the beamline and a photography of the tabletop setup with highlighted IR source, cell, and beamline are presented. As shown, two gold-plated concave spherical mirrors ($f = 150\,\text{mm}$) (cf. Figure 5.6 M1 and M2) are used to focus the beam into the cell and refocus the transmitted beam. Two other mirrors, M3 and M4, guide the beamline to the FTIR spectrometer after optionally passing an optical cell filled with a reference gas for calibration purpose. These mirrors are part of the existing setup for regular operation and are not moved. In the spectrometer, the beam propagates through a Michelson interferometer. The resulting interferogram is collected and converted to an ASCII file with the parameters 'intensity' and 'wavenumber'. The beam path on the spectrometer is simplified. Details on the technique can be found in Section 4.1.

For ensuring a near-nominal instrumental line shape, the alignment status of the FTIR spectrometer is regularly checked by performing gas cell measurements. These cells are filled with HCl, C_2H_2, or N_2O [Has13; Has12]. The resulting spectra are analysed using *LINEFIT* software [Has99].

The spectrometer can reach a spectral resolution of $0.0019\,\text{cm}^{-1}$.

For measurements, different filters can be used that cover in total the spectral range from 1800 to $10\,000\,\text{cm}^{-1}$. The available filters and their spectral range can be found in Table 5.2.
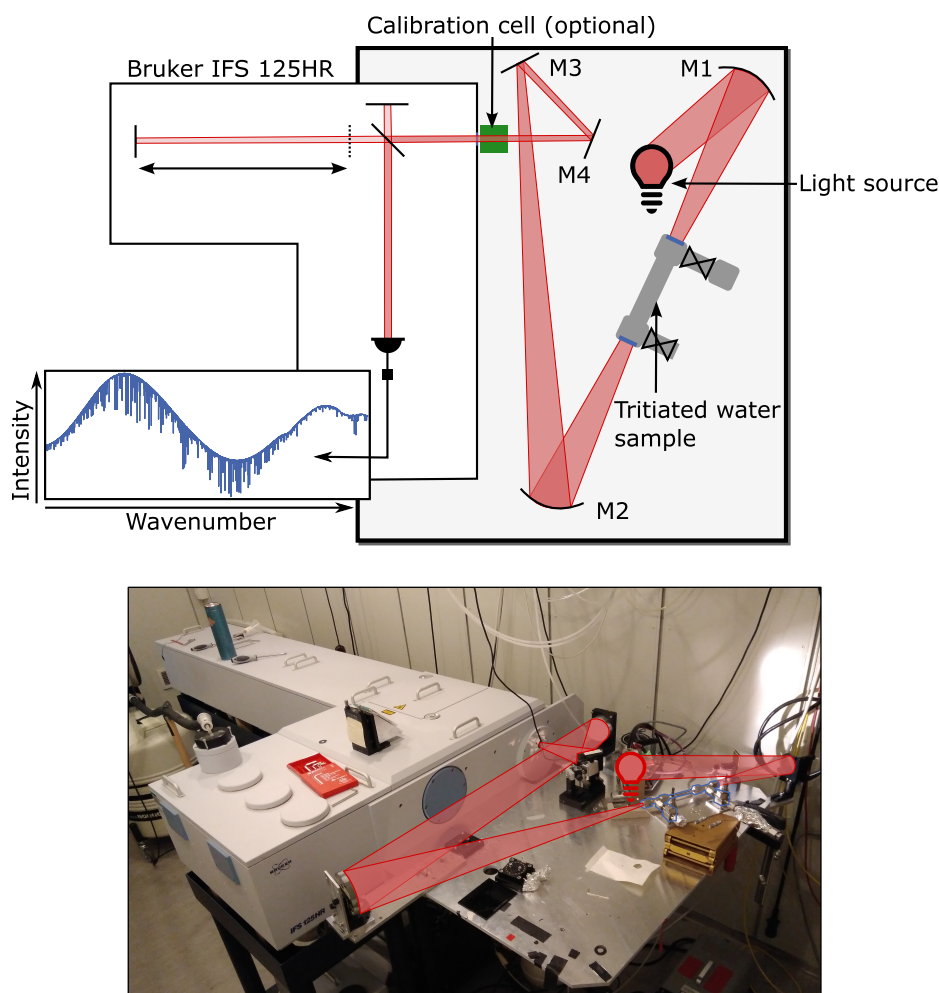
Figure 5.6: The experimental setup. Top: Sketch of the IR beamline of the tabletop setup for the measurements. The light of the IR source is focused in the optical section of the tritiated water sample using a spherical mirror (M1). The light passing through is collected with a second spherical mirror (M2). With mirrors M3 and M4, the light is guided into the FTIR spectrometer, where the light passes a Michelson interferometer. The collected interferogram is Fourier-transformed by the spectrometer providing an ASCII file with the parameters 'intensity' and 'wavenumber'.
Bottom: Photography of the setup with highlighted IR source, beam path (both red) and the tritiated water cell (blue).

Table 5.2: Spectral filters available for measurements with the FTIR spectrometer

Filter name	Spectral range
BE	1800-2300 cm^{-1}
BD	2000-2700 cm^{-1}
BC	2400-3250 cm^{-1}
BB	3000-4000 cm^{-1}
BM	3700-5440 cm^{-1}
BN	5000-10 000 cm^{-1}

5.3.2 Acquisition of the spectra from the 1 GBq sample

> The measurements of the the 1 GBq sample have been performed by Frank Hase, Magnus Schlösser and Johannes Müller prior to this work.

The setup using the cell on a lab jack and the concave mirrors to focus the light into the cell has been set up and the manual alignment of the cell into the existing optical path (M3, M4 and spectrometer) could be realised in less than 5 minutes. The polished inner surfaces of the light pipe cell worked as intended since the cell preserves the divergence of the input cone. This has been verified by checking the output light distribution from which near-grazing incidence reflection can be assumed.

The transmittance of infrared light through the cell is measured by comparing the free-path IR intensity to the scenario with the cell installed in the beam path. The empirical transmission of the cell was determined to be approximately 20%. This result is in a qualitative agreement with the estimation when taking into account transmission and coupling losses in the windows as well as losses from multiple reflections on the polished Al surface (see Section 5.2.3.1). The wavelength-dependent transmission was found to be dominated by the reflectivity of aluminium. A reduction in transmission of less than 4% was measured when comparing 5400 cm^{-1} with 3800 cm^{-1} which is in accordance with aluminium's wavenumber-depended reflectivity.

In total, 9 spectra were recorded. In Table 5.4, the measurement properties, spectral range of the filters, resolution, and number of averaged scans of the individual spectra are presented. For each filter available in Table 5.2 a spectrum with resolutions up to 0.0019 cm^{-1} was recorded. In addition, for filters *BD*, *BC*, and *BB*, a measurement is performed with a calibration cell filled with N$_2$O.

The measurements were performed within 15 hours divided over two days. The restricted availability of the spectrometer limited the acquisition time. However, a longer recording would not have improved the spectra in SNR by a significant factor, which is why additional measurements have not been pursued. In Figure 5.9, the spectra of measurements with each filter without a calibration cell are presented. It is noticeable that the intensity, which represents the transmittance of the beam throughout the whole beam path, is dropping to

Table 5.3: Overview of the properties of measurement for each spectrum obtained from the 1 GBq sample. Some spectra were recorded with calibration cell (Cal. cell) present. The recording time for each spectrum (not listed) depends on the spectral resolution and the amount of averaged scans (Avg. scans).

Name	Filter	Spectral range	Cal. cell	Resolution	Avg. scans
BE/1GBq	BE	1800-2300 $\mathrm{cm^{-1}}$	no	0.0075 $\mathrm{cm^{-1}}$	11
BD/1GBq	BD	2000-2700 $\mathrm{cm^{-1}}$	no	0.0075 $\mathrm{cm^{-1}}$	16
BDc/1GBq	BD	2000-2700 $\mathrm{cm^{-1}}$	yes	0.0075 $\mathrm{cm^{-1}}$	17
BC/1GBq	BC	2400-3250 $\mathrm{cm^{-1}}$	no	0.0075 $\mathrm{cm^{-1}}$	16
BCc/1GBq	BC	2400-3250 $\mathrm{cm^{-1}}$	yes	0.0075 $\mathrm{cm^{-1}}$	17
BB/1GBq	BB	3000-4000 $\mathrm{cm^{-1}}$	no	0.0019 $\mathrm{cm^{-1}}$	41
BBc/1GBq	BB	3000-4000 $\mathrm{cm^{-1}}$	yes	0.0019 $\mathrm{cm^{-1}}$	17
BM/1GBq	BM	3700-5440 $\mathrm{cm^{-1}}$	no	0.0019 $\mathrm{cm^{-1}}$	90
BN/1GBq	BN	5000-10 000 $\mathrm{cm^{-1}}$	no	0.0075 $\mathrm{cm^{-1}}$	119

zero for several spectral areas. This originates from the absorption of water in the ambient air. Reduction of the humidity by e.g. purging with dry nitrogen was considered for the second sample but was not performed as long preparation time (with cell present) would be necessary to narrow down this effect to an acceptable level which was not compatible with the available measuring time.

5.3.3 Acquisition of the spectra from the 10 GBq sample

For the measurement of the 10 GBq sample, the special radioactive handling licence of *SUM* is required. Thanks to the help of this KIT institution, one day of measurement was available to record the spectra.

Two cells are measured, the tritiated water sample itself and a reference cell. To switch between the samples in the setup without realigning the beam path, a sample holder has been produced. As for the reference cell, no radioactive handling licence is necessary, it is used the day before the measurement with tritium to prepare and align the setup.

Overnight, three spectra were recorded with the reference cell.

For the measurement of the tritiated water sample, an additional modification is required. The sample is supposed to contain (tritiated) water vapour of approximately 35 mbar at a container temperature of 20 °C. As presented in Figure 5.8, the vapour pressure for these conditions is exceeded, which will result in the condensation of the water. Not only will the particles in the beamline be reduced significantly, but absorption in water condensed on the windows will produce broad artefacts which spoil accurate assignment.

For this reason, the tritiated water cell, after being transported to the spectrometer container by *SUM* (now radiation supervised area), is wrapped with a heating wire and thermal
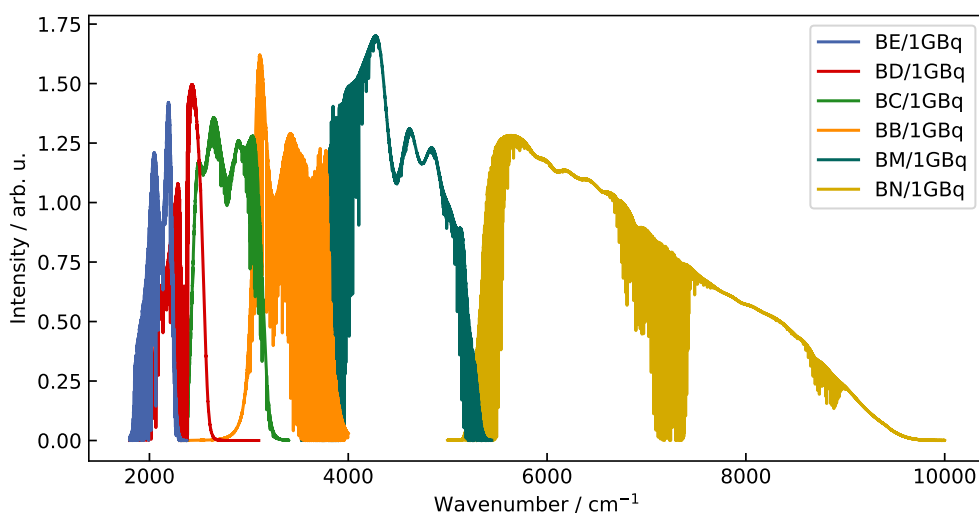
Figure 5.7: Obtained spectra from the $1\,\mathrm{GBq}$ **sample.** Measurements with the calibration cell have been left out in this visualisation.

Table 5.4: Overview of the properties of measurement for each spectrum obtained from the $10\,\mathrm{GBq}$ sample.

Name	Filter	Spectral range	Activity	Resolution	Avg. scans
BD/10GBq	BD	2000-2700 cm^{-1}	yes	0.0075 cm^{-1}	4
BD/Bgr	BD	2000-2700 cm^{-1}	no	0.0075 cm^{-1}	2
BC/10GBq	BC	2400-3250 cm^{-1}	yes	0.0075 cm^{-1}	4
BC/Bgr	BC	2400-3250 cm^{-1}	no	0.0075 cm^{-1}	2
BM/10GBq	BM	3700-5440 cm^{-1}	yes	0.0019 cm^{-1}	35
BM/Bgr	BM	3700-5440 cm^{-1}	no	0.0019 cm^{-1}	10

insulation. A thermal sensor with PID control is used to heat and keep the sample at a target temperature of $35\,°\mathrm{C}$, a temperature that according to Figure 5.8 is high enough to maintain the vapour conditions.

Three measurements were performed with the tritiated water sample heated to $35\,°\mathrm{C}$, using the same filters as for the reference, BC, BD and BM. More measurements, including additional filters, could not be performed within the available measurement time. After recording for 6 hours, the sample is unwrapped and placed in a radioactive transport box. After transport back to TLK it is stored in the storage glovebox and the container is not longer considered as a radioactive supervised area by *SUM*.
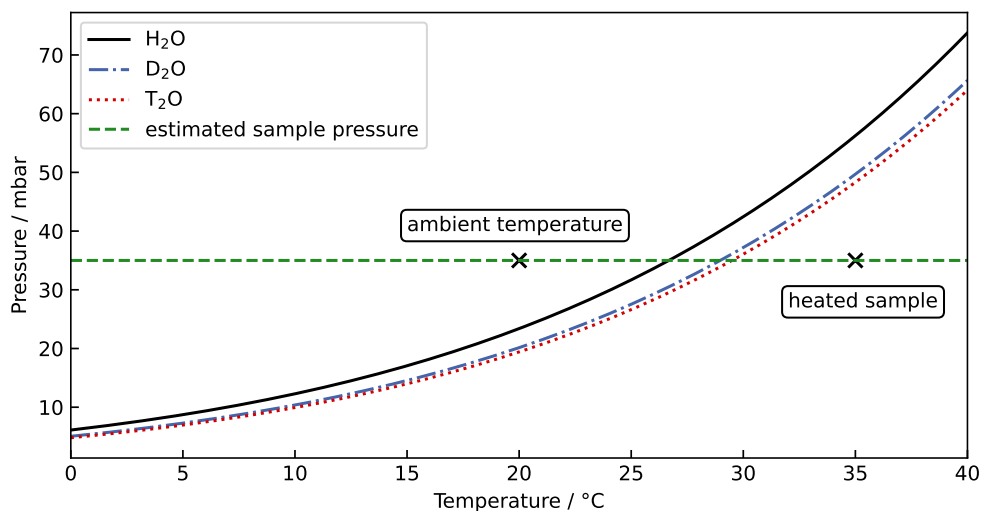
Figure 5.8: Vapour pressure of H$_2$O, D$_2$O and T$_2$O. Data reproduced from [Lid04; Jon03]. The green dashed line indicates the estimated pressure of the sample. At ambient temperature, this pressure exceeds the vapour pressure. Thus, water is condensed and the number of particles in the beamline is reduced. Heating the sample to 35 °C prevents this effect.
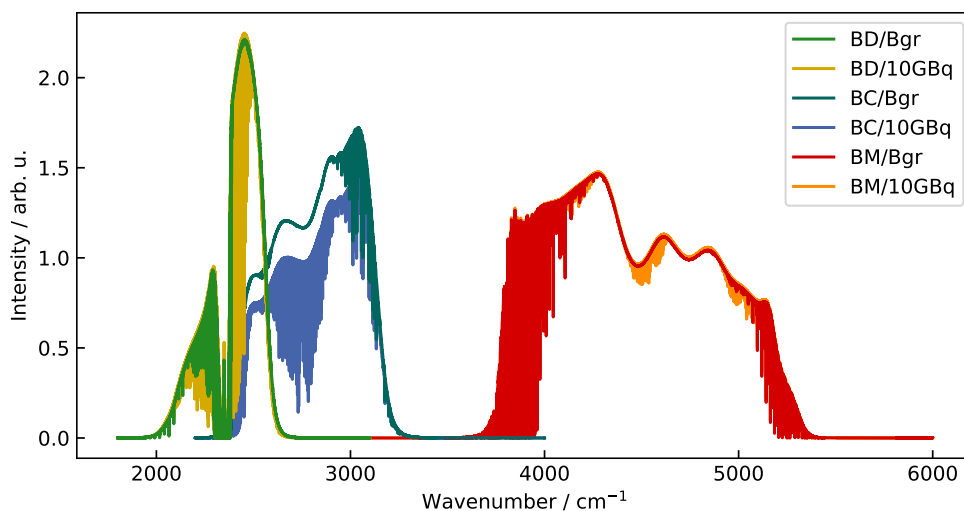
Figure 5.9: Obtained spectra from the 10 GBq **sample.** Absorption features originating from tritiated species can be noticed by eye comparing reference spectra (ending ∼/Bgr) with the tritiated water spectra (ending ∼/10GBq).

5.4 Evaluation of the spectra

The optical cells have been constructed, prepared and filled with tritium. The oxidation to the tritiated water species was performed, and the samples were measured providing high-resolution spectra.

However, these spectra consist of absorption lines of all species present in the beamline, raising the challenge of an unambiguous assignment. In this section, the general concept and procedure of line assignment are presented. To obtain highly accurate data, a calibration of the wavenumber axis is mandatory. The method and consistency checks for the calibration are presented. A Monte Carlo study validates the accuracy of the fit and analyses the best use of the spectra obtained from the reference cell. Finally, in this section, an estimation of the composition of the samples is given using general observations during the evaluation of the spectra.

5.4.1 Concept and procedure of the line assignment

> The general concept of the assignment procedure is based on a program routine developed by Johannes Reinking [Rei18] using the *LINEFIT* software of Frank Hase [Has99].

In Figure 5.10, an overview of the different steps in the assignment process is illustrated. Starting from the spectrum that is evaluated, slices of typically one wavenumber are taken. For each slice, a synthetic spectrum is generated by simulating the line profiles using the line parameters of the HITRAN database (High-resolution Transmission Molecular Absorption Database) [Gor17; Gor22] for non-tritiated gases and the line positions and (relative) intensities from the theoretical predictions in the SPECTRA database for the radioactive water isotopologues [Mik05]. The code used for this step is based on the HAPI (HITRAN Application Programming Interface) [Koc16].

The synthetic spectrum takes into account the convolution of the Voigt profiles of mixing lines and the instrumental line shape of the FTIR spectrometer (details to the FTIR technique in Section 4.1). However, this synthetic spectrum, as visible in the figure (cf. Figure 5.10), generally deviates by orders of $0.1\,\mathrm{cm}^{-1}$ for the predicted tritiated water lines. This fact impedes a purely software-based assignment, as the deviations are up to 20 times larger than the width of the lines ($\sim 0.015\,\mathrm{cm}^{-1}$).

Despite the comparably large deviations of these calculations, the accuracy of the relative line intensities and the relative distance of lines within a vibrational band permit in most cases one to perform an initial visual assignment. Because of the sometimes high line densities in the evaluated spectra, especially for the tritiated water isotopologues, some of the predicted line positions cannot be identified unambiguously and must be discarded.

Throughout the first assigned vibrational bands, an additional method has been implemented to shift the initial positions closer to their actual position. The key is a statistical
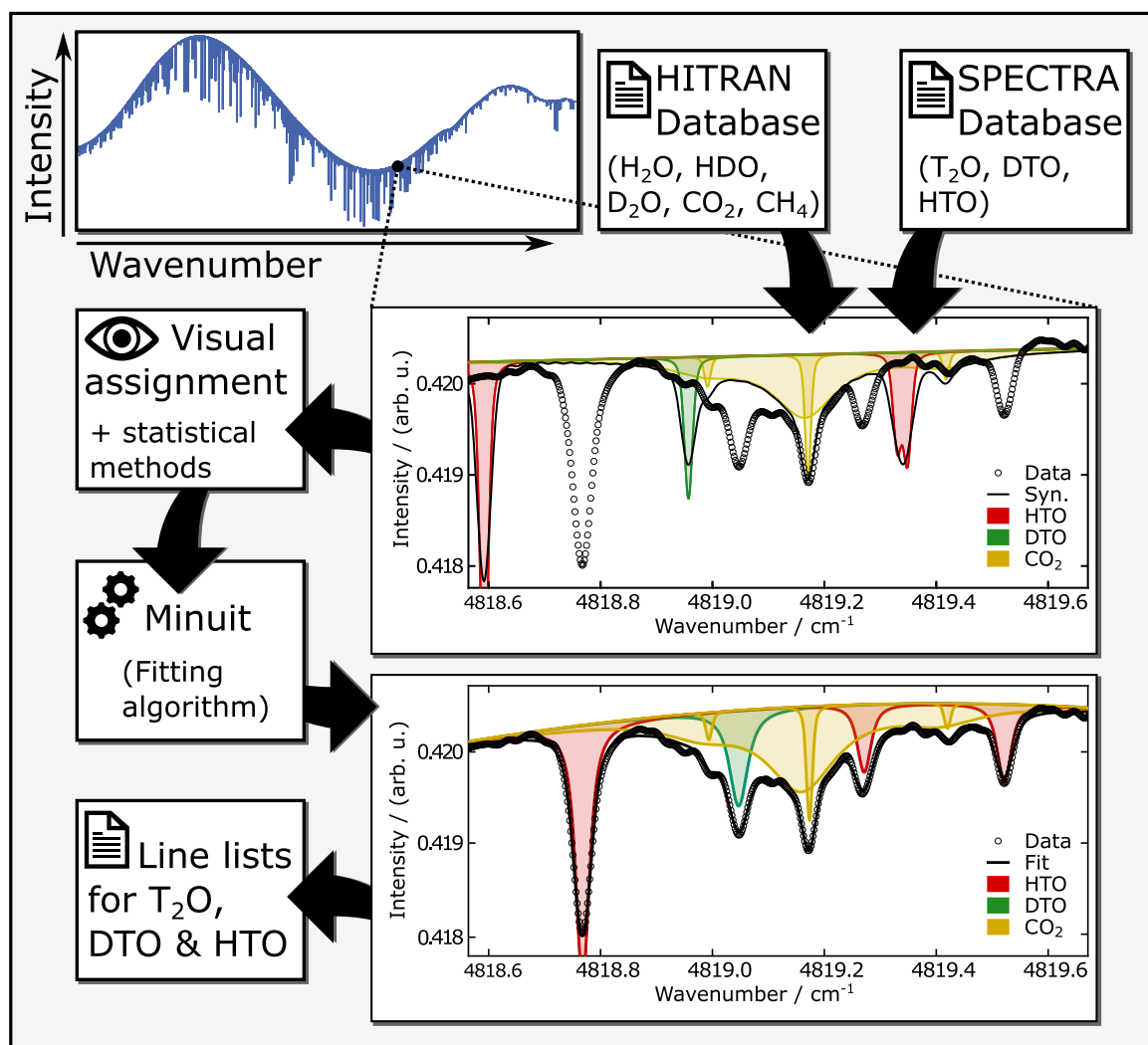
Figure 5.10: General concept of the assignment of the FTIR spectra. The spectrum is subdivided into slices (in order of cm^{-1}). Using spectral data for non-tritiated species from the HITRAN database and ab initio predictions from the SPECTRA database [Mik05] for tritiated water isotopologues, a synthetic spectrum is generated. Then, a visual assignment is performed based on the line intensity and statistical observations. A fit using the *Minuit* algorithm adjusts the synthetic spectrum to the measured one and provides data for position, intensity, and broadening for all tritiated water species.

evaluation of the positional shifts of the tritiated water lines showing a vibrational band-dependent 'base' shift and an often much smaller rotational quantum-number-dependent shift. By assigning some lines of a vibrational band, the base shift can be extracted and the initial position corrected for. A detailed description of these observations can be found in Section 5.8.

Starting from these visually corrected initial line positions, a fit of the synthetic spectrum to the FTIR spectrum was performed using the robust minimisation algorithm *MINUIT* [Jam75] via the iminuit[1] Python library.

For each of the non-tritiated species, one fit parameter determining intensity (scaling), broadening, and a wavenumber-dependent correction of the line position, the calibration factor, is set. As CO_2 and H_2O in the beam path from outside the cell are also contributing to the spectra, models of these broader and different intense lines have been included with their own parameters.

For each of the tritiated water species, each line position is treated as an independent fit parameter, whereas the line intensity (scaling) and broadening are fitted as one parameter for all lines.

The adaptation of the line intensity from the data bases is implemented by introducing an empirical scaling factor. This scaling factor is obtained by adaptation by eye and by extracting the line intensity scaling parameter from the fit of some lines and is performed for each sample and specie independently. The analysis of these scaling factors is the basis for the estimation of the sample composition, found in Section 5.4.4.

The set of parameters fitted for each of the tritiated species with the corresponding uncertainties is collected. The identification of the line is given by its upper and lower vibrational and rotational quantum numbers. These line lists, typically subdivided for vibrational bands of an isotopologue, are the objective of the measurements.

Although the fit uncertainties for the line centres are of the order 10^{-4}cm^{-1}, these line lists are not yet highly accurate. There are three additional steps that must be included:

1. **Calibration of the wavenumber axis:** Although the wavenumber axis is calibrated by an accurate HeNe laser in the spectrometer itself, an additional calibration of the wavenumber axis is mandatory as small misalignment may cause a wavenumber dependent shift. In addition, an estimation of the wavenumber axis accuracy using a HITRAN reference must be given. The calibration is presented in the next Section 5.4.2.

2. **Validation of the fit accuracy:** The fit uncertainties provided by algorithms are not always representing the actual situation. Although the *Minuit* algorithm [Jam75] has been proven to provide true values in various experiments (as CMS [col20], Planck 2015 [Agh16], or cavity ring-down spectroscopy [Dup15]), a potential error

---

[1]https://github.com/scikit-hep/iminuit

in the implementation into the software can cause false output. To validate a correct implementation a Monte-Carlo study was performed in Section 5.4.3.

3. **Validation of the assignment:** As visual assignment is required, misassignments due to the operator's bias needs to be considered. To exclude methodical errors the data sets need to be validated. This is performed by cross-checks with different measurements. This is performed in Section 5.6.

5.4.2 Calibration of wavenumber axis

The *Bruker* IFS 125HR FTIR spectrometer has a HeNe laser that tracks the mirror distance. The resulting interferogram of the mono-energetic laser light propagating through the Michelson interferometer is used for a precise energy (wavenumber) scale calibration.

The alignment status of the FTIR spectrometer is checked by performing gas cell measurements, usually filled with HCl, C_2H_2, or N_2O [Has13; Has12]. The resulting spectra are analysed using the *LINEFIT* software [Has99]. This calibration is regularly performed to ensure a near-nominal instrumental line shape.

The interferometer is operated in vented state, as it is mostly used for atmospheric observations in the region between 4200 and $4340\,\mathrm{cm^{-1}}$. Exposed to thermal and atmospheric fluctuations, the precision of the HeNe laser wavenumber scale ruler suffers from slight changes of the refractive index in the beam path or slight misalignment of the beam leading to a wavenumber dependent scaling error ϵ

$$\nu_{\mathrm{cal.}} = (1 - \epsilon) \cdot \nu_{\mathrm{meas.}}.$$ (5.4)

The differences between the calibrated wavenumber value $\nu_{\mathrm{cal.}}$ and the measured one $\nu_{\mathrm{meas.}}$ is usually in order of 10^{-6}, respectively $\sim 10^{-3}\mathrm{cm^{-1}}$. Therefore, to obtain an precise energy scale additional calibration of the measured spectra are mandatory.

5.4.2.1 Concept of calibration

To correctly attribute a wavenumber dependent scaling error, a comparison with a reference standard is the way to go. Absorption features from non-tritiated molecules can serve as such a reference standard as their line positions have been measured accurately before. For each spectral range, 20 to 50 line positions of non-tritiated molecules are compared with positions provided by HITRAN database.

The assignment software has implemented the calibration factor ϵ for all non-tritiated species allowing the usage of the evaluation tool to obtain the required values. Each fit made is provided with an uncertainty on the calibration factor σ_ϵ provided by the minimisation algorithm.

The species to be compared with the HITRAN database depends on the availability of lines in proximity to the assigned tritiated water lines. For the spectra presented in this work,

CO_2, H_2O, HDO, and N_2O from spectra measured with the calibration cell have been used. Generally, isolated lines with high SNR are used to achieve high fit accuracy.

For CO_2 and H_2O, absorption features originating from absorption in the cell and in the laboratory air overlap, affecting the accuracy of the fit. In the first place, this makes HDO highly favourable. However, CO_2 and H_2O lines often have much better SNR compared to HDO. Water species have much more transitions in the IR compared to CO_2, where lines are only found in few spectral ranges. The calibration cell with N_2O was not used for all spectra as absorption signatures can also only be found in selected spectral ranges. Hence, the best calibration molecule must be individually determined for each range based on the availability and quality of lines of these molecules.

The final fit value ϵ is obtained from the weighted mean value $\bar{\epsilon}$ of the individual fit values ϵ_i where the weight g is depending on the fit uncertainty of each value, $\sigma_{\epsilon,i}$,

$$\bar{\epsilon} = \frac{\sum_{i=1}^{n} \epsilon_i g_i}{\sum_{i=1}^{n} g_i} \tag{5.5}$$

$$\text{with } g_i = \frac{1}{\sigma_{\epsilon,i}{}^2}. \tag{5.6}$$

The use of a weighted average is justified as individual values ϵ_i are independently distributed with the same expected value but different variances $\sigma_{\epsilon_i}{}^2$.

The calibration factor obtained is used to correct the assigned tritiated water lines using Equation 5.4. For each of the spectral ranges used to assign tritiated water lines, such a calibration was performed. Corrections are usually in the order of $1 \cdot 10^{-3}\,\text{cm}^{-1}$ and, therefore, of relevant magnitude.

Uncertainty of the calibration process

This calibration process implies an additional source of uncertainty for the assigned tritiated water lines. From the fitting process, the weighted standard deviation,

$$\sigma_{\bar{\epsilon}}{}^2 = \frac{1}{\sum_{i=1}^{n} g_i} = \frac{1}{\sum_{i=1}^{n} \frac{1}{\sigma_{\epsilon,i}{}^2}} = \sum_{i=1}^{n} \sigma_{\epsilon,i}{}^2, \tag{5.7}$$

is used as one source of uncertainty of the calibration factor. The reduced chi-squared value

$$\chi_v^2 = \frac{1}{(n-1)} \sum_{i=1}^{n} \frac{\left(\epsilon_i - \bar{\epsilon}\right)^2}{\sigma_{\epsilon,i}} \tag{5.8}$$

is checked to be equal or smaller than one to exclude any mistake during the procedure. Usually, values smaller than one are obtained, which argues for an overestimation of the uncertainties in the fitting process.

Using the reduced chi-square value, a standard error of the weighted mean (variance weights, scale corrected) using

$$\hat{\sigma}_{\bar{\epsilon}}^2 = \sigma_{\bar{\epsilon}}^2 \chi_v^2 \tag{5.9}$$

is obtained.

The propagation of uncertainties by the pressure shift and by the air-broadening parameter is not included in the minimisation process. For absorption lines that originate inside the cell, the contribution is negligible ($\sim 1.5 \cdot 10^{-6}\,\mathrm{cm}^{-1}$) due to the low pressure. For calibration using absorption lines of H_2O from the laboratory air path, used for spectrum *BN/1GBq*, the uncertainties have been taken into account by introducing an additional systematic uncertainty of $3.0 \cdot 10^{-4}\,\mathrm{cm}^{-1}$ that takes into account the pressure shift of this atmospheric signature.

For a correct attribution of the calibration uncertainty, the uncertainty of the reference lines of the HITRAN database must also be taken into account. Those are provided from the database as ranges. The lines used are therefore usually provided with an uncertainty range from $1 \cdot 10^{-3}$ to $1 \cdot 10^{-4}\,\mathrm{cm}^{-1}$ or from $1 \cdot 10^{-4}$ to $1 \cdot 10^{-5}\,\mathrm{cm}^{-1}$. Discriminating contributions from less accurate lines, therefore, benefit the overall calibration uncertainty and are taken into consideration when choosing the reference lines. The reference uncertainty is determined by the mean of the stated uncertainty ranges, for example $5 \cdot 10^{-5}\,\mathrm{cm}^{-1}$ for lines with an uncertainty range of $1 \cdot 10^{-4}$ to $1 \cdot 10^{-5}\,\mathrm{cm}^{-1}$. It should be noted that some calibrations are based on the older HITRAN2016 [Gor17] database instead of the updated HITRAN2020[Gor22], which came only recently available.

Both sources of uncertainties from the calibration, from the fitting process and from the accuracy of the reference lines are treated independently, as a statistical and a systematic source. Thus, the total uncertainty for the calibration $\sigma_{cal.}$ is given by

$$\sigma_{\mathrm{cal.}} = \sigma_{\mathrm{HITRAN}} + \hat{\sigma}_{\bar{\epsilon}}. \tag{5.10}$$

The final value must be added to the individual uncertainty of an assigned tritiated water line position.

5.4.2.2 Overview of calibration procedures

> The here presented calibration procedures have been used as presented for the calibration of the tritiated water data published in [Rei20; Her21; Her22; Her23]. The resulting uncertainties from these processes have been reanalyzed for a consistent methodology.

An overview of the calibration procedures is provided in Table 5.5. For four different spectra, six calibrations have been performed using lines of CO_2, H_2O, HDO and N_2O. The calibration procedures provide an additional uncertainty to the assigned lines from $7 \cdot 10^{-5}$

Table 5.5: Overview of the calibration procedures used in this work. Besides the calibrated spectrum and spectral range, the molecule used as reference, the amount of lines and the composition of the uncertainty from the calibration process is listed.

Spectrum	Spec. range in cm^{-1}	Calibration molecule	Number of lines	Uncertainty in cm^{-1}		
				Fit	HITRAN	Total
BCc/1GBq	2450-2950	N_2O	64	$3 \cdot 10^{-5}$	$5 \cdot 10^{-4}$	$5.3 \cdot 10^{-4}$
BM/1GBq	4300-4700	CO_2	20	$2 \cdot 10^{-5}$	$5 \cdot 10^{-5}$	$7 \cdot 10^{-5}$
BM/1GBq	4715-5300	CO_2	21	$4 \cdot 10^{-5}$	$5 \cdot 10^{-4}$	$5.4 \cdot 10^{-4}$
BN/1GBq	5830-6440	H_2O	15	$4.0 \cdot 10^{-4}$	$5 \cdot 10^{-5}$	$4.5 \cdot 10^{-4}$
BM/10GBq	4300-4700	HDO	25	$1.1 \cdot 10^{-4}$	$5 \cdot 10^{-5}$	$1.6 \cdot 10^{-4}$
BM/10GBq	4780-5180	CO_2	20	$3 \cdot 10^{-6}$	$5 \cdot 10^{-4}$	$5 \cdot 10^{-4}$

to $5.4 \cdot 10^{-4}\,cm^{-1}$, where in most cases the uncertainty resulting from the accuracy of the reference lines is the limiting factor.

For the spectra *BM/1GBq* and *BM/10GBq* two different calibrations are performed. As calibration factors may vary within a spectrum and lines in different ranges of the spectra, calibrations in proximity of the assigned tritiated lines were performed.

An analysis of possible changes of the calibration factor has been performed in the framework of a consistency check at the subject of the *BM/1GBq* spectrum.

5.4.2.3 Validation of the calibration procedure

In this study 3 different aspects of consistency are investigated to validate the calibration procedure. These aspects are related to key questions:

1. **Consistency within a species:** Are the obtained calibration factors for a reference molecule agreeing with the stated uncertainties?

2. **Consistency between different molecules:** Are the values obtained using different molecules as reference consistent with each other?

3. **Consistency within the spectrum:** Are the values obtained in different ranges of a spectrum consistent?

To answer these questions, two different ranges in the spectrum *BM/1GBq* were analysed. In the spectral range of 4000 to $4270\,cm^{-1}$, 57 lines of H_2O and 19 lines of HDO were fitted to obtain a value of the calibration factor ϵ. In the range from 4830 to $5160\,cm^{-1}$ 70 lines of CO_2, 7 lines of H_2O and 19 lines of HDO have been fitted. For all lines, the absorption feature originating from inside the cell was used.

For the uncertainty of the individual values, the uncertainty from the reference lines from HITRAN database, σ_{HITRAN}, are converted to equivalent of ϵ using

$$\sigma_{\epsilon,\text{HITRAN}} = \frac{\sigma_{\text{HITRAN}}}{\nu_{meas.}} \tag{5.11}$$

and combined with the uncertainty from the fit (σ_ϵ). This way, the obtained calibration values can be compared and set into relation by taking into account all uncertainties.

In Figure 5.11, the calibration factors obtained ϵ (cf. Equation 5.4) are plotted in the lower plot with the combined uncertainty of the fit σ_ϵ and of the reference line, $\sigma_{\epsilon,\text{HITRAN}}$, for the position of the reference line. The uncertainty of the fit is for all lines of the same order, showing that for most lines the uncertainty of the reference line (σ_{HITRAN}) is the dominant source of uncertainty.

Calibration factors agree very well within a species. This confirms the general suitability of the applied method. Furthermore, some interesting observations can be made when analysing the distribution of calibration factors within a species: Only a very narrow spread is observed for CO_2. The calibration factors for HDO spread the most among the evaluated species, probably originating from a comparable low SNR and, therefore, were obtained with the highest fit uncertainty. Also, for H_2O some lines of low SNR deviate notably from the mean.

Comparing the values of the calibration factor of different species, one can note that they agree on a level much narrower than expected from the stated total uncertainties. The differences between molecules are smaller than $< 1 \cdot 10^{-7}$ while most uncertainties are of the order of $5 \cdot 10^{-7}$. Considering that the large error bars in the figure originate from the uncertainty of the reference lines themselves, it can be inferred that some uncertainties of HITRAN are overestimated.

The comparison between the two spectral ranges reveals agreement of the values. A slight change of order of $1 \cdot 10^{-7}$ is observed in the analysis range, which is, however, covered by the combined uncertainty.

In conclusion, the values obtained for the calibration factor for different reference molecules in different ranges are very consistent with each other, validating the correctness of the procedure.

It is shown that only one calibration of a spectrum is necessary. This could benefit the lines from the *BM/1GBq* and *BM/10GBq* spectra (cf. Table 5.5) as the calibration with smaller uncertainty can be used for both. As the uncertainty of the calibration is mostly governed by the accuracy of the reference lines used, this study suggests the utilisation of only lines with high accuracy stated from all over the analysed spectrum to define the calibration factor.

In addition, by including several molecules and several references (lines from different experiments), one can argue about the necessity of adding the uncertainty of HITRAN lines to the calibration uncertainty. By applying a weighted mean for the calibration factor,
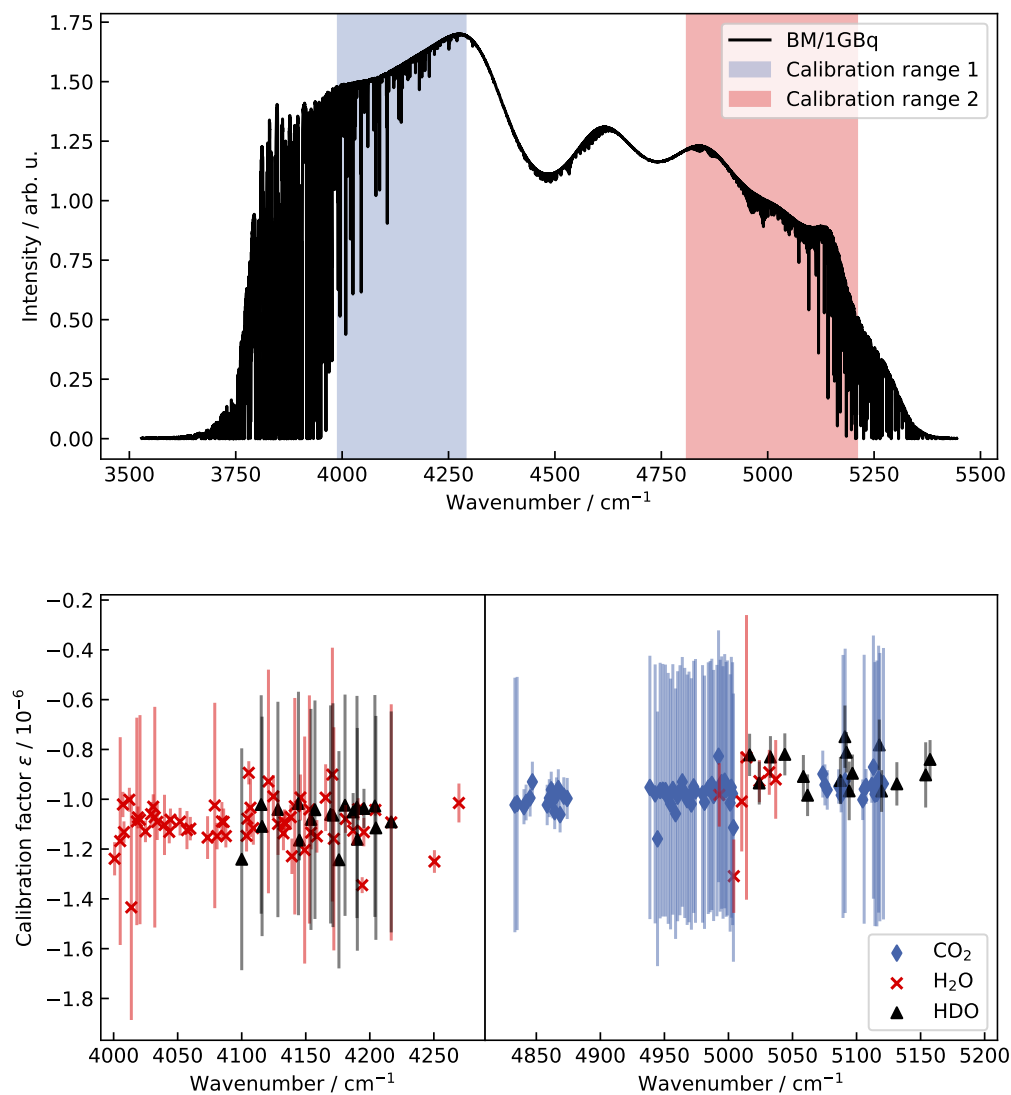
Figure 5.11: Consistency study of calibration factors. In two different ranges (Calibration range 1 & 2) of the *BM/1GBq* spectrum, lines of CO_2, H_2O and HDO have been compared with the HITRAN database. The calibration factors ϵ obtained (cf. Equation 5.4) are plotted in the lower figure with the combined uncertainty of the reference line from fit and HITRAN.

using both the fit and HITRAN uncertainties as weights, and calculating the weighted standard deviation corrected for the reduced chi-square, a reliable value can be determined. It should be noted that this argumentation is only valid if the references are obtained independently.

Implementing these findings, the calibration for the spectra *BM/1GBq* and *BM/10GBq* are revised and optimised:

For the *BM/1GBq* spectrum, all 169 lines analysed have been included, covering with HDO, H_2O and CO_2 three different species and numerous references. The new calibration value is obtained from the weighted mean and is used to recalibrate the data sets obtained from this spectrum. The changes for the line positions are on a much smaller scale than the given uncertainty. The standard error of the weighted mean of the calibration factor is stated as $3.0 \cdot 10^{-5}\,\mathrm{cm}^{-1}$. An additional contribution from uncertainty from the HITRAN database is not needed for this calibration, as a large number of references are used.

For *BM/10GBq*, the data set of the lines compared to HITRAN reference lines does not cover enough references to neglect the additional contribution to the uncertainty of the calibration process. However, as it was shown that calibration factors obtained within a spectrum are valid for the total spectrum, the calibration with the smaller uncertainty can be used for both analysed spectral ranges. This means that the calibration factor of the $4300 - 4700\,\mathrm{cm}^{-1}$ range with the total uncertainty of $1.6 \cdot 10^{-4}\,\mathrm{cm}^{-1}$ is now used for the range of $4780 - 5180\,\mathrm{cm}^{-1}$, too.

5.4.3 Monte-Carlo study of the fit accuracy

> This Monte-Carlo study was performed with Marcel Gaisdörfer in the framework of his bachelor's thesis [Gai22].

The assignment process, in order to obtain spectroscopic properties of tritiated water species and their individual uncertainties, is based on a fitting process of a synthetic FTIR spectrum to the actual spectrum. The valuable output, line position and line intensity, is provided with uncertainties by the algorithm. Although the *Minuit* algorithm has been proven to provide true values at, e.g., CERN experiments for several decades now [Jam75; col20], a validation of the output quality, the correctness of values with regard to the provided uncertainties, must be performed as potential error in the implementation into the software can cause false output.

For this reason a Monte Carlo study has been performed. Three key questions have been identified:

1. **Is the claimed precision of the determined line positions ensured?** Can the true value and uncertainty of line parameters from simulated spectra be reconstructed? Is the determination of position and uncertainty affected by, e.g., strong line mixing?

2. **Is the claimed precision of the measured line intensities ensured?** To what extent does the sample pressure as a fitting parameter affect the correctness of the line intensity determined?

3. **What is the optimal method for implementing the reference spectrum?** For the implementation of the reference spectrum, two approaches are possible: division and subtraction. Which approach provides more accurate and/or true results?

5.4.3.1 Concept of procedure

For the procedure, 5 water lines in the *BM/10GBq* spectrum are selected. Spectrum slices with $\pm 0.5 \, \text{cm}^{-1}$ around these water lines are taken and manipulated using the synthetic spectrum tool from the line fit software. An artificial line with an intensity significantly lower than the line resulting from atmospheric water is added to the spectrum in such a manner that it is strongly mixed.

By generating these strongly mixing lines, the fitting problem becomes rather elaborate, which allows testing more extreme congestion cases. Also, the implementation of the reference spectrum can be tested as it is estimated to benefit in such cases.

The position and intensity of this artificial line is saved and blinded for the duration of the study.

In Figure 5.12, one of the water lines used mixed with an artificial line is presented. A fit was performed that determined the values for the line position, line intensity, and pressure, which, as mentioned in the general assignment procedure, is set as a free parameter to better mimic the line shape. All values are provided with uncertainties.

For the implementation of the reference spectrum two approaches are tested: (i) subtraction of the reference spectrum from the tritiated water spectrum and (ii) division of the water spectrum with the reference spectrum. For both approaches, this is performed for the 5 individual water lines. During first tests it was noted that for both approaches a total discrimination of the water line from atmospheric absorption cannot be achieved. For that reason, fits with and without simulation of the atmospheric contribution were performed for both approaches. For the fits taking the atmospheric contribution into account, the code had to be adapted allowing 'negative' absorption features as atmospheric contribution is stronger in the reference spectrum.

5.4.3.2 Validation of the line fit parameters

An overview of the obtained parameters for the five lines is presented in Table 5.6. The differences of line positions $\Delta_{Pos.}$, are obtained by subtracting the position of the fit from the true value, the uncertainty is provided by the fit $\sigma_{\Delta_{Pos.}}$. The relative line intensities I_{fit}/I_0 are taken from the fit. It should be noted that the expected value for the relative line intensity is not necessarily unity. This is because an empirical scaling value is used,
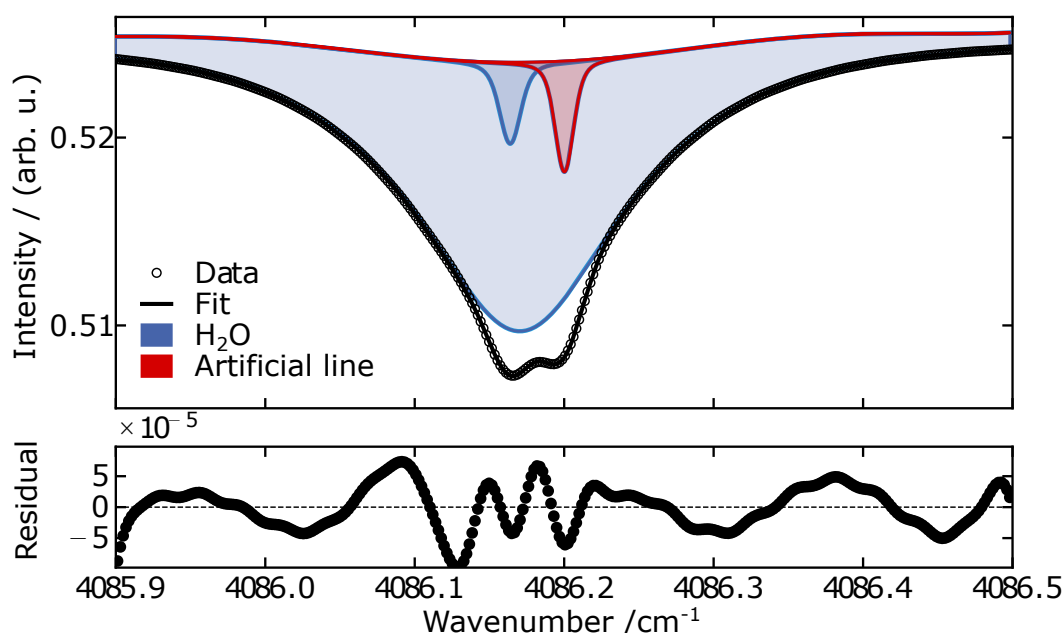
Figure 5.12: A spectrum slice of a water line mixing with an artificial line. The manipulation of the spectrum was performed prior to the fitting procedure. The actual position was blinded till the evaluation of the Monte-Carlo study. Note that the water line has a contribution from the atmosphere (broad line) and from the sample (narrow line).

that is not needed to be accurate. However, the value is expected to be same for all 5 lines. The uncertainty given from the fit is referring to the relative intensity value. The pressure value is also directly taken from the fit. Uncertainties are not included here but are of same order as the values.

For position and intensity, a reduced chi-square value, χ^2_ν, is determined summarising the quality of the uncertainties with respect to the actual deviation.

All positional deviations are smaller than the uncertainty values returned, leading to a chi-square value of 0.33. This shows that even for strong line mixing, the stated uncertainties are rather over- than underestimated and with $1 \cdot 10^{-3} - 1 \cdot 10^{-4}\,\mathrm{cm}^{-1}$ found with high accuracy. As this study only covers a small sample size no statement of a general overestimation of the uncertainty can be given.

The line intensities, however, deviate much more from a mean value than expected from the stated uncertainties. Consequently, the chi-square value is with 80 indicating an underestimation of the uncertainties.

As mentioned in section 5.4.1, the pressure is set as a free parameter to better mimic the line shape. The correlation of pressure and line intensity is not implemented for

Table 5.6: Differences of fit parameters to the actual value and their uncertainties from all 5 manipulated spectra slices from the Monte Carlo study. $\Delta_{Pos.}$ is the difference of the position (set - fit), I_{fit}/I_0 is the relative line intensity. The reduced chi-square value summarizes the consistency of the deviations and the uncertainties.

No.	$\Delta_{Pos.}$ in cm^{-1}	$\sigma_{\Delta_{Pos.}}$ in cm^{-1}	I_{fit}/I_0	$\sigma_{Int.}$	Pressure in mbar
1	$-1.6 \cdot 10^{-4}$	$2.2 \cdot 10^{-4}$	$8.17 \cdot 10^{-1}$	$3.0 \cdot 10^{-2}$	24.6
2	$1.7 \cdot 10^{-4}$	$2.7 \cdot 10^{-4}$	$8.70 \cdot 10^{-1}$	$4.6 \cdot 10^{-2}$	11.3
3	$1.9 \cdot 10^{-4}$	$5.9 \cdot 10^{-4}$	$4.50 \cdot 10^{-1}$	$5.6 \cdot 10^{-2}$	20.0
4	$-4.1 \cdot 10^{-4}$	$1.1 \cdot 10^{-3}$	$1.17 \cdot 10^{-1}$	$2.4 \cdot 10^{-2}$	11.5
5	$-4.7 \cdot 10^{-4}$	$1.1 \cdot 10^{-3}$	$2.50 \cdot 10^{-1}$	$5.9 \cdot 10^{-2}$	72.5
χ_ν^2	0.33		80		

the uncertainties provided by the fit, which might be the origin of the underestimated uncertainties for the line intensities.

Consequently, in this configuration, the uncertainties for the line intensity cannot be used as reliable values.

5.4.3.3 Implementation of the reference spectrum

For the implementation of the reference spectrum two approaches have been identified: (i) the subtraction of the reference spectrum from the actual one, in the following referred as 'Subtraction Method', and (ii) the division of the actual spectrum by the reference spectrum, further referred as 'Division Method'. Both approaches are performed using the 5 individual slices. In addition, as a total correction for the water line from atmospheric absorption cannot be achieved for either approach, fits with and without simulation of the atmospheric contribution are performed. Thus, with the fit of the pure spectrum and the Subtraction/Division with and without fitting atmospheric contribution, in total 5 methods are tested.

In the following, the 'Subtraction / Division Method 1' refers to the method only including the artificial line. The Subtraction and Division Method where the atmospheric water line is included in the simulation and fit is attributed as 'Method 2'. An example of Subtraction Method 1 (subtraction of the reference spectrum only including the artificial line) is shown in Figure 5.13. In this figure, a 'negative' broad absorption feature can be noted. This means that the atmospheric water line is more intense in the reference spectrum, leading to an overcorrection of the atmospheric contribution. A comparable feature can be found for the Division Method.

In Table 5.7, the fit parameters obtained with uncertainties of the five manipulated spectra slices with an artificial line are presented. All approaches including the reference spectrum,
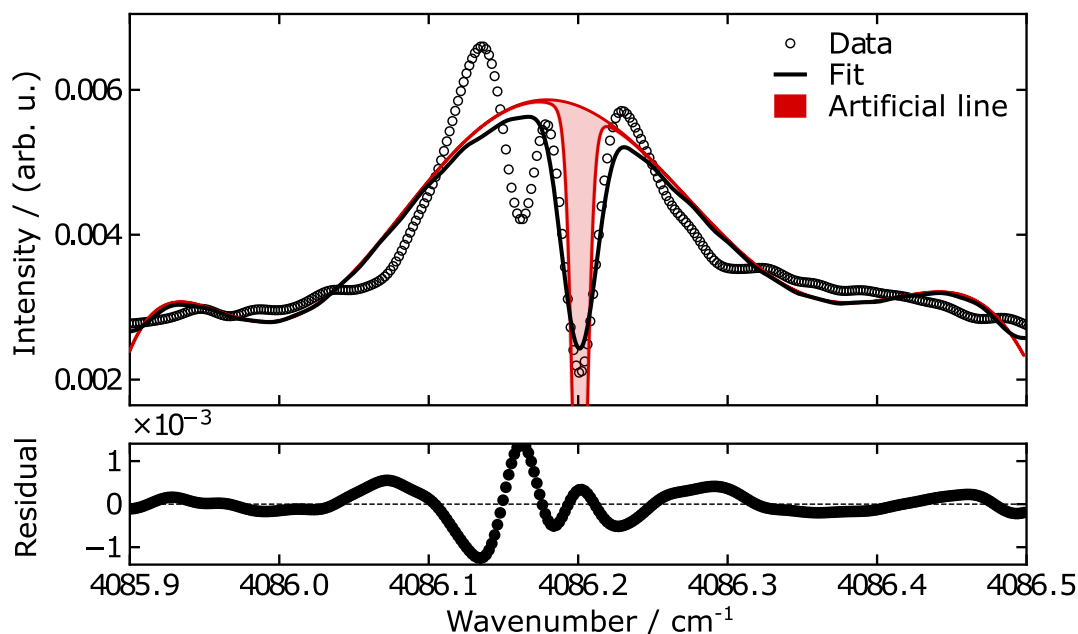
Figure 5.13: Example for the Subtraction Method 1. The reference spectrum is subtracted from the manipulated tritiated water spectrum with the artificial line. The line shape of the artificial line is visualized before the convolution with the baseline profile.

subtraction and division, with and without consideration of the 'negative' absorption feature, do not provide reliable results. The deviations are in most cases larger than the stated uncertainties, reflected for all four methods by reduced chi-square values of larger than 4.

A plausible explanation is that the slight difference in the abundance of atmospheric water during the acquisition of the spectra leads to a mismatch of the line intensities. This creates the 'negative' absorption feature after subtraction / division which is adding a slope to the artificial line. The effect of this slope might not be treated correctly by the software for Methods 1 and 2. An indication for this is given in the Division Method, where the 'negative' feature is more dominant, leading to worse results.

In summary, it can also be noted that the uncertainties provided for all methods are comparable to those of the fit of the pure spectrum. On the one hand, this proves that the software is dealing very efficiently with strong line mixing. On the other hand, the estimated improvement of the implementation of a reference spectrum could not be validated. For this reason, for the evaluation of the *BM/10GBq* spectrum, the reference spectrum is not included.

Table 5.7: The obtained fit parameters with uncertainties from all 5 manipulated spectra slices with artificial line. For the Subtraction Method 1 and Division Method 1 only includes the artificial line. For the Subtraction Method 2 and Division Method 2 the atmospheric water line is included in the simulation and fit of the spectrum.

No.	Pure spectrum $\Delta_{Pos.}$ in cm^{-1}	$\sigma_{\Delta_{Pos.}}$	Subtraction Meth. 1 $\Delta_{Pos.}$ in cm^{-1}	$\sigma_{\Delta_{Pos.}}$	Subtraction Meth. 2 $\Delta_{Pos.}$ in cm^{-1}	$\sigma_{\Delta_{Pos.}}$	Division Meth. 1 $\Delta_{Pos.}$ in cm^{-1}	$\sigma_{\Delta_{Pos.}}$	Division Meth. 2 $\Delta_{Pos.}$ in cm^{-1}	$\sigma_{\Delta_{Pos.}}$
1	$-1.6\cdot10^{-4}$	$2.2\cdot10^{-4}$	$-7.0\cdot10^{-5}$	$2.4\cdot10^{-4}$	$-8.4\cdot10^{-4}$	$2.4\cdot10^{-4}$	$-2.8\cdot10^{-5}$	$1.2\cdot10^{-4}$	$-2.4\cdot10^{-4}$	$1.2\cdot10^{-4}$
2	$1.7\cdot10^{-4}$	$2.7\cdot10^{-4}$	$1.1\cdot10^{-3}$	$4.0\cdot10^{-4}$	$1.2\cdot10^{-3}$	$4.3\cdot10^{-4}$	$1.9\cdot10^{-3}$	$2.0\cdot10^{-4}$	$1.4\cdot10^{-3}$	$2.1\cdot10^{-4}$
3	$1.9\cdot10^{-4}$	$5.9\cdot10^{-4}$	$-1.7\cdot10^{-3}$	$6.0\cdot10^{-4}$	$-2.2\cdot10^{-3}$	$6.3\cdot10^{-4}$	$-1.8\cdot10^{-3}$	$3.1\cdot10^{-4}$	$7.8\cdot10^{-4}$	$2.9\cdot10^{-4}$
4	$-4.1\cdot10^{-4}$	$1.1\cdot10^{-3}$	$-3.7\cdot10^{-4}$	$1.1\cdot10^{-3}$	$8.0\cdot10^{-6}$	$1.2\cdot10^{-3}$	$-1.8\cdot10^{-4}$	$5.8\cdot10^{-4}$	$-3.1\cdot10^{-4}$	$5.9\cdot10^{-4}$
5	$-4.7\cdot10^{-4}$	$1.1\cdot10^{-3}$	$-1.1\cdot10^{-3}$	$1.4\cdot10^{-3}$	$-1.0\cdot10^{-3}$	$1.5\cdot10^{-3}$	$-1.1\cdot10^{-3}$	$7.7\cdot10^{-4}$	$-1.8\cdot10^{-4}$	$1.1\cdot10^{-3}$
χ^2_ν	0.33		4.2		8		32.5		14.6	

5.4.4 Composition of the samples

An important property of the sample is its composition. Taking into account the composition of the sample, the abundance ratios of target molecules in the sample, and the presence of side products, gives important insights into the efficiency of production processes or hints of unknown or not considered processes. Thus, an analysis of the composition is mandatory to improve the efficiency of sample productions.

5.4.4.1 Concept of the determination of the composition

Spectroscopy is a technique that is widely used in application to analyse gas compositions. FTIR spectroscopy also allows for a non-destructive determination of compositions if desired. The disadvantage of this method is that only compounds that interact sufficiently with the light source are determined.

The determination of compositions is usually made by comparison of the line intensities of species present in the spectrum with calibrated references. In this way, accurate measurement of the compositions of the samples is possible.

For the samples used in this work, such a reference is not available. A measurement with a replica of the optical sample filled with a determined amount of a calibrated gas mixture, favourably consisting of several species also present in the tritiated water sample, would be necessary for robust determination of the sample composition. This opportunity has been missed by implementing the reference cell mentioned in Section 5.2.3.1.

However, using the spectra given, an estimation of the composition can be obtained. The base of the estimation is the empirical scaling factor of the line intensities. This empirical scaling factor is an adaption of the line intensity of the databases to the measured ones from the spectrum after correction for natural abundance[2]. The composition is extracted by taking the weight of a scaling factor s_i of a species (IR active) i in the sum of all scaling factors. The estimated concentration c_a of a species a is therefore given with

$$c_a = \frac{s_a}{\sum_i s_i}. \tag{5.12}$$

As the Monte-Carlo study in the previous section pointed out, the line intensities can only be obtained accurately to some extent. The uncertainty of this procedure has been conservatively estimated with 20% of the stated values, which are therefore only recommended for qualitative discussion.

Also, it should be noted that this method only takes into account IR active species with absorption features in the measured range. Potential species that cannot be measured by this method are molecular hydrogen (isotopologues), nitrogen, oxygen (relevant due to the self-radiolysis of tritium [Pen24]), or ^{3}He, tritium's decay product.

---

[2]Line intensities in *SPECTRA* and HITRAN database take the natural abundance into account. This may vary for other databases.
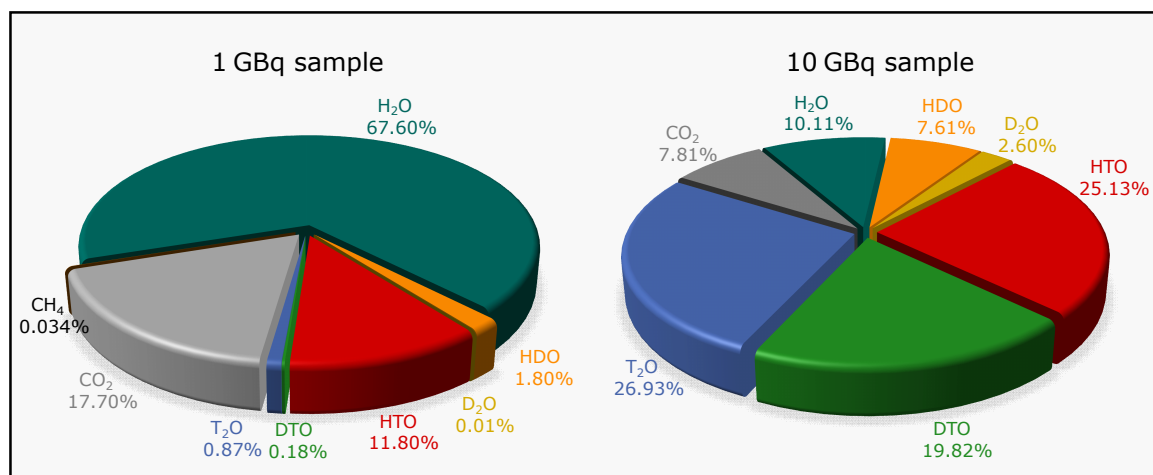
Figure 5.14: Composition of the $1\,\mathrm{GBq}$ **and** $10\,\mathrm{GBq}$ **activity tritiated water samples.** It should be noted that only IR active molecules with known spectra and detectable SNR can be included. The sample may contain unknown amounts of nitrogen and tritiated methane variations that will shift the relative quantities.

5.4.4.2 Composition of the $1\,\mathrm{GBq}$ sample

The optical sample containing the $1\,\mathrm{GBq}$ activity of tritiated water was developed and constructed with the central objective to measure $\mathrm{T}_2^{16}\mathrm{O}$. To enhance the conversion rate to the desired isotopologue, a series of procedures have been implemented to discriminate residuals in the cell, particularly water and copper(II) hydroxide, $\mathrm{Cu(OH)}_2$, both of which sources for protium.

The analysis of the composition of the $1\,\mathrm{GBq}$ sample, presented in the pie chart on the left of Figure 5.14, reveals that the primary target $\mathrm{T}_2\mathrm{O}$ constitutes only approximately $\sim 7\%$ of the tritiated isotopologues. The predominant tritiated species is HTO, accounting for approximately $\sim 92\%$. Remarkably, also DTO is detectable with $\sim 1\%$ of the tritiated species. The deuterium is probably originating from residuals in and/or on the walls from a proof-of-principle test of the oxidation segment prior to the filling procedure.

The composition of the sample also reveals that the tritiated species only cover $\sim 12\%$ of the IR-active content. Note that tritiated methane species, likely as the presence of methane in the cell was measured, can not be evaluated to date in this work because they are not covered by databases.

The high presence of $\mathrm{H}_2\mathrm{O}$ in the cell can be attributed to the valve seat leak that occurred between the preparation and the filling process. However, the origin of methane and CO_2 remains not unambiguously clarified. The potential explanation is a heat- and/or radiation-induced dissociation of hydrocarbons that have persisted from the production process of the components. An additional explanation is found in [Mat91], where the photodesorption of these molecules was observed for different materials in vacuum chambers.

From the line fit tool, an estimation for the sample pressure of 50 to $100\,\mathrm{mbar}$ is given. This pressure is much higher as expected from the filled gas amount proving the seat valve leakage.

5.4.4.3 Composition of the $10\,\mathrm{GBq}$ sample

The composition of this sample is presented in the pie chart on the right side of Figure 5.14. Compared to the previous sample, significantly higher purity was achieved with a relative quantity of tritiated water species of $\sim 72\%$. The tritiated water species subdivide into 37.4% T_2O, 27.6% DTO, and 35% HTO. The predominant non-tritiated species is with 10.1% H_2O.

Several measures and procedures have been included to minimise the amount of protium. A significantly reduced relative amount of H_2O and HTO is observed, but was not completely vanished. The presence of protium (containing species) is expected because the removal of water films and hydrogen in steel components is known to require a great deal of effort and time.

In addition, the presence of CO_2 is reduced compared to the first sample and methane is even not distinguishable from the contribution of the ambient atmosphere. This observation may hint that, either, the measures to remove hydrocarbons from the components were successful and the origin is indeed based on those; or the high presence in the first sample may originate from the valve seat leakage.

Compared to the first sample, the SNR for T_2O has been increased by a factor 50, for DTO by a factor of 174, and for HTO by a factor of 3.

From the line fit tool, an estimate is given for the sample pressure of 25 to $50\,\mathrm{mbar}$ that is in agreement with the loading pressure of $34.4\,\mathrm{mbar}$.

In conclusion, analysis of the composition of the $10\,\mathrm{GBq}$ sample shows a significant improvement in the purity of the sample, reducing the abundance of protium, as well as CO_2 and methane. An approximately equal composition of tritiated water species could be achieved with a significantly higher overall SNR for T_2O and DTO.

Table 5.8: Overview of the number of assigned lines of each of the HTO bands. The numbers are subdivided for the positional uncertainty obtained from the fit. The uncertainty from calibration procedure is not included.

Fit uncertainty in cm^{-1}	Vibrational band					
	$\nu_2 + \nu_3$	$\nu_1 + 2\nu_2$	$\nu_1 + \nu_3$	$2\nu_2 + \nu_3$	$2\nu_1$ (1 GBq)	$2\nu_1$ (10 GBq)
$10^{-4} > \sigma > 10^{-5}$	80				49	18
$10^{-3} > \sigma > 10^{-4}$	288	140	59	16	162	161
$10^{-2} > \sigma > 10^{-3}$	220	281	103	31	143	239
$\sigma > 10^{-2}$	23		25	4	6	16
Total	611	446	165	81	361	454

5.5 Determined ro-vibrational transitions of tritiated water isotopologues

The data presented in this section are published in [Rei20; Her21; Her22; Her23].

In this section, a summary of the data sets of the assigned tritiated water lines is presented. General information about the data sets will be presented including the number of lines, range of fit uncertainty for the line positions, and range of the transition quantum numbers.

The calibration of the used spectra is described in Section 5.4.2. The validation of the data sets is presented in Section 5.6.

5.5.1 Vibrational bands of the HT^{16}O species

Five vibrational bands of HTO were investigated in the frame of this work with a total number of 2001 assigned lines. 1654 individual ro-vibrational transitions were determined for the first time with high accuracy.

The $\nu_2 + \nu_3$ and $\nu_1 + 2\nu_2$ bands and the $\nu_1 + \nu_3$ and $2\nu_2 + \nu_3$ bands were assigned from the same spectrum jointly. These pairs of bands are partially overlapping and are therefore presented as doublets.

The $2\nu_1$ band was analysed twice using two different spectra, from the 1 GBq activity sample and from the 10 GBq activity sample.

In the following the two band doublets and the two analysis of the $2\nu_1$ band are presented. A summary of the number of lines assigned subdivided for fit accuracy is provided in Table 5.8.

The line lists obtained for the HTO species are presented in the Appendix A.2.1.
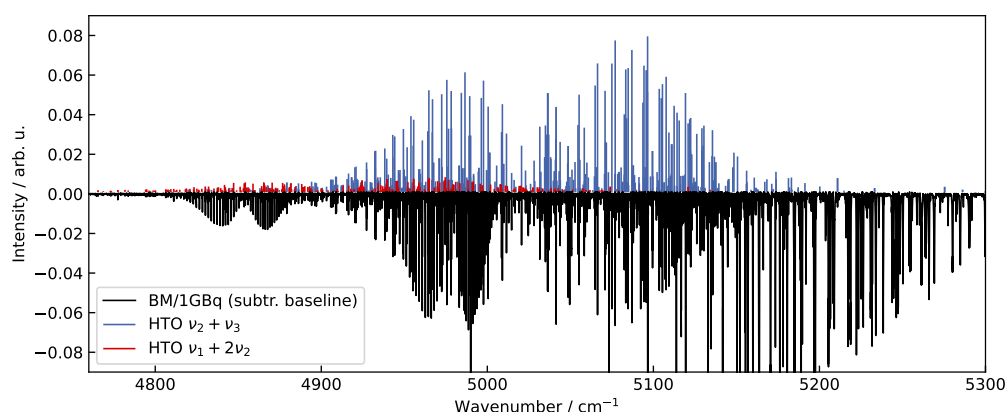
Figure 5.15: The assigned spectral lines of the $\nu_2 + \nu_3$ and $\nu_1 + 2\nu_2$ band. For visualisation, the assigned lines are reversed and presented on top of the analysed spectrum *BM/1GBq*. The spectrum is corrected for the baseline.

5.5.1.1 The $\nu_2 + \nu_3$ and $\nu_1 + 2\nu_2$ band

The assignment of these bands was performed with Marcel Kamrad in the framework of his Bachelor's thesis [Kam21] and published in [Her21].

In the range from 4715 to $5300\,\mathrm{cm}^{-1}$, 446 new experimental line positions assigned to the $\nu_1 + 2\nu_2$ and 611 new line positions belonging to the $\nu_2 + \nu_3$ band are reported.

The 1057 lines cover rotational quantum numbers up to $J = 15$ and $K_a = 7$.

Each line is presented with an individual statistical uncertainty from the fitting procedure in the range of $2.5 \cdot 10^{-5}\,\mathrm{cm}^{-1}$ to $2.8 \cdot 10^{-1}\,\mathrm{cm}^{-1}$. In Table 5.8, the number of lines is subdivided into categories of accuracy of the fit. In addition to the uncertainties presented, the uncertainty from the calibration procedure must be taken into account with $3.0 \cdot 10^{-5}$ cm^{-1}.

In Figure 5.15, the assigned spectral lines are visualised as reversed absorption peaks on the analysed spectrum *BM/1GBq*. To better compare the lines with the spectrum, the baseline is subtracted from the spectrum using a rolling ball approach.

As visible in the plot, the lines of the $\nu_2 + \nu_3$ achieve a much higher SNR and therefore achieve higher accuracy compared to the $\nu_1 + 2\nu_2$ band. The assigned spectrum is subject to strong water absorption in the higher energetic region, leading to a drop of the intensity to zero. In the spectral range around $4850\,\mathrm{cm}^{-1}$ and $4990\,\mathrm{cm}^{-1}$ strong CO_2 bands are visible in the spectrum overlapping with the assigned band. The high line density leads to numerous line mixings and therefore to a worse fit accuracy.

5.5.1.2 The $\nu_1 + \nu_3$ and $2\nu_2 + \nu_3$ band

In the range of 5830 to $6440\,\mathrm{cm}^{-1}$, 165 experimental line positions were determined for the $\nu_1 + \nu_3$ band and 81 line positions to the $2\nu_2 + \nu_3$ band.

The 244 reported lines cover rotational quantum numbers up to $J = 12$ and $K_a = 5$. Individual statistical uncertainties from the fitting procedure range from $4.7 \cdot 10^{-4}\,\mathrm{cm}^{-1}$ to $5.1 \cdot 10^{-2}\,\mathrm{cm}^{-1}$. An additional systematic uncertainty from the calibration process of $4.5 \cdot 10^{-4}\,\mathrm{cm}^{-1}$ must be taken into account.

In the upper plot of Figure 5.16, the lines assigned to the two vibration bands are visualised as reversed absorbance features on top of the analysed spectrum *BN/1GBq*, corrected for the baseline. A close-up plot, the lower plot in Figure 5.16, shows the higher noise level compared to the *BM/1GBq* spectrum. This leads to an overall lower SNR leading to less assigned lines with higher uncertainties for the line parameters compared to the previous presented HTO bands.

5.5.1.3 The $2\nu_1$ band

> The assignment of the $2\nu_1$ band of HTO from the *BM/1GBq* spectrum was performed together with Johannes Reinking and was published in [Rei20].

For the $2\nu_1$ band of HTO two different spectra, the *BM/1GBq* and *BM/10GBq* were analysed.

From the *BM/1GBq* spectrum, 361 experimental line positions were assigned. The uncertainties of the line positions of this data set range from $4.4 \cdot 10^{-5}\,\mathrm{cm}^{-1}$ to $1.9 \cdot 10^{-2}\,\mathrm{cm}^{-1}$. The additional systematic uncertainty from calibration of $3.0 \cdot 10^{-5}\,\mathrm{cm}^{-1}$ must be added.

From the *BM/10GBq* spectrum, 454 experimental line positions could be assigned. The uncertainties of the line positions range from $6.2 \cdot 10^{-5}\,\mathrm{cm}^{-1}$ to $6.4 \cdot 10^{-2}\,\mathrm{cm}^{-1}$. The additional systematic uncertainty of the calibration is $1.6 \cdot 10^{-4}\,\mathrm{cm}^{-1}$.

In Figure 5.17, both spectra, *BM/1GBq* and *BM/10GBq*, are presented. The obtained lines are visualised as reversed absorption lines on top of the spectrum. The increase in the SNR for HTO in the high-activity sample (bottom) compared to the low-activity sample (top) can be observed by eye. Also, DTO and T_2O lines emerged with higher activity leading to an overall higher line density. This leads to numerous line mixings and generally less accurate lines as noted in Table 5.8.

A more detailed comparison of the datasets, especially the line positions obtained, is performed in Section 5.6 as one of the validation methods implemented.
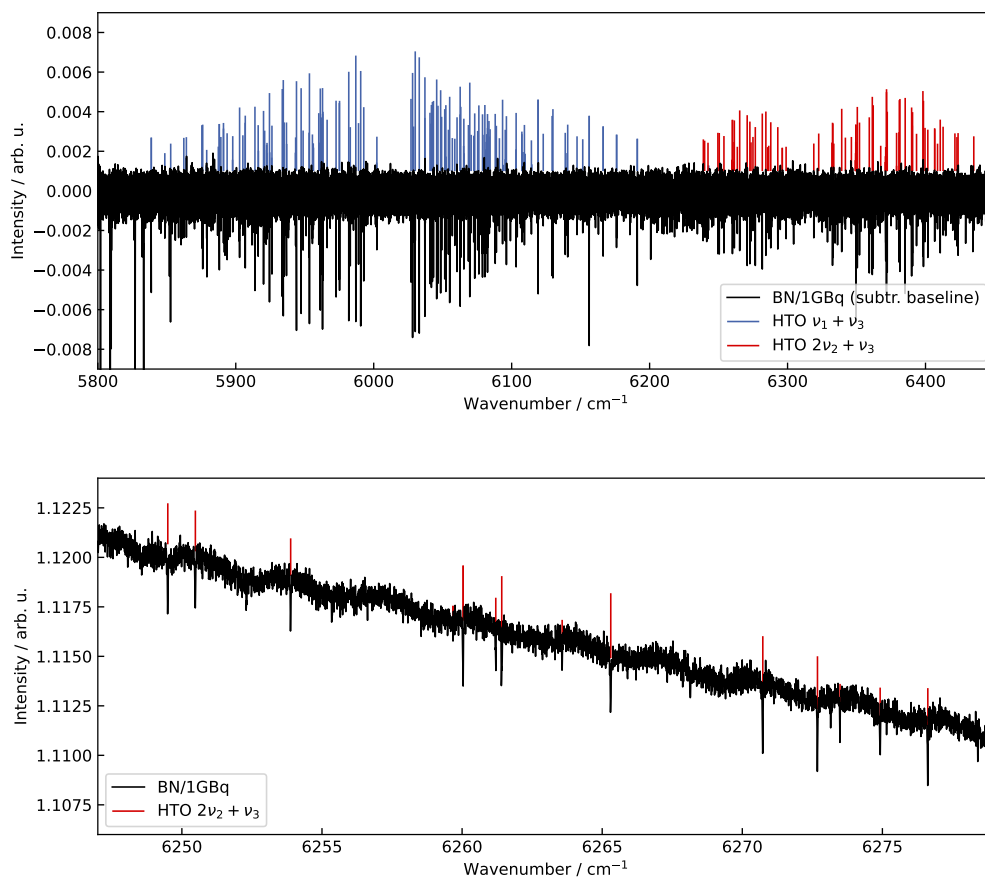
Figure 5.16: The assigned lines from the $\nu_1 + \nu_3$ and $2\nu_2 + \nu_3$ band. Top: The assigned lines from the two vibrational bands, $\nu_1 + \nu_3$ and $2\nu_2 + \nu_3$, are visualized as reversed absorbance features on top of the analysed spectrum *BN/1GBq* corrected for the baseline.
Bottom: A close-up plot from the analysed spectrum shows the high noise level of these spectral data.

5.5.2 Vibrational bands of the DT^{16}O species

In total 1658 lines of the DTO species have been assigned to 5 different vibrational bands. While the concentration of DTO in the first sample was just enough to analyse the fundamental ν_3 band, the high activity sample allowed access to the first overtone and mixing bands with its 173 times higher SNR.

In this section, in addition to the ν_3 band, the $2\nu_1$ and $\nu_1 + 2\nu_2$ bands and the $\nu_1 + \nu_3$ and $2\nu_2 + \nu_3$ bands were assigned. These overlapping band pairs were acquired within the same assignment process and are therefore presented as doublets.

In Table 5.9, an overview of the number of lines assigned to each of the bands is presented. The numbers are subdivided for the fit accuracy of the line positions obtained.
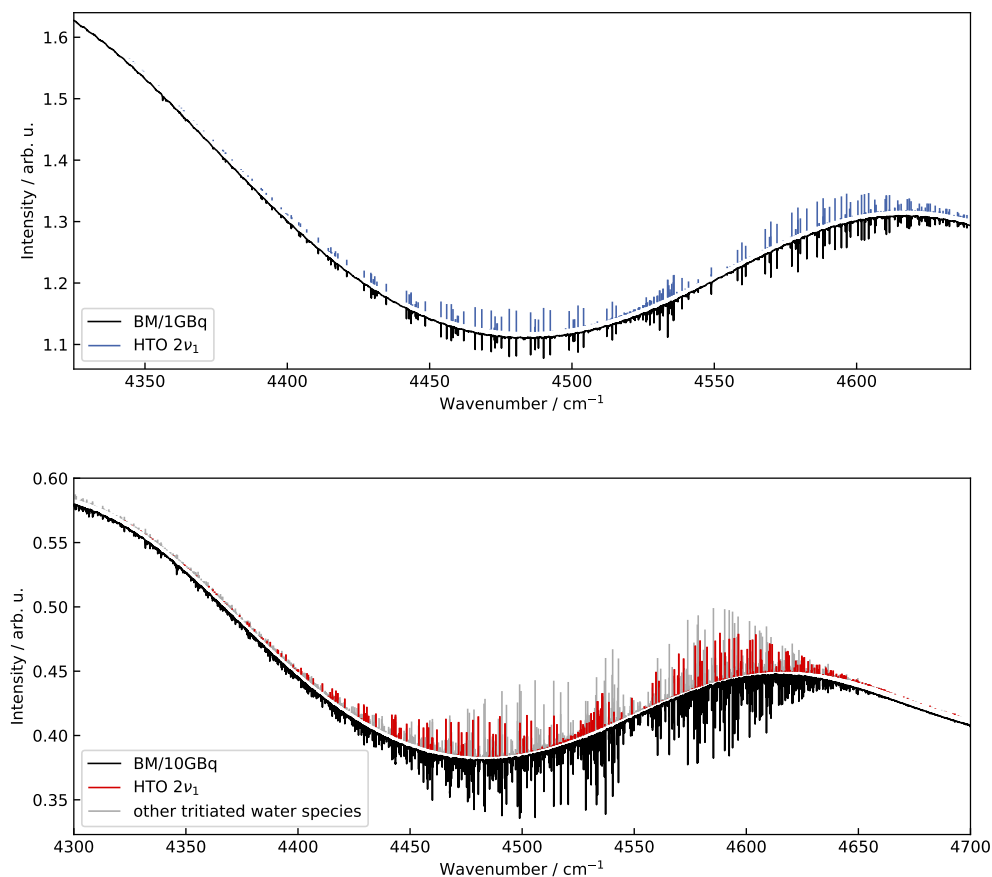
Figure 5.17: Assigned lines of the $2\nu_1$ **band of HTO.** Top: The spectrum *BM/1GBq* and the assigned lines of the $2\nu_1$ band of HTO.
Bottom: The spectrum *BM/10GBq* from the high activity sample and the lines assigned of the $2\nu_1$ band of HTO. In grey assigned lines from other tritiated water species are highlighted.

The line lists obtained for the DTO species are presented in the Appendix A.2.2.

5.5.2.1 The ν_3 band of DT^{16}O

The assignment of the ν_3 band of DTO was performed together with Johannes Reinking published in [Rei20].

In the range from 2570 to $2870\,\text{cm}^{-1}$, a total number of 436 lines were assigned to the fundamental band ν_3 of DTO.

Individual fit uncertainties range from $2.7 \cdot 10^{-4}$ to $2.9 \cdot 10^{-2}\,\text{cm}^{-1}$ with an additional uncertainty from the calibration procedure of $5.3 \cdot 10^{-4}\,\text{cm}^{-1}$.

Table 5.9: Overview of the number of assigned lines of each of the DTO bands. The numbers are subdivided for the positional uncertainty obtained from the fit. The uncertainty from calibration procedure is not included.

Fit uncertainty in cm^{-1}			Vibrational band				
		ν_3	$2\nu_1$	$\nu_1 + 2\nu_2$	$\nu_1 + \nu_3$	$2\nu_2 + \nu_3$
$10^{-3} >$	$\sigma > 10^{-4}$	122	155	36	3	0
$10^{-2} >$	$\sigma > 10^{-3}$	292	135	215	312	141
	$\sigma > 10^{-2}$	22	50	14	7	20
Total		436	440	265	356	161
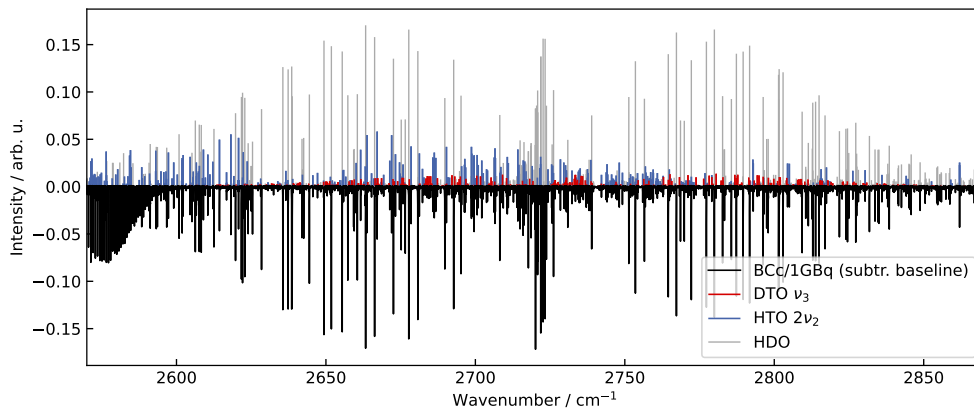
Figure 5.18: The *BCc/1GBq* spectrum with assigned lines of the fundamental band ν_3 of DTO. For visualisation, the assigned lines of the fundamental band ν_3 of DTO (red), the prior to this work assigned $2\nu_2$ [Rei19] (blue), and HDO lines (grey) are presented as reversed peaks. The spectrum is corrected for the baseline.

The SNR of DTO in the analysed *BCc/1GBq* spectrum allowed the assignment of lines with rotational quantum numbers up to $J = 15$ and $K_a = 8$.

In Figure 5.18, the FTIR spectrum with subtracted baseline is presented. The spectrum includes numerous absorption features: In red, blue, and grey, the main contributors to the spectrum, DTO, HTO, and HDO, are highlighted as reversed absorbance lines. It can be noted that the SNR for DTO is the lowest of the named contributing species. This fact, combined with the high density of lines in this spectrum, makes an unambiguous assignment process for DTO challenging. In addition, this affects the acquired accuracy for the line positions of this species.

An assignment of the HTO lines ($2\nu_2$ band) from this spectrum was made prior to this work and was published in [Rei19].
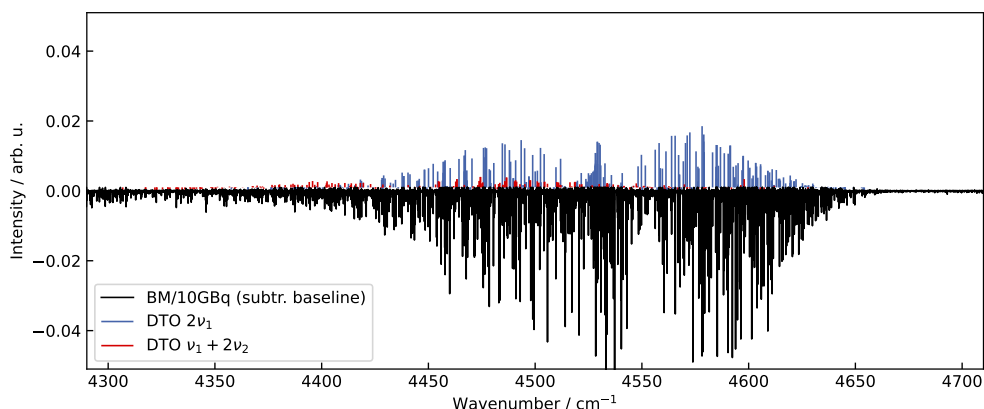
Figure 5.19: Assigned lines of the $2\nu_1$ **and** $\nu_1 + 2\nu_2$ **bands of DTO.** The lines are reversed and presented on top of the analysed spectrum *BM/10GBq*. The spectrum is corrected for the baseline.

5.5.2.2 The $2\nu_1$ and $\nu_1 + 2\nu_2$ band of DT^{16}O

In the range from 4300 to $4700\,\mathrm{cm}^{-1}$, 440 lines were assigned to the $2\nu_1$ band and 265 lines to the $\nu_1 + 2\nu_2$ band obtained from the *BM/10GBq* spectrum. The 705 lines cover rotational quantum numbers up to $J = 18$ and $K_a = 8$.

The positional uncertainty of the fitting process ranges from $1.2 \cdot 10^{-4}$ to $4.6 \cdot 10^{-2}\,\mathrm{cm}^{-1}$ with an additional uncertainty of the calibration procedure of $1.6 \cdot 10^{-4}\,\mathrm{cm}^{-1}$.

In Figure 5.19, the assigned lines are highlighted on top of the analysed FTIR spectrum with subtracted baseline. Naturally, the $\nu_1 + 2\nu_2$ band is less intense than the $2\nu_1$ band.

5.5.2.3 The $\nu_1 + \nu_3$ and $2\nu_2 + \nu_3$ band of DT^{16}O

> The assignment of these bands was performed with Marcel Gaisdörfer in the frame of his Bachelor's thesis [Gai22] and are published in [Her22].

In the higher energetic region of the *BM/10GBq* spectrum, from 4780 to $5180\,\mathrm{cm}^{-1}$, 517 lines have been assigned to the $\nu_1 + \nu_3$ (365 lines) and $2\nu_2 + \nu_3$ (161 lines) bands of DTO.

As visible in Figure 5.20, the line intensities of the assigned DTO signatures are up to an order of magnitude lower than the signatures characterised the spectrum. While species like HTO and CO_2 achieve high SNR (>100), DTO lines rarely exceed a SNR of 10 in this range.

Nonetheless, a substantial number of lines that cover quantum numbers up to $J = 14$ and $K_a = 7$ could be assigned. The positional fit uncertainties are in the range of $1 \cdot 10^{-3}$ to $1 \cdot 10^{-2}\,\mathrm{cm}^{-1}$ for the majority of the lines. The additional uncertainty of $1.6 \cdot 10^{-4}\,\mathrm{cm}^{-1}$ from the calibration must be included.
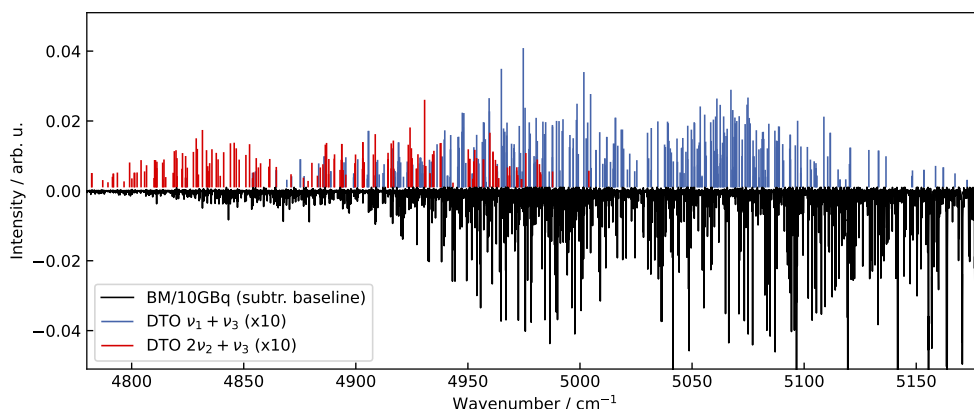
Figure 5.20: Assigned lines of the $\nu_1 + \nu_3$ and $2\nu_2 + \nu_3$ bands of DTO. Lines are reversed and presented on top of the analysed spectrum, *BM/10GBq*, which is subtracted with the baseline. The line intensities are multiplied by 10 for better visualisation.

Table 5.10: Overview of the number of assigned lines of each of the T_2O bands. The numbers are subdivided for the positional uncertainty obtained from the fit. The uncertainty from calibration procedure is not included.

Fit uncertainty in cm^{-1}	Vibrational band			
	$\nu_1 + \nu_3$ (1 GBq)	$\nu_1 + \nu_3$ (10 GBq)	$2\nu_1$	$2\nu_2 + \nu_3$
$10^{-4} > \sigma > 10^{-5}$		39		
$10^{-3} > \sigma > 10^{-4}$	46	243	99	26
$10^{-2} > \sigma > 10^{-3}$	154	303	345	134
$\sigma > 10^{-2}$	6	41	35	12
Total	206	626	479	172

5.5.3 Vibrational bands of the $T_2^{16}O$ species

From the T_2O species, in total 1277 individual lines from 3 different vibrational bands have been assigned for the first time. In addition to this number, there is the $\nu_1 + \nu_3$ band that was assigned from spectra of both samples. An overview of both data sets, originating from the low- and high-activity samples, and the overlap of both data sets is presented.

Overlapping with the $\nu_1 + \nu_3$ band of the 10 GBq activity sample, the $2\nu_1$ and $2\nu_2 + \nu_3$ bands were observed. The results of the assignment process for these three bands are presented in Section 5.5.3.2.

An overview of the lines obtained subdivided for the vibration bands in classes of positional fit accuracy is presented in Table 5.10.

The line lists obtained for the T_2O species are presented in the Appendix A.2.3.
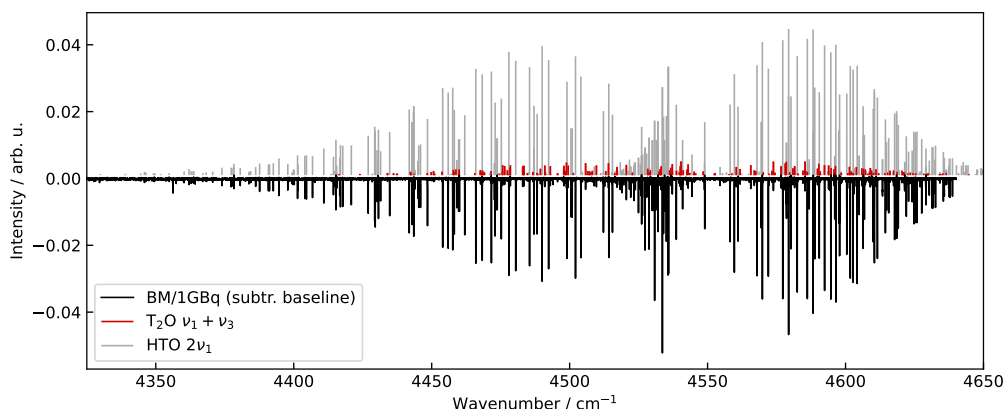
Figure 5.21: The assigned lines of the $\nu_1 + \nu_3$ **band of T$_2$O and the** $2\nu_1$ **band of HTO.** The lines are presented on top of the analysed spectrum *BM/1GBq* with subtracted baseline.

5.5.3.1 The $\nu_1 + \nu_3$ band from the 1 GBq activity sample

> The assignment of this band is performed with Philipp Lingnau in the frame of his Bachelor's thesis [Lin21] and published in [Her22].

The dataset of the $\nu_1 + \nu_3$ band of T$_2$O is obtained from the *BM/1GBq* spectrum of the low-activity sample. It consists of 206 lines from 4410 to $4650\,\text{cm}^{-1}$ with quantum numbers up to $J = 16$ and $K_a = 8$.

In Figure 5.21, the baseline corrected analysed spectrum is presented with the highlighted lines of the HTO $2\nu_1$ and T$_2$O $\nu_1 + \nu_3$ assigned from this spectrum. Despite the dominating HTO lines, presented in light grey in the plot, this large number of highly accurate lines with fit uncertainties of $4.2 \cdot 10^{-4}$ to $2.9 \cdot 10^{-2}\,\text{cm}^{-1}$ could be obtained. This is due to the low line density and therefore rare line mixing.

The additional uncertainty for the line position resulting from calibration is $3.0 \cdot 10^{-5}$ cm^{-1}.

5.5.3.2 The $2\nu_1$, the $\nu_1 + \nu_3$ and the $2\nu_2 + \nu_3$ band

From analysed range from 4300 to $4700\,\text{cm}^{-1}$ of the *BM/10GBq* spectrum, in total 1277 lines were assigned to the $2\nu_1$, $\nu_1 + \nu_3$ and $2\nu_2 + \nu_3$ bands of T$_2$O.

In Figure 5.22, the baseline corrected spectrum slice is presented with the highlighted lines of the three bands. It can be noted that the $\nu_1 + \nu_3$ band is the dominant band in this spectral area, achieving the highest SNR and the highest number of lines assigned from this spectrum for all three species of tritiated water. Due to this high SNR for some lines, very precise fit results could be achieved reaching uncertainties down to $3.4 \cdot 10^{-5}\,\text{cm}^{-1}$.
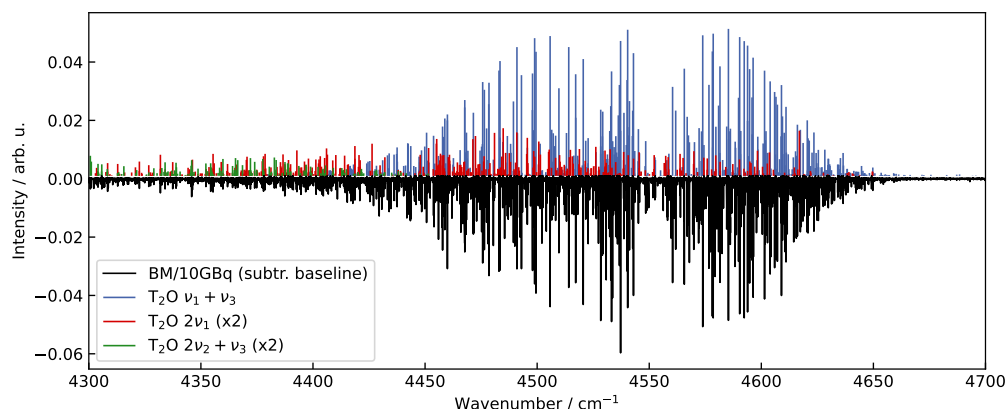
Figure 5.22: The $2\nu_1$, $\nu_1 + \nu_3$ **and** $2\nu_2 + \nu_3$ **band.** The assigned lines from these bands are presented on top of the baseline corrected *BM/10GBq* spectrum. For better visualisation, the intensity for the $2\nu_1$ and $2\nu_2 + \nu_3$ band are doubled.

However, the high density of lines (~ 6 tritiated water lines/cm^{-1}) affects the fit results, especially for lines with low SNR, leading to uncertainties up to $6.9 \cdot 10^{-2}$ cm^{-1}.

The additional uncertainty originating from the calibration process is $1.6 \cdot 10^{-4}$ cm^{-1}

The 206 lines obtained for the $\nu_1 + \nu_3$ of T$_2$O from the 1 GBq activity sample were also assigned from the high-activity sample spectrum. A detailed comparison is presented in the next section in the context of a validation study.

5.6 Validation of the obtained transition energies

In the previous section datasets of absorption lines of all three tritiated water species are presented.

To ensure the reliability of these datasets, a validation is presented in this chapter. This is especially important because the assignment required a visual assignment. In this procedure the initial line positions are corrected by taking the line intensities and observed band- and quantum-number-related deviations into consideration. However, this step adds a potential source of error that must be excluded within a data validation.

The validation methods that will be presented in the following are (i) a cross-check comparing shared lines from spectra of the 1 GBq and 10 GBq activity samples and (ii) a comparison of the dataset with (pure rotational) microwave measurements by using combination differences of the ro-vibrational transitions.

5.6.1 Comparison of shared transitions from the samples with 1 GBq and 10 GBq activity

Due to the measurement of the *BM/1GBq* and *BM/10GBq* spectra, transition energies from different samples and therefore independent measurements could be assigned. In this work, the $2\nu_1$ of HTO and the $\nu_1 + \nu_3$ of T_2O are such data sets that have been obtained from both samples.

To test for the consistency of the two measurements, the shared lines of both data sets were compared with respect to their positions. The difference of each line was statistically analysed in units of cm^{-1} and in units of the total uncertainty σ_{total} of the individual line pairs. The total uncertainty is determined by using the individual fit uncertainty of the line positions of both compared lines and their systematic uncertainty resulting from the calibration of the two spectra.

$$\sigma_{total} = \sqrt{\left(\sigma_{stat,1GBq} + \sigma_{syst,1GBq}\right)^2 + \left(\sigma_{stat,10GBq} + \sigma_{syst,10GBq}\right)^2} \qquad (5.13)$$

Deviations of $> 3\,\sigma_{total}$ are considered as disagreeing lines. It is assumed that in those cases some error has occurred during visual assignment. They are flagged with an asterisk in the line lists presented in the Appendix A.2.1.1 and A.2.3.1.

In Figure 5.23, a histogram of the differences in units of σ_{total} is presented. The disagreeing lines have been excluded for this graph and a Gaussian fit is applied.

It can be noted that the distribution of the differences is Gaussian-like for the T_2O dataset with a width of $1.00\,\sigma_{total}$. This is the expected result when all sources of uncertainties are correctly evaluated. For T_2O, 6 of 206 were excluded due to a too large deviation.

However, for the HTO dataset, the fit yields a width of $0.86\,\sigma_{total}$ a narrower Gaussian. Comparing the Gaussian with the histogram, in the right plot of Figure 5.23, one notices that the Gaussian does not represent the distribution correctly. It seems that the histogram is a mix of two (or more) Gaussian-like distributions, one wider and one narrower. This can be originating from an overestimation of the uncertainty of a subset of the data. This subset has in units of (the overestimated) σ_{total} a narrower distribution. With 23 of 347 shared lines a quite large number of line pairs is disagreeing. These are probably misassignments in the 1 GBq dataset, the first acquired dataset. The visual assignment procedure was to date of the earlier assignments not as elaborated as for the later assignment procedures, and therefore errors are more likely. A detailed description of the quantum number shifts is described in a later comparison with the *SPECTRA* data in Section 5.8.

In Figure 5.24 for the example of the T_2O band, a line-by-line comparison of both datasets is presented. The differences of both datasets are presented for the line positions to exclude any wavenumber-dependent effects. Differences (in cm^{-1}) are summarised in a histogram on the right of the graph. The distribution of the differences does not fit a regular Gaussian. This distribution is likely the result of the fact that the uncertainties of the line positions are
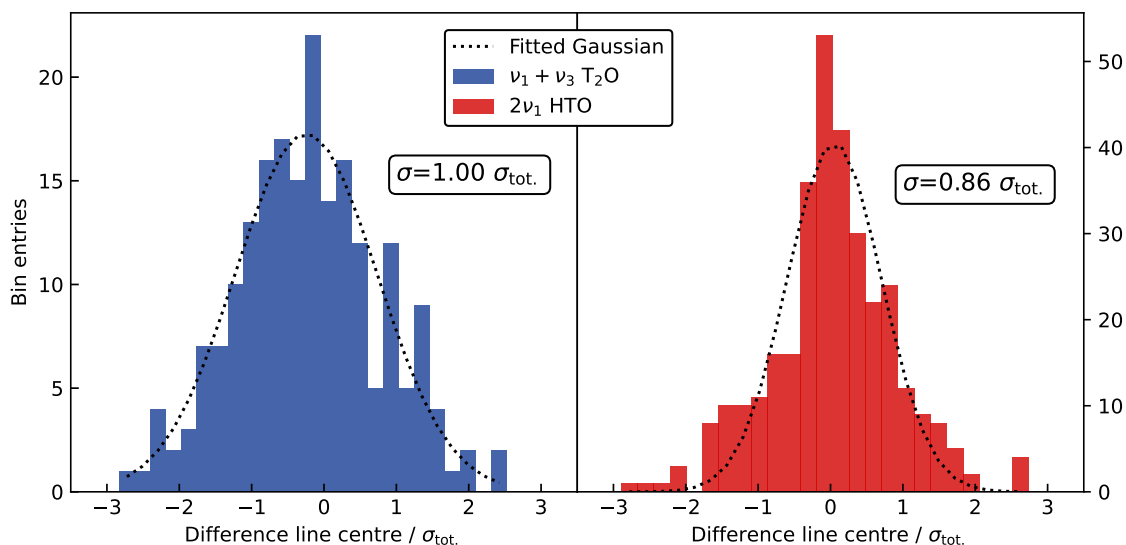
Figure 5.23: Histograms of differences of the line pair centres obtained from the $1\,\mathrm{GBq}$ **and** $10\,\mathrm{GBq}$ **sample.** Left: the $\nu_1 + \nu_3$ band of T_2O; Right: the $2\nu_1$ band of HTO. The differences are calculated in units of σ_{total} taking into account all positional uncertainties of both sets of lines. Gaussian fits have been applied. The standard deviations are $1.00\,\sigma_{\mathrm{total}}$ for T_2O and $0.86\,\sigma_{\mathrm{total}}$ for HTO

not the same for all. Lines with smaller uncertainty on the line centres will be distributed in a narrower (Gaussian-like) distribution. The convolution of a Gaussian with the distribution of line centre uncertainty is leading to this presented distribution. Although the model does not represent the data accurately, a Gaussian fit is used to obtain a mean deviation of the data sets and a standard deviation estimate in units of cm^{-1} for some qualitative analysis.

In Table 5.11 these values in units of cm^{-1} and σ_{total} are presented. The statistical analysis of both bands provides standard deviations up to $3.7 \cdot 10^{-3}\,\mathrm{cm}^{-1}$ and minor shifts up to $6.6 \cdot 10^{-4}\,\mathrm{cm}^{-1}$ (both T_2O). The comparison of both species does not reveal any inconsistency or hint of some unknown systematic effect.

Summarising the comparison of the data sets from the $1\,\mathrm{GBq}$ and the$10\,\mathrm{GBq}$ sample, it can be noted that, besides some disagreeing lines, the data are consistent with each other. The deviations are in accordance with the uncertainties of both data sets. No systematic shifts are observed for both data sets.
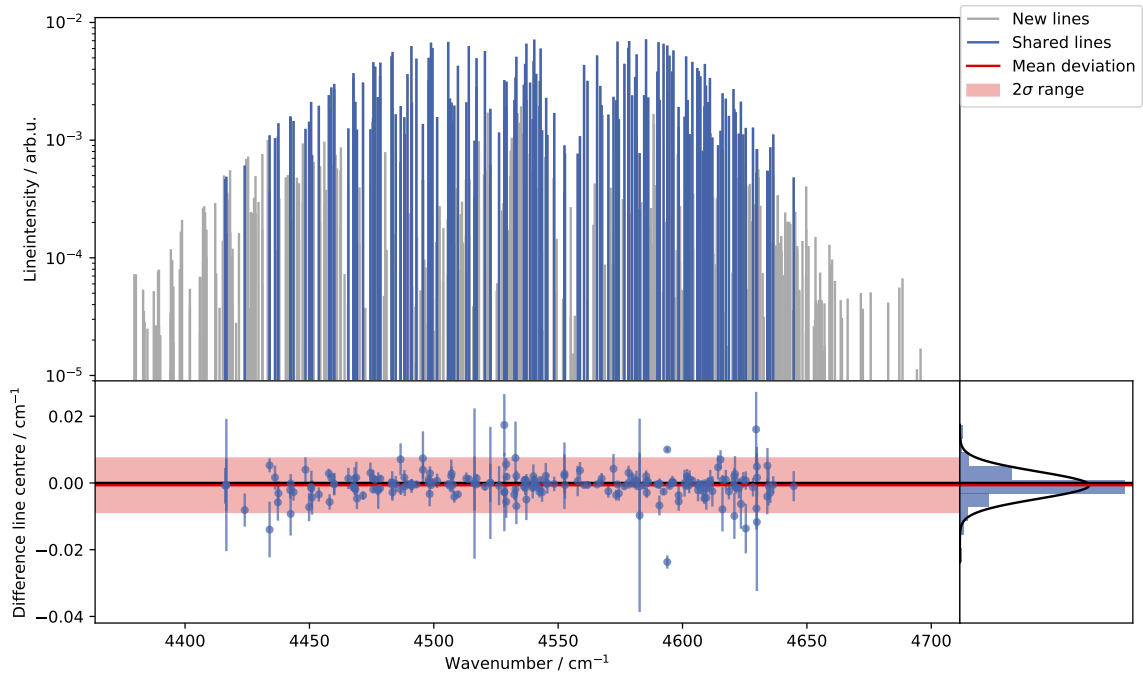
Figure 5.24: Line-by-line comparison of the $\nu_1 + \nu_3$ **band of T$_2$O obtained from the** $1\,\mathrm{GBq}$ **and** $10\,\mathrm{GBq}$ **sample.** For the shared lines (blue) the differences are plotted in the lower part of the graph. To the lower right a histogram of the differences with a Gaussian fit for discussion is added. The 2σ-range from the Gaussian fit is highlighted as red-shaded area.

Table 5.11: Comparison of the two datasets of the HTO $2\nu_1$ **and T$_2$O** $\nu_1+\nu_3$ **bands obtained from the** **10 GBq and 1 GBq activity sample.** The statistical values were found using a Gaussian fit on the histograms of the line-to-line differences. These differences are used in units of wavenumbers and σ_{total}, the individual uncertainty of both compared lines plus their systematic uncertainty. Transitions with differences $> 3\,\sigma_{\mathrm{total}}$ are considered as disagreement and were excluded in the statistics.

Species, band	T$_2$O, $\nu_1+\nu_3$	HTO, $2\nu_1$
Lines '10 GBq '	626	454
Lines '1 GBq '	206	361
New lines in '10 GBq '	420	107
Shared lines	206	347
Mean difference position (cm^{-1})	$-6.6 \cdot 10^{-4}$	$-3.5 \cdot 10^{-5}$
STD difference position (cm^{-1})	$3.7 \cdot 10^{-3}$	$3.3 \cdot 10^{-3}$
STD difference position (σ_{total})	1.00	0.86
Disagreeing lines	6	23

5.6.2 Comparison of rotational spacings with microwave measurements

Although the first validation method does not show hints of any misunderstood or unknown systematic contribution, it is still not excluded that such a potential effect would occur in a similar way for both measurements.

For this reason, an additional independent method is implemented that is based on the comparison of the obtained ro-vibrational transitions with pure rotational transitions from microwave measurement.

The microwave measurements have been performed for HTO, DTO and T_2O by Helminger et al. and De Lucia et al. published in [Hel74; De 73]. Those data are not provided with uncertainties, but a conservative estimate of $0.1 \, \mathrm{MHz}$ or $3.4 \cdot 10^{-6} \, \mathrm{cm}^{-1}$ is assumed.

5.6.2.1 Fit of Watson's ground state

A direct comparison of the microwave measurements with these high-resolution data, however, is not possible because the vibrational excitation must be removed first. This can be performed by creating combination differences of lines with the same upper state. By subtracting two lines with the same upper state quantum numbers, the difference between their ground state is determined as a pure rotational transition.

Note that the rotational ground state quantum numbers of the higher energetic transition are the ground state and the rotational ground state quantum numbers of the lower energetic transition the upper state of the created pure rotational transition.

Despite these combination differences, a comparison of these data one-by-one with data of Helminger and De Lucia is not possible because the microwave transition is an one-photon transition and the combination differences include two photons. Hence, the change of quanta is different for the to-be compared data sets.

An approach to compare these data is provided by Helminger and De Lucia within their publications. They determined spectroscopic parameters of Watson's A-reduced Hamiltonian (cf. Equation 2.26) using pure rotational measurements. This Hamiltonian describes the rotational energy states and can be determined using a sufficient number of rotational transitions.

The Watson A-reduced Hamiltonian is described in detail in Section 2.1.3. For the used parameters the Hamiltonian is given with:

$$
\begin{aligned}
H_{\text{red}}^{A} = \Bigg[& \frac{1}{2}(A+B)\hat{J}^2 + \left(C - \frac{1}{2}(A+B) \right) \hat{J}_z^2 - \Delta_J(\hat{J}^2)^2 - \Delta_{JK}\hat{J}^2\hat{J}_z^2 - \Delta_K\hat{J}_z^4 \\
& + H_J \left(\hat{J}^2 \right)^3 + H_{JK}\left(\hat{J}^2 \right)^2 \hat{J}_z^2 + H_{KJ}\hat{J}^2\hat{J}_z^4 + H_K\hat{J}_z^6 \\
& + L_{JJK}\left(\hat{J}^2 \right)^3 \hat{J}_z^2 + L_{JK}\left(\hat{J}^2 \right)^2 \hat{J}_z^4 + L_{KKJ}\hat{J}^2\hat{J}_z^6 + L_K\hat{J}_z^8 \\
& + P_{JJK}\left(\hat{J}^2 \right)^3 \hat{J}_z^4 + P_{KJ}\left(\hat{J}^2 \right)^2 \hat{J}_z^6 + P_{KKJ}\hat{J}^2\hat{J}_z^8 + P_K\hat{J}_z^{10} \Bigg] \\
& + \Bigg[\left(\hat{J}_x^2 - \hat{J}_y^2 \right) \left(\frac{1}{4}(A-B) - \delta_J\hat{J}^2 - \delta_K\hat{J}_z^2 + h_J\left(\hat{J}^2 \right)^2 + h_{JK}\hat{J}^2\hat{J}_z^2 \right. \\
& \left. + h_K\hat{J}_z^4 + l_{KJ}\hat{J}^2\hat{J}_z^4 + l_K\hat{J}_z^6 + p_{KKJ}\hat{J}^2\hat{J}_z^6 + p_K\hat{J}_z^8 \right) \\
& + \left(\frac{1}{4}(A-B) - \delta_J\hat{J}^2 - \delta_K\hat{J}_z^2 + h_J\left(\hat{J}^2 \right)^2 + h_{JK}\hat{J}^2\hat{J}_z^2 \right. \\
& \left. + h_K\hat{J}_z^4 + l_{KJ}\hat{J}^2\hat{J}_z^4 + l_K\hat{J}_z^6 + p_{KKJ}\hat{J}^2\hat{J}_z^6 + p_K\hat{J}_z^8 \right) \left(\hat{J}_x^2 - \hat{J}_y^2 \right) \Bigg] \quad .
\end{aligned}
\tag{5.14}
$$

Using this model, the experimental pure-rotational data can be compared. This is performed by first finding the mentioned combinational differences for all vibrational bands. Each pure rotational transition is provided with its experimental uncertainty, $\sigma_{\text{exp.}}$, with

$$
\sigma_{\text{exp.}} = \sqrt{(\sigma_{\text{line 1}})^2 + (\sigma_{\text{line 2}})^2}, \tag{5.15}
$$

where only fit uncertainty of each line ($\sigma_{\text{line 1/2}}$) is taken into account. The systematic uncertainty of the calibration is canceling out during the subtraction. Then, for each species, a fit of the Watson parameters is performed using the FORTRAN-based fitting programme *SPFIT* [Pic91]. Except for HTO, the choice of parameters and initial values from Helminger and De Lucia is used for a better comparison. For HTO, the choice is based on personal communication with Kentarou Kawaguchi who found a better working set of parameters [Kaw23].

5.6.2.2 The obtained parameters

The obtained parameters are listed in Tables 5.12,5.13 and 5.14 for HTO, DTO and T_2O, respectively. In these tables, the original data from Helminger et al. and De Lucia et al., respectively, have been added for comparison. In addition, for HTO, the parameters of Cope et al. [Cop88] are added.

Table 5.12: Comparison of spectroscopic constants A-reduced Watson Hamiltonian for the vibrational ground state of HTO. Parameters of Helminger et al. [Hel74], Cope et al. [Cop88] and those obtained in this work using combination differences of the infrared measurements (CD) combined with the microwave measurements (MW) from Helminger et al. in cm^{-1} are presented.

Watson Parameter		[Hel74] Value	2σ	[Cop88] Value	2σ	this work Value	2σ
	A	22.610 610 1	(56)	22.610 47	(57)	22.610 600 364	(69)
	B	6.611 156 6	(42)	6.611 18	(15)	6.611 131 816	(28)
	C	5.018 885 8	(42)	5.019 02	(13)	5.018 903 963	(27)
$10^3\cdot$	Δ_J	0.173 85	(10)	0.175 12	(96)	0.173 489 40	(94)
$10^3\cdot$	Δ_{JK}	1.6185	(7)	1.6168	(140)	1.616 471	(12)
$10^3\cdot$	Δ_K	9.049	(2)	8.9836	(369)	9.046 778	(41)
$10^3\cdot$	δ_J	0.047 170	(17)	0.047 183	(690)	0.047 151 03	(18)
$10^3\cdot$	δ_K	1.7121	(23)	1.6767	(214)	1.699 799	(14)
$10^8\cdot$	h_J	0.59	(3)	0.48	(42)	0.474 53	(25)
$10^7\cdot$	h_{JK}	5.71	(7)	5.71	fixed	6.165 02	(69)
$10^5\cdot$	h_K	1.796	(43)	1.142	(194)	1.558 48	(25)
$10^7\cdot$	H_J	0.1731	(133)	0.1731	fixed	0.110 75	(12)
$10^6\cdot$	H_{JK}	1.315	(20)	1.112	(191)	1.278 89	(25)
$10^5\cdot$	H_{KJ}	−0.212	(6)	−0.195	(78)	−0.227 91	(41)
$10^4\cdot$	H_K	0.2990	(36)	0.2395	(239)	0.296 36	(18)
$10^9\cdot$	L_{JJK}					−0.5079	(12)
$10^7\cdot$	L_{JK}					−0.153 62	(20)
$10^7\cdot$	L_{KKJ}	0.662	(27)			0.7139	(43)
$10^7\cdot$	L_K	−2.78	(23)			−2.794	(22)
$10^9\cdot$	l_{KJ}	−3.04	(67)			−9.979	(11)
$10^8\cdot$	l_K	−27.2	(23)			−11.87	(12)
$10^9\cdot$	P_{KKJ}					−0.874	(18)
$10^9\cdot$	P_K	3.68	(57)			5.056	(85)
$10^9\cdot$	p_K	1.99	(37)				
RMS MW		0.000002		?		0.000003	
RMS CD		-		0.011		0.00830	
No. of MW		48		48		48	
No. of CD		0		133 [1]		3389	

[1] reproduced from data [Cop88]

Table 5.13: Comparison of spectroscopic constants A-reduced Watson Hamiltonian for the vibrational ground state of DTO. Parameters of Helminger et al. [Hel74] and those obtained in this work using combination differences of the infrared measurements (CD) combined with the microwave measurements (MW) from Helminger et al. in cm^{-1} are presented.

Watson Parameter		[Hel74] Value	2σ	this work Value	2σ
	A	13.681 936 8	(26)	13.681 930 380	(45)
	B	5.740 703 2	(15)	5.740 702 609	(26)
	C	3.973 677 3	(15)	3.973 678 80	(16)
$10^3\cdot$	Δ_J	0.173 42	(10)	0.173 441 23	(14)
$10^3\cdot$	Δ_{JK}	-0.517 16	(50)	-0.517 179 4	(74)
$10^3\cdot$	Δ_K	6.014 51	(33)	6.012 745 7	(31)
$10^3\cdot$	δ_J	0.064 753	(33)	0.064 787 42	(49)
$10^3\cdot$	δ_K	0.042 994	(40)	0.428 784 6	(53)
$10^7\cdot$	h_J	0.0990	(53)	0.100 654	(79)
$10^7\cdot$	h_{JK}	0.99	(14)	1.1536	(20)
$10^5\cdot$	h_K	0.2698	(53)	0.240 243	(38)
$10^7\cdot$	H_J	0.198	(23)	0.203 26	(36)
$10^6\cdot$	H_{JK}	0.138	(27)	0.145 91	(39)
$10^5\cdot$	H_{KJ}	-0.2150	(33)	-0.214 672	(39)
$10^4\cdot$	H_K	0.115 65	(30)	0.114 319 0	(21)
$10^9\cdot$	L_{JJK}	0.44	(13)	0.3606	(13)
$10^7\cdot$	L_{KKJ}	0.0595	(67)	0.056 596	(57)
$10^7\cdot$	L_K	-0.2740	(67)	-0.240 570	(51)
$10^8\cdot$	l_K	-0.020 61	(27)	-0.723 08	(85)
RMS MW		0.000002		0.000005	
RMS CD		-		0.01074	
No. of MW		44		44	
No. of CD		0		1955	

Table 5.14: Comparison of spectroscopic constants A-reduced Watson Hamiltonian for the vibrational ground state of T_2O. Parameters of De Lucia et al. [De 73] and those obtained in this work using combination differences of the infrared measurements (CD) combined with the microwave measurements (MW) from De Lucia et al. in cm^{-1} are presented.

Watson Parameter		[De 73] Value	2σ	this work Value	2σ
	A	11.301 515 9	(25)	11.301 515 654	(32)
	B	4.858 861 4	(15)	4.858 875 051	(16)
	C	3.344 294 1	(15)	3.344 294 289	(13)
$10^3\cdot$	Δ_J	0.138 282	(47)	0.138 276 43	(49)
$10^3\cdot$	Δ_{JK}	$-0.735\,14$	(27)	$-0.735\,147\,7$	(29)
$10^3\cdot$	Δ_K	4.807 91	(20)	4.807 889 8	(19)
$10^3\cdot$	δ_J	0.053 698	(27)	0.053 695 42	(24)
$10^3\cdot$	δ_K	0.181 49	(33)	0.181 387 2	(35)
$10^8\cdot$	h_J	0.895	(33)	0.895 01	(36)
$10^7\cdot$	h_{JK}	0.093	(80)	0.068 16	(78)
$10^5\cdot$	h_K	0.1213	(13)	0.121 058	(13)
$10^7\cdot$	H_J	0.1859	(60)	0.184 924	(61)
$10^6\cdot$	H_{JK}	-0.0818	(60)	$-0.082\,274$	(64)
$10^5\cdot$	H_{KJ}	-0.0912	(11)	$-0.091\,176$	(11)
$10^4\cdot$	H_K	0.067 92	(10)	0.067 904 11	(98)
$10^7\cdot$	L_{JK}	0.006 35	(80)	0.006 247 7	(82)
$10^7\cdot$	L_K	-0.1260	(13)	$-0.125\,864$	(13)
$10^9\cdot$	l_J	0.0023	(17)	0.002 036	(17)
$10^9\cdot$	l_{JK}	0.105	(47)	$-0.095\,28$	(45)
$10^9\cdot$	P_{KJ}	0.0055	(2)	0.005 076	(17)
$10^9\cdot$	P_K	0.0184	(11)	0.019 494	(11)
$10^9\cdot$	p_{KKJ}	-0.0114	(33)	$-0.010\,353$	(35)
RMS MW		0.000003		0.000003	
RMS CD		-		0.01281	*
No. of MW		51		51	
No. of CD		0		1781	

*For T_2O 1 CD with very large deviation is excluded.
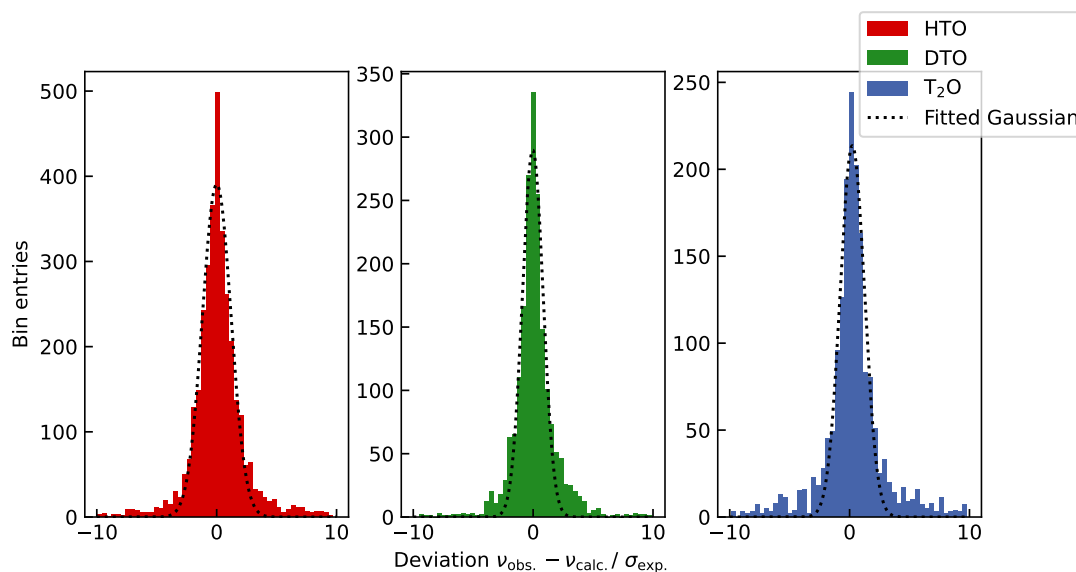
Figure 5.25: Histograms of the deviations of the observed pure rotational combination differences, $\nu_{obs.}$**, to the calculated transitions,** $\nu_{calc.}$**, in units of the experimental uncertainty** $\sigma_{exp.}$ **for all three species.** A Gaussian fit was applied. The obtained standard deviations are listed in Table 5.15.

The fits achieve RMS values for the microwave data of at least $5 \cdot 10^{-6}\,\mathrm{cm}^{-1}$, $150\,\mathrm{MHz}$, respectively. This is in the order of the estimated uncertainty. The authors did not provide experimental uncertainties in their publications.

The parameters obtained for DTO and T_2O do agree with those obtained from microwave measurements. It can be noted that the combined data sets allow for further improvement of the uncertainty and therefore in the description of the vibrational ground state.

For HTO, a different set of parameters to Helminger et al. is used. Moments of inertia (A,B,C) as well as the other shared parameters do not agree within their uncertainties although both sets achieve low and almost the same RMS values for the microwave data. This discrepancy points out that the obtained Watson parameters including the choice of the parameters only provide an 'effective' Hamiltonian, describing the vibrational ground state within the frame of the data set. A (systematic) error in the IR data set leading to this mismatch and achieving RMS values for the microwave data of all three species on such a level is unlikely. However, such a case would likely be noticed in a statistical analysis of the fits.

Table 5.15: Statistical analysis of the fit of the pure rotational A-reduced Watson model. The fit is applied on the microwave measurements (MW) of Helminger and De Lucia [Hel74; De 73] and combination differences (CD) of the IR data. The statistical analysis includes a Gaussian fit on the histograms presented in Figure 5.25.

Species	HTO	DTO	T_2O
Number MW lines	48	44	51
Number CDs	3389	1955	1781
RMS MW / MHz	0.091	0.150	0.076
STD Gaussian / $\sigma_{\text{exp.}}$	1.19	0.87	1.01
Deviation CD >5 $\sigma_{\text{exp.}}$	232	118	267

5.6.2.3 Statistical analysis of the Watson fits

To further exclude any systematic errors in the IR data a statistical analysis of the fitted model with the experimental data was performed. An overview of key values of this analysis is given in Table 5.15.

For the combination differences obtained from the IR measurements, the first deviations from the calculated transitions are found. Histograms of these deviations in units of the experimental uncertainty $\sigma_{\text{exp.}}$, as presented in Figure 5.25, show a Gaussian-like distribution. Gaussian standard deviations of up to $1.19\ \sigma_{\text{exp.}}$ are found showing agreement of the lines with the model in units of the individual uncertainty. The Gaussian-like distribution and the absence of any substructure also indicate that there is no systematic problem with the obtained model.

However, it should also be noted that up to 15% of the combinations deviate more than $5\ \sigma$. This might be an indication of potential misassignment or arises from a limitation of the model. An analysis of the quantum number of these transitions does not show any trend.

In summary, agreement of the found combination differences with the microwave data can be attested. For all three species, parameters of the Watson Hamiltonian are found describing both datasets, microwave and IR. The deviations from the data to the model reflect the experimental uncertainty. The number of lines deviating from the model is small enough that a systematic problem in the assignment procedure is not expected.

5.7 Determination of spectroscopic constants for the vibrational states

The Watson Hamiltonian, a model for describing the rotational states of a molecule, is useful not only when pure rotational transitions are compared with a set of combination differences. Moreover, the determination of the parameters allows to reconstruct the entire band of rotational transitions and is therefore a condensed representation of the experimental obtained data. By implementing an additional parameter for the vibrational energy, the Watson Hamiltonian can also be determined for vibrational bands.

In this section, five of the vibrational bands of the HTO and DTO spectroscopic parameters of the A-reduced Watson Hamiltonian are found and presented. First, a general overview of the fitting procedure is presented. The parameters obtained are then presented for the fits that have been successfully performed. A subsequent analysis of the parameters shows the different quality of applicability of the model for some bands, explaining the breakdown of the fit for the remaining bands.

5.7.1 Fitting procedure

The fitting of the spectroscopic data to the Watson Hamiltonian is performed with *SPFIT* [Pic91].

To fit the IR data two sets of parameters of the Watson Hamiltonian are needed, (i) one for the rotational states of the vibrational ground state and (ii) one for the vibrational excited state. Both sets are different because vibrational motion affects the moment of inertia.

For the set of parameters for the ground states, the parameters of this work are used. They have been determined in the previous section using combination differences of IR data and microwave measurements by Helminger et al. and De Lucia et al. [Hel74; De 73] (cf. Section 5.6.2). These ground-state values are fixed for the fit of the vibrational upper states.

For the vibrational energy, separating the two rotational bands, an additional parameter ν_0 is introduced. An initial value for this data set is found by taking the mean of the IR data of the analysed band.

For the excited state parameter, the right choice of parameters and initial values is crucial for a successful fit. The following routine has shown the best results: First, fits with low power series parameters (quartic and sextic order) are performed by testing different initial values for the main moments of inertia (A, B and C). Then, fits with parameters of higher power have been added as long as the RMS value keeps decreasing.

The obtained set of parameters is checked to determine whether some parameters with high uncertainty and/or small value can be omitted with no or very small increase in RMS.

The uncertainty of the IR data provided to the fit is only the fit uncertainty of the individual line as the uncertainty of the calibration is expected to be similar for all lines of a band and will only affect the vibrational energy. For the $2\nu_1$ band of HTO and the $\nu_1 + \nu_3$ band of T_2O data of both measurements were used. There, the uncertainty of the calibration is included. The provided uncertainty is determining the weight of a line in the fit.

5.7.2 Determined spectroscopic parameters

For the $2\nu_1$ and $\nu_1 + \nu_3$ band of HTO, as well as for the ν_3, the $\nu_1 + \nu_3$ and $2\nu_2 + \nu_3$ DTO, set of parameters have been found. In Table 5.16, results for the HTO bands are presented, in Table 5.17 for the DTO bands. Similar sets of parameters and parameters for additional bands have been published [Rei20; Her21; Her22]. It should be noted that the tool and for some of the fits the approach is different, therefore other results are obtained.

The RMS values range from $5.3 \cdot 10^{-3}$ to $1.2 \cdot 10^{-2}\,\mathrm{cm}^{-1}$ when ignoring up to 10 lines per set that deviate more than the range of the spectral line estimated with $0.04\,\mathrm{cm}^{-1}$. For the remaining bands, the best achievable RMS and the number of lines to be excluded are much higher and therefore are not included in this chapter.

5.7.3 Statistical analysis and breakdown of the fit

Analogous to the ground state fits, the fits for the vibrational excited states are statistically analysed. This is useful to visualise how effective the set of parameters obtained is representing the actual data. In Figures 5.26 and 5.27 the histograms of the deviations of the lines of a band from the fitted models in units of their individual fit uncertainty $\sigma_{\mathrm{exp.}}$ are presented. In addition to the five vibrational bands presented, an HTO band is included as an example of a band that could not be fitted using the presented approach.

A summary of the relevant parameters of the statistical analysis is presented in Table 5.18.

For DTO (cf. Figure 5.27), all three histograms show a Gaussian-like distribution. The standard deviations obtained from the histograms span from 0.89 to $1.93\,\sigma_{\mathrm{exp.}}$, and most of the lines agree within the experimental acceptance ($5\,\sigma_{\mathrm{exp.}}$).

For HTO (cf. Figure 5.26), the fit results presented are of very different quality: While the $2\nu_2$ band of HTO can be described by the Watson parameters, resulting in a Gaussian-like distribution with a standard deviation of $1.01\,\sigma_{\mathrm{exp.}}$, the $\nu_1 + \nu_3$ band reveals a substructure in the distribution, indicator of systematic problems. However, these Watson parameters are included in this work as the RMS value is with $0.0101\,\mathrm{cm}^{-1}$ better than the accuracy of the SPECTRA database ($\sim 0.1\,\mathrm{cm}^{-1}$). The third histogram, the band $\nu_1 + 2\nu_2$, is representative of all bands that could not be fitted. Standard deviations of over $> 10\,\sigma_{\mathrm{exp.}}$ and RMS values in the order of $1\,\mathrm{cm}^{-1}$ are the best results obtained for these bands using the described procedure.

Table 5.16: Spectroscopic constants of A-reduced Watson Hamiltonian for the vibrational excited states $2\nu_2$ and $\nu_1 + \nu_3$ of HTO in cm^{-1}. For the RMS only lines with deviations smaller than $< 0.04\,\text{cm}^{-1}$ are taken into account. A detailed statistical analysis of the deviations is presented in the next section 5.7.3.

Watson Parameter		HTO $2\nu_1$ Value	2σ	HTO $\nu_1 + \nu_3$ Value	2σ
	ν_0	4537.732 186	(64)	6010.6273	(12)
	A	22.211 951	(34)	21.5652	(11)
	B	6.362 213	(14)	6.463 56	(84)
	C	4.873 765	(12)	4.904 24	(73)
$10^3\cdot$	Δ_J	0.167 42	(93)	0.210	(55)
$10^3\cdot$	Δ_{JK}	1.661 16	(91)	2.61	(10)
$10^3\cdot$	Δ_K	7.9618	(57)	7.32	(17)
$10^3\cdot$	δ_J	0.043 821	(65)	−0.1167	(71)
$10^3\cdot$	δ_K	1.6949	(58)	−6.05	(43)
$10^8\cdot$	h_J	0.333	(31)	−43.4	(35)
$10^7\cdot$	h_{JK}	4.87	(20)	−155.2	(66)
$10^5\cdot$	h_K	1.169	(66)	11.95	(67)
$10^7\cdot$	H_J	0.0742	(58)	2.80	(54)
$10^6\cdot$	H_{JK}	1.074	(41)	−31.6	(44)
$10^5\cdot$	H_{KJ}	−0.179	(15)	37.8	(18)
$10^4\cdot$	H_K	0.2391	(30)	−1.50	(11)
$10^7\cdot$	L_{JJK}			7.95	(43)
$10^7\cdot$	L_{JK}			−75.1	(44)
$10^7\cdot$	L_K	−0.582	(42)		
$10^7\cdot$	l_{KJ}			270	(13)
$10^9\cdot$	P_{JK}			35.2	(33)
$10^9\cdot$	P_K			96.0	(42)
$10^9\cdot$	p_{JJK}			3.77	(20)
$10^9\cdot$	p_{JK}			−92.9	(58)
No. of lines		815		165	
Dev. $> 0.04\,\text{cm}^{-1}$		2		10	
RMS remaining lines		0.00525		0.0101	

Table 5.17: Spectroscopic constants A-reduced Watson Hamiltonian for the vibrational excited states ν_3, $nu_1 + \nu_3$ and $2\nu_2 + \nu_3$ of DTO in cm^{-1}. For the RMS only lines with deviations smaller than $< 0.04\,\text{cm}^{-1}$ are taken into account. A detailed statistical analysis of the deviations is presented in the next section 5.7.3.

Watson Parameter		DTO ν_3 Value	2σ	DTO $\nu_1 + \nu_3$ Value	2σ	DTO $2\nu_2 + \nu_3$ Value	2σ
	ν_0	2737.395 13	(52)	5021.0770	(11)	4880.8085	(13)
	A	13.248 84	(15)	13.121 61	(54)	15.176 62	(57)
	B	5.724 940	(63)	5.650 34	(20)	5.836 40	(14)
	C	3.934 728	(41)	3.887 65	(14)	3.853 043	(78)
$10^3 \cdot$	Δ_J	0.179 58	(59)	0.1568	(29)	0.2148	(12)
$10^3 \cdot$	Δ_{JK}	-0.5855	(47)	-0.062	(23)	-0.9035	(99)
$10^3 \cdot$	Δ_K	5.6037	(79)	5.025	(65)	1.267 21	(64)
$10^3 \cdot$	δ_J	0.0678	(44)	0.0538	(18)	0.086 46	(63)
$10^3 \cdot$	δ_K	0.3834	(33)	0.641	(49)	1.022	(13)
$10^8 \cdot$	h_J	1.47	(24)	-7.5	(13)		
$10^7 \cdot$	h_{JK}			-64.4	(29)		
$10^5 \cdot$	h_K	0.173	(26)	-6.29	(49)		
$10^7 \cdot$	H_J	0.0279	(33)	-1.99	(26)		
$10^6 \cdot$	H_{JK}			-8.17	(67)		
$10^5 \cdot$	H_{KJ}	-0.153	(15)	6.41	(34)		
$10^4 \cdot$	H_K	0.0798	(16)	-0.421	(33)	0.224	(14)
$10^7 \cdot$	L_{KKJ}			-6.78	(53)		
$10^7 \cdot$	L_K			8.06	(57)		
No. of lines		436		365		161	
Dev. $> 0.04\,\text{cm}^{-1}$		1		9		3	
RMS remaining lines		0.00530		0.01246		0.00788	

Table 5.18: Overview of the statistical analysis of the Watson fits of the vibrational upper state. The corresponding histograms are displayed in Figure 5.26 and Figure 5.27.

Species	Band	STD Gaussian / $\sigma_{\text{exp.}}$	No. lines	Dev. $> 5\,\sigma_{\text{exp.}}$
HTO	$2\nu_1$	1.05	815	23
	$\nu_1 + \nu_3$	4.65	165	57
	$\nu_1 + 2\nu_2$	10.71	446	332
DTO	ν_3	1.25	436	26
	$\nu_1 + \nu_3$	1.93	356	46
	$2\nu_2 + \nu_3$	0.89	161	4
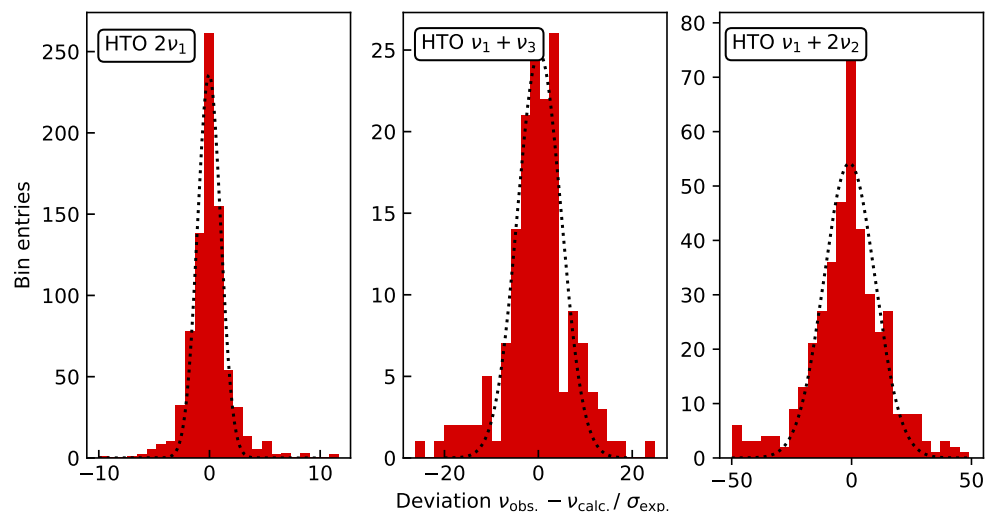
Figure 5.26: Histograms of deviations of the assigned lines of different HTO bands from the fitted Watson model. The used parameters are listed in Table 5.16. Statistical properties are presented in Table 5.18. The $\nu_1 + 2\nu_2$ band is included for discussion.
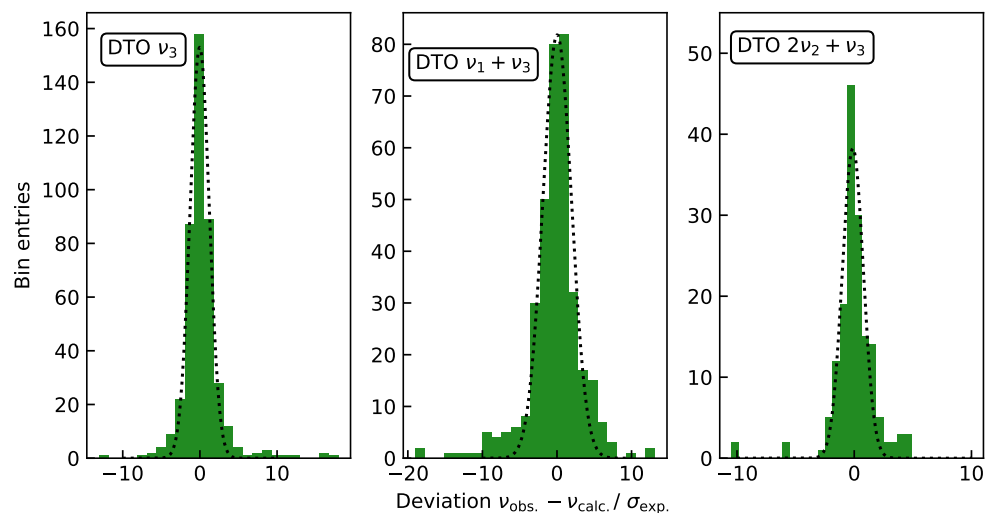
Figure 5.27: Histograms of deviations of the assigned lines of DTO bands from the fitted Watson model. The used parameters are listed in Table 5.17. Statistical properties are presented in Table 5.18.

Resonances as reason for the breakdown of Watson fits

A reason for the breakdown of the fits could be that a working combination of parameters and initial values could not yet be found. Assuming that this is not the case, the breakdown of the fit for these bands could be rooted in the resonance of vibrational bands.

Resonances occur when the ro-vibrational states (for example, A and B) have similar energies, leading to an overlap of the wave functions $\Psi(\nu, J, K_a, K_c)_{A,B}$. The symmetry of the motion determines whether and how the interaction manifests itself. Known resonances are the Fermi resonance (i.e. [Orp94; Kis09]) and three Coriolis resonances (i.e. [Kwa04; Kis08]). Note that only one Coriolis resonance is relevant for (tritiated) water, as the other two require out-of-plane motion.

Bands that could not be fitted successfully within this work are part of polyads, groups of vibrational bands with similar energies and therefore potentially influenced by resonances. When analysing the theortically predicted lines (see also Figure 2.6), one can find following polyads including <u>observed bands of this work</u>:

Table 5.19: **Overview of vibrational polyads.** The spectral range is given by the outer band centres. Vibrational bands presented in this work are underlined.

Species	Polyad	Spectral range
HTO:	$\underline{\nu_1 + 2\nu_2}$, $\underline{\nu_2 + \nu_3}$ and $4\nu_2$	$3630 - 3960\,\mathrm{cm}^{-1}$
	$2\nu_1 + \nu_2$, $\underline{\nu_1 + \nu_3}$, $\nu_1 + 3\nu_2$, $\underline{2\nu_2 + \nu_3}$ and $5\nu_2$	$4920 - 5130\,\mathrm{cm}^{-1}$
DTO:	$4\nu_2$, $\underline{\nu_1 + 2\nu_2}$ and $\underline{2\nu_1}$	$4200 - 4540\,\mathrm{cm}^{-1}$
	$\underline{\nu_1 + \nu_3}$ and $\underline{2\nu_2 + \nu_3}$	$4880 - 5021\,\mathrm{cm}^{-1}$
T$_2$O:	$\nu_1 + 2\nu_2$, $\underline{2\nu_2 + \nu_3}$, $\underline{2\nu_1}$, $\underline{\nu_1 + \nu_3}$ and $2\nu_3$	$4220 - 4720\,\mathrm{cm}^{-1}$

In addition, the fitted $2\nu_1$ of HTO and ν_3 of DTO are energetically isolated, as well as the successfully fitted bands of HTO (ν_1 [Cop88], ν_2 [Ule91] and $2\nu_2$ [Rei19]) and T$_2$O (ν_2 [Fry84]) in observations before this work. These observations support the hypothesis of the influence of resonances within the fit process of the upper states. On the other side, exceptions, the $\nu_1 + \nu_3$ and $2\nu_2 + \nu_3$ of DTO and the ν_3 [Tin12] and $\nu_1 + \nu_3$ of HTO and ν_3 of T$_2$O [Cop86], seem to be not or weakly influenced by resonances. The presence of resonances on a relevant scale for the fit of the upper states can only be proven by including parameters in the model to determine the coupling strength. However, this requires further investigations that are beyond the scope of this work.
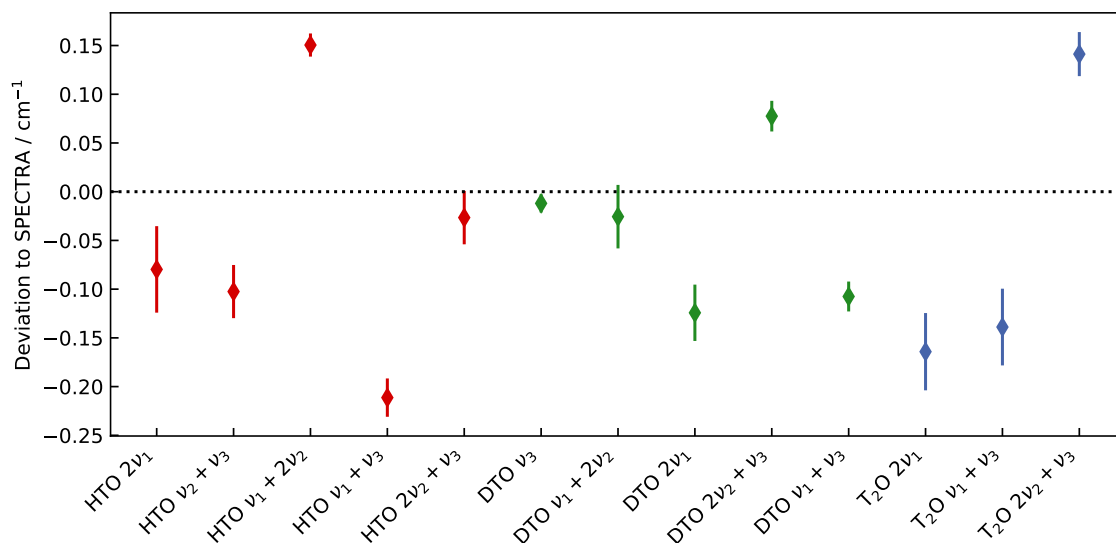
Figure 5.28: Comparison of experimental data with ab-initio predictions from SPECTRA for the individual vibrational bands. The mean deviation of the vibrational bands with the standard deviation as error-bar is compared to the ab-initio calculations from SPECTRA database.

5.8 Comparison to the theoretical predictions from SPECTRA database

The ab initio calculations for the tritiated water species from the SPECTRA database [Mik05] are one of the key elements for the determination process of the ro-vibrational spacings. These data were produced with the PES (potential energy surface) from Partridge and Schwenke 1997. The precision of these calculations for HDO was tested, revealing a root mean square deviation of $0.25\,\mathrm{cm}^{-1}$ [Par97; Sch00].

For tritiated species, this test has not been performed, but previous observations indicate a similar precision [Bra15; Dow13]. In this section a comparison of the experimentally acquired data with the ab initio calculation is performed. First, the precision of the prediction for the vibrational energy is investigated. Then, further insights are gained by investigating the correlation with rotational quantum numbers.

5.8.1 Precision of theoretical predictions on the vibrational energy

Deviation of experimental data to the SPECTRA database has already been observed by Down et al. [Dow13] (Dev.$= -0.103\,\mathrm{cm}^{-1}$), by Bray et al. [Bra15] (-0.067 to $-0.128\,\mathrm{cm}^{-1}$) and Reinking et al. [Rei19] - all in HTO. However, these data sets are limited to lines of a single vibrational band, which allowed no systematic investigation on the precision of the ab initio predictions for the vibrational energies.

Using the 13 bands of tritiated water species (3 T_2O, 5 DTO, and 5 HTO) counting a total number of 4589 individual highly accurate lines, for the first time an analysis can be performed. In Figure 5.28, the mean deviation of the experimental data to SPECTRA database is presented.

The deviations range from 0.15 to $-0.25\,\mathrm{cm}^{-1}$. It can be noted that the deviations are band-specific. For all species, positive and negative values can be observed. The spread of the deviations for each band, characterised by the standard deviation, is presented in the figure as an error bar. As the centre value, the spread is also different for the individual bands. The dependency between the vibrational quantum number and the deviations was tested, but was not found. A statistical analysis including all bands provides for the vibrational energy a precision of $0.11\,\mathrm{cm}^{-1}$ with a mean deviation of $-0.05\,\mathrm{cm}^{-1}$.

5.8.2 Rotational quantum number dependent deviations from theoretical predictions

Although the deviations have, as presented previously, a significant contribution from the vibrational energy, the large spread within a band (peak-to-peak up to $0.3\,\mathrm{cm}^{-1}$) indicates also a significant contribution from rotational energies.

In this section, these deviations are investigated in relation to their dependency on the quantum numbers J and K_a.

For the dependence on the quantum number K_a the difference between the experimental data and the SPECTRA database [Mik05] ($\nu_{\mathrm{obs.}} - \nu_{\mathrm{pred.}}$) is found and plotted for the position of the individual line. In Figure 5.29, the DTO $\nu_1 + 2\nu_2$ and HTO $2\nu_1$ from the $10\,\mathrm{GBq}$ sample are presented as an example. Lines with $K'_a = 3$, 4 and 5 of these data sets are highlighted in blue, black, and red to show the correlation of the rotational quantum number with the differences to the SPECTRA database. In the Appendix A.3.2 plots for all bands of this work are presented.

Analysing all bands, in general the deviation from the theoretical predictions is shifted to the negative for increasing K'_a (and K''_a). As deviations are defined as $\nu_{\mathrm{obs.}} - \nu_{\mathrm{pred.}}$, this means that the energy is generally overestimated for increasing K_a. This K'_a-dependent shift is different for each band.

When analysing the general shape of the data points in these plots, its parabolic shape is striking. This characteristic indicates a dependency of the deviations on the quantum number J.

In Figure 5.30, for the T_2O $2\nu_1$ band the $J'(J'+1)$ value is plotted for the deviations from theoretical predictions. It can be noted that with increasing J and fixed K'_a the deviations are shifted to the positive, meaning an underestimation of the energy with increasing J (respectively, $J(J+1)$). As for the K'_a-dependency, these shifts are also different for each
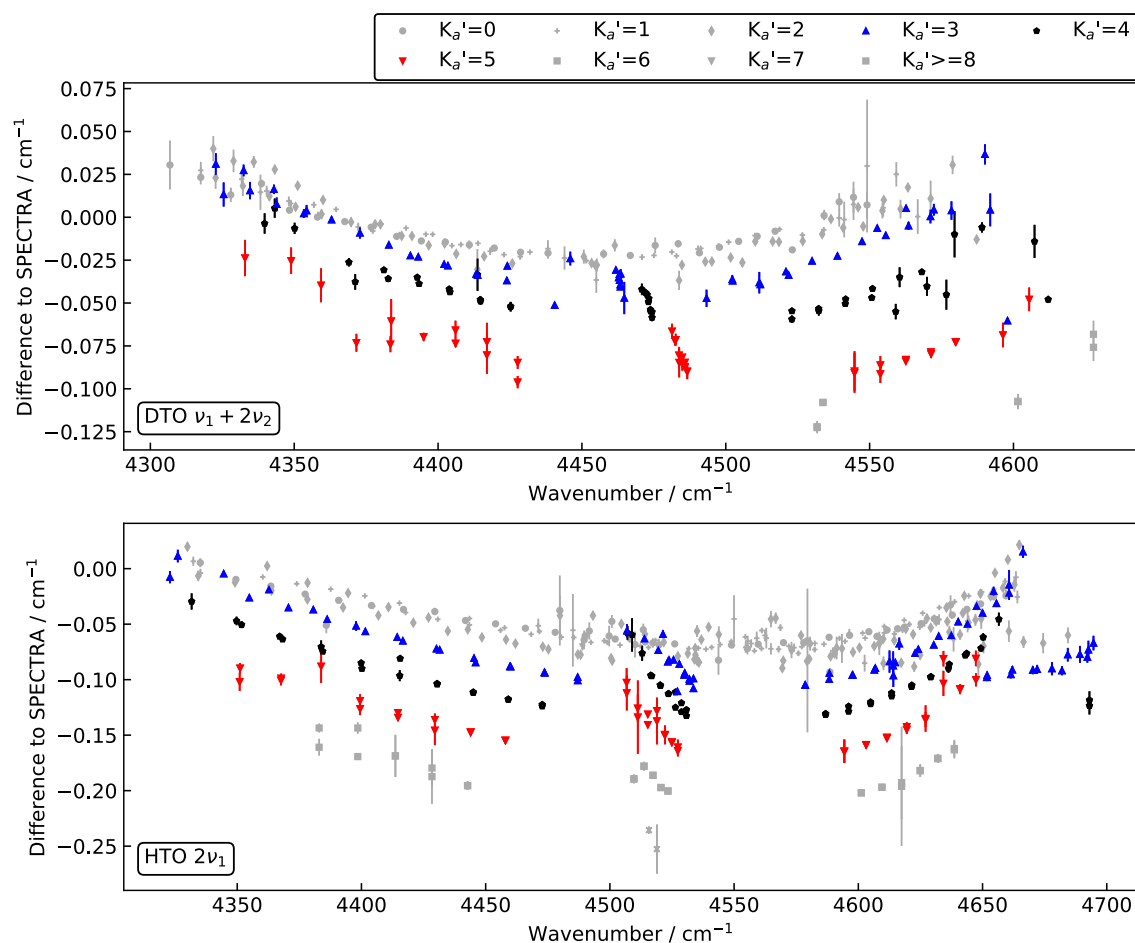
Figure 5.29: Visualisation of the K_a-dependency of the deviations of experimental data and predictions. The differences of the experimental data of the DTO $\nu_1 + 2\nu_2$ and HTO $2\nu_1$ from the 10 GBq sample to SPECTRA database [Mik05] for the individual line positions are presented. Lines with quantum number $K_a' = 3,\ 4$ and 5 are highlighted.

band and for a few bands almost neglectable. An example for such a weak J-dependency is presented in Figure 5.31.

Plots for all bands showing this correlation can be found in the Appendix A.3.1.
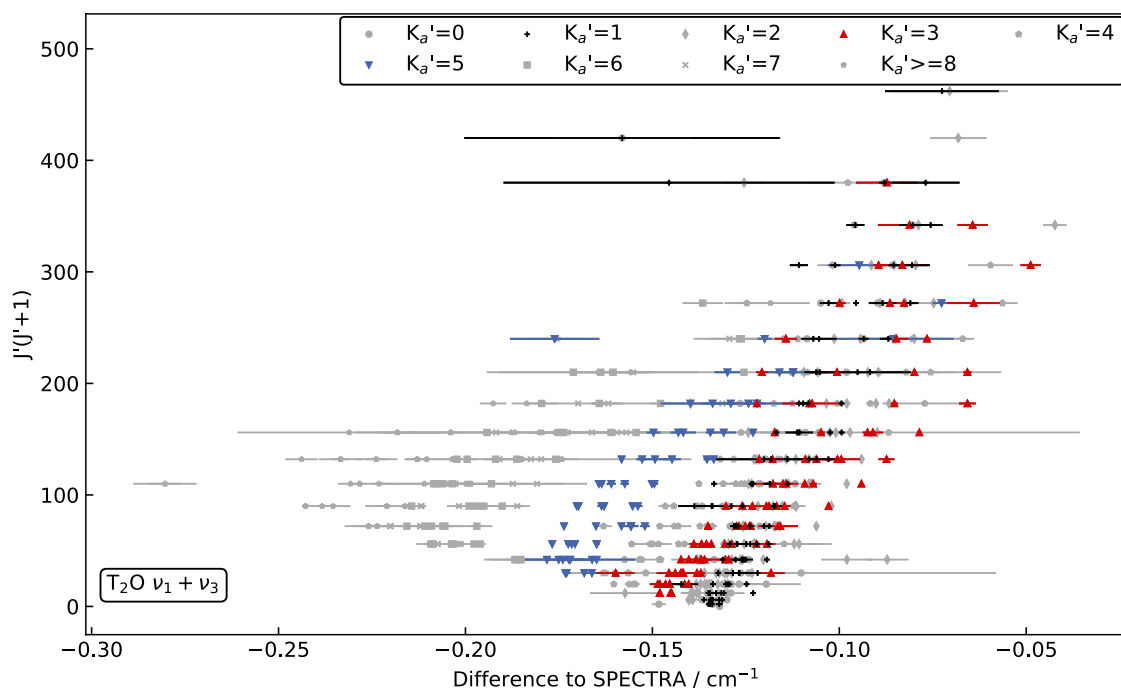
Figure 5.30: Visualisation of a strong $J'(J'+1)$**-dependency of deviations of experimental data to predictions.** The differences of the experimental data of the T_2O $2\nu_1$ to SPECTRA database[Mik05] for individual values of $J'(J'+1)$ are presented. Lines with quantum number K'_a = 1, 3 and 5 are highlighted. The strong $J'(J'+1)$-dependency is visible from the change of the deviations with increasing J' and for constant K'_a.
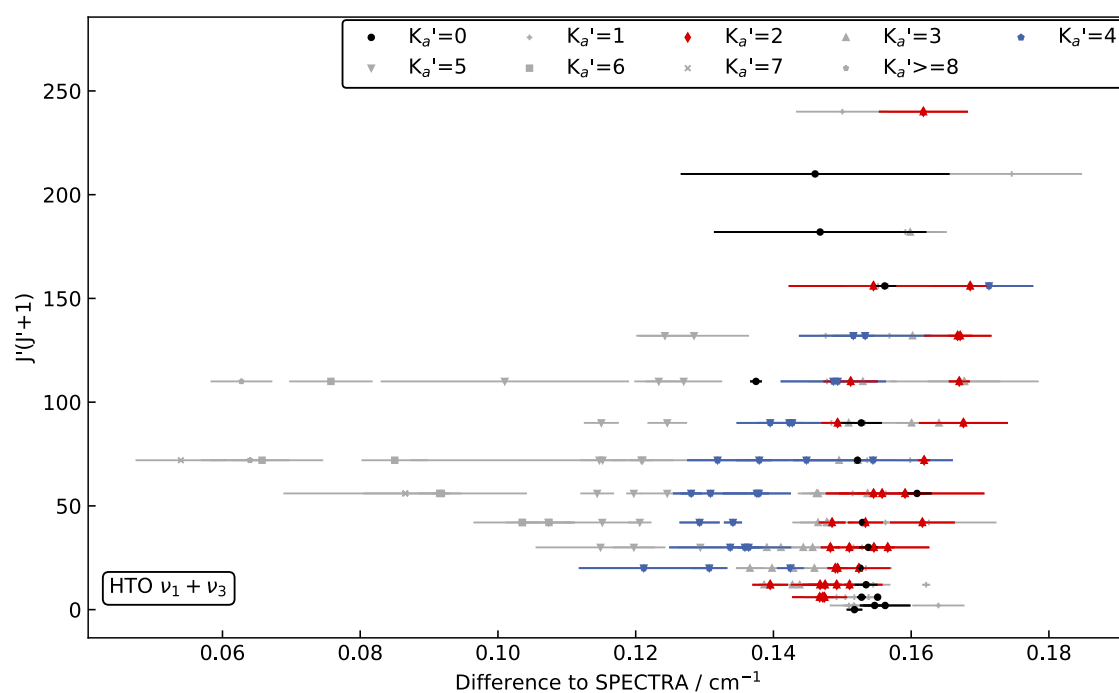
Figure 5.31: Visualisation of a weak $J'(J' + 1)$-dependency of deviations of experimental data to predictions. The differences of the experimental data of the HTO $\nu_1 + \nu_3$ to SPECTRA database[Mik05] for individual values of $J'(J' + 1)$ are presented. Lines with quantum number $K_a' = 0, 2$ and 4 are highlighted. The weak $J'(J' + 1)$-dependency is visible from (almost) constant deviations for lines with same K_a'.

5.9 Conclusion and discussion

Starting from a tritiated water vapour sample of $1\,\mathrm{GBq}$ activity, which development and measurement performed by Müller et al.[Mül19; Mül18; Rei19] are described in detail in the first part of this chapter, improvements in design and preparation have been developed and implemented in a new sample.

In this sample (i) a higher reflective silver light-pipe for less signal loss, (ii) an optimised oxidation unit for reduction of impurities, (iii) additional cleaning cycles for reduction of hydrocarbons and residual water, and (iv) a ten times higher activity tritium-deuterium mixture filling contributed to a sample with an almost equal hydrogen isotope abundance.

This, compared to the $1\,\mathrm{GBq}$ sample, increased the SNR for DTO and T_2O by factors 174 and 50. For HTO, the most abundant tritiated isotopologue in the $1\,\mathrm{GBq}$ sample, the SNR increased by 3. The signatures of residual water, CO_2, and methane have been reduced.

Using a high-resolution FTIR located outside the radiation-supervised laboratory, spectra within the range of 1800 to $10\,000\,\mathrm{cm}^{-1}$ and a resolution up to $0.0019\,\mathrm{cm}^{-1}$ have been obtained from both samples.

These spectra were calibrated by comparing the spectral position of the signatures of CO_2, HDO and H_2O from the samples with highly accurate data from the HITRAN database [Gor17; Gor22][3]. While for most measured spectra the accuracy of the database is limiting the accuracy of the wavenumber scale, for the *BM/1GBq* spectrum an extensive analysis with 169 lines covering the 3 reference species and numerous references is performed. Ensuring consistency of the references with each other and throughout the spectrum, a wavenumber accuracy of $3 \cdot 10^{-5}\,\mathrm{cm}^{-1}$ is achieved.

The assignment of tritiated water lines from the measured spectra was performed using initial line positions and intensities from ab initio predictions available from the SPECTRA database [Mik05][4]. These predictions deviate up to 10 line width ($\approx 0.3\,\mathrm{cm}^{-1}$) which requires a visual assignment. After this assignment procedure that takes into account intensities and statistical observations, a fit is performed using the *Minuit* algorithm.

The reliability of the fit procedure and the resulting line position, intensity, and uncertainties were investigated in a Monte Carlo study, revealing great consistency for the line position and its uncertainty and a high fluctuation in the intensities. However, the results for the intensities are expected as for an optimal line shape reproduction pressure and intensity (broadening and amplitude) is set as a free parameter.

From both samples, in total 4589 different lines of 13 vibrational bands of $HT^{16}O$, $DT^{16}O$ and $T_2^{16}O$ have been assigned for the first time, achieving accuracy up to $5.6 \cdot 10^{-5}\,\mathrm{cm}^{-1}$ including fit and wavenumber axis uncertainty.

---

[3]https://hitran.org/
[4]https://spectra.iao.ru/
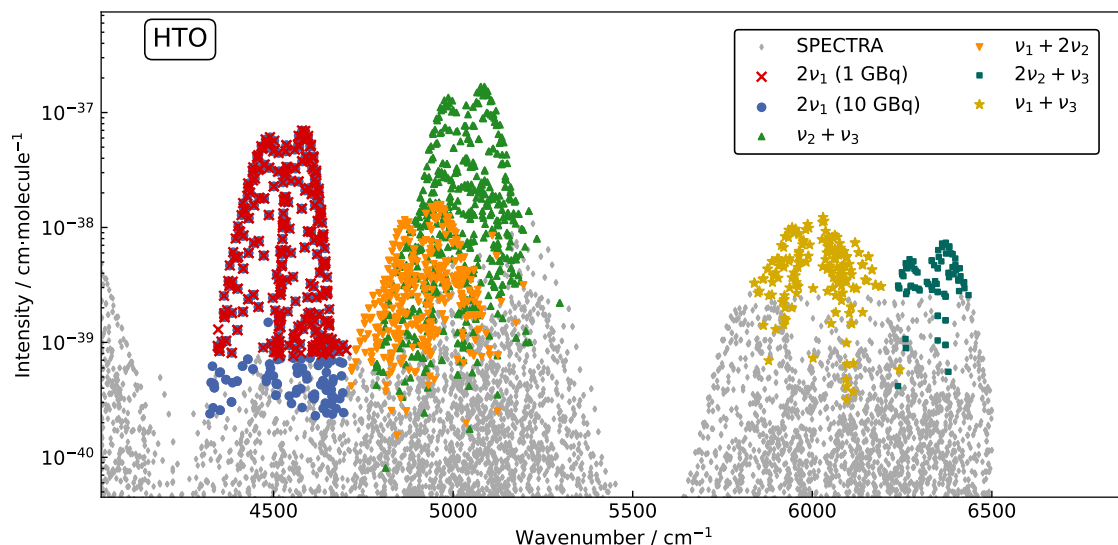
Figure 5.32: Illustration of the measured lines of HTO in this work. Predictions from SPECTRA database are provided for comparison. The line intensities are corrected for the natural abundance of HTO.

Illustrations of the size and coverage of these datasets are presented in Figures 5.32, 5.33 and 5.34.

The $2\nu_1$ band of HTO and the $\nu_1 + \nu_3$ band of T_2O have been measured and assigned from spectra of both samples. In total, 553 remeasured lines have been used for a line-by-line cross-check as one of the implemented validation methods. The standard deviation of both measurements is with $1.0\,\sigma_{\text{total}}$ and $0.9\,\sigma_{\text{total}}$ in units of the combined uncertainties of both measurements σ_{total}, which shows great consistency.

Another validation method is the comparison of the obtained data with microwave measurements performed by De Lucia et al. [De 73] and Helminger et al. [Hel74]. For this method, first combination differences of the lines with same upper vibrational and rotational quanta are found to obtain rotational spacings of the vibrational ground state. To compare both data sets, a fit of Watson's ground state [Wat67] is performed combining the microwave and IR combination differences.

The fits show agreement with the microwave data. The RMS values for the microwave data are lower than $< 150\,\text{kHz}$, a comparable value to the fits performed in the mentioned publications [De 73; Hel74]. The combination differences obtained from the measured lines deviate from the fitted model in a Gaussian-like distribution with a standard deviation of less than $< 1.2\,\sigma_{\text{exp.}}$, where $\sigma_{\text{exp.}}$ is the combined uncertainty of the fitted lines.

For all three species, ground state parameters with smaller stated uncertainties than reported by any publication to date of this work are found. However, it should be mentioned that up to 15% of the fitted combinations disagree with more than $< 5\,\sigma_{\text{exp.}}$. This is
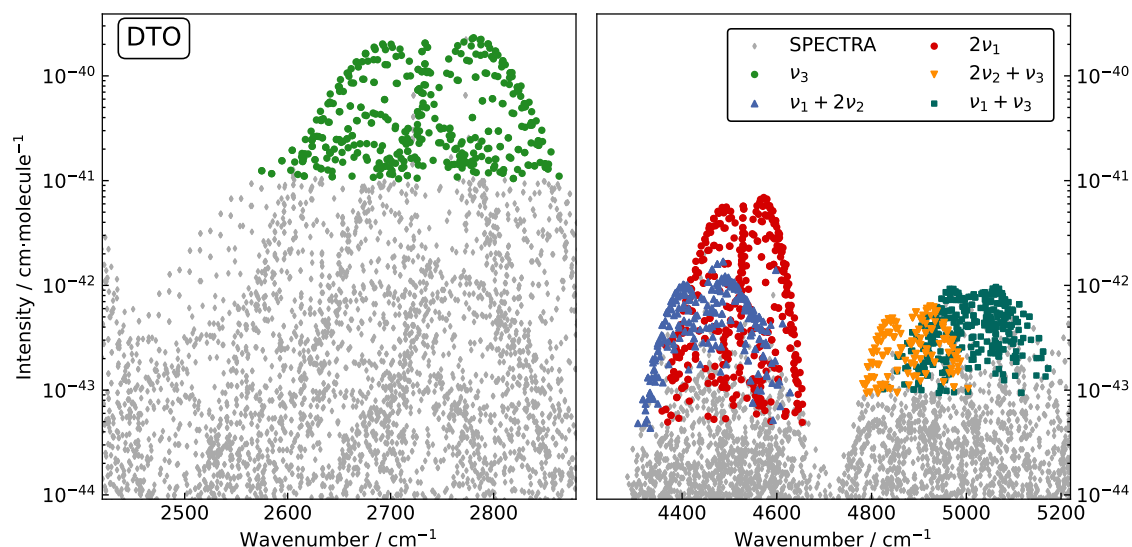
Figure 5.33: Illustration of the measured lines of DTO. Predictions from SPECTRA database are provided for comparison. The line intensities are corrected for the natural abundance of the molecules.

either resulting from misassigned lines, resonances shifting the upper states, or a general limitation of the model for the tritiated water species. A hint of problems with the model is shown by the example of the parameters for the HTO ground state. A different set of parameters was used as in [Hel74] yielding better results for the combined data sets. This raises the question whether the parameters presented describe the rotational states of the molecule or if they are only 'effective' parameters that describe a subset of $\sim 85\%$ and the microwave measurements.

A hint for the influence of resonances unfolds when finding the spectroscopic parameters of the vibrational upper state. The fits were performed using the IR data of a band for a species and an additional Watson parameter for the vibrational energy. Only for 5 bands (out of 13) satisfactory results were obtained. It is suspected that interaction between vibrational bands, the Fermi and Coriolis resonances, is (strongly) influencing these upper states, leading to failure of the model. This assumption is supported by the fact that for all energetic isolated bands the fits of the upper state were performed with great satisfaction. An answer to this topic can only be obtained by further investigation of the fits, including the potential resonances. In addition, the usage of Euler series as a complementary approach could reveal further insights. Pickett et al. performed this work for water achieving better results than with Watson's power series [Pic05]. However, both are beyond the scope of this work.

In the last section of this chapter, a comparison of the acquired data to the ab initio predictions of SPECTRA is presented. Deviations of the order of $0.1\,\mathrm{cm}^{-1}$ have been observed in agreement with the observations of Down, Bray, and Reinking [Dow13; Bra15;
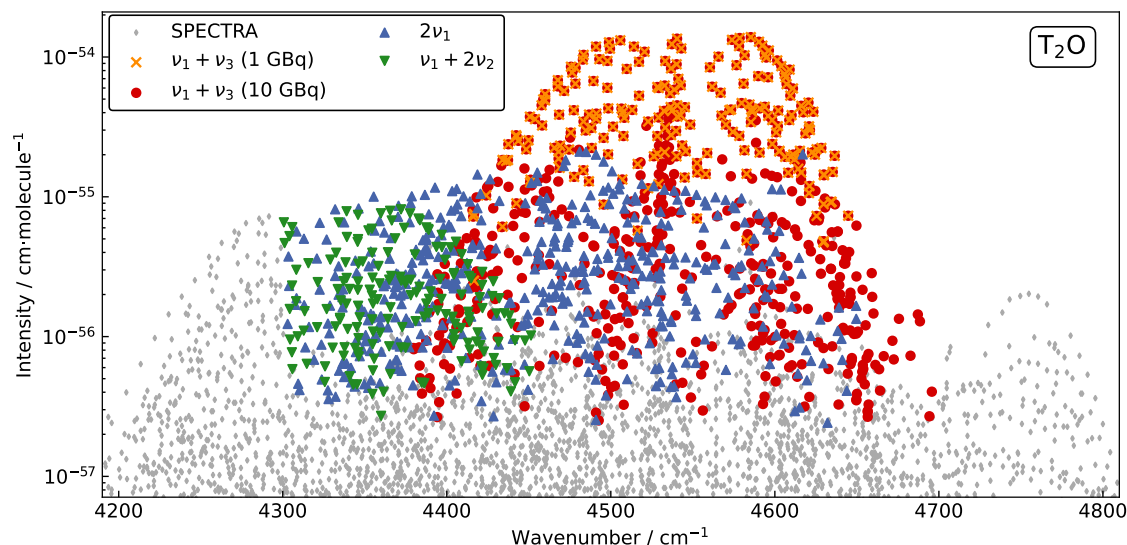
Figure 5.34: Illustration of the measured lines of T$_2$O in this work. Predictions from SPECTRA database are provided for comparison. The line intensities are corrected for the natural abundance of the molecules.

Rei19]. Due to the large data set an analysis on the precision of the vibrational energy and on a potential correlation with rotational quantum number could be performed. The deviations of the measured lines to the predictions are shown to be more or less scattered around a band-specific value that can be positive or negative. This shows that the precision of the vibrational energy is significantly contributing to the deviations. The precision of the vibrational energy is determined with $0.11\,\mathrm{cm}^{-1}$.

An analysis of the individual bands revealed that, in addition to the contribution of vibrational energy, a dependence on rotational quantum number influences the deviation of the prediction on the $0.1\,\mathrm{cm}^{-1}$ scale. It has been shown that for increasing J (respectively, $J(J+1)$) the energies have been underestimated, for increasing K_a in general overestimated. The impact of both dependencies on the vibrational bands varies individually. A link to vibrational quantum number was not found.

With in total 4589 individual lines, a significant data set of water isotopologue lines containing tritium was measured for the first time. This data set is indispensable for tritium detection and tritium monitoring, both fields of growing importance due to the growing and supported fusion branch (see, e.g. for Germany[5]). In nuclear facilities such as nuclear power plants and spent fuel reprocessing facilities, tritium is continuously discharged into the environment [Con17; Hir21], requiring a monitoring device (e.g. [Tan22]) that can be performed with optical methods using these data.

---

[5]Bundesministerium für Bildung und Forschung: https://www.bmbf.de/SharedDocs/Downloads/de/2024/fusion2040_programm.pdf?__blob=publicationFile&v=1

6 Determination of ro-vibrational transitions of HT using NICE-OHMS

The NICE-OHMS experiment on HT was performed in collaboration with the LaserLaB of the Department of Physics and Astronomy at Vrije Universiteit Amsterdam (VU) in Netherlands. The following publications have been obtained from this project: [Coz22a; Coz24a; Her24; Coz24b].

6.1 Overview

The application of the sensitive and precise NICE-OHMS technique on a tritium-bearing molecule is a technological challenge, as cutting-edge spectroscopy and tritium handling need to be combined. Both, spectroscopy and radiation safety, have strict requirements that need to be fulfilled simultaneously. Any unforeseen event during the measurement that interferes with either aspect would lead to an immediate halt of the progress. Therefore, careful development of a rugged concept is required, including tests prior to tritium operation.

In Section 6.2 first the challenges will be outlined and the concept of measurement with regard to principal challenges will be presented. Then, in Section 6.3, the experimental setup is described in three subsystems: (i) the optical setup, including frequency generation, analysis and standard, (ii) the cavity and tritium system, which describes all components in contact with tritium, and (iii) the non-evaporable getter as HT source, which is the key component to generate and store the hydrogen-tritium mixture.

To validate the concept of the sample preparation, a study with this getter type prior to the NICE-OHMS experiment was performed to determine its characteristics for the operation with tritium. This includes a calibrated temperature read-out method by the measurement of the resistance of the getter itself. These sorption tests are performed at TLK and are presented in Section 6.4. The results are presented with implications for the NICE-OHMS experiment. In Section 6.5, an investigation of the optical properties of the cavity is carried out with HD, ensuring proper operational state. In addition to high-resolution measurement of the P(3) $\nu = 0 \rightarrow 2$ line of HD, a general proof-of-principle with the getter was proven in the NICE-OHMS setup. Finally, in Section 6.6, the NICE-OHMS experiment measurement of the R(0), R(1), and P(1) lines of the $\nu = 0 \rightarrow 2$ of HT are presented. The results are subdivided into the general performance of the novel tritium sample cycle system and the spectroscopic findings.

6.2 Challenges and concept of measurement of HT using NICE-OHMS

6.2.1 Tritium-related challenges for NICE-OHMS

The following paragraphs address challenges related to operation with tritium, which subdivide into two main aspects: (i) tritium confinement and (ii) sample production.

(i) **Tritium confinement:** Ensuring the containment of tritium is a mandatory requirement. This can be achieved by using tightly sealed vessels made from materials compatible with tritium. However, for this experiment, the confinement needs to comply with the requirements of the NICE-OHMS technique. This includes two highly reflective mirrors with small tolerance in the parallelism and an optical beam path and a piezo that allows the control of the position of one mirror.

In addition, for this experiment, it is crucial to avoid halogen-containing components, as their radiation-induced decomposition can lead to the formation of halogen hydrides / tritides (e.g., TF, TCl, etc.)[Sch64; Tan65; Kun70] that could lead to the degradation of the high-reflective mirrors [Fis15].

In addition, the setup needs to be decoupled from exterior influences to obtain stability in temperature and motion such that operational stability of the cavity is guaranteed.

(ii) **Sample production:** There are several requirements for the samples to be examined:
(a) Under European law, the total amount of tritium that can be handled outside licensed laboratories is limited to an activity of $1\,\mathrm{GBq}$. This corresponds to an amount of gas of $1183\,\mathrm{Pa\,L}$ of T_2. Being limited to this amount, the generation of samples up to $2\,\mathrm{Pa}$ poses significant challenges to sample production procedures.
(b) An important requirement of this experiment is a correct attribution of the pressure shift of the transition frequencies. For this reason, measurements at different sample pressures must carried out to extrapolate to $p = 0\,\mathrm{Pa}$ and correctly determine the pressure-dependent shift. As confinement does not allow for conventional pumps, this means that a method needs to be considered to regulate the sample pressure without removing tritium from the closed system. In addition, an accurate pressure sensor is required.
(c) The composition of the sample should be reproducible and, to some extent, identical.Any changes in the composition will affect the accurate attribution of the pressure shift to the determined line positions and change the spectral line shape. The hydrogen and hydrogen-containing molecules will, as expected, shift the composition of the tritium-containing sample by exchange reactions. With water in the system, tritium would undergo exchange reactions and stick to the inner surface of the vessels.

6.2.2 Non-evapoarable getter as tritium source

The concept of NICE-OHMS on HT is to utilise the spectroscopic sensitivity of the NICE-OHMS technique in combination with a tritium-compatible high-finesse cavity within a closed hydrogen-tritium gas system.

For the tritium-compatible high-finesse cavity, a method has been developed which provides HT samples at different pressures. At the end of each measurement on a sample, the gas is recovered. In this way, repeated sample productions with different sample pressures can be performed while being restricted to a small and limited tritium reservoir.

The key component is a non-evaporable getter (NEG), here the St171 getter type, from *SAES*. The general function of this getter is described in [Mac12]. It is used in NICE-OHMS to set the partial pressure of the target molecule HT in a range of $0.05\,\text{Pa}$ to $3\,\text{Pa}$ within an experimental setup volume of $\sim 140\,\text{cm}^3$.

The application of NEGs in tritium technology is not entirely unprecedented. James et al. explored the utilisation of NEGs for tritium recovery from molecules, such as ammonia, that dissociate in the getter following their absorption [Jam18]. For tritium extraction from breeding blankets in fusion reactors, helium is intended to be employed as a purge gas where tritium accumulates. Substantial quantities of NEGs will thus be utilised to remove the tritium in a semi-continuous process, enabling its return to the fusion chamber [Ana24]. Santucci et al. further evaluated this capability to eliminate tritium impurities as well from the helium coolant of breeding blankets in fusion reactors, where it permeates in trace amounts, but should be as free as possible from tritium [San20].

In addition to their extensive application in fusion-related activities, NEGs have been utilised for the precise dosing of small amounts of tritium and/or deuterium gas. Specifically, the Project8 experiment employed similar types of getters to introduce small amounts of tritium into a measurement cell [Ash23], while Das et al. [Das20] and Yamamoto et al. [Yam17] used NEGs to supply fusion-based neutron sources with D_2 and T_2:DT:D_2, respectively.

Pictures of the non-evaporable getter by *SAES* of St171 LHI/1,5-7 type welded onto a CF16 electrical feedthrough are displayed in Figure 6.1. The NEG has a cylindrical shape ($\ell = 7\,\text{mm}$, $d = 1.5\,\text{mm}$) and contains $38\,\text{mg}$ of zirconium alloy powder as an active material that is sintered around a $0.2\,\text{mm}$ thick molybdenum wire acting as a heater.

Upon thermal activation at $T = 900\,°\text{C}$, this type of NEG can absorb non-noble gases from a vacuum system through its reactive surface into the bulk when applying high temperatures of $T \geq 450\,°\text{C}$.

Unlike other non-noble gases, the St171 does not form chemical compounds with hydrogen below a certain concentration. Instead, the hydrogen diffuses into the bulk forming a solution following Sievert's law for this type of getter:

$$\log(P) = 3.6 + 2\log(C) - \frac{5200}{T} \tag{6.1}$$
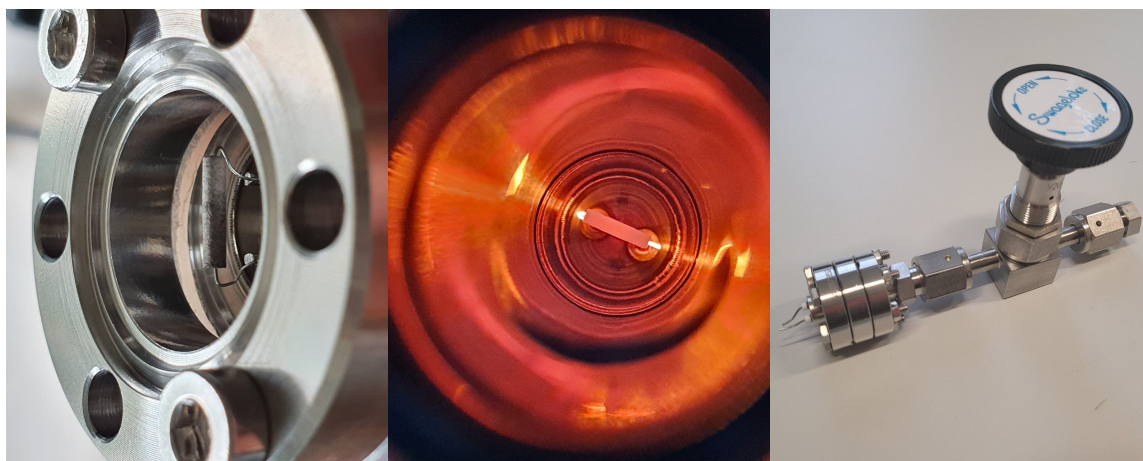
Figure 6.1: Pictures of the tritium getter before and during operation and its containment. Left: The St171 LHI/1,5-7 getter from *SAES* welded on an electrical CF16-feedthrough. Middle: View from location of the optical pyrometer during operation at 900 °C. Right: Getter installed in a small CF16-cell with a valve.

Equation (6.1) describes the relation between the hydrogen concentration inside of the bulk (C in L Torr g^{-1}) of the getter and the hydrogen partial pressure outside of it (P in Torr) which is highly temperature-dependent (T in K).
At room temperature, the partial pressure is very low, at $1.3 \cdot 10^{-10}$ Pa, which allows the use as a hydrogen pump. The here presented information regarding the getter properties and the parameters in Equation (6.1) are provided by *SAES* [1].

6.2.3 Concept of sample production and measurement

The concept of sample production and measurement can be divided into three main aspects: (i) the filling and shipment of the tritium, (ii) the provision of the sample at target pressure and, (iii) maintenance procedures that are implemented to guarantee the stability and reproducibility of the samples:

(i) **Filling and shipment of the tritium:** The loading of the getter, encapsulated in a small CF16-cell with a valve (see Figure 6.1, right picture) for connection to vacuum systems, is performed at the TLK tritium gas-mixture infrastructure *TRIHYDE* [Nie21b]. A defined amount of H$_2$:HT:T$_2$ mixture (with H:T=1:1) equivalent to $1\,\mathrm{GBq}$ activity is filled into the cell with the getter. The activated cold getter material absorbs the gas and traps it inside the bulk. After the valve is closed and the infrastructure is disconnected, the outer surface of the cell is decontaminated and shipped to LaserLaB Amsterdam, where it is installed in the NICE-OHMS setup. A correct installation

---

[1] *SAES*, St171 and St172 - Sintered Porous Getters, https://www.saesgetters.com/industrial/wp-content/uploads/sites/8/2024/02/St-171-172_Sintered-Porous-Getters_1.pdf

is ensured by a leak test with the getter valve still closed. This is followed by an extensive pumping cycle to remove water films on the inside surfaces of the setup, accumulated during installation.

(ii) **Sample preparation:** To release the gas mixture and generate HT samples at specific pressure according to Sievert's law, the getter material must be heated to a specific temperature. This is achieved by applying a DC current to the wire heater of the getter. The temperature is read out in situ from the electrical resistivity of the getter which has been previously calibrated against a pyrometer prior to loading with tritium. The temperature ranges from 500 to $900\,°C$. Sievert's law, providing the relation between the equilibrium pressure of the desorbed hydrogen above the getter surface and the temperature, is provided from *SAES* only for pure hydrogen. Therefore, a sorption study on this getter was performed that includes all isotopes H_2, D_2 and T_2 and a H_2:HT:T_2 mixture (with H:T=1:1). A detailed description and results of this study are presented in the following section.

(iii) **Procedures maintaining sample integrity:** Several maintenance procedures are implemented to ensure the integrity and reproducibility of the samples:

(a) For optimal measurement conditions, high stability of the sample pressure and of the cavity temperature is required. The measurement can take several hours, and continuous heating of the getter is not advised as it would be detrimental to both stability criteria. A valve is used to decouple the getter from the cavity after setting the target conditions. The getter can then be turned off and the thermal perturbation is reduced to a minimum. After measurement, opening the valve is sufficient for the sample gas to be reabsorbed by the tritium getter. Any tritium-hydrogen mixture that comes in contact with the getter material when cold will be absorbed. An accurate pressure gauge connected to the sample volume serves as the process monitor.

(b) The outgassing of hydrogen and residual water from the inner walls of a vacuum system can be a challenging problem, especially when the operating system is decoupled from any exterior gas system due to tritium handling. To handle this challenge, a getter of the same type as the tritium getter but with ten times more getter material is used as a small vacuum pump to remove other species from cell volume. This getter is separated with a valve from the sample volume to not interfere with sample production. It is mostly used after measurement breaks of several hours. In addition, for this procedure, the pressure sensor connected to the sample volume serves as a process monitor. Note that this vacuum getter was implemented to not burden the capacity of the tritium getter with outgassing residual gases. A change in the capacity of the getter can alter its performance and therefore harm the reproducibility of the sample production.

(c) Despite these procedures, the production of (tritiated) water during measurements, possibly enhanced by the radiochemistry of tritium, cannot be excluded. To avoid any impact on measurement performance by absorption from (tritiated) water species,
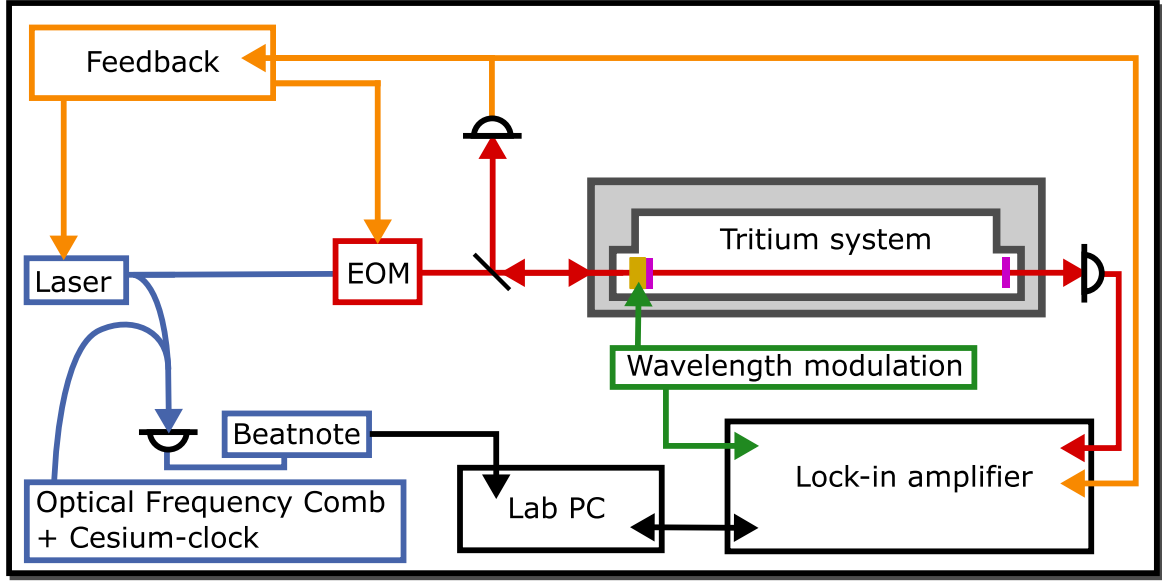
Figure 6.2: Schematical layout of the optical setup of NICE-OHMS. The setup is subdivided in colour-coded themes. Further information are provided in the text.

a cryo-trap cooled by LN_2 is implemented to freeze any produced water or other species during measurements.

6.3 Experimental setup of NICE-OHMS on HT

The setup can be subdivided into the cavity/tritium gas system, which is built only for HT and complies with the tritium-specific requirements and the optical setup.

6.3.1 Optical setup

The optical setup was developed for the operation with the HT cavity used in this work and, including minor alteration, another cavity of the Amsterdam group, from which transition frequencies for water [Dio23], HD [Dio19; Coz22b] and H_2 [Coz23; Dio24] were obtained with high accuracy. Its mostly developed by Frank Cozijn in the frame of his PhD thesis [Coz24b]. The NICE-OHMS technique is described in Section 4.2.

A schematic of the optical setup is presented in Figure 6.2. It is divided into colour-coded subsystems matching with the presented schematical layout:

- **High-accurate laser light generation** ▮ : The carrier laser light is generated by a *Toptica* DL Pro diode laser with a spectral range from 1430 to 1520 nm. By creating a beatnote with a frequency comb laser (*Menlo Systems* FC1500-250-WG) accurate

frequency measurement of the laser on kHz level is implemented. For absolute accuracy on long-term scale, the reference is compared with a cesium atomic clock.

- **Frequency modulation in the cavity** ■ : A custom-built electro-optical modulator (EOM) from *Qubig* generates the sidebands to the carrier with $f_c \pm f_{\mathrm{FSR}}$ where the free spectral range (FSR) is $f_{\mathrm{FSR}} = 405\,\mathrm{MHz}$. The beam consisting of carrier and sidebands propagates through the cavity with two high-reflective mirrors and is recorded with a fast-readout photodiode from *New Focus 1611FS-AC* behind the cavity. The reflection from the first cavity mirror is recorded for feedback mechanisms.

- **Feedback mechanisms** ■ : The collected reflection is used to lock the laser and the sidebands to the length of the cavity. The Pound-Drever-Hall (PDH) locking of the laser [Dre83] and the DeVoe-Brewer locking for the sidebands [DeV84] are implemented by using the reflection from the cavity entrance and are applied on the laser and the EOM. Details are provided in Section 4.2.

- **Frequency scanning and wavelength modulation** ■ : To scan the frequency and therefore generate a line profile, the length of the cavity is varied using a piezo on one of the high-reflective mirrors. Due to the feedback-loop that assures the lock of the carrier and the sidebands, resonance conditions are maintained during the scan. The wavelength modulation is implemented by applying a low-frequency dither ($f_{\mathrm{dit.}} = 395\,\mathrm{Hz}$) on the piezo. By subdividing a triple-stack piezo into two for scanning and one for the wavelength modulation, the so-called dither, the technical implementation is realised. The applied amplitude of the modulation is varying peak-to-peak amplitudes, in this application set to $100\,\mathrm{kHz}$.

- **Recording of the NICE-OHMS signal** ■ : The NICE-OHMS signal is recorded by a fast-readout photodiode from *New Focus 1611FS-AC*. To obtain the dispersion, a demodulation with f_{FSR} is performed using a *Zurich-Instruments* HF2LI Lock-in amplifier. The phases need to be set correctly to separate absorption and dispersion signals. By demodulation with $f_{\mathrm{dit.}}$ the derivative signals $1f$ is obtained. The corresponding accurate frequency values are obtained from the beatnote measurement.

The laser beam, photo-detectors, EOM and further optics are installed into thermally isolated and controlled enclosures in front and behind the cavity, both purged with dry nitrogen. These enclosures ensure (i) low thermal drift, especially important for the EOM; (ii) low absorption of the beam on atmospheric water, and (iii) a quick exchange of the optical instrumentation between both cavities of the Amsterdam group. A picture of the open box in front of the cavity is presented in Figure 6.3.
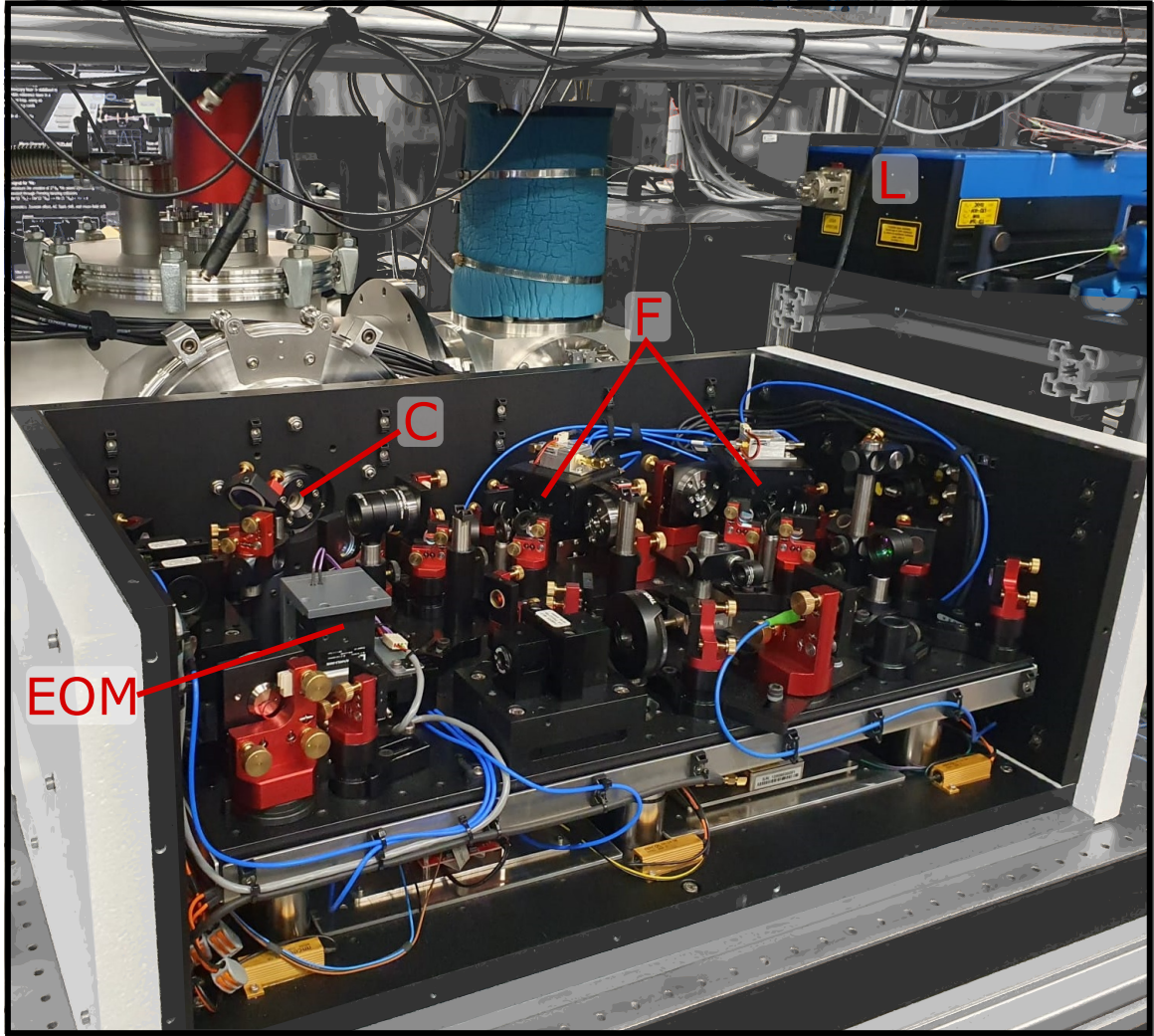
Figure 6.3: Picture of the optical setup with open box. Compact beam path setup fixed in front of the cavity (C) mounted on a breadboard in a thermally controlled and isolated box. One of two lasers (L) can be coupled in. Most important devices are the electro-optical modifier (EOM) and two feedback photo-detectors (F) for short and longterm stabilization and locking of the cavity.
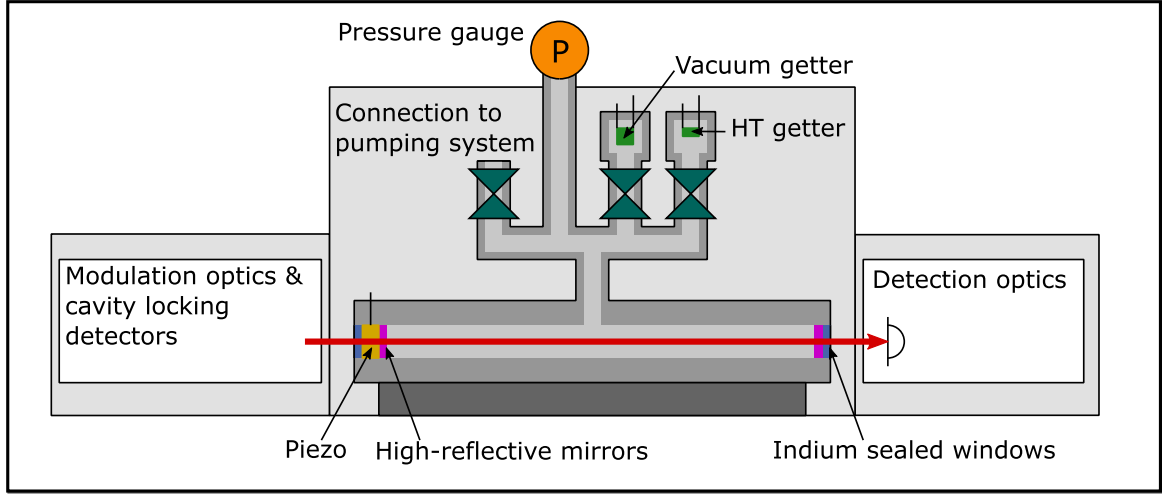
Figure 6.4: Sketch of the cavity and the tritium gas system of NICE-OHMS. A cavity consisting of two high-reflective mirrors and a piezo is connected to a gas system with a smaller getter, containing the tritium-hydrogen mixture, a larger getter, acting as vacuum pump, a process-monitoring pressure gauge, and a connection to a pumping system which is sealed off, before first tritium exposure. The entire cavity assembly is housed in a secondary, evacuated enclosure.

6.3.2 Cavity and tritium gas system

A sketch of the cavity and the tritium gas system is presented in Figure 6.4. The setup consists of a fully custom-built cavity made from aluminium with indium-sealed windows at each rear end. The $37\,\mathrm{cm}$ long cavity is hemispherical with a curved mirror at a radius of curvature of $2\,\mathrm{m}$. The two mirrors are custom-produced by *Layertec* with a reflectivity of $R = 99.996\%$ for the wavelength of the laser (TOPTICA DL Pro) of $1430\,\mathrm{nm} < \lambda < 1520\,\mathrm{nm}$. A triple-stack piezoactuator at one of the mirrors allows for small-scale adaptation of the cavity length, also used for the wavelength modulation.

Stainless steel tubing connections from the cavity grants access to a *Pfeiffer* 365CMR pressure gauge, a (larger volume) non-evaporable getter *SAES* St171 HI/7,5-7 acts as a vacuum pump and a (smaller volume) non-evaporable getter *SAES* St171 LHI/1,5-7 loaded with a H_2:HT:T_2 mixture (with H:T ratio = 1:1) equivalent to $1\,\mathrm{GBq}$ activity for the HT sample provision and removal from/to the laser-gas interaction volume.

Before the initial exposure to tritium, the system was evacuated using a connection to a pumping system. Furthermore, a LN_2-cooled cryotrap is included to capture any potentially generated (tritiated) water or other species. This part of the system exposed to tritium has a volume of $\sim 140\,\mathrm{cm}^3$ and was tested for leaks below the detection limit of $1 \cdot 10^{-9}\,\mathrm{Pa\,L\,s^{-1}}$. To isolate the cavity from acoustic and thermal disturbances, it is surrounded by a secondary enclosure evacuated to below $1 \cdot 10^{-2}\,\mathrm{Pa}$. The valves between the attachments of the cavity assembly can be operated from outside of the secondary enclosure through rotational feedthroughs. A picture of the tritium setup with open secondary enclosure is depicted in Figure 6.5.
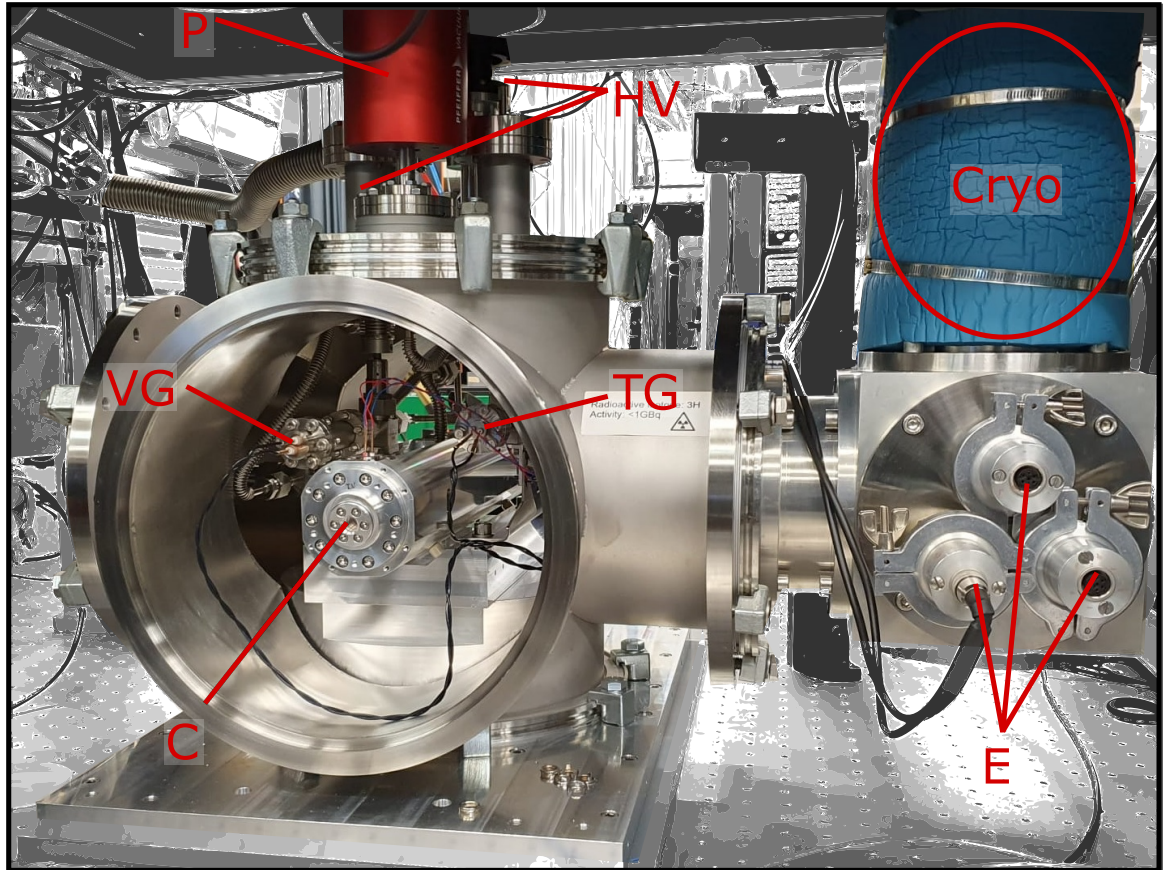
Figure 6.5: Picture of the NICE-OHMS setup with open second shield. Front view of the closed and sealed cavity (C) with the two getter components, the vacuum getter (VG) and the tritium getter (TG). The hole assembly is housed in a secondary shield which will be closed with a ISO-flange with a window and evacuated with a turbomolecular pump. To operate the getters and the piezo of the cavity, electrical feedthrough (E) have been installed. The valves in front of the getter components can be operated by mechanical feedthroughs on the top (HV). The pressure sensor (P) is placed outside of the evacuated secondary shield. A cryo trap is been included to trap (tritiated) water produced during operation.

6.4 Sorption study with getter tritium source

> The sorption study was developed with Benedict Rothmund in the frame of his Bachelor's thesis [Rot21].

For the NICE-OHMS experiment on HT, the reversible tritium storage using the NEG St171 from *SAES* is a crucial asset. It offers repetitive measurements with tritium at different pressures although being restricted to small activity. The performance of this component depends on the sorption properties of hydrogen isotopologues, while those containing tritium have not yet been studied in great detail. To determine these properties, a study on the *SAES* St171 getter using H_2, D_2, T_2 and a H_2:HT:T_2 mixture (with H:T=1:1) has been performed in the TLK prior to the construction of the NICE-OHMS experiment. The study is designed to mimic the dimensions of the planned NICE-OHMS experiment. The study is presented in the following of this section, describing concept, experimental setup, measurements and results.

6.4.1 Concept of getter temperature measurement and control

Hydrogen sorption by the St171 getter is temperature-dependent (cf. Equation 6.1), thus reliable in-situ temperature measurement is mandatory. This can be performed by pyrometric measurement. For the final getter assembly, incorporating such a sensor is very challenging due to experimental restrictions in the tritium glove system and in the NICE-OHMS setup.

Thus, the method of choice is the read-out of the temperature from the electrical resistivity of the getter heater itself, previously calibrated against the pyrometric standard. Note that the temperature of the getter material is not homogeneous throughout its surface. Differences of up to $20\,\mathrm{K}$ have been observed, which is taken into account when considering the accuracy of temperature measurements or temperature-dependent effects.
In Figure 6.6, the concept of measurement and calibration of the getter temperature is shown.

6.4.2 Experimental setups

According to the concept, the *Calibration system* is used to measure the current-temperature dependence, $I(T)$, while the *Tritium system* is employed for measuring the resistance-current dependence, $R(I)$, as part of the calibration process and for the actual sorption measurements, including tritium. A sketch of both setups can be found in Figure 6.7. The contributions of systematic effects by all measurement devices are listed in Table 6.1.
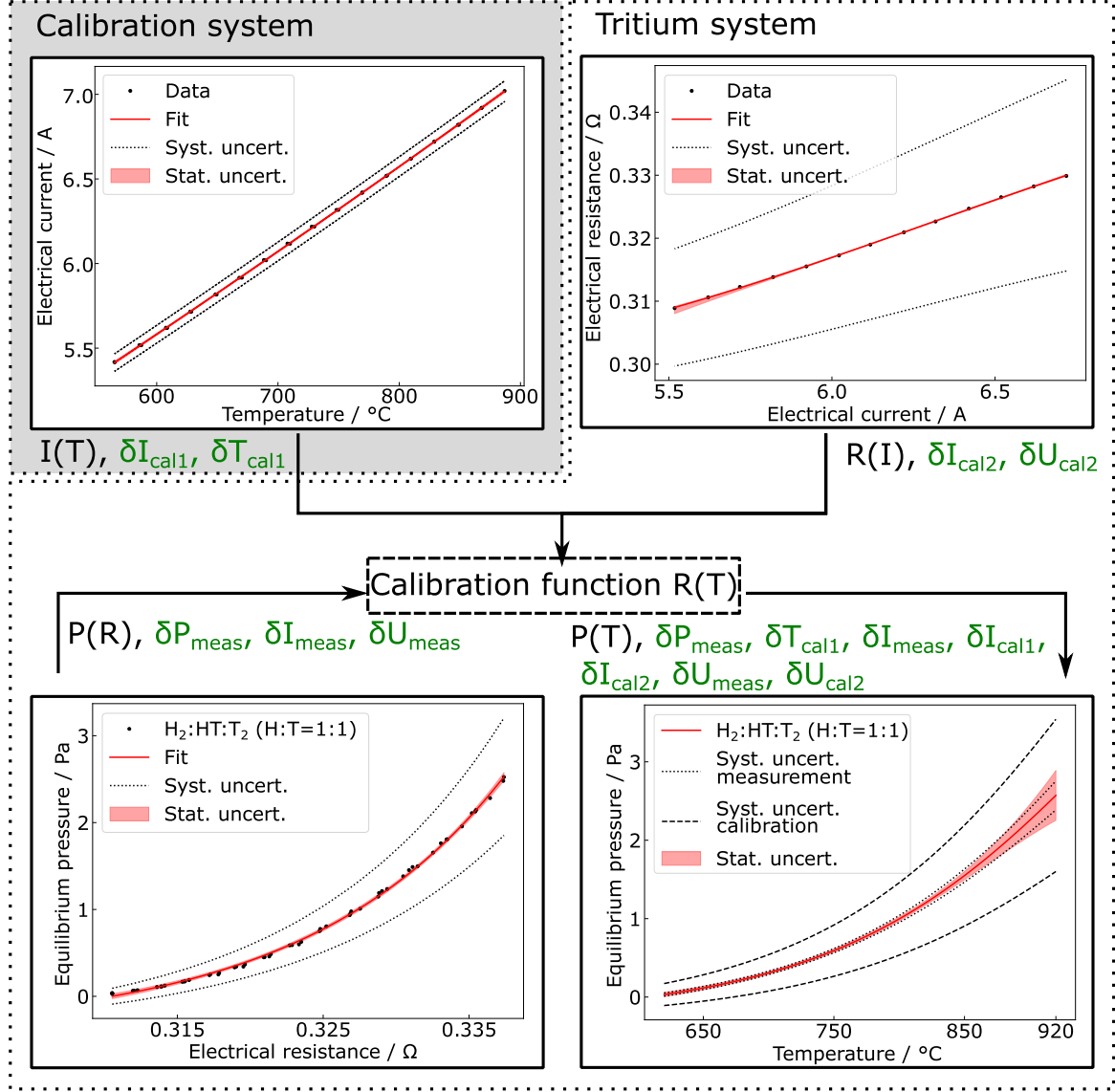
Figure 6.6: Concept of the measurement procedure. Top left: Optical pyrometry combined with a measurement of the operation current of the getter in a dedicated *Calibration system* provide the relation $I(T)$. Top right: At the final location of the getter in the *Tritium system*, the relation of resistance to heating current curve $R(I)$ are calibrated. Bottom left: In addition, in this system the pressure is measured with a pressure gauge as a function of the resistance P(R). These functional dependencies are put together in order to obtain a relation of pressure and temperature in the actual sorption measurement, P(T). The contributions to the systematic uncertainties have been indicated for each step in green with the symbol of the physical quantity. Values can be found in Table 6.1.

Table 6.1: Overview of the sources of systematic uncertainties resulting from each measurement device. Since multiple measurements have been combined for calibration, certain uncertainties may contribute multiple times to the final results. These contributions can depend on the value ($val.$) as-well as on the full scale ($F.S.$) of the device.

Device	Phys. quantity	Symbol	Description	1σ uncertainty
Pfeiffer CMR 365	Pressure	δ_{P}	Uncertainty	$5 \cdot 10^{-3}$ $val.$
			Resolution	$3 \cdot 10^{-5}$ F.S.
			Effect temp. zero point	$2 \cdot 10^{-4}$ F.S.
			Effect temp. range	$3 \cdot 10^{-4}$ $val.$
Pfeiffer TPG 362	Pressure	δ_{P}	Measurement gain	$1 \cdot 10^{-4}$ F.S.
			Offset	$1 \cdot 10^{-4}$ F.S.
			Resolution A/D conv.	$1 \cdot 10^{-5}$ F.S.
Optris CTLaser 1ML	Temperature	δ_{T}	Uncertainty	$3 \cdot 10^{-3}$ $val.$ $+2\,°C$
			Transmission window	$2\,°C$
			Emissivity getter	$2\,°C$
Fluke 117	Current$< 6\,A$	δ_{I}	Uncertainty	0.01 $val.$ $+3 \cdot 10^{-3}\,A$
	Current$> 6\,A$	δ_{I}	Uncertainty	0.01 val $+3 \cdot 10^{-2}\,A$
Fluke 114	Voltage	δ_{U}	Uncertainty	$5 \cdot 10^{-3}$ $val.$ $+2 \cdot 10^{-3}\,V$

6.4.2.1 Calibration system

The *Calibration system* consists of the welded getter mounted on a vacuum cell (VC / a). The temperature of the getter is measured through a glass window using an optical pyrometer *Optris* CTLaser 1ML. A connection to a pumping system is used to create and maintain vacuum conditions. The inner volume of the *Calibration system* is given by $30\,\mathrm{mL}$.

6.4.2.2 Tritium system

The *Tritium setup* reuses the same getter-feedthrough assembly as for the calibration to preserve the thermoelectrical properties. The vacuum cell (VC/b) is identical to the *Calibration system*, but with a blind flange replacing the pyrometer window. Using mostly the same parts as for the calibration, from the perspective of the getter, the direct environment is identical within $99.5\,\%$ of the spatial angle. Note that the geometry of the surrounding vessels affects the power balance of thermal radiation by a different fraction of losses and reflections. A reference volume (RV) combined with a *Pfeiffer* CMR 365 pressure sensor is connected by valves on either of the two sides to the getter-cell (VC/b) and the
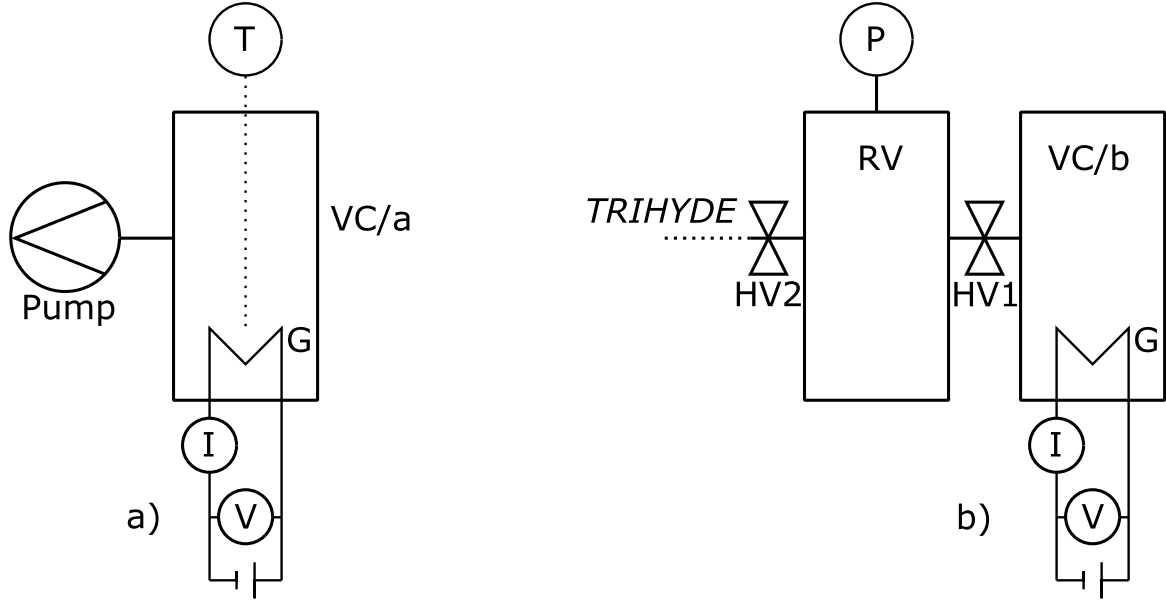
Figure 6.7: (a) Calibration system: The *SAES* St171 LHI/1,5-7 getter (G) powered with current (I) and
voltage (V) readout. A pyrometer *Optris* CTLaser 1ML (T) is measuring the temperature through a
glass window. The vacuum cell (VC/a) is evacuated through a pumping system (Pump); **(b) Tritium
system:** The system is consisting of vacuum cell of the getter (VC/b), reference volume (RV), a *Pfeiffer*
CMR 365 pressure sensor (P) and valves (HV1&2) to separate vessels and the reference volume from
the TLK infrastructure *TRIHYDE* [Nie21b] providing tritium-gas mixtures and a pumping system.

tritium gas-mixture infrastructure *TRIHYDE* [Nie21b], respectively. The inner volume of
the *Tritium setup* is given by (61.8 ± 0.4) mL.

6.4.3 Measurements of tritium sorption study

The measurements are performed according to the concept depicted in Figure 6.6, with (i)
calibration measurements for temperature and (ii) sorption measurements for hydrogen
mixtures.

6.4.3.1 Calibration of temperature measurement

The getter-feedthrough assembling is calibrated in a two step process. First, the surface
temperature (T) is measured in the *Calibration system* with an optical pyrometer as a
function of the getter heating currents (I) in steps of $\Delta I = 0.1$ A between 5.4 A and
7.0 A at high vacuum conditions ($< 4 \cdot 10^{-2}$ Pa). The upper limit for the temperature is
$T_{\mathrm{max}} = 900$ °C which is recommended from the manufacturer *SAES*.
In a second step, the getter-feedthrough assembling is installed to the *Tritium system* at
the tritium gas-mixture infrastructure *TRIHYDE* [Nie21b] of the TLK. Under high vacuum

conditions, the electrical resistance (R) is measured for the same operation parameter as used in the calibration setup.

Using the current-temperature relation $I(T)$ of the first step (calibration) and the resistance-current relation $R(I)$ of the second step, we can find a functional relation of $R(T)$ during a measurement of the sorption at different operation powers.

6.4.3.2 Sorption measurement

Initially, the getter material is activated by operating it at $900\,^\circ\mathrm{C}$ for 10 minutes in a high vacuum. The required current to reach this temperature, i.e. $7.0\,\mathrm{A}$, is taken from the calibration process.

For comparability of sorption measurements of the different hydrogen mixtures, the amount of the investigated gas mixture has to be well defined. For that purpose, a reference volume (RV) with a capacitance pressure sensor (P), connected to a valve (HV1) to the cell (VC/b) with the getter (G), is filled with a defined amount of gas. The subsequent loading to the getter is then performed by opening the valve HV1.

After opening the valve (HV1) into the getter cell, the defined amount of hydrogen is absorbed by the getter, recorded by the drop in pressure below the lower range of the pressure sensor of $<4 \cdot 10^{-2}\,\mathrm{Pa}$ (except for the loading of tritium where $^3\mathrm{He}$ remains). During the measurements, the parameters: (i) pressure of the desorbed gas, (ii) electric current (I) and (iii) voltage (V) applied to the heater of the getter are recorded for the operation range of 5.4 to $7.0\,\mathrm{A}$ in steps of $0.1\,\mathrm{A}$.

For each current set-point, certain amount of settle time, typically about $5-10\,\mathrm{min}$, is spent in order to allow for stabilization of the system. Static conditions are assumed when the pressure value reaches a plateau. The unloading of the getter is performed by operating at $900\,^\circ\mathrm{C}$ while evacuating for $30\,\mathrm{min}$. Note that the duration of the unloading process depends on the loaded amount, pumping speed of the system, and the temperature of the getter.

For the D_2 and H_2 measurements, the amount of $(2.20 \pm 0.02)\,\mathrm{Pa\,L}$ is loaded at room temperature. For reproducibility proof, the H_2 measurement is repeated with equal amounts of gas.

The tritium gas supplied for the experiments contained approximately 2% of the tritium decay product $^3\mathrm{He}$, which is not absorbed by the getter. For that reason, the loading of T_2 and of a mixture of H_2:HT:T_2 (with H:T ratio = 1:1) is performed with an additional step, where the remaining amount of $^3\mathrm{He}$ after the first loading is replaced by the same amount of $^1/_2\,\mathrm{T}_2$.

The amounts of loaded tritium gas in this work are $(2.22 \pm 0.02)\,\mathrm{Pa\,L}$ for T_2 and $(2.21 \pm 0.02)\,\mathrm{Pa\,L}$ for H_2:HT:T_2. The amount of gas corresponds for a mixture of H_2:HT:T_2 (with H:T = 1:1) to the total activity of $1\,\mathrm{GBq}$. This is the same amount of gas that is planned for the NICE-OHMS experiment.

6.4.4 Results and discussion

The results of the sorption study are subdivided into (i) calibration and (ii) sorption measurements.

6.4.4.1 Calibration

The calibration is performed as described in the Section 6.4.1 and sketched in Figure 6.6. In the range of 5.4 to $7.0\,\mathrm{A}$, 34 temperature/current data points are recorded at the *Calibration system* to obtain the operating current-temperature function $I(T)$ by a polynomial fit. At the *Tritium system*, 25 data points of applied voltage and current from 5.4 to $7.0\,\mathrm{A}$ are measured. The function $R(I)$ resulting from a polynomial fit of the voltage-current measurement and the function $I(T)$ are then combined with the calibration function $R(T)$. Both systematic uncertainties resulting from the pyrometer, amperemeter, and voltmeter, as well as statistical uncertainties, are taken into account. In Figure 6.6, the contributions are indicated in green with the symbol of the associated physical quantity. In Table 6.1 the individual contributions from each measurement device are shown. When propagating the calibration from the pyrometer to the resistance / temperature dependence of the getter, these uncertainties lead to a rather high systematic uncertainty in the absolute temperature ($\Delta_{\mathrm{sys}}T_{\mathrm{calibration}} \approx 50\,\mathrm{K}$). This will affect the sorption curves of all species at the same time. All calibration fit parameters can be found in the Appendix B.1.3.

6.4.4.2 Sorption measurements

In Figure 6.8, for each gas sample the recorded pressure is plotted as a function of the electrical resistance of the getter, obtained from the voltage and current measurement. Note that the change of the electrical resistance is assumed to depend on the temperature of the getter. All four gas samples are covering a pressure range from $2.5\,\mathrm{Pa}$ down to the lower range of the pressure sensor of $4 \cdot 10^{-2}\,\mathrm{Pa}$. For H_2, both measurements show no significant difference which demonstrates the reproducibility of the method.

Resistance offset correction   For each of the four samples, an exponential fit was performed showing a slightly different offset for each cycle in electrical resistance. This offset is independent of the pressure in the cell but increased throughout the measurement campaign.
The data and the exponential fits are corrected by these systematic offsets using the mean value of the measured resistance of all measurements at operation at lowest pressure.
Due to the different offsets of the resistance for each cycle, in addition to the systematic uncertainty of the calibration, there is a second smaller systematic uncertainty ($\Delta_{\mathrm{sys}}T_{\mathrm{measurement}} \leq 7\,\mathrm{K}$) that affects the curves individually.
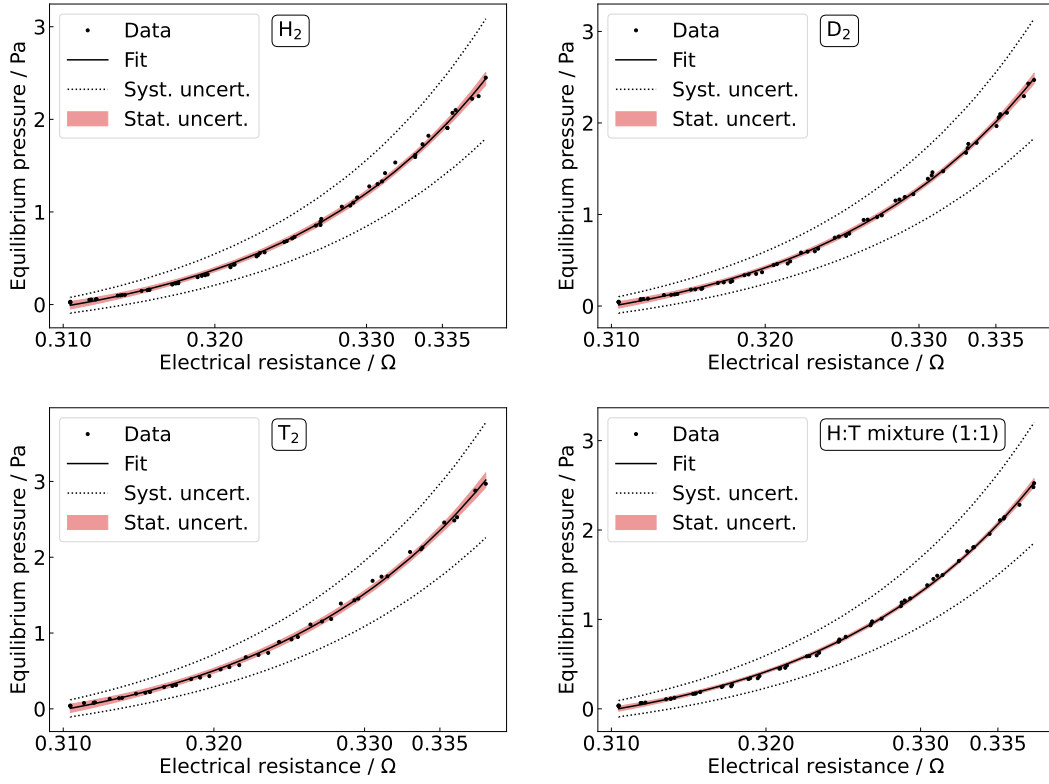
Figure 6.8: Recorded equilibrium pressures for all four loaded gases over the electrical resistance of the getter. The equilibrium pressures of the desorbed gas from a *SAES* St171 LHI/1,5-7 getter after almost equal H_2, D_2, T_2 and H_2:HT:T_2 mixture (with H:T=1:1) loadings for operations between 5.4 and 7.0 A. The resistance is formed by the simultaneous measurement of the current and the applied voltage.

Sorption results on the temperature scale Figure 6.9 shows a comparison of the pressure of the desorbed gases as a function of the getter temperature for the four samples. The functions were found from the sorption data set for the individual gases after converting the corrected resistance values using $R(T)$ from the calibration to a temperature. The fit functions are arbitrarily chosen with

$$P = \mathrm{A} \times \exp\left(\mathrm{B} \times (T - T_0)\right) + \mathrm{C}, \tag{6.2}$$

in units of Pa and °C. T_0 is $770\,°\mathrm{C}$. The parameters can be found in Table 6.2. The stated uncertainties to these parameters were found using Monte-Carlo in order to be in accordance with the uncertainties of the experiment.

Using the properties given by the manufacturer *SAES* (cf. Equation 6.1) and combining it with the loaded amount and volume of the sorption experiment, the expected equilibrium pressures for this experiment can be found. A comparison of the data reveals that all of
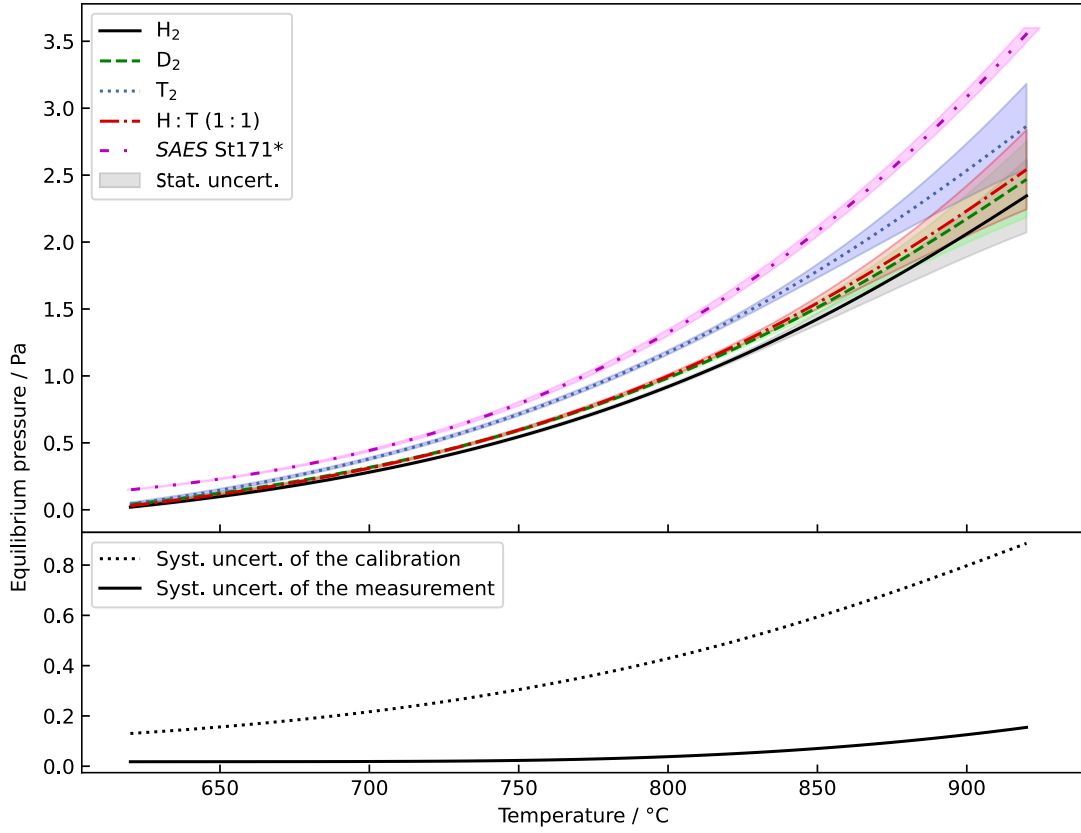
Figure 6.9: P(T) functions obtained from sorption measurements of H$_2$, D$_2$, T$_2$ and a H$_2$:HT:T$_2$ mixture (with H:T=1:1) for the selected operation range. The curves are generated by combining the sorption measurement (P(R)) and the calibration function ($R(T)$). The systematic uncertainty of the calibration affects all curves equally, while the systematic uncertainty of the measurements may be different for different measurements. The expected equilibrium pressures taking the loaded amount, system volume and getter properties from *SAES* are plotted for comparison.

the curves fall below the expected values, although they remain within the experimental uncertainties. A general pressure offset highly supports the hypothesis that the temperature might be overestimated. For calibration temperature differences, up to $20\,\mathrm{K}$ could be observed and the hottest part was measured, so an overestimation is plausible.

Potential isotope effect Isotopic effects were observed for similar *SAES* getter types, for the St172 by Yamamoto et al. [Yam17], and for the St101 and St707 by Boffito et al. [Bof83]. In the case of Yamamoto et al. investigating the St172 type, a significantly lower desorption for tritium was observed compared to hydrogen. Boffito et al. observed slightly higher desorption properties for deuterium compared to hydrogen using the St101 and St707 types.

Table 6.2: Obtained parameters for the desorbed hydrogen samples H_2, D_2, T_2 and a H:T mixture with (almost) equal loadings in the sorption experiment. The fit function for the pressure is given with: $P = A \times \exp{(B \times (T - 770))} + C$ in units of Pa and for temperatures (T) in °C. The measured electrical resistance has been obtained from the desorption measurement and is converted to a temperature using the calibration process described in the text. Note that these relations are only valid for the analysed range. Uncertainties were derived using a Monte-Carlo approach. Covariance matrix elements Cov_{ij} are provided as well.

Gas species	H_2		D_2		T_2		H:T mixture	
Parameter	Value	2σ	Value	2σ	Value	2σ	Value	2σ
$A \times 1$	1.2	(0.4)	1.2	(0.4)	1.6	(0.7)	1.3	(0.3)
$B \times 1 \cdot 10^3$	6	(1)	6	(1)	5	(2)	6	(1)
$C \times 1 \cdot 10^1$	−4	(4)	−5	(4)	−7	(6)	−5	(3)
$\text{Cov}_{AB} \times 1 \cdot 10^4$	−2		−2		−4		−1	
$\text{Cov}_{AC} \times 1 \cdot 10^2$	−4		−4		−1		−3	
$\text{Cov}_{BC} \times 1 \cdot 10^4$	2		2		3		1	

Taking into account individual and statistical systematic uncertainties, there are no significant differences in the desorption of various hydrogen species at a temperature greater than 850 °C. For T_2, however, an overall higher pressure can be observed for temperatures below 850 °C. The difference of H_2 and D_2 in this range is not significant.

The curves for H_2 and D_2 in the measurement agree on the level of the stated uncertainties. For the H_2:HT:T_2 mixture, the curve is between those of H_2 and T_2, which is plausible.

The measured differences in desorption can affect the composition of the desorbed gas for isotope mixtures such as the one here for the mixture H_2:HT:T_2. Based on the measurements of pure T_2 and H_2, an estimation of the composition of the desorbed gas can be made using the following assumptions:

- Even at 900 °C more than 90% of the gas is absorbed in the getter material. Therefore, the difference in hydrogen (isotope) concentration within the getter at each temperature can be neglected and is assumed to be the same for H and T (difference of concentration < 1.5 %).

- The different isotopes have very limited influence on each other within the bulk. This assumption may be justified in the given cases as the ratio of gas atoms to getter atoms is less than 6 ppm.

The recorded desorption pressures of H_2 and T_2 together with the temperature-dependent equilibrium constants for H_2:HT:T_2 mixtures [Jon48], the gas composition can be estimated for a sample of a mixture H_2:HT:T_2 (with H:T = 1: 1) as a function of temperature, as shown in Figure 6.10. During desorption, the gas temperature is significantly higher than after it is isolated at room temperature, which is the measurement condition in NICE-OHMS. The
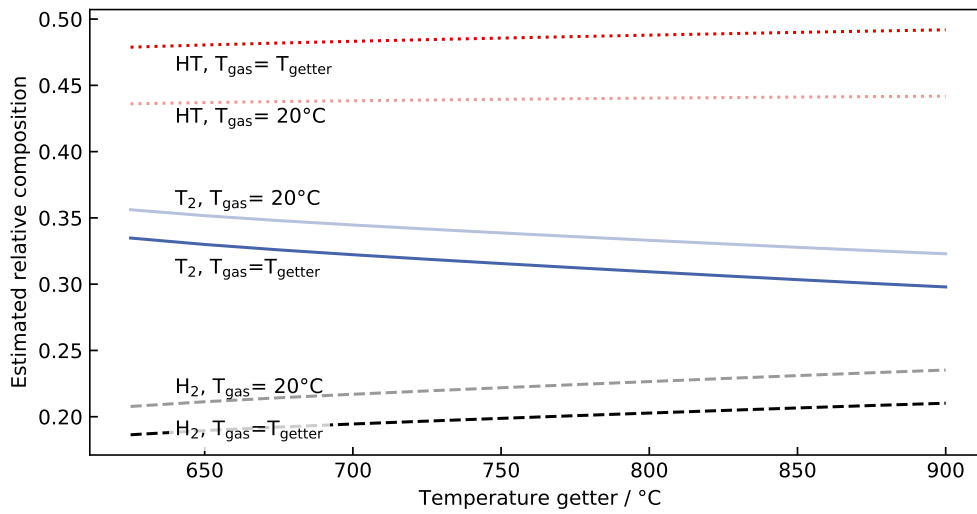
Figure 6.10: The estimated composition of the desorbed gas from a St171 getter loaded with a H_2**:HT:**T_2 **mixture (with H:T=1:1).** The estimation is calculated from the sorption measurements of the pure H_2 and T_2 measurements. The composition is given for equilibrium at getter temperature and at 20 °C and obtained using the equilibrium constant for the corresponding temperature from [Jon48].

impact on the equilibrium constant leads to a shift in the composition as indicated in the figure.

Throughout the operation range, the composition remains stable (change of concentration from peak to peak for HT $< 0.7\%$). However, a cooling of the gas, which usually occurs by collision of gas particles with the walls of the experimental setup, can have a significant impact on the composition (see the shaded lines in Figure 6.10).

In [Nie21a] an investigation on the self-equilibration times of such gas mixtures has been performed for pressures in the range of 200 to $900\,\mathrm{mbar}$. It has been shown that for low pressures the self-equilibration times are drastically increased, however, remaining on the order of few hours. In addition, the influence of surface interactions is yet unknown, which is required for further discussion about the expected composition.

Attention has been paid to this potential effect during the NICE-OHMS measurements, but no noticeable impact was observed.

6.5 Validation of the experimental setup and measurement of the P(3) transition of HD

Once tritium is released into the cavity/tritium system, no changes of the setup can be made. For this reason, it is indispensable to test every component in advance for correct installation and functionality. A good method to ensure functionality and quality of the cavity and to validate the general concept using the two-getter gas sample provision is to perform measurements with HD. HD has very similar physical and chemical properties (except for properties related to radioactivity) and has a transition, the P(3) of the $\nu = 0 \rightarrow 2$ (J=3 $\rightarrow$ 2), within the ranges of high reflectivity of the mirrors and of the laser that will be used for HT.

This study has the objectives: (i) proof of applicability of the two-getter gas sample provision, (ii) test of performance of cavity, and (iii) determine general differences during measurements with pure HD and H_2:HD:D_2 gas mixtures when using the getter.

The experimental setup consists of the same cavity/tritium gas system as presented in Section 6.3.2 except for the secondary containment but with an additional connection to a HD gas bottle.

6.5.1 Proof-of-principle of two-getter gas sample provision

Although it has been proven in the sorption study (cf. Section 6.4) that the getter will reversibly absorb tritium and achieve the required pressures, its applicability must be confirmed in the environment of the intended operation. The cavity/tritium gas system with two SAES getters (St171 LHI/1,5-7 for H:D storage and St171 HI/7,5-7 as a vacuum pump) is used. Note that the getters are renewed for tritium operation.

By filling a segment of the setup of known volume with HD from the gas bottle up to a certain pressure, the storage getter can be loaded with the amount of $2.2\,\mathrm{Pa\,L}$, corresponding to $1\,\mathrm{GBq}$ activity of HT. After loading, the system is evacuated with a turbo-molecular pump below detection limit of $1 \cdot 10^{-2}\,\mathrm{Pa}$.

The proof-of-principle is demonstrated by targeting different sample pressures in the range of 0.05 to $10\,\mathrm{Pa}$ and capturing back the gas using the properties of the getter when not heated. The applicability of the vacuum getter is proven by evacuating the system below $1 \cdot 10^{-2}\,\mathrm{Pa}$ every few days for a period of 3 weeks. Note that for this validation, the gas load for the vacuum getter is significantly larger than for the tritium campaign, where an extensive cleaning and pumping cycle is intended.

The following results were obtained:

- With a loaded amount corresponding to the amount of $1\,\mathrm{GBq}$ H:T (50:50), sample pressures of $\sim 3\,\mathrm{Pa}$ can be achieved inside the cavity. This is consistent with the results of the sorption measurements (cf. Section 6.4).

- Reabsorption of the gas into the getter required several reactivation procedures of the getter. This is performed by heating it to $\sim 850\,°C$ for a few minutes. Closing the valve of the getter module during reactivation hinders a rise of the pressure in the system and is therefore helpful for reaching low pressures.
  It is estimated that residual gas in the system that out-gassed during the measurement is picked up by the reactive surface of the getter, which is subsequently blocked for hydrogen absorption. Only by reactivation do the collected residual gases move into the bulk and the reactive surface is restored.

- The St171 LHI/7,5-7 getter was shown to have sufficient pumping speed and capacity to restore vacuum quality below the limit of the pressure sensor of $1 \cdot 10^{-2}\,\mathrm{Pa}$.

- The outgassing was observed to be strong. This can be explained by the small volume-surface ratio of the system and by the fact that, for the proof-of-principle, no bake-out or cleaning procedures have been implemented.

  However, in response to this observation, a cryo trap is added to the setup to freeze and cryo-pump potentially formed or outgassing water during measurements such that the performance of the measurement is not impacted. During the first operation with tritium, the amount of frozen water was found to be negligible.

6.5.2 Validation of the optical performance of the cavity

To measure the optical properties of the cavity and ensure clean and well-orientated mirrors and correctly operating piezo, (i) the laser must be locked to the cavity, (ii) the finesse of the cavity is measured, and (iii) NICE-OHMS measurements with residual water in the system and (iv) HD are performed.

Locking of laser to cavity   First, the laser is coupled to the cavity. As described in the experimental setup in Section 6.3.1, this is performed by recording the back-reflection of the laser light from the cavity. A PID controller regulates the wavelength using the Pound-Drever-Hall technique. The laser is locked in such a way that resonance conditions ($\lambda = 2\,\mathrm{FSR}/n, \ \ n \in \mathbb{N}^+$) are maintained. Small drifts and motions of the cavity are corrected by the locking.

To obtain a good estimate of the quality of the cavity, the in-coupling efficiency η_{inc} of the laser into the cavity is an appropriate observable. It is determined by taking the ratio of the back-reflection in $I_{\mathrm{in\ lock}}$ and out $I_{\mathrm{out\ lock}}$ of the resonance.

$$\eta_{\mathrm{inc}} = \frac{I_{\mathrm{in\ lock}}}{I_{\mathrm{out\ lock}}}.\tag{6.3}$$

For this cavity, the determined in-coupling efficiency is found to be $\sim 70\%$, which shows clean mirrors and proper installation.

Measurement of the finesse   A finesse of the cavity of $F = 80000$, stable at the level of $\Delta F = \pm 5000$ due to the wavelength dependence of the mirror reflectivity, has been derived from the width of the resonance fringes. With a maximum laser power of $P_{\text{in}} = 26\,\text{mW}$ and the incoupling efficiency of $\eta = 70\%$, this adds up to

$$P_{\text{eff}} = P_{\text{in}} \cdot \eta \cdot \frac{F}{\pi} \approx 460\,\text{W}. \tag{6.4}$$

Note, that the incoupling efficiency needs to be measured regularly.

Measurement of H$_2$O lines   To ensure operation of the piezo, a measurement with NICE-OHMS was performed. NICE-OHMS measurements require the ability to scan over a certain frequency range and dither. The dither, an additional wavelength modulation, is applied by modulating the cavity length with a small amplitude, corresponding to a modulation of $100\,\text{kHz}$, and with a frequency of $395\,\text{Hz}$. Both the scanning and the dithering are performed via the triple-stacked piezo, two stacks for the scanning, and one for the dither, which are tested with this measurement.

Water measurement is performed by targeting water lines from the HITRAN database [Gor22] or predicted by SNAPS [Tób20]. The cavity is in an evacuated state with closed valves and turned off pumps. Sufficient residual water in the system is evaporating so that measurements could be performed. Usually, these water lines are only used to correctly set the dispersion and absorption phases so that the best measurement conditions are met. The measurements of various water lines were performed such that correct functionality of the piezo was proven. In Figure 6.11, an example of a single scan of a saturated water line is shown.

Measurement of the P(3) $\nu = 0 \rightarrow 2$ line of HD

> The measurement of the P(3) $\nu = 0 \rightarrow 2$ of HD is performed with Frank Cozijn, Meissa Diouf and Wim Ubachs at Vrije Universiteit Amsterdam. The spectroscopic results are discussed and published in [Coz22a].

For the high-precision measurement of the line position, pure HD from a gas bottle is used. The position of the P(3) line is predicted by H2Spectre[2] vers. 7.3 [Kom19a] which was targeted after setting the parameters on the bases of a nearby water line.
For pressures of 1.0 and $2.5\,\text{Pa}$ up to 60 scans of duration of 6-8 min are performed. The transition is determined with high precision to be 203821936.805 (0.060) MHz [Coz22a]. The recorded line shape did not reveal a Lamb dip as observed for the water line (cf. Figure 6.11). However, the despersive lineshape is in agreement with previous observations of other lines in HD using the same the other cavity of the Amsterdam group [Dio19; Dio20; Coz22b]. A detailed presentation of the results and discussion of the line shape in HD can be found in the individual publications and in the PhD thesis of Meissa Diouf [Dio23].

---

[2]https://qcg.home.amu.edu.pl/H2Spectre.html
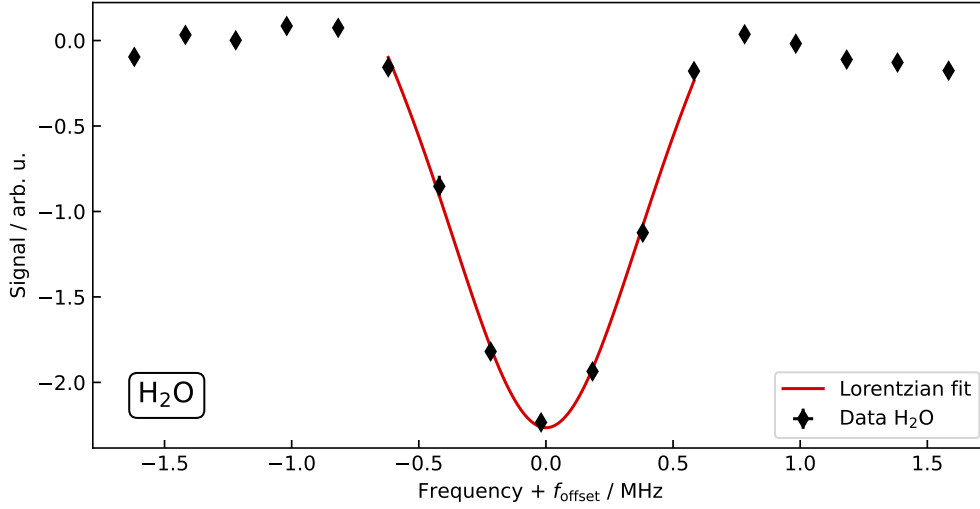
Figure 6.11: Example of a single scan of a saturated water line used for adjustment and calibration of parameters. The scanning area is focused on the saturation feature, the Lamb-dip. Each data point is an average of 3 measurement points. On the basis of such water line measurements parameters are optimized.

In summary, the high-precise measurement of the HD is ensuring operational state of the optical setup. The consistency of the typical lines shapes of water, revealing a Lamb dip, and of HD, reproducing the lineshapes of HD of different measurements, was shown. This rules out any mistake in the signal acquisition.

6.5.3 Comparison of measurements of HD from the getter and from the gas bottle

Sample provision and measurement of the P(3) transition using HD from the getter were performed to prove operation of the sample provision from the getter, as planned for HT. By comparing to measurement of HD using the gas bottle, presented in Section 6.5.2, following observations were made :

- **Gas composition:** By comparison of the line intensities at different sample pressures from measurements with pure HD and from the getter, a relative abundance of HD in the getter sample of $40 - 50\%$ is derived. This agrees with the expectations.

- **Heat propagation:** It was observed that for operations of the getter longer than 15 min heat propagates to the cavity, leading to a drift in the cavity length in the recorded signal. The heat propagation is affected on a very long time scale, such that thermal equilibrium is not reachable within a reasonable time. The resulting drift requires readjustments every few scans, which which would induce unstable

measurement conditions.

As a consequence, setting of the pressures is performed by carefully opening the valve in front of the getter for dosing. Operation of the getter at a current corresponding to a temperature of $\sim 850\,°C$ was chosen for this procedure. This reduces the operation of the getter to a minimum.

- **Temperature of the gas:** A check was made to see if there was a change in the line parameters due to the increased temperature of the sample gas. In agreement with expectations no influence on the line shape was observed.

6.6 Measurement of $\nu = 0 \to 2$ transitions in HT

The measurements of transitions of the $\nu = 0 \to 2$ in HT is performed with Frank Cozijn, Meissa Diouf and Wim Ubachs at Vrije Universiteit Amsterdam. The spectroscopic results presented in this section were published in [Coz24a].

In this section the measurements with HT are briefly described. Subsequently, the results are presented focussing on general achievements and observations regarding the operation of such an experiment with tritium. Then, the spectroscopic measurements, namely the ultra-precise acquisition of the R(0), R(1) and P(1) transitions of the $\nu = 0 \to 2$ are presented.

6.6.1 Measurement procedure

Loading and installation of the getter: The tritium getter is loaded at the TRIHYDE infrastructure at TLK with $2.2\,Pa\,L$ of H_2:HT:T_2 gas mixture with H:T 1:1. This corresponds to $1\,GBq$ activity. The getter cell is closed, disconnected, the hand wheel is dismantled and the cell is decontaminated before being shipped to VU.

At the VU Amsterdam, the cell is connected to the dedicated VCR-connection of the cavity/getter system (cf. Figure 6.5). The rotational feedthrough of the valve is attached and the secondary containment is closed. To reduce the amount of water on the inner walls of the system, it is pumped for four weeks using a turbomolecular pump stand. The getter valve remains closed during this procedure.

Before initial tritium operation, the valve to the pumping system is closed and disconnected. The secondary containment is evacuated below $1 \cdot 10^{-2}\,Pa$ and the boxes containing the optics (cf. Section 6.3.1) are installed in the front and the back of the cavity.

Decay product ^{3}He: The time between the loading of the getter with tritium and first NICE-OHMS experiments was 176 days.

When opening the valve to the tritium getter, an increase in pressure of $0.085\,Pa$ is observed that most likely originates from ^{3}He, the tritium decay product. As a noble gas, it cannot

be pumped by the getter and leads to a constant pressure offset. Using the half-life of tritium of ~ 4500 days (≈ 12.3 years) [Luc00] and the available volume of $\sim 140\,\mathrm{cm}^3$, this released amount corresponds to approximately $\sim 20\%$ of the total decay product ^{3}He. It is well known that ^{3}He can be trapped in metal after beta decay of tritium, solved in the bulk (see, e.g. [Sch89]). The pressure gauge is zeroed before starting the measurement campaign. In the following, the sample pressures presented are using this offset.

Sample preparation: To prepare the samples the tritium getter is operated at a current corresponding to $850\,°\mathrm{C}$ with closed valve and the pressure is set by controlled opening of the valve. The in-situ temperature measurement, presented in Section 6.4.1, has therefore only been included for monitoring of the operation of the getter. Sample pressures from 0.1 to $2.4\,\mathrm{Pa}$ (relative to the ^{3}He level) have been used.

Sample resorption: To return the tritium back to the getter, the valve to the getter-cell needs to be opened without heating the getter. Usually after measurement of a sample for several hours a strong reduction of the pumping speed of the tritium getter is observed. It is assumed that residual gases block the surface of the cold getter material and hinder the hydrogen (tritium) gettering process. A reactivation of the getter material by operating it at $850\,°\mathrm{C}$ with closed valve for $2\,\mathrm{min}$ is sufficient to restore the pumping properties. The origin of residual gas remains not fully clarified. Potential explanation is a radiation-induced dissociation of hydrocarbons that have persisted from production process of the components.

Test of cyro trap and dealing with accumulations of residual gas: The cryo trap was tested once for accumulated residual gases, achieving temperatures down to $78\,\mathrm{K}$, with no pressure reduction observed. The trap is therefore not included in the measurement procedure.
The residual gas, collected in the system after a longer period of time, is absorbed down to the ^{3}He pressure level by the cold vacuum getter and is therefore identified as mainly hydrogen. Thus, opening the valve to the vacuum getter without heating as a vacuum restoring procedure prior to measurements is often sufficient. Only after several cycles the degradation of the pumping speed of the getter becomes noticeable, a sign that the surface of the getter is blocked by non-hydrogen residuals. Then, an operation at a current corresponding to $850\,°\mathrm{C}$ is performed for less than $15\,\mathrm{min}$.

Preparation of measurement parameters: Before the actual HT measurement can be performed, adjustment and calibration of different parameters is essential. This mainly includes the phase separation of dispersion and absorption but also a general verification of operational state of the optical setup. This procedure is usually performed on a water line close to the frequency of the HT target line. Despite the extensive pumping procedure
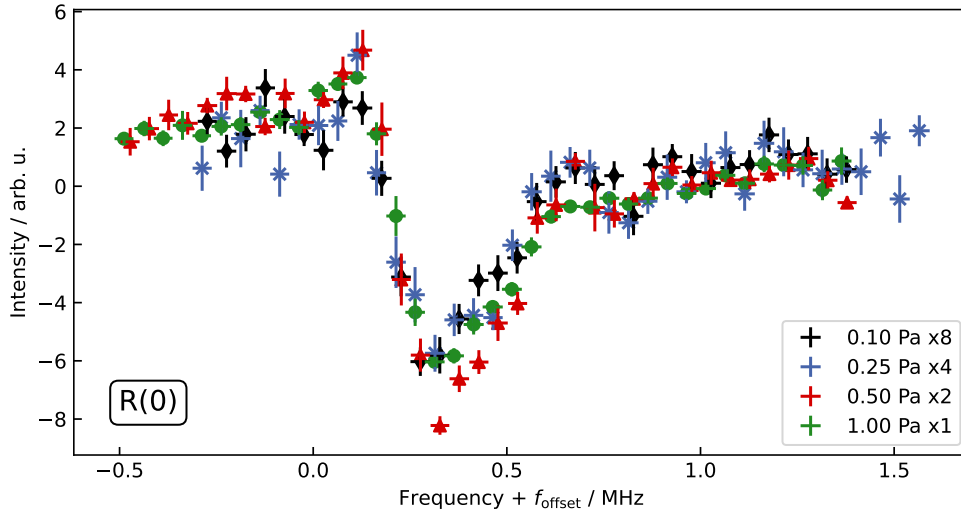
Figure 6.12: Averaged measurements of the $1f$ **signal for the R(0) line of HT for different sample pressures.** Up to 120 scans with an acquisition time of 6-12 min were performed for each sample pressure. The dither amplitude is corresponding to a modulation of 100 kHz and the intracavity power is 400 W. Intensity of the different samples pressures is multiplied with a factor for better comparison, as indicated in the legend.

prior to this campaign, the little amount of water vapour remaining is sufficient for this procedure. Further reduction of the water content with repeated operations throughout the measurement campaign is observed, which necessitated to chose stronger water lines over time. An example of a single scan of $\nu_1 = 0 \rightarrow 2$ (J, K$_A$, K$_C$ = 6, 4, 3 $\rightarrow$ 5, 1, 4) of H$_2$O is given in Figure 6.11 showing the Doppler-free Lamb dip feature recognisable by its Lorentzian-like profile.

Measurement properties: In total, three lines of the $\nu = 0 \rightarrow 2$ band are measured. For the P(1) (J=1 $\rightarrow$ 0) and R(1) (J=1 $\rightarrow$ 2) lines, measurements at pressures of $0.25, 0.50$ and 1.0 Pa, relative to the constant ^{3}He level, are performed. For the R(0) (J=0 $\rightarrow$ 1), measurements at 0.1 Pa are recorded additionally. The averaged first derivatives of the NICE-OHMS signals ($1f$) for all pressures are shown in Figure 6.12.

For all measurements, the dither amplitude was set to correspond to a modulation of 100 kHz. Most of the measurements are performed with the maximum intracavity power of 400 W. Typical recordings took about 12 hours of averaging, where single scans covering 1.4 MHz lasted 6 minutes. For each sample pressure and line, up to 120 scans were recorded. For the R(0) and R(1), additionally, measurements at 0.5 Pa with reduced laser power have been recorded. Here, the intracavity power is estimated to be ~ 80 W. During the ~ 300 h of measurement and about 120 sample provisions, no degradation of the getter/sample production performance is observed.

6.6.2 Assignment using the hyperfine splitting

The spectroscopic analysis of the HT overtone profits from its favourable ordering of hyperfine components, exhibiting an isolated narrow feature, not found in HD [Coz18b; Dio19], where all hyperfine components overlap.

In this section, the accurate assignment of the R(0) and R(1) using this feature is presented. Afterwards a discussion of the sources of uncertainty for these HT lines is provided. For the P(1) of HT line, a similar approach using the isolated hyperfine component is used and is presented separately.

6.6.2.1 Assignment of the R(0)

As visible from the R(0) in Figure 6.12, the shape of the recorded line does not reflect the expectations of a symmetrical line shape as observed in the water lines. The spectral structure consists of a broad dispersion-shaped resonance, reminiscent of the features observed in HD [Tao18; Coz18b; Dio19; Hua20; Coz22a]. However, this structure can be associated with the overlapping features of 5 hyperfine components as shown in the lower and right panels of Figure 6.13.

The hyperfine components from computations by Jozwiak et al. [Jóź21] include only the couplings between nuclear spin and rotation. It should be noted that hyperfine splittings in $J = 0$ rotational levels, between $F = 0$ and $F = 1$ components, are determined to be zero in these computations, while in refined calculations of the spin-spin interaction a splitting of 0.3 kHz is found for HT [Puc18]. This discrepancy, however, is below the resolution of the experiment and the assumption of degeneracy is therefore justified.

Unlike for the case of HD, in HT there is a single isolated hyperfine component for excitation to the level $|JF\rangle = |10\rangle$ located on the positive side of the main feature by 444 kHz [Jóź21]. This component is resolved as a narrow symmetric Lamb dip in the spectrum, measured at the lower intracavity power of $80\,\mathrm{W}$. As visualised in Figure 6.13, this feature is used to fit the position of this hyperfine component and consequently accurately assign the line using Jozwiak's et al. computations. Only data points covering the isolated hyperfine component, as displayed in the plot, are included in the fit. Lorentzian fit is applied which is in accordance with the expected line shape of a $1f$-demodulated NICE-OHMS signal [Fol09].

6.6.2.2 Assignment of the R(1)

The R(1) line in the $\nu = 0 \rightarrow 2$ band, displayed in Figure 6.14, reveals a very similar line shape as the R(0): on the high-frequency side of the broad dispersion-shaped feature, an isolated Lamb dip feature appears, specifically in the low-power recording of $80\,\mathrm{W}$ intracavity. Its centre position is determined analogously to the R(0) using a Lorentzian fit. For the R(1) line, this feature corresponds not just to one but to three hyperfine components,
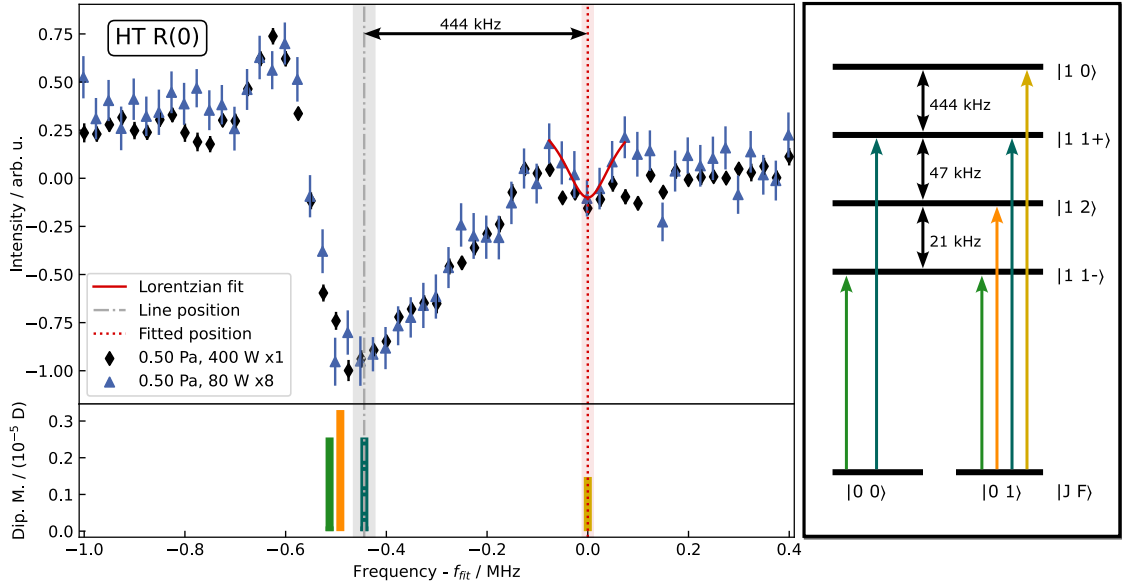
Figure 6.13: Assignment of the R(0) line. Recorded spectra of the R(0) line at the total hydrogen pressure of 0.5 Pa (50% HT) for intracavity powers of 80 W and 400 W. The frequency scale is given by f_{fit} = 203 396 427.135 MHz. The single isolated hyperfine component is used for the fit of the line. The red shaded area represents the fit uncertainty, while the grey line and grey shaded area represent the line position with all uncertainty contributing to the assignment. In the lower, hyperfine components in the magnitude of their dipole moment are visualised as a stick spectrum. A level scheme of hyperfine components is provided to the right, matching the color coding of the stick spectrum.

for which an intensity-weighted average is taken at a frequency offset of 440 kHz [Jóź21] from the position of the (hyperfineless) line.

6.6.2.3 Uncertainties on the assignment

Uncertainty from the fit: The statistical uncertainty from the fit of the R(0) line amounts to 11 kHz and 6 kHz for the R(1), due to its higher signal-to-noise ratio. For both lines, no sign of asymmetry is found in the fitting procedures to the experimental data. This supports the assumption that the isolated components are absorption Lamb dips.

The resulting values are transformed into frequencies of the hyperfineless or purely rovibrational transitions by including the shift of the isolated hyperfine component based on accurately computed values [Jóź21], as discussed above and illustrated in Figures 6.13 and 6.14.
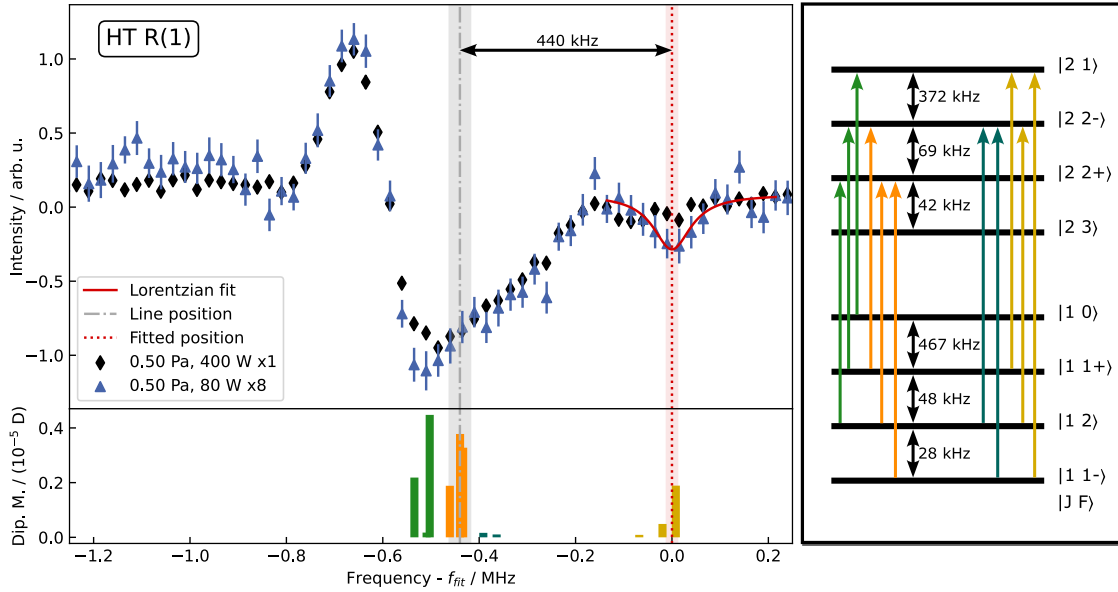
Figure 6.14: Assignment of the R(1) line. The recorded spectra of the R(1) line at two different intracavity powers, show an isolated Lamb dip at the high frequency side covering three hyperfine components. The absolute frequency scale is given by f_{fit} = 205 380 034.083 MHz, corresponding to the fitted center position of the isolated Lamb dip as shown in red. The shaded area represents the sum of the statistical uncertainty and the uncertainty contribution of the three components (see text). The grey bar represents the location and final uncertainty of the purely rovibrational transition frequency. A hyperfine stick spectrum for this transition and a corresponding level scheme of hyperfine components, in identical colour coding, is provided to the lower and right respectively.

Composed Lamb dip for R(1):   Since for the R(1) line the isolated Lamb dip is composed of 3 overlapping hyperfine components, a weighted average is taken, adding an uncertainty of $6\,\mathrm{kHz}$. The saturated absorption spectra do not exhibit a first-order Doppler effect, but are subject to a second-order relativistic Doppler effect of $f_{2D} = hf_0^2 v^2/2mc^2$, which amounts to $1.4\,\mathrm{kHz}$ for HT at room temperature. Here, f_0 is the transition frequency, m is the mass, h is the Planck constant, and c is the speed of light.

Pressure shift: The overall pattern of the isolated components in the spectra shows that the spectra overlap for different pressure recordings (cf. Figure 6.12). Quantitative analysis reveals that a pressure shift should be on the order of $5\,\mathrm{kHz\,Pa^{-1}}$, which would be in agreement with the pressure shifts found in HD (at $10\,\mathrm{kHz\,Pa^{-1}}$) [Coz18b; Dio19] and in H_2 (at $15\,\mathrm{kHz\,Pa^{-1}}$) [Coz23]. Due to helium present in the system and limited measurement time, a systematic measurement could not be performed. For this reason, a conservative estimate of $10\,\mathrm{kHz}$ is added to the error budget.

The recoil effect: The recoil caused by the interaction of the photon with the comparably light molecule has a non-negligible impact on the measured transitions. In the saturation regime, a red and a blue shifted recoil component is observed [Hal76; Bar79; Bag91] at frequencies $f_{rec} = \pm h f_0^2 / 2mc^2$.

For the case of the $\nu = 0 \rightarrow 2$ band transitions in HT, the recoil shift corresponds to $\pm 22\,\mathrm{kHz}$.

From the line-profile fits it could be noted that the resonance widths are narrower than expected from transit-time broadening. In comparable observations in HD [Coz18b] it has been concluded that under weak saturation conditions, the selection of cold molecules occurs. The widths for HT are $\Gamma = (90 \pm 40)\,\mathrm{kHz}$ (FWHM) for the R(0) line, and $\Gamma = (180 \pm 25)\,\mathrm{kHz}$ for R(1). At the same time, these narrow line profiles are incompatible with the expectation of a recoil doublet.

In addition, in the case of a recent observation of a Lamb dip in the very weak quadrupole spectrum of H_2 [Coz23] only a single recoil component was observed, which was interpreted as the blue recoil.

In the present case of HT, the combination of widths and noise levels does not allow for a decision on whether the observed spectra cover both recoil components or only one.

For the publication [Coz24a], the authors agreed on the generally accepted approach to the recoil phenomenon in saturation that the blue and the red recoil components average out to no shift in the molecular resonance frequency.

If suppression of the red recoil components in intracavity saturation spectroscopy of weak transitions is an ubiquitous feature, then the measured frequencies as presented in Table 6.3 (and in the publication) should be lowered by $22\,\mathrm{kHz}$.

Considering the presented systematic effects and contributions to the uncertainty budget, the final transition frequencies and uncertainties are determined and listed in Table 6.3.

6.6.2.4 Assignment of the Lamb-dip-less P(1)

Spectra of the P(1) line were recorded for the sample pressures of 0.25 and $0.5\,\mathrm{Pa}$ and the intracavity power of $400\,\mathrm{W}$, which are shown in Figure 6.15. As shown in the lower and right panels, there are 6 hyperfine components contributing to the signal of one of these being isolated. This component is red-shifted from the hyperfineless, purely rovibrational transition by $467\,\mathrm{kHz}$ according to computations [Jóź21].

Similarly to the case of the P(1) line in HD [Dio20], the saturation features for the isolated hyperfine component and the composite feature appear as peaks, rather than as Lamb dips. For HD, these reversed signal amplitudes were interpreted as originating from the contribution of crossover resonances, that were included in a comprehensive model based on optical Bloch equations [Dio19]. For the presented HT, this assumption can be disproved, as crossovers cannot interfere with regular hyperfine components at the location of the isolated component.

To date of this work, there is no explanation for the phenomenon of signal inversion,
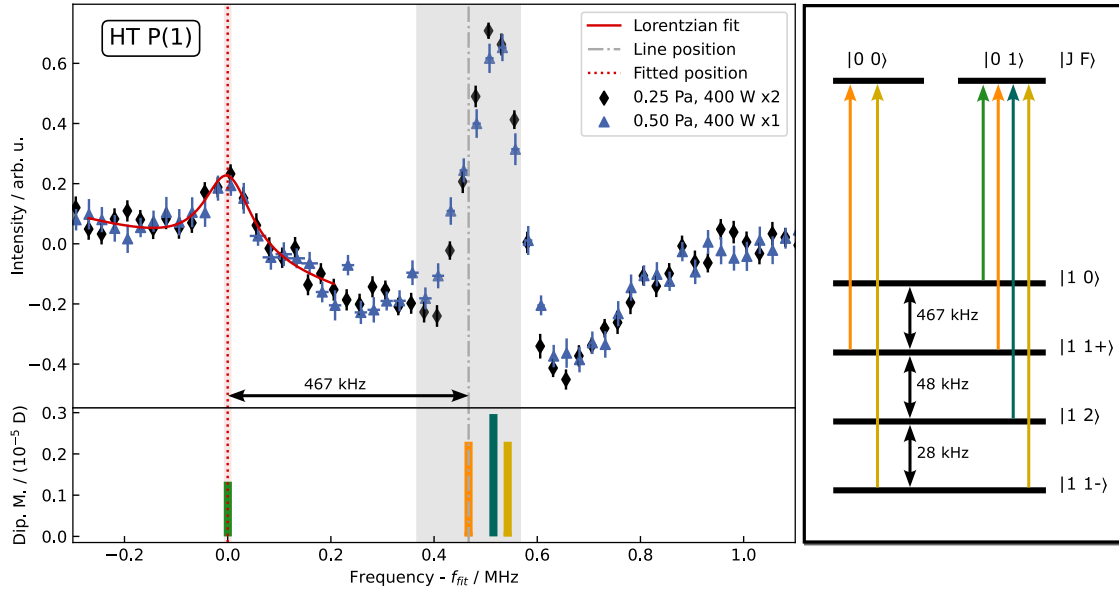
Figure 6.15: Recorded saturated absorption spectra of the P(1) line. The measurements are performed at intracavity power of 400 W and H_2:HT:T_2 pressures as indicated. The absolute frequency scale is given by f_{fit} = 198 824 820.185 MHz. The red bar represents the location and the statistical uncertainty of the single isolated hyperfine component. The grey bar shows the position and final uncertainty of the purely rovibrational transition. A stick spectrum of the hyperfine components and the corresponding level scheme in matching colours are provided on the lower and on the right.

neither in HT nor in HD. Also, the dispersive-like line shapes of the composite features in both isotopologues, HD and HT, for the R lines remain an open issue.

As the P(1) is not observed as a regular Lamb dip, the presented procedure for precise determination of the transition energy for the R lines needs to be adapted and used with care. Using an inverted Lorenzian with slope as a fit model, the position for the single hyperfine component is extracted, from which the rovibrational transition frequency of 198 824 820.600 MHz is obtained. For positional uncertainty, a conservative estimate of 100 kHz is taken.

6.6.2.5 Comparison to theory

The obtained transitions, as presented in Table 6.3, are compared with recent calculations for the tritium bearing hydrogen isotopologues [Pac22].
These calculations are based on a direct non-adiabatic approach [Puc19b; Puc19a], including non-adiabatic James-Coolidge wave functions, and refined with computations of relativistic and quantum electrodynamical (QED) corrections [Kom19b] giving the final theoretical uncertainties of 0.9 MHz for the transitions presented in HT [Pac22].
This data have been incorporated into the H2SPECTRE programme, version 7.4 [Kom19a].

Table 6.3: Measured transition frequencies of the purely rovibrational (hyperfineless) lines R(0), R(1) and P(1) in the $\nu = 0 \rightarrow 2$ band of HT. The results are compared with results from a calculation in which the non-relativistic energy is computed via the direct non-adiabatic approach [Pac22] from H2SPECTRE [Kom19a]. The differences are also presented in terms of the combined standard deviation (σ) of experiment and theory. Note that P(1) is not obtained from a Lamb dip and is therefore stated with higher uncertainty. Details can be found in the text.

Line	Obs. / MHz	Calc. [Kom19a] / MHz	Diff. / MHz	Diff. / σ
R(0)	203 396 426.692 (21)	203 396 424.9 (9)	1.8 (1.1)	1.8
R(1)	205 380 033.644 (22)	205 380 031.7 (9)	1.8 (1.0)	1.8
P(1)	198 824 820.600 (100)	198 824 819.0 (9)	1.9 (1.1)	1.7

H2SPECTRE introduces an uncertainty in the computation of the level energies of $4.2\,\mathrm{MHz}$, but cancellation of uncertainty when computing the transition frequencies reduces the uncertainties to the presented $0.9\,\mathrm{MHz}$.

Note that H2SPECTRE also reveals the origin of the estimated uncertainty, which is in the $E^{(5)}$ or $m\alpha^5$-term in the level energy expansion of the fine structure constant, the leading-order QED correction.

The comparison of the obtained transitions with this computations, presented in Table 6.3, show a systematic deviation between experiment and theory at the level of $1.8\,\sigma$.

The exact same deviations of $1.8\,\sigma$ were found for the vibrational bands $\nu = 0 \rightarrow 2$ in HD [Fas20; Coz22b], in H_2 [Fle23; Coz23], and in D_2 [Zab20]. For all mentioned deviations, the precision of theory is the leading contribution for the total uncertainty.

Even for the more advanced treatment of the leading-order QED term, which was recently recomputed [Sił23], the discrepancies persist.

6.7 Conclusion and discussion

In this chapter, an experiment that merges the sub-Doppler NICE-OHMS technology with tritium confinement and sample preparation technology is presented. Starting from requirements from the side of the spectroscopy and from the tritium confinement, a cavity/tritium system was developed.

Its key component is the *SAES* getter that is loaded with $1\,\mathrm{GBq}$ of a H_2:HT:T_2 (H:T 1:1) mixture. The ability of the getter to reversibly store hydrogen allows to set sample pressures of the loaded gas mixture up to $2.4\,\mathrm{Pa}$ in the cavity while retaining safe tritium confinement. This approach is a novelty for such applications, whereas the idea was first proposed by Yamamoto [Yam17].

A validation of the applicability of such a getter as a reversible tritium storage is a mandatory step in order to develop a working setup. This was carried out with a TLK sorption study, in which the sorption properties for H_2, D_2, T_2 and H_2:HT:T_2 (H:T 1:1) were measured in

dependence on the temperature of the getter in a set-up that mimics the dimensions of NICE-OHMS.

The problem of measuring the temperature of the small getter device ($7 \times 1.5 \times 1.5\,\text{mm}$) was solved by calibration of the temperature-resistance dependency. The temperature measurement by resistance led to comparably high uncertainty, but is also applicable within the small NICE-OHMS setup.

The results of the sorption study confirmed the applicability of the tritium storage getter by revealing similar desorption pressures for all gas mixtures. Differences between H_2 and T_2 were observed. The potential impact on the NICE-OHMS experiment was shown to be negligible, using calculations of the reaction kinetics from the observed differences.

For NICE-OHMS, the optical setup is mostly replicated from a NICE-OHMS setup measuring ultra-precisely transitions in HD [Coz18b; Dio19; Dio20; Coz22b; Coz22a] and H_2[Coz23]. Optics and laser were selected to fit to the optical range of the targeted HT transitions. To ensure operational state of the setup, measurements on residual water in the system were performed, providing Lamb dips in the $1f$ NICE-OHMS signal. In addition, HD was measured as part of an extensive study using the getter storage approach and pure HD from the bottle. From this study, precise transition frequency for the P(3) $\nu = 2 \rightarrow 0$ in HD [Coz22a] were obtained, which were inaccessible from the other NICE-OHMS setup of the Amsterdam group.

After ensuring operation of all crucial components of the setup, a getter was filled with $1\,\text{GBq}$ activity hydrogen-tritium mixture (1:1) and shipped to the VU laboratory where it was installed. Before starting the measurements, a release of the tritium decay product ^{3}He from the installed getter cell was observed, leading to a constant base pressure of $0.085\,\text{Pa}$.

HT experiments were carried out, measuring for the first time the R(0), R(1) and P(1) $\nu = 2 \rightarrow 0$ transitions. Data were obtained at sample pressures from 0.1 to $1\,\text{Pa}$ with an estimated HT content of $40 - 50\%$. For R(0) and R(1) additional measurements were performed at reduced intracavity power, $80\,\text{W}$ instead of the maximum power of $400\,\text{W}$.

For both lines a dispersive line shape was observed, reminiscent of the features observed in HD [Tao18; Coz18b; Dio19; Hua20; Coz22a]. An isolated Lamb dip on the higher frequency scale, especially for the lower intracavity power, is notable for both lines. The Lamb dips agree in distance to the main feature with theoretical computations of the hyperfine splitting [Jóź21] in HT. Assigning these Lamp dips to isolated hyperfine components, the positions of the hyperfineless, pure rovibrational transitions were obtained with precision up to $21\,\text{kHz}$.

For P(1), a peak-like line shape is observed, comparable to the observation of P(1) in HD [Dio20]. Also, here a hyperfine component is isolated, but at lower frequency. However, it is also revealing itself as a peak.

To date of this work, there is no explanation for (i) the dispersive line shapes of the R lines and (ii) the peak-like line shapes for P(1). As P(1) is not observed as regular Lamb dip, a

conservatively estimated uncertainty on the position of $100\,\text{kHz}$ is stated. Future studies may reveal whether these phenomena are related to optical pumping, collisional relaxation, or trapping effects of molecules at the nodes of intense standing waves in the cavity.

The precision of the experimental transition frequencies assigned in this work is among the highest in hydrogen isotopologues, with those of HD [Fas20] and H_2 [Coz23]. This is an ideal precondition for testing current theory. The comparison with differences of recent computations of the energy levels [Kom19a] show deviation of $0.9\,\text{MHz}$ ($1.8\,\sigma$), which is in good agreement with similarly deviating observations from high-precision experiments of hydrogen molecules (HD [Fas20; Coz22b], H_2 [Fle23; Coz23], D_2 [Zab20]).

The presented results of the HT frequencies form an accurate testing ground for future computations of the non-adiabatic QED term $m\alpha^5$ in molecular hydrogen isotopologues.

This experiment achieved for the first time ultra-precise rovibrational transition energies from a tritiated hydrogen molecule, a thousand times better than for any previously observed transition in a tritiated hydrogen molecule [Lai20]. The combination of the NICE-OHMS technique and the novel getter tritium storage and sample preparation showed that measurement campaigns of extended duration can be performed in a cavity-enhanced configuration without radioactive tritium degrading the highly reflective mirror coatings or having detrimental effects on the instrumentation.

This opens the perspective of adding all three tritiated hydrogen molecules to the set of benchmark systems to test molecular quantum theory and potentially probe new physics [Uba16].

7 Conclusion and future outlook

The primary objective of this work was the accurate determination of ro-vibrational transitions in the simplest molecules containing tritium: tritiated water and tritium hydride. These data are required as benchmark for theoretical models to test and improve mass-dependent contributions.

In Chapter 5, FTIR spectroscopy and a custom-built optical cell were used to measure in total 4589 lines of 13 vibrational bands of tritiated water. To access all species, HTO, DTO and T_2O, the production of the sample was improved. For each species, more than 1200 lines were measured for the first time with an accuracy up to $5.6 \cdot 10^{-5}\,\mathrm{cm}^{-1}$. This large data set withstood an extensive validation using a cross-check and a comparison with microwave measurements. Therefore, a first study of the accuracy of theoretical predictions could be performed revealing that accuracy is limited by vibrational and rotational contributions.

In Chapter 6, three vibrational overtone transitions of the tritiated heteronuclear version tritium hydride (HT) were measured with an accuracy of up to $21\,\mathrm{kHz}$. These data are the most precise for a tritium-variant and integrate in precision with the most accurate measurements of ro-vibrational transitions in molecular hydrogen [Coz23; Coz22a]. In addition, further insights into the line shape generation of molecular hydrogen in NICE-OHMS were obtained. Although previous observations in HD [Dio19; Dio20] already linked its asymmetrical line shape to the underlying hyperfine components, only HT could confirm this hypothesis by resolving its isolated hyperfine component. The remaining hyperfine components reproduced the asymmetric line shape of the R lines and the peak-like shape of P(1), previously observed in HD. The determined transition frequencies in HT were found to deviate by $1.8\,\mathrm{MHz}$ or $1.8\,\sigma$ with current theory which is perfectly in accordance with observations from different isotopologues [Coz22b; Coz23; Zab20] but poses a challenge to theory.

Both experiments successfully dealt with tritium-specific requirements: (i) limitation to a small amount of tritium due to its activity, (ii) suppression of the production of impurities due to tritium's radiochemical activity, and (iii) safe confinement. The scientific results obtained and also the methodology used are starting points for various future prospects, some of them already starting.

Future outlook: Tritiated water These new transitions obtained are substantial for process and environmental monitoring in and around tritium facilities such as fusion plants. As a result, the International Atomic Energy Agency (IAEA) will host these data in its

open-access database for measurements related to fission and fusion [Hil24], making these findings accessible for future research and industry use.

Recognising the need for more accurate models, Jonathan Tennyson intends to use these results to improve theoretical predictions by at least an order of magnitude [Ten24].

In astronomy, tritiated water has not yet been considered due to the low formation rate of tritium in space and its short half-life. However, recent proposals, such as the work by Haqq-Misra et al., suggest that tritiated species could serve as potential technosignatures [Haq24]. Incorporating the spectral data obtained here could open new possibilities for astronomical detection of tritiated compounds, particularly in environments similar to those where deuterated species have been observed, such as in the protostar *IRAS 16293-2422* [Cou12].

Furthermore, the measurement techniques developed in this work can be applied to other tritiated species, such as tritiated methane and ammonia, which are relevant for fusion research. This is a great opportunity for further investigation of tritium-containing molecules, expanding the role of precision spectroscopy in fusion-related applications. Measurements for tritiated methane in a setup similar to that for water are currently in preparation.

Future outlook: Tritium hydride   The NICE-OHMS measurement on HT provided valuable information on the line shape generation. For better understanding of the underlying processes, NICE-OHMS studies in H_2 were performed, where the suppression of the red-shifted recoil component was shown [Coz23] and hyperfine components of the quadrupole-allowed transition were resolved [Dio24].

In precision spectroscopy of simple systems, molecular hydrogen ions are of great interest. The three-body problem can be calculated with much higher precision [Kor21] but also spectroscopy achieves due to modern ion traps (e.g., [Sch23]) precision in the Hertz regime [Ali20]. Measurement of a tritiated molecular hydrogen ion might potentially be of interest for such measurements, which, with their high accuracy, aim to improve the determination of fundamental constants such as the Rydberg constant [Ali23] and are searching for physics beyond the standard model [Uba16]. The key technology for accessing those molecular hydrogen ions with tritium could be the getter gas supply used in the NICE-OHMS experiment in this work. The ability to deliver small amounts of hydrogen samples that in addition need to be ionised in the suggested application could replace the yet-common approach of using gas bottles. This experiment, which targets HT+, is currently in development in cooperation with Stephan Schiller and Soroosh Alighanbari [Sch24].

In summary, this work has successfully provided high-accuracy spectral data on tritiated water and HT, offering valuable benchmarks for future theoretical developments and potential future applications. The experimental techniques developed here are well-suited for further exploration of tritiated species and provide valuable insights into both environmental monitoring and fundamental physics.

Appendix A

Supplemental material to tritiated water spectroscopy

Additional material for the tritiated water spectroscopy is provided. The material is only recommended in combination with the main work presented in Section 5.

A.1 Composition of the 1 GBq and 10 GBq samples

Here, the composition presented in the main work (Section 5.4.4) is listed as table.

Table A.1: Composition of the 1 GBq and 10 GBq activity tritiated water samples. Note that only IR active molecules with known spectra and detectable SNR can be included. The sample may contain unknown amounts of nitrogen and tritiated methane variations that will change the relative quantities.

Molecule	Relative quantity sample "1 GBq" /%	Relative quantity sample "10 GBq" /%
H_2O	67.6	10.1
HDO	1.8	7.6
D_2O	0.01	2.6
HTO	11.8	25.1
DTO	0.18	19.8
T_2O	0.87	26.9
CO_2	17.7	7.8
CH_4	0.034	-

A.2 List of assigned tritiated water lines

In this section the assigned line positions with uncertainty, line intensities, transition quantum numbers and the deviation to SPECTRA database are presented.

A.2.1 Linelists of HTO

A.2.1.1 HTO $2\nu_1$ band from the 1 GBq sample

Here, the lines assigned to the $2\nu_1$ from the 1 GBq sample are presented. These lines are published in [Rei20]. For further information, see Section 5.5.1.

Table A.2: Linelist of the $2\nu_1$ from the 1 GBq sample. The columns present the assigned line position, the uncertainty on the position $\sigma_{\text{Pos.}}$, the line intensity taking natural abundance into account, lower and upper vibrational quanta, lower and upper rotational quanta and the deviation to the predictions from SPECTRA database $\Delta_{\text{SPEC.}}$.

Position	$\sigma_{\text{Pos.}}$	Intensity	$\nu_1\,\nu_2\,\nu_3$	$\nu_1'\,\nu_2'\,\nu_3'$	J K_a K_c	J' K_a' K_c'	$\Delta_{\text{SPEC.}}$
4344.55439	0.00292	9.3×10^{-40}	0 0 0	2 0 0	13 3 10	12 3 9	-0.001
4345.89863	0.00148	1.3×10^{-39}	0 0 0	2 0 0	13 2 11	12 2 10	0.011
4346.41708	0.00361	9.2×10^{-40}	0 0 0	2 0 0	14 1 13	13 1 12	-0.004
4349.11090	0.00265	8.9×10^{-40}	0 0 0	2 0 0	14 2 13	13 2 12	-0.008
4349.46711	0.00238	8.4×10^{-40}	0 0 0	2 0 0	15 0 15	14 0 14	-0.010
4349.56762	0.00281	8.4×10^{-40}	0 0 0	2 0 0	15 1 15	14 1 14	-0.009
4354.86035	0.00535	1.0×10^{-39}	0 0 0	2 0 0	13 3 11	12 3 10	-0.028
4362.04417	0.00122	2.5×10^{-39}	0 0 0	2 0 0	12 2 10	11 2 9	-0.001
4362.79283	0.00134	1.8×10^{-39}	0 0 0	2 0 0	12 3 9	11 3 8	-0.019
4363.53492	0.00143	1.7×10^{-39}	0 0 0	2 0 0	14 0 14	13 0 13	-0.018
4363.69595	0.00137	1.7×10^{-39}	0 0 0	2 0 0	14 1 14	13 1 13	-0.016
4363.74864	0.00135	1.7×10^{-39}	0 0 0	2 0 0	13 2 12	12 2 11	-0.021
4367.08773	0.00283	1.0×10^{-39}	0 0 0	2 0 0	12 4 8	11 4 7	-0.064
4368.26711	0.00199	1.0×10^{-39}	0 0 0	2 0 0	12 4 9	11 4 8	-0.064
4370.62311	0.00144	1.9×10^{-39}	0 0 0	2 0 0	12 3 10	11 3 9	-0.036
4373.96934	0.00110	3.4×10^{-39}	0 0 0	2 0 0	12 1 11	11 1 10	-0.012
4377.32509	0.00085	3.1×10^{-39}	0 0 0	2 0 0	13 0 13	12 0 12	-0.024
4377.57245	0.00074	3.1×10^{-39}	0 0 0	2 0 0	13 1 13	12 1 12	-0.024
4378.24631	0.00093	3.2×10^{-39}	0 0 0	2 0 0	12 2 11	11 2 10	-0.028
4378.32051	0.00081	4.7×10^{-39}	0 0 0	2 0 0	11 2 9	10 2 8	-0.012
4380.61408	0.00091	3.2×10^{-39}	0 0 0	2 0 0	11 3 8	10 3 7	-0.038
4383.78120	0.00231	1.8×10^{-39}	0 0 0	2 0 0	11 4 7	10 4 6	-0.078
4383.79641	0.00834	8.1×10^{-40}	0 0 0	2 0 0	11 5 6	10 5 5	-0.071
4383.75428	0.00367	8.1×10^{-40}	0 0 0	2 0 0	11 5 7	10 5 6	-0.144
4384.42500	0.00140	1.8×10^{-39}	0 0 0	2 0 0	11 4 8	10 4 7	-0.075
4386.20325	0.00074	3.4×10^{-39}	0 0 0	2 0 0	11 3 9	10 3 8	-0.047
4387.63468	0.00042	6.1×10^{-39}	0 0 0	2 0 0	11 1 10	10 1 9	-0.018
4390.82890	0.00044	5.5×10^{-39}	0 0 0	2 0 0	12 0 12	11 0 11	-0.027
4391.20701	0.00044	5.5×10^{-39}	0 0 0	2 0 0	12 1 12	11 1 11	-0.030
4392.60277	0.00060	5.6×10^{-39}	0 0 0	2 0 0	11 2 10	10 2 9	-0.034

Position	$\sigma_{\text{Pos.}}$	Intensity	$\nu_1\,\nu_2\,\nu_3$	$\nu_1'\,\nu_2'\,\nu_3'$	J K_a K_c	J' K_a' K_c'	$\Delta_{\text{SPEC.}}$
4394.63567	0.00033	8.0×10^{-39}	0 0 0	2 0 0	10 2 8	9 2 7	-0.023
4397.85438	0.00011	5.4×10^{-39}	0 0 0	2 0 0	10 3 7	9 3 6	-0.050
4399.45460	0.00328	1.3×10^{-39}	0 0 0	2 0 0	10 5 5	9 5 4	-0.120
4399.46363	0.00334	1.3×10^{-39}	0 0 0	2 0 0	10 5 6	9 5 5	-0.123
4399.87582	0.00089	2.9×10^{-39}	0 0 0	2 0 0	10 4 6	9 4 5	-0.085
4400.19696	0.00090	2.9×10^{-39}	0 0 0	2 0 0	10 4 7	9 4 6	-0.087
4401.38740	0.00027	1.0×10^{-38}	0 0 0	2 0 0	10 1 9	9 1 8	-0.024
4401.56786	0.00049	5.6×10^{-39}	0 0 0	2 0 0	10 3 8	9 3 7	-0.056
4404.03350	0.00030	9.3×10^{-39}	0 0 0	2 0 0	11 0 11	10 0 10	-0.033
4404.60385	0.00029	9.2×10^{-39}	0 0 0	2 0 0	11 1 11	10 1 10	-0.035
4406.81412	0.00029	9.2×10^{-39}	0 0 0	2 0 0	10 2 9	9 2 8	-0.042
4410.89424	0.00023	1.3×10^{-38}	0 0 0	2 0 0	9 2 7	8 2 6	-0.035
4414.39633	0.00035	8.4×10^{-39}	0 0 0	2 0 0	9 3 6	8 3 5	-0.062
4414.71295	0.00323	1.8×10^{-39}	0 0 0	2 0 0	9 5 4	8 5 3	-0.132
4414.71295	0.00323	1.8×10^{-39}	0 0 0	2 0 0	9 5 5	8 5 4	-0.136
4415.29502	0.00017	1.6×10^{-38}	0 0 0	2 0 0	9 1 8	8 1 7	-0.031
4415.41455	0.00067	4.4×10^{-39}	0 0 0	2 0 0	9 4 5	8 4 4	-0.095
4415.56525*	0.00075	4.4×10^{-39}	0 0 0	2 0 0	9 4 6	8 4 5	-0.093
4416.67521	0.00032	8.5×10^{-39}	0 0 0	2 0 0	9 3 7	8 3 6	-0.066
4416.93473*	0.00019	1.5×10^{-38}	0 0 0	2 0 0	10 0 10	9 0 9	-0.038
4417.77077	0.00019	1.5×10^{-38}	0 0 0	2 0 0	10 1 10	9 1 9	-0.040
4420.87671	0.00021	1.4×10^{-38}	0 0 0	2 0 0	9 2 8	8 2 7	-0.049
4426.99587*	0.00015	1.9×10^{-38}	0 0 0	2 0 0	8 2 6	7 2 5	-0.045
4429.35297	0.00013	2.4×10^{-38}	0 0 0	2 0 0	8 1 7	7 1 6	-0.038
4429.54025	0.00077	2.2×10^{-38}	0 0 0	2 0 0	9 0 9	8 0 8	-0.041
4429.54025	0.00536	2.4×10^{-39}	0 0 0	2 0 0	8 5 3	7 5 2	-0.146
4429.54025	0.00532	2.4×10^{-39}	0 0 0	2 0 0	8 5 4	7 5 3	-0.148
4430.20714	0.00023	1.2×10^{-38}	0 0 0	2 0 0	8 3 5	7 3 4	-0.072
4430.44610	0.00048	6.0×10^{-39}	0 0 0	2 0 0	8 4 4	7 4 3	-0.103
4430.50743	0.00047	6.0×10^{-39}	0 0 0	2 0 0	8 4 5	7 4 4	-0.104
4430.71758	0.00014	2.2×10^{-38}	0 0 0	2 0 0	9 1 9	8 1 8	-0.045
4431.48589	0.00024	1.2×10^{-38}	0 0 0	2 0 0	8 3 6	7 3 5	-0.074
4434.77381	0.00015	2.0×10^{-38}	0 0 0	2 0 0	8 2 7	7 2 6	-0.056
4441.86897	0.00010	3.1×10^{-38}	0 0 0	2 0 0	8 0 8	7 0 7	-0.046
4442.81345	0.00012	2.6×10^{-38}	0 0 0	2 0 0	7 2 5	6 2 4	-0.055
4443.45447	0.00011	3.0×10^{-38}	0 0 0	2 0 0	8 1 8	7 1 7	-0.050
4443.49581	0.00010	3.3×10^{-38}	0 0 0	2 0 0	7 1 6	6 1 5	-0.045
4443.95849	0.00586	2.6×10^{-39}	0 0 0	2 0 0	7 5 2	6 5 1	-0.148
4443.95849	0.00586	2.6×10^{-39}	0 0 0	2 0 0	7 5 3	6 5 2	-0.148
4445.00104	0.00043	7.3×10^{-39}	0 0 0	2 0 0	7 4 3	6 4 2	-0.110
4445.02174	0.00041	7.3×10^{-39}	0 0 0	2 0 0	7 4 4	6 4 3	-0.112

Position	$\sigma_{\text{Pos.}}$	Intensity	$\nu_1\,\nu_2\,\nu_3$	$\nu_1{}'\,\nu_2{}'\,\nu_3{}'$	J K_a K_c	J' $K_a{}'$ $K_c{}'$	$\Delta_{\text{SPEC.}}$
4445.31381	0.00019	1.6×10^{-38}	0 0 0	2 0 0	7 3 4	6 3 3	-0.081
4445.96000*	0.00019	1.6×10^{-38}	0 0 0	2 0 0	7 3 5	6 3 4	-0.082
4448.48495	0.00012	2.7×10^{-38}	0 0 0	2 0 0	7 2 6	6 2 5	-0.062
4453.98703	0.00008	4.1×10^{-38}	0 0 0	2 0 0	7 0 7	6 0 6	-0.050
4455.98903	0.00008	4.0×10^{-38}	0 0 0	2 0 0	7 1 7	6 1 6	-0.055
4457.62831*	0.00008	4.3×10^{-38}	0 0 0	2 0 0	6 1 5	5 1 4	-0.051
4457.95225	0.00180	2.0×10^{-39}	0 0 0	2 0 0	6 5 1	5 5 0	-0.155
4457.95225	0.00180	2.0×10^{-39}	0 0 0	2 0 0	6 5 2	5 5 1	-0.155
4458.19629	0.00010	3.2×10^{-38}	0 0 0	2 0 0	6 2 4	5 2 3	-0.064
4459.10140	0.00112	7.6×10^{-39}	0 0 0	2 0 0	6 4 2	5 4 1	-0.116
4459.10501	0.00112	7.6×10^{-39}	0 0 0	2 0 0	6 4 3	5 4 2	-0.119
4459.77705	0.00017	1.8×10^{-38}	0 0 0	2 0 0	6 3 3	5 3 2	-0.088
4460.06375	0.00017	1.8×10^{-38}	0 0 0	2 0 0	6 3 4	5 3 3	-0.088
4461.98415	0.00011	3.2×10^{-38}	0 0 0	2 0 0	6 2 5	5 2 4	-0.068
4465.98956	0.00006	5.1×10^{-38}	0 0 0	2 0 0	6 0 6	5 0 5	-0.054
4468.32508	0.00007	4.8×10^{-38}	0 0 0	2 0 0	6 1 6	5 1 5	-0.059
4471.18593	0.00346	9.0×10^{-40}	0 0 0	2 0 0	8 1 7	8 1 8	-0.041
4471.65134	0.00006	4.9×10^{-38}	0 0 0	2 0 0	5 1 4	4 1 3	-0.057
4472.76086	0.00080	5.7×10^{-39}	0 0 0	2 0 0	5 4 1	4 4 0	-0.123
4472.76086	0.00080	5.7×10^{-39}	0 0 0	2 0 0	5 4 2	4 4 1	-0.125
4472.99115	0.00009	3.5×10^{-38}	0 0 0	2 0 0	5 2 3	4 2 2	-0.071
4473.66397	0.00017	1.8×10^{-38}	0 0 0	2 0 0	5 3 2	4 3 1	-0.094
4473.77031	0.00018	1.8×10^{-38}	0 0 0	2 0 0	5 3 3	4 3 2	-0.094
4475.24300	0.00009	3.5×10^{-38}	0 0 0	2 0 0	5 2 4	4 2 3	-0.073
4477.98361	0.00005	5.8×10^{-38}	0 0 0	2 0 0	5 0 5	4 0 4	-0.057
4480.46098	0.00013	5.4×10^{-38}	0 0 0	2 0 0	5 1 5	4 1 4	-0.063
4485.47601	0.00006	5.1×10^{-38}	0 0 0	2 0 0	4 1 3	3 1 2	-0.062
4487.03202	0.00029	1.3×10^{-38}	0 0 0	2 0 0	4 3 1	3 3 0	-0.099
4487.06027	0.00030	1.3×10^{-38}	0 0 0	2 0 0	4 3 2	3 3 1	-0.100
4487.09096	0.00011	3.3×10^{-38}	0 0 0	2 0 0	4 2 2	3 2 1	-0.077
4488.23386	0.00012	3.3×10^{-38}	0 0 0	2 0 0	4 2 3	3 2 2	-0.078
4490.03518	0.00005	6.1×10^{-38}	0 0 0	2 0 0	4 0 4	3 0 3	-0.060
4492.38578	0.00006	5.4×10^{-38}	0 0 0	2 0 0	4 1 4	3 1 3	-0.066
4493.17852	0.00351	9.8×10^{-40}	0 0 0	2 0 0	9 2 7	9 2 8	-0.043
4497.77735*	0.00142	2.4×10^{-39}	0 0 0	2 0 0	6 1 5	6 1 6	-0.056
4499.02977	0.00007	4.6×10^{-38}	0 0 0	2 0 0	3 1 2	2 1 1	-0.066
4500.47232	0.00014	2.3×10^{-38}	0 0 0	2 0 0	3 2 1	2 2 0	-0.081
4500.73359*	0.00467	8.3×10^{-40}	0 0 0	2 0 0	5 1 4	5 0 5	-0.110
4500.92639*	0.00014	2.3×10^{-38}	0 0 0	2 0 0	3 2 2	2 2 1	-0.081
4502.13276	0.00006	5.7×10^{-38}	0 0 0	2 0 0	3 0 3	2 0 2	-0.063
4504.08219	0.00007	4.7×10^{-38}	0 0 0	2 0 0	3 1 3	2 1 2	-0.069

Position	$\sigma_{\text{Pos.}}$	Intensity	$\nu_1\,\nu_2\,\nu_3$	$\nu_1'\,\nu_2'\,\nu_3'$	J K_a K_c	J' K_a' K_c'	$\Delta_{\text{SPEC.}}$
4504.62233	0.00166	1.9×10^{-39}	0 0 0	2 0 0	8 2 6	8 2 7	-0.051
4506.85365	0.00332	8.2×10^{-40}	0 0 0	2 0 0	10 3 7	10 3 8	-0.061
4507.98835	0.00301	1.0×10^{-39}	0 0 0	2 0 0	4 1 3	4 0 4	-0.062
4508.91641	0.00952	3.9×10^{-39}	0 0 0	2 0 0	5 1 4	5 1 5	-0.059
4512.10438	0.00345	9.1×10^{-40}	0 0 0	2 0 0	10 4 6	10 4 7	-0.090
4512.25351	0.00010	3.1×10^{-38}	0 0 0	2 0 0	2 1 1	1 1 0	-0.070
4512.98271	0.00286	9.1×10^{-40}	0 0 0	2 0 0	10 4 7	10 4 6	-0.089
4513.43437	0.00278	1.1×10^{-39}	0 0 0	2 0 0	3 1 2	3 0 3	-0.064
4513.72900	0.00388	8.4×10^{-40}	0 0 0	2 0 0	9 6 3	9 6 4	-0.180
4513.72900	0.00384	8.4×10^{-40}	0 0 0	2 0 0	9 6 4	9 6 3	-0.180
4513.92054	0.00174	1.7×10^{-39}	0 0 0	2 0 0	9 3 6	9 3 7	-0.063
4514.13661	0.00099	3.5×10^{-39}	0 0 0	2 0 0	7 2 5	7 2 6	-0.062
4514.19468	0.00007	4.4×10^{-38}	0 0 0	2 0 0	2 0 2	1 0 1	-0.066
4515.28547	0.00269	1.4×10^{-39}	0 0 0	2 0 0	9 5 4	9 5 5	-0.130
4515.28547	0.00267	1.4×10^{-39}	0 0 0	2 0 0	9 5 5	9 5 4	-0.139
4515.52538	0.00010	3.1×10^{-38}	0 0 0	2 0 0	2 1 2	1 1 1	-0.071
4515.71969	0.00278	7.7×10^{-40}	0 0 0	2 0 0	8 7 1	8 7 2	-0.237
4515.71969	0.00278	7.7×10^{-40}	0 0 0	2 0 0	8 7 2	8 7 1	-0.237
4516.45867	0.00151	1.8×10^{-39}	0 0 0	2 0 0	9 4 5	9 4 6	-0.095
4516.83919	0.00138	1.8×10^{-39}	0 0 0	2 0 0	9 4 6	9 4 5	-0.097
4517.29382	0.00322	1.0×10^{-39}	0 0 0	2 0 0	2 1 1	2 0 2	-0.072
4517.35483	0.00142	1.6×10^{-39}	0 0 0	2 0 0	8 6 2	8 6 3	-0.185
4517.35483	0.00142	1.6×10^{-39}	0 0 0	2 0 0	8 6 3	8 6 2	-0.185
4518.35742	0.00052	6.2×10^{-39}	0 0 0	2 0 0	4 1 3	4 1 4	-0.064
4518.92594	0.01088	2.6×10^{-39}	0 0 0	2 0 0	8 5 3	8 5 4	-0.137
4518.92594	0.01088	2.6×10^{-39}	0 0 0	2 0 0	8 5 4	8 5 3	-0.140
4518.92594	0.01674	1.4×10^{-39}	0 0 0	2 0 0	7 7 1	7 7 0	-0.251
4518.92594	0.01674	1.4×10^{-39}	0 0 0	2 0 0	7 7 0	7 7 1	-0.251
4519.46465	0.00090	3.2×10^{-39}	0 0 0	2 0 0	8 3 5	8 3 6	-0.075
4519.99985	0.00351	8.2×10^{-40}	0 0 0	2 0 0	10 3 8	10 3 7	-0.055
4520.24454	0.00084	3.4×10^{-39}	0 0 0	2 0 0	8 4 4	8 4 5	-0.104
4520.39314	0.00083	3.4×10^{-39}	0 0 0	2 0 0	8 4 5	8 4 4	-0.105
4520.56967	0.00615	2.8×10^{-39}	0 0 0	2 0 0	7 6 2	7 6 1	-0.192
4520.56967	0.00615	2.8×10^{-39}	0 0 0	2 0 0	7 6 1	7 6 2	-0.192
4521.35642	0.00244	1.7×10^{-39}	0 0 0	2 0 0	9 3 7	9 3 6	-0.067
4521.68891*	0.00060	6.4×10^{-39}	0 0 0	2 0 0	6 2 4	6 2 5	-0.074
4522.14456	0.00050	4.6×10^{-39}	0 0 0	2 0 0	7 5 2	7 5 3	-0.149
4522.14456	0.00049	4.6×10^{-39}	0 0 0	2 0 0	7 5 3	7 5 2	-0.150
4523.32277	0.00090	3.2×10^{-39}	0 0 0	2 0 0	8 3 6	8 3 5	-0.075
4523.37612	0.00078	4.8×10^{-39}	0 0 0	2 0 0	6 6 1	6 6 0	-0.201
4523.37612	0.00078	4.8×10^{-39}	0 0 0	2 0 0	6 6 0	6 6 1	-0.201

Position	$\sigma_{\text{Pos.}}$	Intensity	$\nu_1\,\nu_2\,\nu_3$	$\nu_1{}'\,\nu_2{}'\,\nu_3{}'$	$J\,K_a\,K_c$	$J'\,K_a{}'\,K_c{}'$	$\Delta_{\text{SPEC.}}$
4523.53829	0.00044	6.1×10^{-39}	0 0 0	2 0 0	7 4 3	7 4 4	-0.112
4523.58786	0.00045	6.1×10^{-39}	0 0 0	2 0 0	7 4 4	7 4 3	-0.113
4523.80201	0.00048	5.9×10^{-39}	0 0 0	2 0 0	7 3 4	7 3 5	-0.083
4524.95392	0.00199	7.9×10^{-39}	0 0 0	2 0 0	6 5 1	6 5 2	-0.159
4524.95975	0.00200	7.9×10^{-39}	0 0 0	2 0 0	6 5 2	6 5 1	-0.153
4525.60120	0.00052	5.9×10^{-39}	0 0 0	2 0 0	7 3 5	7 3 4	-0.082
4525.99097	0.00030	1.0×10^{-38}	0 0 0	2 0 0	3 1 2	3 1 3	-0.068
4526.10247	0.00012	2.5×10^{-38}	0 0 0	2 0 0	1 0 1	0 0 0	-0.068
4526.38391	0.00044	1.0×10^{-38}	0 0 0	2 0 0	6 4 2	6 4 3	-0.117
4526.39362	0.00044	1.0×10^{-38}	0 0 0	2 0 0	6 4 3	6 4 2	-0.121
4527.20216	0.00028	1.0×10^{-38}	0 0 0	2 0 0	6 3 3	6 3 4	-0.089
4527.36430	0.00191	1.1×10^{-38}	0 0 0	2 0 0	5 2 3	5 2 4	-0.082
4527.36430	0.00169	1.3×10^{-38}	0 0 0	2 0 0	5 5 0	5 5 1	-0.160
4527.36430	0.00169	1.3×10^{-38}	0 0 0	2 0 0	5 5 1	5 5 0	-0.160
4527.93425	0.00028	1.0×10^{-38}	0 0 0	2 0 0	6 3 4	6 3 3	-0.089
4528.80133	0.00090	1.7×10^{-38}	0 0 0	2 0 0	5 4 1	5 4 2	-0.124
4528.80133	0.00090	1.7×10^{-38}	0 0 0	2 0 0	5 4 2	5 4 1	-0.126
4529.88202	0.00019	1.7×10^{-38}	0 0 0	2 0 0	5 3 2	5 3 3	-0.095
4530.12840	0.00037	1.7×10^{-38}	0 0 0	2 0 0	5 3 3	5 3 2	-0.095
4530.80700	0.00101	2.8×10^{-38}	0 0 0	2 0 0	4 4 0	4 4 1	-0.128
4530.80320	0.00101	2.8×10^{-38}	0 0 0	2 0 0	4 4 1	4 4 0	-0.132
4531.37940	0.00020	1.8×10^{-38}	0 0 0	2 0 0	4 2 2	4 2 3	-0.078
4531.75183	0.00019	1.7×10^{-38}	0 0 0	2 0 0	2 1 1	2 1 2	-0.071
4531.99102	0.00011	2.8×10^{-38}	0 0 0	2 0 0	4 3 1	4 3 2	-0.099
4532.05267	0.00011	2.8×10^{-38}	0 0 0	2 0 0	4 3 2	4 3 1	-0.100
4533.62599	0.00044	4.6×10^{-38}	0 0 0	2 0 0	3 3 0	3 3 1	-0.099
4533.62599	0.00044	4.6×10^{-38}	0 0 0	2 0 0	3 3 1	3 3 0	-0.108
4534.02466	0.00010	3.0×10^{-38}	0 0 0	2 0 0	3 2 1	3 2 2	-0.081
4534.35102	0.00030	1.1×10^{-38}	0 0 0	2 0 0	5 2 4	5 2 3	-0.073
4534.45419	0.00016	1.8×10^{-38}	0 0 0	2 0 0	4 2 3	4 2 2	-0.078
4535.06532	0.00294	6.3×10^{-39}	0 0 0	2 0 0	6 2 5	6 2 4	-0.066
4535.06532	0.00062	3.0×10^{-38}	0 0 0	2 0 0	3 2 2	3 2 1	-0.081
4535.60440	0.00010	3.4×10^{-38}	0 0 0	2 0 0	1 1 0	1 1 1	-0.072
4535.64852	0.00006	5.2×10^{-38}	0 0 0	2 0 0	2 2 0	2 2 1	-0.084
4535.85805	0.00006	5.2×10^{-38}	0 0 0	2 0 0	2 2 1	2 2 0	-0.084
4536.82842	0.00082	3.5×10^{-39}	0 0 0	2 0 0	7 2 6	7 2 5	-0.058
4538.67093	0.00011	3.4×10^{-38}	0 0 0	2 0 0	1 1 1	1 1 0	-0.072
4539.75547	0.00176	1.9×10^{-39}	0 0 0	2 0 0	8 2 7	8 2 6	-0.053
4540.94686	0.00017	1.7×10^{-38}	0 0 0	2 0 0	2 1 2	2 1 1	-0.071
4543.86832	0.00262	9.4×10^{-40}	0 0 0	2 0 0	9 2 8	9 2 7	-0.045
4544.35964	0.00032	9.8×10^{-39}	0 0 0	2 0 0	3 1 3	3 1 2	-0.069

Position	$\sigma_{\text{Pos.}}$	Intensity	$\nu_1\,\nu_2\,\nu_3$	$\nu_1{}'\,\nu_2{}'\,\nu_3{}'$	J K_a K_c	J' $K_a{}'$ $K_c{}'$	$\Delta_{\text{SPEC.}}$
4548.89538	0.00049	6.0×10^{-39}	0 0 0	2 0 0	4 1 4	4 1 3	-0.065
4548.96746	0.00023	2.5×10^{-38}	0 0 0	2 0 0	0 0 0	1 0 1	-0.069
4554.51643	0.00074	3.7×10^{-39}	0 0 0	2 0 0	5 1 5	5 1 4	-0.060
4554.66183	0.00365	7.6×10^{-40}	0 0 0	2 0 0	1 0 1	1 1 0	-0.070
4555.46041	0.00236	1.1×10^{-39}	0 0 0	2 0 0	2 0 2	2 1 1	-0.067
4556.86419	0.00211	1.2×10^{-39}	0 0 0	2 0 0	3 0 3	3 1 2	-0.066
4558.16908	0.00009	3.3×10^{-38}	0 0 0	2 0 0	1 1 1	2 1 2	-0.073
4559.10275	0.00263	1.1×10^{-39}	0 0 0	2 0 0	4 0 4	4 1 3	-0.063
4559.70658	0.00006	4.7×10^{-38}	0 0 0	2 0 0	1 0 1	2 0 2	-0.068
4561.02636	0.00009	3.2×10^{-38}	0 0 0	2 0 0	1 1 0	2 1 1	-0.072
4561.14152	0.00124	2.3×10^{-39}	0 0 0	2 0 0	6 1 6	6 1 5	-0.056
4562.40872	0.00422	8.9×10^{-40}	0 0 0	2 0 0	5 0 5	5 1 4	-0.056
4566.87901	0.00274	1.1×10^{-39}	0 0 0	2 0 0	3 1 3	4 0 4	-0.062
4567.90916	0.00018	5.2×10^{-38}	0 0 0	2 0 0	2 1 2	3 1 3	-0.072
4568.63807	0.00189	1.4×10^{-39}	0 0 0	2 0 0	7 1 7	7 1 6	-0.054
4569.41007	0.00011	2.5×10^{-38}	0 0 0	2 0 0	2 2 1	3 2 2	-0.085
4569.78765	0.00012	2.5×10^{-38}	0 0 0	2 0 0	2 2 0	3 2 1	-0.084
4569.86315	0.00013	6.3×10^{-38}	0 0 0	2 0 0	2 0 2	3 0 3	-0.067
4572.02969	0.00006	5.0×10^{-38}	0 0 0	2 0 0	2 1 1	3 1 2	-0.070
4574.16293	0.00308	9.6×10^{-40}	0 0 0	2 0 0	1 0 1	2 1 2	-0.068
4576.82674	0.00466	8.1×10^{-40}	0 0 0	2 0 0	8 1 8	8 1 7	-0.034
4577.24159	0.00004	6.2×10^{-38}	0 0 0	2 0 0	3 1 3	4 1 4	-0.070
4578.03285	0.00173	1.4×10^{-39}	0 0 0	2 0 0	4 1 4	5 0 5	-0.063
4578.58949	0.00026	1.5×10^{-38}	0 0 0	2 0 0	3 3 1	4 3 2	-0.104
4578.61248	0.00027	1.5×10^{-38}	0 0 0	2 0 0	3 3 0	4 3 1	-0.104
4579.35410	0.00010	3.8×10^{-38}	0 0 0	2 0 0	3 2 2	4 2 3	-0.082
4579.37857	0.00005	7.0×10^{-38}	0 0 0	2 0 0	3 0 3	4 0 4	-0.064
4580.24558	0.00008	3.7×10^{-38}	0 0 0	2 0 0	3 2 1	4 2 2	-0.081
4582.42160	0.00223	1.3×10^{-39}	0 0 0	2 0 0	2 0 2	3 1 3	-0.069
4582.50083	0.00005	5.8×10^{-38}	0 0 0	2 0 0	3 1 2	4 1 3	-0.067
4586.16021	0.00005	6.4×10^{-38}	0 0 0	2 0 0	4 1 4	5 1 5	-0.068
4586.84491	0.00149	6.7×10^{-39}	0 0 0	2 0 0	4 4 1	5 4 2	-0.131
4586.84491	0.00149	6.7×10^{-39}	0 0 0	2 0 0	4 4 0	5 4 1	-0.132
4588.23885	0.00004	6.9×10^{-38}	0 0 0	2 0 0	4 0 4	5 0 5	-0.062
4588.26957	0.00017	2.1×10^{-38}	0 0 0	2 0 0	4 3 2	5 3 3	-0.101
4588.34888	0.00014	2.1×10^{-38}	0 0 0	2 0 0	4 3 1	5 3 2	-0.100
4588.59825	0.00193	1.6×10^{-39}	0 0 0	2 0 0	5 1 5	6 0 6	-0.064
4588.83738	0.00007	4.2×10^{-38}	0 0 0	2 0 0	4 2 3	5 2 4	-0.079
4589.74541	0.00163	1.6×10^{-39}	0 0 0	2 0 0	3 0 3	4 1 4	-0.068
4590.48810	0.00007	4.1×10^{-38}	0 0 0	2 0 0	4 2 2	5 2 3	-0.077
4592.41196	0.00007	5.8×10^{-38}	0 0 0	2 0 0	4 1 3	5 1 4	-0.063

Position	$\sigma_{\text{Pos.}}$	Intensity	$\nu_1\ \nu_2\ \nu_3$	$\nu_1'\ \nu_2'\ \nu_3'$	J K_a K_c	J' K_a' K_c'	$\Delta_{\text{SPEC.}}$
4594.36579	0.00081	2.5×10^{-39}	0 0 0	2 0 0	5 5 1	6 5 2	-0.164
4594.36579	0.00081	2.5×10^{-39}	0 0 0	2 0 0	5 5 0	6 5 1	-0.164
4594.66538	0.00004	5.9×10^{-38}	0 0 0	2 0 0	5 1 5	6 1 6	-0.065
4596.08708	0.00042	9.2×10^{-39}	0 0 0	2 0 0	5 4 2	6 4 3	-0.124
4596.08708	0.00042	9.2×10^{-39}	0 0 0	2 0 0	5 4 1	6 4 2	-0.129
4596.36683	0.00165	1.8×10^{-39}	0 0 0	2 0 0	4 0 4	5 1 5	-0.066
4596.49024	0.00005	6.2×10^{-38}	0 0 0	2 0 0	5 0 5	6 0 6	-0.060
4597.55335	0.00012	2.2×10^{-38}	0 0 0	2 0 0	5 3 3	6 3 4	-0.096
4597.75183	0.00012	2.2×10^{-38}	0 0 0	2 0 0	5 3 2	6 3 3	-0.096
4597.85132	0.00007	3.9×10^{-38}	0 0 0	2 0 0	5 2 4	6 2 5	-0.075
4598.43588	0.00197	1.6×10^{-39}	0 0 0	2 0 0	6 1 6	7 0 7	-0.058
4600.45492	0.00007	3.8×10^{-38}	0 0 0	2 0 0	5 2 3	6 2 4	-0.071
4601.73150	0.00006	5.1×10^{-38}	0 0 0	2 0 0	5 1 4	6 1 5	-0.058
4602.55560	0.00159	1.8×10^{-39}	0 0 0	2 0 0	5 0 5	6 1 6	-0.063
4602.76430	0.00005	5.1×10^{-38}	0 0 0	2 0 0	6 1 6	7 1 7	-0.063
4603.14191	0.00062	3.2×10^{-39}	0 0 0	2 0 0	6 5 2	7 5 3	-0.159
4603.14191	0.00062	3.2×10^{-39}	0 0 0	2 0 0	6 5 1	7 5 2	-0.159
4604.22756	0.00005	5.2×10^{-38}	0 0 0	2 0 0	6 0 6	7 0 7	-0.058
4604.93474	0.00106	9.2×10^{-39}	0 0 0	2 0 0	6 4 3	7 4 4	-0.119
4604.94642	0.00106	9.2×10^{-39}	0 0 0	2 0 0	6 4 2	7 4 3	-0.122
4606.39085	0.00009	3.3×10^{-38}	0 0 0	2 0 0	6 2 5	7 2 6	-0.070
4606.42237	0.00015	2.0×10^{-38}	0 0 0	2 0 0	6 3 4	7 3 5	-0.091
4606.84305	0.00014	2.0×10^{-38}	0 0 0	2 0 0	6 3 3	7 3 4	-0.090
4607.48722	0.00179	1.4×10^{-39}	0 0 0	2 0 0	7 1 7	8 0 8	-0.062
4608.44634	0.00294	8.7×10^{-40}	0 0 0	2 0 0	1 1 0	2 2 1	-0.074
4608.55404	0.00152	1.7×10^{-39}	0 0 0	2 0 0	6 0 6	7 1 7	-0.064
4609.52351	0.00200	9.2×10^{-40}	0 0 0	2 0 0	7 6 2	8 6 3	-0.197
4609.52351	0.00200	9.2×10^{-40}	0 0 0	2 0 0	7 6 1	8 6 2	-0.197
4610.03888	0.00009	3.2×10^{-38}	0 0 0	2 0 0	6 2 4	7 2 5	-0.063
4610.11971	0.00365	8.3×10^{-40}	0 0 0	2 0 0	1 1 1	2 2 0	-0.084
4610.42930	0.00007	4.2×10^{-38}	0 0 0	2 0 0	6 1 5	7 1 6	-0.052
4610.46915	0.00008	4.0×10^{-38}	0 0 0	2 0 0	7 1 7	8 1 8	-0.059
4611.55576	0.00007	4.1×10^{-38}	0 0 0	2 0 0	7 0 7	8 0 8	-0.055
4611.51794	0.00111	3.1×10^{-39}	0 0 0	2 0 0	7 5 3	8 5 4	-0.153
4611.51794	0.00111	3.1×10^{-39}	0 0 0	2 0 0	7 5 2	8 5 3	-0.154
4613.38592	0.00036	7.8×10^{-39}	0 0 0	2 0 0	7 4 4	8 4 5	-0.114
4613.42271	0.00037	7.8×10^{-39}	0 0 0	2 0 0	7 4 3	8 4 4	-0.115
4614.45287	0.00010	2.6×10^{-38}	0 0 0	2 0 0	7 2 6	8 2 7	-0.065
4614.53261	0.00168	1.5×10^{-39}	0 0 0	2 0 0	7 0 7	8 1 8	-0.058
4614.85946	0.00017	1.6×10^{-38}	0 0 0	2 0 0	7 3 5	8 3 6	-0.084
4615.63856	0.00025	1.6×10^{-38}	0 0 0	2 0 0	7 3 4	8 3 5	-0.084

Position	$\sigma_{\text{Pos.}}$	Intensity	$\nu_1\,\nu_2\,\nu_3$	$\nu_1'\,\nu_2'\,\nu_3'$	J K_a K_c	J' K_a' K_c'	$\Delta_{\text{SPEC.}}$
4615.80891	0.00188	1.2×10^{-39}	0 0 0	2 0 0	8 1 8	9 0 9	-0.054
4617.25984	0.00348	9.5×10^{-40}	0 0 0	2 0 0	2 1 1	3 2 2	-0.076
4617.42168	0.00293	8.3×10^{-40}	0 0 0	2 0 0	8 6 3	9 6 4	-0.190
4617.42168	0.00293	8.3×10^{-40}	0 0 0	2 0 0	8 6 2	9 6 3	-0.190
4617.79427	0.00009	3.0×10^{-38}	0 0 0	2 0 0	8 1 8	9 1 9	-0.056
4618.47934	0.00009	3.1×10^{-38}	0 0 0	2 0 0	7 1 6	8 1 7	-0.046
4618.55314	0.00009	3.0×10^{-38}	0 0 0	2 0 0	8 0 8	9 0 9	-0.052
4619.12223	0.00011	2.4×10^{-38}	0 0 0	2 0 0	7 2 5	8 2 6	-0.055
4619.49175	0.00081	2.5×10^{-39}	0 0 0	2 0 0	8 5 4	9 5 5	-0.144
4619.49175	0.00081	2.5×10^{-39}	0 0 0	2 0 0	8 5 3	9 5 4	-0.147
4620.54116	0.00205	1.3×10^{-39}	0 0 0	2 0 0	8 0 8	9 1 9	-0.052
4621.43509	0.00044	5.9×10^{-39}	0 0 0	2 0 0	8 4 5	9 4 6	-0.107
4621.51969	0.00044	5.9×10^{-39}	0 0 0	2 0 0	8 4 4	9 4 5	-0.107
4622.04080	0.00014	1.9×10^{-38}	0 0 0	2 0 0	8 2 7	9 2 8	-0.059
4622.50216	0.00362	8.5×10^{-40}	0 0 0	2 0 0	2 1 2	3 2 1	-0.076
4622.84606	0.00023	1.1×10^{-38}	0 0 0	2 0 0	8 3 6	9 3 7	-0.076
4623.46984	0.00534	9.4×10^{-40}	0 0 0	2 0 0	9 1 9	10 0 10	-0.042
4624.15009	0.00034	1.1×10^{-38}	0 0 0	2 0 0	8 3 5	9 3 6	-0.072
4624.75399	0.00012	2.1×10^{-38}	0 0 0	2 0 0	9 1 9	10 1 10	-0.052
4624.87338	0.00343	1.0×10^{-39}	0 0 0	2 0 0	3 1 2	4 2 3	-0.073
4625.25968	0.00012	2.1×10^{-38}	0 0 0	2 0 0	9 0 9	10 0 10	-0.049
4625.86940	0.00014	2.2×10^{-38}	0 0 0	2 0 0	8 1 7	9 1 8	-0.041
4626.55739	0.00262	9.6×10^{-40}	0 0 0	2 0 0	9 0 9	10 1 10	-0.045
4627.06078	0.00187	1.8×10^{-39}	0 0 0	2 0 0	9 5 5	10 5 6	-0.133
4627.06078	0.00186	1.8×10^{-39}	0 0 0	2 0 0	9 5 4	10 5 5	-0.140
4627.61619	0.00016	1.7×10^{-38}	0 0 0	2 0 0	8 2 6	9 2 7	-0.045
4629.07201	0.00074	4.0×10^{-39}	0 0 0	2 0 0	9 4 6	10 4 7	-0.098
4629.16019	0.00024	1.3×10^{-38}	0 0 0	2 0 0	9 2 8	10 2 9	-0.053
4629.24443	0.00076	4.0×10^{-39}	0 0 0	2 0 0	9 4 5	10 4 6	-0.098
4630.36484	0.00032	7.7×10^{-39}	0 0 0	2 0 0	9 3 7	10 3 8	-0.068
4631.30417	0.00251	1.0×10^{-39}	0 0 0	2 0 0	4 1 3	5 2 4	-0.075
4631.36157	0.00018	1.3×10^{-38}	0 0 0	2 0 0	10 1 10	11 1 11	-0.047
4631.68629	0.00018	1.4×10^{-38}	0 0 0	2 0 0	10 0 10	11 0 11	-0.046
4632.35308	0.00038	7.5×10^{-39}	0 0 0	2 0 0	9 3 6	10 3 7	-0.061
4632.61475	0.00019	1.4×10^{-38}	0 0 0	2 0 0	9 1 8	10 1 9	-0.035
4634.21661	0.00348	1.1×10^{-39}	0 0 0	2 0 0	10 5 6	11 5 7	-0.124
4634.22714	0.00338	1.1×10^{-39}	0 0 0	2 0 0	10 5 5	11 5 6	-0.129
4635.46801	0.00025	1.1×10^{-38}	0 0 0	2 0 0	9 2 7	10 2 8	-0.034
4635.82265	0.00089	8.1×10^{-39}	0 0 0	2 0 0	10 2 9	11 2 10	-0.047
4635.82265	0.00839	7.8×10^{-40}	0 0 0	2 0 0	3 1 3	4 2 2	-0.063
4636.28436	0.00093	2.6×10^{-39}	0 0 0	2 0 0	10 4 7	11 4 8	-0.088

Position	$\sigma_{\text{Pos.}}$	Intensity	$\nu_1\,\nu_2\,\nu_3$	$\nu_1'\,\nu_2'\,\nu_3'$	J K_a K_c	J' K_a' K_c'	$\Delta_{\text{SPEC.}}$
4636.60431	0.00100	2.6×10^{-39}	0 0 0	2 0 0	10 4 6	11 4 7	-0.087
4636.62946	0.00351	9.4×10^{-40}	0 0 0	2 0 0	5 1 4	6 2 5	-0.066
4637.40339	0.00053	4.8×10^{-39}	0 0 0	2 0 0	10 3 8	11 3 9	-0.060
4637.62703	0.00029	8.3×10^{-39}	0 0 0	2 0 0	11 1 11	12 1 12	-0.043
4637.83037	0.00029	8.4×10^{-39}	0 0 0	2 0 0	11 0 11	12 0 12	-0.042
4638.76555	0.00032	8.7×10^{-39}	0 0 0	2 0 0	10 1 9	11 1 10	-0.030
4640.19525	0.00061	4.6×10^{-39}	0 0 0	2 0 0	10 3 7	11 3 8	-0.048
4640.93468	0.00407	8.4×10^{-40}	0 0 0	2 0 0	6 1 5	7 2 6	-0.058
4642.04322	0.00064	4.8×10^{-39}	0 0 0	2 0 0	11 2 10	12 2 11	-0.040
4642.65463	0.00040	6.6×10^{-39}	0 0 0	2 0 0	10 2 8	11 2 9	-0.024
4643.05684	0.00158	1.5×10^{-39}	0 0 0	2 0 0	11 4 8	12 4 9	-0.079
4643.55961	0.00052	4.9×10^{-39}	0 0 0	2 0 0	12 1 12	13 1 13	-0.037
4643.60757	0.00172	1.5×10^{-39}	0 0 0	2 0 0	11 4 7	12 4 8	-0.075
4643.68360	0.00051	4.9×10^{-39}	0 0 0	2 0 0	12 0 12	13 0 13	-0.036
4643.95441	0.00099	2.8×10^{-39}	0 0 0	2 0 0	11 3 9	12 3 10	-0.050
4644.40668	0.00053	5.1×10^{-39}	0 0 0	2 0 0	11 1 10	12 1 11	-0.025
4647.59221	0.00110	2.6×10^{-39}	0 0 0	2 0 0	11 3 8	12 3 9	-0.034
4647.83723	0.00098	2.7×10^{-39}	0 0 0	2 0 0	12 2 11	13 2 12	-0.032
4649.16103	0.00124	3.7×10^{-39}	0 0 0	2 0 0	11 2 9	12 2 10	-0.021
4649.17026	0.00180	2.7×10^{-39}	0 0 0	2 0 0	13 1 13	14 1 14	-0.023
4649.23550	0.00279	2.7×10^{-39}	0 0 0	2 0 0	13 0 13	14 0 14	-0.032
4649.37517	0.00280	8.4×10^{-40}	0 0 0	2 0 0	12 4 9	13 4 10	-0.069
4649.63009	0.00092	2.8×10^{-39}	0 0 0	2 0 0	12 1 11	13 1 12	-0.021
4650.01757	0.00158	1.5×10^{-39}	0 0 0	2 0 0	12 3 10	13 3 11	-0.038
4650.25863	0.00276	8.3×10^{-40}	0 0 0	2 0 0	12 4 8	13 4 9	-0.063
4651.72815	0.00322	1.1×10^{-39}	0 0 0	2 0 0	2 2 0	3 3 1	-0.094
4651.84251	0.00266	1.1×10^{-39}	0 0 0	2 0 0	2 2 1	3 3 0	-0.095
4653.21931	0.00150	1.4×10^{-39}	0 0 0	2 0 0	13 2 12	14 2 13	-0.028
4654.43754	0.00281	1.4×10^{-39}	0 0 0	2 0 0	14 1 14	15 1 15	-0.026
4654.44728	0.00328	1.4×10^{-39}	0 0 0	2 0 0	12 3 9	13 3 10	-0.020
4654.48059	0.00212	1.4×10^{-39}	0 0 0	2 0 0	14 0 14	15 0 15	-0.027
4654.51503	0.00193	1.5×10^{-39}	0 0 0	2 0 0	13 1 12	14 1 13	-0.018
4655.01265	0.00140	1.9×10^{-39}	0 0 0	2 0 0	12 2 10	13 2 11	-0.004
4655.59012	0.00248	8.0×10^{-40}	0 0 0	2 0 0	13 3 11	14 3 12	-0.030
4660.19686	0.00403	9.6×10^{-40}	0 0 0	2 0 0	13 2 11	14 2 12	0.000
4661.41394	0.00280	1.1×10^{-39}	0 0 0	2 0 0	3 2 1	4 3 2	-0.095
4661.99880	0.00317	1.1×10^{-39}	0 0 0	2 0 0	3 2 2	4 3 1	-0.091
4670.24076	0.00256	9.8×10^{-40}	0 0 0	2 0 0	4 2 2	5 3 3	-0.089
4671.98209	0.00351	9.7×10^{-40}	0 0 0	2 0 0	4 2 3	5 3 2	-0.091
4681.97639	0.00497	8.4×10^{-40}	0 0 0	2 0 0	5 2 4	6 3 3	-0.083
4693.02821	0.01869	9.5×10^{-40}	0 0 0	2 0 0	3 3 0	4 4 1	-0.118

Position	$\sigma_{\mathrm{Pos.}}$	Intensity	$\nu_1\ \nu_2\ \nu_3$	$\nu_1'\ \nu_2'\ \nu_3'$	J K_a K_c	J' K_a' K_c'	$\Delta_{\mathrm{SPEC.}}$
4693.02821	0.01873	9.5×10^{-40}	0 0 0	2 0 0	3 3 1	4 4 0	-0.123
4702.48142	0.00498	8.6×10^{-40}	0 0 0	2 0 0	4 3 1	5 4 2	-0.107
4702.50911	0.00277	8.6×10^{-40}	0 0 0	2 0 0	4 3 2	5 4 1	-0.115

A.2.1.2 HTO $2\nu_1$ band from the 10 GBq sample

Here, the lines assigned to the $2\nu_1$ from the $10\,\mathrm{GBq}$ sample are presented. These lines are published in [Her23]. For further information, see Section 5.5.1.

Table A.3: Linelist of the $2\nu_1$ from the 10 GBq sample. The columns present the assigned line position, the uncertainty on the position $\sigma_{\mathrm{Pos.}}$, the line intensity taking natural abundance into account, lower and upper vibrational quanta, lower and upper rotational quanta and the deviation to the predictions from SPECTRA database $\Delta_{\mathrm{SPEC.}}$.

Position	$\sigma_{\mathrm{Pos.}}$	Intensity	$\nu_1\ \nu_2\ \nu_3$	$\nu_1'\ \nu_2'\ \nu_3'$	J K_a K_c	J' K_a' K_c'	$\Delta_{\mathrm{SPEC.}}$
4322.92414	0.00548	2.4×10^{-40}	0 0 0	2 0 0	15 3 13	14 3 12	-0.008
4326.07501	0.00566	4.5×10^{-40}	0 0 0	2 0 0	14 3 11	13 3 10	0.011
4329.96420	0.00373	6.2×10^{-40}	0 0 0	2 0 0	14 2 12	13 2 11	0.020
4331.65440	0.00729	2.7×10^{-40}	0 0 0	2 0 0	14 4 10	13 4 9	-0.030
4332.31865	0.00417	4.4×10^{-40}	0 0 0	2 0 0	15 1 14	14 1 13	0.007
4334.30253	0.00474	4.3×10^{-40}	0 0 0	2 0 0	15 2 14	14 2 13	-0.007
4335.13397	0.00406	4.0×10^{-40}	0 0 0	2 0 0	16 0 16	15 0 15	0.005
4335.18649	0.00387	4.0×10^{-40}	0 0 0	2 0 0	16 1 16	15 1 15	-0.004
4344.55035	0.00218	9.3×10^{-40}	0 0 0	2 0 0	13 3 10	12 3 9	-0.005
4349.10621	0.00218	8.9×10^{-40}	0 0 0	2 0 0	14 2 13	13 2 12	-0.012
4349.46776	0.00204	8.4×10^{-40}	0 0 0	2 0 0	15 0 15	14 0 14	-0.010
4349.56787	0.00222	8.4×10^{-40}	0 0 0	2 0 0	15 1 15	14 1 14	-0.009
4349.73014	0.00383	5.5×10^{-40}	0 0 0	2 0 0	13 4 9	12 4 8	-0.047
4350.99379	0.00823	2.6×10^{-40}	0 0 0	2 0 0	13 5 8	12 5 7	-0.102
4351.15492	0.00468	2.6×10^{-40}	0 0 0	2 0 0	13 5 9	12 5 8	-0.090
4351.75581	0.00304	5.5×10^{-40}	0 0 0	2 0 0	13 4 10	12 4 9	-0.051
4354.86244	0.00207	1.0×10^{-39}	0 0 0	2 0 0	13 3 11	12 3 10	-0.026
4360.27239	0.00118	1.8×10^{-39}	0 0 0	2 0 0	13 1 12	12 1 11	-0.007
4362.04721	0.00126	2.5×10^{-39}	0 0 0	2 0 0	12 2 10	11 2 9	0.002
4362.79316	0.00184	1.8×10^{-39}	0 0 0	2 0 0	12 3 9	11 3 8	-0.019
4363.53764	0.00121	1.7×10^{-39}	0 0 0	2 0 0	14 0 14	13 0 13	-0.016
4363.69594	0.00143	1.7×10^{-39}	0 0 0	2 0 0	14 1 14	13 1 13	-0.016
4363.75029	0.00170	1.7×10^{-39}	0 0 0	2 0 0	13 2 12	12 2 11	-0.020
4367.09048	0.00192	1.0×10^{-39}	0 0 0	2 0 0	12 4 8	11 4 7	-0.061
4367.61249	0.00454	4.7×10^{-40}	0 0 0	2 0 0	12 5 7	11 5 6	-0.101
4367.68444	0.00427	4.7×10^{-40}	0 0 0	2 0 0	12 5 8	11 5 7	-0.099
4368.26745	0.00183	1.0×10^{-39}	0 0 0	2 0 0	12 4 9	11 4 8	-0.064
4370.62383	0.00129	1.9×10^{-39}	0 0 0	2 0 0	12 3 10	11 3 9	-0.035
4373.96816	0.00146	3.4×10^{-39}	0 0 0	2 0 0	12 1 11	11 1 10	-0.014
4377.32615	0.00110	3.1×10^{-39}	0 0 0	2 0 0	13 0 13	12 0 12	-0.023
4377.57202	0.00078	3.1×10^{-39}	0 0 0	2 0 0	13 1 13	12 1 12	-0.024
4378.24633	0.00089	3.2×10^{-39}	0 0 0	2 0 0	12 2 11	11 2 10	-0.028

Position	$\sigma_{\text{Pos.}}$	Intensity	$\nu_1\ \nu_2\ \nu_3$	$\nu_1'\ \nu_2'\ \nu_3'$	J K_a K_c	J' K_a' K_c'	$\Delta_{\text{SPEC.}}$
4378.31956	0.00067	4.7×10^{-39}	0 0 0	2 0 0	11 2 9	10 2 8	-0.013
4380.61457	0.00126	3.2×10^{-39}	0 0 0	2 0 0	11 3 8	10 3 7	-0.037
4382.96154	0.00766	3.0×10^{-40}	0 0 0	2 0 0	11 6 6	10 6 5	-0.161
4382.97809	0.00419	3.0×10^{-40}	0 0 0	2 0 0	11 6 5	10 6 4	-0.144
4383.77936	0.01509	8.1×10^{-40}	0 0 0	2 0 0	11 5 6	10 5 5	-0.088
4383.78872	0.00583	1.8×10^{-39}	0 0 0	2 0 0	11 4 7	10 4 6	-0.070
4384.42576	0.00176	1.8×10^{-39}	0 0 0	2 0 0	11 4 8	10 4 7	-0.075
4385.85946	0.00723	4.5×10^{-40}	0 0 0	2 0 0	6 2 4	5 0 5	-0.051
4386.20415	0.00077	3.4×10^{-39}	0 0 0	2 0 0	11 3 9	10 3 8	-0.046
4387.63433	0.00046	6.1×10^{-39}	0 0 0	2 0 0	11 1 10	10 1 9	-0.019
4390.82777	0.00049	5.5×10^{-39}	0 0 0	2 0 0	12 0 12	11 0 11	-0.029
4391.20834	0.00057	5.5×10^{-39}	0 0 0	2 0 0	12 1 12	11 1 11	-0.028
4392.60133	0.00055	5.6×10^{-39}	0 0 0	2 0 0	11 2 10	10 2 9	-0.035
4394.63657	0.00040	8.0×10^{-39}	0 0 0	2 0 0	10 2 8	9 2 7	-0.022
4397.85279	0.00434	5.4×10^{-39}	0 0 0	2 0 0	10 3 7	9 3 6	-0.052
4398.51475	0.00314	4.6×10^{-40}	0 0 0	2 0 0	10 6 4	9 6 3	-0.169
4398.54071	0.00527	4.6×10^{-40}	0 0 0	2 0 0	10 6 5	9 6 4	-0.144
4399.45520	0.00579	1.3×10^{-39}	0 0 0	2 0 0	10 5 5	9 5 4	-0.119
4399.46005	0.00576	1.3×10^{-39}	0 0 0	2 0 0	10 5 6	9 5 5	-0.126
4399.87554	0.00084	2.9×10^{-39}	0 0 0	2 0 0	10 4 6	9 4 5	-0.085
4400.19356	0.00072	2.9×10^{-39}	0 0 0	2 0 0	10 4 7	9 4 6	-0.090
4401.38727	0.00029	1.0×10^{-38}	0 0 0	2 0 0	10 1 9	9 1 8	-0.025
4401.56729	0.00056	5.6×10^{-39}	0 0 0	2 0 0	10 3 8	9 3 7	-0.057
4404.03312	0.00038	9.3×10^{-39}	0 0 0	2 0 0	11 0 11	10 0 10	-0.033
4404.60471	0.00043	9.2×10^{-39}	0 0 0	2 0 0	11 1 11	10 1 10	-0.034
4406.81399	0.00032	9.2×10^{-39}	0 0 0	2 0 0	10 2 9	9 2 8	-0.042
4410.89466	0.00105	1.3×10^{-38}	0 0 0	2 0 0	9 2 7	8 2 6	-0.035
4413.66783	0.01898	6.2×10^{-40}	0 0 0	2 0 0	9 6 3	8 6 2	-0.169
4413.66783	0.01898	6.2×10^{-40}	0 0 0	2 0 0	9 6 4	8 6 3	-0.169
4414.39688	0.00036	8.4×10^{-39}	0 0 0	2 0 0	9 3 6	8 3 5	-0.062
4414.71481	0.00271	1.8×10^{-39}	0 0 0	2 0 0	9 5 4	8 5 3	-0.130
4414.71481	0.00271	1.8×10^{-39}	0 0 0	2 0 0	9 5 5	8 5 4	-0.134
4415.29517	0.00023	1.6×10^{-38}	0 0 0	2 0 0	9 1 8	8 1 7	-0.031
4415.41328	0.00496	4.4×10^{-39}	0 0 0	2 0 0	9 4 5	8 4 4	-0.096
4415.57777	0.00189	4.4×10^{-39}	0 0 0	2 0 0	9 4 6	8 4 5	-0.081
4416.67583	0.00042	8.5×10^{-39}	0 0 0	2 0 0	9 3 7	8 3 6	-0.065
4416.93644	0.00027	1.5×10^{-38}	0 0 0	2 0 0	10 0 10	9 0 9	-0.037
4417.77141	0.00055	1.5×10^{-38}	0 0 0	2 0 0	10 1 10	9 1 9	-0.040
4420.87677	0.00023	1.4×10^{-38}	0 0 0	2 0 0	9 2 8	8 2 7	-0.049
4426.99725	0.00019	1.9×10^{-38}	0 0 0	2 0 0	8 2 6	7 2 5	-0.044
4428.39348	0.02461	7.1×10^{-40}	0 0 0	2 0 0	8 6 3	7 6 2	-0.187

Position	$\sigma_{\text{Pos.}}$	Intensity	$\nu_1\,\nu_2\,\nu_3$	$\nu_1'\,\nu_2'\,\nu_3'$	J K_a K_c	J' K_a' K_c'	$\Delta_{\text{SPEC.}}$
4428.40122	0.01682	7.1×10^{-40}	0 0 0	2 0 0	8 6 2	7 6 1	-0.180
4429.35311	0.00038	2.4×10^{-38}	0 0 0	2 0 0	8 1 7	7 1 6	-0.038
4429.54225	0.01336	2.4×10^{-39}	0 0 0	2 0 0	8 5 4	7 5 3	-0.146
4429.54225	0.00179	2.2×10^{-38}	0 0 0	2 0 0	9 0 9	8 0 8	-0.039
4429.55052	0.00554	2.4×10^{-39}	0 0 0	2 0 0	8 5 3	7 5 2	-0.136
4430.20701	0.00096	1.2×10^{-38}	0 0 0	2 0 0	8 3 5	7 3 4	-0.072
4430.44588	0.00086	6.0×10^{-39}	0 0 0	2 0 0	8 4 4	7 4 3	-0.104
4430.50693	0.00054	6.0×10^{-39}	0 0 0	2 0 0	8 4 5	7 4 4	-0.104
4430.71740	0.00017	2.2×10^{-38}	0 0 0	2 0 0	9 1 9	8 1 8	-0.046
4431.48664	0.00039	1.2×10^{-38}	0 0 0	2 0 0	8 3 6	7 3 5	-0.073
4434.77316	0.00071	2.0×10^{-38}	0 0 0	2 0 0	8 2 7	7 2 6	-0.056
4441.86844	0.00013	3.1×10^{-38}	0 0 0	2 0 0	8 0 8	7 0 7	-0.047
4442.72309	0.00391	5.9×10^{-40}	0 0 0	2 0 0	7 6 1	6 6 0	-0.195
4442.72309	0.00391	5.9×10^{-40}	0 0 0	2 0 0	7 6 2	6 6 1	-0.195
4442.81401	0.00028	2.6×10^{-38}	0 0 0	2 0 0	7 2 5	6 2 4	-0.055
4443.45405	0.00014	3.0×10^{-38}	0 0 0	2 0 0	8 1 8	7 1 7	-0.051
4443.49551	0.00019	3.3×10^{-38}	0 0 0	2 0 0	7 1 6	6 1 5	-0.045
4443.95886	0.00160	2.6×10^{-39}	0 0 0	2 0 0	7 5 3	6 5 2	-0.147
4443.95886	0.00160	2.6×10^{-39}	0 0 0	2 0 0	7 5 2	6 5 1	-0.147
4444.99964	0.00097	7.3×10^{-39}	0 0 0	2 0 0	7 4 3	6 4 2	-0.112
4445.02222	0.00066	7.3×10^{-39}	0 0 0	2 0 0	7 4 4	6 4 3	-0.111
4445.31377	0.00022	1.6×10^{-38}	0 0 0	2 0 0	7 3 4	6 3 3	-0.081
4445.95699	0.00077	1.6×10^{-38}	0 0 0	2 0 0	7 3 5	6 3 4	-0.085
4448.48475	0.00017	2.7×10^{-38}	0 0 0	2 0 0	7 2 6	6 2 5	-0.062
4453.98717	0.00033	4.1×10^{-38}	0 0 0	2 0 0	7 0 7	6 0 6	-0.050
4455.98825	0.00071	4.0×10^{-38}	0 0 0	2 0 0	7 1 7	6 1 6	-0.056
4457.62599	0.00025	4.3×10^{-38}	0 0 0	2 0 0	6 1 5	5 1 4	-0.053
4457.95294	0.00132	2.0×10^{-39}	0 0 0	2 0 0	6 5 2	5 5 1	-0.155
4457.95294	0.00132	2.0×10^{-39}	0 0 0	2 0 0	6 5 1	5 5 0	-0.155
4458.19606	0.00013	3.2×10^{-38}	0 0 0	2 0 0	6 2 4	5 2 3	-0.064
4459.10012	0.00264	7.6×10^{-39}	0 0 0	2 0 0	6 4 2	5 4 1	-0.118
4459.10643	0.00264	7.6×10^{-39}	0 0 0	2 0 0	6 4 3	5 4 2	-0.118
4459.77696	0.00020	1.8×10^{-38}	0 0 0	2 0 0	6 3 3	5 3 2	-0.088
4460.06375	0.00021	1.8×10^{-38}	0 0 0	2 0 0	6 3 4	5 3 3	-0.088
4461.98418	0.00014	3.2×10^{-38}	0 0 0	2 0 0	6 2 5	5 2 4	-0.067
4465.98953	0.00010	5.1×10^{-38}	0 0 0	2 0 0	6 0 6	5 0 5	-0.054
4468.32513	0.00010	4.8×10^{-38}	0 0 0	2 0 0	6 1 6	5 1 5	-0.059
4471.17583	0.00640	9.0×10^{-40}	0 0 0	2 0 0	8 1 7	8 1 8	-0.051
4471.65134	0.00009	4.9×10^{-38}	0 0 0	2 0 0	5 1 4	4 1 3	-0.057
4472.76177	0.00083	5.7×10^{-39}	0 0 0	2 0 0	5 4 1	4 4 0	-0.122
4472.76177	0.00083	5.7×10^{-39}	0 0 0	2 0 0	5 4 2	4 4 1	-0.124

Position	$\sigma_{\text{Pos.}}$	Intensity	$\nu_1\,\nu_2\,\nu_3$	$\nu_1{'}\,\nu_2{'}\,\nu_3{'}$	J $K_a\,K_c$	J' $K_a{'}\,K_c{'}$	$\Delta_{\text{SPEC.}}$
4472.99160	0.00012	3.5×10^{-38}	0 0 0	2 0 0	5 2 3	4 2 2	-0.070
4473.66455	0.00049	1.8×10^{-38}	0 0 0	2 0 0	5 3 2	4 3 1	-0.093
4473.77024	0.00128	1.8×10^{-38}	0 0 0	2 0 0	5 3 3	4 3 2	-0.094
4475.24373	0.00014	3.5×10^{-38}	0 0 0	2 0 0	5 2 4	4 2 3	-0.073
4477.98353	0.00044	5.8×10^{-38}	0 0 0	2 0 0	5 0 5	4 0 4	-0.057
4479.85315	0.03158	4.6×10^{-40}	0 0 0	2 0 0	4 1 4	3 0 3	-0.038
4479.91651	0.01830	4.9×10^{-40}	0 0 0	2 0 0	10 2 8	10 2 9	-0.042
4480.46188	0.00042	5.4×10^{-38}	0 0 0	2 0 0	5 1 5	4 1 4	-0.062
4485.11374	0.03279	1.5×10^{-39}	0 0 0	2 0 0	7 1 6	7 1 7	-0.055
4485.47597	0.00197	5.1×10^{-38}	0 0 0	2 0 0	4 1 3	3 1 2	-0.062
4487.03276	0.00036	1.3×10^{-38}	0 0 0	2 0 0	4 3 1	3 3 0	-0.098
4487.05952	0.00036	1.3×10^{-38}	0 0 0	2 0 0	4 3 2	3 3 1	-0.101
4487.09082	0.00014	3.3×10^{-38}	0 0 0	2 0 0	4 2 2	3 2 1	-0.077
4488.23383	0.00016	3.3×10^{-38}	0 0 0	2 0 0	4 2 3	3 2 2	-0.078
4488.80139	0.00468	5.3×10^{-40}	0 0 0	2 0 0	3 2 1	3 1 2	-0.068
4489.01022	0.00431	6.5×10^{-40}	0 0 0	2 0 0	4 2 2	4 1 3	-0.069
4489.63005	0.00839	5.1×10^{-40}	0 0 0	2 0 0	3 1 3	2 0 2	-0.064
4490.03509	0.00019	6.1×10^{-38}	0 0 0	2 0 0	4 0 4	3 0 3	-0.060
4491.70848	0.00778	5.9×10^{-40}	0 0 0	2 0 0	6 1 5	6 0 6	-0.056
4492.38532	0.00015	5.4×10^{-38}	0 0 0	2 0 0	4 1 4	3 1 3	-0.066
4493.17879	0.00402	9.8×10^{-40}	0 0 0	2 0 0	9 2 7	9 2 8	-0.042
4497.76846	0.00197	2.4×10^{-39}	0 0 0	2 0 0	6 1 5	6 1 6	-0.065
4499.02951	0.00010	4.6×10^{-38}	0 0 0	2 0 0	3 1 2	2 1 1	-0.067
4499.69036	0.00927	5.1×10^{-40}	0 0 0	2 0 0	2 1 2	1 0 1	-0.061
4500.47273	0.00021	2.3×10^{-38}	0 0 0	2 0 0	3 2 1	2 2 0	-0.081
4500.79605	0.00580	8.3×10^{-40}	0 0 0	2 0 0	5 1 4	5 0 5	-0.048
4500.92488	0.00021	2.3×10^{-38}	0 0 0	2 0 0	3 2 2	2 2 1	-0.083
4502.13275	0.00008	5.7×10^{-38}	0 0 0	2 0 0	3 0 3	2 0 2	-0.063
4504.08196	0.00011	4.7×10^{-38}	0 0 0	2 0 0	3 1 3	2 1 2	-0.069
4504.62335	0.00228	1.9×10^{-39}	0 0 0	2 0 0	8 2 6	8 2 7	-0.050
4506.73403	0.01293	3.5×10^{-40}	0 0 0	2 0 0	11 5 6	11 5 7	-0.103
4506.79808	0.01579	3.5×10^{-40}	0 0 0	2 0 0	11 5 7	11 5 6	-0.112
4506.85843	0.00617	8.2×10^{-40}	0 0 0	2 0 0	10 3 7	10 3 8	-0.056
4507.10158	0.00622	4.4×10^{-40}	0 0 0	2 0 0	11 4 7	11 4 8	-0.058
4507.98807	0.00402	1.0×10^{-39}	0 0 0	2 0 0	4 1 3	4 0 4	-0.063
4508.91695	0.00141	3.9×10^{-39}	0 0 0	2 0 0	5 1 4	5 1 5	-0.059
4508.93805	0.01500	4.4×10^{-40}	0 0 0	2 0 0	11 4 8	11 4 7	-0.060
4509.67734	0.00396	4.3×10^{-40}	0 0 0	2 0 0	10 6 4	10 6 5	-0.189
4509.67734	0.00396	4.3×10^{-40}	0 0 0	2 0 0	10 6 5	10 6 4	-0.190
4510.11313	0.01175	4.3×10^{-40}	0 0 0	2 0 0	1 1 1	0 0 0	-0.068
4511.21803	0.01233	7.1×10^{-40}	0 0 0	2 0 0	10 5 5	10 5 6	-0.126

Position	$\sigma_{\text{Pos.}}$	Intensity	$\nu_1\,\nu_2\,\nu_3$	$\nu_1{}'\,\nu_2{}'\,\nu_3{}'$	J $\text{K}_a\,\text{K}_c$	J' $\text{K}_a{}'\,\text{K}_c{}'$	$\Delta_{\text{SPEC.}}$
4511.23787	0.03306	7.1×10^{-40}	0 0 0	2 0 0	10 5 6	10 5 5	-0.134
4512.25377	0.00037	3.1×10^{-38}	0 0 0	2 0 0	2 1 1	1 1 0	-0.070
4512.99596	0.00681	9.1×10^{-40}	0 0 0	2 0 0	10 4 7	10 4 6	-0.076
4513.44334	0.00549	1.1×10^{-39}	0 0 0	2 0 0	3 1 2	3 0 3	-0.055
4513.73077	0.00395	8.4×10^{-40}	0 0 0	2 0 0	9 6 3	9 6 4	-0.178
4513.73077	0.00395	8.4×10^{-40}	0 0 0	2 0 0	9 6 4	9 6 3	-0.178
4513.92041	0.00223	1.7×10^{-39}	0 0 0	2 0 0	9 3 6	9 3 7	-0.063
4514.13911	0.00138	3.5×10^{-39}	0 0 0	2 0 0	7 2 5	7 2 6	-0.059
4514.19464	0.00010	4.4×10^{-38}	0 0 0	2 0 0	2 0 2	1 0 1	-0.066
4515.28413	0.00195	1.4×10^{-39}	0 0 0	2 0 0	9 5 4	9 5 5	-0.131
4515.28413	0.00195	1.4×10^{-39}	0 0 0	2 0 0	9 5 5	9 5 4	-0.141
4515.52511	0.00014	3.1×10^{-38}	0 0 0	2 0 0	2 1 2	1 1 1	-0.071
4515.72125	0.00318	7.7×10^{-40}	0 0 0	2 0 0	8 7 1	8 7 2	-0.236
4515.72125	0.00318	7.7×10^{-40}	0 0 0	2 0 0	8 7 2	8 7 1	-0.236
4516.45730	0.00154	1.8×10^{-39}	0 0 0	2 0 0	9 4 5	9 4 6	-0.096
4516.83984	0.00165	1.8×10^{-39}	0 0 0	2 0 0	9 4 6	9 4 5	-0.097
4517.29884	0.00431	1.0×10^{-39}	0 0 0	2 0 0	2 1 1	2 0 2	-0.067
4517.35353	0.00123	1.6×10^{-39}	0 0 0	2 0 0	8 6 2	8 6 3	-0.186
4517.35353	0.00123	1.6×10^{-39}	0 0 0	2 0 0	8 6 3	8 6 2	-0.186
4518.35713	0.00071	6.2×10^{-39}	0 0 0	2 0 0	4 1 3	4 1 4	-0.065
4518.92437	0.02217	1.4×10^{-39}	0 0 0	2 0 0	7 7 0	7 7 1	-0.253
4518.92438	0.02196	1.4×10^{-39}	0 0 0	2 0 0	7 7 1	7 7 0	-0.253
4518.92559	0.02105	2.6×10^{-39}	0 0 0	2 0 0	8 5 3	8 5 4	-0.137
4518.93750	0.00401	2.6×10^{-39}	0 0 0	2 0 0	8 5 4	8 5 3	-0.128
4519.46645	0.00108	3.2×10^{-39}	0 0 0	2 0 0	8 3 5	8 3 6	-0.074
4519.76296	0.00551	7.3×10^{-40}	0 0 0	2 0 0	1 1 0	1 0 1	-0.069
4520.24382	0.00085	3.4×10^{-39}	0 0 0	2 0 0	8 4 4	8 4 5	-0.105
4520.39256	0.00081	3.4×10^{-39}	0 0 0	2 0 0	8 4 5	8 4 4	-0.105
4520.56452	0.00167	2.8×10^{-39}	0 0 0	2 0 0	7 6 1	7 6 2	-0.197
4520.56452	0.00167	2.8×10^{-39}	0 0 0	2 0 0	7 6 2	7 6 1	-0.197
4521.36415	0.00351	1.7×10^{-39}	0 0 0	2 0 0	9 3 7	9 3 6	-0.059
4521.69627	0.00150	6.4×10^{-39}	0 0 0	2 0 0	6 2 4	6 2 5	-0.066
4522.14439	0.00820	4.6×10^{-39}	0 0 0	2 0 0	7 5 3	7 5 2	-0.150
4522.14439	0.00820	4.6×10^{-39}	0 0 0	2 0 0	7 5 2	7 5 3	-0.149
4523.31354	0.00130	3.2×10^{-39}	0 0 0	2 0 0	8 3 6	8 3 5	-0.084
4523.37632	0.00048	4.8×10^{-39}	0 0 0	2 0 0	6 6 0	6 6 1	-0.200
4523.37632	0.00048	4.8×10^{-39}	0 0 0	2 0 0	6 6 1	6 6 0	-0.200
4523.53763	0.00048	6.1×10^{-39}	0 0 0	2 0 0	7 4 3	7 4 4	-0.113
4523.58812	0.00048	6.1×10^{-39}	0 0 0	2 0 0	7 4 4	7 4 3	-0.113
4523.80217	0.00079	5.9×10^{-39}	0 0 0	2 0 0	7 3 4	7 3 5	-0.082
4524.95674	0.00122	7.9×10^{-39}	0 0 0	2 0 0	6 5 1	6 5 2	-0.156

Position	$\sigma_{\text{Pos.}}$	Intensity	$\nu_1\ \nu_2\ \nu_3$	$\nu_1'\ \nu_2'\ \nu_3'$	J K_a K_c	J' K_a' K_c'	$\Delta_{\text{SPEC.}}$
4524.95674	0.00122	7.9×10^{-39}	0 0 0	2 0 0	6 5 2	6 5 1	-0.156
4525.60063	0.00056	5.9×10^{-39}	0 0 0	2 0 0	7 3 5	7 3 4	-0.082
4525.99187	0.00045	1.0×10^{-38}	0 0 0	2 0 0	3 1 2	3 1 3	-0.067
4526.10262	0.00042	2.5×10^{-38}	0 0 0	2 0 0	1 0 1	0 0 0	-0.068
4526.39004	0.00222	1.0×10^{-38}	0 0 0	2 0 0	6 4 3	6 4 2	-0.125
4526.39004	0.00223	1.0×10^{-38}	0 0 0	2 0 0	6 4 2	6 4 3	-0.111
4527.18078	0.00048	1.0×10^{-38}	0 0 0	2 0 0	6 3 3	6 3 4	-0.111
4527.35979	0.00509	1.3×10^{-38}	0 0 0	2 0 0	5 5 0	5 5 1	-0.164
4527.36311	0.00676	1.3×10^{-38}	0 0 0	2 0 0	5 5 1	5 5 0	-0.161
4527.36719	0.00344	1.1×10^{-38}	0 0 0	2 0 0	5 2 3	5 2 4	-0.079
4527.93703	0.00273	1.0×10^{-38}	0 0 0	2 0 0	6 3 4	6 3 3	-0.086
4528.79590	0.00093	1.7×10^{-38}	0 0 0	2 0 0	5 4 1	5 4 2	-0.129
4528.80672	0.00099	1.7×10^{-38}	0 0 0	2 0 0	5 4 2	5 4 1	-0.121
4529.88074	0.00027	1.7×10^{-38}	0 0 0	2 0 0	5 3 2	5 3 3	-0.096
4530.12914	0.00022	1.7×10^{-38}	0 0 0	2 0 0	5 3 3	5 3 2	-0.094
4530.80192	0.00082	2.8×10^{-38}	0 0 0	2 0 0	4 4 0	4 4 1	-0.133
4530.80770	0.00083	2.8×10^{-38}	0 0 0	2 0 0	4 4 1	4 4 0	-0.127
4531.38083	0.00028	1.8×10^{-38}	0 0 0	2 0 0	4 2 2	4 2 3	-0.077
4531.75039	0.00053	1.7×10^{-38}	0 0 0	2 0 0	2 1 1	2 1 2	-0.072
4531.99073	0.00018	2.8×10^{-38}	0 0 0	2 0 0	4 3 1	4 3 2	-0.100
4532.05104	0.00082	2.8×10^{-38}	0 0 0	2 0 0	4 3 2	4 3 1	-0.101
4533.62568	0.00077	4.6×10^{-38}	0 0 0	2 0 0	3 3 1	3 3 0	-0.108
4533.62568	0.00077	4.6×10^{-38}	0 0 0	2 0 0	3 3 0	3 3 1	-0.099
4534.02413	0.00015	3.0×10^{-38}	0 0 0	2 0 0	3 2 1	3 2 2	-0.082
4534.35214	0.00054	1.1×10^{-38}	0 0 0	2 0 0	5 2 4	5 2 3	-0.072
4534.45431	0.00027	1.8×10^{-38}	0 0 0	2 0 0	4 2 3	4 2 2	-0.078
4535.06381	0.00135	3.0×10^{-38}	0 0 0	2 0 0	3 2 2	3 2 1	-0.083
4535.07517	0.00532	6.3×10^{-39}	0 0 0	2 0 0	6 2 5	6 2 4	-0.056
4535.60503	0.00013	3.4×10^{-38}	0 0 0	2 0 0	1 1 0	1 1 1	-0.072
4535.64867	0.00009	5.2×10^{-38}	0 0 0	2 0 0	2 2 0	2 2 1	-0.084
4535.85774	0.00008	5.2×10^{-38}	0 0 0	2 0 0	2 2 1	2 2 0	-0.084
4536.82215	0.00132	3.5×10^{-39}	0 0 0	2 0 0	7 2 6	7 2 5	-0.064
4538.67064	0.00018	3.4×10^{-38}	0 0 0	2 0 0	1 1 1	1 1 0	-0.073
4539.75552	0.00368	1.9×10^{-39}	0 0 0	2 0 0	8 2 7	8 2 6	-0.053
4540.94684	0.00028	1.7×10^{-38}	0 0 0	2 0 0	2 1 2	2 1 1	-0.071
4543.70303	0.01310	3.4×10^{-40}	0 0 0	2 0 0	1 1 1	2 0 2	-0.083
4543.85408	0.00735	9.4×10^{-40}	0 0 0	2 0 0	9 2 8	9 2 7	-0.059
4544.35980	0.00053	9.8×10^{-39}	0 0 0	2 0 0	3 1 3	3 1 2	-0.068
4548.89510	0.00070	6.0×10^{-39}	0 0 0	2 0 0	4 1 4	4 1 3	-0.066
4548.96743	0.00031	2.5×10^{-38}	0 0 0	2 0 0	0 0 0	1 0 1	-0.069
4549.96634	0.02137	2.9×10^{-40}	0 0 0	2 0 0	4 2 3	5 1 4	-0.045

Position	$\sigma_{\text{Pos.}}$	Intensity	$\nu_1\,\nu_2\,\nu_3$	$\nu_1{}'\,\nu_2{}'\,\nu_3{}'$	J K_a K_c	J' $K_a{}'$ $K_c{}'$	$\Delta_{\text{SPEC.}}$
4554.51514	0.00113	3.7×10^{-39}	0 0 0	2 0 0	5 1 5	5 1 4	-0.061
4554.66126	0.00497	7.6×10^{-40}	0 0 0	2 0 0	1 0 1	1 1 0	-0.071
4555.34800	0.00522	7.3×10^{-40}	0 0 0	2 0 0	2 1 2	3 0 3	-0.072
4555.46210	0.00487	1.1×10^{-39}	0 0 0	2 0 0	2 0 2	2 1 1	-0.065
4556.86272	0.00377	1.2×10^{-39}	0 0 0	2 0 0	3 0 3	3 1 2	-0.067
4558.16816	0.00067	3.3×10^{-38}	0 0 0	2 0 0	1 1 1	2 1 2	-0.074
4559.10268	0.00598	1.1×10^{-39}	0 0 0	2 0 0	4 0 4	4 1 3	-0.063
4559.70639	0.00008	4.7×10^{-38}	0 0 0	2 0 0	1 0 1	2 0 2	-0.068
4561.02624	0.00013	3.2×10^{-38}	0 0 0	2 0 0	1 1 0	2 1 1	-0.072
4561.14222	0.00215	2.3×10^{-39}	0 0 0	2 0 0	6 1 6	6 1 5	-0.056
4562.40468	0.00526	8.8×10^{-40}	0 0 0	2 0 0	5 0 5	5 1 4	-0.060
4562.95739	0.00932	3.6×10^{-40}	0 0 0	2 0 0	5 2 4	6 1 5	-0.063
4564.80909	0.00518	6.1×10^{-40}	0 0 0	2 0 0	0 0 0	1 1 1	-0.072
4564.83544	0.00746	3.9×10^{-40}	0 0 0	2 0 0	8 1 7	8 2 6	-0.045
4566.74152	0.00511	5.4×10^{-40}	0 0 0	2 0 0	7 1 6	7 2 5	-0.045
4567.90835	0.00302	5.2×10^{-38}	0 0 0	2 0 0	2 1 2	3 1 3	-0.073
4568.63877	0.00307	1.4×10^{-39}	0 0 0	2 0 0	7 1 7	7 1 6	-0.053
4569.40504	0.00150	2.5×10^{-38}	0 0 0	2 0 0	2 2 1	3 2 2	-0.090
4569.78864	0.00087	2.5×10^{-38}	0 0 0	2 0 0	2 2 0	3 2 1	-0.083
4569.86303	0.00040	6.3×10^{-38}	0 0 0	2 0 0	2 0 2	3 0 3	-0.067
4572.02986	0.00009	5.0×10^{-38}	0 0 0	2 0 0	2 1 1	3 1 2	-0.070
4573.11974	0.00736	7.4×10^{-40}	0 0 0	2 0 0	5 1 4	5 2 3	-0.073
4574.15993	0.00374	9.6×10^{-40}	0 0 0	2 0 0	1 0 1	2 1 2	-0.071
4575.87312	0.00237	4.0×10^{-40}	0 0 0	2 0 0	6 2 5	7 1 6	-0.076
4576.93505	0.00331	7.2×10^{-40}	0 0 0	2 0 0	4 1 3	4 2 2	-0.060
4577.24157	0.00006	6.2×10^{-38}	0 0 0	2 0 0	3 1 3	4 1 4	-0.070
4578.02953	0.00258	1.4×10^{-39}	0 0 0	2 0 0	4 1 4	5 0 5	-0.067
4578.58843	0.00043	1.5×10^{-38}	0 0 0	2 0 0	3 3 1	4 3 2	-0.105
4578.61178	0.00054	1.5×10^{-38}	0 0 0	2 0 0	3 3 0	4 3 1	-0.105
4579.35261	0.00018	3.8×10^{-38}	0 0 0	2 0 0	3 2 2	4 2 3	-0.083
4579.37786	0.00011	7.0×10^{-38}	0 0 0	2 0 0	3 0 3	4 0 4	-0.065
4579.52141	0.06478	2.7×10^{-40}	0 0 0	2 0 0	8 0 8	8 1 7	-0.083
4580.24521	0.00010	3.7×10^{-38}	0 0 0	2 0 0	3 2 1	4 2 2	-0.081
4580.58913	0.00631	6.0×10^{-40}	0 0 0	2 0 0	3 1 2	3 2 1	-0.068
4582.41773	0.00250	1.3×10^{-39}	0 0 0	2 0 0	2 0 2	3 1 3	-0.073
4582.50087	0.00020	5.8×10^{-38}	0 0 0	2 0 0	3 1 2	4 1 3	-0.067
4586.16025	0.00021	6.4×10^{-38}	0 0 0	2 0 0	4 1 4	5 1 5	-0.068
4586.84496	0.00233	6.7×10^{-39}	0 0 0	2 0 0	4 4 0	5 4 1	-0.132
4586.84496	0.00233	6.7×10^{-39}	0 0 0	2 0 0	4 4 1	5 4 2	-0.131
4588.23919	0.00006	6.9×10^{-38}	0 0 0	2 0 0	4 0 4	5 0 5	-0.062
4588.27129	0.00022	2.1×10^{-38}	0 0 0	2 0 0	4 3 2	5 3 3	-0.100

Position	$\sigma_{\text{Pos.}}$	Intensity	$\nu_1\,\nu_2\,\nu_3$	$\nu_1{'}\,\nu_2{'}\,\nu_3{'}$	$J\,K_a\,K_c$	$J'\,K_a{'}\,K_c{'}$	$\Delta_{\text{SPEC.}}$
4588.35505	0.00103	2.1×10^{-38}	0 0 0	2 0 0	4 3 1	5 3 2	-0.094
4588.56887	0.00351	1.6×10^{-39}	0 0 0	2 0 0	5 1 5	6 0 6	-0.093
4588.83714	0.00009	4.2×10^{-38}	0 0 0	2 0 0	4 2 3	5 2 4	-0.079
4589.73987	0.00313	1.6×10^{-39}	0 0 0	2 0 0	3 0 3	4 1 4	-0.074
4590.48819	0.00011	4.1×10^{-38}	0 0 0	2 0 0	4 2 2	5 2 3	-0.077
4591.26691	0.01026	5.2×10^{-40}	0 0 0	2 0 0	4 1 4	4 2 3	-0.071
4592.41189	0.00019	5.8×10^{-38}	0 0 0	2 0 0	4 1 3	5 1 4	-0.063
4593.40922	0.01304	4.8×10^{-40}	0 0 0	2 0 0	5 1 5	5 2 4	-0.072
4594.36480	0.01051	2.5×10^{-39}	0 0 0	2 0 0	5 5 0	6 5 1	-0.165
4594.36480	0.01051	2.5×10^{-39}	0 0 0	2 0 0	5 5 1	6 5 2	-0.165
4594.66535	0.00006	5.9×10^{-38}	0 0 0	2 0 0	5 1 5	6 1 6	-0.065
4596.08716	0.00028	9.2×10^{-39}	0 0 0	2 0 0	5 4 1	6 4 2	-0.129
4596.08716	0.00028	9.2×10^{-39}	0 0 0	2 0 0	5 4 2	6 4 3	-0.124
4596.37452	0.00430	1.8×10^{-39}	0 0 0	2 0 0	4 0 4	5 1 5	-0.059
4596.49017	0.00006	6.2×10^{-38}	0 0 0	2 0 0	5 0 5	6 0 6	-0.060
4597.55335	0.00015	2.2×10^{-38}	0 0 0	2 0 0	5 3 3	6 3 4	-0.096
4597.75184	0.00014	2.2×10^{-38}	0 0 0	2 0 0	5 3 2	6 3 3	-0.096
4597.85107	0.00009	3.9×10^{-38}	0 0 0	2 0 0	5 2 4	6 2 5	-0.075
4600.45446	0.00013	3.8×10^{-38}	0 0 0	2 0 0	5 2 3	6 2 4	-0.071
4601.21781	0.00265	7.3×10^{-40}	0 0 0	2 0 0	6 6 1	7 6 2	-0.202
4601.21781	0.00265	7.3×10^{-40}	0 0 0	2 0 0	6 6 0	7 6 1	-0.202
4601.73122	0.00008	5.1×10^{-38}	0 0 0	2 0 0	5 1 4	6 1 5	-0.058
4602.53391	0.00761	1.8×10^{-39}	0 0 0	2 0 0	5 0 5	6 1 6	-0.085
4602.76424	0.00007	5.1×10^{-38}	0 0 0	2 0 0	6 1 6	7 1 7	-0.063
4603.14241	0.00326	3.2×10^{-39}	0 0 0	2 0 0	6 5 2	7 5 3	-0.159
4603.14241	0.00326	3.2×10^{-39}	0 0 0	2 0 0	6 5 1	7 5 2	-0.159
4604.22848	0.00134	5.2×10^{-38}	0 0 0	2 0 0	6 0 6	7 0 7	-0.057
4604.93393	0.00092	9.2×10^{-39}	0 0 0	2 0 0	6 4 3	7 4 4	-0.120
4604.94660	0.00092	9.2×10^{-39}	0 0 0	2 0 0	6 4 2	7 4 3	-0.122
4606.39094	0.00010	3.3×10^{-38}	0 0 0	2 0 0	6 2 5	7 2 6	-0.070
4606.42178	0.00019	2.0×10^{-38}	0 0 0	2 0 0	6 3 4	7 3 5	-0.091
4606.84290	0.00015	2.0×10^{-38}	0 0 0	2 0 0	6 3 3	7 3 4	-0.090
4607.48817	0.00317	1.4×10^{-39}	0 0 0	2 0 0	7 1 7	8 0 8	-0.061
4608.43821	0.01052	3.4×10^{-40}	0 0 0	2 0 0	9 0 9	9 2 8	-0.067
4608.45280	0.00586	8.6×10^{-40}	0 0 0	2 0 0	1 1 0	2 2 1	-0.067
4608.55637	0.00212	1.7×10^{-39}	0 0 0	2 0 0	6 0 6	7 1 7	-0.061
4609.52365	0.00224	9.2×10^{-40}	0 0 0	2 0 0	7 6 2	8 6 3	-0.197
4609.52365	0.00224	9.2×10^{-40}	0 0 0	2 0 0	7 6 1	8 6 2	-0.197
4610.03862	0.00026	3.2×10^{-38}	0 0 0	2 0 0	6 2 4	7 2 5	-0.063
4610.11840	0.00621	8.3×10^{-40}	0 0 0	2 0 0	1 1 1	2 2 0	-0.085
4610.42944	0.00022	4.2×10^{-38}	0 0 0	2 0 0	6 1 5	7 1 6	-0.052

Position	$\sigma_{\text{Pos.}}$	Intensity	$\nu_1\ \nu_2\ \nu_3$	$\nu_1\text{'}\ \nu_2\text{'}\ \nu_3\text{'}$	J K_a K_c	J' $\text{K}_a\text{'}$ $\text{K}_c\text{'}$	$\Delta_{\text{SPEC.}}$
4610.47048	0.00069	4.0×10^{-38}	0 0 0	2 0 0	7 1 7	8 1 8	-0.058
4611.51877	0.00106	3.1×10^{-39}	0 0 0	2 0 0	7 5 3	8 5 4	-0.152
4611.51877	0.00108	3.1×10^{-39}	0 0 0	2 0 0	7 5 2	8 5 3	-0.153
4611.55577	0.00009	4.1×10^{-38}	0 0 0	2 0 0	7 0 7	8 0 8	-0.055
4612.55117	0.01000	3.2×10^{-40}	0 0 0	2 0 0	6 2 5	6 3 4	-0.084
4613.38794	0.00123	7.8×10^{-39}	0 0 0	2 0 0	7 4 4	8 4 5	-0.112
4613.42253	0.00040	7.8×10^{-39}	0 0 0	2 0 0	7 4 3	8 4 4	-0.115
4614.02338	0.01294	3.3×10^{-40}	0 0 0	2 0 0	4 2 2	4 3 1	-0.088
4614.09216	0.01012	3.6×10^{-40}	0 0 0	2 0 0	5 2 4	5 3 3	-0.096
4614.45322	0.00116	2.6×10^{-38}	0 0 0	2 0 0	7 2 6	8 2 7	-0.065
4614.53143	0.00209	1.5×10^{-39}	0 0 0	2 0 0	7 0 7	8 1 8	-0.059
4614.85903	0.00076	1.6×10^{-38}	0 0 0	2 0 0	7 3 5	8 3 6	-0.085
4615.80838	0.00316	1.2×10^{-39}	0 0 0	2 0 0	8 1 8	9 0 9	-0.054
4616.48127	0.00553	2.3×10^{-40}	0 0 0	2 0 0	3 2 1	3 3 0	-0.068
4617.25150	0.00365	9.5×10^{-40}	0 0 0	2 0 0	2 1 1	3 2 2	-0.085
4617.41586	0.05374	8.3×10^{-40}	0 0 0	2 0 0	8 6 2	9 6 3	-0.196
4617.41916	0.03288	8.3×10^{-40}	0 0 0	2 0 0	8 6 3	9 6 4	-0.193
4617.79419	0.00010	3.0×10^{-38}	0 0 0	2 0 0	8 1 8	9 1 9	-0.056
4618.47924	0.00012	3.1×10^{-38}	0 0 0	2 0 0	7 1 6	8 1 7	-0.046
4618.55288	0.00011	3.0×10^{-38}	0 0 0	2 0 0	8 0 8	9 0 9	-0.053
4619.12266	0.00027	2.4×10^{-38}	0 0 0	2 0 0	7 2 5	8 2 6	-0.054
4619.49376	0.00410	2.5×10^{-39}	0 0 0	2 0 0	8 5 4	9 5 5	-0.142
4619.49376	0.00409	2.5×10^{-39}	0 0 0	2 0 0	8 5 3	9 5 4	-0.145
4620.54265	0.00239	1.3×10^{-39}	0 0 0	2 0 0	8 0 8	9 1 9	-0.050
4621.43530	0.00050	5.9×10^{-39}	0 0 0	2 0 0	8 4 5	9 4 6	-0.106
4621.52148	0.00168	5.9×10^{-39}	0 0 0	2 0 0	8 4 4	9 4 5	-0.105
4622.04075	0.00023	1.9×10^{-38}	0 0 0	2 0 0	8 2 7	9 2 8	-0.059
4622.49009	0.00463	8.4×10^{-40}	0 0 0	2 0 0	2 1 2	3 2 1	-0.088
4622.84635	0.00116	1.1×10^{-38}	0 0 0	2 0 0	8 3 6	9 3 7	-0.076
4624.14961	0.00049	1.1×10^{-38}	0 0 0	2 0 0	8 3 5	9 3 6	-0.073
4624.75291	0.00077	2.1×10^{-38}	0 0 0	2 0 0	9 1 9	10 1 10	-0.053
4624.86798	0.00377	1.0×10^{-39}	0 0 0	2 0 0	3 1 2	4 2 3	-0.078
4624.90946	0.00573	6.3×10^{-40}	0 0 0	2 0 0	9 6 3	10 6 4	-0.182
4624.90948	0.00572	6.3×10^{-40}	0 0 0	2 0 0	9 6 4	10 6 5	-0.182
4625.25932	0.00018	2.1×10^{-38}	0 0 0	2 0 0	9 0 9	10 0 10	-0.050
4625.87014	0.00015	2.2×10^{-38}	0 0 0	2 0 0	8 1 7	9 1 8	-0.040
4626.55366	0.00319	9.6×10^{-40}	0 0 0	2 0 0	9 0 9	10 1 10	-0.049
4627.05838	0.00675	1.8×10^{-39}	0 0 0	2 0 0	9 5 5	10 5 6	-0.136
4627.06563	0.01189	1.8×10^{-39}	0 0 0	2 0 0	9 5 4	10 5 5	-0.135
4627.61636	0.00020	1.7×10^{-38}	0 0 0	2 0 0	8 2 6	9 2 7	-0.045
4629.07220	0.00063	4.0×10^{-39}	0 0 0	2 0 0	9 4 6	10 4 7	-0.098

Position	$\sigma_{\mathrm{Pos.}}$	Intensity	$\nu_1\ \nu_2\ \nu_3$	$\nu_1'\ \nu_2'\ \nu_3'$	J K_a K_c	J' K_a' K_c'	$\Delta_{\mathrm{SPEC.}}$
4629.16048	0.00022	1.3×10^{-38}	0 0 0	2 0 0	9 2 8	10 2 9	-0.053
4629.24457	0.00065	4.0×10^{-39}	0 0 0	2 0 0	9 4 5	10 4 6	-0.097
4630.36447	0.00044	7.7×10^{-39}	0 0 0	2 0 0	9 3 7	10 3 8	-0.069
4630.53738	0.00380	6.8×10^{-40}	0 0 0	2 0 0	10 1 10	11 0 11	-0.045
4631.35936	0.00039	1.3×10^{-38}	0 0 0	2 0 0	10 1 10	11 1 11	-0.050
4631.68616	0.00020	1.4×10^{-38}	0 0 0	2 0 0	10 0 10	11 0 11	-0.046
4631.98516	0.00389	4.3×10^{-40}	0 0 0	2 0 0	10 6 5	11 6 6	-0.171
4631.98516	0.00389	4.3×10^{-40}	0 0 0	2 0 0	10 6 4	11 6 5	-0.171
4632.35321	0.00040	7.5×10^{-39}	0 0 0	2 0 0	9 3 6	10 3 7	-0.061
4632.51276	0.00457	6.9×10^{-40}	0 0 0	2 0 0	10 0 10	11 1 11	-0.046
4632.61480	0.00023	1.4×10^{-38}	0 0 0	2 0 0	9 1 8	10 1 9	-0.035
4634.25253	0.01135	1.2×10^{-39}	0 0 0	2 0 0	10 5 5	11 5 6	-0.103
4634.25976	0.00698	1.2×10^{-39}	0 0 0	2 0 0	10 5 6	11 5 7	-0.081
4635.46734	0.00029	1.1×10^{-38}	0 0 0	2 0 0	9 2 7	10 2 8	-0.035
4635.82218	0.00055	8.1×10^{-39}	0 0 0	2 0 0	10 2 9	11 2 10	-0.048
4636.28262	0.00398	2.6×10^{-39}	0 0 0	2 0 0	10 4 7	11 4 8	-0.090
4636.60519	0.00113	2.6×10^{-39}	0 0 0	2 0 0	10 4 6	11 4 7	-0.086
4636.63846	0.00570	9.4×10^{-40}	0 0 0	2 0 0	5 1 4	6 2 5	-0.057
4637.11776	0.00861	4.6×10^{-40}	0 0 0	2 0 0	11 1 11	12 0 12	-0.033
4637.40297	0.00053	4.8×10^{-39}	0 0 0	2 0 0	10 3 8	11 3 9	-0.060
4637.62706	0.00030	8.3×10^{-39}	0 0 0	2 0 0	11 1 11	12 1 12	-0.043
4637.83019	0.00031	8.4×10^{-39}	0 0 0	2 0 0	11 0 11	12 0 12	-0.042
4638.32787	0.01101	4.7×10^{-40}	0 0 0	2 0 0	11 0 11	12 1 12	-0.064
4638.64072	0.00787	2.7×10^{-40}	0 0 0	2 0 0	11 6 5	12 6 6	-0.163
4638.64072	0.00786	2.7×10^{-40}	0 0 0	2 0 0	11 6 6	12 6 7	-0.162
4638.76605	0.00037	8.7×10^{-39}	0 0 0	2 0 0	10 1 9	11 1 10	-0.030
4640.19585	0.00063	4.6×10^{-39}	0 0 0	2 0 0	10 3 7	11 3 8	-0.048
4640.93342	0.00453	8.3×10^{-40}	0 0 0	2 0 0	6 1 5	7 2 6	-0.059
4640.96258	0.00453	6.9×10^{-40}	0 0 0	2 0 0	11 5 7	12 5 8	-0.109
4640.99506	0.00422	6.9×10^{-40}	0 0 0	2 0 0	11 5 6	12 5 7	-0.108
4642.04270	0.00056	4.8×10^{-39}	0 0 0	2 0 0	11 2 10	12 2 11	-0.040
4642.65399	0.00045	6.6×10^{-39}	0 0 0	2 0 0	10 2 8	11 2 9	-0.024
4643.05751	0.00162	1.5×10^{-39}	0 0 0	2 0 0	11 4 8	12 4 9	-0.078
4643.55903	0.00050	4.9×10^{-39}	0 0 0	2 0 0	12 1 12	13 1 13	-0.038
4643.60656	0.00176	1.5×10^{-39}	0 0 0	2 0 0	11 4 7	12 4 8	-0.076
4643.68337	0.00051	4.9×10^{-39}	0 0 0	2 0 0	12 0 12	13 0 13	-0.037
4643.95491	0.00091	2.8×10^{-39}	0 0 0	2 0 0	11 3 9	12 3 10	-0.050
4643.99556	0.01021	3.0×10^{-40}	0 0 0	2 0 0	12 0 12	13 1 13	-0.047
4644.36937	0.00635	7.0×10^{-40}	0 0 0	2 0 0	7 1 6	8 2 7	-0.049
4644.40704	0.00065	5.1×10^{-39}	0 0 0	2 0 0	11 1 10	12 1 11	-0.025
4647.12650	0.00550	5.5×10^{-40}	0 0 0	2 0 0	8 1 7	9 2 8	-0.046

Position	$\sigma_{\text{Pos.}}$	Intensity	$\nu_1\,\nu_2\,\nu_3$	$\nu_1'\,\nu_2'\,\nu_3'$	J K_a K_c	J' K_a' K_c'	$\Delta_{\text{SPEC.}}$
4647.30088	0.00701	3.8×10^{-40}	0 0 0	2 0 0	12 5 8	13 5 9	-0.081
4647.34388	0.00590	3.9×10^{-40}	0 0 0	2 0 0	12 5 7	13 5 8	-0.100
4647.59258	0.00102	2.6×10^{-39}	0 0 0	2 0 0	11 3 8	12 3 9	-0.034
4647.83641	0.00090	2.7×10^{-39}	0 0 0	2 0 0	12 2 11	13 2 12	-0.033
4648.30131	0.01113	2.4×10^{-40}	0 0 0	2 0 0	3 0 3	4 2 2	-0.086
4649.15946	0.00107	3.7×10^{-39}	0 0 0	2 0 0	11 2 9	12 2 10	-0.023
4649.17258	0.00165	2.7×10^{-39}	0 0 0	2 0 0	13 1 13	14 1 14	-0.021
4649.23596	0.00088	2.7×10^{-39}	0 0 0	2 0 0	13 0 13	14 0 14	-0.032
4649.37280	0.00307	8.3×10^{-40}	0 0 0	2 0 0	12 4 9	13 4 10	-0.072
4649.46134	0.00911	4.1×10^{-40}	0 0 0	2 0 0	9 1 8	10 2 9	-0.045
4649.63039	0.00103	2.8×10^{-39}	0 0 0	2 0 0	12 1 11	13 1 12	-0.021
4650.01582	0.00164	1.5×10^{-39}	0 0 0	2 0 0	12 3 10	13 3 11	-0.040
4650.25939	0.00348	8.2×10^{-40}	0 0 0	2 0 0	12 4 8	13 4 9	-0.062
4650.37612	0.00670	6.5×10^{-40}	0 0 0	2 0 0	4 1 4	5 2 3	-0.070
4651.72434	0.00325	1.1×10^{-39}	0 0 0	2 0 0	2 2 0	3 3 1	-0.098
4651.84172	0.00319	1.1×10^{-39}	0 0 0	2 0 0	2 2 1	3 3 0	-0.096
4653.22246	0.00325	1.4×10^{-39}	0 0 0	2 0 0	13 2 12	14 2 13	-0.025
4654.43874	0.00358	1.4×10^{-39}	0 0 0	2 0 0	14 1 14	15 1 15	-0.025
4654.44719	0.00399	1.4×10^{-39}	0 0 0	2 0 0	12 3 9	13 3 10	-0.020
4654.48285	0.00195	1.4×10^{-39}	0 0 0	2 0 0	14 0 14	15 0 15	-0.025
4654.51444	0.00205	1.5×10^{-39}	0 0 0	2 0 0	13 1 12	14 1 13	-0.019
4655.01292	0.00142	1.9×10^{-39}	0 0 0	2 0 0	12 2 10	13 2 11	-0.004
4655.58847	0.00244	8.0×10^{-40}	0 0 0	2 0 0	13 3 11	14 3 12	-0.031
4656.55554	0.00591	4.2×10^{-40}	0 0 0	2 0 0	13 4 9	14 4 10	-0.046
4658.21683	0.00275	7.1×10^{-40}	0 0 0	2 0 0	14 2 13	15 2 14	-0.017
4659.11184	0.00306	7.3×10^{-40}	0 0 0	2 0 0	14 1 13	15 1 14	-0.012
4659.38648	0.00374	7.1×10^{-40}	0 0 0	2 0 0	15 1 15	16 1 16	-0.023
4659.41056	0.00311	7.1×10^{-40}	0 0 0	2 0 0	15 0 15	16 0 16	-0.024
4660.20492	0.00264	9.6×10^{-40}	0 0 0	2 0 0	13 2 11	14 2 12	0.008
4660.59426	0.00968	2.9×10^{-40}	0 0 0	2 0 0	4 0 4	5 2 3	-0.056
4660.66735	0.00453	6.9×10^{-40}	0 0 0	2 0 0	13 3 10	14 3 11	-0.022
4660.69002	0.01347	3.9×10^{-40}	0 0 0	2 0 0	14 3 12	15 3 13	-0.015
4661.41328	0.00346	1.1×10^{-39}	0 0 0	2 0 0	3 2 1	4 3 2	-0.095
4661.99833	0.00328	1.1×10^{-39}	0 0 0	2 0 0	3 2 2	4 3 1	-0.091
4662.83130	0.00644	3.4×10^{-40}	0 0 0	2 0 0	15 2 14	16 2 15	-0.014
4663.43261	0.00546	3.4×10^{-40}	0 0 0	2 0 0	15 1 14	16 1 15	-0.008
4664.01651	0.00580	2.4×10^{-40}	0 0 0	2 0 0	16 1 16	17 1 17	-0.025
4664.77601	0.00431	4.5×10^{-40}	0 0 0	2 0 0	14 2 12	15 2 13	0.021
4666.26133	0.00543	3.2×10^{-40}	0 0 0	2 0 0	14 3 11	15 3 12	0.015
4666.49480	0.00545	4.8×10^{-40}	0 0 0	2 0 0	5 1 5	6 2 4	-0.066
4670.23817	0.00367	9.8×10^{-40}	0 0 0	2 0 0	4 2 2	5 3 3	-0.091

Position	$\sigma_{\text{Pos.}}$	Intensity	$\nu_1\,\nu_2\,\nu_3$	$\nu_1{}'\,\nu_2{}'\,\nu_3{}'$	$J\,K_a\,K_c$	$J'\,K_a{}'\,K_c{}'$	$\Delta_{\text{SPEC.}}$
4671.98235	0.00397	9.7×10^{-40}	0 0 0	2 0 0	4 2 3	5 3 2	-0.091
4674.38192	0.00911	2.7×10^{-40}	0 0 0	2 0 0	5 0 5	6 2 4	-0.067
4677.93907	0.00593	8.4×10^{-40}	0 0 0	2 0 0	5 2 3	6 3 4	-0.090
4681.96761	0.00413	8.3×10^{-40}	0 0 0	2 0 0	5 2 4	6 3 3	-0.092
4684.30831	0.00612	6.8×10^{-40}	0 0 0	2 0 0	6 2 4	7 3 5	-0.078
4684.38366	0.00717	3.2×10^{-40}	0 0 0	2 0 0	6 1 6	7 2 5	-0.060
4689.19703	0.00764	5.1×10^{-40}	0 0 0	2 0 0	7 2 5	8 3 6	-0.077
4692.19636	0.00499	6.6×10^{-40}	0 0 0	2 0 0	6 2 5	7 3 4	-0.080
4692.61470	0.00824	3.6×10^{-40}	0 0 0	2 0 0	8 2 6	9 3 7	-0.073
4693.02756	0.00791	9.5×10^{-40}	0 0 0	2 0 0	3 3 1	4 4 0	-0.123
4693.02756	0.00793	9.5×10^{-40}	0 0 0	2 0 0	3 3 0	4 4 1	-0.118
4694.65188	0.00654	2.4×10^{-40}	0 0 0	2 0 0	9 2 7	10 3 8	-0.067

A.2.1.3 HTO $\nu_2 + \nu_3$ band

Here, the lines assigned to the $\nu_2 + \nu_3$ band obtained from the $1\,\text{GBq}$ sample are presented. These lines are published in [Her21]. For further information, see Section 5.5.1.

Table A.4: Linelist of the $\nu_2 + \nu_3$ band. The columns present the assigned line position, the uncertainty on the position $\sigma_{\text{Pos.}}$, the line intensity taking natural abundance into account, lower and upper vibrational quanta, lower and upper rotational quanta and the deviation to the predictions from SPECTRA database $\Delta_{\text{SPEC.}}$.

Position	$\sigma_{\text{Pos.}}$	Intensity	$\nu_1\,\nu_2\,\nu_3$	$\nu_1{}'\,\nu_2{}'\,\nu_3{}'$	$J\,K_a\,K_c$	$J'\,K_a{}'\,K_c{}'$	$\Delta_{\text{SPEC.}}$
4785.54629	0.00436	6.1×10^{-40}	0 0 0	0 1 1	10 5 5	9 4 6	-0.120
4786.61120	0.00719	4.3×10^{-40}	0 0 0	0 1 1	10 5 6	9 4 5	-0.078
4787.80303	0.00931	6.5×10^{-40}	0 0 0	0 1 1	8 6 2	7 5 3	-0.161
4787.80303	0.00931	6.5×10^{-40}	0 0 0	0 1 1	8 6 3	7 5 2	-0.161
4795.92619	0.00500	5.6×10^{-40}	0 0 0	0 1 1	11 4 7	10 3 8	-0.098
4796.97768	0.00376	1.0×10^{-39}	0 0 0	0 1 1	9 5 4	8 4 5	-0.103
4797.12866	0.00297	9.9×10^{-40}	0 0 0	0 1 1	9 5 5	8 4 4	-0.124
4799.46716	0.00385	9.6×10^{-40}	0 0 0	0 1 1	7 6 1	6 5 2	-0.164
4799.46716	0.00385	9.6×10^{-40}	0 0 0	0 1 1	7 6 2	6 5 1	-0.164
4805.58989	0.00373	5.5×10^{-40}	0 0 0	0 1 1	11 4 8	10 3 7	-0.100
4808.43485	0.00184	1.6×10^{-39}	0 0 0	0 1 1	8 5 3	7 4 4	-0.131
4808.48921	0.00161	1.6×10^{-39}	0 0 0	0 1 1	8 5 4	7 4 3	-0.127
4808.61443	0.00286	1.0×10^{-39}	0 0 0	0 1 1	10 4 6	9 3 7	-0.098
4811.14417	0.00576	1.3×10^{-39}	0 0 0	0 1 1	6 6 1	5 5 0	-0.167
4811.14417	0.00576	1.3×10^{-39}	0 0 0	0 1 1	6 6 0	5 5 1	-0.167
4812.00282	0.02567	8.1×10^{-41}	0 0 0	0 1 1	9 3 6	8 1 7	-0.087
4814.01942	0.00252	1.0×10^{-39}	0 0 0	0 1 1	10 4 7	9 3 6	-0.101

Position	$\sigma_{\text{Pos.}}$	Intensity	$\nu_1\ \nu_2\ \nu_3$	$\nu_1'\ \nu_2'\ \nu_3'$	J K_a K_c	J' K_a' K_c'	$\Delta_{\text{SPEC.}}$
4819.26657	0.00305	1.1×10^{-39}	0 0 0	0 1 1	9 2 7	8 1 8	-0.068
4819.98459	0.00250	2.3×10^{-39}	0 0 0	0 1 1	7 5 2	6 4 3	-0.131
4819.99216	0.00258	2.3×10^{-39}	0 0 0	0 1 1	7 5 3	6 4 2	-0.137
4820.06954	0.00145	2.1×10^{-39}	0 0 0	0 1 1	10 3 7	9 2 8	-0.055
4820.78254	0.00225	1.7×10^{-39}	0 0 0	0 1 1	9 4 5	8 3 6	-0.101
4823.54146	0.00216	1.7×10^{-39}	0 0 0	0 1 1	9 4 6	8 3 5	-0.101
4831.57802	0.00119	3.2×10^{-39}	0 0 0	0 1 1	6 5 2	5 4 1	-0.138
4831.57802	0.00119	3.2×10^{-39}	0 0 0	0 1 1	6 5 1	5 4 2	-0.136
4832.64263	0.00113	2.7×10^{-39}	0 0 0	0 1 1	8 4 4	7 3 5	-0.107
4833.89310	0.00111	2.7×10^{-39}	0 0 0	0 1 1	8 4 5	7 3 4	-0.109
4837.59513	0.00112	3.0×10^{-39}	0 0 0	0 1 1	9 3 6	8 2 7	-0.087
4843.20001	0.00250	4.3×10^{-39}	0 0 0	0 1 1	5 5 1	4 4 0	-0.141
4843.20001	0.00252	4.3×10^{-39}	0 0 0	0 1 1	5 5 0	4 4 1	-0.141
4844.34821	0.00096	4.1×10^{-39}	0 0 0	0 1 1	7 4 3	6 3 4	-0.111
4844.83156	0.00077	4.1×10^{-39}	0 0 0	0 1 1	7 4 4	6 3 3	-0.112
4846.16439	0.00174	1.7×10^{-39}	0 0 0	0 1 1	8 2 6	7 1 7	-0.078
4850.56466	0.00964	3.8×10^{-40}	0 0 0	0 1 1	16 1 15	15 1 14	-0.101
4851.85918	0.00368	8.9×10^{-40}	0 0 0	0 1 1	11 3 9	10 2 8	-0.039
4853.54882	0.00083	4.5×10^{-39}	0 0 0	0 1 1	8 3 5	7 2 6	-0.094
4855.99174	0.00114	5.7×10^{-39}	0 0 0	0 1 1	6 4 2	5 3 3	-0.115
4856.13341	0.00048	5.7×10^{-39}	0 0 0	0 1 1	6 4 3	5 3 2	-0.115
4859.29607	0.00746	3.3×10^{-40}	0 0 0	0 1 1	15 2 14	14 1 13	-0.073
4859.79988	0.00262	9.8×10^{-40}	0 0 0	0 1 1	15 1 15	14 0 14	-0.060
4859.89561	0.00179	1.6×10^{-39}	0 0 0	0 1 1	15 0 15	14 0 14	-0.062
4859.94176	0.00193	1.6×10^{-39}	0 0 0	0 1 1	15 1 15	14 1 14	-0.061
4860.04360	0.00281	9.8×10^{-40}	0 0 0	0 1 1	15 0 15	14 1 14	-0.057
4863.05845	0.00082	3.1×10^{-39}	0 0 0	0 1 1	9 3 7	8 2 6	-0.102
4865.64215	0.21055	4.6×10^{-40}	0 0 0	0 1 1	15 3 13	14 3 12	-0.085
4867.63773	0.00111	7.5×10^{-39}	0 0 0	0 1 1	5 4 1	4 3 2	-0.114
4867.63773	0.00109	7.6×10^{-39}	0 0 0	0 1 1	5 4 2	4 3 1	-0.120
4868.06806	0.00045	6.6×10^{-39}	0 0 0	0 1 1	7 3 4	6 2 5	-0.097
4869.12983	0.00461	6.4×10^{-40}	0 0 0	0 1 1	14 2 13	13 1 12	-0.077
4869.63957	0.00069	4.7×10^{-39}	0 0 0	0 1 1	8 3 6	7 2 5	-0.101
4870.66175	0.00103	3.1×10^{-39}	0 0 0	0 1 1	7 2 5	6 1 6	-0.082
4871.34966	0.00251	1.2×10^{-39}	0 0 0	0 1 1	14 2 12	13 2 11	-0.078
4872.25300	0.00163	1.8×10^{-39}	0 0 0	0 1 1	14 1 14	13 0 13	-0.063
4872.41717	0.00092	3.2×10^{-39}	0 0 0	0 1 1	14 0 14	13 0 13	-0.063
4872.49409	0.00084	3.1×10^{-39}	0 0 0	0 1 1	14 1 14	13 1 13	-0.064
4872.66177	0.00152	1.8×10^{-39}	0 0 0	0 1 1	14 0 14	13 1 13	-0.061
4873.25830	0.00195	1.8×10^{-39}	0 0 0	0 1 1	14 1 13	13 1 12	-0.069
4874.73119	0.00144	1.7×10^{-39}	0 0 0	0 1 1	14 2 13	13 2 12	-0.072

Position	$\sigma_{\text{Pos.}}$	Intensity	$\nu_1\ \nu_2\ \nu_3$	$\nu_1'\ \nu_2'\ \nu_3'$	J K_a K_c	J' K_a' K_c'	$\Delta_{\text{SPEC.}}$
4877.15548	0.00423	9.8×10^{-40}	0 0 0	0 1 1	14 3 12	13 3 11	-0.079
4877.36892	0.00048	6.8×10^{-39}	0 0 0	0 1 1	7 3 5	6 2 4	-0.101
4878.18415	0.00262	1.2×10^{-39}	0 0 0	0 1 1	13 2 12	12 1 11	-0.077
4879.23356	0.00047	9.7×10^{-39}	0 0 0	0 1 1	4 4 0	3 3 1	-0.118
4879.24453	0.00048	9.7×10^{-39}	0 0 0	0 1 1	4 4 1	3 3 0	-0.122
4880.95437	0.00381	4.9×10^{-40}	0 0 0	0 1 1	14 4 10	13 4 9	-0.084
4881.49982	0.00033	9.1×10^{-39}	0 0 0	0 1 1	6 3 3	5 2 4	-0.100
4882.15657	0.00112	2.6×10^{-39}	0 0 0	0 1 1	13 2 11	12 2 10	-0.081
4884.15370	0.00173	1.8×10^{-39}	0 0 0	0 1 1	13 3 10	12 3 9	-0.056
4884.21921	0.00115	3.6×10^{-39}	0 0 0	0 1 1	13 1 12	12 1 11	-0.076
4884.46337	0.00085	3.2×10^{-39}	0 0 0	0 1 1	13 1 13	12 0 12	-0.067
4884.67169	0.00340	7.5×10^{-40}	0 0 0	0 1 1	6 2 4	5 0 5	-0.084
4884.73553	0.00046	6.0×10^{-39}	0 0 0	0 1 1	13 0 13	12 0 12	-0.067
4884.86813	0.00044	6.0×10^{-39}	0 0 0	0 1 1	13 1 13	12 1 12	-0.067
4885.14040	0.00086	3.2×10^{-39}	0 0 0	0 1 1	13 0 13	12 1 12	-0.067
4886.27454	0.00036	9.2×10^{-39}	0 0 0	0 1 1	6 3 4	5 2 3	-0.103
4886.30433	0.00102	3.4×10^{-39}	0 0 0	0 1 1	13 2 12	12 2 11	-0.074
4886.39677	0.00147	1.9×10^{-39}	0 0 0	0 1 1	12 2 11	11 1 10	-0.078
4888.70487	0.00180	2.0×10^{-39}	0 0 0	0 1 1	13 3 11	12 3 10	-0.083
4892.34093	0.00249	1.1×10^{-39}	0 0 0	0 1 1	13 1 12	12 2 11	-0.072
4892.65069	0.00055	5.3×10^{-39}	0 0 0	0 1 1	6 2 4	5 1 5	-0.084
4893.22195	0.00060	5.1×10^{-39}	0 0 0	0 1 1	12 2 10	11 2 9	-0.084
4893.36095	0.00271	9.8×10^{-40}	0 0 0	0 1 1	13 4 9	12 4 8	-0.097
4894.16642	0.25241	1.2×10^{-38}	0 0 0	0 1 1	5 3 2	4 2 3	-0.103
4894.63485	0.25774	1.0×10^{-39}	0 0 0	0 1 1	13 4 10	12 4 9	-0.097
4895.00271	0.27890	6.8×10^{-39}	0 0 0	0 1 1	12 1 11	11 1 10	-0.072
4896.24038	0.00026	1.2×10^{-38}	0 0 0	0 1 1	5 3 3	4 2 2	-0.104
4896.39281	0.00052	5.4×10^{-39}	0 0 0	0 1 1	12 1 12	11 0 11	-0.070
4896.56151	0.00088	3.6×10^{-39}	0 0 0	0 1 1	12 3 9	11 3 8	-0.076
4896.84005	0.00027	1.1×10^{-38}	0 0 0	0 1 1	12 0 12	11 0 11	-0.069
4897.06411	0.00027	1.1×10^{-38}	0 0 0	0 1 1	12 1 12	11 1 11	-0.069
4897.51036	0.00063	5.4×10^{-39}	0 0 0	0 1 1	12 0 12	11 1 11	-0.069
4897.76187	0.00046	6.3×10^{-39}	0 0 0	0 1 1	12 2 11	11 2 10	-0.074
4900.31676	0.00086	3.7×10^{-39}	0 0 0	0 1 1	12 3 10	11 3 9	-0.085
4900.59837	0.00072	4.6×10^{-39}	0 0 0	0 1 1	10 2 9	9 1 8	-0.081
4900.97054	0.00493	7.5×10^{-40}	0 0 0	0 1 1	5 5 0	5 4 1	-0.162
4900.98826	0.01001	7.5×10^{-40}	0 0 0	0 1 1	5 5 1	5 4 2	-0.142
4900.98826	0.00814	1.0×10^{-39}	0 0 0	0 1 1	6 5 1	6 4 2	-0.147
4900.98826	0.00814	1.0×10^{-39}	0 0 0	0 1 1	6 5 2	6 4 3	-0.135
4901.03314	0.00277	9.7×10^{-40}	0 0 0	0 1 1	7 5 3	7 4 4	-0.141
4901.07828	0.00301	9.7×10^{-40}	0 0 0	0 1 1	7 5 2	7 4 3	-0.144

Position	$\sigma_{\text{Pos.}}$	Intensity	$\nu_1\ \nu_2\ \nu_3$	$\nu_1'\ \nu_2'\ \nu_3'$	J K_a K_c	J' K_a' K_c'	$\Delta_{\text{SPEC.}}$
4901.16261	0.00331	7.9×10^{-40}	0 0 0	0 1 1	8 5 4	8 4 5	-0.139
4901.67879	0.00291	8.0×10^{-40}	0 0 0	0 1 1	5 2 3	4 0 4	-0.092
4903.16722	0.00047	6.7×10^{-39}	0 0 0	0 1 1	11 2 9	10 2 8	-0.029
4905.69529	0.00053	1.2×10^{-38}	0 0 0	0 1 1	11 1 10	10 1 9	-0.074
4905.73140	0.00304	1.8×10^{-39}	0 0 0	0 1 1	12 4 8	11 4 7	-0.088
4906.33469	0.00025	1.4×10^{-38}	0 0 0	0 1 1	4 3 1	3 2 2	-0.102
4906.61487	0.00184	1.9×10^{-39}	0 0 0	0 1 1	12 4 9	11 4 8	-0.103
4906.96027	0.00080	6.4×10^{-39}	0 0 0	0 1 1	9 2 8	8 1 7	-0.087
4907.02526	0.00023	1.4×10^{-38}	0 0 0	0 1 1	4 3 2	3 2 1	-0.105
4907.98432	0.00035	8.7×10^{-39}	0 0 0	0 1 1	11 1 11	10 0 10	-0.071
4908.70531	0.00016	1.8×10^{-38}	0 0 0	0 1 1	11 0 11	10 0 10	-0.072
4908.95482	0.00030	1.0×10^{-38}	0 0 0	0 1 1	11 2 10	10 2 9	-0.051
4909.01761	0.00046	6.5×10^{-39}	0 0 0	0 1 1	11 3 8	10 3 7	-0.084
4909.08076	0.00018	1.8×10^{-38}	0 0 0	0 1 1	11 1 11	10 1 10	-0.073
4909.80315	0.00034	8.7×10^{-39}	0 0 0	0 1 1	11 0 11	10 1 10	-0.072
4911.99434	0.00048	6.6×10^{-39}	0 0 0	0 1 1	11 3 9	10 3 8	-0.089
4912.19378	0.00040	8.2×10^{-39}	0 0 0	0 1 1	5 2 3	4 1 4	-0.090
4913.17744	0.00038	8.4×10^{-39}	0 0 0	0 1 1	8 2 7	7 1 6	-0.091
4915.53830	0.00020	1.6×10^{-38}	0 0 0	0 1 1	10 2 8	9 2 7	-0.084
4916.42129	0.00079	2.1×10^{-38}	0 0 0	0 1 1	10 1 9	9 1 8	-0.077
4916.59737	0.00486	7.3×10^{-40}	0 0 0	0 1 1	12 5 7	11 5 6	-0.130
4916.62157	0.00468	7.3×10^{-40}	0 0 0	0 1 1	12 5 8	11 5 7	-0.135
4917.96229	0.00106	3.1×10^{-39}	0 0 0	0 1 1	11 4 7	10 4 6	-0.097
4918.19526	0.00020	1.5×10^{-38}	0 0 0	0 1 1	3 3 0	2 2 1	-0.107
4918.33279	0.00046	1.6×10^{-38}	0 0 0	0 1 1	3 3 1	2 2 0	-0.107
4918.63959	0.00092	3.3×10^{-39}	0 0 0	0 1 1	11 4 8	10 4 7	-0.104
4919.10582	0.00024	1.4×10^{-38}	0 0 0	0 1 1	10 1 10	9 0 9	-0.071
4919.54731	0.00033	1.1×10^{-38}	0 0 0	0 1 1	7 2 6	6 1 5	-0.094
4919.84051	0.00916	2.4×10^{-40}	0 0 0	0 1 1	13 3 11	13 2 12	-0.089
4920.25635	0.00029	2.8×10^{-38}	0 0 0	0 1 1	10 0 10	9 0 9	-0.070
4920.83154	0.00117	2.9×10^{-39}	0 0 0	0 1 1	11 1 10	10 2 9	-0.047
4920.90780	0.00013	2.8×10^{-38}	0 0 0	0 1 1	10 1 10	9 1 9	-0.075
4920.93535	0.01059	5.5×10^{-40}	0 0 0	0 1 1	8 3 6	8 1 7	-0.094
4921.50778	0.00023	1.5×10^{-38}	0 0 0	0 1 1	10 2 9	9 2 8	-0.056
4921.54249	0.00032	1.1×10^{-38}	0 0 0	0 1 1	10 3 7	9 3 6	-0.088
4922.05781	0.00025	1.4×10^{-38}	0 0 0	0 1 1	10 0 10	9 1 9	-0.074
4923.74105	0.00030	1.1×10^{-38}	0 0 0	0 1 1	10 3 8	9 3 7	-0.092
4924.28280	0.00625	5.9×10^{-40}	0 0 0	0 1 1	11 4 8	11 3 9	-0.109
4925.13027	0.00349	9.9×10^{-40}	0 0 0	0 1 1	10 4 7	10 3 8	-0.107
4925.58070	0.00240	1.5×10^{-39}	0 0 0	0 1 1	9 4 6	9 3 7	-0.108
4925.68338	0.00758	2.3×10^{-39}	0 0 0	0 1 1	4 4 1	4 3 2	-0.119

Position	$\sigma_{\text{Pos.}}$	Intensity	$\nu_1\ \nu_2\ \nu_3$	ν_1' ν_2' ν_3'	J K_a K_c	J' K_a' K_c'	$\Delta_{\text{SPEC.}}$
4925.68338	0.00749	2.3×10^{-39}	0 0 0	0 1 1	4 4 0	4 3 1	-0.124
4925.69427	0.00242	3.2×10^{-39}	0 0 0	0 1 1	5 4 2	5 3 3	-0.122
4925.74195	0.00326	3.3×10^{-39}	0 0 0	0 1 1	6 4 3	6 3 4	-0.121
4925.75516	0.00227	2.2×10^{-39}	0 0 0	0 1 1	8 4 5	8 3 6	-0.117
4925.78258	0.00176	2.8×10^{-39}	0 0 0	0 1 1	7 4 4	7 3 5	-0.119
4925.82886	0.00112	3.3×10^{-39}	0 0 0	0 1 1	5 4 1	5 3 2	-0.120
4926.19164	0.00092	3.3×10^{-39}	0 0 0	0 1 1	6 4 2	6 3 3	-0.120
4926.33408	0.00027	1.3×10^{-38}	0 0 0	0 1 1	6 2 5	5 1 4	-0.094
4926.92412	0.00111	2.8×10^{-39}	0 0 0	0 1 1	7 4 3	7 3 4	-0.118
4927.26025	0.00040	3.4×10^{-38}	0 0 0	0 1 1	9 1 8	8 1 7	-0.080
4927.35823	0.00013	2.6×10^{-38}	0 0 0	0 1 1	9 2 7	8 2 6	-0.088
4928.21701	0.00110	2.2×10^{-39}	0 0 0	0 1 1	8 4 4	8 3 5	-0.115
4928.86719	0.00275	1.2×10^{-39}	0 0 0	0 1 1	11 5 6	10 5 5	-0.132
4928.88719	0.00298	1.2×10^{-39}	0 0 0	0 1 1	11 5 7	10 5 6	-0.129
4929.39009	0.00197	1.6×10^{-39}	0 0 0	0 1 1	10 2 9	10 1 10	-0.078
4929.51504	0.00030	1.1×10^{-38}	0 0 0	0 1 1	4 2 2	3 1 3	-0.093
4929.62501	0.00687	4.0×10^{-40}	0 0 0	0 1 1	3 2 1	2 0 2	-0.096
4930.07207	0.00403	9.1×10^{-40}	0 0 0	0 1 1	11 1 10	11 0 11	-0.070
4930.27784	0.00236	1.6×10^{-39}	0 0 0	0 1 1	9 4 5	9 3 6	-0.113
4930.45084	0.00042	1.0×10^{-38}	0 0 0	0 1 1	9 1 9	8 0 8	-0.068
4930.68603	0.00130	5.3×10^{-39}	0 0 0	0 1 1	10 4 7	9 4 6	-0.108
4931.24340	0.00134	3.8×10^{-39}	0 0 0	0 1 1	10 4 6	9 4 5	-0.065
4932.24893	0.00007	4.7×10^{-38}	0 0 0	0 1 1	9 0 9	8 0 8	-0.066
4932.55401	0.00012	2.8×10^{-38}	0 0 0	0 1 1	9 2 8	8 2 7	-0.085
4932.74453	0.00007	4.8×10^{-38}	0 0 0	0 1 1	9 1 9	8 1 8	-0.078
4933.73467	0.00023	1.4×10^{-38}	0 0 0	0 1 1	5 2 4	4 1 3	-0.096
4934.05314	0.00045	1.7×10^{-38}	0 0 0	0 1 1	9 3 6	8 3 5	-0.093
4934.54277	0.00025	1.3×10^{-38}	0 0 0	0 1 1	9 0 9	8 1 8	-0.077
4935.54861	0.00020	1.7×10^{-38}	0 0 0	0 1 1	9 3 7	8 3 6	-0.095
4937.25064	0.00713	6.5×10^{-40}	0 0 0	0 1 1	11 4 7	11 3 8	-0.095
4937.32766	0.00119	2.7×10^{-39}	0 0 0	0 1 1	10 1 9	9 2 8	-0.054
4938.20801	0.00593	1.8×10^{-39}	0 0 0	0 1 1	10 3 8	10 2 9	-0.058
4938.25755	0.00008	5.1×10^{-38}	0 0 0	0 1 1	8 1 7	7 1 6	-0.084
4939.11188	0.00145	2.6×10^{-39}	0 0 0	0 1 1	9 2 8	9 1 9	-0.082
4939.41700	0.00009	3.9×10^{-38}	0 0 0	0 1 1	8 2 6	7 2 5	-0.089
4940.35718	0.00023	2.0×10^{-38}	0 0 0	0 1 1	8 1 8	7 0 7	-0.083
4941.11195	0.00233	2.0×10^{-39}	0 0 0	0 1 1	10 5 6	9 5 5	-0.139
4941.11196	0.00229	2.0×10^{-39}	0 0 0	0 1 1	10 5 5	9 5 4	-0.131
4941.88583	0.00023	1.6×10^{-38}	0 0 0	0 1 1	4 2 3	3 1 2	-0.096
4942.68677	0.00045	7.9×10^{-39}	0 0 0	0 1 1	9 4 5	8 4 4	-0.113
4942.73485	0.00045	7.9×10^{-39}	0 0 0	0 1 1	9 4 6	8 4 5	-0.112

Position	$\sigma_{\text{Pos.}}$	Intensity	$\nu_1\,\nu_2\,\nu_3$	$\nu_1'\,\nu_2'\,\nu_3'$	J K_a K_c	J' K_a' K_c'	$\Delta_{\text{SPEC.}}$
4943.10211	0.00039	6.7×10^{-38}	0 0 0	0 1 1	8 0 8	7 0 7	-0.081
4943.57539	0.00215	1.6×10^{-39}	0 0 0	0 1 1	9 3 7	9 2 8	-0.068
4943.91909	0.00009	4.0×10^{-38}	0 0 0	0 1 1	8 2 7	7 2 6	-0.089
4944.11658	0.00179	1.7×10^{-39}	0 0 0	0 1 1	10 1 9	10 0 10	-0.072
4944.24011	0.00005	6.5×10^{-38}	0 0 0	0 1 1	8 1 8	7 1 7	-0.082
4944.93886	0.00025	1.4×10^{-38}	0 0 0	0 1 1	3 2 1	2 1 2	-0.095
4946.47599	0.00015	2.4×10^{-38}	0 0 0	0 1 1	8 3 5	7 3 4	-0.097
4946.52112	0.00109	3.3×10^{-39}	0 0 0	0 1 1	8 3 6	8 2 7	-0.100
4946.98441	0.00017	2.0×10^{-38}	0 0 0	0 1 1	8 0 8	7 1 7	-0.081
4947.40519	0.00014	2.4×10^{-38}	0 0 0	0 1 1	8 3 6	7 3 5	-0.098
4948.13059	0.00140	4.3×10^{-39}	0 0 0	0 1 1	8 2 7	8 1 8	-0.083
4948.94114	0.00074	4.8×10^{-39}	0 0 0	0 1 1	7 3 5	7 2 6	-0.105
4949.45516	0.00005	7.1×10^{-38}	0 0 0	0 1 1	7 1 6	6 1 5	-0.086
4949.94077	0.00014	2.5×10^{-38}	0 0 0	0 1 1	7 1 7	6 0 6	-0.086
4950.68868	0.00061	6.0×10^{-39}	0 0 0	0 1 1	6 3 4	6 2 5	-0.105
4950.86919	0.00020	1.6×10^{-38}	0 0 0	0 1 1	3 2 2	2 1 1	-0.097
4951.70966	0.00007	5.3×10^{-38}	0 0 0	0 1 1	7 2 5	6 2 4	-0.091
4951.85936	0.00056	6.7×10^{-39}	0 0 0	0 1 1	5 3 3	5 2 4	-0.099
4952.55364	0.00152	6.4×10^{-39}	0 0 0	0 1 1	4 3 2	4 2 3	-0.110
4952.85232	0.00075	4.6×10^{-39}	0 0 0	0 1 1	9 1 8	8 2 7	-0.079
4952.93025	0.00081	4.4×10^{-39}	0 0 0	0 1 1	3 3 1	3 2 2	-0.110
4953.30901	0.00120	2.8×10^{-39}	0 0 0	0 1 1	9 5 4	8 5 3	-0.137
4953.30901	0.00120	2.8×10^{-39}	0 0 0	0 1 1	9 5 5	8 5 4	-0.140
4953.58332	0.00088	4.5×10^{-39}	0 0 0	0 1 1	3 3 0	3 2 1	-0.111
4954.00407	0.00004	8.9×10^{-38}	0 0 0	0 1 1	7 0 7	6 0 6	-0.084
4954.46115	0.00054	6.6×10^{-39}	0 0 0	0 1 1	4 3 1	4 2 2	-0.109
4954.73684	0.00034	1.1×10^{-38}	0 0 0	0 1 1	8 4 4	7 4 3	-0.115
4954.77075	0.00034	1.1×10^{-38}	0 0 0	0 1 1	8 4 5	7 4 4	-0.116
4955.35948	0.00007	5.5×10^{-38}	0 0 0	0 1 1	7 2 6	6 2 5	-0.092
4955.66409	0.00016	8.5×10^{-38}	0 0 0	0 1 1	7 1 7	6 1 6	-0.085
4955.99765	0.00056	6.4×10^{-39}	0 0 0	0 1 1	7 2 6	7 1 7	-0.089
4956.09176	0.00050	7.2×10^{-39}	0 0 0	0 1 1	5 3 2	5 2 3	-0.110
4957.60978	0.00124	2.7×10^{-39}	0 0 0	0 1 1	9 1 8	9 0 9	-0.071
4958.61177	0.00052	6.8×10^{-39}	0 0 0	0 1 1	6 3 3	6 2 4	-0.108
4958.76886	0.00013	3.1×10^{-38}	0 0 0	0 1 1	7 3 4	6 3 3	-0.101
4958.82223	0.00024	1.6×10^{-38}	0 0 0	0 1 1	2 2 0	1 1 1	-0.098
4959.01036	0.00016	2.9×10^{-38}	0 0 0	0 1 1	6 1 6	5 0 5	-0.087
4959.29248	0.00011	3.1×10^{-38}	0 0 0	0 1 1	7 3 5	6 3 4	-0.101
4959.72815	0.00022	2.5×10^{-38}	0 0 0	0 1 1	7 0 7	6 1 6	-0.083
4960.72739	0.00023	1.7×10^{-38}	0 0 0	0 1 1	2 2 1	1 1 0	-0.099
4960.87281	0.00005	9.1×10^{-38}	0 0 0	0 1 1	6 1 5	5 1 4	-0.088

Position	$\sigma_{\text{Pos.}}$	Intensity	$\nu_1\,\nu_2\,\nu_3$	$\nu_1'\,\nu_2'\,\nu_3'$	J $K_a\,K_c$	J' $K_a'\,K_c'$	$\Delta_{\text{SPEC.}}$
4961.95777	0.00062	5.8×10^{-39}	0 0 0	0 1 1	7 3 4	7 2 5	-0.108
4962.91461	0.00048	8.8×10^{-39}	0 0 0	0 1 1	6 2 5	6 1 6	-0.092
4964.15700	0.00005	6.6×10^{-38}	0 0 0	0 1 1	6 2 4	5 2 3	-0.093
4964.80298	0.00005	1.1×10^{-37}	0 0 0	0 1 1	6 0 6	5 0 5	-0.086
4965.85136	0.00084	4.6×10^{-39}	0 0 0	0 1 1	8 3 5	8 2 6	-0.108
4966.76395	0.00044	1.3×10^{-38}	0 0 0	0 1 1	7 4 4	6 4 3	-0.133
4966.77665	0.00045	1.3×10^{-38}	0 0 0	0 1 1	7 4 3	6 4 2	-0.105
4966.85055	0.00006	6.7×10^{-38}	0 0 0	0 1 1	6 2 5	5 2 4	-0.093
4966.99015	0.00004	1.0×10^{-37}	0 0 0	0 1 1	6 1 6	5 1 5	-0.087
4967.71757	0.00012	3.1×10^{-38}	0 0 0	0 1 1	5 1 5	4 0 4	-0.089
4968.75749	0.01359	7.0×10^{-40}	0 0 0	0 1 1	9 6 4	8 6 3	-0.171
4968.75749	0.01363	7.0×10^{-40}	0 0 0	0 1 1	9 6 3	8 6 2	-0.171
4968.80397	0.00062	1.1×10^{-38}	0 0 0	0 1 1	5 2 4	5 1 5	-0.095
4968.99826	0.00063	5.9×10^{-39}	0 0 0	0 1 1	8 1 7	7 2 6	-0.083
4969.81630	0.00120	3.3×10^{-39}	0 0 0	0 1 1	9 3 6	9 2 7	-0.104
4970.91392	0.00070	8.4×10^{-39}	0 0 0	0 1 1	8 1 7	8 0 8	-0.069
4970.92627	0.00014	3.6×10^{-38}	0 0 0	0 1 1	6 3 3	5 3 2	-0.103
4971.19045	0.00010	3.6×10^{-38}	0 0 0	0 1 1	6 3 4	5 3 3	-0.103
4972.51078	0.00009	1.1×10^{-37}	0 0 0	0 1 1	5 1 4	4 1 3	-0.089
4972.78305	0.00015	2.7×10^{-38}	0 0 0	0 1 1	6 0 6	5 1 5	-0.085
4973.19818	0.00227	1.3×10^{-39}	0 0 0	0 1 1	8 1 7	8 1 8	-0.089
4973.65761	0.00031	1.2×10^{-38}	0 0 0	0 1 1	4 2 3	4 1 4	-0.097
4975.60723	0.00003	1.3×10^{-37}	0 0 0	0 1 1	5 0 5	4 0 4	-0.087
4976.33657	0.00014	3.0×10^{-38}	0 0 0	0 1 1	4 1 4	3 0 3	-0.090
4976.62949	0.00005	7.4×10^{-38}	0 0 0	0 1 1	5 2 3	4 2 2	-0.095
4977.48939	0.00030	1.2×10^{-38}	0 0 0	0 1 1	3 2 2	3 1 3	-0.097
4977.54514	0.00125	3.9×10^{-39}	0 0 0	0 1 1	7 5 3	6 5 2	-0.147
4977.54514	0.00125	3.9×10^{-39}	0 0 0	0 1 1	7 5 2	6 5 1	-0.147
4978.23104	0.00003	1.2×10^{-37}	0 0 0	0 1 1	5 1 5	4 1 4	-0.088
4978.38641	0.00005	7.4×10^{-38}	0 0 0	0 1 1	5 2 4	4 2 3	-0.095
4978.73911	0.00039	1.4×10^{-38}	0 0 0	0 1 1	6 4 2	5 4 1	-0.119
4978.73911	0.00039	1.4×10^{-38}	0 0 0	0 1 1	6 4 3	5 4 2	-0.124
4980.32364	0.00047	8.2×10^{-39}	0 0 0	0 1 1	2 2 1	2 1 2	-0.099
4981.13869	0.00149	2.9×10^{-39}	0 0 0	0 1 1	10 2 8	10 1 9	-0.080
4982.01764	0.00084	1.1×10^{-38}	0 0 0	0 1 1	7 1 6	7 0 7	-0.087
4982.95455	0.00010	3.6×10^{-38}	0 0 0	0 1 1	5 3 2	4 3 1	-0.105
4983.08577	0.00048	3.6×10^{-38}	0 0 0	0 1 1	5 3 3	4 3 2	-0.104
4984.35549	0.00003	1.1×10^{-37}	0 0 0	0 1 1	4 1 3	3 1 2	-0.090
4985.18893	0.00014	2.7×10^{-38}	0 0 0	0 1 1	3 1 3	2 0 2	-0.091
4985.26718	0.00056	6.8×10^{-39}	0 0 0	0 1 1	7 1 6	6 2 5	-0.084
4985.59047	0.00042	9.4×10^{-39}	0 0 0	0 1 1	2 2 0	2 1 1	-0.100

Position	$\sigma_{\text{Pos.}}$	Intensity	$\nu_1\ \nu_2\ \nu_3$	$\nu_1{}'\ \nu_2{}'\ \nu_3{}'$	J K_a K_c	J' $\text{K}_a{}'$ $\text{K}_c{}'$	$\Delta_{\text{SPEC.}}$
4986.12144	0.00014	2.7×10^{-38}	0 0 0	0 1 1	5 0 5	4 1 4	-0.086
4986.54370	0.00004	1.4×10^{-37}	0 0 0	0 1 1	4 0 4	3 0 3	-0.088
4987.67662	0.00024	1.5×10^{-38}	0 0 0	0 1 1	3 2 1	3 1 2	-0.100
4988.99206	0.00005	7.0×10^{-38}	0 0 0	0 1 1	4 2 2	3 2 1	-0.097
4989.39932	0.00003	1.2×10^{-37}	0 0 0	0 1 1	4 1 4	3 1 3	-0.090
4989.57036	0.00194	3.1×10^{-39}	0 0 0	0 1 1	6 5 1	5 5 0	-0.150
4989.57036	0.00203	3.1×10^{-39}	0 0 0	0 1 1	6 5 2	5 5 1	-0.151
4989.87083	0.00021	1.8×10^{-38}	0 0 0	0 1 1	4 2 2	4 1 3	-0.101
4989.96450	0.00020	7.0×10^{-38}	0 0 0	0 1 1	4 2 3	3 2 2	-0.097
4990.65192	0.00105	1.0×10^{-38}	0 0 0	0 1 1	5 4 2	4 4 1	-0.124
4990.65192	0.00105	1.0×10^{-38}	0 0 0	0 1 1	5 4 1	4 4 0	-0.123
4990.70453	0.00047	8.8×10^{-39}	0 0 0	0 1 1	8 2 6	8 1 7	-0.090
4991.72370	0.00145	1.7×10^{-38}	0 0 0	0 1 1	6 1 5	6 0 6	-0.092
4991.72841	0.00130	1.9×10^{-38}	0 0 0	0 1 1	5 2 3	5 1 4	-0.094
4992.54429	0.00063	1.3×10^{-38}	0 0 0	0 1 1	7 2 5	7 1 6	-0.093
4992.75935	0.00022	1.7×10^{-38}	0 0 0	0 1 1	6 2 4	6 1 5	-0.098
4994.55367	0.00017	2.2×10^{-38}	0 0 0	0 1 1	2 1 2	1 0 1	-0.092
4994.87171	0.00022	2.6×10^{-38}	0 0 0	0 1 1	4 3 1	3 3 0	-0.108
4994.88953	0.00023	2.6×10^{-38}	0 0 0	0 1 1	4 3 2	3 3 1	-0.109
4996.38458	0.00004	1.0×10^{-37}	0 0 0	0 1 1	3 1 2	2 1 1	-0.091
4997.45316	0.00070	5.3×10^{-39}	0 0 0	0 1 1	6 1 5	6 1 6	-0.086
4997.69270	0.00003	1.3×10^{-37}	0 0 0	0 1 1	3 0 3	2 0 2	-0.089
4999.60120	0.00045	2.3×10^{-38}	0 0 0	0 1 1	4 0 4	3 1 3	-0.093
4999.60570	0.00045	2.3×10^{-38}	0 0 0	0 1 1	5 1 4	5 0 5	-0.083
5000.50133	0.00005	1.0×10^{-37}	0 0 0	0 1 1	3 1 3	2 1 2	-0.092
5001.15731	0.00014	4.9×10^{-38}	0 0 0	0 1 1	3 2 1	2 2 0	-0.098
5001.38968	0.00058	6.9×10^{-39}	0 0 0	0 1 1	6 1 5	5 2 4	-0.086
5001.57669	0.00009	4.9×10^{-38}	0 0 0	0 1 1	3 2 2	2 2 1	-0.098
5004.62047	0.00057	1.5×10^{-38}	0 0 0	0 1 1	1 1 1	0 0 0	-0.092
5005.61359	0.00013	3.0×10^{-38}	0 0 0	0 1 1	4 1 3	4 0 4	-0.091
5007.58074	0.00045	8.7×10^{-39}	0 0 0	0 1 1	5 1 4	5 1 5	-0.087
5008.57439	0.00013	6.8×10^{-38}	0 0 0	0 1 1	2 1 1	1 1 0	-0.093
5009.06474	0.00004	1.0×10^{-37}	0 0 0	0 1 1	2 0 2	1 0 1	-0.090
5009.94260	0.00012	3.3×10^{-38}	0 0 0	0 1 1	3 1 2	3 0 3	-0.092
5011.53442	0.00006	6.9×10^{-38}	0 0 0	0 1 1	2 1 2	1 1 1	-0.093
5012.21093	0.00372	1.2×10^{-39}	0 0 0	0 1 1	2 2 0	3 1 3	-0.101
5012.62002	0.00764	5.2×10^{-40}	0 0 0	0 1 1	9 7 2	9 7 3	-0.108
5012.63574	0.00892	5.2×10^{-40}	0 0 0	0 1 1	9 7 3	9 7 2	-0.092
5012.85996	0.01135	9.8×10^{-40}	0 0 0	0 1 1	8 7 2	8 7 1	-0.329
5012.85996	0.00050	3.0×10^{-38}	0 0 0	0 1 1	2 1 1	2 0 2	-0.091
5012.89434	0.00968	9.8×10^{-40}	0 0 0	0 1 1	8 7 1	8 7 2	-0.295

Position	$\sigma_{\text{Pos.}}$	Intensity	$\nu_1\,\nu_2\,\nu_3$	$\nu_1\text{'}\,\nu_2\text{'}\,\nu_3\text{'}$	J K_a K_c	J' K_a' K_c'	$\Delta_{\text{SPEC.}}$
5013.00520	0.00023	1.7×10^{-38}	0 0 0	0 1 1	3 0 3	2 1 2	-0.090
5013.36356	0.00265	1.8×10^{-39}	0 0 0	0 1 1	7 7 1	7 7 0	-0.238
5013.38069	0.00233	1.8×10^{-39}	0 0 0	0 1 1	7 7 0	7 7 1	-0.221
5014.63266	0.00028	2.2×10^{-38}	0 0 0	0 1 1	1 1 0	1 0 1	-0.093
5016.12723	0.00031	1.4×10^{-38}	0 0 0	0 1 1	4 1 3	4 1 4	-0.090
5016.31742	0.00260	3.2×10^{-39}	0 0 0	0 1 1	8 2 6	8 2 7	-0.069
5017.16198	0.00066	6.3×10^{-39}	0 0 0	0 1 1	5 1 4	4 2 3	-0.089
5017.18132	0.00321	1.8×10^{-39}	0 0 0	0 1 1	8 2 6	7 3 5	-0.087
5019.44746	0.00198	1.9×10^{-39}	0 0 0	0 1 1	3 2 1	4 1 4	-0.101
5020.50772	0.00538	6.8×10^{-40}	0 0 0	0 1 1	5 3 2	6 2 5	-0.111
5020.61008	0.00006	5.6×10^{-38}	0 0 0	0 1 1	1 0 1	0 0 0	-0.091
5023.00402	0.00028	2.3×10^{-38}	0 0 0	0 1 1	3 1 2	3 1 3	-0.093
5023.28456	0.00208	6.9×10^{-39}	0 0 0	0 1 1	7 2 5	7 2 6	-0.093
5026.04620	0.00042	8.9×10^{-39}	0 0 0	0 1 1	2 0 2	1 1 1	-0.091
5027.71585	0.00354	9.0×10^{-40}	0 0 0	0 1 1	11 3 8	11 3 9	-0.087
5028.17125	0.00011	3.8×10^{-38}	0 0 0	0 1 1	2 1 1	2 1 2	-0.093
5028.30057	0.00444	1.3×10^{-39}	0 0 0	0 1 1	5 2 3	6 1 6	-0.100
5028.57144	0.00031	1.3×10^{-38}	0 0 0	0 1 1	6 2 4	6 2 5	-0.096
5028.95868	0.00428	9.3×10^{-40}	0 0 0	0 1 1	5 3 3	6 2 4	-0.119
5029.00898	0.00376	1.0×10^{-39}	0 0 0	0 1 1	9 2 8	8 3 5	-0.094
5029.21179	0.00458	7.0×10^{-40}	0 0 0	0 1 1	6 2 4	7 1 7	-0.091
5031.61362	0.00005	7.7×10^{-38}	0 0 0	0 1 1	1 1 0	1 1 1	-0.094
5032.23999	0.00017	2.3×10^{-38}	0 0 0	0 1 1	5 2 3	5 2 4	-0.098
5032.44018	0.00091	4.7×10^{-39}	0 0 0	0 1 1	4 1 3	3 2 2	-0.084
5032.65133	0.00209	1.9×10^{-39}	0 0 0	0 1 1	10 3 7	10 3 8	-0.097
5033.63095	0.00266	2.1×10^{-39}	0 0 0	0 1 1	7 2 5	6 3 4	-0.093
5034.52341	0.00009	4.0×10^{-38}	0 0 0	0 1 1	4 2 2	4 2 3	-0.099
5034.99262	0.00005	7.7×10^{-38}	0 0 0	0 1 1	1 1 1	1 1 0	-0.095
5035.75515	0.00006	6.7×10^{-38}	0 0 0	0 1 1	3 2 1	3 2 2	-0.100
5036.09196	0.00092	3.8×10^{-39}	0 0 0	0 1 1	9 3 6	9 3 7	-0.101
5036.29849	0.00003	1.2×10^{-37}	0 0 0	0 1 1	2 2 0	2 2 1	-0.101
5036.54270	0.00003	1.2×10^{-37}	0 0 0	0 1 1	2 2 1	2 2 0	-0.101
5036.71256	0.00237	1.5×10^{-39}	0 0 0	0 1 1	7 1 7	6 2 4	-0.093
5036.84842	0.00239	1.5×10^{-39}	0 0 0	0 1 1	8 2 7	7 3 4	-0.090
5036.96649	0.00006	6.7×10^{-38}	0 0 0	0 1 1	3 2 2	3 2 1	-0.101
5037.84735	0.00196	3.2×10^{-39}	0 0 0	0 1 1	3 2 2	4 1 3	-0.103
5038.09324	0.00010	4.0×10^{-38}	0 0 0	0 1 1	4 2 3	4 2 2	-0.101
5038.30225	0.00011	3.8×10^{-38}	0 0 0	0 1 1	2 1 2	2 1 1	-0.095
5038.33982	0.00089	7.2×10^{-39}	0 0 0	0 1 1	8 3 5	8 3 6	-0.103
5038.49910	0.00189	2.3×10^{-39}	0 0 0	0 1 1	6 1 6	5 2 3	-0.093
5039.27547	0.00059	7.5×10^{-39}	0 0 0	0 1 1	1 1 1	2 0 2	-0.096

Position	$\sigma_{\text{Pos.}}$	Intensity	$\nu_1\ \nu_2\ \nu_3$	$\nu_1{'}\ \nu_2{'}\ \nu_3{'}$	J K_a K_c	J' $K_a{'}$ $K_c{'}$	$\Delta_{\text{SPEC.}}$
5039.72159	0.00028	1.3×10^{-38}	0 0 0	0 1 1	7 3 4	7 3 5	-0.106
5040.31241	0.28176	2.4×10^{-38}	0 0 0	0 1 1	5 2 4	5 2 3	-0.101
5040.53471	0.27892	2.2×10^{-38}	0 0 0	0 1 1	6 3 3	6 3 4	-0.108
5041.00848	0.27831	3.7×10^{-38}	0 0 0	0 1 1	5 3 2	5 3 3	-0.110
5041.27709	0.00011	3.7×10^{-38}	0 0 0	0 1 1	5 3 3	5 3 2	-0.110
5041.30620	0.00008	5.9×10^{-38}	0 0 0	0 1 1	4 3 1	4 3 2	-0.109
5041.34275	0.00007	6.0×10^{-38}	0 0 0	0 1 1	4 3 2	4 3 1	-0.112
5041.39009	0.00017	2.2×10^{-38}	0 0 0	0 1 1	6 3 4	6 3 3	-0.108
5041.46945	0.00006	9.6×10^{-38}	0 0 0	0 1 1	3 3 0	3 3 1	-0.093
5041.87033	0.00028	1.3×10^{-38}	0 0 0	0 1 1	7 3 5	7 3 4	-0.106
5042.98045	0.00054	7.2×10^{-39}	0 0 0	0 1 1	8 3 6	8 3 5	-0.105
5043.23942	0.00018	2.3×10^{-38}	0 0 0	0 1 1	3 1 3	3 1 2	-0.096
5043.83752	0.00006	5.9×10^{-38}	0 0 0	0 1 1	0 0 0	1 0 1	-0.093
5043.96094	0.00028	1.4×10^{-38}	0 0 0	0 1 1	6 2 5	6 2 4	-0.103
5044.10317	0.00700	4.2×10^{-40}	0 0 0	0 1 1	12 4 8	12 4 9	-0.112
5044.58749	0.00482	9.3×10^{-40}	0 0 0	0 1 1	6 3 4	7 2 5	-0.107
5045.04689	0.00095	3.8×10^{-39}	0 0 0	0 1 1	9 3 7	9 3 6	-0.103
5045.42783	0.00326	9.0×10^{-40}	0 0 0	0 1 1	11 4 7	11 4 8	-0.118
5046.06598	0.00267	1.9×10^{-39}	0 0 0	0 1 1	7 2 6	6 3 3	-0.089
5046.32020	0.00306	1.8×10^{-39}	0 0 0	0 1 1	10 4 6	10 4 7	-0.118
5046.32020	0.02450	1.8×10^{-40}	0 0 0	0 1 1	10 3 8	9 4 5	-0.109
5046.94353	0.00095	3.6×10^{-39}	0 0 0	0 1 1	9 4 5	9 4 6	-0.120
5047.09050	0.00166	2.4×10^{-39}	0 0 0	0 1 1	3 1 2	2 2 1	-0.094
5047.16153	0.00183	1.8×10^{-39}	0 0 0	0 1 1	10 4 7	10 4 6	-0.111
5047.41361	0.00052	6.7×10^{-39}	0 0 0	0 1 1	8 4 4	8 4 5	-0.124
5047.55966	0.00430	9.0×10^{-40}	0 0 0	0 1 1	11 4 8	11 4 7	-0.107
5047.63802	0.00092	6.6×10^{-39}	0 0 0	0 1 1	8 4 5	8 4 4	-0.150
5047.80165	0.00029	1.2×10^{-38}	0 0 0	0 1 1	7 4 3	7 4 4	-0.125
5047.87824	0.00030	1.2×10^{-38}	0 0 0	0 1 1	7 4 4	7 4 3	-0.125
5048.13782	0.00018	2.0×10^{-38}	0 0 0	0 1 1	6 4 2	6 4 3	-0.127
5048.15711	0.00018	2.0×10^{-38}	0 0 0	0 1 1	6 4 3	6 4 2	-0.128
5048.21002	0.00155	2.4×10^{-39}	0 0 0	0 1 1	9 4 6	9 4 5	-0.075
5048.43297	0.00017	3.4×10^{-38}	0 0 0	0 1 1	5 4 1	5 4 2	-0.131
5048.43680	0.00130	3.4×10^{-38}	0 0 0	0 1 1	5 4 2	5 4 1	-0.131
5048.69480	0.00032	5.4×10^{-38}	0 0 0	0 1 1	4 4 1	4 4 0	-0.131
5048.69480	0.00032	5.4×10^{-38}	0 0 0	0 1 1	4 4 0	4 4 1	-0.131
5048.87649	0.00119	2.9×10^{-39}	0 0 0	0 1 1	4 1 4	3 2 1	-0.094
5049.24779	0.00050	7.5×10^{-39}	0 0 0	0 1 1	7 2 6	7 2 5	-0.103
5049.75546	0.00027	1.4×10^{-38}	0 0 0	0 1 1	4 1 4	4 1 3	-0.097
5050.98299	0.00017	2.4×10^{-38}	0 0 0	0 1 1	1 0 1	1 1 0	-0.093
5051.85989	0.00029	1.4×10^{-38}	0 0 0	0 1 1	2 1 2	3 0 3	-0.096

Position	$\sigma_{\text{Pos.}}$	Intensity	$\nu_1\ \nu_2\ \nu_3$	$\nu_1'\ \nu_2'\ \nu_3'$	J K_a K_c	J' K_a' K_c'	$\Delta_{\text{SPEC.}}$
5052.81372	0.00051	3.4×10^{-38}	0 0 0	0 1 1	2 0 2	2 1 1	-0.094
5053.18843	0.00094	4.3×10^{-39}	0 0 0	0 1 1	4 2 3	5 1 4	-0.104
5053.24744	0.00642	5.5×10^{-40}	0 0 0	0 1 1	9 3 6	8 4 5	-0.104
5054.58842	0.00005	7.7×10^{-38}	0 0 0	0 1 1	1 1 1	2 1 2	-0.096
5055.26646	0.00004	1.1×10^{-37}	0 0 0	0 1 1	1 0 1	2 0 2	-0.094
5055.74288	0.00013	3.7×10^{-38}	0 0 0	0 1 1	3 0 3	3 1 2	-0.095
5056.22077	0.00147	4.0×10^{-39}	0 0 0	0 1 1	8 2 7	8 2 6	-0.104
5056.27363	0.00278	2.0×10^{-39}	0 0 0	0 1 1	6 2 5	5 3 2	-0.099
5056.31596	0.00992	1.2×10^{-39}	0 0 0	0 1 1	10 5 5	10 5 6	-0.146
5056.35918	0.00358	1.2×10^{-39}	0 0 0	0 1 1	10 5 6	10 5 5	-0.144
5056.72193	0.00272	1.8×10^{-39}	0 0 0	0 1 1	3 1 3	2 2 0	-0.092
5056.93569	0.00253	2.3×10^{-39}	0 0 0	0 1 1	9 5 4	9 5 5	-0.144
5056.94430	0.00247	2.3×10^{-39}	0 0 0	0 1 1	9 5 5	9 5 4	-0.150
5057.51460	0.00182	4.3×10^{-39}	0 0 0	0 1 1	8 5 4	8 5 3	-0.153
5057.51460	0.00182	4.3×10^{-39}	0 0 0	0 1 1	8 5 3	8 5 4	-0.149
5057.75964	0.27224	8.7×10^{-39}	0 0 0	0 1 1	5 1 5	5 1 4	-0.098
5058.05225	0.27248	7.6×10^{-39}	0 0 0	0 1 1	7 5 2	7 5 3	-0.153
5058.05225	0.27248	7.6×10^{-39}	0 0 0	0 1 1	7 5 3	7 5 2	-0.154
5058.38150	0.27261	7.6×10^{-38}	0 0 0	0 1 1	1 1 0	2 1 1	-0.097
5058.54029	0.00050	1.3×10^{-38}	0 0 0	0 1 1	6 5 2	6 5 1	-0.159
5058.54347	0.27258	1.3×10^{-38}	0 0 0	0 1 1	6 5 1	6 5 2	-0.156
5058.97900	0.27194	2.1×10^{-38}	0 0 0	0 1 1	5 5 0	5 5 1	-0.158
5058.97900	0.27194	2.1×10^{-38}	0 0 0	0 1 1	5 5 1	5 5 0	-0.158
5059.96269	0.00011	3.4×10^{-38}	0 0 0	0 1 1	4 0 4	4 1 3	-0.095
5060.81854	0.00025	1.6×10^{-38}	0 0 0	0 1 1	0 0 0	1 1 1	-0.094
5063.47124	0.00271	1.6×10^{-39}	0 0 0	0 1 1	5 2 3	4 3 2	-0.098
5064.49766	0.00021	1.8×10^{-38}	0 0 0	0 1 1	3 1 3	4 0 4	-0.097
5064.77531	0.00213	2.1×10^{-39}	0 0 0	0 1 1	9 2 8	9 2 7	-0.102
5064.92246	0.00003	1.2×10^{-37}	0 0 0	0 1 1	2 1 2	3 1 3	-0.096
5065.65050	0.00015	2.8×10^{-38}	0 0 0	0 1 1	5 0 5	5 1 4	-0.096
5066.37170	0.00003	1.5×10^{-37}	0 0 0	0 1 1	2 0 2	3 0 3	-0.094
5067.10046	0.00095	5.4×10^{-39}	0 0 0	0 1 1	6 1 6	6 1 5	-0.098
5067.18080	0.00582	1.7×10^{-39}	0 0 0	0 1 1	5 2 4	4 3 1	-0.091
5067.34838	0.00652	6.7×10^{-40}	0 0 0	0 1 1	8 3 5	7 4 4	-0.109
5068.91440	0.00096	4.7×10^{-39}	0 0 0	0 1 1	5 2 4	6 1 5	-0.106
5070.57956	0.00019	2.1×10^{-38}	0 0 0	0 1 1	1 0 1	2 1 2	-0.094
5070.90924	0.00003	1.2×10^{-37}	0 0 0	0 1 1	2 1 1	3 1 2	-0.098
5071.14025	0.00008	5.9×10^{-38}	0 0 0	0 1 1	2 2 1	3 2 2	-0.104
5071.68779	0.00007	5.9×10^{-38}	0 0 0	0 1 1	2 2 0	3 2 1	-0.105
5072.44702	0.00151	1.9×10^{-39}	0 0 0	0 1 1	8 6 2	8 6 3	-0.185
5072.44702	0.00151	1.9×10^{-39}	0 0 0	0 1 1	8 6 3	8 6 2	-0.185

188

Position	$\sigma_{\text{Pos.}}$	Intensity	$\nu_1\,\nu_2\,\nu_3$	$\nu_1'\,\nu_2'\,\nu_3'$	J K_a K_c	J' K_a' K_c'	$\Delta_{\text{SPEC.}}$
5072.89540	0.00020	2.0×10^{-38}	0 0 0	0 1 1	6 0 6	6 1 5	-0.094
5075.01165	0.00004	1.5×10^{-37}	0 0 0	0 1 1	3 1 3	4 1 4	-0.096
5076.84595	0.00023	2.0×10^{-38}	0 0 0	0 1 1	4 1 4	5 0 5	-0.096
5077.00208	0.00002	1.7×10^{-37}	0 0 0	0 1 1	3 0 3	4 0 4	-0.095
5077.54216	0.00166	3.3×10^{-39}	0 0 0	0 1 1	7 1 7	7 1 6	-0.101
5078.49989	0.00057	2.2×10^{-38}	0 0 0	0 1 1	6 1 5	6 2 4	-0.096
5079.08842	0.00018	2.4×10^{-38}	0 0 0	0 1 1	5 1 4	5 2 3	-0.095
5079.15527	0.00025	1.8×10^{-38}	0 0 0	0 1 1	7 1 6	7 2 5	-0.096
5079.43388	0.00044	2.5×10^{-38}	0 0 0	0 1 1	2 0 2	3 1 3	-0.094
5080.56253	0.00018	2.3×10^{-38}	0 0 0	0 1 1	4 1 3	4 2 2	-0.095
5081.30104	0.00038	1.3×10^{-38}	0 0 0	0 1 1	8 1 7	8 2 6	-0.097
5081.60866	0.00031	1.4×10^{-38}	0 0 0	0 1 1	7 0 7	7 1 6	-0.096
5082.48068	0.00044	1.9×10^{-38}	0 0 0	0 1 1	3 1 2	3 2 1	-0.097
5082.49719	0.00006	8.9×10^{-38}	0 0 0	0 1 1	3 2 2	4 2 3	-0.104
5083.36059	0.00014	1.4×10^{-37}	0 0 0	0 1 1	3 1 2	4 1 3	-0.100
5083.88389	0.00005	8.9×10^{-38}	0 0 0	0 1 1	3 2 1	4 2 2	-0.105
5084.38979	0.00035	1.2×10^{-38}	0 0 0	0 1 1	2 1 1	2 2 0	-0.096
5084.82506	0.00005	1.6×10^{-37}	0 0 0	0 1 1	4 1 4	5 1 5	-0.096
5085.07434	0.00051	8.1×10^{-39}	0 0 0	0 1 1	9 1 8	9 2 7	-0.096
5087.05254	0.00003	1.7×10^{-37}	0 0 0	0 1 1	4 0 4	5 0 5	-0.094
5087.51560	0.00016	2.6×10^{-38}	0 0 0	0 1 1	3 0 3	4 1 4	-0.094
5087.90372	0.00026	3.1×10^{-38}	0 0 0	0 1 1	3 3 1	4 3 2	-0.115
5087.90372	0.00026	3.2×10^{-38}	0 0 0	0 1 1	3 3 0	4 3 1	-0.115
5088.61688	0.00020	1.9×10^{-38}	0 0 0	0 1 1	5 1 5	6 0 6	-0.097
5089.00920	0.00038	1.1×10^{-38}	0 0 0	0 1 1	2 1 2	2 2 1	-0.097
5091.31756	0.00028	1.5×10^{-38}	0 0 0	0 1 1	3 1 3	3 2 2	-0.097
5091.52245	0.00051	8.9×10^{-39}	0 0 0	0 1 1	8 0 8	8 1 7	-0.096
5093.70357	0.00004	1.0×10^{-37}	0 0 0	0 1 1	4 2 3	5 2 4	-0.105
5094.34125	0.00003	1.5×10^{-37}	0 0 0	0 1 1	5 1 5	6 1 6	-0.095
5094.40892	0.00027	1.7×10^{-38}	0 0 0	0 1 1	4 1 4	4 2 3	-0.095
5095.03217	0.00017	2.5×10^{-38}	0 0 0	0 1 1	4 0 4	5 1 5	-0.094
5095.65644	0.00003	1.4×10^{-37}	0 0 0	0 1 1	4 1 3	5 1 4	-0.100
5096.44887	0.00005	9.8×10^{-38}	0 0 0	0 1 1	4 2 2	5 2 3	-0.106
5096.50749	0.00016	1.5×10^{-37}	0 0 0	0 1 1	5 0 5	6 0 6	-0.094
5098.27649	0.00029	1.5×10^{-38}	0 0 0	0 1 1	5 1 5	5 2 4	-0.097
5098.38680	0.00195	2.6×10^{-39}	0 0 0	0 1 1	11 1 10	11 2 9	-0.104
5099.39708	0.00013	4.6×10^{-38}	0 0 0	0 1 1	4 3 2	5 3 3	-0.116
5099.49762	0.00024	4.6×10^{-38}	0 0 0	0 1 1	4 3 1	5 3 2	-0.115
5099.66833	0.00024	1.7×10^{-38}	0 0 0	0 1 1	6 1 6	7 0 7	-0.094
5100.45342	0.00765	1.1×10^{-39}	0 0 0	0 1 1	9 1 9	9 1 8	-0.079
5100.53662	0.00112	3.9×10^{-39}	0 0 0	0 1 1	7 2 6	8 1 7	-0.103

Position	$\sigma_{\text{Pos.}}$	Intensity	$\nu_1\,\nu_2\,\nu_3$	$\nu_1'\,\nu_2'\,\nu_3'$	J K_a K_c	J' K_a' K_c'	$\Delta_{\text{SPEC.}}$
5102.23150	0.00138	2.2×10^{-38}	0 0 0	0 1 1	5 0 5	6 1 6	-0.093
5102.23536	0.00596	5.4×10^{-39}	0 0 0	0 1 1	9 0 9	9 1 8	-0.094
5102.91313	0.00034	1.3×10^{-38}	0 0 0	0 1 1	6 1 6	6 2 5	-0.096
5103.55008	0.00003	1.2×10^{-37}	0 0 0	0 1 1	6 1 6	7 1 7	-0.094
5104.61960	0.00159	2.1×10^{-39}	0 0 0	0 1 1	11 2 9	11 3 8	-0.084
5104.72620	0.00005	9.6×10^{-38}	0 0 0	0 1 1	5 2 4	6 2 5	-0.105
5105.46018	0.00005	1.3×10^{-37}	0 0 0	0 1 1	6 0 6	7 0 7	-0.094
5106.48064	0.00215	1.3×10^{-38}	0 0 0	0 1 1	4 4 1	5 4 2	-0.134
5106.48064	0.00213	1.3×10^{-38}	0 0 0	0 1 1	4 4 0	5 4 1	-0.136
5106.48064	0.00538	3.4×10^{-39}	0 0 0	0 1 1	10 2 8	10 3 7	-0.085
5107.69044	0.00004	1.3×10^{-37}	0 0 0	0 1 1	5 1 4	6 1 5	-0.100
5108.28591	0.00042	9.6×10^{-39}	0 0 0	0 1 1	7 1 7	7 2 6	-0.096
5109.08988	0.00024	1.9×10^{-38}	0 0 0	0 1 1	1 1 0	2 2 1	-0.097
5109.34448	0.00070	1.9×10^{-38}	0 0 0	0 1 1	6 0 6	7 1 7	-0.091
5109.35061	0.00057	9.3×10^{-38}	0 0 0	0 1 1	5 2 3	6 2 4	-0.107
5109.35061	0.01024	5.1×10^{-39}	0 0 0	0 1 1	9 2 7	9 3 6	-0.085
5110.20229	0.00023	1.8×10^{-38}	0 0 0	0 1 1	7 1 7	8 0 8	-0.082
5110.80652	0.00024	1.9×10^{-38}	0 0 0	0 1 1	1 1 1	2 2 0	-0.099
5110.88614	0.00008	4.9×10^{-38}	0 0 0	0 1 1	5 3 3	6 3 4	-0.115
5111.20797	0.00009	4.9×10^{-38}	0 0 0	0 1 1	5 3 2	6 3 3	-0.115
5112.49620	0.00004	9.6×10^{-38}	0 0 0	0 1 1	7 1 7	8 1 8	-0.092
5112.75857	0.00059	7.1×10^{-39}	0 0 0	0 1 1	8 2 6	8 3 5	-0.092
5113.32384	0.00128	3.2×10^{-39}	0 0 0	0 1 1	10 0 10	10 1 9	-0.088
5114.26608	0.00009	9.0×10^{-38}	0 0 0	0 1 1	7 0 7	8 0 8	-0.080
5114.37432	0.00067	6.7×10^{-39}	0 0 0	0 1 1	8 1 8	8 2 7	-0.092
5115.53573	0.00005	8.3×10^{-38}	0 0 0	0 1 1	6 2 5	7 2 6	-0.104
5115.82439	0.00141	3.0×10^{-39}	0 0 0	0 1 1	8 2 7	9 1 8	-0.099
5116.20225	0.00064	9.1×10^{-39}	0 0 0	0 1 1	7 2 5	7 3 4	-0.105
5116.55978	0.00023	1.8×10^{-38}	0 0 0	0 1 1	7 0 7	8 1 8	-0.090
5117.84116	0.00094	1.9×10^{-38}	0 0 0	0 1 1	5 4 1	6 4 2	-0.145
5117.85066	0.00094	1.9×10^{-38}	0 0 0	0 1 1	5 4 2	6 4 3	-0.124
5119.33303	0.00005	1.0×10^{-37}	0 0 0	0 1 1	6 1 5	7 1 6	-0.099
5120.93186	0.00006	7.8×10^{-38}	0 0 0	0 1 1	8 1 8	9 1 9	-0.090
5121.34703	0.00139	3.8×10^{-39}	0 0 0	0 1 1	9 1 9	9 2 8	-0.069
5121.66629	0.00036	1.2×10^{-38}	0 0 0	0 1 1	5 2 3	5 3 2	-0.100
5121.87529	0.00005	7.8×10^{-38}	0 0 0	0 1 1	8 0 8	9 0 9	-0.084
5122.34194	0.00010	4.4×10^{-38}	0 0 0	0 1 1	6 3 4	7 3 5	-0.114
5122.45991	0.00007	7.9×10^{-38}	0 0 0	0 1 1	6 2 4	7 2 5	-0.107
5123.11205	0.00010	4.4×10^{-38}	0 0 0	0 1 1	6 3 3	7 3 4	-0.114
5123.14384	0.00674	7.7×10^{-40}	0 0 0	0 1 1	9 0 9	9 2 8	-0.070
5123.31074	0.00039	1.1×10^{-38}	0 0 0	0 1 1	4 2 2	4 3 1	-0.102

Position	$\sigma_{\text{Pos.}}$	Intensity	$\nu_1\ \nu_2\ \nu_3$	$\nu_1'\ \nu_2'\ \nu_3'$	J K$_a$ K$_c$	J' K$_a'$ K$_c'$	$\Delta_{\text{SPEC.}}$
5123.66771	0.03650	3.5×10^{-40}	0 0 0	0 1 1	11 1 11	11 1 10	-0.088
5123.67535	0.00062	6.5×10^{-39}	0 0 0	0 1 1	8 0 8	9 1 9	-0.089
5124.29392	0.00058	7.3×10^{-39}	0 0 0	0 1 1	3 2 1	3 3 0	-0.104
5124.38393	0.00306	1.8×10^{-39}	0 0 0	0 1 1	11 0 11	11 1 10	-0.093
5124.39956	0.00029	1.6×10^{-38}	0 0 0	0 1 1	2 1 2	3 2 1	-0.100
5124.83205	0.00062	7.2×10^{-39}	0 0 0	0 1 1	3 2 2	3 3 1	-0.104
5124.93871	0.00041	1.1×10^{-38}	0 0 0	0 1 1	4 2 3	4 3 2	-0.101
5125.22804	0.00037	1.1×10^{-38}	0 0 0	0 1 1	5 2 4	5 3 3	-0.102
5125.88285	0.00059	1.0×10^{-38}	0 0 0	0 1 1	6 2 5	6 3 4	-0.104
5126.13025	0.00007	6.5×10^{-38}	0 0 0	0 1 1	7 2 6	8 2 7	-0.101
5127.01365	0.00108	8.5×10^{-39}	0 0 0	0 1 1	7 2 6	7 3 5	-0.099
5127.31018	0.00154	2.6×10^{-39}	0 0 0	0 1 1	10 1 10	10 2 9	-0.062
5127.95349	0.00104	4.2×10^{-39}	0 0 0	0 1 1	5 5 1	6 5 2	-0.162
5127.95349	0.00104	4.2×10^{-39}	0 0 0	0 1 1	5 5 0	6 5 1	-0.162
5128.01263	0.00027	1.6×10^{-38}	0 0 0	0 1 1	3 1 2	4 2 3	-0.099
5128.13318	0.00138	5.1×10^{-39}	0 0 0	0 1 1	9 1 9	10 0 10	-0.090
5128.70893	0.00066	6.3×10^{-39}	0 0 0	0 1 1	8 2 7	8 3 6	-0.099
5129.23092	0.00045	5.4×10^{-38}	0 0 0	0 1 1	9 1 9	10 1 10	-0.090
5129.23884	0.00149	1.9×10^{-38}	0 0 0	0 1 1	6 4 3	7 4 4	-0.092
5129.93179	0.00008	5.5×10^{-38}	0 0 0	0 1 1	9 0 9	10 0 10	-0.088
5130.44318	0.00005	7.8×10^{-38}	0 0 0	0 1 1	7 1 6	8 1 7	-0.096
5131.02827	0.00092	5.1×10^{-39}	0 0 0	0 1 1	9 0 9	10 1 10	-0.090
5131.05038	0.00121	4.3×10^{-39}	0 0 0	0 1 1	9 2 8	9 3 7	-0.099
5133.73291	0.00025	3.6×10^{-38}	0 0 0	0 1 1	7 3 5	8 3 6	-0.113
5134.09219	0.00182	2.7×10^{-39}	0 0 0	0 1 1	10 2 9	10 3 8	-0.095
5135.29790	0.00012	3.5×10^{-38}	0 0 0	0 1 1	7 3 4	8 3 5	-0.112
5135.58624	0.00007	6.1×10^{-38}	0 0 0	0 1 1	7 2 5	8 2 6	-0.107
5136.16870	0.00048	1.4×10^{-38}	0 0 0	0 1 1	4 1 3	5 2 4	-0.103
5136.54540	0.00127	3.2×10^{-39}	0 0 0	0 1 1	10 1 10	11 0 11	-0.090
5136.73450	0.00010	4.3×10^{-38}	0 0 0	0 1 1	8 2 7	9 2 8	-0.073
5137.21764	0.00011	3.6×10^{-38}	0 0 0	0 1 1	10 1 10	11 1 11	-0.088
5137.69772	0.00011	3.6×10^{-38}	0 0 0	0 1 1	10 0 10	11 0 11	-0.088
5137.84941	0.00240	1.6×10^{-39}	0 0 0	0 1 1	11 2 10	11 3 9	-0.096
5138.36524	0.00116	3.2×10^{-39}	0 0 0	0 1 1	10 0 10	11 1 11	-0.090
5139.05139	0.00057	5.6×10^{-39}	0 0 0	0 1 1	6 5 1	7 5 2	-0.162
5139.05139	0.00057	5.6×10^{-39}	0 0 0	0 1 1	6 5 2	7 5 3	-0.161
5139.44693	0.00035	1.2×10^{-38}	0 0 0	0 1 1	3 1 3	4 2 2	-0.101
5140.55634	0.00025	1.6×10^{-38}	0 0 0	0 1 1	7 4 4	8 4 5	-0.132
5140.69576	0.00024	1.6×10^{-38}	0 0 0	0 1 1	7 4 3	8 4 4	-0.132
5140.90404	0.00018	5.5×10^{-38}	0 0 0	0 1 1	8 1 7	9 1 8	-0.092
5143.50315	0.00040	1.2×10^{-38}	0 0 0	0 1 1	5 1 4	6 2 5	-0.097

Position	$\sigma_{\text{Pos.}}$	Intensity	$\nu_1\ \nu_2\ \nu_3$	$\nu_1'\ \nu_2'\ \nu_3'$	J K_a K_c	J' K_a' K_c'	$\Delta_{\text{SPEC.}}$
5144.92139	0.00019	2.3×10^{-38}	0 0 0	0 1 1	11 1 11	12 1 12	-0.088
5145.01941	0.00016	2.6×10^{-38}	0 0 0	0 1 1	8 3 6	9 3 7	-0.112
5145.24078	0.00017	2.3×10^{-38}	0 0 0	0 1 1	11 0 11	12 0 12	-0.085
5145.51381	0.00014	2.8×10^{-38}	0 0 0	0 1 1	9 2 8	10 2 9	-0.069
5147.83744	0.00018	2.6×10^{-38}	0 0 0	0 1 1	8 3 5	9 3 6	-0.112
5148.51923	0.00010	4.3×10^{-38}	0 0 0	0 1 1	8 2 6	9 2 7	-0.105
5150.07357	0.00051	9.0×10^{-39}	0 0 0	0 1 1	6 1 5	7 2 6	-0.098
5150.11273	0.00145	5.4×10^{-39}	0 0 0	0 1 1	7 5 3	8 5 4	-0.159
5150.11273	0.00145	5.4×10^{-39}	0 0 0	0 1 1	7 5 2	8 5 3	-0.161
5150.67405	0.00011	3.6×10^{-38}	0 0 0	0 1 1	9 1 8	10 1 9	-0.092
5151.92272	0.00033	1.2×10^{-38}	0 0 0	0 1 1	8 4 5	9 4 6	-0.129
5152.35818	0.00028	1.3×10^{-38}	0 0 0	0 1 1	12 1 12	13 1 13	-0.085
5152.56238	0.00025	1.3×10^{-38}	0 0 0	0 1 1	12 0 12	13 0 13	-0.085
5152.88992	0.00044	8.7×10^{-39}	0 0 0	0 1 1	8 4 4	9 4 5	-0.085
5156.03848	0.00068	6.8×10^{-39}	0 0 0	0 1 1	7 1 6	8 2 7	-0.093
5156.15657	0.00023	1.8×10^{-38}	0 0 0	0 1 1	9 3 7	10 3 8	-0.110
5156.33341	0.00053	8.5×10^{-39}	0 0 0	0 1 1	4 1 4	5 2 3	-0.102
5159.54529	0.00023	2.0×10^{-38}	0 0 0	0 1 1	2 2 0	3 3 1	-0.115
5159.67271	0.00024	2.0×10^{-38}	0 0 0	0 1 1	2 2 1	3 3 0	-0.114
5159.68986	0.00072	7.5×10^{-39}	0 0 0	0 1 1	13 0 13	14 0 14	-0.059
5159.79750	0.00023	2.3×10^{-38}	0 0 0	0 1 1	10 1 9	11 1 10	-0.091
5160.24704	0.00127	3.5×10^{-39}	0 0 0	0 1 1	8 3 5	8 4 4	-0.111
5160.31484	0.00022	2.1×10^{-38}	0 0 0	0 1 1	9 2 7	10 2 8	-0.052
5160.75567	0.00025	1.7×10^{-38}	0 0 0	0 1 1	9 3 6	10 3 7	-0.108
5161.14619	0.00657	4.4×10^{-39}	0 0 0	0 1 1	8 5 3	9 5 4	-0.162
5161.14619	0.00656	4.4×10^{-39}	0 0 0	0 1 1	8 5 4	9 5 5	-0.155
5161.80920	0.00095	5.2×10^{-39}	0 0 0	0 1 1	8 1 7	9 2 8	-0.071
5161.82196	0.00111	4.4×10^{-39}	0 0 0	0 1 1	7 3 4	7 4 3	-0.108
5162.17745	0.00122	3.4×10^{-39}	0 0 0	0 1 1	8 3 6	8 4 5	-0.113
5164.59756	0.00035	1.2×10^{-38}	0 0 0	0 1 1	11 2 10	12 2 11	-0.094
5166.46488	0.00096	4.0×10^{-39}	0 0 0	0 1 1	14 1 14	15 1 15	-0.080
5166.54375	0.00087	4.0×10^{-39}	0 0 0	0 1 1	14 0 14	15 0 15	-0.082
5167.09764	0.00039	1.2×10^{-38}	0 0 0	0 1 1	10 3 8	11 3 9	-0.108
5168.35755	0.00036	1.3×10^{-38}	0 0 0	0 1 1	11 1 10	12 1 11	-0.090
5171.28533	0.00031	1.7×10^{-38}	0 0 0	0 1 1	3 2 2	4 3 1	-0.106
5172.15865	0.00280	3.2×10^{-39}	0 0 0	0 1 1	9 5 5	10 5 6	-0.154
5172.17758	0.00294	3.2×10^{-39}	0 0 0	0 1 1	9 5 4	10 5 5	-0.155
5173.84623	0.00083	1.7×10^{-38}	0 0 0	0 1 1	10 2 8	11 2 9	-0.094
5173.96455	0.00040	1.1×10^{-38}	0 0 0	0 1 1	10 3 7	11 3 8	-0.105
5174.63168	0.00076	5.7×10^{-39}	0 0 0	0 1 1	10 4 7	11 4 8	-0.127
5175.23930	0.00119	5.6×10^{-39}	0 0 0	0 1 1	10 4 6	11 4 7	-0.121

Position	$\sigma_{\text{Pos.}}$	Intensity	$\nu_1\ \nu_2\ \nu_3$	ν_1'$\ \nu_2$'$\ \nu_3$'	J K_a K_c	J' K_a' K_c'	$\Delta_{\text{SPEC.}}$
5175.25406	0.00822	1.1×10^{-39}	0 0 0	0 1 1	8 6 2	9 6 3	-0.194
5175.25406	0.00822	1.1×10^{-39}	0 0 0	0 1 1	8 6 3	9 6 4	-0.194
5175.39014	0.00102	5.3×10^{-39}	0 0 0	0 1 1	5 1 5	6 2 4	-0.103
5181.36877	0.00283	1.3×10^{-38}	0 0 0	0 1 1	4 2 2	5 3 3	-0.103
5181.96308	0.00135	3.8×10^{-39}	0 0 0	0 1 1	13 2 12	14 2 13	-0.095
5183.13126	0.00049	1.3×10^{-38}	0 0 0	0 1 1	4 2 3	5 3 2	-0.106
5187.19606	0.00108	5.8×10^{-39}	0 0 0	0 1 1	11 3 8	12 3 9	-0.085
5187.23534	0.00478	3.4×10^{-39}	0 0 0	0 1 1	11 4 7	12 4 8	-0.128
5191.27848	0.00271	9.8×10^{-39}	0 0 0	0 1 1	5 2 3	6 3 4	-0.102
5195.42961	0.00076	9.5×10^{-39}	0 0 0	0 1 1	5 2 4	6 3 3	-0.105
5200.22479	0.00086	6.8×10^{-39}	0 0 0	0 1 1	6 2 4	7 3 5	-0.104
5202.50751	0.00445	1.0×10^{-39}	0 0 0	0 1 1	9 4 5	9 5 4	-0.133
5202.60199	0.00435	1.3×10^{-39}	0 0 0	0 1 1	6 0 6	7 2 5	-0.098
5210.91438	0.00120	1.4×10^{-38}	0 0 0	0 1 1	3 3 1	4 4 0	-0.128
5210.92055	0.00122	1.4×10^{-38}	0 0 0	0 1 1	3 3 0	4 4 1	-0.116
5212.25689	0.00652	1.0×10^{-39}	0 0 0	0 1 1	13 4 9	14 4 10	-0.111
5233.15239	0.00129	8.0×10^{-39}	0 0 0	0 1 1	5 3 2	6 4 3	-0.124
5233.29954	0.00155	8.0×10^{-39}	0 0 0	0 1 1	5 3 3	6 4 2	-0.124
5296.87435	0.00424	2.2×10^{-39}	0 0 0	0 1 1	7 4 3	8 5 4	-0.149
5296.91104	0.00492	2.2×10^{-39}	0 0 0	0 1 1	7 4 4	8 5 3	-0.143

A.2.1.4 HTO $\nu_1 + 2\nu_2$ band

Here, the lines assigned to the $\nu_1 + 2\nu_2$ band obtained from the 1 GBq sample are presented. These lines are published in [Her21]. For further information, see Section 5.5.1.

Table A.5: Linelist of the $\nu_1 + 2\nu_2$ band. The columns present the assigned line position, the uncertainty on the position $\sigma_{\text{Pos.}}$, the line intensity taking natural abundance into account, lower and upper vibrational quanta, lower and upper rotational quanta and the deviation to the predictions from SPECTRA database $\Delta_{\text{SPEC.}}$.

Position	$\sigma_{\text{Pos.}}$	Intensity	$\nu_1\ \nu_2\ \nu_3$	ν_1'$\ \nu_2$'$\ \nu_3$'	J K_a K_c	J' K_a' K_c'	$\Delta_{\text{SPEC.}}$
4717.09216	0.00405	4.2×10^{-40}	0 0 0	1 2 0	9 4 5	8 3 6	0.152
4717.67733	0.00528	5.6×10^{-40}	0 0 0	1 2 0	8 5 3	7 4 4	0.138
4717.70929	0.00448	5.6×10^{-40}	0 0 0	1 2 0	8 5 4	7 4 3	0.140
4719.80037	0.00314	6.0×10^{-40}	0 0 0	1 2 0	7 6 2	6 5 1	0.143
4719.80037	0.00314	6.0×10^{-40}	0 0 0	1 2 0	7 6 1	6 5 2	0.143
4729.44034	0.00368	6.7×10^{-40}	0 0 0	1 2 0	8 4 4	7 3 5	0.143
4729.55053	0.00513	8.5×10^{-40}	0 0 0	1 2 0	7 5 2	6 4 3	0.135
4729.56254	0.00532	8.5×10^{-40}	0 0 0	1 2 0	7 5 3	6 4 2	0.138
4731.55847	0.00667	8.7×10^{-40}	0 0 0	1 2 0	6 6 0	5 5 1	0.140

Position	$\sigma_{\text{Pos.}}$	Intensity	$\nu_1\ \nu_2\ \nu_3$	$\nu_1'\ \nu_2'\ \nu_3'$	J K_a K_c	J' K_a' K_c'	$\Delta_{\text{SPEC.}}$
4731.55847	0.00667	8.7×10^{-40}	0 0 0	1 2 0	6 6 1	5 5 0	0.140
4741.41437	0.00181	1.2×10^{-39}	0 0 0	1 2 0	6 5 2	5 4 1	0.131
4741.41437	0.00181	1.2×10^{-39}	0 0 0	1 2 0	6 5 1	5 4 2	0.133
4741.58556	0.00276	1.0×10^{-39}	0 0 0	1 2 0	7 4 3	6 3 4	0.140
4742.02246	0.00274	9.9×10^{-40}	0 0 0	1 2 0	7 4 4	6 3 3	0.137
4753.25205	0.00350	1.6×10^{-39}	0 0 0	1 2 0	5 5 0	4 4 1	0.130
4753.25205	0.00350	1.6×10^{-39}	0 0 0	1 2 0	5 5 1	4 4 0	0.130
4753.60895	0.00180	1.5×10^{-39}	0 0 0	1 2 0	6 4 2	5 3 3	0.135
4753.75346	0.00223	1.4×10^{-39}	0 0 0	1 2 0	6 4 3	5 3 2	0.135
4754.93634	0.00289	1.1×10^{-39}	0 0 0	1 2 0	7 3 4	6 2 5	0.152
4755.29447	0.00386	8.1×10^{-40}	0 0 0	1 2 0	8 3 6	7 2 5	0.159
4763.72922	0.00268	1.2×10^{-39}	0 0 0	1 2 0	7 3 5	6 2 4	0.156
4765.56121	0.00153	2.0×10^{-39}	0 0 0	1 2 0	5 4 1	4 3 2	0.131
4765.59546	0.00181	2.0×10^{-39}	0 0 0	1 2 0	5 4 2	4 3 1	0.131
4768.75895	0.00202	1.6×10^{-39}	0 0 0	1 2 0	6 3 3	5 2 4	0.141
4772.13255	0.00348	6.7×10^{-40}	0 0 0	1 2 0	12 1 12	11 0 11	0.180
4772.57312	0.00416	7.5×10^{-40}	0 0 0	1 2 0	12 0 12	11 0 11	0.174
4772.85532	0.00322	8.3×10^{-40}	0 0 0	1 2 0	6 2 4	5 1 5	0.145
4773.11539	0.00358	7.6×10^{-40}	0 0 0	1 2 0	12 1 12	11 1 11	0.174
4773.24032	0.00158	1.6×10^{-39}	0 0 0	1 2 0	6 3 4	5 2 3	0.145
4773.56961	0.00498	6.8×10^{-40}	0 0 0	1 2 0	12 0 12	11 1 11	0.182
4777.45361	0.00164	2.5×10^{-39}	0 0 0	1 2 0	4 4 0	3 3 1	0.125
4777.46804	0.00162	2.5×10^{-39}	0 0 0	1 2 0	4 4 1	3 3 0	0.135
4781.77355	0.00150	2.1×10^{-39}	0 0 0	1 2 0	5 3 2	4 2 3	0.140
4783.70362	0.00140	2.2×10^{-39}	0 0 0	1 2 0	5 3 3	4 2 2	0.138
4784.49923	0.00278	1.1×10^{-39}	0 0 0	1 2 0	11 1 11	10 0 10	0.171
4785.22115	0.00216	1.3×10^{-39}	0 0 0	1 2 0	11 0 11	10 0 10	0.171
4786.04704	0.00195	1.3×10^{-39}	0 0 0	1 2 0	11 1 11	10 1 10	0.172
4786.42846	0.00297	1.0×10^{-39}	0 0 0	1 2 0	11 1 10	10 1 9	0.183
4786.76653	0.00253	1.1×10^{-39}	0 0 0	1 2 0	11 0 11	10 1 10	0.170
4787.42536	0.00325	9.1×10^{-40}	0 0 0	1 2 0	9 2 8	8 1 7	0.167
4788.17163	0.00313	8.8×10^{-40}	0 0 0	1 2 0	11 2 9	10 2 8	0.191
4792.84685	0.00259	1.4×10^{-39}	0 0 0	1 2 0	5 2 3	4 1 4	0.151
4793.68816	0.00365	1.3×10^{-39}	0 0 0	1 2 0	8 2 7	7 1 6	0.164
4794.22391	0.00113	2.7×10^{-39}	0 0 0	1 2 0	4 3 1	3 2 2	0.137
4794.63132	0.00365	9.9×10^{-40}	0 0 0	1 2 0	11 2 10	10 2 9	0.180
4794.86735	0.00112	2.7×10^{-39}	0 0 0	1 2 0	4 3 2	3 2 1	0.138
4796.34041	0.00172	1.7×10^{-39}	0 0 0	1 2 0	10 1 10	9 0 9	0.166
4796.96118	0.00206	1.7×10^{-39}	0 0 0	1 2 0	10 1 9	9 1 8	0.169
4797.49124	0.00157	2.2×10^{-39}	0 0 0	1 2 0	10 0 10	9 0 9	0.167
4798.71632	0.00136	2.2×10^{-39}	0 0 0	1 2 0	10 1 10	9 1 9	0.166

Position	$\sigma_{\text{Pos.}}$	Intensity	$\nu_1\,\nu_2\,\nu_3$	ν_1' ν_2' ν_3'	J K$_a$ K$_c$	J' K$_a$' K$_c$'	$\Delta_{\text{SPEC.}}$
4799.86697	0.00162	1.7×10^{-39}	0 0 0	1 2 0	10 0 10	9 1 9	0.167
4800.20166	0.00165	1.6×10^{-39}	0 0 0	1 2 0	7 2 6	6 1 5	0.160
4800.32231	0.00183	1.7×10^{-39}	0 0 0	1 2 0	10 2 8	9 2 7	0.173
4803.96903	0.00326	1.2×10^{-39}	0 0 0	1 2 0	11 3 8	10 3 7	0.139
4806.30717	0.00096	3.2×10^{-39}	0 0 0	1 2 0	3 3 0	2 2 1	0.135
4806.43339	0.00379	3.2×10^{-39}	0 0 0	1 2 0	3 3 1	2 2 0	0.133
4806.54205	0.00190	1.7×10^{-39}	0 0 0	1 2 0	10 2 9	9 2 8	0.168
4807.18198	0.00161	2.0×10^{-39}	0 0 0	1 2 0	6 2 5	5 1 4	0.153
4807.21343	0.00499	7.4×10^{-40}	0 0 0	1 2 0	11 3 9	10 3 8	0.177
4807.58247	0.00127	2.4×10^{-39}	0 0 0	1 2 0	9 1 9	8 0 8	0.164
4807.72488	0.00110	2.8×10^{-39}	0 0 0	1 2 0	9 1 8	8 1 7	0.174
4809.38062	0.00110	3.5×10^{-39}	0 0 0	1 2 0	9 0 9	8 0 8	0.165
4810.52985	0.00158	1.9×10^{-39}	0 0 0	1 2 0	4 2 2	3 1 3	0.151
4811.14417	0.00266	3.5×10^{-39}	0 0 0	1 2 0	9 1 9	8 1 8	0.160
4811.98789	0.00209	1.8×10^{-39}	0 0 0	1 2 0	9 2 7	8 2 6	0.158
4812.93793	0.05269	3.7×10^{-40}	0 0 0	1 2 0	12 4 8	11 4 7	0.161
4812.94495	0.01028	2.4×10^{-39}	0 0 0	1 2 0	9 0 9	8 1 8	0.163
4813.94802	0.00809	4.2×10^{-40}	0 0 0	1 2 0	12 4 9	11 4 8	0.162
4814.79059	0.00133	2.4×10^{-39}	0 0 0	1 2 0	5 2 4	4 1 3	0.148
4818.16134	0.00087	3.2×10^{-39}	0 0 0	1 2 0	8 1 8	7 0 7	0.160
4818.44462	0.00117	2.6×10^{-39}	0 0 0	1 2 0	9 2 8	8 2 7	0.165
4818.76645	0.00071	4.4×10^{-39}	0 0 0	1 2 0	8 1 7	7 1 6	0.170
4819.51827	0.00231	1.3×10^{-39}	0 0 0	1 2 0	10 3 8	9 3 7	0.165
4820.90676	0.00071	5.2×10^{-39}	0 0 0	1 2 0	8 0 8	7 0 7	0.162
4822.06019	0.00522	5.2×10^{-40}	0 0 0	1 2 0	8 4 5	8 3 6	0.132
4822.36731	0.00357	6.8×10^{-40}	0 0 0	1 2 0	10 1 9	9 2 8	0.175
4822.58956	0.00311	6.9×10^{-40}	0 0 0	1 2 0	7 4 4	7 3 5	0.141
4823.13259	0.00111	2.7×10^{-39}	0 0 0	1 2 0	4 2 3	3 1 2	0.144
4823.35839	0.00061	5.1×10^{-39}	0 0 0	1 2 0	8 1 8	7 1 7	0.160
4825.06812	0.00092	3.5×10^{-39}	0 0 0	1 2 0	8 2 6	7 2 5	0.167
4825.97097	0.00437	6.8×10^{-40}	0 0 0	1 2 0	11 4 7	10 4 6	0.159
4826.10065	0.00095	3.3×10^{-39}	0 0 0	1 2 0	8 0 8	7 1 7	0.159
4826.22113	0.00127	2.5×10^{-39}	0 0 0	1 2 0	3 2 1	2 1 2	0.141
4826.52154	0.00641	7.2×10^{-40}	0 0 0	1 2 0	11 4 8	10 4 7	0.166
4826.52981	0.00573	8.0×10^{-40}	0 0 0	1 2 0	8 2 7	8 1 8	0.154
4828.07209	0.00075	4.0×10^{-39}	0 0 0	1 2 0	7 1 7	6 0 6	0.157
4828.23226	0.01098	2.5×10^{-40}	0 0 0	1 2 0	10 4 6	10 3 7	0.119
4828.60865	0.00491	5.5×10^{-40}	0 0 0	1 2 0	9 3 7	9 2 8	0.155
4830.00461	0.00217	1.5×10^{-39}	0 0 0	1 2 0	9 3 6	8 3 5	0.155
4830.10601	0.00052	6.2×10^{-39}	0 0 0	1 2 0	7 1 6	6 1 5	0.164
4830.33522	0.00079	4.0×10^{-39}	0 0 0	1 2 0	8 2 7	7 2 6	0.160

Position	$\sigma_{\text{Pos.}}$	Intensity	$\nu_1\ \nu_2\ \nu_3$	$\nu_1'\ \nu_2'\ \nu_3'$	J K_a K_c	J' K_a' K_c'	$\Delta_{\text{SPEC.}}$
4831.86142	0.00148	2.0×10^{-39}	0 0 0	1 2 0	9 3 7	8 3 6	0.162
4832.13492	0.00044	7.1×10^{-39}	0 0 0	1 2 0	7 0 7	6 0 6	0.158
4832.27027	0.00101	2.9×10^{-39}	0 0 0	1 2 0	3 2 2	2 1 1	0.141
4832.40628	0.00384	8.0×10^{-40}	0 0 0	1 2 0	8 3 6	8 2 7	0.144
4834.84517	0.00411	6.2×10^{-40}	0 0 0	1 2 0	9 1 8	9 0 9	0.167
4835.11318	0.00247	1.2×10^{-39}	0 0 0	1 2 0	7 2 6	7 1 7	0.150
4835.35357	0.01015	1.2×10^{-39}	0 0 0	1 2 0	7 3 5	7 2 6	0.140
4835.37006	0.00066	7.0×10^{-39}	0 0 0	1 2 0	7 1 7	6 1 6	0.156
4837.39523	0.00081	4.6×10^{-39}	0 0 0	1 2 0	6 1 6	5 0 5	0.154
4837.55585	0.00229	1.5×10^{-39}	0 0 0	1 2 0	6 3 4	6 2 5	0.143
4838.06435	0.00061	5.1×10^{-39}	0 0 0	1 2 0	7 2 5	6 2 4	0.160
4838.74009	0.00391	9.0×10^{-40}	0 0 0	1 2 0	9 1 8	8 2 7	0.168
4838.80452	0.00271	1.1×10^{-39}	0 0 0	1 2 0	10 4 6	9 4 5	0.161
4839.07590	0.00281	1.2×10^{-39}	0 0 0	1 2 0	10 4 7	9 4 6	0.156
4839.11637	0.00225	1.6×10^{-39}	0 0 0	1 2 0	5 3 3	5 2 4	0.140
4839.43391	0.00074	4.0×10^{-39}	0 0 0	1 2 0	7 0 7	6 1 6	0.158
4840.16140	0.00201	1.5×10^{-39}	0 0 0	1 2 0	4 3 2	4 2 3	0.134
4840.29381	0.00109	2.9×10^{-39}	0 0 0	1 2 0	2 2 0	1 1 1	0.139
4840.82081	0.00278	1.1×10^{-39}	0 0 0	1 2 0	3 3 1	3 2 2	0.131
4841.42614	0.00274	1.1×10^{-39}	0 0 0	1 2 0	3 3 0	3 2 1	0.132
4841.72138	0.00040	8.1×10^{-39}	0 0 0	1 2 0	6 1 5	5 1 4	0.160
4841.92882	0.00334	1.6×10^{-39}	0 0 0	1 2 0	4 3 1	4 2 2	0.137
4842.22484	0.00311	5.5×10^{-39}	0 0 0	1 2 0	7 2 6	6 2 5	0.155
4842.24167	0.00184	3.0×10^{-39}	0 0 0	1 2 0	2 2 1	1 1 0	0.142
4842.62040	0.00167	1.6×10^{-39}	0 0 0	1 2 0	6 2 5	6 1 6	0.149
4843.05880	0.00181	1.7×10^{-39}	0 0 0	1 2 0	5 3 2	5 2 3	0.139
4843.12940	0.00114	2.5×10^{-39}	0 0 0	1 2 0	8 3 5	7 3 4	0.153
4843.18976	0.00107	9.1×10^{-39}	0 0 0	1 2 0	6 0 6	5 0 5	0.158
4844.20664	0.00103	2.9×10^{-39}	0 0 0	1 2 0	8 3 6	7 3 5	0.156
4844.34821	0.01740	1.5×10^{-40}	0 0 0	1 2 0	12 2 10	12 1 11	0.162
4844.96741	0.00204	1.6×10^{-39}	0 0 0	1 2 0	6 3 3	6 2 4	0.144
4846.33145	0.00061	4.9×10^{-39}	0 0 0	1 2 0	5 1 5	4 0 4	0.152
4847.20556	0.00043	8.9×10^{-39}	0 0 0	1 2 0	6 1 6	5 1 5	0.153
4847.60991	0.00239	1.3×10^{-39}	0 0 0	1 2 0	7 3 4	7 2 5	0.149
4848.06191	0.01217	1.1×10^{-39}	0 0 0	1 2 0	8 1 7	8 0 8	0.179
4849.01926	0.00194	2.1×10^{-39}	0 0 0	1 2 0	5 2 4	5 1 5	0.145
4850.47982	0.01301	1.0×10^{-39}	0 0 0	1 2 0	8 3 5	8 2 6	0.137
4851.12346	0.00043	6.7×10^{-39}	0 0 0	1 2 0	6 2 4	5 2 3	0.155
4851.45516	0.00155	1.8×10^{-39}	0 0 0	1 2 0	9 4 5	8 4 4	0.156
4851.58495	0.00150	1.8×10^{-39}	0 0 0	1 2 0	9 4 6	8 4 5	0.156
4852.99764	0.00074	4.5×10^{-39}	0 0 0	1 2 0	6 0 6	5 1 5	0.154

Position	$\sigma_{\text{Pos.}}$	Intensity	$\nu_1\ \nu_2\ \nu_3$	$\nu_1'\ \nu_2'\ \nu_3'$	J K_a K_c	J' K_a' K_c'	$\Delta_{\text{SPEC.}}$
4853.56705	0.00034	9.7×10^{-39}	0 0 0	1 2 0	5 1 4	4 1 3	0.155
4854.09655	0.00872	3.2×10^{-40}	0 0 0	1 2 0	11 2 9	11 1 10	0.129
4854.11486	0.00046	6.9×10^{-39}	0 0 0	1 2 0	6 2 5	5 2 4	0.153
4854.22131	0.00028	1.1×10^{-38}	0 0 0	1 2 0	5 0 5	4 0 4	0.153
4854.30873	0.00129	2.3×10^{-39}	0 0 0	1 2 0	4 2 3	4 1 4	0.143
4854.59644	0.00487	6.5×10^{-40}	0 0 0	1 2 0	9 3 6	9 2 7	0.148
4855.16730	0.00059	4.8×10^{-39}	0 0 0	1 2 0	4 1 4	3 0 3	0.150
4855.41165	0.00228	1.2×10^{-39}	0 0 0	1 2 0	8 1 7	7 2 6	0.164
4855.96417	0.00392	3.5×10^{-39}	0 0 0	1 2 0	7 3 4	6 3 3	0.152
4856.53306	0.00076	3.8×10^{-39}	0 0 0	1 2 0	7 3 5	6 3 4	0.153
4858.49728	0.00140	2.2×10^{-39}	0 0 0	1 2 0	3 2 2	3 1 3	0.140
4858.88135	0.00033	1.0×10^{-38}	0 0 0	1 2 0	5 1 5	4 1 4	0.150
4859.82754	0.00166	1.8×10^{-39}	0 0 0	1 2 0	7 1 6	7 0 7	0.161
4860.99623	0.00293	7.2×10^{-40}	0 0 0	1 2 0	10 5 5	9 5 4	0.169
4861.01725	0.00494	7.2×10^{-40}	0 0 0	1 2 0	10 5 6	9 5 5	0.181
4863.95944	0.00122	2.5×10^{-39}	0 0 0	1 2 0	8 4 4	7 4 3	0.154
4864.01195	0.00121	2.5×10^{-39}	0 0 0	1 2 0	8 4 5	7 4 4	0.152
4864.09491	0.00040	7.7×10^{-39}	0 0 0	1 2 0	5 2 3	4 2 2	0.150
4864.20678	0.00068	4.5×10^{-39}	0 0 0	1 2 0	3 1 3	2 0 2	0.146
4865.37344	0.22788	1.2×10^{-38}	0 0 0	1 2 0	4 0 4	3 0 3	0.151
4865.60309	0.22478	1.0×10^{-38}	0 0 0	1 2 0	4 1 3	3 1 2	0.152
4865.99382	0.23034	7.8×10^{-39}	0 0 0	1 2 0	5 2 4	4 2 3	0.149
4866.77339	0.00068	4.5×10^{-39}	0 0 0	1 2 0	5 0 5	4 1 4	0.154
4866.99219	0.00165	1.8×10^{-39}	0 0 0	1 2 0	2 2 0	2 1 1	0.138
4868.54694	0.00071	4.3×10^{-39}	0 0 0	1 2 0	6 3 3	5 3 2	0.149
4868.80978	0.00069	4.5×10^{-39}	0 0 0	1 2 0	6 3 4	5 3 3	0.149
4868.92340	0.00112	2.8×10^{-39}	0 0 0	1 2 0	3 2 1	3 1 2	0.141
4869.55911	0.01275	2.5×10^{-40}	0 0 0	1 2 0	11 6 6	10 6 5	0.188
4869.55911	0.01275	2.5×10^{-40}	0 0 0	1 2 0	11 6 5	10 6 4	0.188
4869.85989	0.00115	2.9×10^{-39}	0 0 0	1 2 0	6 1 5	6 0 6	0.156
4870.40944	0.00080	1.1×10^{-38}	0 0 0	1 2 0	4 1 4	3 1 3	0.150
4870.92815	0.00087	3.4×10^{-39}	0 0 0	1 2 0	4 2 2	4 1 3	0.144
4871.16653	0.00186	1.8×10^{-39}	0 0 0	1 2 0	8 2 6	8 1 7	0.161
4872.13567	0.00204	1.4×10^{-39}	0 0 0	1 2 0	7 1 6	6 2 5	0.166
4872.57257	0.00087	3.5×10^{-39}	0 0 0	1 2 0	5 2 3	5 1 4	0.149
4873.05276	0.00195	2.5×10^{-39}	0 0 0	1 2 0	7 2 5	7 1 6	0.160
4873.39978	0.00104	3.2×10^{-39}	0 0 0	1 2 0	6 2 4	6 1 5	0.142
4873.71314	0.00082	3.7×10^{-39}	0 0 0	1 2 0	2 1 2	1 0 1	0.145
4876.32769	0.00103	3.1×10^{-39}	0 0 0	1 2 0	7 4 3	6 4 2	0.151
4876.34720	0.00102	3.1×10^{-39}	0 0 0	1 2 0	7 4 4	6 4 3	0.150
4876.71180	0.00029	1.1×10^{-38}	0 0 0	1 2 0	3 0 3	2 0 2	0.149

Position	$\sigma_{\text{Pos.}}$	Intensity	$\nu_1\,\nu_2\,\nu_3$	$\nu_1'\,\nu_2'\,\nu_3'$	J K_a K_c	J' K_a' K_c'	$\Delta_{\text{SPEC.}}$
4876.83397	0.00046	7.5×10^{-39}	0 0 0	1 2 0	4 2 2	3 2 1	0.146
4877.15548	0.00651	5.7×10^{-40}	0 0 0	1 2 0	6 1 5	6 1 6	0.152
4877.78830	0.00033	9.5×10^{-39}	0 0 0	1 2 0	3 1 2	2 1 1	0.149
4877.85569	0.00043	7.5×10^{-39}	0 0 0	1 2 0	4 2 3	3 2 2	0.145
4877.98626	0.00078	4.1×10^{-39}	0 0 0	1 2 0	5 1 4	5 0 5	0.154
4880.61466	0.00075	4.0×10^{-39}	0 0 0	1 2 0	4 0 4	3 1 3	0.150
4880.91232	0.00073	4.5×10^{-39}	0 0 0	1 2 0	5 3 2	4 3 1	0.146
4881.01174	0.00066	4.6×10^{-39}	0 0 0	1 2 0	5 3 3	4 3 2	0.144
4881.78532	0.00084	9.6×10^{-39}	0 0 0	1 2 0	3 1 3	2 1 2	0.146
4883.85438	0.00108	2.7×10^{-39}	0 0 0	1 2 0	1 1 1	0 0 0	0.143
4884.22977	0.00074	5.2×10^{-39}	0 0 0	1 2 0	4 1 3	4 0 4	0.152
4885.67378	0.00164	1.4×10^{-39}	0 0 0	1 2 0	8 5 3	7 5 2	0.159
4885.68704	0.00168	1.4×10^{-39}	0 0 0	1 2 0	8 5 4	7 5 3	0.171
4887.79866	0.00300	9.0×10^{-40}	0 0 0	1 2 0	5 1 4	5 1 5	0.155
4888.22498	0.00040	8.9×10^{-39}	0 0 0	1 2 0	2 0 2	1 0 1	0.147
4888.57632	0.00196	3.3×10^{-39}	0 0 0	1 2 0	6 4 2	5 4 1	0.151
4888.57632	0.00196	3.3×10^{-39}	0 0 0	1 2 0	6 4 3	5 4 2	0.145
4888.65255	0.00220	1.4×10^{-39}	0 0 0	1 2 0	6 1 5	5 2 4	0.159
4888.77166	0.00060	5.7×10^{-39}	0 0 0	1 2 0	3 1 2	3 0 3	0.147
4889.25854	0.00058	5.3×10^{-39}	0 0 0	1 2 0	3 2 1	2 2 0	0.143
4889.68922	0.00062	5.3×10^{-39}	0 0 0	1 2 0	3 2 2	2 2 1	0.144
4890.08699	0.00049	6.5×10^{-39}	0 0 0	1 2 0	2 1 1	1 1 0	0.146
4891.87881	0.00095	5.3×10^{-39}	0 0 0	1 2 0	2 1 1	2 0 2	0.146
4893.00604	0.00047	6.5×10^{-39}	0 0 0	1 2 0	2 1 2	1 1 1	0.144
4893.08772	0.00160	3.4×10^{-39}	0 0 0	1 2 0	4 3 1	3 3 0	0.141
4893.11507	0.00198	3.4×10^{-39}	0 0 0	1 2 0	4 3 2	3 3 1	0.140
4893.81513	0.00088	3.8×10^{-39}	0 0 0	1 2 0	1 1 0	1 0 1	0.166
4893.91991	0.02043	5.5×10^{-40}	0 0 0	1 2 0	9 6 3	8 6 2	0.181
4893.91991	0.02045	5.5×10^{-40}	0 0 0	1 2 0	9 6 4	8 6 3	0.181
4894.28959	0.25084	3.0×10^{-39}	0 0 0	1 2 0	3 0 3	2 1 2	0.148
4896.17094	0.00909	5.5×10^{-40}	0 0 0	1 2 0	9 2 7	8 3 6	0.186
4896.77871	0.00201	1.4×10^{-39}	0 0 0	1 2 0	4 1 3	4 1 4	0.150
4897.88070	0.00269	1.6×10^{-39}	0 0 0	1 2 0	7 5 2	6 5 1	0.162
4897.88070	0.00269	1.6×10^{-39}	0 0 0	1 2 0	7 5 3	6 5 2	0.162
4899.84580	0.00062	5.1×10^{-39}	0 0 0	1 2 0	1 0 1	0 0 0	0.145
4900.70155	0.00493	2.5×10^{-39}	0 0 0	1 2 0	5 4 2	4 4 1	0.144
4900.70155	0.00488	2.5×10^{-39}	0 0 0	1 2 0	5 4 1	4 4 0	0.145
4904.01110	0.00126	2.2×10^{-39}	0 0 0	1 2 0	3 1 2	3 1 3	0.144
4904.76988	0.00230	1.3×10^{-39}	0 0 0	1 2 0	5 1 4	4 2 3	0.155
4907.51820	0.00218	1.6×10^{-39}	0 0 0	1 2 0	2 0 2	1 1 1	0.147
4909.45450	0.00086	3.7×10^{-39}	0 0 0	1 2 0	2 1 1	2 1 2	0.144

Position	$\sigma_{\text{Pos.}}$	Intensity	$\nu_1\ \nu_2\ \nu_3$	$\nu_1{}'\ \nu_2{}'\ \nu_3{}'$	J K_a K_c	J' $\text{K}_a{}'$ $\text{K}_c{}'$	$\Delta_{\text{SPEC.}}$
4909.69974	0.00394	9.3×10^{-40}	0 0 0	1 2 0	7 2 5	7 2 6	0.156
4909.98715	0.00292	1.3×10^{-39}	0 0 0	1 2 0	6 5 2	5 5 1	0.159
4909.98715	0.00292	1.3×10^{-39}	0 0 0	1 2 0	6 5 1	5 5 0	0.159
4913.08600	0.00044	7.4×10^{-39}	0 0 0	1 2 0	1 1 0	1 1 1	0.144
4914.10171	0.00272	1.1×10^{-39}	0 0 0	1 2 0	11 2 10	10 3 7	0.129
4915.43486	0.00197	1.7×10^{-39}	0 0 0	1 2 0	6 2 4	6 2 5	0.149
4916.50442	0.00045	7.4×10^{-39}	0 0 0	1 2 0	1 1 1	1 1 0	0.144
4917.77725	0.00098	3.2×10^{-39}	0 0 0	1 2 0	10 2 9	9 3 6	0.135
4918.29570	0.00272	1.3×10^{-39}	0 0 0	1 2 0	1 1 1	2 0 2	0.143
4919.50328	0.00113	2.8×10^{-39}	0 0 0	1 2 0	5 2 3	5 2 4	0.147
4919.70495	0.00096	3.6×10^{-39}	0 0 0	1 2 0	2 1 2	2 1 1	0.144
4922.13016	0.00072	4.7×10^{-39}	0 0 0	1 2 0	4 2 2	4 2 3	0.144
4922.99776	0.00059	5.4×10^{-39}	0 0 0	1 2 0	0 0 0	1 0 1	0.144
4923.06513	0.00376	8.4×10^{-40}	0 0 0	1 2 0	7 1 7	6 2 4	0.156
4923.14092	0.00391	9.8×10^{-40}	0 0 0	1 2 0	8 1 8	7 2 5	0.159
4923.64626	0.00044	7.8×10^{-39}	0 0 0	1 2 0	3 2 1	3 2 2	0.141
4924.40983	0.00026	1.3×10^{-38}	0 0 0	1 2 0	2 2 0	2 2 1	0.140
4924.48607	0.00162	2.1×10^{-39}	0 0 0	1 2 0	3 1 3	3 1 2	0.144
4924.64387	0.00029	1.3×10^{-38}	0 0 0	1 2 0	2 2 1	2 2 0	0.140
4924.80790	0.00046	7.8×10^{-39}	0 0 0	1 2 0	3 2 2	3 2 1	0.141
4924.96748	0.00286	1.3×10^{-39}	0 0 0	1 2 0	9 2 8	8 3 5	0.162
4925.46711	0.00104	4.1×10^{-39}	0 0 0	1 2 0	9 1 9	8 2 6	0.150
4925.46711	0.00381	8.9×10^{-40}	0 0 0	1 2 0	6 1 6	5 2 3	0.157
4925.55920	0.00069	4.8×10^{-39}	0 0 0	1 2 0	4 2 3	4 2 2	0.144
4927.26025	0.00444	2.9×10^{-39}	0 0 0	1 2 0	5 2 4	5 2 3	0.128
4927.29120	0.00171	2.5×10^{-39}	0 0 0	1 2 0	9 0 9	8 2 6	0.177
4930.13130	0.00514	9.0×10^{-40}	0 0 0	1 2 0	5 1 5	4 2 2	0.151
4930.31624	0.00265	1.8×10^{-39}	0 0 0	1 2 0	6 2 5	6 2 4	0.150
4930.68603	0.00252	2.5×10^{-39}	0 0 0	1 2 0	2 1 2	3 0 3	0.139
4930.81501	0.00253	1.3×10^{-39}	0 0 0	1 2 0	4 1 4	4 1 3	0.150
4930.87984	0.00325	1.0×10^{-39}	0 0 0	1 2 0	7 2 5	6 3 4	0.169
4931.34561	0.01080	4.2×10^{-40}	0 0 0	1 2 0	10 1 10	9 2 7	0.152
4932.49451	0.00078	4.2×10^{-39}	0 0 0	1 2 0	1 0 1	1 1 0	0.145
4933.50088	0.00256	1.2×10^{-39}	0 0 0	1 2 0	8 2 7	7 3 4	0.159
4933.59813	0.00251	1.5×10^{-39}	0 0 0	1 2 0	10 1 9	9 3 6	0.138
4934.05314	0.00771	8.3×10^{-40}	0 0 0	1 2 0	4 2 3	5 1 4	0.159
4934.21641	0.00058	6.0×10^{-39}	0 0 0	1 2 0	2 0 2	2 1 1	0.146
4934.28567	0.00037	1.0×10^{-38}	0 0 0	1 2 0	1 0 1	2 0 2	0.144
4934.65647	0.00318	1.1×10^{-39}	0 0 0	1 2 0	8 3 5	8 3 6	0.158
4934.90307	0.00264	1.2×10^{-39}	0 0 0	1 2 0	7 2 6	7 2 5	0.157
4935.20745	0.00575	5.1×10^{-40}	0 0 0	1 2 0	3 1 2	2 2 1	0.152

Position	$\sigma_{\text{Pos.}}$	Intensity	$\nu_1\ \nu_2\ \nu_3$	ν_1' ν_2' ν_3'	J K$_a$ K$_c$	J' K$_a$' K$_c$'	$\Delta_{\text{SPEC.}}$
4935.87176	0.00046	7.6×10^{-39}	0 0 0	1 2 0	1 1 1	2 1 2	0.141
4936.52337	0.00221	2.0×10^{-39}	0 0 0	1 2 0	7 3 4	7 3 5	0.148
4936.71961	0.00401	7.7×10^{-40}	0 0 0	1 2 0	4 1 4	3 2 1	0.150
4936.99047	0.00053	6.5×10^{-39}	0 0 0	1 2 0	3 0 3	3 1 2	0.147
4937.77471	0.00099	3.6×10^{-39}	0 0 0	1 2 0	6 3 3	6 3 4	0.145
4938.52549	0.00140	2.3×10^{-39}	0 0 0	1 2 0	7 3 5	7 3 4	0.146
4938.58502	0.00101	3.8×10^{-39}	0 0 0	1 2 0	6 3 4	6 3 3	0.144
4938.60399	0.00476	7.8×10^{-40}	0 0 0	1 2 0	5 1 5	5 1 4	0.145
4938.62731	0.00066	5.9×10^{-39}	0 0 0	1 2 0	5 3 2	5 3 3	0.141
4938.89681	0.00059	6.1×10^{-39}	0 0 0	1 2 0	5 3 3	5 3 2	0.140
4938.93402	0.00263	1.5×10^{-39}	0 0 0	1 2 0	8 3 6	8 3 5	0.146
4939.23430	0.00071	9.5×10^{-39}	0 0 0	1 2 0	4 3 1	4 3 2	0.141
4939.29955	0.00037	9.6×10^{-39}	0 0 0	1 2 0	4 3 2	4 3 1	0.139
4939.68155	0.00619	1.5×10^{-38}	0 0 0	1 2 0	3 3 1	3 3 0	0.132
4939.68251	0.00619	1.5×10^{-38}	0 0 0	1 2 0	3 3 0	3 3 1	0.143
4939.78471	0.00113	7.4×10^{-39}	0 0 0	1 2 0	1 1 0	2 1 1	0.143
4939.84319	0.00333	1.4×10^{-39}	0 0 0	1 2 0	9 3 7	9 3 6	0.122
4941.01832	0.00058	6.0×10^{-39}	0 0 0	1 2 0	4 0 4	4 1 3	0.149
4942.29105	0.00123	2.9×10^{-39}	0 0 0	1 2 0	0 0 0	1 1 1	0.144
4943.25651	0.00253	1.3×10^{-39}	0 0 0	1 2 0	7 2 6	6 3 3	0.159
4945.20206	0.00027	1.4×10^{-38}	0 0 0	1 2 0	2 0 2	3 0 3	0.146
4945.92932	0.00036	1.2×10^{-38}	0 0 0	1 2 0	2 1 2	3 1 3	0.141
4946.49751	0.00081	4.8×10^{-39}	0 0 0	1 2 0	5 0 5	5 1 4	0.151
4946.69668	0.00316	1.1×10^{-39}	0 0 0	1 2 0	6 2 4	5 3 3	0.163
4947.76204	0.00535	4.7×10^{-40}	0 0 0	1 2 0	6 1 6	6 1 5	0.162
4952.15579	0.00031	1.2×10^{-38}	0 0 0	1 2 0	2 1 1	3 1 2	0.142
4953.54721	0.00145	3.5×10^{-39}	0 0 0	1 2 0	6 0 6	6 1 5	0.157
4953.89124	0.00700	1.3×10^{-39}	0 0 0	1 2 0	6 2 5	5 3 2	0.149
4955.23053	0.00109	3.6×10^{-39}	0 0 0	1 2 0	4 1 4	5 0 5	0.145
4955.61641	0.00024	1.6×10^{-38}	0 0 0	1 2 0	3 0 3	4 0 4	0.146
4955.66557	0.00087	1.5×10^{-38}	0 0 0	1 2 0	3 1 3	4 1 4	0.146
4956.26328	0.00263	1.2×10^{-39}	0 0 0	1 2 0	8 4 4	8 4 5	0.144
4956.43656	0.00354	1.2×10^{-39}	0 0 0	1 2 0	8 4 5	8 4 4	0.149
4957.70675	0.00081	4.2×10^{-39}	0 0 0	1 2 0	6 4 3	6 4 2	0.126
4957.72282	0.00083	4.2×10^{-39}	0 0 0	1 2 0	6 4 2	6 4 3	0.158
4958.27407	0.00129	7.3×10^{-39}	0 0 0	1 2 0	5 4 1	5 4 2	0.142
4958.27407	0.00129	7.3×10^{-39}	0 0 0	1 2 0	5 4 2	5 4 1	0.139
4958.74615	0.00050	1.2×10^{-38}	0 0 0	1 2 0	4 4 1	4 4 0	0.139
4958.74615	0.00050	1.2×10^{-38}	0 0 0	1 2 0	4 4 0	4 4 1	0.140
4959.03365	0.00060	6.7×10^{-39}	0 0 0	1 2 0	2 2 1	3 2 2	0.140
4959.52991	0.00054	6.7×10^{-39}	0 0 0	1 2 0	2 2 0	3 2 1	0.138

Position	$\sigma_{\mathrm{Pos.}}$	Intensity	$\nu_1\,\nu_2\,\nu_3$	$\nu_1{}'\,\nu_2{}'\,\nu_3{}'$	J K_a K_c	J' $K_a{}'$ $K_c{}'$	$\Delta_{\mathrm{SPEC.}}$
4960.44316	0.00080	4.5×10^{-39}	0 0 0	1 2 0	2 0 2	3 1 3	0.145
4962.11842	0.00189	2.3×10^{-39}	0 0 0	1 2 0	7 0 7	7 1 6	0.159
4964.41807	0.00044	1.4×10^{-38}	0 0 0	1 2 0	3 1 2	4 1 3	0.146
4964.83701	0.00233	3.6×10^{-39}	0 0 0	1 2 0	6 1 5	6 2 4	0.138
4965.04048	0.00025	1.5×10^{-38}	0 0 0	1 2 0	4 1 4	5 1 5	0.144
4965.44320	0.00032	1.6×10^{-38}	0 0 0	1 2 0	4 0 4	5 0 5	0.153
4966.05489	0.00086	4.3×10^{-39}	0 0 0	1 2 0	5 1 4	5 2 3	0.153
4966.75077	0.00193	3.5×10^{-39}	0 0 0	1 2 0	5 1 5	6 0 6	0.149
4968.16776	0.00080	4.7×10^{-39}	0 0 0	1 2 0	3 0 3	4 1 4	0.146
4969.85712	0.00198	1.8×10^{-39}	0 0 0	1 2 0	9 1 8	9 2 7	0.159
4970.10463	0.00036	1.0×10^{-38}	0 0 0	1 2 0	3 2 2	4 2 3	0.140
4970.32383	0.00096	3.7×10^{-39}	0 0 0	1 2 0	3 1 2	3 2 1	0.147
4971.34848	0.00065	1.0×10^{-38}	0 0 0	1 2 0	3 2 1	4 2 2	0.138
4972.51078	0.00300	2.4×10^{-39}	0 0 0	1 2 0	2 1 1	2 2 0	0.165
4974.04664	0.00026	1.4×10^{-38}	0 0 0	1 2 0	5 1 5	6 1 6	0.146
4974.63950	0.00063	1.4×10^{-38}	0 0 0	1 2 0	5 0 5	6 0 6	0.150
4975.24697	0.00080	4.5×10^{-39}	0 0 0	1 2 0	4 0 4	5 1 5	0.146
4976.50486	0.00039	1.4×10^{-38}	0 0 0	1 2 0	4 1 3	5 1 4	0.148
4977.12299	0.00166	2.2×10^{-39}	0 0 0	1 2 0	2 1 2	2 2 1	0.146
4977.46644	0.00127	3.1×10^{-39}	0 0 0	1 2 0	6 1 6	7 0 7	0.142
4977.58606	0.00363	1.6×10^{-39}	0 0 0	1 2 0	8 5 3	8 5 4	0.150
4977.59592	0.00275	1.6×10^{-39}	0 0 0	1 2 0	8 5 4	8 5 3	0.156
4978.27717	0.00119	2.9×10^{-39}	0 0 0	1 2 0	7 5 3	7 5 2	0.154
4978.27717	0.00119	2.9×10^{-39}	0 0 0	1 2 0	7 5 2	7 5 3	0.155
4978.87802	0.00080	5.1×10^{-39}	0 0 0	1 2 0	6 5 1	6 5 2	0.153
4978.87802	0.00080	5.1×10^{-39}	0 0 0	1 2 0	6 5 2	6 5 1	0.153
4979.20841	0.00123	3.2×10^{-39}	0 0 0	1 2 0	3 1 3	3 2 2	0.144
4979.39657	0.00045	8.6×10^{-39}	0 0 0	1 2 0	5 5 1	5 5 0	0.152
4979.39657	0.00045	8.6×10^{-39}	0 0 0	1 2 0	5 5 0	5 5 1	0.152
4980.96781	0.00034	1.1×10^{-38}	0 0 0	1 2 0	4 2 3	5 2 4	0.141
4981.93632	0.00089	4.0×10^{-39}	0 0 0	1 2 0	5 0 5	6 1 6	0.147
4982.02876	0.00335	3.4×10^{-39}	0 0 0	1 2 0	4 1 4	4 2 3	0.161
4982.66719	0.00037	1.2×10^{-38}	0 0 0	1 2 0	6 1 6	7 1 7	0.147
4983.26498	0.00031	1.2×10^{-38}	0 0 0	1 2 0	6 0 6	7 0 7	0.150
4983.41454	0.00045	1.1×10^{-38}	0 0 0	1 2 0	4 2 2	5 2 3	0.141
4985.53868	0.00188	3.1×10^{-39}	0 0 0	1 2 0	5 1 5	5 2 4	0.147
4985.84123	0.00090	5.0×10^{-39}	0 0 0	1 2 0	3 3 1	4 3 2	0.144
4988.34202	0.00049	1.2×10^{-38}	0 0 0	1 2 0	5 1 4	6 1 5	0.151
4989.77651	0.00141	2.5×10^{-39}	0 0 0	1 2 0	6 1 6	6 2 5	0.149
4990.89893	0.00038	9.8×10^{-39}	0 0 0	1 2 0	7 1 7	8 1 8	0.149
4991.39761	0.00037	9.8×10^{-39}	0 0 0	1 2 0	7 0 7	8 0 8	0.151

Position	$\sigma_{\text{Pos.}}$	Intensity	$\nu_1\ \nu_2\ \nu_3$	$\nu_1'\ \nu_2'\ \nu_3'$	J K_a K_c	J' K_a' K_c'	$\Delta_{\text{SPEC.}}$
4991.59154	0.00172	1.1×10^{-38}	0 0 0	1 2 0	5 2 4	6 2 5	0.142
4995.70632	0.00035	1.1×10^{-38}	0 0 0	1 2 0	5 2 3	6 2 4	0.145
4997.01590	0.00061	7.3×10^{-39}	0 0 0	1 2 0	4 3 2	5 3 3	0.136
4997.11610	0.00048	7.4×10^{-39}	0 0 0	1 2 0	4 3 1	5 3 2	0.134
4998.74020	0.00048	7.3×10^{-39}	0 0 0	1 2 0	8 1 8	9 1 9	0.151
4998.90773	0.00097	3.7×10^{-39}	0 0 0	1 2 0	1 1 1	2 2 0	0.142
4999.11013	0.00050	7.3×10^{-39}	0 0 0	1 2 0	8 0 8	9 0 9	0.153
4999.84236	0.00036	1.0×10^{-38}	0 0 0	1 2 0	6 1 5	7 1 6	0.155
5001.95181	0.00041	9.3×10^{-39}	0 0 0	1 2 0	6 2 5	7 2 6	0.145
5004.13955	0.00116	3.3×10^{-39}	0 0 0	1 2 0	9 2 7	9 3 6	0.132
5006.19537	0.00069	5.1×10^{-39}	0 0 0	1 2 0	9 1 9	10 1 10	0.153
5006.44743	0.00067	5.1×10^{-39}	0 0 0	1 2 0	9 0 9	10 0 10	0.155
5006.87844	0.00100	3.5×10^{-39}	0 0 0	1 2 0	2 1 1	3 2 2	0.143
5008.11170	0.00172	9.0×10^{-39}	0 0 0	1 2 0	6 2 4	7 2 5	0.150
5008.12844	0.00160	7.7×10^{-39}	0 0 0	1 2 0	5 3 3	6 3 4	0.140
5008.40209	0.00049	7.8×10^{-39}	0 0 0	1 2 0	5 3 2	6 3 3	0.137
5008.70760	0.00112	3.4×10^{-39}	0 0 0	1 2 0	8 2 6	8 3 5	0.154
5010.90966	0.00065	7.6×10^{-39}	0 0 0	1 2 0	7 1 6	8 1 7	0.159
5012.01993	0.00053	7.0×10^{-39}	0 0 0	1 2 0	7 2 6	8 2 7	0.148
5012.23429	0.00136	3.2×10^{-39}	0 0 0	1 2 0	2 1 2	3 2 1	0.136
5012.27960	0.00565	7.0×10^{-40}	0 0 0	1 2 0	10 1 10	11 0 11	0.154
5012.85064	0.00294	3.8×10^{-39}	0 0 0	1 2 0	7 2 5	7 3 4	0.140
5013.27477	0.00275	3.4×10^{-39}	0 0 0	1 2 0	10 1 10	11 1 11	0.160
5013.43248	0.00108	3.3×10^{-39}	0 0 0	1 2 0	10 0 10	11 0 11	0.158
5015.62112	0.00107	3.1×10^{-39}	0 0 0	1 2 0	3 1 2	4 2 3	0.146
5016.30113	0.00144	3.1×10^{-39}	0 0 0	1 2 0	4 4 0	5 4 1	0.117
5016.31742	0.00268	3.1×10^{-39}	0 0 0	1 2 0	4 4 1	5 4 2	0.135
5016.46849	0.00087	4.2×10^{-39}	0 0 0	1 2 0	6 2 4	6 3 3	0.155
5019.14430	0.00055	6.9×10^{-39}	0 0 0	1 2 0	6 3 4	7 3 5	0.140
5019.28634	0.00088	4.3×10^{-39}	0 0 0	1 2 0	5 2 3	5 3 2	0.150
5019.76648	0.00054	6.9×10^{-39}	0 0 0	1 2 0	6 3 3	7 3 4	0.137
5019.96577	0.00169	2.1×10^{-39}	0 0 0	1 2 0	11 1 11	12 1 12	0.156
5020.06596	0.00177	2.1×10^{-39}	0 0 0	1 2 0	11 0 11	12 0 12	0.158
5020.21815	0.00066	7.1×10^{-39}	0 0 0	1 2 0	7 2 5	8 2 6	0.141
5021.26861	0.00096	3.9×10^{-39}	0 0 0	1 2 0	4 2 2	4 3 1	0.149
5021.45377	0.00075	5.4×10^{-39}	0 0 0	1 2 0	8 1 7	9 1 8	0.163
5021.77038	0.00067	5.3×10^{-39}	0 0 0	1 2 0	8 2 7	9 2 8	0.152
5022.51058	0.00144	2.6×10^{-39}	0 0 0	1 2 0	3 2 1	3 3 0	0.146
5022.84912	0.00113	3.6×10^{-39}	0 0 0	1 2 0	5 2 4	5 3 3	0.151
5022.86392	0.00114	3.6×10^{-39}	0 0 0	1 2 0	4 2 3	4 3 2	0.146
5023.06061	0.00122	2.6×10^{-39}	0 0 0	1 2 0	3 2 2	3 3 1	0.148

Position	$\sigma_{\text{Pos.}}$	Intensity	$\nu_1\ \nu_2\ \nu_3$	$\nu_1'\ \nu_2'\ \nu_3'$	J K_a K_c	J' K_a' K_c'	$\Delta_{\text{SPEC.}}$
5023.12383	0.00123	3.1×10^{-39}	0 0 0	1 2 0	6 2 5	6 3 4	0.150
5023.43840	0.00150	2.7×10^{-39}	0 0 0	1 2 0	4 1 3	5 2 4	0.149
5023.81378	0.00174	2.4×10^{-39}	0 0 0	1 2 0	7 2 6	7 3 5	0.153
5026.29745	0.00270	1.2×10^{-39}	0 0 0	1 2 0	12 1 12	13 1 13	0.162
5026.35626	0.00279	1.2×10^{-39}	0 0 0	1 2 0	12 0 12	13 0 13	0.163
5026.82993	0.00310	1.1×10^{-39}	0 0 0	1 2 0	9 2 8	9 3 7	0.160
5026.91077	0.00147	2.5×10^{-39}	0 0 0	1 2 0	3 1 3	4 2 2	0.142
5027.40953	0.00176	4.2×10^{-39}	0 0 0	1 2 0	5 4 2	6 4 3	0.135
5027.41902	0.00426	4.3×10^{-39}	0 0 0	1 2 0	5 4 1	6 4 2	0.138
5029.30609	0.00418	6.6×10^{-40}	0 0 0	1 2 0	10 2 9	10 3 8	0.166
5030.04629	0.00070	5.5×10^{-39}	0 0 0	1 2 0	7 3 5	8 3 6	0.144
5030.36750	0.00180	2.1×10^{-39}	0 0 0	1 2 0	5 1 4	6 2 5	0.148
5031.17877	0.00200	3.6×10^{-39}	0 0 0	1 2 0	9 2 8	10 2 9	0.150
5031.24841	0.00101	5.5×10^{-39}	0 0 0	1 2 0	7 3 4	8 3 5	0.136
5031.40963	0.00111	3.6×10^{-39}	0 0 0	1 2 0	9 1 8	10 1 9	0.167
5033.30402	0.00111	4.1×10^{-39}	0 0 0	1 2 0	8 2 6	9 2 7	0.152
5036.35917	0.01084	2.0×10^{-40}	0 0 0	1 2 0	12 2 11	12 3 10	0.176
5036.48611	0.00298	1.6×10^{-39}	0 0 0	1 2 0	6 1 5	7 2 6	0.147
5038.44273	0.00097	4.2×10^{-39}	0 0 0	1 2 0	6 4 2	7 4 3	0.118
5038.45952	0.00107	4.2×10^{-39}	0 0 0	1 2 0	6 4 3	7 4 4	0.156
5040.25138	0.28539	2.3×10^{-39}	0 0 0	1 2 0	10 2 9	11 2 10	0.162
5040.76012	0.28820	2.3×10^{-39}	0 0 0	1 2 0	10 1 9	11 1 10	0.169
5040.79984	0.27993	4.0×10^{-39}	0 0 0	1 2 0	8 3 6	9 3 7	0.148
5043.29571	0.00310	1.7×10^{-39}	0 0 0	1 2 0	4 1 4	5 2 3	0.141
5045.31418	0.00139	2.8×10^{-39}	0 0 0	1 2 0	9 2 7	10 2 8	0.163
5046.86135	0.00445	8.1×10^{-40}	0 0 0	1 2 0	8 1 7	9 2 8	0.171
5048.28792	0.00290	1.7×10^{-39}	0 0 0	1 2 0	5 5 0	6 5 1	0.146
5048.28792	0.00290	1.7×10^{-39}	0 0 0	1 2 0	5 5 1	6 5 2	0.146
5049.40420	0.00113	3.5×10^{-39}	0 0 0	1 2 0	7 4 4	8 4 5	0.134
5049.45611	0.00108	3.5×10^{-39}	0 0 0	1 2 0	7 4 3	8 4 4	0.129
5051.36999	0.00140	2.7×10^{-39}	0 0 0	1 2 0	9 3 7	10 3 8	0.150
5057.12085	0.00196	1.7×10^{-39}	0 0 0	1 2 0	10 2 8	11 2 9	0.175
5057.30934	0.00512	7.7×10^{-40}	0 0 0	1 2 0	12 2 11	13 2 12	0.175
5057.78338	0.26979	4.2×10^{-39}	0 0 0	1 2 0	2 2 0	3 3 1	0.146
5057.89577	0.26877	4.2×10^{-39}	0 0 0	1 2 0	2 2 1	3 3 0	0.142
5059.27256	0.00241	2.3×10^{-39}	0 0 0	1 2 0	6 5 1	7 5 2	0.143
5059.27543	0.00171	2.3×10^{-39}	0 0 0	1 2 0	6 5 2	7 5 3	0.146
5060.31586	0.00187	2.6×10^{-39}	0 0 0	1 2 0	8 4 5	9 4 6	0.138
5060.44810	0.00171	2.6×10^{-39}	0 0 0	1 2 0	8 4 4	9 4 5	0.139
5061.72732	0.00272	1.7×10^{-39}	0 0 0	1 2 0	10 3 8	11 3 9	0.156
5061.74057	0.00449	1.0×10^{-39}	0 0 0	1 2 0	5 1 5	6 2 4	0.144

Position	$\sigma_{\mathrm{Pos.}}$	Intensity	$\nu_1\,\nu_2\,\nu_3$	ν_1' ν_2' ν_3'	J K_a K_c	J' K_a' K_c'	$\Delta_{\mathrm{SPEC.}}$
5067.51904	0.00306	1.3×10^{-39}	0 0 0	1 2 0	10 3 7	11 3 8	0.146
5068.65633	0.00158	2.9×10^{-39}	0 0 0	1 2 0	3 2 1	4 3 2	0.144
5069.24308	0.00159	2.6×10^{-39}	0 0 0	1 2 0	3 2 2	4 3 1	0.145
5070.19318	0.00915	2.1×10^{-39}	0 0 0	1 2 0	7 5 3	8 5 4	0.149
5070.19318	0.00918	2.1×10^{-39}	0 0 0	1 2 0	7 5 2	8 5 3	0.148
5071.17414	0.00274	1.7×10^{-39}	0 0 0	1 2 0	9 4 6	10 4 7	0.148
5072.52693	0.00203	1.3×10^{-39}	0 0 0	1 2 0	6 3 3	6 4 2	0.166
5078.98241	0.00205	1.9×10^{-39}	0 0 0	1 2 0	4 2 2	5 3 3	0.143
5079.60266	0.00562	7.5×10^{-40}	0 0 0	1 2 0	11 3 8	12 3 9	0.164
5081.03605	0.00263	1.7×10^{-39}	0 0 0	1 2 0	8 5 3	9 5 4	0.144
5081.03605	0.00263	1.7×10^{-39}	0 0 0	1 2 0	8 5 4	9 5 5	0.150
5091.80300	0.00425	1.2×10^{-39}	0 0 0	1 2 0	9 5 5	10 5 6	0.145
5091.81655	0.00310	1.2×10^{-39}	0 0 0	1 2 0	9 5 4	10 5 5	0.145
5100.67814	0.02230	8.7×10^{-40}	0 0 0	1 2 0	8 6 2	9 6 3	0.161
5100.68115	0.02237	8.7×10^{-40}	0 0 0	1 2 0	8 6 3	9 6 4	0.164
5102.50690	0.00549	7.7×10^{-40}	0 0 0	1 2 0	10 5 6	11 5 7	0.151
5102.53161	0.00515	7.7×10^{-40}	0 0 0	1 2 0	10 5 5	11 5 6	0.142
5109.28332	0.00068	8.5×10^{-39}	0 0 0	1 2 0	7 0 7	8 2 6	0.139
5120.97048	0.00177	5.7×10^{-39}	0 0 0	1 2 0	3 3 0	4 4 1	0.152
5120.97048	0.00177	5.7×10^{-39}	0 0 0	1 2 0	3 3 1	4 4 0	0.147
5123.66771	0.05113	2.5×10^{-40}	0 0 0	1 2 0	12 5 8	13 5 9	0.148
5125.05253	0.00636	7.7×10^{-40}	0 0 0	1 2 0	7 4 3	7 5 2	0.177
5125.06991	0.00622	7.7×10^{-40}	0 0 0	1 2 0	7 4 4	7 5 3	0.167
5134.12628	0.00229	2.3×10^{-39}	0 0 0	1 2 0	8 0 8	9 2 7	0.150
5175.22331	0.00424	1.5×10^{-39}	0 0 0	1 2 0	8 3 6	9 4 5	0.161
5195.73771	0.00339	3.2×10^{-39}	0 0 0	1 2 0	5 4 2	6 5 1	0.160
5195.73771	0.00339	3.2×10^{-39}	0 0 0	1 2 0	5 4 1	6 5 2	0.162

A.2.1.5 HTO $\nu_1 + \nu_3$ band

Here, the lines assigned to the $\nu_1 + \nu_3$ band obtained from the $1\,\mathrm{GBq}$ sample are presented. These lines are published in [Her21]. For further information, see Section 5.5.1.

Table A.6: Linelist of the $\nu_1 + \nu_3$ band. The columns present the assigned line position, the uncertainty on the position $\sigma_{\mathrm{Pos.}}$, the line intensity taking natural abundance into account, lower and upper vibrational quanta, lower and upper rotational quanta and the deviation to the predictions from SPECTRA database $\Delta_{\mathrm{SPEC.}}$.

Position	$\sigma_{\mathrm{Pos.}}$	Intensity	$\nu_1\,\nu_2\,\nu_3$	ν_1' ν_2' ν_3'	J K_a K_c	J' K_a' K_c'	$\Delta_{\mathrm{SPEC.}}$
5838.76257	0.00220	3.3×10^{-39}	0 0 0	1 0 1	4 4 0	3 3 1	-0.239
5838.76257	0.00220	3.3×10^{-39}	0 0 0	1 0 1	4 4 1	3 3 0	-0.245

Position	$\sigma_{\text{Pos.}}$	Intensity	$\nu_1\ \nu_2\ \nu_3$	$\nu_1'\ \nu_2'\ \nu_3'$	J K_a K_c	J' K_a' K_c'	$\Delta_{\text{SPEC.}}$
5848.57203	0.00289	2.7×10^{-39}	0 0 0	1 0 1	6 3 3	5 2 4	-0.210
5852.83590	0.00156	2.8×10^{-39}	0 0 0	1 0 1	6 3 4	5 2 3	-0.216
5862.35364	0.00152	3.5×10^{-39}	0 0 0	1 0 1	5 3 2	4 2 3	-0.219
5863.82178	0.00265	1.4×10^{-39}	0 0 0	1 0 1	10 2 9	9 1 8	-0.200
5864.20068	0.00142	3.6×10^{-39}	0 0 0	1 0 1	5 3 3	4 2 2	-0.219
5875.43105	0.00116	4.3×10^{-39}	0 0 0	1 0 1	4 3 1	3 2 2	-0.221
5876.04572	0.00103	4.4×10^{-39}	0 0 0	1 0 1	4 3 2	3 2 1	-0.221
5878.43873	0.00600	6.9×10^{-40}	0 0 0	1 0 1	8 4 5	8 3 6	-0.230
5878.93670	0.00209	2.6×10^{-39}	0 0 0	1 0 1	11 1 11	10 0 10	-0.187
5887.35908	0.00172	2.6×10^{-39}	0 0 0	1 0 1	5 2 3	4 1 4	-0.205
5887.98548	0.00093	5.1×10^{-39}	0 0 0	1 0 1	3 3 0	2 2 1	-0.225
5888.10736	0.00096	5.1×10^{-39}	0 0 0	1 0 1	3 3 1	2 2 0	-0.225
5889.20239	0.00152	3.3×10^{-39}	0 0 0	1 0 1	7 2 6	6 1 5	-0.201
5891.09789	0.00124	3.8×10^{-39}	0 0 0	1 0 1	10 1 10	9 0 9	-0.186
5893.73504	0.00114	3.8×10^{-39}	0 0 0	1 0 1	10 0 10	9 1 9	-0.185
5897.68021	0.00481	1.3×10^{-39}	0 0 0	1 0 1	10 1 9	9 2 8	-0.182
5897.81205	0.00174	4.0×10^{-39}	0 0 0	1 0 1	6 2 5	5 1 4	-0.207
5902.78260	0.00095	5.4×10^{-39}	0 0 0	1 0 1	9 1 9	8 0 8	-0.186
5905.15229	0.00150	3.6×10^{-39}	0 0 0	1 0 1	4 2 2	3 1 3	-0.207
5906.80050	0.00107	4.6×10^{-39}	0 0 0	1 0 1	5 2 4	4 1 3	-0.207
5906.89659	0.00091	5.3×10^{-39}	0 0 0	1 0 1	9 0 9	8 1 8	-0.191
5913.90987	0.00070	7.0×10^{-39}	0 0 0	1 0 1	8 1 8	7 0 7	-0.192
5916.25698	0.00093	5.1×10^{-39}	0 0 0	1 0 1	4 2 3	3 1 2	-0.208
5916.43620	0.00192	2.2×10^{-39}	0 0 0	1 0 1	6 3 4	6 2 5	-0.220
5920.13469	0.00071	6.7×10^{-39}	0 0 0	1 0 1	8 0 8	7 1 7	-0.185
5920.48800	0.00262	1.4×10^{-39}	0 0 0	1 0 1	8 2 7	8 1 8	-0.194
5920.74595	0.00235	2.3×10^{-39}	0 0 0	1 0 1	4 3 2	4 2 3	-0.221
5920.94289	0.00126	4.5×10^{-39}	0 0 0	1 0 1	3 2 1	2 1 2	-0.210
5922.42467	0.00199	2.4×10^{-39}	0 0 0	1 0 1	4 3 1	4 2 2	-0.221
5922.60485	0.00289	1.6×10^{-39}	0 0 0	1 0 1	3 3 0	3 2 1	-0.227
5922.65204	0.00168	2.6×10^{-39}	0 0 0	1 0 1	5 3 2	5 2 3	-0.224
5924.44246	0.00060	8.4×10^{-39}	0 0 0	1 0 1	7 1 7	6 0 6	-0.191
5924.62137	0.00266	2.0×10^{-39}	0 0 0	1 0 1	7 3 4	7 2 5	-0.222
5926.04342	0.00339	1.6×10^{-39}	0 0 0	1 0 1	8 3 5	8 2 6	-0.209
5926.23610	0.00094	5.3×10^{-39}	0 0 0	1 0 1	3 2 2	2 1 1	-0.212
5933.72051	0.00060	8.2×10^{-39}	0 0 0	1 0 1	7 0 7	6 1 6	-0.194
5934.45884	0.00054	9.5×10^{-39}	0 0 0	1 0 1	6 1 6	5 0 5	-0.198
5935.07635	0.00099	5.1×10^{-39}	0 0 0	1 0 1	2 2 0	1 1 1	-0.214
5936.77175	0.00088	5.4×10^{-39}	0 0 0	1 0 1	2 2 1	1 1 0	-0.212
5936.90709	0.00172	3.0×10^{-39}	0 0 0	1 0 1	6 2 5	6 1 6	-0.203
5943.24125	0.00274	2.0×10^{-39}	0 0 0	1 0 1	8 1 7	8 0 8	-0.191

Position	$\sigma_{\text{Pos.}}$	Intensity	$\nu_1 \, \nu_2 \, \nu_3$	$\nu_1' \, \nu_2' \, \nu_3'$	J $\text{K}_a \, \text{K}_c$	J' K_a' K_c'	$\Delta_{\text{SPEC.}}$
5943.41114	0.00124	3.7×10^{-39}	0 0 0	1 0 1	5 2 4	5 1 5	-0.208
5944.02254	0.00051	1.0×10^{-38}	0 0 0	1 0 1	5 1 5	4 0 4	-0.201
5947.38945	0.00054	9.0×10^{-39}	0 0 0	1 0 1	6 0 6	5 1 5	-0.198
5948.82303	0.00117	4.0×10^{-39}	0 0 0	1 0 1	4 2 3	4 1 4	-0.212
5953.12560	0.00129	3.8×10^{-39}	0 0 0	1 0 1	3 2 2	3 1 3	-0.213
5953.41259	0.00052	9.7×10^{-39}	0 0 0	1 0 1	4 1 4	3 0 3	-0.205
5955.57040	0.00167	3.3×10^{-39}	0 0 0	1 0 1	7 1 6	7 0 7	-0.196
5956.18357	0.00158	3.2×10^{-39}	0 0 0	1 0 1	8 2 6	8 1 7	-0.198
5956.32608	0.00307	2.7×10^{-39}	0 0 0	1 0 1	2 2 1	2 1 2	-0.215
5960.17611	0.00154	4.5×10^{-39}	0 0 0	1 0 1	7 2 5	7 1 6	-0.203
5960.96265	0.00172	3.1×10^{-39}	0 0 0	1 0 1	2 2 0	2 1 1	-0.211
5961.28659	0.00060	8.9×10^{-39}	0 0 0	1 0 1	5 0 5	4 1 4	-0.201
5962.04690	0.00102	4.9×10^{-39}	0 0 0	1 0 1	3 2 1	3 1 2	-0.213
5962.41392	0.00091	5.6×10^{-39}	0 0 0	1 0 1	6 2 4	6 1 5	-0.205
5962.89934	0.00056	8.7×10^{-39}	0 0 0	1 0 1	3 1 3	2 0 2	-0.205
5962.93725	0.00092	6.0×10^{-39}	0 0 0	1 0 1	4 2 2	4 1 3	-0.211
5963.20534	0.00075	6.2×10^{-39}	0 0 0	1 0 1	5 2 3	5 1 4	-0.208
5966.23003	0.00129	5.1×10^{-39}	0 0 0	1 0 1	6 1 5	6 0 6	-0.193
5972.71496	0.00069	7.1×10^{-39}	0 0 0	1 0 1	2 1 2	1 0 1	-0.205
5975.04836	0.00067	7.5×10^{-39}	0 0 0	1 0 1	5 1 4	5 0 5	-0.200
5975.24242	0.00062	7.7×10^{-39}	0 0 0	1 0 1	4 0 4	3 1 3	-0.203
5981.91841	0.00054	9.6×10^{-39}	0 0 0	1 0 1	4 1 3	4 0 4	-0.203
5983.01106	0.00103	5.0×10^{-39}	0 0 0	1 0 1	1 1 1	0 0 0	-0.210
5987.01909	0.00058	1.1×10^{-38}	0 0 0	1 0 1	3 1 2	3 0 3	-0.206
5989.00881	0.00093	5.6×10^{-39}	0 0 0	1 0 1	3 0 3	2 1 2	-0.204
5990.56884	0.00052	9.9×10^{-39}	0 0 0	1 0 1	2 1 1	2 0 2	-0.207
5992.79401	0.00069	7.1×10^{-39}	0 0 0	1 0 1	1 1 0	1 0 1	-0.207
6002.15860	0.00392	7.3×10^{-40}	0 0 0	1 0 1	7 2 6	6 3 3	-0.222
6002.30043	0.00139	2.9×10^{-39}	0 0 0	1 0 1	2 0 2	1 1 1	-0.207
6027.02551	0.00071	7.9×10^{-39}	0 0 0	1 0 1	1 0 1	1 1 0	-0.209
6028.18200	0.00047	1.1×10^{-38}	0 0 0	1 0 1	2 0 2	2 1 1	-0.208
6028.93883	0.00110	4.6×10^{-39}	0 0 0	1 0 1	2 1 2	3 0 3	-0.208
6030.11264	0.00047	1.2×10^{-38}	0 0 0	1 0 1	3 0 3	3 1 2	-0.208
6033.02774	0.00048	1.1×10^{-38}	0 0 0	1 0 1	4 0 4	4 1 3	-0.207
6037.07273	0.00105	5.3×10^{-39}	0 0 0	1 0 1	0 0 0	1 1 1	-0.210
6037.13096	0.00064	9.3×10^{-39}	0 0 0	1 0 1	5 0 5	5 1 4	-0.206
6040.80170	0.00078	6.0×10^{-39}	0 0 0	1 0 1	3 1 3	4 0 4	-0.210
6041.49294	0.00135	4.3×10^{-39}	0 0 0	1 0 1	8 1 7	8 2 6	-0.198
6041.82512	0.00088	6.0×10^{-39}	0 0 0	1 0 1	7 1 6	7 2 5	-0.203
6042.49209	0.00208	2.8×10^{-39}	0 0 0	1 0 1	9 1 8	9 2 7	-0.196
6042.54762	0.00087	6.8×10^{-39}	0 0 0	1 0 1	6 0 6	6 1 5	-0.204

Position	$\sigma_{\mathrm{Pos.}}$	Intensity	$\nu_1\ \nu_2\ \nu_3$	$\nu_1'\ \nu_2'\ \nu_3'$	J K_a K_c	J' K_a' K_c'	$\Delta_{\mathrm{SPEC.}}$
6043.30116	0.00082	7.5×10^{-39}	0 0 0	1 0 1	6 1 5	6 2 4	-0.205
6045.65031	0.00066	8.3×10^{-39}	0 0 0	1 0 1	5 1 4	5 2 3	-0.207
6046.58176	0.00075	7.1×10^{-39}	0 0 0	1 0 1	1 0 1	2 1 2	-0.210
6048.52273	0.00064	8.0×10^{-39}	0 0 0	1 0 1	4 1 3	4 2 2	-0.210
6049.24352	0.00129	4.6×10^{-39}	0 0 0	1 0 1	7 0 7	7 1 6	-0.202
6051.50261	0.00074	6.6×10^{-39}	0 0 0	1 0 1	3 1 2	3 2 1	-0.212
6052.29534	0.00080	6.6×10^{-39}	0 0 0	1 0 1	4 1 4	5 0 5	-0.206
6052.43278	0.00326	1.5×10^{-39}	0 0 0	1 0 1	6 2 5	7 1 6	-0.209
6054.16485	0.00149	4.1×10^{-39}	0 0 0	1 0 1	2 1 1	2 2 0	-0.214
6055.07208	0.00067	8.2×10^{-39}	0 0 0	1 0 1	2 0 2	3 1 3	-0.207
6057.00045	0.00207	3.0×10^{-39}	0 0 0	1 0 1	8 0 8	8 1 7	-0.204
6058.80071	0.00147	3.7×10^{-39}	0 0 0	1 0 1	2 1 2	2 2 1	-0.215
6060.41635	0.00096	5.3×10^{-39}	0 0 0	1 0 1	3 1 3	3 2 2	-0.213
6062.59434	0.00113	5.8×10^{-39}	0 0 0	1 0 1	4 1 4	4 2 3	-0.212
6062.68171	0.00068	8.6×10^{-39}	0 0 0	1 0 1	3 0 3	4 1 4	-0.208
6063.11846	0.00093	6.5×10^{-39}	0 0 0	1 0 1	5 1 5	6 0 6	-0.202
6065.20260	0.00207	2.6×10^{-39}	0 0 0	1 0 1	8 2 6	8 3 5	-0.210
6065.34617	0.00106	5.3×10^{-39}	0 0 0	1 0 1	5 1 5	5 2 4	-0.209
6065.46963	0.00336	1.8×10^{-39}	0 0 0	1 0 1	9 0 9	9 1 8	-0.202
6068.66151	0.00104	4.5×10^{-39}	0 0 0	1 0 1	6 1 6	6 2 5	-0.209
6069.63836	0.00065	8.2×10^{-39}	0 0 0	1 0 1	4 0 4	5 1 5	-0.207
6070.64195	0.00131	3.3×10^{-39}	0 0 0	1 0 1	7 2 5	7 3 4	-0.215
6072.52279	0.00153	3.4×10^{-39}	0 0 0	1 0 1	7 1 7	7 2 6	-0.209
6073.21744	0.00084	5.8×10^{-39}	0 0 0	1 0 1	6 1 6	7 0 7	-0.207
6075.37937	0.00151	3.9×10^{-39}	0 0 0	1 0 1	6 2 4	6 3 3	-0.217
6076.22421	0.00072	7.3×10^{-39}	0 0 0	1 0 1	5 0 5	6 1 6	-0.204
6078.87993	0.00083	6.6×10^{-39}	0 0 0	1 0 1	1 1 0	2 2 1	-0.216
6079.16383	0.00128	4.2×10^{-39}	0 0 0	1 0 1	5 2 3	5 3 2	-0.221
6080.58305	0.00082	6.3×10^{-39}	0 0 0	1 0 1	1 1 1	2 2 0	-0.215
6081.38999	0.00240	2.3×10^{-39}	0 0 0	1 0 1	8 2 7	8 3 6	-0.214
6081.53113	0.00172	3.1×10^{-39}	0 0 0	1 0 1	7 2 6	7 3 5	-0.220
6081.94032	0.00132	3.9×10^{-39}	0 0 0	1 0 1	4 2 2	4 3 1	-0.223
6082.00391	0.00144	3.8×10^{-39}	0 0 0	1 0 1	6 2 5	6 3 4	-0.224
6082.49305	0.00094	6.1×10^{-39}	0 0 0	1 0 1	6 0 6	7 1 7	-0.197
6082.52790	0.00115	4.6×10^{-39}	0 0 0	1 0 1	7 1 7	8 0 8	-0.206
6082.71157	0.00121	4.2×10^{-39}	0 0 0	1 0 1	5 2 4	5 3 3	-0.222
6083.53223	0.00147	3.9×10^{-39}	0 0 0	1 0 1	4 2 3	4 3 2	-0.225
6083.81898	0.00198	2.7×10^{-39}	0 0 0	1 0 1	3 2 1	3 3 0	-0.220
6084.36586	0.00218	2.7×10^{-39}	0 0 0	1 0 1	3 2 2	3 3 1	-0.220
6088.08549	0.00089	6.2×10^{-39}	0 0 0	1 0 1	2 1 1	3 2 2	-0.216
6088.91443	0.00122	4.8×10^{-39}	0 0 0	1 0 1	7 0 7	8 1 8	-0.203

Position	$\sigma_{\text{Pos.}}$	Intensity	$\nu_1\,\nu_2\,\nu_3$	ν_1' ν_2' ν_3'	J K_a K_c	J' K_a' K_c'	$\Delta_{\text{SPEC.}}$
6091.11963	0.00150	3.4×10^{-39}	0 0 0	1 0 1	8 1 8	9 0 9	-0.203
6093.41883	0.00134	5.4×10^{-39}	0 0 0	1 0 1	2 1 2	3 2 1	-0.217
6093.86203	0.00839	4.8×10^{-40}	0 0 0	1 0 1	8 0 8	9 0 9	-0.204
6095.32155	0.00551	9.9×10^{-40}	0 0 0	1 0 1	9 3 6	9 4 5	-0.220
6095.35306	0.00181	3.5×10^{-39}	0 0 0	1 0 1	8 0 8	9 1 9	-0.199
6095.77413	0.00824	3.2×10^{-40}	0 0 0	1 0 1	7 2 5	8 2 6	-0.213
6095.96660	0.00754	4.1×10^{-40}	0 0 0	1 0 1	7 1 6	8 1 7	-0.160
6096.19885	0.00090	5.6×10^{-39}	0 0 0	1 0 1	3 1 2	4 2 3	-0.215
6096.50420	0.00991	6.4×10^{-40}	0 0 0	1 0 1	10 3 8	10 4 7	-0.218
6103.10492	0.00437	1.8×10^{-39}	0 0 0	1 0 1	7 3 4	7 4 3	-0.224
6103.24198	0.00151	4.8×10^{-39}	0 0 0	1 0 1	4 1 3	5 2 4	-0.211
6107.40714	0.00155	4.2×10^{-39}	0 0 0	1 0 1	3 1 3	4 2 2	-0.216
6107.94996	0.00260	2.0×10^{-39}	0 0 0	1 0 1	5 3 2	5 4 1	-0.245
6108.08486	0.00245	2.0×10^{-39}	0 0 0	1 0 1	5 3 3	5 4 2	-0.243
6109.25116	0.00169	3.9×10^{-39}	0 0 0	1 0 1	5 1 4	6 2 5	-0.211
6109.61027	0.00373	1.5×10^{-39}	0 0 0	1 0 1	4 3 1	4 4 0	-0.255
6109.65532	0.00341	1.5×10^{-39}	0 0 0	1 0 1	4 3 2	4 4 1	-0.244
6114.04202	0.01772	3.7×10^{-40}	0 0 0	1 0 1	11 0 11	12 0 12	-0.161
6114.31294	0.00215	3.0×10^{-39}	0 0 0	1 0 1	6 1 5	7 2 6	-0.208
6114.48737	0.00703	6.6×10^{-40}	0 0 0	1 0 1	11 0 11	12 1 12	-0.189
6119.08128	0.00068	7.4×10^{-39}	0 0 0	1 0 1	2 2 0	3 3 1	-0.229
6119.19819	0.00067	7.4×10^{-39}	0 0 0	1 0 1	2 2 1	3 3 0	-0.229
6122.89153	0.00250	2.9×10^{-39}	0 0 0	1 0 1	4 1 4	5 2 3	-0.219
6129.32370	0.00086	6.1×10^{-39}	0 0 0	1 0 1	3 2 1	4 3 2	-0.228
6129.91524	0.00081	6.0×10^{-39}	0 0 0	1 0 1	3 2 2	4 3 1	-0.227
6138.84415	0.00127	4.8×10^{-39}	0 0 0	1 0 1	4 2 2	5 3 3	-0.230
6140.18485	0.00240	1.8×10^{-39}	0 0 0	1 0 1	5 1 5	6 2 4	-0.218
6140.62803	0.00114	4.7×10^{-39}	0 0 0	1 0 1	4 2 3	5 3 2	-0.227
6147.39352	0.00409	3.5×10^{-39}	0 0 0	1 0 1	5 2 3	6 3 4	-0.228
6151.53490	0.00148	3.4×10^{-39}	0 0 0	1 0 1	5 2 4	6 3 3	-0.226
6156.21527	0.00205	5.6×10^{-39}	0 0 0	1 0 1	3 3 0	4 4 1	-0.248
6156.21527	0.00205	5.6×10^{-39}	0 0 0	1 0 1	3 3 1	4 4 0	-0.253
6166.30728	0.00126	4.3×10^{-39}	0 0 0	1 0 1	4 3 1	5 4 2	-0.246
6166.34254	0.00133	4.3×10^{-39}	0 0 0	1 0 1	4 3 2	5 4 1	-0.247
6176.02216	0.00154	3.1×10^{-39}	0 0 0	1 0 1	5 3 2	6 4 3	-0.245
6176.16798	0.00145	3.1×10^{-39}	0 0 0	1 0 1	5 3 3	6 4 2	-0.243
6191.08067	0.00152	3.1×10^{-39}	0 0 0	1 0 1	4 4 1	5 5 0	-0.282
6191.08067	0.00151	3.1×10^{-39}	0 0 0	1 0 1	4 4 0	5 5 1	-0.282
6242.57919	0.01116	5.8×10^{-40}	0 0 0	1 0 1	7 5 2	8 6 3	-0.135
6242.61196	0.01712	5.8×10^{-40}	0 0 0	1 0 1	7 5 3	8 6 2	-0.103

A.2.1.6 HTO $2\nu_2 + \nu_3$ band

Here, the lines assigned to the $2\nu_2 + \nu_3$ band obtained from the $1\,\mathrm{GBq}$ sample are presented. These lines are published in [Her21]. For further information, see Section 5.5.1.

Table A.7: Linelist of the $2\nu_2 + \nu_3$ band. The columns present the assigned line position, the uncertainty on the position $\sigma_{\mathrm{Pos.}}$, the line intensity taking natural abundance into account, lower and upper vibrational quanta, lower and upper rotational quanta and the deviation to the predictions from SPECTRA database $\Delta_{\mathrm{SPEC.}}$.

Position	$\sigma_{\mathrm{Pos.}}$	Intensity	$\nu_1\,\nu_2\,\nu_3$	$\nu_1'\,\nu_2'\,\nu_3'$	J $\mathrm{K}_a\,\mathrm{K}_c$	J' $\mathrm{K}_a'\,\mathrm{K}_c'$	$\Delta_{\mathrm{SPEC.}}$
6238.77199	0.00640	4.2×10^{-40}	0 0 0	0 2 1	3 2 2	2 1 1	-0.002
6238.94922	0.00159	3.1×10^{-39}	0 0 0	0 2 1	7 0 7	6 0 6	0.005
6239.88094	0.00155	3.0×10^{-39}	0 0 0	0 2 1	7 1 6	6 1 5	-0.006
6242.32758	0.00168	3.0×10^{-39}	0 0 0	0 2 1	7 1 7	6 1 6	0.000
6249.49748	0.00124	4.1×10^{-39}	0 0 0	0 2 1	6 0 6	5 0 5	0.002
6250.48136	0.00131	3.9×10^{-39}	0 0 0	0 2 1	6 1 5	5 1 4	-0.005
6253.88215	0.00136	3.8×10^{-39}	0 0 0	0 2 1	6 1 6	5 1 5	-0.002
6259.67562	0.00391	1.1×10^{-39}	0 0 0	0 2 1	6 0 6	5 1 5	0.001
6260.03743	0.00097	4.9×10^{-39}	0 0 0	0 2 1	5 0 5	4 0 4	0.001
6260.52615	0.00468	8.9×10^{-40}	0 0 0	0 2 1	4 1 4	3 0 3	-0.000
6261.20222	0.00181	2.6×10^{-39}	0 0 0	0 2 1	6 2 4	5 2 3	-0.029
6261.41510	0.00123	4.6×10^{-39}	0 0 0	0 2 1	5 1 4	4 1 3	-0.008
6263.57145	0.00208	2.8×10^{-39}	0 0 0	0 2 1	6 2 5	5 2 4	-0.029
6265.30580	0.00132	4.4×10^{-39}	0 0 0	0 2 1	5 1 5	4 1 4	-0.006
6270.73204	0.00087	5.3×10^{-39}	0 0 0	0 2 1	4 0 4	3 0 3	0.001
6272.68285	0.00101	4.8×10^{-39}	0 0 0	0 2 1	4 1 3	3 1 2	-0.010
6273.48856	0.00166	3.1×10^{-39}	0 0 0	0 2 1	5 2 3	4 2 2	-0.031
6274.91995	0.00145	3.1×10^{-39}	0 0 0	0 2 1	5 2 4	4 2 3	-0.032
6276.62089	0.00111	4.6×10^{-39}	0 0 0	0 2 1	4 1 4	3 1 3	-0.008
6281.68579	0.00100	5.1×10^{-39}	0 0 0	0 2 1	3 0 3	2 0 2	-0.000
6284.27487	0.00131	4.4×10^{-39}	0 0 0	0 2 1	3 1 2	2 1 1	-0.009
6285.53854	0.00204	3.0×10^{-39}	0 0 0	0 2 1	4 2 2	3 2 1	-0.036
6286.35343	0.00246	3.0×10^{-39}	0 0 0	0 2 1	4 2 3	3 2 2	-0.034
6287.83178	0.00110	4.2×10^{-39}	0 0 0	0 2 1	3 1 3	2 1 2	-0.011
6292.92235	0.00112	4.1×10^{-39}	0 0 0	0 2 1	2 0 2	1 0 1	-0.002
6296.16708	0.00210	2.9×10^{-39}	0 0 0	0 2 1	2 1 1	1 1 0	-0.012
6298.93882	0.00184	2.8×10^{-39}	0 0 0	0 2 1	2 1 2	1 1 1	-0.013
6319.01814	0.00182	3.4×10^{-39}	0 0 0	0 2 1	1 1 0	1 1 1	-0.014
6322.58169	0.00182	3.2×10^{-39}	0 0 0	0 2 1	1 1 1	1 1 0	-0.017
6332.14632	0.00198	3.1×10^{-39}	0 0 0	0 2 1	3 2 1	3 2 2	-0.036
6332.58825	0.00103	5.2×10^{-39}	0 0 0	0 2 1	2 2 0	2 2 1	-0.037
6332.86657	0.00106	5.1×10^{-39}	0 0 0	0 2 1	2 2 1	2 2 0	-0.040

Position	$\sigma_{\text{Pos.}}$	Intensity	$\nu_1\ \nu_2\ \nu_3$	$\nu_1'\ \nu_2'\ \nu_3'$	J K_a K_c	J' K_a' K_c'	$\Delta_{\text{SPEC.}}$
6333.51346	0.00197	2.9×10^{-39}	0 0 0	0 2 1	3 2 2	3 2 1	-0.040
6339.25941	0.00110	4.7×10^{-39}	0 0 0	0 2 1	1 0 1	2 0 2	-0.005
6341.92001	0.00147	3.4×10^{-39}	0 0 0	0 2 1	1 1 1	2 1 2	-0.014
6346.27019	0.00191	3.2×10^{-39}	0 0 0	0 2 1	1 1 0	2 1 1	-0.016
6349.06134	0.00501	1.0×10^{-39}	0 0 0	0 2 1	6 3 3	6 3 4	-0.057
6349.31160	0.00331	1.7×10^{-39}	0 0 0	0 2 1	5 3 2	5 3 3	-0.056
6349.42689	0.00190	2.7×10^{-39}	0 0 0	0 2 1	4 3 1	4 3 2	-0.064
6349.50489	0.01294	2.7×10^{-39}	0 0 0	0 2 1	4 3 2	4 3 1	-0.059
6349.50489	0.00903	4.4×10^{-39}	0 0 0	0 2 1	3 3 0	3 3 1	-0.062
6349.50489	0.00902	4.4×10^{-39}	0 0 0	0 2 1	3 3 1	3 3 0	-0.073
6349.60068	0.00323	1.7×10^{-39}	0 0 0	0 2 1	5 3 3	5 3 2	-0.062
6350.56053	0.00075	6.4×10^{-39}	0 0 0	0 2 1	2 0 2	3 0 3	-0.005
6352.14354	0.00100	5.5×10^{-39}	0 0 0	0 2 1	2 1 2	3 1 3	-0.014
6359.23769	0.00098	5.1×10^{-39}	0 0 0	0 2 1	2 1 1	3 1 2	-0.017
6361.43154	0.00086	7.2×10^{-39}	0 0 0	0 2 1	3 0 3	4 0 4	-0.007
6362.08701	0.00081	6.8×10^{-39}	0 0 0	0 2 1	3 1 3	4 1 4	-0.013
6367.52908	0.00230	2.6×10^{-39}	0 0 0	0 2 1	2 2 1	3 2 2	-0.042
6370.93282	0.00534	9.5×10^{-40}	0 0 0	0 2 1	6 4 2	6 4 3	-0.097
6370.95272	0.00550	9.5×10^{-40}	0 0 0	0 2 1	6 4 3	6 4 2	-0.095
6371.05888	0.01129	1.6×10^{-39}	0 0 0	0 2 1	5 4 1	5 4 2	-0.094
6371.06268	0.01158	1.6×10^{-39}	0 0 0	0 2 1	5 4 2	5 4 1	-0.093
6371.17676	0.00163	2.5×10^{-39}	0 0 0	0 2 1	4 4 0	4 4 1	-0.096
6371.17676	0.00163	2.5×10^{-39}	0 0 0	0 2 1	4 4 1	4 4 0	-0.097
6371.71555	0.00087	7.1×10^{-39}	0 0 0	0 2 1	4 1 4	5 1 5	-0.012
6371.74881	0.00085	7.4×10^{-39}	0 0 0	0 2 1	4 0 4	5 0 5	-0.004
6372.26466	0.00082	5.9×10^{-39}	0 0 0	0 2 1	3 1 2	4 1 3	-0.019
6379.03097	0.05125	5.5×10^{-40}	0 0 0	0 2 1	3 1 2	3 2 1	-0.032
6379.03096	0.00733	4.0×10^{-39}	0 0 0	0 2 1	3 2 2	4 2 3	-0.041
6380.73879	0.00164	3.7×10^{-39}	0 0 0	0 2 1	3 2 1	4 2 2	-0.045
6381.00422	0.00089	6.7×10^{-39}	0 0 0	0 2 1	5 1 5	6 1 6	-0.010
6381.45269	0.00093	6.8×10^{-39}	0 0 0	0 2 1	5 0 5	6 0 6	-0.005
6385.26525	0.00084	6.0×10^{-39}	0 0 0	0 2 1	4 1 3	5 1 4	-0.017
6389.93317	0.00083	5.9×10^{-39}	0 0 0	0 2 1	6 1 6	7 1 7	-0.009
6390.42628	0.00109	4.5×10^{-39}	0 0 0	0 2 1	4 2 3	5 2 4	-0.039
6390.60412	0.00089	5.9×10^{-39}	0 0 0	0 2 1	6 0 6	7 0 7	-0.004
6393.49631	0.00157	3.9×10^{-39}	0 0 0	0 2 1	4 2 2	5 2 3	-0.040
6398.12028	0.00127	5.4×10^{-39}	0 0 0	0 2 1	5 1 4	6 1 5	-0.015
6398.50630	0.00150	4.7×10^{-39}	0 0 0	0 2 1	7 1 7	8 1 8	-0.010
6399.63607	0.00129	4.3×10^{-39}	0 0 0	0 2 1	7 0 7	8 0 8	0.006
6401.67666	0.00122	4.4×10^{-39}	0 0 0	0 2 1	5 2 4	6 2 5	-0.037
6406.64071	0.00161	3.5×10^{-39}	0 0 0	0 2 1	8 1 8	9 1 9	-0.002

Position	$\sigma_{\text{Pos.}}$	Intensity	$\nu_1\,\nu_2\,\nu_3$	$\nu_1{}'\,\nu_2{}'\,\nu_3{}'$	J K_a K_c	J' $K_a{}'$ $K_c{}'$	$\Delta_{\text{SPEC.}}$
6406.69380	0.00186	3.4×10^{-39}	0 0 0	0 2 1	8 0 8	9 0 9	0.013
6408.72107	0.00187	2.8×10^{-39}	0 0 0	0 2 1	5 2 3	6 2 4	-0.059
6410.67993	0.00145	4.4×10^{-39}	0 0 0	0 2 1	6 1 5	7 1 6	-0.016
6412.74639	0.00186	3.8×10^{-39}	0 0 0	0 2 1	6 2 5	7 2 6	-0.034
6421.31707	0.00195	3.3×10^{-39}	0 0 0	0 2 1	6 2 4	7 2 5	-0.043
6422.78391	0.00147	3.3×10^{-39}	0 0 0	0 2 1	7 1 6	8 1 7	-0.013
6423.60359	0.00197	3.0×10^{-39}	0 0 0	0 2 1	7 2 6	8 2 7	-0.034
6434.99560	0.00171	2.6×10^{-39}	0 0 0	0 2 1	7 2 5	8 2 6	-0.039

A.2.2 Linelists of DTO

A.2.2.1 DTO ν_3 band

Here, the lines assigned to the ν_3 band of DTO obtained from the $1\,\text{GBq}$ sample are presented. These lines are published in [Rei20]. For further information, see Section 5.5.2.

Table A.8: Linelist of the DTO ν_3 band. The columns present the assigned line position, the uncertainty on the position $\sigma_{\text{Pos.}}$, the line intensity taking natural abundance into account, lower and upper vibrational quanta, lower and upper rotational quanta and the deviation to the predictions from SPECTRA database $\Delta_{\text{SPEC.}}$.

Position	$\sigma_{\text{Pos.}}$	Intensity	$\nu_1\,\nu_2\,\nu_3$	$\nu_1{}'\,\nu_2{}'\,\nu_3{}'$	J K_a K_c	J' $K_a{}'$ $K_c{}'$	$\Delta_{\text{SPEC.}}$
2574.83706	0.00508	1.2×10^{-41}	0 0 0	0 0 1	6 6 0	5 5 1	-0.028
2574.84771	0.00519	1.2×10^{-41}	0 0 0	0 0 1	6 6 1	5 5 0	-0.017
2584.36989	0.00267	1.2×10^{-41}	0 0 0	0 0 1	7 5 2	6 4 3	-0.034
2584.49632	0.00351	1.2×10^{-41}	0 0 0	0 0 1	7 5 3	6 4 2	-0.018
2594.41678	0.00398	1.5×10^{-41}	0 0 0	0 0 1	6 5 1	5 4 2	-0.017
2594.43775	0.00409	1.5×10^{-41}	0 0 0	0 0 1	6 5 2	5 4 1	-0.019
2602.97077	0.00569	1.3×10^{-41}	0 0 0	0 0 1	7 4 3	6 3 4	-0.007
2604.43362	0.00661	1.9×10^{-41}	0 0 0	0 0 1	5 5 0	4 4 1	-0.019
2604.42045	0.00615	1.9×10^{-41}	0 0 0	0 0 1	5 5 1	4 4 0	-0.035
2606.86787	0.00351	1.5×10^{-41}	0 0 0	0 0 1	12 3 9	11 3 8	0.001
2609.85588	0.00416	1.1×10^{-41}	0 0 0	0 0 1	12 4 9	11 4 8	-0.007
2613.50660	0.00348	1.7×10^{-41}	0 0 0	0 0 1	6 4 2	5 3 3	-0.016
2613.94837	0.00561	1.8×10^{-41}	0 0 0	0 0 1	12 2 10	11 2 9	0.004
2614.34668	0.00526	1.7×10^{-41}	0 0 0	0 0 1	6 4 3	5 3 2	-0.011
2614.43943	0.01133	1.5×10^{-41}	0 0 0	0 0 1	13 1 12	12 1 11	-0.002
2614.55511	0.00377	1.5×10^{-41}	0 0 0	0 0 1	13 2 12	12 2 11	0.001
2614.73436	0.00467	1.6×10^{-41}	0 0 0	0 0 1	14 0 14	13 0 13	0.001
2614.73436	0.00468	1.6×10^{-41}	0 0 0	0 0 1	14 1 14	13 1 13	-0.000
2615.67543	0.00562	1.7×10^{-41}	0 0 0	0 0 1	12 3 10	11 3 9	-0.002

Position	$\sigma_{\text{Pos.}}$	Intensity	$\nu_1\,\nu_2\,\nu_3$	$\nu_1'\,\nu_2'\,\nu_3'$	J K$_a$ K$_c$	J' K$_a$' K$_c$'	$\Delta_{\text{SPEC.}}$
2615.78839	0.00558	1.1×10^{-41}	0 0 0	0 0 1	11 5 6	10 5 5	-0.013
2616.22370	0.00584	1.1×10^{-41}	0 0 0	0 0 1	11 5 7	10 5 6	-0.017
2616.76255	0.00720	1.8×10^{-41}	0 0 0	0 0 1	11 4 7	10 4 6	-0.007
2617.20225	0.00235	2.5×10^{-41}	0 0 0	0 0 1	11 3 8	10 3 7	-0.000
2619.91667	0.00422	1.8×10^{-41}	0 0 0	0 0 1	11 4 8	10 4 7	-0.008
2622.75781	0.00194	3.0×10^{-41}	0 0 0	0 0 1	11 2 9	10 2 8	0.002
2623.31773	0.00196	2.5×10^{-41}	0 0 0	0 0 1	12 1 11	11 1 10	-0.001
2623.53178	0.00236	2.4×10^{-41}	0 0 0	0 0 1	12 2 11	11 2 10	-0.007
2623.63996	0.02110	2.4×10^{-41}	0 0 0	0 0 1	13 0 13	12 0 12	-0.009
2623.64892	0.01428	2.4×10^{-41}	0 0 0	0 0 1	13 1 13	12 1 12	-0.003
2623.69914	0.00568	2.1×10^{-41}	0 0 0	0 0 1	5 4 1	4 3 2	-0.019
2623.92615	0.00243	2.1×10^{-41}	0 0 0	0 0 1	5 4 2	4 3 1	-0.004
2625.08250	0.00211	2.6×10^{-41}	0 0 0	0 0 1	11 3 9	10 3 8	-0.001
2626.44578	0.00355	1.6×10^{-41}	0 0 0	0 0 1	10 5 5	9 5 4	-0.010
2626.64072	0.00335	1.6×10^{-41}	0 0 0	0 0 1	10 5 6	9 5 5	-0.012
2627.96513	0.00151	3.8×10^{-41}	0 0 0	0 0 1	10 3 7	9 3 6	0.003
2628.10918	0.00500	1.4×10^{-41}	0 0 0	0 0 1	6 3 3	5 2 4	-0.011
2628.14816	0.00345	2.7×10^{-41}	0 0 0	0 0 1	10 4 6	9 4 5	-0.007
2630.09429	0.00200	2.6×10^{-41}	0 0 0	0 0 1	10 4 7	9 4 6	-0.004
2631.83146	0.00114	4.6×10^{-41}	0 0 0	0 0 1	10 2 8	9 2 7	0.003
2631.97043	0.00460	1.3×10^{-41}	0 0 0	0 0 1	7 3 5	6 2 4	-0.007
2632.08390	0.00143	3.8×10^{-41}	0 0 0	0 0 1	11 1 10	10 1 9	-0.001
2632.49203	0.01471	1.3×10^{-41}	0 0 0	0 0 1	12 1 12	11 0 11	0.007
2632.48211	0.00364	3.7×10^{-41}	0 0 0	0 0 1	11 2 10	10 2 9	-0.013
2632.50607	0.00279	3.8×10^{-41}	0 0 0	0 0 1	12 0 12	11 0 11	0.007
2632.49203	0.00635	3.8×10^{-41}	0 0 0	0 0 1	12 1 12	11 1 11	-0.015
2632.49203	0.01475	1.3×10^{-41}	0 0 0	0 0 1	12 0 12	11 1 11	-0.030
2633.74115	0.00260	2.6×10^{-41}	0 0 0	0 0 1	4 4 0	3 3 1	-0.015
2633.77117	0.00244	2.6×10^{-41}	0 0 0	0 0 1	4 4 1	3 3 0	-0.015
2634.60265	0.00128	3.9×10^{-41}	0 0 0	0 0 1	10 3 8	9 3 7	-0.002
2636.94197	0.00249	2.1×10^{-41}	0 0 0	0 0 1	9 5 4	8 5 3	-0.013
2637.01738	0.00242	2.1×10^{-41}	0 0 0	0 0 1	9 5 5	8 5 4	-0.015
2638.05187	0.00340	1.6×10^{-41}	0 0 0	0 0 1	6 3 4	5 2 3	-0.008
2639.00990	0.00424	1.3×10^{-41}	0 0 0	0 0 1	10 2 9	9 1 8	-0.000
2639.08500	0.00092	5.4×10^{-41}	0 0 0	0 0 1	9 3 6	8 3 5	0.001
2639.29571	0.00142	3.6×10^{-41}	0 0 0	0 0 1	9 4 5	8 4 4	-0.006
2640.34565	0.00122	3.6×10^{-41}	0 0 0	0 0 1	9 4 6	8 4 5	-0.008
2640.72280	0.00418	5.6×10^{-41}	0 0 0	0 0 1	10 1 9	9 1 8	-0.001
2640.76211	0.00920	1.9×10^{-41}	0 0 0	0 0 1	5 3 2	4 2 3	-0.007
2641.25039	0.00865	1.8×10^{-41}	0 0 0	0 0 1	11 1 11	10 0 10	-0.002
2641.28076	0.00238	5.6×10^{-41}	0 0 0	0 0 1	11 0 11	10 0 10	-0.002

Position	$\sigma_{\mathrm{Pos.}}$	Intensity	$\nu_1\,\nu_2\,\nu_3$	$\nu_1\text{'}\,\nu_2\text{'}\,\nu_3\text{'}$	J K_a K_c	J' $\mathrm{K}_a\text{'}$ $\mathrm{K}_c\text{'}$	$\Delta_{\mathrm{SPEC.}}$
2641.29727	0.00083	5.6×10^{-41}	0 0 0	0 0 1	11 1 11	10 1 10	-0.002
2641.32000	0.00168	6.7×10^{-41}	0 0 0	0 0 1	9 2 7	8 2 6	0.001
2641.32874	0.01065	1.8×10^{-41}	0 0 0	0 0 1	11 0 11	10 1 10	-0.002
2641.44605	0.00215	5.5×10^{-41}	0 0 0	0 0 1	10 2 9	9 2 8	-0.002
2643.15835	0.00510	1.2×10^{-41}	0 0 0	0 0 1	10 1 9	9 2 8	-0.003
2643.27888	0.00726	1.1×10^{-41}	0 0 0	0 0 1	8 6 2	7 6 1	-0.021
2643.27888	0.00726	1.1×10^{-41}	0 0 0	0 0 1	8 6 3	7 6 2	-0.022
2644.25814	0.00096	5.5×10^{-41}	0 0 0	0 0 1	9 3 7	8 3 6	-0.004
2645.24823	0.00292	2.0×10^{-41}	0 0 0	0 0 1	5 3 3	4 2 2	-0.010
2646.26502	0.00346	1.6×10^{-41}	0 0 0	0 0 1	9 2 8	8 1 7	-0.001
2647.31866	0.00222	2.5×10^{-41}	0 0 0	0 0 1	8 5 3	7 5 2	-0.014
2647.34457	0.00223	2.5×10^{-41}	0 0 0	0 0 1	8 5 4	7 5 3	-0.014
2649.24763	0.00101	7.9×10^{-41}	0 0 0	0 0 1	9 1 8	8 1 7	-0.000
2649.93078	0.00206	2.5×10^{-41}	0 0 0	0 0 1	10 1 10	9 0 9	-0.000
2649.99189	0.00081	7.9×10^{-41}	0 0 0	0 0 1	10 0 10	9 0 9	-0.002
2650.02883	0.00102	7.9×10^{-41}	0 0 0	0 0 1	10 1 10	9 1 9	-0.002
2650.09259	0.00220	2.5×10^{-41}	0 0 0	0 0 1	10 0 10	9 1 9	-0.001
2650.14630	0.00116	4.6×10^{-41}	0 0 0	0 0 1	8 4 4	7 4 3	-0.009
2650.42679	0.00461	7.6×10^{-41}	0 0 0	0 0 1	9 2 8	8 2 7	-0.002
2650.42946	0.00491	7.1×10^{-41}	0 0 0	0 0 1	8 3 5	7 3 4	-0.003
2650.63956	0.00091	4.5×10^{-41}	0 0 0	0 0 1	8 4 5	7 4 4	-0.009
2651.27775	0.00055	9.2×10^{-41}	0 0 0	0 0 1	8 2 6	7 2 5	-0.000
2652.05197	0.00349	2.3×10^{-41}	0 0 0	0 0 1	4 3 1	3 2 2	-0.015
2652.81139	0.00332	1.9×10^{-41}	0 0 0	0 0 1	8 2 7	7 1 6	-0.004
2653.41446	0.00471	1.5×10^{-41}	0 0 0	0 0 1	9 1 8	8 2 7	0.003
2653.59083	0.00249	2.4×10^{-41}	0 0 0	0 0 1	4 3 2	3 2 1	-0.011
2654.05510	0.00076	7.1×10^{-41}	0 0 0	0 0 1	8 3 6	7 3 5	-0.005
2657.59730	0.00713	2.5×10^{-41}	0 0 0	0 0 1	7 5 2	6 5 1	-0.013
2657.59407	0.00717	2.5×10^{-41}	0 0 0	0 0 1	7 5 3	6 5 2	-0.023
2657.74837	0.00052	1.1×10^{-40}	0 0 0	0 0 1	8 1 7	7 1 6	-0.003
2658.49478	0.00164	3.1×10^{-41}	0 0 0	0 0 1	9 1 9	8 0 8	-0.003
2658.62334	0.00048	1.1×10^{-40}	0 0 0	0 0 1	9 0 9	8 0 8	-0.003
2658.70071	0.00048	1.1×10^{-40}	0 0 0	0 0 1	9 1 9	8 1 8	-0.004
2658.76952	0.00254	2.1×10^{-41}	0 0 0	0 0 1	7 2 6	6 1 5	-0.005
2658.83023	0.00169	3.1×10^{-41}	0 0 0	0 0 1	9 0 9	8 1 8	-0.003
2659.46738	0.00057	9.9×10^{-41}	0 0 0	0 0 1	8 2 7	7 2 6	-0.006
2660.73256	0.00096	5.2×10^{-41}	0 0 0	0 0 1	7 4 3	6 4 2	-0.011
2660.92763	0.00094	5.2×10^{-41}	0 0 0	0 0 1	7 4 4	6 4 3	-0.012
2661.67542	0.00044	1.2×10^{-40}	0 0 0	0 0 1	7 2 5	6 2 4	-0.002
2661.77237	0.00061	8.6×10^{-41}	0 0 0	0 0 1	7 3 4	6 3 3	-0.006
2662.51426	0.00750	1.1×10^{-41}	0 0 0	0 0 1	4 2 2	3 1 3	-0.010

Position	$\sigma_{\text{Pos.}}$	Intensity	$\nu_1\,\nu_2\,\nu_3$	$\nu_1'\,\nu_2'\,\nu_3'$	J K_a K_c	J' K_a' K_c'	$\Delta_{\text{SPEC.}}$
2662.52939	0.00296	2.7×10^{-41}	0 0 0	0 0 1	3 3 0	2 2 1	-0.017
2662.83469	0.00234	2.7×10^{-41}	0 0 0	0 0 1	3 3 1	2 2 0	-0.018
2663.98069	0.00062	8.5×10^{-41}	0 0 0	0 0 1	7 3 5	6 3 4	-0.007
2664.40779	0.00346	1.7×10^{-41}	0 0 0	0 0 1	8 1 7	7 2 6	-0.002
2664.47725	0.00254	2.2×10^{-41}	0 0 0	0 0 1	6 2 5	5 1 4	-0.008
2666.42431	0.00039	1.4×10^{-40}	0 0 0	0 0 1	7 1 6	6 1 5	-0.004
2666.90632	0.00142	3.7×10^{-41}	0 0 0	0 0 1	8 1 8	7 0 7	-0.003
2667.16510	0.00059	1.4×10^{-40}	0 0 0	0 0 1	8 0 8	7 0 7	-0.005
2667.32391	0.00038	1.3×10^{-40}	0 0 0	0 0 1	8 1 8	7 1 7	-0.005
2667.58346	0.00141	3.7×10^{-41}	0 0 0	0 0 1	8 0 8	7 1 7	-0.005
2667.78275	0.00479	1.8×10^{-41}	0 0 0	0 0 1	6 5 1	5 5 0	-0.018
2667.78275	0.00479	1.8×10^{-41}	0 0 0	0 0 1	6 5 2	5 5 1	-0.019
2668.62103	0.00042	1.2×10^{-40}	0 0 0	0 0 1	7 2 6	6 2 5	0.003
2670.37188	0.00282	2.2×10^{-41}	0 0 0	0 0 1	5 2 4	4 1 3	-0.005
2671.11069	0.00106	5.0×10^{-41}	0 0 0	0 0 1	6 4 2	5 4 1	-0.013
2671.17399	0.00105	5.0×10^{-41}	0 0 0	0 0 1	6 4 3	5 4 2	-0.013
2672.44811	0.00040	1.4×10^{-40}	0 0 0	0 0 1	6 2 4	5 2 3	-0.003
2672.87372	0.00057	9.3×10^{-41}	0 0 0	0 0 1	6 3 3	5 3 2	-0.009
2674.00562	0.00192	9.3×10^{-41}	0 0 0	0 0 1	6 3 4	5 3 3	-0.009
2675.09446	0.00155	4.2×10^{-41}	0 0 0	0 0 1	7 1 7	6 0 6	-0.001
2675.48479	0.00032	1.6×10^{-40}	0 0 0	0 0 1	6 1 5	5 1 4	-0.004
2675.60234	0.00032	1.6×10^{-40}	0 0 0	0 0 1	7 0 7	6 0 6	-0.006
2675.91207	0.00032	1.6×10^{-40}	0 0 0	0 0 1	7 1 7	6 1 6	-0.006
2676.26786	0.00258	1.7×10^{-41}	0 0 0	0 0 1	7 1 6	6 2 5	-0.003
2676.42639	0.00122	4.2×10^{-41}	0 0 0	0 0 1	7 0 7	6 1 6	-0.003
2676.79336	0.00278	2.3×10^{-41}	0 0 0	0 0 1	4 2 3	3 1 2	-0.011
2677.33831	0.00399	1.6×10^{-41}	0 0 0	0 0 1	3 2 1	2 1 2	-0.012
2677.88060	0.00040	1.4×10^{-40}	0 0 0	0 0 1	6 2 5	5 2 4	-0.007
2681.33547	0.00227	3.6×10^{-41}	0 0 0	0 0 1	5 4 1	4 4 0	-0.013
2681.34549	0.00230	3.6×10^{-41}	0 0 0	0 0 1	5 4 2	4 4 1	-0.017
2682.95028	0.00123	4.4×10^{-41}	0 0 0	0 0 1	6 1 6	5 0 5	-0.006
2683.18383	0.00520	1.1×10^{-41}	0 0 0	0 0 1	7 3 5	7 2 6	-0.010
2683.48829	0.00038	1.4×10^{-40}	0 0 0	0 0 1	5 2 3	4 2 2	-0.006
2683.61662	0.00063	8.7×10^{-41}	0 0 0	0 0 1	5 3 2	4 3 1	-0.010
2683.92755	0.00030	1.9×10^{-40}	0 0 0	0 0 1	6 0 6	5 0 5	-0.005
2683.97815	0.00335	2.2×10^{-41}	0 0 0	0 0 1	3 2 2	2 1 1	-0.007
2684.08376	0.00063	8.7×10^{-41}	0 0 0	0 0 1	5 3 3	4 3 2	-0.010
2684.48945	0.00029	1.8×10^{-40}	0 0 0	0 0 1	6 1 6	5 1 5	-0.006
2685.02087	0.00029	1.8×10^{-40}	0 0 0	0 0 1	5 1 4	4 1 3	-0.004
2685.46653	0.00125	4.3×10^{-41}	0 0 0	0 0 1	6 0 6	5 1 5	-0.006
2686.60443	0.00377	1.3×10^{-41}	0 0 0	0 0 1	6 3 4	6 2 5	-0.008

Position	$\sigma_{\text{Pos.}}$	Intensity	$\nu_1\ \nu_2\ \nu_3$	$\nu_1'\ \nu_2'\ \nu_3'$	J K_a K_c	J' K_a' K_c'	$\Delta_{\text{SPEC.}}$
2687.28777	0.00039	1.4×10^{-40}	0 0 0	0 0 1	5 2 4	4 2 3	-0.008
2688.88744	0.00418	1.5×10^{-41}	0 0 0	0 0 1	6 1 5	5 2 4	-0.003
2689.03316	0.00398	1.4×10^{-41}	0 0 0	0 0 1	5 3 3	5 2 4	-0.014
2689.44450	0.00533	1.1×10^{-41}	0 0 0	0 0 1	6 2 5	6 1 6	-0.009
2689.95662	0.00485	1.9×10^{-41}	0 0 0	0 0 1	2 2 0	1 1 1	-0.014
2690.39599	0.00325	4.3×10^{-41}	0 0 0	0 0 1	5 1 5	4 0 4	-0.007
2690.60943	0.01070	1.3×10^{-41}	0 0 0	0 0 1	4 3 2	4 2 3	-0.022
2692.01084	0.00268	2.2×10^{-41}	0 0 0	0 0 1	2 2 1	1 1 0	-0.010
2692.17327	0.00027	2.0×10^{-40}	0 0 0	0 0 1	5 0 5	4 0 4	-0.007
2693.08522	0.00028	1.9×10^{-40}	0 0 0	0 0 1	5 1 5	4 1 4	-0.007
2694.01765	0.00089	5.9×10^{-41}	0 0 0	0 0 1	4 3 1	3 3 0	-0.013
2694.16120	0.00093	5.9×10^{-41}	0 0 0	0 0 1	4 3 2	3 3 1	-0.012
2694.27353	0.00477	1.4×10^{-41}	0 0 0	0 0 1	4 3 1	4 2 2	-0.014
2694.59778	0.00042	1.3×10^{-40}	0 0 0	0 0 1	4 2 2	3 2 1	-0.008
2694.86336	0.00135	4.0×10^{-41}	0 0 0	0 0 1	5 0 5	4 1 4	-0.006
2694.98619	0.00030	1.8×10^{-40}	0 0 0	0 0 1	4 1 3	3 1 2	-0.006
2695.54122	0.00572	1.4×10^{-41}	0 0 0	0 0 1	5 2 4	5 1 5	-0.010
2696.42587	0.00305	1.6×10^{-41}	0 0 0	0 0 1	5 3 2	5 2 3	-0.017
2696.82757	0.00046	1.3×10^{-40}	0 0 0	0 0 1	4 2 3	3 2 2	-0.009
2697.46813	0.00149	3.8×10^{-41}	0 0 0	0 0 1	4 1 4	3 0 3	-0.007
2698.86165	0.00262	1.6×10^{-41}	0 0 0	0 0 1	6 3 3	6 2 4	-0.008
2699.04462	0.00480	1.2×10^{-41}	0 0 0	0 0 1	8 2 6	8 1 7	-0.002
2699.62318	0.00661	1.3×10^{-41}	0 0 0	0 0 1	6 1 5	6 0 6	-0.012
2700.44881	0.00490	1.2×10^{-41}	0 0 0	0 0 1	6 1 5	6 1 6	-0.008
2700.48382	0.00029	2.0×10^{-40}	0 0 0	0 0 1	4 0 4	3 0 3	-0.007
2700.65606	0.00357	1.5×10^{-41}	0 0 0	0 0 1	4 2 3	4 1 4	-0.017
2700.78102	0.00348	1.5×10^{-41}	0 0 0	0 0 1	7 3 4	7 2 5	-0.009
2701.37112	0.00424	1.2×10^{-41}	0 0 0	0 0 1	8 3 5	8 2 6	-0.009
2701.73383	0.00049	1.9×10^{-40}	0 0 0	0 0 1	4 1 4	3 1 3	-0.007
2701.94346	0.00639	1.1×10^{-41}	0 0 0	0 0 1	5 1 4	4 2 3	-0.000
2704.43495	0.00209	3.1×10^{-41}	0 0 0	0 0 1	3 1 3	2 0 2	-0.012
2704.74776	0.00619	1.5×10^{-41}	0 0 0	0 0 1	3 2 2	3 1 3	-0.001
2704.74776	0.00295	3.3×10^{-41}	0 0 0	0 0 1	4 0 4	3 1 3	-0.009
2705.27042	0.00035	1.5×10^{-40}	0 0 0	0 0 1	3 1 2	2 1 1	-0.007
2705.49039	0.00066	8.5×10^{-41}	0 0 0	0 0 1	3 2 1	2 2 0	-0.009
2706.22367	0.00200	1.8×10^{-41}	0 0 0	0 0 1	7 2 5	7 1 6	-0.012
2706.48156	0.00067	8.5×10^{-41}	0 0 0	0 0 1	3 2 2	2 2 1	-0.009
2707.75348	0.00650	1.0×10^{-41}	0 0 0	0 0 1	2 2 1	2 1 2	-0.010
2708.65501	0.00315	1.9×10^{-41}	0 0 0	0 0 1	5 1 4	5 0 5	-0.005
2709.09710	0.00032	1.8×10^{-40}	0 0 0	0 0 1	3 0 3	2 0 2	-0.008
2710.20273	0.00389	1.6×10^{-41}	0 0 0	0 0 1	5 1 4	5 1 5	0.003

Position	$\sigma_{\mathrm{Pos.}}$	Intensity	$\nu_1\,\nu_2\,\nu_3$	ν_1'$\,\nu_2$'$\,\nu_3$'	J K$_a$ K$_c$	J' K$_a$' K$_c$'	$\Delta_{\mathrm{SPEC.}}$
2710.45755	0.00036	1.6×10^{-40}	0 0 0	0 0 1	3 1 3	2 1 2	-0.008
2710.97418	0.00437	1.3×10^{-41}	0 0 0	0 0 1	8 8 1	8 8 0	-0.052
2711.01746	0.00614	1.3×10^{-41}	0 0 0	0 0 1	8 8 0	8 8 1	-0.009
2711.14866	0.00260	2.5×10^{-41}	0 0 0	0 0 1	6 2 4	6 1 5	-0.012
2711.74088	0.00228	2.4×10^{-41}	0 0 0	0 0 1	2 1 2	1 0 1	-0.009
2712.85188	0.00544	1.4×10^{-41}	0 0 0	0 0 1	2 2 0	2 1 1	-0.010
2712.88846	0.00429	1.5×10^{-41}	0 0 0	0 0 1	7 2 5	7 2 6	-0.005
2713.88321	0.00337	2.9×10^{-41}	0 0 0	0 0 1	5 2 3	5 1 4	0.002
2714.14922	0.00341	2.3×10^{-41}	0 0 0	0 0 1	3 2 1	3 1 2	-0.010
2714.70903	0.00226	2.9×10^{-41}	0 0 0	0 0 1	4 2 2	4 1 3	-0.008
2715.11438	0.00298	2.2×10^{-41}	0 0 0	0 0 1	3 0 3	2 1 2	-0.010
2715.75906	0.00053	9.9×10^{-41}	0 0 0	0 0 1	2 1 1	1 1 0	-0.008
2716.17107	0.00216	2.5×10^{-41}	0 0 0	0 0 1	4 1 3	4 0 4	-0.001
2716.21317	0.00338	1.1×10^{-41}	0 0 0	0 0 1	9 7 2	9 7 3	-0.034
2716.21317	0.00338	1.1×10^{-41}	0 0 0	0 0 1	9 7 3	9 7 2	-0.034
2716.58786	0.02879	1.9×10^{-41}	0 0 0	0 0 1	8 7 1	8 7 2	-0.035
2716.58786	0.02890	1.9×10^{-41}	0 0 0	0 0 1	8 7 2	8 7 1	-0.035
2716.91725	0.00151	3.1×10^{-41}	0 0 0	0 0 1	7 7 0	7 7 1	-0.044
2716.91725	0.00151	3.1×10^{-41}	0 0 0	0 0 1	7 7 1	7 7 0	-0.044
2718.17943	0.00037	1.4×10^{-40}	0 0 0	0 0 1	2 0 2	1 0 1	-0.008
2718.85485	0.00254	2.3×10^{-41}	0 0 0	0 0 1	4 1 3	4 1 4	-0.006
2719.26292	0.00057	1.0×10^{-40}	0 0 0	0 0 1	2 1 2	1 1 1	-0.008
2719.74204	0.00363	1.6×10^{-41}	0 0 0	0 0 1	1 1 1	0 0 0	-0.012
2723.44172	0.02316	1.7×10^{-41}	0 0 0	0 0 1	8 3 5	8 3 6	-0.013
2725.32637	0.00280	1.6×10^{-41}	0 0 0	0 0 1	9 5 4	9 5 5	-0.016
2725.47758	0.00195	3.0×10^{-41}	0 0 0	0 0 1	2 1 1	2 0 2	-0.012
2725.60134	0.00349	1.6×10^{-41}	0 0 0	0 0 1	9 5 5	9 5 4	-0.024
2725.71867	0.00695	1.1×10^{-41}	0 0 0	0 0 1	2 0 2	1 1 1	0.009
2725.76924	0.00217	2.7×10^{-41}	0 0 0	0 0 1	8 5 3	8 5 4	-0.028
2725.85600	0.00221	2.7×10^{-41}	0 0 0	0 0 1	8 5 4	8 5 3	-0.026
2726.03371	0.00140	3.4×10^{-41}	0 0 0	0 0 1	3 1 2	3 1 3	-0.007
2726.16103	0.00056	4.5×10^{-41}	0 0 0	0 0 1	7 5 2	7 5 3	0.000
2726.16103	0.00056	4.5×10^{-41}	0 0 0	0 0 1	7 5 3	7 5 2	-0.020
2726.44149	0.00057	7.3×10^{-41}	0 0 0	0 0 1	6 5 1	6 5 2	-0.029
2726.45618	0.00056	7.3×10^{-41}	0 0 0	0 0 1	6 5 2	6 5 1	-0.017
2726.72051	0.00038	1.2×10^{-40}	0 0 0	0 0 1	5 5 0	5 5 1	-0.017
2726.70650	0.00038	1.2×10^{-40}	0 0 0	0 0 1	5 5 1	5 5 0	-0.031
2726.88144	0.00362	1.4×10^{-41}	0 0 0	0 0 1	9 4 5	9 4 6	-0.011
2727.27523	0.00124	4.1×10^{-41}	0 0 0	0 0 1	5 2 3	5 2 4	-0.008
2727.64055	0.00217	2.3×10^{-41}	0 0 0	0 0 1	1 1 0	1 0 1	-0.008
2727.68156	0.00062	7.6×10^{-41}	0 0 0	0 0 1	1 0 1	0 0 0	-0.009

Position	$\sigma_{\text{Pos.}}$	Intensity	$\nu_1\ \nu_2\ \nu_3$	$\nu_1'\ \nu_2'\ \nu_3'$	J K_a K_c	J' K_a' K_c'	$\Delta_{\text{SPEC.}}$
2728.05198	0.00177	3.0×10^{-41}	0 0 0	0 0 1	7 3 4	7 3 5	-0.005
2728.50715	0.00178	2.5×10^{-41}	0 0 0	0 0 1	8 4 4	8 4 5	-0.011
2729.40429	0.00141	4.2×10^{-41}	0 0 0	0 0 1	7 4 3	7 4 4	-0.015
2729.91739	0.00216	6.9×10^{-41}	0 0 0	0 0 1	6 4 2	6 4 3	-0.017
2730.07048	0.00174	4.2×10^{-41}	0 0 0	0 0 1	7 4 4	7 4 3	-0.007
2730.10382	0.00092	6.9×10^{-41}	0 0 0	0 0 1	6 4 3	6 4 2	-0.017
2730.24587	0.00061	1.1×10^{-40}	0 0 0	0 0 1	5 4 1	5 4 2	-0.018
2730.28322	0.00076	1.1×10^{-40}	0 0 0	0 0 1	5 4 2	5 4 1	-0.019
2730.37868	0.00682	2.5×10^{-41}	0 0 0	0 0 1	8 4 5	8 4 4	-0.013
2730.47906	0.00074	1.7×10^{-40}	0 0 0	0 0 1	4 4 0	4 4 1	-0.025
2730.49566	0.00061	1.7×10^{-40}	0 0 0	0 0 1	4 4 1	4 4 0	-0.013
2730.86821	0.00117	5.1×10^{-41}	0 0 0	0 0 1	6 3 3	6 3 4	-0.012
2731.41103	0.00425	1.4×10^{-41}	0 0 0	0 0 1	9 4 6	9 4 5	-0.011
2731.50050	0.00106	5.5×10^{-41}	0 0 0	0 0 1	2 1 1	2 1 2	-0.009
2731.62438	0.00090	6.8×10^{-41}	0 0 0	0 0 1	4 2 2	4 2 3	-0.011
2732.38486	0.00073	8.2×10^{-41}	0 0 0	0 0 1	5 3 2	5 3 3	-0.012
2733.10499	0.00061	1.3×10^{-40}	0 0 0	0 0 1	4 3 1	4 3 2	-0.019
2733.43595	0.00034	2.1×10^{-40}	0 0 0	0 0 1	3 3 0	3 3 1	-0.021
2733.49300	0.00056	1.3×10^{-40}	0 0 0	0 0 1	4 3 2	4 3 1	0.004
2733.47452	0.00040	2.1×10^{-40}	0 0 0	0 0 1	3 3 1	3 3 0	-0.035
2733.78980	0.00090	8.2×10^{-41}	0 0 0	0 0 1	5 3 3	5 3 2	-0.020
2734.17363	0.00058	1.1×10^{-40}	0 0 0	0 0 1	3 2 1	3 2 2	-0.018
2734.87397	0.00120	5.0×10^{-41}	0 0 0	0 0 1	6 3 4	6 3 3	-0.012
2735.15946	0.00051	1.1×10^{-40}	0 0 0	0 0 1	1 1 0	1 1 1	-0.010
2735.35521	0.00030	1.9×10^{-40}	0 0 0	0 0 1	2 2 0	2 2 1	-0.012
2735.90011	0.00031	1.9×10^{-40}	0 0 0	0 0 1	2 2 1	2 2 0	-0.012
2736.81863	0.00055	1.1×10^{-40}	0 0 0	0 0 1	3 2 2	3 2 1	-0.012
2737.22209	0.00201	2.9×10^{-41}	0 0 0	0 0 1	7 3 5	7 3 4	-0.008
2738.71427	0.00068	1.1×10^{-40}	0 0 0	0 0 1	1 1 1	1 1 0	-0.008
2739.04643	0.00093	6.6×10^{-41}	0 0 0	0 0 1	4 2 3	4 2 2	-0.011
2741.25081	0.00389	1.6×10^{-41}	0 0 0	0 0 1	8 3 6	8 3 5	-0.009
2742.15052	0.00102	5.3×10^{-41}	0 0 0	0 0 1	2 1 2	2 1 1	-0.012
2742.95991	0.00165	3.9×10^{-41}	0 0 0	0 0 1	5 2 4	5 2 3	-0.010
2746.64867	0.00262	2.3×10^{-41}	0 0 0	0 0 1	1 0 1	1 1 0	-0.011
2747.05390	0.00074	7.7×10^{-41}	0 0 0	0 0 1	0 0 0	1 0 1	-0.010
2747.27743	0.00329	3.3×10^{-41}	0 0 0	0 0 1	3 1 3	3 1 2	0.002
2748.59148	0.00255	3.1×10^{-41}	0 0 0	0 0 1	2 0 2	2 1 1	-0.009
2748.62823	0.00791	2.3×10^{-41}	0 0 0	0 0 1	6 2 5	6 2 4	-0.009
2751.91321	0.00655	3.2×10^{-41}	0 0 0	0 0 1	3 0 3	3 1 2	-0.020
2753.92521	0.00292	2.1×10^{-41}	0 0 0	0 0 1	4 1 4	4 1 3	-0.007
2754.44688	0.00063	1.1×10^{-40}	0 0 0	0 0 1	1 1 1	2 1 2	-0.018

Position	$\sigma_{\text{Pos.}}$	Intensity	$\nu_1\ \nu_2\ \nu_3$	ν_1' ν_2' ν_3'	J K_a K_c	J' K_a' K_c'	$\Delta_{\text{SPEC.}}$
2754.56756	0.00541	1.5×10^{-41}	0 0 0	0 0 1	0 0 0	1 1 1	-0.018
2755.89405	0.00468	1.3×10^{-41}	0 0 0	0 0 1	7 2 6	7 2 5	-0.009
2756.37186	0.00038	1.5×10^{-40}	0 0 0	0 0 1	1 0 1	2 0 2	-0.010
2756.93740	0.00232	2.7×10^{-41}	0 0 0	0 0 1	4 0 4	4 1 3	-0.011
2757.23643	0.00217	3.1×10^{-41}	0 0 0	0 0 1	4 1 3	4 2 2	-0.009
2757.59727	0.00329	3.2×10^{-41}	0 0 0	0 0 1	5 1 4	5 2 3	-0.020
2758.04976	0.00060	1.0×10^{-40}	0 0 0	0 0 1	1 1 0	2 1 1	-0.011
2758.10375	0.00272	2.5×10^{-41}	0 0 0	0 0 1	3 1 2	3 2 1	-0.018
2759.63317	0.00225	2.7×10^{-41}	0 0 0	0 0 1	6 1 5	6 2 4	-0.007
2759.65225	0.00511	1.4×10^{-41}	0 0 0	0 0 1	2 1 1	2 2 0	-0.006
2761.85990	0.00538	1.4×10^{-41}	0 0 0	0 0 1	5 1 5	5 1 4	-0.003
2762.38670	0.00324	2.0×10^{-41}	0 0 0	0 0 1	1 0 1	2 1 2	-0.015
2762.91518	0.00036	1.7×10^{-40}	0 0 0	0 0 1	2 1 2	3 1 3	-0.011
2763.54866	0.00350	2.0×10^{-41}	0 0 0	0 0 1	7 1 6	7 2 5	-0.008
2763.63083	0.00349	2.0×10^{-41}	0 0 0	0 0 1	5 0 5	5 1 4	-0.009
2764.58655	0.00072	9.1×10^{-41}	0 0 0	0 0 1	2 2 1	3 2 2	-0.018
2764.64271	0.00667	1.1×10^{-41}	0 0 0	0 0 1	2 1 2	2 2 1	-0.025
2765.08853	0.00033	1.9×10^{-40}	0 0 0	0 0 1	2 0 2	3 0 3	-0.010
2765.69332	0.00071	9.1×10^{-41}	0 0 0	0 0 1	2 2 0	3 2 1	-0.013
2765.74012	0.00437	1.4×10^{-41}	0 0 0	0 0 1	8 2 6	8 3 5	-0.005
2766.92355	0.00327	1.7×10^{-41}	0 0 0	0 0 1	7 2 5	7 3 4	-0.006
2767.27959	0.00087	1.5×10^{-41}	0 0 0	0 0 1	3 1 3	3 2 2	-0.028
2768.30694	0.00037	1.6×10^{-40}	0 0 0	0 0 1	2 1 1	3 1 2	-0.012
2768.44378	0.00298	2.2×10^{-41}	0 0 0	0 0 1	3 1 3	4 0 4	-0.011
2769.26487	0.00507	1.8×10^{-41}	0 0 0	0 0 1	6 2 4	6 3 3	-0.013
2769.34560	0.00360	2.3×10^{-41}	0 0 0	0 0 1	2 0 2	3 1 3	-0.019
2769.37754	0.00771	1.3×10^{-41}	0 0 0	0 0 1	8 1 7	8 2 6	-0.015
2770.83928	0.00401	1.6×10^{-41}	0 0 0	0 0 1	4 1 4	4 2 3	-0.012
2771.13238	0.00030	2.1×10^{-40}	0 0 0	0 0 1	3 1 3	4 1 4	-0.012
2771.58753	0.00507	1.5×10^{-41}	0 0 0	0 0 1	6 0 6	6 1 5	-0.012
2772.03858	0.00433	1.8×10^{-41}	0 0 0	0 0 1	5 2 3	5 3 2	-0.007
2773.84658	0.00047	1.4×10^{-40}	0 0 0	0 0 1	3 2 2	4 2 3	-0.013
2774.48443	0.00539	1.5×10^{-41}	0 0 0	0 0 1	4 2 2	4 3 1	-0.008
2776.39932	0.00050	1.4×10^{-40}	0 0 0	0 0 1	3 2 1	4 2 2	-0.013
2777.54975	0.00320	2.5×10^{-41}	0 0 0	0 0 1	4 1 4	5 0 5	-0.018
2777.88022	0.00524	1.4×10^{-41}	0 0 0	0 0 1	4 2 3	4 3 2	-0.014
2778.22217	0.00035	1.9×10^{-40}	0 0 0	0 0 1	3 1 2	4 1 3	-0.011
2778.91979	0.00415	1.5×10^{-41}	0 0 0	0 0 1	5 2 4	5 3 3	-0.004
2779.10875	0.00059	2.3×10^{-40}	0 0 0	0 0 1	4 1 4	5 1 5	0.002
2779.40618	0.00223	4.0×10^{-41}	0 0 0	0 0 1	4 4 1	5 4 2	-0.018
2779.41964	0.00241	4.0×10^{-41}	0 0 0	0 0 1	4 4 0	5 4 1	-0.023

Position	$\sigma_{\text{Pos.}}$	Intensity	$\nu_1\,\nu_2\,\nu_3$	$\nu_1\text{'}\,\nu_2\text{'}\,\nu_3\text{'}$	$J\,K_a\,K_c$	$J\text{'}\,K_a\text{'}\,K_c\text{'}$	$\Delta_{\text{SPEC.}}$
2780.45459	0.00624	1.2×10^{-41}	0 0 0	0 0 1	6 1 6	6 2 5	-0.011
2780.55612	0.00760	1.8×10^{-41}	0 0 0	0 0 1	1 1 0	2 2 1	-0.010
2780.57269	0.00033	2.3×10^{-40}	0 0 0	0 0 1	4 0 4	5 0 5	-0.011
2780.63657	0.00468	1.4×10^{-41}	0 0 0	0 0 1	6 2 5	6 3 4	-0.011
2782.11224	0.00260	2.6×10^{-41}	0 0 0	0 0 1	4 0 4	5 1 5	-0.010
2782.24219	0.00071	9.7×10^{-41}	0 0 0	0 0 1	4 3 2	5 3 3	-0.017
2782.60670	0.00435	1.6×10^{-41}	0 0 0	0 0 1	1 1 1	2 2 0	-0.007
2782.83079	0.00422	9.7×10^{-41}	0 0 0	0 0 1	4 3 1	5 3 2	-0.009
2782.83545	0.00248	1.6×10^{-40}	0 0 0	0 0 1	4 2 3	5 2 4	-0.012
2783.14967	0.00450	1.2×10^{-41}	0 0 0	0 0 1	7 2 6	7 3 5	-0.021
2785.37611	0.00631	2.1×10^{-41}	0 0 0	0 0 1	5 5 1	6 5 2	-0.031
2785.39664	0.00381	2.1×10^{-41}	0 0 0	0 0 1	5 5 0	6 5 1	-0.012
2786.81900	0.00030	2.2×10^{-40}	0 0 0	0 0 1	5 1 5	6 1 6	-0.012
2787.29372	0.00045	1.6×10^{-40}	0 0 0	0 0 1	4 2 2	5 2 3	-0.015
2787.62107	0.00034	2.0×10^{-40}	0 0 0	0 0 1	4 1 3	5 1 4	-0.011
2787.77492	0.00030	2.2×10^{-40}	0 0 0	0 0 1	5 0 5	6 0 6	-0.011
2788.33979	0.00478	1.7×10^{-41}	0 0 0	0 0 1	2 1 1	3 2 2	-0.011
2788.60206	0.00358	2.4×10^{-41}	0 0 0	0 0 1	5 0 5	6 1 6	-0.006
2789.09071	0.00115	5.8×10^{-41}	0 0 0	0 0 1	5 4 2	6 4 3	-0.022
2789.17516	0.00115	5.8×10^{-41}	0 0 0	0 0 1	5 4 1	6 4 2	-0.022
2791.50838	0.00043	1.6×10^{-40}	0 0 0	0 0 1	5 2 4	6 2 5	-0.013
2791.79374	0.00068	1.1×10^{-40}	0 0 0	0 0 1	5 3 3	6 3 4	-0.013
2793.25319	0.00067	1.1×10^{-40}	0 0 0	0 0 1	5 3 2	6 3 3	-0.016
2793.91829	0.00365	2.0×10^{-41}	0 0 0	0 0 1	6 1 6	7 0 7	-0.013
2794.33765	0.00034	2.0×10^{-40}	0 0 0	0 0 1	6 1 6	7 1 7	-0.012
2794.89645	0.00034	2.0×10^{-40}	0 0 0	0 0 1	6 0 6	7 0 7	-0.011
2794.99249	0.01882	1.2×10^{-41}	0 0 0	0 0 1	2 1 2	3 2 1	-0.015
2795.00423	0.01259	3.0×10^{-41}	0 0 0	0 0 1	6 5 2	7 5 3	-0.020
2794.99996	0.01720	3.0×10^{-41}	0 0 0	0 0 1	6 5 1	7 5 2	-0.034
2795.13654	0.00514	1.6×10^{-41}	0 0 0	0 0 1	3 1 2	4 2 3	-0.015
2795.31406	0.00358	2.0×10^{-41}	0 0 0	0 0 1	6 0 6	7 1 7	-0.013
2796.31715	0.00117	1.8×10^{-40}	0 0 0	0 0 1	5 1 4	6 1 5	-0.009
2798.02086	0.00052	1.5×10^{-40}	0 0 0	0 0 1	5 2 3	6 2 4	-0.012
2798.77465	0.00145	6.1×10^{-41}	0 0 0	0 0 1	6 4 3	7 4 4	-0.022
2799.05156	0.00118	6.0×10^{-41}	0 0 0	0 0 1	6 4 2	7 4 3	-0.020
2799.83426	0.00065	1.5×10^{-40}	0 0 0	0 0 1	6 2 5	7 2 6	-0.019
2800.13222	0.00564	1.3×10^{-41}	0 0 0	0 0 1	7 6 2	8 6 3	-0.039
2800.13222	0.00564	1.3×10^{-41}	0 0 0	0 0 1	7 6 1	8 6 2	-0.040
2801.01635	0.00537	1.4×10^{-41}	0 0 0	0 0 1	4 1 3	5 2 4	-0.018
2801.14150	0.00160	1.0×10^{-40}	0 0 0	0 0 1	6 3 4	7 3 5	-0.023
2801.48146	0.00145	1.6×10^{-41}	0 0 0	0 0 1	7 1 7	8 0 8	-0.010

Position	$\sigma_{\text{Pos.}}$	Intensity	$\nu_1\ \nu_2\ \nu_3$	$\nu_1'\ \nu_2'\ \nu_3'$	J K_a K_c	J' K_a' K_c'	$\Delta_{\text{SPEC.}}$
2801.67903	0.00044	1.7×10^{-40}	0 0 0	0 0 1	7 1 7	8 1 8	-0.019
2801.99160	0.00039	1.7×10^{-40}	0 0 0	0 0 1	7 0 7	8 0 8	-0.012
2802.19809	0.00461	1.6×10^{-41}	0 0 0	0 0 1	7 0 7	8 1 8	-0.012
2804.10723	0.00070	9.9×10^{-41}	0 0 0	0 0 1	6 3 3	7 3 4	-0.015
2804.18864	0.00043	1.6×10^{-40}	0 0 0	0 0 1	6 1 5	7 1 6	-0.010
2804.61890	0.00252	3.0×10^{-41}	0 0 0	0 0 1	7 5 3	8 5 4	-0.027
2804.65681	0.00243	3.0×10^{-41}	0 0 0	0 0 1	7 5 2	8 5 3	-0.028
2806.16165	0.00732	1.2×10^{-41}	0 0 0	0 0 1	5 1 4	6 2 5	-0.008
2806.26249	0.00371	2.1×10^{-41}	0 0 0	0 0 1	2 2 0	3 3 1	-0.015
2806.55296	0.00396	2.1×10^{-41}	0 0 0	0 0 1	2 2 1	3 3 0	-0.016
2807.82305	0.00057	1.2×10^{-40}	0 0 0	0 0 1	7 2 6	8 2 7	-0.012
2808.27816	0.00050	1.3×10^{-40}	0 0 0	0 0 1	6 2 4	7 2 5	-0.011
2808.42739	0.00125	5.4×10^{-41}	0 0 0	0 0 1	7 4 4	8 4 5	-0.013
2808.78088	0.00441	1.2×10^{-41}	0 0 0	0 0 1	8 1 8	9 0 9	-0.026
2808.89475	0.00049	1.4×10^{-40}	0 0 0	0 0 1	8 1 8	9 1 9	-0.012
2809.05481	0.00049	1.4×10^{-40}	0 0 0	0 0 1	8 0 8	9 0 9	-0.012
2809.14545	0.00146	5.4×10^{-41}	0 0 0	0 0 1	7 4 3	8 4 4	-0.017
2809.13346	0.00672	1.2×10^{-41}	0 0 0	0 0 1	8 0 8	9 1 9	-0.034
2809.66512	0.02409	1.3×10^{-41}	0 0 0	0 0 1	8 6 3	9 6 4	-0.032
2809.66512	0.02407	1.3×10^{-41}	0 0 0	0 0 1	8 6 2	9 6 3	-0.037
2810.23625	0.00081	8.6×10^{-41}	0 0 0	0 0 1	7 3 5	8 3 6	-0.015
2811.31607	0.00055	1.3×10^{-40}	0 0 0	0 0 1	7 1 6	8 1 7	-0.010
2814.24363	0.00264	2.6×10^{-41}	0 0 0	0 0 1	8 5 4	9 5 5	-0.026
2814.36695	0.00272	2.6×10^{-41}	0 0 0	0 0 1	8 5 3	9 5 4	-0.024
2815.24131	0.00374	1.7×10^{-41}	0 0 0	0 0 1	3 2 1	4 3 2	-0.007
2815.24131	0.00109	8.3×10^{-41}	0 0 0	0 0 1	7 3 4	8 3 5	-0.015
2815.45802	0.00128	9.6×10^{-41}	0 0 0	0 0 1	8 2 7	9 2 8	-0.028
2815.98360	0.00215	1.1×10^{-40}	0 0 0	0 0 1	9 1 9	10 1 10	-0.014
2816.06673	0.00062	1.1×10^{-40}	0 0 0	0 0 1	9 0 9	10 0 10	-0.012
2816.70310	0.00448	1.6×10^{-41}	0 0 0	0 0 1	3 2 2	4 3 1	-0.014
2817.86706	0.00062	1.1×10^{-40}	0 0 0	0 0 1	7 2 5	8 2 6	-0.010
2817.96054	0.00233	4.4×10^{-41}	0 0 0	0 0 1	8 4 5	9 4 6	-0.021
2817.97315	0.00092	9.9×10^{-41}	0 0 0	0 0 1	8 1 7	9 1 8	-0.010
2818.98509	0.00155	6.7×10^{-41}	0 0 0	0 0 1	8 3 6	9 3 7	-0.013
2819.18984	0.01202	1.0×10^{-41}	0 0 0	0 0 1	9 6 4	10 6 5	-0.025
2819.17873	0.01233	1.0×10^{-41}	0 0 0	0 0 1	9 6 3	10 6 4	-0.053
2819.56414	0.00312	4.4×10^{-41}	0 0 0	0 0 1	8 4 4	9 4 5	-0.023
2822.82883	0.00096	7.1×10^{-41}	0 0 0	0 0 1	9 2 8	10 2 9	-0.012
2822.96898	0.00092	7.8×10^{-41}	0 0 0	0 0 1	10 1 10	11 1 11	-0.013
2823.01104	0.00093	7.8×10^{-41}	0 0 0	0 0 1	10 0 10	11 0 11	-0.012
2823.25950	0.00538	1.3×10^{-41}	0 0 0	0 0 1	4 2 2	5 3 3	-0.003

Position	$\sigma_{\text{Pos.}}$	Intensity	$\nu_1\ \nu_2\ \nu_3$	$\nu_1{}'\ \nu_2{}'\ \nu_3{}'$	J K_a K_c	J' $K_a{}'$ $K_c{}'$	$\Delta_{\text{SPEC.}}$
2823.85675	0.00350	2.0×10^{-41}	0 0 0	0 0 1	9 5 5	10 5 6	-0.022
2824.17963	0.00311	2.0×10^{-41}	0 0 0	0 0 1	9 5 4	10 5 5	-0.025
2824.45250	0.00099	7.2×10^{-41}	0 0 0	0 0 1	9 1 8	10 1 9	-0.011
2826.31166	0.00162	6.4×10^{-41}	0 0 0	0 0 1	8 3 5	9 3 6	-0.011
2826.62708	0.00086	8.0×10^{-41}	0 0 0	0 0 1	8 2 6	9 2 7	-0.009
2827.31660	0.00185	3.3×10^{-41}	0 0 0	0 0 1	9 4 6	10 4 7	-0.025
2827.33971	0.00127	4.9×10^{-41}	0 0 0	0 0 1	9 3 7	10 3 8	-0.020
2827.65669	0.00286	1.2×10^{-41}	0 0 0	0 0 1	4 2 3	5 3 2	0.047
2829.84795	0.00162	5.4×10^{-41}	0 0 0	0 0 1	11 1 11	12 1 12	-0.021
2829.86692	0.00176	5.4×10^{-41}	0 0 0	0 0 1	11 0 11	12 0 12	-0.022
2829.92869	0.00223	5.0×10^{-41}	0 0 0	0 0 1	10 2 9	11 2 10	-0.021
2830.18136	0.00387	1.9×10^{-41}	0 0 0	0 0 1	3 3 0	4 4 1	-0.023
2830.20700	0.00384	1.9×10^{-41}	0 0 0	0 0 1	3 3 1	4 4 0	-0.025
2830.40968	0.00596	3.2×10^{-41}	0 0 0	0 0 1	9 4 5	10 4 6	-0.020
2830.92004	0.00138	5.1×10^{-41}	0 0 0	0 0 1	10 1 9	11 1 10	-0.011
2833.41687	0.00490	1.4×10^{-41}	0 0 0	0 0 1	10 5 6	11 5 7	-0.022
2834.18138	0.00481	1.4×10^{-41}	0 0 0	0 0 1	10 5 5	11 5 6	-0.022
2834.44072	0.00126	5.6×10^{-41}	0 0 0	0 0 1	9 2 7	10 2 8	-0.008
2835.30373	0.00181	3.4×10^{-41}	0 0 0	0 0 1	10 3 8	11 3 9	-0.013
2836.41977	0.00280	2.3×10^{-41}	0 0 0	0 0 1	10 4 7	11 4 8	-0.015
2836.65267	0.01369	3.6×10^{-41}	0 0 0	0 0 1	12 1 12	13 1 13	-0.008
2836.65267	0.01368	3.6×10^{-41}	0 0 0	0 0 1	12 0 12	13 0 13	-0.018
2836.84552	0.00187	3.4×10^{-41}	0 0 0	0 0 1	11 2 10	12 2 11	-0.011
2836.92220	0.00144	4.6×10^{-41}	0 0 0	0 0 1	9 3 6	10 3 7	-0.009
2837.40897	0.00192	3.4×10^{-41}	0 0 0	0 0 1	11 1 10	12 1 11	-0.012
2839.65138	0.00503	1.4×10^{-41}	0 0 0	0 0 1	4 3 1	5 4 2	-0.018
2839.84286	0.00512	1.4×10^{-41}	0 0 0	0 0 1	4 3 2	5 4 1	-0.018
2841.33156	0.00209	3.7×10^{-41}	0 0 0	0 0 1	10 2 8	11 2 9	-0.006
2841.61159	0.00332	2.2×10^{-41}	0 0 0	0 0 1	10 4 6	11 4 7	-0.015
2842.86612	0.00235	2.2×10^{-41}	0 0 0	0 0 1	11 3 9	12 3 10	-0.010
2843.34696	0.02053	2.4×10^{-41}	0 0 0	0 0 1	13 1 13	14 1 14	-0.012
2843.33191	0.00516	2.4×10^{-41}	0 0 0	0 0 1	13 0 13	14 0 14	-0.030
2843.58889	0.00258	2.2×10^{-41}	0 0 0	0 0 1	12 2 11	13 2 12	-0.012
2843.90486	0.00278	2.2×10^{-41}	0 0 0	0 0 1	12 1 11	13 1 12	-0.012
2845.16185	0.00570	1.5×10^{-41}	0 0 0	0 0 1	11 4 8	12 4 9	-0.021
2846.79142	0.00224	3.0×10^{-41}	0 0 0	0 0 1	10 3 7	11 3 8	-0.006
2847.51832	0.00311	2.4×10^{-41}	0 0 0	0 0 1	11 2 9	12 2 10	-0.007
2849.95116	0.01882	1.5×10^{-41}	0 0 0	0 0 1	14 1 14	15 1 15	-0.013
2849.95116	0.01879	1.5×10^{-41}	0 0 0	0 0 1	14 0 14	15 0 15	-0.015
2850.05558	0.00473	1.4×10^{-41}	0 0 0	0 0 1	12 3 10	13 3 11	-0.015
2850.19410	0.00408	1.3×10^{-41}	0 0 0	0 0 1	13 2 12	14 2 13	-0.015

Position	$\sigma_{\text{Pos.}}$	Intensity	$\nu_1\,\nu_2\,\nu_3$	ν_1' ν_2' ν_3'	J K_a K_c	J' K_a' K_c'	$\Delta_{\text{SPEC.}}$
2850.36545	0.00482	1.3×10^{-41}	0 0 0	0 0 1	13 1 12	14 1 13	-0.011
2852.75274	0.00859	1.3×10^{-41}	0 0 0	0 0 1	4 4 0	5 5 1	-0.036
2852.76277	0.00780	1.3×10^{-41}	0 0 0	0 0 1	4 4 1	5 5 0	-0.028
2852.88148	0.00452	1.4×10^{-41}	0 0 0	0 0 1	11 4 7	12 4 8	-0.018
2853.33826	0.00474	1.4×10^{-41}	0 0 0	0 0 1	12 2 10	13 2 11	-0.015
2855.72706	0.00360	1.9×10^{-41}	0 0 0	0 0 1	11 3 8	12 3 9	-0.007
2863.61398	0.00829	1.1×10^{-41}	0 0 0	0 0 1	12 3 9	13 3 10	-0.004

A.2.2.2 DTO $2\nu_1$ band

Here, the lines assigned to the $2\nu_1$ band of DTO obtained from the $10\,\text{GBq}$ sample are presented. These lines are published in [Her23]. For further information, see Section 5.5.2.

Table A.9: Linelist of the DTO $2\nu_1$ band. The columns present the assigned line position, the uncertainty on the position $\sigma_{\text{Pos.}}$, the line intensity taking natural abundance into account, lower and upper vibrational quanta, lower and upper rotational quanta and the deviation to the predictions from SPECTRA database $\Delta_{\text{SPEC.}}$.

Position	$\sigma_{\text{Pos.}}$	Intensity	$\nu_1\,\nu_2\,\nu_3$	ν_1' ν_2' ν_3'	J K_a K_c	J' K_a' K_c'	$\Delta_{\text{SPEC.}}$
4357.70701	0.02442	6.3×10^{-44}	0 0 0	2 0 0	13 6 7	12 6 6	-0.113
4365.40457	0.00870	6.5×10^{-44}	0 0 0	2 0 0	17 1 17	16 1 16	-0.083
4365.40457	0.00870	6.5×10^{-44}	0 0 0	2 0 0	17 0 17	16 0 16	-0.083
4365.63194	0.00502	2.7×10^{-43}	0 0 0	2 0 0	9 3 6	8 2 7	-0.060
4369.69529	0.01480	5.0×10^{-44}	0 0 0	2 0 0	9 4 5	8 3 6	-0.125
4376.37879	0.00601	1.3×10^{-43}	0 0 0	2 0 0	16 1 16	15 1 15	-0.089
4376.37879	0.00601	1.3×10^{-43}	0 0 0	2 0 0	16 0 16	15 0 15	-0.087
4376.56276	0.00895	5.8×10^{-44}	0 0 0	2 0 0	12 7 5	11 7 4	-0.149
4376.56276	0.00895	5.8×10^{-44}	0 0 0	2 0 0	12 7 6	11 7 5	-0.154
4378.41124	0.00323	1.9×10^{-43}	0 0 0	2 0 0	13 3 10	12 3 9	-0.058
4379.61952	0.00242	3.0×10^{-43}	0 0 0	2 0 0	8 3 5	7 1 6	-0.102
4379.77797	0.00502	1.2×10^{-43}	0 0 0	2 0 0	9 4 6	8 3 5	-0.111
4382.44909	0.00505	1.5×10^{-43}	0 0 0	2 0 0	11 6 6	10 6 5	-0.118
4382.44909	0.00505	1.5×10^{-43}	0 0 0	2 0 0	11 6 5	10 6 4	-0.081
4386.52937	0.00480	1.3×10^{-43}	0 0 0	2 0 0	13 4 10	12 4 9	-0.074
4387.11208	0.00259	2.2×10^{-43}	0 0 0	2 0 0	15 1 15	14 1 14	-0.069
4387.18643	0.00242	2.5×10^{-43}	0 0 0	2 0 0	15 0 15	14 0 14	-0.093
4388.01086	0.00223	2.4×10^{-43}	0 0 0	2 0 0	13 2 11	12 2 10	-0.075
4388.16185	0.00237	2.1×10^{-43}	0 0 0	2 0 0	14 1 13	13 1 12	-0.087
4388.32573	0.00247	2.1×10^{-43}	0 0 0	2 0 0	14 2 13	13 2 12	-0.089
4388.76260	0.00555	8.5×10^{-44}	0 0 0	2 0 0	11 7 4	10 7 3	-0.167
4388.76260	0.00555	8.5×10^{-44}	0 0 0	2 0 0	11 7 5	10 7 4	-0.168

Position	$\sigma_{\text{Pos.}}$	Intensity	$\nu_1\,\nu_2\,\nu_3$	$\nu_1'\,\nu_2'\,\nu_3'$	J K_a K_c	J' K_a' K_c'	$\Delta_{\text{SPEC.}}$
4390.12832	0.00188	3.4×10^{-43}	0 0 0	2 0 0	12 3 9	11 3 8	-0.066
4390.79681	0.00302	2.2×10^{-43}	0 0 0	2 0 0	13 3 11	12 3 10	-0.085
4391.82822	0.00255	2.3×10^{-43}	0 0 0	2 0 0	12 4 8	11 4 7	-0.073
4392.90939	0.01082	5.4×10^{-44}	0 0 0	2 0 0	7 2 5	6 0 6	-0.109
4394.14854	0.00827	1.4×10^{-43}	0 0 0	2 0 0	7 3 4	6 1 5	-0.109
4394.34092	0.00473	2.0×10^{-43}	0 0 0	2 0 0	10 6 5	9 6 4	-0.087
4394.34092	0.00472	2.0×10^{-43}	0 0 0	2 0 0	10 6 4	9 6 3	-0.075
4397.79992	0.01390	3.7×10^{-43}	0 0 0	2 0 0	14 1 14	13 1 13	-0.103
4397.80340	0.01872	4.2×10^{-43}	0 0 0	2 0 0	12 2 10	11 2 9	-0.105
4398.16165	0.00476	2.3×10^{-43}	0 0 0	2 0 0	12 4 9	11 4 8	-0.084
4398.56222	0.00368	3.6×10^{-43}	0 0 0	2 0 0	13 1 12	12 1 11	-0.088
4398.83439	0.00182	3.5×10^{-43}	0 0 0	2 0 0	13 2 12	12 2 11	-0.096
4399.20598	0.00242	1.0×10^{-43}	0 0 0	2 0 0	12 5 7	11 5 6	-0.072
4400.42436	0.00485	1.0×10^{-43}	0 0 0	2 0 0	12 5 8	11 5 7	-0.077
4401.52950	0.00208	3.5×10^{-43}	0 0 0	2 0 0	12 3 10	11 3 9	-0.078
4402.47689	0.00389	5.7×10^{-43}	0 0 0	2 0 0	11 3 8	10 3 7	-0.086
4405.72028	0.00187	3.7×10^{-43}	0 0 0	2 0 0	11 4 7	10 4 6	-0.094
4405.89212	0.00194	2.5×10^{-43}	0 0 0	2 0 0	9 6 4	8 6 3	-0.138
4405.89212	0.00194	2.5×10^{-43}	0 0 0	2 0 0	9 6 3	8 6 2	-0.135
4406.06013	0.01822	1.1×10^{-43}	0 0 0	2 0 0	6 3 3	5 1 4	-0.127
4407.79741	0.00095	7.1×10^{-43}	0 0 0	2 0 0	11 2 9	10 2 8	-0.089
4408.23711	0.00415	5.9×10^{-43}	0 0 0	2 0 0	13 0 13	12 0 12	-0.103
4408.24385	0.00729	5.9×10^{-43}	0 0 0	2 0 0	13 1 13	12 1 12	-0.105
4408.73022	0.00158	5.9×10^{-43}	0 0 0	2 0 0	12 1 11	11 1 10	-0.100
4409.22219	0.00104	5.8×10^{-43}	0 0 0	2 0 0	12 2 11	11 2 10	-0.101
4409.91032	0.00228	3.7×10^{-43}	0 0 0	2 0 0	11 4 8	10 4 7	-0.102
4411.77855	0.00348	1.7×10^{-43}	0 0 0	2 0 0	11 5 6	10 5 5	-0.092
4412.36032	0.00357	1.7×10^{-43}	0 0 0	2 0 0	11 5 7	10 5 6	-0.090
4412.52941	0.00522	1.3×10^{-43}	0 0 0	2 0 0	9 7 2	8 7 1	-0.190
4412.52941	0.00522	1.3×10^{-43}	0 0 0	2 0 0	9 7 3	8 7 2	-0.190
4412.56716	0.00122	6.0×10^{-43}	0 0 0	2 0 0	11 3 9	10 3 8	-0.102
4415.41646	0.01089	7.9×10^{-44}	0 0 0	2 0 0	6 2 4	5 0 5	-0.095
4415.56264	0.00109	7.5×10^{-43}	0 0 0	2 0 0	10 3 7	9 3 6	-0.095
4417.23806	0.00467	2.6×10^{-43}	0 0 0	2 0 0	8 6 2	7 6 1	-0.147
4417.24970	0.00463	2.6×10^{-43}	0 0 0	2 0 0	8 6 3	7 6 2	-0.136
4418.16516	0.00094	1.1×10^{-42}	0 0 0	2 0 0	10 2 8	9 2 7	-0.093
4418.48998	0.00558	9.3×10^{-43}	0 0 0	2 0 0	12 0 12	11 0 11	-0.109
4418.51096	0.00208	9.2×10^{-43}	0 0 0	2 0 0	12 1 12	11 1 11	-0.106
4418.65474	0.00301	9.3×10^{-43}	0 0 0	2 0 0	11 1 10	10 1 9	-0.105
4419.26090	0.00122	5.7×10^{-43}	0 0 0	2 0 0	10 4 6	9 4 5	-0.108
4419.49918	0.00079	9.1×10^{-43}	0 0 0	2 0 0	11 2 10	10 2 9	-0.107

Position	$\sigma_{\text{Pos.}}$	Intensity	$\nu_1\ \nu_2\ \nu_3$	$\nu_1\text{'}\ \nu_2\text{'}\ \nu_3\text{'}$	J K_a K_c	J' K_a' K_c'	$\Delta_{\text{SPEC.}}$
4421.72469	0.00449	5.7×10^{-43}	0 0 0	2 0 0	10 4 7	9 4 6	-0.112
4423.96476	0.00305	2.6×10^{-43}	0 0 0	2 0 0	10 5 5	9 5 4	-0.100
4424.20607	0.00254	2.6×10^{-43}	0 0 0	2 0 0	10 5 6	9 5 5	-0.105
4428.08051	0.00058	1.2×10^{-42}	0 0 0	2 0 0	9 3 6	8 3 5	-0.101
4428.29977	0.00178	1.4×10^{-42}	0 0 0	2 0 0	10 1 9	9 1 8	-0.121
4428.34595	0.01742	2.0×10^{-43}	0 0 0	2 0 0	7 6 1	6 6 0	-0.160
4428.36191	0.04667	2.0×10^{-43}	0 0 0	2 0 0	7 6 2	6 6 1	-0.144
4428.52425	0.00372	2.2×10^{-43}	0 0 0	2 0 0	11 1 11	10 0 10	-0.117
4428.55753	0.00074	1.4×10^{-42}	0 0 0	2 0 0	11 0 11	10 0 10	-0.114
4428.59280	0.00075	1.4×10^{-42}	0 0 0	2 0 0	11 1 11	10 1 10	-0.114
4428.61937	0.00471	2.2×10^{-43}	0 0 0	2 0 0	11 0 11	10 1 10	-0.118
4429.05272	0.00046	1.7×10^{-42}	0 0 0	2 0 0	9 2 7	8 2 6	-0.103
4429.68959	0.00055	1.4×10^{-42}	0 0 0	2 0 0	10 2 9	9 2 8	-0.113
4432.24868	0.00042	8.1×10^{-43}	0 0 0	2 0 0	9 4 5	8 4 4	-0.118
4433.52160	0.00087	8.1×10^{-43}	0 0 0	2 0 0	9 4 6	8 4 5	-0.122
4434.58327	0.00052	1.3×10^{-42}	0 0 0	2 0 0	9 3 7	8 3 6	-0.118
4435.81465	0.00167	3.7×10^{-43}	0 0 0	2 0 0	9 5 4	8 5 3	-0.118
4435.90707	0.00172	3.7×10^{-43}	0 0 0	2 0 0	9 5 5	8 5 4	-0.117
4437.69898	0.00111	2.0×10^{-42}	0 0 0	2 0 0	9 1 8	8 1 7	-0.111
4438.43530	0.00040	2.0×10^{-42}	0 0 0	2 0 0	10 0 10	9 0 9	-0.116
4438.50626	0.00047	2.0×10^{-42}	0 0 0	2 0 0	10 1 10	9 1 9	-0.117
4440.44936	0.00063	2.4×10^{-42}	0 0 0	2 0 0	8 2 6	7 2 5	-0.111
4441.37400	0.00138	1.7×10^{-42}	0 0 0	2 0 0	8 3 5	7 3 4	-0.119
4444.64946	0.00069	1.0×10^{-42}	0 0 0	2 0 0	8 4 4	7 4 3	-0.131
4445.22286	0.00070	1.0×10^{-42}	0 0 0	2 0 0	8 4 5	7 4 4	-0.133
4445.71895	0.00137	1.8×10^{-42}	0 0 0	2 0 0	8 3 6	7 3 5	-0.123
4447.39637	0.00250	4.6×10^{-43}	0 0 0	2 0 0	8 5 3	7 5 2	-0.128
4447.42103	0.00314	4.6×10^{-43}	0 0 0	2 0 0	8 5 4	7 5 3	-0.132
4447.97735	0.00292	3.1×10^{-43}	0 0 0	2 0 0	9 1 9	8 0 8	-0.121
4448.09889	0.00102	2.8×10^{-42}	0 0 0	2 0 0	9 0 9	8 0 8	-0.129
4448.24743	0.00029	2.8×10^{-42}	0 0 0	2 0 0	9 1 9	8 1 8	-0.122
4448.37642	0.00284	3.1×10^{-43}	0 0 0	2 0 0	9 0 9	8 1 8	-0.122
4449.25273	0.00452	1.6×10^{-43}	0 0 0	2 0 0	7 2 6	6 1 5	-0.118
4450.04986	0.00036	2.6×10^{-42}	0 0 0	2 0 0	8 2 7	7 2 6	-0.123
4452.25187	0.00026	3.1×10^{-42}	0 0 0	2 0 0	7 2 5	6 2 4	-0.118
4454.33756	0.00089	2.2×10^{-42}	0 0 0	2 0 0	7 3 4	6 3 3	-0.130
4454.80918	0.01312	5.6×10^{-44}	0 0 0	2 0 0	11 2 9	11 2 10	-0.132
4454.99759	0.01404	1.2×10^{-43}	0 0 0	2 0 0	9 2 8	9 0 9	-0.134
4456.57296	0.00141	1.2×10^{-42}	0 0 0	2 0 0	7 4 3	6 4 2	-0.109
4456.76132	0.00072	1.2×10^{-42}	0 0 0	2 0 0	7 4 4	6 4 3	-0.140
4456.87642	0.00081	2.2×10^{-42}	0 0 0	2 0 0	7 3 5	6 3 4	-0.133

Position	$\sigma_{\text{Pos.}}$	Intensity	$\nu_1\,\nu_2\,\nu_3$	$\nu_1{}'\,\nu_2{}'\,\nu_3{}'$	J K$_a$ K$_c$	J' K$_a$' K$_c$'	$\Delta_{\text{SPEC.}}$
4456.90628	0.00029	3.5×10^{-42}	0 0 0	2 0 0	7 1 6	6 1 5	-0.118
4457.46958	0.00044	3.5×10^{-42}	0 0 0	2 0 0	8 0 8	7 0 7	-0.119
4457.81810	0.00109	3.7×10^{-42}	0 0 0	2 0 0	8 1 8	7 1 7	-0.111
4458.73456	0.00137	4.9×10^{-43}	0 0 0	2 0 0	7 5 2	6 5 1	-0.133
4458.73456	0.00137	4.9×10^{-43}	0 0 0	2 0 0	7 5 3	6 5 2	-0.140
4460.20863	0.00035	3.2×10^{-42}	0 0 0	2 0 0	7 2 6	6 2 5	-0.128
4462.57904	0.00632	1.4×10^{-43}	0 0 0	2 0 0	5 2 4	4 1 3	-0.127
4464.32298	0.00022	3.7×10^{-42}	0 0 0	2 0 0	6 2 4	5 2 3	-0.126
4466.31528	0.00259	4.0×10^{-43}	0 0 0	2 0 0	7 1 7	6 0 6	-0.127
4466.74679	0.00037	2.4×10^{-42}	0 0 0	2 0 0	6 3 3	5 3 2	-0.138
4466.82527	0.00056	4.4×10^{-42}	0 0 0	2 0 0	7 0 7	6 0 6	-0.129
4466.83701	0.00070	4.3×10^{-42}	0 0 0	2 0 0	6 1 5	5 1 4	-0.121
4467.24711	0.00987	5.3×10^{-44}	0 0 0	2 0 0	6 3 4	6 1 5	-0.118
4467.28139	0.00045	4.3×10^{-42}	0 0 0	2 0 0	7 1 7	6 1 6	-0.134
4467.79972	0.00263	4.0×10^{-43}	0 0 0	2 0 0	7 0 7	6 1 6	-0.128
4467.99924	0.00085	2.4×10^{-42}	0 0 0	2 0 0	6 3 4	5 3 3	-0.139
4468.01129	0.00183	1.2×10^{-42}	0 0 0	2 0 0	6 4 2	5 4 1	-0.148
4468.07830	0.00080	1.2×10^{-42}	0 0 0	2 0 0	6 4 3	5 4 2	-0.149
4469.33408	0.00451	1.7×10^{-43}	0 0 0	2 0 0	8 1 7	8 1 8	-0.121
4469.76325	0.00582	1.2×10^{-43}	0 0 0	2 0 0	4 2 3	3 1 2	-0.133
4469.83246	0.01075	3.7×10^{-43}	0 0 0	2 0 0	6 5 2	5 5 1	-0.145
4469.83246	0.01075	3.7×10^{-43}	0 0 0	2 0 0	6 5 1	5 5 0	-0.143
4470.40712	0.00031	3.7×10^{-42}	0 0 0	2 0 0	6 2 5	5 2 4	-0.133
4474.84087	0.00206	3.7×10^{-43}	0 0 0	2 0 0	6 1 6	5 0 5	-0.132
4475.81983	0.00027	5.1×10^{-42}	0 0 0	2 0 0	6 0 6	5 0 5	-0.130
4476.49309	0.00074	3.9×10^{-42}	0 0 0	2 0 0	5 2 3	4 2 2	-0.133
4476.61868	0.00018	5.0×10^{-42}	0 0 0	2 0 0	6 1 6	5 1 5	-0.132
4477.22603	0.00018	4.9×10^{-42}	0 0 0	2 0 0	5 1 4	4 1 3	-0.128
4477.59351	0.00251	3.7×10^{-43}	0 0 0	2 0 0	6 0 6	5 1 5	-0.134
4478.52089	0.00072	2.3×10^{-42}	0 0 0	2 0 0	5 3 2	4 3 1	-0.136
4479.01086	0.00038	2.3×10^{-42}	0 0 0	2 0 0	5 3 3	4 3 2	-0.145
4479.13282	0.00230	8.8×10^{-43}	0 0 0	2 0 0	5 4 1	4 4 0	-0.150
4479.13991	0.00228	8.8×10^{-43}	0 0 0	2 0 0	5 4 2	4 4 1	-0.158
4479.84255	0.01082	2.4×10^{-43}	0 0 0	2 0 0	6 2 5	6 0 6	-0.135
4480.63396	0.00106	3.9×10^{-42}	0 0 0	2 0 0	5 2 4	4 2 3	-0.137
4481.41737	0.00613	1.3×10^{-43}	0 0 0	2 0 0	6 1 5	5 2 4	-0.127
4484.63977	0.00018	5.5×10^{-42}	0 0 0	2 0 0	5 0 5	4 0 4	-0.132
4484.89320	0.01216	1.1×10^{-43}	0 0 0	2 0 0	10 8 3	10 8 2	-0.170
4484.89320	0.01218	1.1×10^{-43}	0 0 0	2 0 0	10 8 2	10 8 3	-0.170
4485.82278	0.00264	2.5×10^{-43}	0 0 0	2 0 0	5 2 4	5 0 5	-0.206
4485.86911	0.00020	5.4×10^{-42}	0 0 0	2 0 0	5 1 5	4 1 4	-0.134

Position	$\sigma_{\text{Pos.}}$	Intensity	$\nu_1\,\nu_2\,\nu_3$	$\nu_1'\,\nu_2'\,\nu_3'$	J K_a K_c	J' K_a' K_c'	$\Delta_{\text{SPEC.}}$
4486.62447	0.00861	1.7×10^{-43}	0 0 0	2 0 0	9 8 1	9 8 2	-0.190
4486.69385	0.00935	1.7×10^{-43}	0 0 0	2 0 0	9 8 2	9 8 1	-0.120
4487.64635	0.00337	3.1×10^{-43}	0 0 0	2 0 0	5 0 5	4 1 4	-0.134
4487.95154	0.00017	4.9×10^{-42}	0 0 0	2 0 0	4 1 3	3 1 2	-0.133
4488.02529	0.00203	2.8×10^{-43}	0 0 0	2 0 0	8 8 1	8 8 0	-0.228
4488.02529	0.00203	2.8×10^{-43}	0 0 0	2 0 0	8 8 0	8 8 1	-0.228
4488.49813	0.00025	3.5×10^{-42}	0 0 0	2 0 0	4 2 2	3 2 1	-0.141
4488.61929	0.00529	1.2×10^{-43}	0 0 0	2 0 0	11 6 5	11 6 6	-0.118
4488.70344	0.00610	1.2×10^{-43}	0 0 0	2 0 0	11 6 6	11 6 5	-0.123
4489.69391	0.00133	1.6×10^{-42}	0 0 0	2 0 0	4 3 1	3 3 0	-0.151
4489.84147	0.00056	1.6×10^{-42}	0 0 0	2 0 0	4 3 2	3 3 1	-0.150
4490.43126	0.00523	2.4×10^{-43}	0 0 0	2 0 0	4 1 4	3 0 3	-0.140
4490.44798	0.00485	2.1×10^{-43}	0 0 0	2 0 0	4 2 3	4 0 4	-0.129
4490.85811	0.00030	3.5×10^{-42}	0 0 0	2 0 0	4 2 3	3 2 2	-0.143
4491.81602	0.00265	3.4×10^{-43}	0 0 0	2 0 0	6 1 5	6 1 6	-0.139
4491.89383	0.01412	5.3×10^{-44}	0 0 0	2 0 0	12 7 6	12 7 5	-0.212
4492.72175	0.00355	3.7×10^{-43}	0 0 0	2 0 0	9 6 3	9 6 4	-0.134
4492.72204	0.00349	3.7×10^{-43}	0 0 0	2 0 0	9 6 4	9 6 3	-0.141
4493.45204	0.01184	1.3×10^{-43}	0 0 0	2 0 0	3 2 2	3 0 3	-0.128
4493.45204	0.00031	5.6×10^{-42}	0 0 0	2 0 0	4 0 4	3 0 3	-0.135
4494.38897	0.00337	6.3×10^{-43}	0 0 0	2 0 0	8 6 2	8 6 3	-0.148
4494.39726	0.00337	6.3×10^{-43}	0 0 0	2 0 0	8 6 3	8 6 2	-0.141
4494.48082	0.00693	1.1×10^{-43}	0 0 0	2 0 0	11 7 4	11 7 5	-0.161
4494.48082	0.00694	1.1×10^{-43}	0 0 0	2 0 0	11 7 5	11 7 4	-0.164
4495.06291	0.00019	5.2×10^{-42}	0 0 0	2 0 0	4 1 4	3 1 3	-0.137
4495.84344	0.02437	1.0×10^{-42}	0 0 0	2 0 0	7 6 1	7 6 2	-0.148
4495.84344	0.02437	1.0×10^{-42}	0 0 0	2 0 0	7 6 2	7 6 1	-0.148
4496.81912	0.00238	2.0×10^{-43}	0 0 0	2 0 0	10 7 3	10 7 4	-0.174
4496.81912	0.00238	2.0×10^{-43}	0 0 0	2 0 0	10 7 4	10 7 3	-0.175
4497.08011	0.00078	1.6×10^{-42}	0 0 0	2 0 0	6 6 0	6 6 1	-0.152
4497.08011	0.00078	1.6×10^{-42}	0 0 0	2 0 0	6 6 1	6 6 0	-0.152
4498.07255	0.00339	2.2×10^{-43}	0 0 0	2 0 0	4 0 4	3 1 3	-0.143
4498.83803	0.00023	4.3×10^{-42}	0 0 0	2 0 0	3 1 2	2 1 1	-0.138
4498.95224	0.00309	3.5×10^{-43}	0 0 0	2 0 0	9 7 2	9 7 3	-0.189
4498.95224	0.00309	3.5×10^{-43}	0 0 0	2 0 0	9 7 3	9 7 2	-0.189
4500.02632	0.00055	2.4×10^{-42}	0 0 0	2 0 0	3 2 1	2 2 0	-0.145
4500.88386	0.00231	6.1×10^{-43}	0 0 0	2 0 0	8 7 1	8 7 2	-0.193
4500.88386	0.00231	6.1×10^{-43}	0 0 0	2 0 0	8 7 2	8 7 1	-0.193
4501.04615	0.00047	2.4×10^{-42}	0 0 0	2 0 0	3 2 2	2 2 1	-0.145
4502.33963	0.00216	4.6×10^{-43}	0 0 0	2 0 0	5 1 4	5 1 5	-0.115
4502.49997	0.00016	5.1×10^{-42}	0 0 0	2 0 0	3 0 3	2 0 2	-0.137

Position	$\sigma_{\text{Pos.}}$	Intensity	$\nu_1\,\nu_2\,\nu_3$	$\nu_1{}'\,\nu_2{}'\,\nu_3{}'$	J K$_a$ K$_c$	J' K$_a$' K$_c$'	$\Delta_{\text{SPEC.}}$
4502.59246	0.00049	1.0×10^{-42}	0 0 0	2 0 0	7 7 1	7 7 0	-0.205
4502.59246	0.00049	1.0×10^{-42}	0 0 0	2 0 0	7 7 0	7 7 1	-0.205
4503.46464	0.00210	4.2×10^{-43}	0 0 0	2 0 0	7 2 5	7 2 6	-0.128
4504.21515	0.00020	4.4×10^{-42}	0 0 0	2 0 0	3 1 3	2 1 2	-0.140
4506.91406	0.00995	8.2×10^{-44}	0 0 0	2 0 0	4 2 2	4 1 3	-0.132
4508.62698	0.01128	7.1×10^{-44}	0 0 0	2 0 0	4 1 3	4 0 4	-0.137
4508.88810	0.01008	1.3×10^{-43}	0 0 0	2 0 0	3 0 3	2 1 2	-0.125
4509.74964	0.00048	2.8×10^{-42}	0 0 0	2 0 0	2 1 1	1 1 0	-0.140
4511.64653	0.00882	6.6×10^{-43}	0 0 0	2 0 0	4 1 3	4 1 4	-0.126
4511.91281	0.00056	3.9×10^{-42}	0 0 0	2 0 0	2 0 2	1 0 1	-0.140
4512.59493	0.00137	7.0×10^{-43}	0 0 0	2 0 0	6 2 4	6 2 5	-0.127
4513.77475	0.00422	4.3×10^{-43}	0 0 0	2 0 0	8 3 5	8 3 6	-0.119
4514.74099	0.01078	9.0×10^{-44}	0 0 0	2 0 0	3 1 2	3 0 3	-0.131
4518.51382	0.00326	3.2×10^{-43}	0 0 0	2 0 0	9 4 5	9 4 6	-0.117
4519.36276	0.00080	9.9×10^{-43}	0 0 0	2 0 0	3 1 2	3 1 3	-0.138
4519.70983	0.00128	7.7×10^{-43}	0 0 0	2 0 0	7 3 4	7 3 5	-0.129
4519.80181	0.00081	1.2×10^{-42}	0 0 0	2 0 0	5 2 3	5 2 4	-0.134
4520.82299	0.00542	1.5×10^{-43}	0 0 0	2 0 0	10 5 5	10 5 6	-0.096
4521.59579	0.00036	2.2×10^{-42}	0 0 0	2 0 0	1 0 1	0 0 0	-0.140
4521.67298	0.00775	5.9×10^{-43}	0 0 0	2 0 0	8 4 4	8 4 5	-0.136
4522.51191	0.00238	3.2×10^{-43}	0 0 0	2 0 0	9 4 6	9 4 5	-0.124
4522.57297	0.00403	1.6×10^{-43}	0 0 0	2 0 0	10 4 7	10 4 6	-0.106
4522.91036	0.00447	2.8×10^{-43}	0 0 0	2 0 0	9 5 4	9 5 5	-0.091
4523.14230	0.00196	2.8×10^{-43}	0 0 0	2 0 0	9 5 5	9 5 4	-0.092
4523.33261	0.00098	5.9×10^{-43}	0 0 0	2 0 0	8 4 5	8 4 4	-0.124
4523.76549	0.00106	1.3×10^{-42}	0 0 0	2 0 0	6 3 3	6 3 4	-0.136
4523.98844	0.00086	1.0×10^{-42}	0 0 0	2 0 0	7 4 3	7 4 4	-0.138
4524.56485	0.00068	1.0×10^{-42}	0 0 0	2 0 0	7 4 4	7 4 3	-0.138
4524.66227	0.00511	5.1×10^{-43}	0 0 0	2 0 0	8 5 3	8 5 4	-0.127
4524.73403	0.00137	5.1×10^{-43}	0 0 0	2 0 0	8 5 4	8 5 3	-0.125
4524.75271	0.00743	1.3×10^{-43}	0 0 0	2 0 0	6 2 4	7 0 7	-0.135
4524.96780	0.00109	1.9×10^{-42}	0 0 0	2 0 0	4 2 2	4 2 3	-0.143
4525.25857	0.00056	1.6×10^{-42}	0 0 0	2 0 0	2 1 1	2 1 2	-0.140
4525.75029	0.00041	1.7×10^{-42}	0 0 0	2 0 0	6 4 2	6 4 3	-0.146
4525.91313	0.00043	1.7×10^{-42}	0 0 0	2 0 0	6 4 3	6 4 2	-0.146
4526.22990	0.00275	8.9×10^{-43}	0 0 0	2 0 0	7 5 3	7 5 2	-0.142
4526.22990	0.00274	8.9×10^{-43}	0 0 0	2 0 0	7 5 2	7 5 3	-0.126
4526.37481	0.00054	2.2×10^{-42}	0 0 0	2 0 0	5 3 2	5 3 3	-0.146
4527.14925	0.00054	2.8×10^{-42}	0 0 0	2 0 0	5 4 1	5 4 2	-0.154
4527.19966	0.00063	2.8×10^{-42}	0 0 0	2 0 0	5 4 2	5 4 1	-0.137
4527.43904	0.00075	1.3×10^{-42}	0 0 0	2 0 0	6 3 4	6 3 3	-0.136

Position	$\sigma_{\text{Pos.}}$	Intensity	$\nu_1\,\nu_2\,\nu_3$	$\nu_1'\,\nu_2'\,\nu_3'$	J K_a K_c	J' K_a' K_c'	$\Delta_{\text{SPEC.}}$
4527.58708	0.00095	1.5×10^{-42}	0 0 0	2 0 0	6 5 1	6 5 2	-0.141
4527.58708	0.00095	1.5×10^{-42}	0 0 0	2 0 0	6 5 2	6 5 1	-0.144
4527.66875	0.00035	2.2×10^{-42}	0 0 0	2 0 0	5 3 3	5 3 2	-0.143
4528.03779	0.00134	3.6×10^{-42}	0 0 0	2 0 0	4 3 1	4 3 2	-0.148
4528.16551	0.00128	7.4×10^{-43}	0 0 0	2 0 0	7 3 5	7 3 4	-0.125
4528.21283	0.00027	3.2×10^{-42}	0 0 0	2 0 0	3 2 1	3 2 2	-0.143
4528.28324	0.00074	4.4×10^{-42}	0 0 0	2 0 0	4 4 1	4 4 0	-0.160
4528.28324	0.00075	4.4×10^{-42}	0 0 0	2 0 0	4 4 0	4 4 1	-0.156
4528.36933	0.00261	3.6×10^{-42}	0 0 0	2 0 0	4 3 2	4 3 1	-0.150
4528.76300	0.00035	2.4×10^{-42}	0 0 0	2 0 0	5 5 1	5 5 0	-0.150
4528.76300	0.00035	2.4×10^{-42}	0 0 0	2 0 0	5 5 0	5 5 1	-0.149
4529.12037	0.00027	5.7×10^{-42}	0 0 0	2 0 0	3 3 0	3 3 1	-0.155
4529.16724	0.00026	5.7×10^{-42}	0 0 0	2 0 0	3 3 1	3 3 0	-0.156
4529.21756	0.00058	3.1×10^{-42}	0 0 0	2 0 0	1 1 0	1 1 1	-0.138
4529.91941	0.00021	5.4×10^{-42}	0 0 0	2 0 0	2 2 0	2 2 1	-0.148
4530.17945	0.00236	3.6×10^{-43}	0 0 0	2 0 0	8 3 6	8 3 5	-0.178
4530.43702	0.00015	5.4×10^{-42}	0 0 0	2 0 0	2 2 1	2 2 0	-0.147
4530.72274	0.00063	3.1×10^{-42}	0 0 0	2 0 0	3 2 2	3 2 1	-0.140
4532.05640	0.00259	1.9×10^{-42}	0 0 0	2 0 0	4 2 3	4 2 2	-0.133
4532.70216	0.00024	3.1×10^{-42}	0 0 0	2 0 0	1 1 1	1 1 0	-0.143
4534.83101	0.00288	1.1×10^{-42}	0 0 0	2 0 0	5 2 4	5 2 3	-0.136
4535.72151	0.00291	1.5×10^{-42}	0 0 0	2 0 0	2 1 2	2 1 1	-0.139
4536.98771	0.00311	8.4×10^{-44}	0 0 0	2 0 0	7 3 4	8 1 7	-0.133
4539.20125	0.00130	6.5×10^{-43}	0 0 0	2 0 0	6 2 5	6 2 4	-0.128
4540.22935	0.00096	9.2×10^{-43}	0 0 0	2 0 0	3 1 3	3 1 2	-0.138
4540.78831	0.00036	2.3×10^{-42}	0 0 0	2 0 0	0 0 0	1 0 1	-0.141
4542.15734	0.00568	1.2×10^{-43}	0 0 0	2 0 0	2 0 2	2 1 1	-0.141
4545.06491	0.00230	3.7×10^{-43}	0 0 0	2 0 0	7 2 6	7 2 5	-0.121
4546.12909	0.00128	5.9×10^{-43}	0 0 0	2 0 0	4 1 4	4 1 3	-0.133
4548.21089	0.00044	3.1×10^{-42}	0 0 0	2 0 0	1 1 1	2 1 2	-0.143
4549.48596	0.00599	1.3×10^{-43}	0 0 0	2 0 0	5 1 4	5 2 3	-0.130
4549.77472	0.00017	4.3×10^{-42}	0 0 0	2 0 0	1 0 1	2 0 2	-0.140
4550.22204	0.00767	1.1×10^{-43}	0 0 0	2 0 0	6 1 5	6 2 4	-0.111
4550.24018	0.00516	1.3×10^{-43}	0 0 0	2 0 0	4 1 3	4 2 2	-0.137
4551.61806	0.00025	3.0×10^{-42}	0 0 0	2 0 0	1 1 0	2 1 1	-0.141
4552.01601	0.01080	1.0×10^{-43}	0 0 0	2 0 0	3 1 2	3 2 1	-0.139
4552.18504	0.00881	2.1×10^{-43}	0 0 0	2 0 0	8 2 7	8 2 6	-0.109
4553.20512	0.00221	3.9×10^{-43}	0 0 0	2 0 0	5 1 5	5 1 4	-0.128
4554.98092	0.00894	8.8×10^{-44}	0 0 0	2 0 0	5 0 5	5 1 4	-0.129
4556.24452	0.00016	5.1×10^{-42}	0 0 0	2 0 0	2 1 2	3 1 3	-0.141
4557.12007	0.01293	5.9×10^{-44}	0 0 0	2 0 0	8 1 7	8 2 6	-0.109

Position	$\sigma_{\text{Pos.}}$	Intensity	$\nu_1\,\nu_2\,\nu_3$	ν_1' ν_2' ν_3'	J K_a K_c	J' K_a' K_c'	$\Delta_{\text{SPEC.}}$
4557.89009	0.01004	7.8×10^{-44}	0 0 0	2 0 0	7 2 5	7 3 4	-0.101
4558.05676	0.00013	5.8×10^{-42}	0 0 0	2 0 0	2 0 2	3 0 3	-0.138
4558.62270	0.00032	2.7×10^{-42}	0 0 0	2 0 0	2 2 1	3 2 2	-0.146
4559.59392	0.00031	2.6×10^{-42}	0 0 0	2 0 0	2 2 0	3 2 1	-0.146
4560.17832	0.00643	1.2×10^{-43}	0 0 0	2 0 0	9 2 8	9 2 7	-0.106
4560.93081	0.00838	9.8×10^{-44}	0 0 0	2 0 0	8 4 5	9 3 6	-0.104
4561.09632	0.00456	2.5×10^{-43}	0 0 0	2 0 0	6 1 6	6 1 5	-0.122
4561.27279	0.00017	4.8×10^{-42}	0 0 0	2 0 0	2 1 1	3 1 2	-0.138
4561.32476	0.01183	7.1×10^{-44}	0 0 0	2 0 0	3 1 3	3 2 2	-0.147
4561.85456	0.01090	8.4×10^{-44}	0 0 0	2 0 0	6 2 4	6 3 3	-0.112
4563.91525	0.00013	6.2×10^{-42}	0 0 0	2 0 0	3 1 3	4 1 4	-0.140
4564.18872	0.01076	7.7×10^{-44}	0 0 0	2 0 0	4 1 4	4 2 3	-0.138
4564.56267	0.02840	2.6×10^{-43}	0 0 0	2 0 0	6 6 1	7 6 2	-0.155
4564.56267	0.02840	2.6×10^{-43}	0 0 0	2 0 0	6 6 0	7 6 1	-0.155
4565.56865	0.00012	6.6×10^{-42}	0 0 0	2 0 0	3 0 3	4 0 4	-0.137
4565.90998	0.01307	8.3×10^{-44}	0 0 0	2 0 0	5 2 3	5 3 2	-0.138
4565.99196	0.00708	1.1×10^{-43}	0 0 0	2 0 0	3 0 3	3 2 2	-0.138
4567.19183	0.00726	1.7×10^{-43}	0 0 0	2 0 0	4 0 4	4 2 3	-0.150
4567.19183	0.00036	4.1×10^{-42}	0 0 0	2 0 0	3 2 2	4 2 3	-0.143
4567.51167	0.00056	1.9×10^{-42}	0 0 0	2 0 0	3 3 1	4 3 2	-0.153
4567.65041	0.00064	1.9×10^{-42}	0 0 0	2 0 0	3 3 0	4 3 1	-0.152
4568.58648	0.01308	7.0×10^{-44}	0 0 0	2 0 0	10 2 9	10 2 8	-0.094
4569.40980	0.00267	4.1×10^{-42}	0 0 0	2 0 0	3 2 1	4 2 2	-0.135
4569.54332	0.00800	1.2×10^{-43}	0 0 0	2 0 0	7 1 7	7 1 6	-0.099
4569.56133	0.00578	2.0×10^{-43}	0 0 0	2 0 0	5 0 5	5 2 4	-0.134
4570.42718	0.00013	5.7×10^{-42}	0 0 0	2 0 0	3 1 2	4 1 3	-0.135
4571.22464	0.00027	6.7×10^{-42}	0 0 0	2 0 0	4 1 4	5 1 5	-0.138
4572.46503	0.00012	6.9×10^{-42}	0 0 0	2 0 0	4 0 4	5 0 5	-0.135
4572.99104	0.01096	3.6×10^{-43}	0 0 0	2 0 0	7 6 2	8 6 3	-0.152
4572.99104	0.01098	3.6×10^{-43}	0 0 0	2 0 0	7 6 1	8 6 2	-0.153
4573.00343	0.01175	1.9×10^{-43}	0 0 0	2 0 0	6 0 6	6 2 5	-0.158
4573.54350	0.00680	7.5×10^{-44}	0 0 0	2 0 0	6 2 5	6 3 4	-0.125
4574.87060	0.00937	6.4×10^{-44}	0 0 0	2 0 0	7 2 6	7 3 5	-0.082
4575.35967	0.00017	4.7×10^{-42}	0 0 0	2 0 0	4 2 3	5 2 4	-0.140
4576.23512	0.00028	2.8×10^{-42}	0 0 0	2 0 0	4 3 2	5 3 3	-0.148
4576.30994	0.00159	1.1×10^{-42}	0 0 0	2 0 0	4 4 1	5 4 2	-0.154
4576.31763	0.00154	1.1×10^{-42}	0 0 0	2 0 0	4 4 0	5 4 1	-0.160
4576.69577	0.00046	2.8×10^{-42}	0 0 0	2 0 0	4 3 1	5 3 2	-0.146
4577.39250	0.00407	1.5×10^{-43}	0 0 0	2 0 0	7 0 7	7 2 6	-0.136
4578.19531	0.00019	6.6×10^{-42}	0 0 0	2 0 0	5 1 5	6 1 6	-0.134
4578.97159	0.00016	5.8×10^{-42}	0 0 0	2 0 0	4 1 3	5 1 4	-0.130

Position	$\sigma_{\mathrm{Pos.}}$	Intensity	$\nu_1\ \nu_2\ \nu_3$	$\nu_1'\ \nu_2'\ \nu_3'$	J K_a K_c	J' K_a' K_c'	$\Delta_{\mathrm{SPEC.}}$
4578.99911	0.00015	6.7×10^{-42}	0 0 0	2 0 0	5 0 5	6 0 6	-0.134
4579.17050	0.00018	4.6×10^{-42}	0 0 0	2 0 0	4 2 2	5 2 3	-0.136
4581.21615	0.00277	3.6×10^{-43}	0 0 0	2 0 0	8 6 3	9 6 4	-0.151
4581.22858	0.00280	3.6×10^{-43}	0 0 0	2 0 0	8 6 2	9 6 3	-0.140
4583.10393	0.00083	4.7×10^{-42}	0 0 0	2 0 0	5 2 4	6 2 5	-0.136
4584.68523	0.00024	3.0×10^{-42}	0 0 0	2 0 0	5 3 3	6 3 4	-0.143
4584.81920	0.00013	5.8×10^{-42}	0 0 0	2 0 0	6 1 6	7 1 7	-0.131
4584.92108	0.00129	1.5×10^{-42}	0 0 0	2 0 0	5 4 2	6 4 3	-0.153
4584.98481	0.00050	1.5×10^{-42}	0 0 0	2 0 0	5 4 1	6 4 2	-0.150
4585.20020	0.00014	5.5×10^{-42}	0 0 0	2 0 0	6 0 6	7 0 7	-0.126
4585.81748	0.00051	3.0×10^{-42}	0 0 0	2 0 0	5 3 2	6 3 3	-0.141
4586.51162	0.00343	4.6×10^{-43}	0 0 0	2 0 0	5 5 1	6 5 2	-0.153
4586.52375	0.00334	4.6×10^{-43}	0 0 0	2 0 0	5 5 0	6 5 1	-0.142
4586.79862	0.00054	5.4×10^{-42}	0 0 0	2 0 0	5 1 4	6 1 5	-0.124
4587.30281	0.00306	1.8×10^{-43}	0 0 0	2 0 0	8 7 1	9 7 2	-0.196
4587.30281	0.00306	1.8×10^{-43}	0 0 0	2 0 0	8 7 2	9 7 3	-0.196
4587.52807	0.01403	5.0×10^{-44}	0 0 0	2 0 0	5 3 3	5 4 2	-0.151
4587.69268	0.00778	7.7×10^{-44}	0 0 0	2 0 0	9 0 9	9 2 8	-0.126
4588.59647	0.00022	4.5×10^{-42}	0 0 0	2 0 0	5 2 3	6 2 4	-0.129
4589.24131	0.00265	3.0×10^{-43}	0 0 0	2 0 0	9 6 3	10 6 4	-0.144
4589.24131	0.00265	3.0×10^{-43}	0 0 0	2 0 0	9 6 4	10 6 5	-0.136
4590.42021	0.00021	4.2×10^{-42}	0 0 0	2 0 0	6 2 5	7 2 6	-0.132
4591.23274	0.00047	5.1×10^{-42}	0 0 0	2 0 0	7 1 7	8 1 8	-0.130
4591.47428	0.00014	5.1×10^{-42}	0 0 0	2 0 0	7 0 7	8 0 8	-0.130
4592.80726	0.00059	2.8×10^{-42}	0 0 0	2 0 0	6 3 4	7 3 5	-0.140
4593.35971	0.00047	1.6×10^{-42}	0 0 0	2 0 0	6 4 3	7 4 4	-0.144
4593.55473	0.00112	1.6×10^{-42}	0 0 0	2 0 0	6 4 2	7 4 3	-0.143
4594.08282	0.00047	3.9×10^{-42}	0 0 0	2 0 0	6 1 5	7 1 6	-0.099
4595.01223	0.00364	1.6×10^{-43}	0 0 0	2 0 0	9 7 2	10 7 3	-0.188
4595.05138	0.00032	2.8×10^{-42}	0 0 0	2 0 0	6 3 3	7 3 4	-0.131
4595.08146	0.00125	6.2×10^{-43}	0 0 0	2 0 0	6 5 2	7 5 3	-0.138
4595.08146	0.00125	6.2×10^{-43}	0 0 0	2 0 0	6 5 1	7 5 2	-0.144
4596.89329	0.00032	2.1×10^{-42}	0 0 0	2 0 0	7 2 6	8 2 7	-0.085
4597.06261	0.00616	2.3×10^{-43}	0 0 0	2 0 0	10 6 5	11 6 6	-0.102
4597.07850	0.01043	2.3×10^{-43}	0 0 0	2 0 0	10 6 4	11 6 5	-0.111
4597.37136	0.00017	4.1×10^{-42}	0 0 0	2 0 0	8 1 8	9 1 9	-0.128
4597.44978	0.00019	3.9×10^{-42}	0 0 0	2 0 0	6 2 4	7 2 5	-0.122
4597.49685	0.00019	4.2×10^{-42}	0 0 0	2 0 0	8 0 8	9 0 9	-0.128
4599.76806	0.00022	3.6×10^{-42}	0 0 0	2 0 0	7 1 6	8 1 7	-0.120
4600.56047	0.00115	2.4×10^{-42}	0 0 0	2 0 0	7 3 5	8 3 6	-0.130
4601.59527	0.00051	1.4×10^{-42}	0 0 0	2 0 0	7 4 4	8 4 5	-0.136

Position	$\sigma_{\text{Pos.}}$	Intensity	$\nu_1\,\nu_2\,\nu_3$	$\nu_1{}'\,\nu_2{}'\,\nu_3{}'$	J K_a K_c	J' $K_a{}'$ $K_c{}'$	$\Delta_{\text{SPEC.}}$
4602.09246	0.00082	1.4×10^{-42}	0 0 0	2 0 0	7 4 3	8 4 4	-0.135
4602.54889	0.01091	1.3×10^{-43}	0 0 0	2 0 0	10 7 4	11 7 5	-0.157
4602.55862	0.00946	1.3×10^{-43}	0 0 0	2 0 0	10 7 3	11 7 4	-0.148
4603.28029	0.00034	3.2×10^{-42}	0 0 0	2 0 0	9 1 9	10 1 10	-0.125
4603.34350	0.00021	3.2×10^{-42}	0 0 0	2 0 0	9 0 9	10 0 10	-0.124
4603.50885	0.00112	6.1×10^{-43}	0 0 0	2 0 0	7 5 3	8 5 4	-0.129
4603.52967	0.00110	6.1×10^{-43}	0 0 0	2 0 0	7 5 2	8 5 3	-0.132
4603.71707	0.00028	2.8×10^{-42}	0 0 0	2 0 0	8 2 7	9 2 8	-0.122
4604.24425	0.01892	2.2×10^{-42}	0 0 0	2 0 0	7 3 4	8 3 5	-0.110
4604.58990	0.00365	1.6×10^{-43}	0 0 0	2 0 0	11 6 6	12 6 7	-0.125
4604.65576	0.00349	1.6×10^{-43}	0 0 0	2 0 0	11 6 5	12 6 6	-0.125
4605.56402	0.00048	2.9×10^{-42}	0 0 0	2 0 0	8 1 7	9 1 8	-0.116
4605.60021	0.00027	3.1×10^{-42}	0 0 0	2 0 0	7 2 5	8 2 6	-0.113
4607.90319	0.00036	1.9×10^{-42}	0 0 0	2 0 0	8 3 6	9 3 7	-0.122
4608.97010	0.00039	2.3×10^{-42}	0 0 0	2 0 0	10 1 10	11 1 11	-0.122
4609.00238	0.00080	2.3×10^{-42}	0 0 0	2 0 0	10 0 10	11 0 11	-0.120
4609.59498	0.00061	1.1×10^{-42}	0 0 0	2 0 0	8 4 5	9 4 6	-0.125
4609.83476	0.00034	2.1×10^{-42}	0 0 0	2 0 0	9 2 8	10 2 9	-0.118
4610.67756	0.00057	1.1×10^{-42}	0 0 0	2 0 0	8 4 4	9 4 5	-0.123
4611.02366	0.00132	2.1×10^{-42}	0 0 0	2 0 0	9 1 8	10 1 9	-0.115
4611.80792	0.00149	5.0×10^{-43}	0 0 0	2 0 0	8 5 4	9 5 5	-0.120
4611.88148	0.00228	5.0×10^{-43}	0 0 0	2 0 0	8 5 3	9 5 4	-0.118
4612.95915	0.00030	2.3×10^{-42}	0 0 0	2 0 0	8 2 6	9 2 7	-0.106
4613.92465	0.00053	1.3×10^{-42}	0 0 0	2 0 0	8 3 5	9 3 6	-0.094
4614.44747	0.00623	1.6×10^{-42}	0 0 0	2 0 0	11 1 11	12 1 12	-0.118
4614.46390	0.00231	1.6×10^{-42}	0 0 0	2 0 0	11 0 11	12 0 12	-0.116
4614.83103	0.00197	1.3×10^{-42}	0 0 0	2 0 0	9 3 7	10 3 8	-0.114
4616.33135	0.00047	1.5×10^{-42}	0 0 0	2 0 0	10 1 9	11 1 10	-0.111
4617.04815	0.01022	5.7×10^{-44}	0 0 0	2 0 0	12 7 6	13 7 7	-0.134
4617.04815	0.01022	5.7×10^{-44}	0 0 0	2 0 0	12 7 5	13 7 6	-0.143
4617.31376	0.00074	8.2×10^{-43}	0 0 0	2 0 0	9 4 6	10 4 7	-0.116
4618.93106	0.01124	6.2×10^{-44}	0 0 0	2 0 0	13 6 8	14 6 9	-0.111
4619.27076	0.01122	6.2×10^{-44}	0 0 0	2 0 0	13 6 7	14 6 8	-0.102
4619.36332	0.00077	8.1×10^{-43}	0 0 0	2 0 0	9 4 5	10 4 6	-0.110
4619.48125	0.00213	1.6×10^{-42}	0 0 0	2 0 0	9 2 7	10 2 8	-0.098
4619.71939	0.00142	1.1×10^{-42}	0 0 0	2 0 0	12 1 12	13 1 13	-0.110
4619.71939	0.00142	1.1×10^{-42}	0 0 0	2 0 0	12 0 12	13 0 13	-0.116
4619.98247	0.00151	3.7×10^{-43}	0 0 0	2 0 0	9 5 5	10 5 6	-0.106
4620.16577	0.00161	3.7×10^{-43}	0 0 0	2 0 0	9 5 4	10 5 5	-0.108
4621.12195	0.00101	9.7×10^{-43}	0 0 0	2 0 0	11 2 10	12 2 11	-0.111
4621.15278	0.00088	8.7×10^{-43}	0 0 0	2 0 0	10 3 8	11 3 9	-0.095

Position	$\sigma_{\text{Pos.}}$	Intensity	$\nu_1\ \nu_2\ \nu_3$	$\nu_1'\ \nu_2'\ \nu_3'$	J K_a K_c	J' K_a' K_c'	$\Delta_{\text{SPEC.}}$
4621.52101	0.00260	9.7×10^{-43}	0 0 0	2 0 0	11 1 10	12 1 11	-0.109
4622.19609	0.00053	1.2×10^{-42}	0 0 0	2 0 0	9 3 6	10 3 7	-0.096
4624.69968	0.00269	5.6×10^{-43}	0 0 0	2 0 0	13 1 13	14 1 14	-0.086
4624.71003	0.00403	5.5×10^{-43}	0 0 0	2 0 0	10 4 7	11 4 8	-0.108
4624.78112	0.00275	6.4×10^{-43}	0 0 0	2 0 0	13 0 13	14 0 14	-0.108
4625.20654	0.00074	1.0×10^{-42}	0 0 0	2 0 0	10 2 8	11 2 9	-0.095
4626.38295	0.00092	6.2×10^{-43}	0 0 0	2 0 0	12 2 11	13 2 12	-0.104
4626.58807	0.00103	6.2×10^{-43}	0 0 0	2 0 0	12 1 11	13 1 12	-0.103
4627.30453	0.00094	6.0×10^{-43}	0 0 0	2 0 0	11 3 9	12 3 10	-0.098
4628.01851	0.00238	2.5×10^{-43}	0 0 0	2 0 0	10 5 6	11 5 7	-0.097
4628.12045	0.00121	5.4×10^{-43}	0 0 0	2 0 0	10 4 6	11 4 7	-0.096
4628.43801	0.00247	2.5×10^{-43}	0 0 0	2 0 0	10 5 5	11 5 6	-0.093
4629.61306	0.03051	4.2×10^{-43}	0 0 0	2 0 0	14 0 14	15 0 15	-0.106
4629.61306	0.03051	4.2×10^{-43}	0 0 0	2 0 0	14 1 14	15 1 15	-0.106
4630.04042	0.00081	8.0×10^{-43}	0 0 0	2 0 0	10 3 7	11 3 8	-0.085
4630.32461	0.00123	6.4×10^{-43}	0 0 0	2 0 0	11 2 9	12 2 10	-0.090
4631.36907	0.00286	3.6×10^{-43}	0 0 0	2 0 0	13 2 12	14 2 13	-0.071
4631.49962	0.00151	3.6×10^{-43}	0 0 0	2 0 0	13 1 12	14 1 13	-0.095
4631.76340	0.00179	3.5×10^{-43}	0 0 0	2 0 0	11 4 8	12 4 9	-0.094
4633.00881	0.00147	3.6×10^{-43}	0 0 0	2 0 0	12 3 10	13 3 11	-0.091
4635.09242	0.00154	3.8×10^{-43}	0 0 0	2 0 0	12 2 10	13 2 11	-0.084
4635.91795	0.00571	1.6×10^{-43}	0 0 0	2 0 0	11 5 7	12 5 8	-0.076
4636.18062	0.00277	1.8×10^{-43}	0 0 0	2 0 0	14 2 13	15 2 14	-0.091
4636.28048	0.00904	1.8×10^{-43}	0 0 0	2 0 0	14 1 13	15 1 14	-0.079
4636.74882	0.00400	1.6×10^{-43}	0 0 0	2 0 0	11 5 6	12 5 7	-0.075
4636.79309	0.00207	3.4×10^{-43}	0 0 0	2 0 0	11 4 7	12 4 8	-0.078
4637.15579	0.00165	4.9×10^{-43}	0 0 0	2 0 0	11 3 8	12 3 9	-0.072
4638.32744	0.00649	6.1×10^{-44}	0 0 0	2 0 0	5 0 5	6 2 4	-0.157
4638.38328	0.00257	2.1×10^{-43}	0 0 0	2 0 0	13 3 11	14 3 12	-0.083
4638.45976	0.00255	2.1×10^{-43}	0 0 0	2 0 0	12 4 9	13 4 10	-0.079
4638.67917	0.00276	1.4×10^{-43}	0 0 0	2 0 0	16 1 16	17 1 17	-0.093
4638.67917	0.00276	1.4×10^{-43}	0 0 0	2 0 0	16 0 16	17 0 17	-0.093
4639.71830	0.00302	2.2×10^{-43}	0 0 0	2 0 0	13 2 11	14 2 12	-0.074
4640.76098	0.00602	1.2×10^{-43}	0 0 0	2 0 0	15 2 14	16 2 15	-0.088
4640.77976	0.00631	1.2×10^{-43}	0 0 0	2 0 0	15 1 14	16 1 15	-0.087
4642.90027	0.00688	7.5×10^{-44}	0 0 0	2 0 0	17 0 17	18 0 18	-0.080
4642.90027	0.00688	7.5×10^{-44}	0 0 0	2 0 0	17 1 17	18 1 18	-0.080
4643.48894	0.01163	2.8×10^{-43}	0 0 0	2 0 0	12 3 9	13 3 10	-0.068
4643.49725	0.02894	1.2×10^{-43}	0 0 0	2 0 0	14 3 12	15 3 13	-0.058
4644.29324	0.00637	1.2×10^{-43}	0 0 0	2 0 0	14 2 12	15 2 13	-0.072
4644.80323	0.00529	1.1×10^{-43}	0 0 0	2 0 0	13 4 10	14 4 11	-0.071

Position	$\sigma_{\text{Pos.}}$	Intensity	$\nu_1\,\nu_2\,\nu_3$	$\nu_1'\,\nu_2'\,\nu_3'$	J K_a K_c	J' K_a' K_c'	$\Delta_{\text{SPEC.}}$
4645.13659	0.00279	1.9×10^{-43}	0 0 0	2 0 0	12 4 8	13 4 9	-0.057
4645.13659	0.00614	9.1×10^{-44}	0 0 0	2 0 0	12 5 7	13 5 8	-0.062
4645.16570	0.03101	6.6×10^{-44}	0 0 0	2 0 0	16 1 15	17 1 16	-0.083
4645.17022	0.03050	6.6×10^{-44}	0 0 0	2 0 0	16 2 15	17 2 16	-0.066
4649.10774	0.00338	1.5×10^{-43}	0 0 0	2 0 0	13 3 10	14 3 11	-0.049
4652.92616	0.00487	1.0×10^{-43}	0 0 0	2 0 0	13 4 9	14 4 10	-0.034
4653.63336	0.00633	4.9×10^{-44}	0 0 0	2 0 0	13 5 8	14 5 9	-0.024
4654.15881	0.00747	7.3×10^{-44}	0 0 0	2 0 0	14 3 11	15 3 12	-0.041

A.2.2.3 DTO $\nu_1 + 2\nu_2$ band

Here, the lines assigned to the $\nu_1 + 2\nu_2$ band of DTO obtained from the $10\,\text{GBq}$ sample are presented. These lines are published in [Her23]. For further information, see Section 5.5.2.

Table A.10: Linelist of the DTO $\nu_1 + 2\nu_2$ band. The columns present the assigned line position, the uncertainty on the position $\sigma_{\text{Pos.}}$, the line intensity taking natural abundance into account, lower and upper vibrational quanta, lower and upper rotational quanta and the deviation to the predictions from SPECTRA database $\Delta_{\text{SPEC.}}$.

Position	$\sigma_{\text{Pos.}}$	Intensity	$\nu_1\,\nu_2\,\nu_3$	$\nu_1'\,\nu_2'\,\nu_3'$	J K_a K_c	J' K_a' K_c'	$\Delta_{\text{SPEC.}}$
4306.80887	0.01427	4.8×10^{-44}	0 0 0	1 2 0	15 0 15	14 0 14	0.030
4317.50765	0.00415	8.2×10^{-44}	0 0 0	1 2 0	14 0 14	13 0 13	0.023
4317.53252	0.00492	8.2×10^{-44}	0 0 0	1 2 0	14 1 14	13 1 13	0.027
4321.87414	0.00738	4.9×10^{-44}	0 0 0	1 2 0	14 2 12	13 2 11	0.040
4322.68593	0.00641	6.4×10^{-44}	0 0 0	1 2 0	14 2 13	13 2 12	0.023
4322.75507	0.00637	7.4×10^{-44}	0 0 0	1 2 0	13 3 10	12 3 9	0.031
4325.47051	0.00701	5.2×10^{-44}	0 0 0	1 2 0	14 3 12	13 3 11	0.013
4327.95145	0.00422	1.3×10^{-43}	0 0 0	1 2 0	13 0 13	12 0 12	0.013
4328.00962	0.00311	1.3×10^{-43}	0 0 0	1 2 0	13 1 13	12 1 12	0.014
4328.90788	0.00657	8.2×10^{-44}	0 0 0	1 2 0	13 2 11	12 2 10	0.033
4331.75787	0.00510	9.3×10^{-44}	0 0 0	1 2 0	13 1 12	12 1 11	0.022
4332.15549	0.00587	9.5×10^{-44}	0 0 0	1 2 0	13 2 12	12 2 11	0.018
4332.41551	0.00341	1.2×10^{-43}	0 0 0	1 2 0	12 3 9	11 3 8	0.027
4332.90798	0.01057	4.3×10^{-44}	0 0 0	1 2 0	14 5 9	13 5 8	-0.024
4334.63812	0.00504	8.7×10^{-44}	0 0 0	1 2 0	13 3 11	12 3 10	0.016
4335.94103	0.00346	1.3×10^{-43}	0 0 0	1 2 0	12 2 10	11 2 9	0.032
4338.26181	0.01027	2.0×10^{-43}	0 0 0	1 2 0	12 1 12	11 1 11	0.015
4338.64221	0.00224	1.8×10^{-43}	0 0 0	1 2 0	12 0 12	11 0 11	0.020
4339.71646	0.00591	8.2×10^{-44}	0 0 0	1 2 0	13 4 10	12 4 9	-0.004
4340.42299	0.00308	1.6×10^{-43}	0 0 0	1 2 0	12 1 11	11 1 10	0.015
4341.37145	0.00247	1.6×10^{-43}	0 0 0	1 2 0	12 2 11	11 2 10	0.012

Position	$\sigma_{\text{Pos.}}$	Intensity	$\nu_1\ \nu_2\ \nu_3$	$\nu_1'\ \nu_2'\ \nu_3'$	J K_a K_c	J' K_a' K_c'	$\Delta_{\text{SPEC.}}$
4342.94770	0.00273	1.9×10^{-43}	0 0 0	1 2 0	11 3 8	10 3 7	0.016
4343.21962	0.00561	1.2×10^{-43}	0 0 0	1 2 0	12 4 8	11 4 7	0.005
4343.25935	0.00271	2.0×10^{-43}	0 0 0	1 2 0	11 2 9	10 2 8	0.028
4343.91000	0.00401	1.4×10^{-43}	0 0 0	1 2 0	12 3 10	11 3 9	0.008
4348.12532	0.00277	2.6×10^{-43}	0 0 0	1 2 0	11 1 11	10 1 10	0.009
4348.34842	0.00197	2.8×10^{-43}	0 0 0	1 2 0	11 0 11	10 0 10	0.004
4348.79817	0.00216	2.3×10^{-43}	0 0 0	1 2 0	11 1 10	10 1 9	0.008
4348.93146	0.00775	7.4×10^{-44}	0 0 0	1 2 0	13 5 9	12 5 8	-0.025
4350.14637	0.00328	1.3×10^{-43}	0 0 0	1 2 0	12 4 9	11 4 8	-0.006
4350.48859	0.00185	2.4×10^{-43}	0 0 0	1 2 0	11 2 10	10 2 9	0.006
4351.21590	0.00204	3.0×10^{-43}	0 0 0	1 2 0	10 2 8	9 2 7	0.018
4353.34801	0.00252	2.1×10^{-43}	0 0 0	1 2 0	11 3 9	10 3 8	0.002
4354.29477	0.00336	2.8×10^{-43}	0 0 0	1 2 0	10 3 7	9 3 6	0.004
4356.82213	0.00188	3.4×10^{-43}	0 0 0	1 2 0	10 1 9	9 1 8	0.007
4358.07511	0.00172	4.2×10^{-43}	0 0 0	1 2 0	10 0 10	9 0 9	0.000
4358.29424	0.00245	4.2×10^{-43}	0 0 0	1 2 0	10 1 10	9 1 9	0.001
4359.34061	0.00991	1.2×10^{-43}	0 0 0	1 2 0	12 5 7	11 5 6	-0.040
4359.49162	0.00271	3.3×10^{-43}	0 0 0	1 2 0	10 2 9	9 2 8	0.002
4360.01268	0.00145	4.2×10^{-43}	0 0 0	1 2 0	9 2 7	8 2 6	0.010
4362.98887	0.00178	3.0×10^{-43}	0 0 0	1 2 0	10 3 8	9 3 7	-0.001
4364.56157	0.00127	4.6×10^{-43}	0 0 0	1 2 0	9 1 8	8 1 7	0.005
4367.55647	0.00121	5.6×10^{-43}	0 0 0	1 2 0	9 0 9	8 0 8	-0.003
4367.87564	0.00111	5.6×10^{-43}	0 0 0	1 2 0	9 1 9	8 1 8	-0.002
4369.00117	0.00246	2.6×10^{-43}	0 0 0	1 2 0	10 4 6	9 4 5	-0.026
4369.76888	0.00285	5.4×10^{-43}	0 0 0	1 2 0	8 2 6	7 2 5	-0.003
4371.20964	0.00459	2.9×10^{-43}	0 0 0	1 2 0	10 4 7	9 4 6	-0.038
4371.61455	0.00521	1.8×10^{-43}	0 0 0	1 2 0	11 5 6	10 5 5	-0.073
4372.25227	0.00252	6.0×10^{-43}	0 0 0	1 2 0	8 1 7	7 1 6	-0.006
4372.84050	0.00329	4.1×10^{-43}	0 0 0	1 2 0	9 3 7	8 3 6	-0.009
4376.74995	0.00098	7.0×10^{-43}	0 0 0	1 2 0	8 0 8	7 0 7	-0.006
4377.30387	0.00130	7.1×10^{-43}	0 0 0	1 2 0	8 1 8	7 1 7	-0.008
4378.12450	0.00099	5.9×10^{-43}	0 0 0	1 2 0	8 2 7	7 2 6	-0.004
4379.96572	0.00098	6.8×10^{-43}	0 0 0	1 2 0	7 2 5	6 2 4	-0.004
4380.26685	0.00146	7.4×10^{-43}	0 0 0	1 2 0	7 1 6	6 1 5	-0.004
4381.16218	0.00135	3.4×10^{-43}	0 0 0	1 2 0	9 4 5	8 4 4	-0.031
4382.66967	0.00200	2.8×10^{-43}	0 0 0	1 2 0	9 4 6	8 4 5	-0.036
4382.89403	0.00118	5.2×10^{-43}	0 0 0	1 2 0	8 3 6	7 3 5	-0.016
4383.44233	0.00465	2.4×10^{-43}	0 0 0	1 2 0	10 5 5	9 5 4	-0.074
4383.71560	0.01290	2.4×10^{-43}	0 0 0	1 2 0	10 5 6	9 5 5	-0.061
4385.62568	0.00107	8.5×10^{-43}	0 0 0	1 2 0	7 0 7	6 0 6	-0.011
4386.58340	0.00110	8.5×10^{-43}	0 0 0	1 2 0	7 1 7	6 1 6	-0.010

Position	$\sigma_{\text{Pos.}}$	Intensity	$\nu_1\ \nu_2\ \nu_3$	$\nu_1\text{'}\ \nu_2\text{'}\ \nu_3\text{'}$	J K_a K_c	J' $K_a\text{'}$ $K_c\text{'}$	$\Delta_{\text{SPEC.}}$
4387.35070	0.00101	7.2×10^{-43}	0 0 0	1 2 0	7 2 6	6 2 5	-0.011
4388.86809	0.00086	8.7×10^{-43}	0 0 0	1 2 0	6 1 5	5 1 4	-0.006
4390.37746	0.00115	5.4×10^{-43}	0 0 0	1 2 0	7 3 4	6 3 3	-0.022
4390.92279	0.00078	7.8×10^{-43}	0 0 0	1 2 0	6 2 4	5 2 3	-0.011
4392.76006	0.00181	4.2×10^{-43}	0 0 0	1 2 0	8 4 4	7 4 3	-0.035
4393.10900	0.00114	6.1×10^{-43}	0 0 0	1 2 0	7 3 5	6 3 4	-0.023
4393.40004	0.00164	3.9×10^{-43}	0 0 0	1 2 0	8 4 5	7 4 4	-0.039
4394.18852	0.00107	9.6×10^{-43}	0 0 0	1 2 0	6 0 6	5 0 5	-0.014
4394.99773	0.00240	3.1×10^{-43}	0 0 0	1 2 0	9 5 5	8 5 4	-0.070
4395.74694	0.00061	9.6×10^{-43}	0 0 0	1 2 0	6 1 6	5 1 5	-0.010
4396.75998	0.00176	8.1×10^{-43}	0 0 0	1 2 0	6 2 5	5 2 4	-0.016
4398.12607	0.00082	9.5×10^{-43}	0 0 0	1 2 0	5 1 4	4 1 3	-0.010
4402.09660	0.00125	6.1×10^{-43}	0 0 0	1 2 0	6 3 3	5 3 2	-0.027
4402.26567	0.00231	8.1×10^{-43}	0 0 0	1 2 0	5 2 3	4 2 2	-0.015
4402.52539	0.00082	1.0×10^{-42}	0 0 0	1 2 0	5 0 5	4 0 4	-0.014
4403.42562	0.00124	6.5×10^{-43}	0 0 0	1 2 0	6 3 4	5 3 3	-0.028
4403.89364	0.00158	4.6×10^{-43}	0 0 0	1 2 0	7 4 3	6 4 2	-0.042
4404.13118	0.00170	4.5×10^{-43}	0 0 0	1 2 0	7 4 4	6 4 3	-0.044
4404.82881	0.00076	1.0×10^{-42}	0 0 0	1 2 0	5 1 5	4 1 4	-0.017
4406.06471	0.00549	3.6×10^{-43}	0 0 0	1 2 0	8 5 3	7 5 2	-0.066
4406.08733	0.00223	3.6×10^{-43}	0 0 0	1 2 0	8 5 4	7 5 3	-0.073
4406.32375	0.00090	8.2×10^{-43}	0 0 0	1 2 0	5 2 4	4 2 3	-0.021
4407.93235	0.00077	9.3×10^{-43}	0 0 0	1 2 0	4 1 3	3 1 2	-0.016
4410.86801	0.00257	1.0×10^{-42}	0 0 0	1 2 0	4 0 4	3 0 3	-0.016
4413.24161	0.00139	5.7×10^{-43}	0 0 0	1 2 0	5 3 2	4 3 1	-0.033
4413.66743	0.01184	7.2×10^{-43}	0 0 0	1 2 0	4 2 2	3 2 1	-0.030
4413.72032	0.00939	1.6×10^{-43}	0 0 0	1 2 0	10 3 7	9 4 6	-0.033
4413.76741	0.00161	6.0×10^{-43}	0 0 0	1 2 0	5 3 3	4 3 2	-0.034
4413.88370	0.00100	9.7×10^{-43}	0 0 0	1 2 0	4 1 4	3 1 3	-0.015
4414.68137	0.00202	4.4×10^{-43}	0 0 0	1 2 0	6 4 2	5 4 1	-0.048
4414.75274	0.00207	4.4×10^{-43}	0 0 0	1 2 0	6 4 3	5 4 2	-0.049
4416.01849	0.00109	7.3×10^{-43}	0 0 0	1 2 0	4 2 3	3 2 2	-0.023
4416.97413	0.01109	3.6×10^{-43}	0 0 0	1 2 0	7 5 2	6 5 1	-0.073
4416.97413	0.01108	3.6×10^{-43}	0 0 0	1 2 0	7 5 3	6 5 2	-0.080
4418.12914	0.00223	8.0×10^{-43}	0 0 0	1 2 0	3 1 2	2 1 1	-0.020
4419.52761	0.00086	9.1×10^{-43}	0 0 0	1 2 0	3 0 3	2 0 2	-0.018
4422.91862	0.00109	8.1×10^{-43}	0 0 0	1 2 0	3 1 3	2 1 2	-0.022
4423.90643	0.00180	3.9×10^{-43}	0 0 0	1 2 0	4 3 1	3 3 0	-0.037
4424.07126	0.00153	4.1×10^{-43}	0 0 0	1 2 0	4 3 2	3 3 1	-0.028
4425.21267	0.00261	3.1×10^{-43}	0 0 0	1 2 0	5 4 1	4 4 0	-0.052
4425.22829	0.00273	3.1×10^{-43}	0 0 0	1 2 0	5 4 2	4 4 1	-0.052

Position	$\sigma_{\text{Pos.}}$	Intensity	$\nu_1\,\nu_2\,\nu_3$	$\nu_1\text{'}\,\nu_2\text{'}\,\nu_3\text{'}$	J K_a K_c	J' K_a' K_c'	$\Delta_{\text{SPEC.}}$
4425.80078	0.00152	4.8×10^{-43}	0 0 0	1 2 0	3 2 2	2 2 1	-0.027
4427.65787	0.00355	2.6×10^{-43}	0 0 0	1 2 0	6 5 1	5 5 0	-0.096
4427.67073	0.00375	2.6×10^{-43}	0 0 0	1 2 0	6 5 2	5 5 1	-0.085
4428.57135	0.00169	5.1×10^{-43}	0 0 0	1 2 0	2 1 1	1 1 0	-0.023
4428.67082	0.00134	6.9×10^{-43}	0 0 0	1 2 0	2 0 2	1 0 1	-0.020
4431.94512	0.00074	5.2×10^{-43}	0 0 0	1 2 0	2 1 2	1 1 1	-0.020
4438.18086	0.00497	1.8×10^{-43}	0 0 0	1 2 0	3 1 2	3 1 3	-0.018
4438.21658	0.00326	3.8×10^{-43}	0 0 0	1 2 0	1 0 1	0 0 0	-0.021
4440.53357	0.00136	7.6×10^{-43}	0 0 0	1 2 0	9 2 8	8 3 5	-0.051
4443.96017	0.00679	2.8×10^{-43}	0 0 0	1 2 0	2 1 1	2 1 2	-0.024
4445.96348	0.00400	7.4×10^{-43}	0 0 0	1 2 0	8 1 7	7 3 4	-0.024
4450.66150	0.00409	3.9×10^{-43}	0 0 0	1 2 0	4 2 2	4 2 3	-0.023
4451.52423	0.00152	5.6×10^{-43}	0 0 0	1 2 0	1 1 1	1 1 0	-0.025
4453.36937	0.00146	6.4×10^{-43}	0 0 0	1 2 0	3 2 1	3 2 2	-0.027
4454.67597	0.00078	1.1×10^{-42}	0 0 0	1 2 0	2 2 0	2 2 1	-0.028
4454.99759	0.00746	2.8×10^{-43}	0 0 0	1 2 0	2 1 2	2 1 1	-0.037
4455.19564	0.00380	1.1×10^{-42}	0 0 0	1 2 0	2 2 1	2 2 0	-0.028
4457.54629	0.00258	3.9×10^{-43}	0 0 0	1 2 0	0 0 0	1 0 1	-0.021
4461.43552	0.00357	2.5×10^{-43}	0 0 0	1 2 0	5 2 4	5 2 3	-0.016
4461.80594	0.00167	5.8×10^{-43}	0 0 0	1 2 0	5 3 2	5 3 3	-0.031
4462.79587	0.00106	9.1×10^{-43}	0 0 0	1 2 0	4 3 1	4 3 2	-0.035
4463.01775	0.00214	6.1×10^{-43}	0 0 0	1 2 0	5 3 3	5 3 2	-0.033
4463.10010	0.00101	9.3×10^{-43}	0 0 0	1 2 0	4 3 2	4 3 1	-0.037
4463.34374	0.00087	1.4×10^{-42}	0 0 0	1 2 0	3 3 0	3 3 1	-0.039
4463.38157	0.00160	1.4×10^{-42}	0 0 0	1 2 0	3 3 1	3 3 0	-0.041
4463.47488	0.00270	4.1×10^{-43}	0 0 0	1 2 0	6 3 4	6 3 3	-0.033
4464.72455	0.00939	3.2×10^{-43}	0 0 0	1 2 0	7 3 5	7 3 4	-0.047
4466.80044	0.00149	7.4×10^{-43}	0 0 0	1 2 0	1 0 1	2 0 2	-0.022
4466.91693	0.00149	5.5×10^{-43}	0 0 0	1 2 0	1 1 1	2 1 2	-0.022
4470.82852	0.00334	2.7×10^{-43}	0 0 0	1 2 0	8 4 4	8 4 5	-0.042
4470.90919	0.00163	5.5×10^{-43}	0 0 0	1 2 0	1 1 0	2 1 1	-0.023
4472.16572	0.00189	4.3×10^{-43}	0 0 0	1 2 0	7 4 3	7 4 4	-0.044
4472.67210	0.00185	4.3×10^{-43}	0 0 0	1 2 0	7 4 4	7 4 3	-0.045
4473.12010	0.00113	6.8×10^{-43}	0 0 0	1 2 0	6 4 2	6 4 3	-0.049
4473.26548	0.00107	6.8×10^{-43}	0 0 0	1 2 0	6 4 3	6 4 2	-0.047
4473.82418	0.00090	1.0×10^{-42}	0 0 0	1 2 0	5 4 1	5 4 2	-0.054
4473.85256	0.00090	1.0×10^{-42}	0 0 0	1 2 0	5 4 2	5 4 1	-0.055
4474.36651	0.00215	1.6×10^{-42}	0 0 0	1 2 0	4 4 1	4 4 0	-0.058
4474.36651	0.00215	1.6×10^{-42}	0 0 0	1 2 0	4 4 0	4 4 1	-0.055
4475.06221	0.00106	9.0×10^{-43}	0 0 0	1 2 0	2 1 2	3 1 3	-0.022
4475.47554	0.00463	1.0×10^{-42}	0 0 0	1 2 0	2 0 2	3 0 3	-0.016

Position	$\sigma_{\text{Pos.}}$	Intensity	$\nu_1\,\nu_2\,\nu_3$	$\nu_1'\,\nu_2'\,\nu_3'$	J K_a K_c	J' K_a' K_c'	$\Delta_{\text{SPEC.}}$
4481.25465	0.00095	8.8×10^{-43}	0 0 0	1 2 0	2 1 1	3 1 2	-0.020
4481.33398	0.00437	1.5×10^{-43}	0 0 0	1 2 0	10 5 6	10 5 5	-0.066
4482.39426	0.00267	2.6×10^{-43}	0 0 0	1 2 0	9 5 4	9 5 5	-0.072
4482.61468	0.00347	2.6×10^{-43}	0 0 0	1 2 0	9 5 5	9 5 4	-0.071
4482.87494	0.00072	1.1×10^{-42}	0 0 0	1 2 0	3 1 3	4 1 4	-0.022
4483.45770	0.00217	1.2×10^{-42}	0 0 0	1 2 0	3 0 3	4 0 4	-0.015
4483.75235	0.00479	4.4×10^{-43}	0 0 0	1 2 0	8 5 3	8 5 4	-0.080
4483.77234	0.00564	5.3×10^{-43}	0 0 0	1 2 0	2 2 1	3 2 2	-0.037
4483.81316	0.00867	4.4×10^{-43}	0 0 0	1 2 0	8 5 4	8 5 3	-0.085
4484.77080	0.00182	5.3×10^{-43}	0 0 0	1 2 0	2 2 0	3 2 1	-0.028
4484.88170	0.00187	7.0×10^{-43}	0 0 0	1 2 0	7 5 2	7 5 3	-0.082
4484.89320	0.00391	7.0×10^{-43}	0 0 0	1 2 0	7 5 3	7 5 2	-0.086
4485.82278	0.00077	1.1×10^{-42}	0 0 0	1 2 0	6 5 1	6 5 2	-0.085
4485.82278	0.00077	1.1×10^{-42}	0 0 0	1 2 0	6 5 2	6 5 1	-0.087
4486.60101	0.00438	1.7×10^{-42}	0 0 0	1 2 0	5 5 0	5 5 1	-0.090
4486.60101	0.00438	1.7×10^{-42}	0 0 0	1 2 0	5 5 1	5 5 0	-0.090
4490.34992	0.00204	1.2×10^{-42}	0 0 0	1 2 0	4 1 4	5 1 5	-0.018
4490.83186	0.00150	1.2×10^{-42}	0 0 0	1 2 0	4 0 4	5 0 5	-0.021
4491.32544	0.00087	1.1×10^{-42}	0 0 0	1 2 0	3 1 2	4 1 3	-0.018
4492.88310	0.00092	8.4×10^{-43}	0 0 0	1 2 0	3 2 2	4 2 3	-0.026
4493.31879	0.00502	1.8×10^{-43}	0 0 0	1 2 0	8 2 6	8 3 5	-0.047
4495.17373	0.00111	8.4×10^{-43}	0 0 0	1 2 0	3 2 1	4 2 2	-0.026
4497.49024	0.00062	1.2×10^{-42}	0 0 0	1 2 0	5 1 5	6 1 6	-0.017
4497.79778	0.00096	1.2×10^{-42}	0 0 0	1 2 0	5 0 5	6 0 6	-0.018
4501.00347	0.00093	1.1×10^{-42}	0 0 0	1 2 0	4 1 3	5 1 4	-0.014
4501.71233	0.00088	9.8×10^{-43}	0 0 0	1 2 0	4 2 3	5 2 4	-0.023
4502.27362	0.00241	4.7×10^{-43}	0 0 0	1 2 0	3 3 1	4 3 2	-0.036
4502.38307	0.00177	4.7×10^{-43}	0 0 0	1 2 0	3 3 0	4 3 1	-0.037
4504.31878	0.00083	1.1×10^{-42}	0 0 0	1 2 0	6 1 6	7 1 7	-0.014
4504.47992	0.00082	1.1×10^{-42}	0 0 0	1 2 0	6 0 6	7 0 7	-0.014
4505.76487	0.00259	9.7×10^{-43}	0 0 0	1 2 0	4 2 2	5 2 3	-0.026
4510.15859	0.00113	1.1×10^{-42}	0 0 0	1 2 0	5 1 4	6 1 5	-0.011
4510.25132	0.00189	9.9×10^{-43}	0 0 0	1 2 0	5 2 4	6 2 5	-0.014
4510.85976	0.00105	9.3×10^{-43}	0 0 0	1 2 0	7 1 7	8 1 8	-0.012
4510.92479	0.00095	9.3×10^{-43}	0 0 0	1 2 0	7 0 7	8 0 8	-0.011
4511.66068	0.00624	7.1×10^{-43}	0 0 0	1 2 0	4 3 2	5 3 3	-0.038
4512.04169	0.00141	7.2×10^{-43}	0 0 0	1 2 0	4 3 1	5 3 2	-0.039
4516.31108	0.00103	9.8×10^{-43}	0 0 0	1 2 0	5 2 3	6 2 4	-0.014
4517.13996	0.00154	7.4×10^{-43}	0 0 0	1 2 0	8 0 8	9 0 9	-0.008
4518.49385	0.00103	9.1×10^{-43}	0 0 0	1 2 0	6 2 5	7 2 6	-0.014
4518.69813	0.00086	9.6×10^{-43}	0 0 0	1 2 0	6 1 5	7 1 6	-0.007

Position	$\sigma_{\text{Pos.}}$	Intensity	$\nu_1\ \nu_2\ \nu_3$	$\nu_1{'}\ \nu_2{'}\ \nu_3{'}$	J K$_a$ K$_c$	J' K$_a${'} K$_c${'}	$\Delta_{\text{SPEC.}}$
4520.91974	0.00094	8.0×10^{-43}	0 0 0	1 2 0	5 3 3	6 3 4	-0.032
4521.85693	0.00098	8.1×10^{-43}	0 0 0	1 2 0	5 3 2	6 3 3	-0.034
4522.97895	0.00210	3.9×10^{-43}	0 0 0	1 2 0	4 4 1	5 4 2	-0.059
4522.99375	0.00160	3.9×10^{-43}	0 0 0	1 2 0	4 4 0	5 4 1	-0.055
4523.12156	0.00138	4.2×10^{-43}	0 0 0	1 2 0	9 0 9	10 0 10	-0.019
4526.62432	0.00142	8.0×10^{-43}	0 0 0	1 2 0	7 1 6	8 1 7	-0.010
4526.76866	0.00124	7.5×10^{-43}	0 0 0	1 2 0	6 2 4	7 2 5	-0.014
4529.98946	0.00120	7.7×10^{-43}	0 0 0	1 2 0	6 3 4	7 3 5	-0.026
4531.74917	0.00333	2.4×10^{-43}	0 0 0	1 2 0	8 6 3	8 6 2	-0.123
4531.74917	0.00333	2.4×10^{-43}	0 0 0	1 2 0	8 6 2	8 6 3	-0.122
4532.29396	0.00177	5.8×10^{-43}	0 0 0	1 2 0	5 4 2	6 4 3	-0.053
4532.33464	0.00277	5.8×10^{-43}	0 0 0	1 2 0	5 4 1	6 4 2	-0.055
4533.51707	0.00108	6.1×10^{-43}	0 0 0	1 2 0	8 2 7	9 2 8	-0.010
4533.78612	0.00065	7.4×10^{-43}	0 0 0	1 2 0	6 6 0	6 6 1	-0.108
4533.78612	0.00065	7.4×10^{-43}	0 0 0	1 2 0	6 6 1	6 6 0	-0.108
4534.06719	0.00120	6.4×10^{-43}	0 0 0	1 2 0	8 1 7	9 1 8	-0.007
4534.17972	0.00271	2.8×10^{-43}	0 0 0	1 2 0	11 0 11	12 0 12	0.001
4534.21445	0.00269	2.8×10^{-43}	0 0 0	1 2 0	11 1 11	12 1 12	0.002
4536.55980	0.00111	7.3×10^{-43}	0 0 0	1 2 0	7 2 5	8 2 6	-0.001
4538.81666	0.00119	6.8×10^{-43}	0 0 0	1 2 0	7 3 5	8 3 6	-0.023
4539.43113	0.00506	1.9×10^{-43}	0 0 0	1 2 0	12 0 12	13 0 13	0.009
4539.43113	0.00502	1.9×10^{-43}	0 0 0	1 2 0	12 1 12	13 1 13	-0.000
4540.82242	0.00191	4.8×10^{-43}	0 0 0	1 2 0	9 2 8	10 2 9	-0.006
4541.16802	0.01041	4.9×10^{-43}	0 0 0	1 2 0	9 1 8	10 1 9	-0.001
4541.53653	0.00139	6.2×10^{-43}	0 0 0	1 2 0	6 4 3	7 4 4	-0.050
4541.66420	0.00133	6.2×10^{-43}	0 0 0	1 2 0	6 4 2	7 4 3	-0.048
4544.40016	0.00909	1.2×10^{-43}	0 0 0	1 2 0	13 0 13	14 0 14	0.012
4544.40016	0.00909	1.2×10^{-43}	0 0 0	1 2 0	13 1 13	14 1 14	0.007
4544.75467	0.01163	3.3×10^{-43}	0 0 0	1 2 0	5 5 1	6 5 2	-0.090
4544.75467	0.01163	3.3×10^{-43}	0 0 0	1 2 0	5 5 0	6 5 1	-0.091
4546.01019	0.00136	5.8×10^{-43}	0 0 0	1 2 0	8 2 6	9 2 7	0.006
4547.36997	0.00104	5.6×10^{-43}	0 0 0	1 2 0	8 3 6	9 3 7	-0.014
4547.76513	0.00223	3.5×10^{-43}	0 0 0	1 2 0	10 2 9	11 2 10	-0.005
4549.10530	0.00737	7.6×10^{-44}	0 0 0	1 2 0	14 0 14	15 0 15	0.007
4549.13016	0.03872	7.6×10^{-44}	0 0 0	1 2 0	14 1 14	15 1 15	0.030
4550.74575	0.00123	5.4×10^{-43}	0 0 0	1 2 0	7 4 4	8 4 5	-0.047
4551.01201	0.00116	5.8×10^{-43}	0 0 0	1 2 0	7 4 3	8 4 4	-0.042
4552.64526	0.00139	5.1×10^{-43}	0 0 0	1 2 0	8 3 5	9 3 6	-0.006
4553.74039	0.00528	4.8×10^{-43}	0 0 0	1 2 0	6 5 2	7 5 3	-0.086
4553.74039	0.00530	4.8×10^{-43}	0 0 0	1 2 0	6 5 1	7 5 2	-0.091
4554.44311	0.00444	2.5×10^{-43}	0 0 0	1 2 0	11 2 10	12 2 11	0.004

Position	$\sigma_{\text{Pos.}}$	Intensity	$\nu_1\ \nu_2\ \nu_3$	$\nu_1'\ \nu_2'\ \nu_3'$	J K$_a$ K$_c$	J' K$_a$' K$_c$'	$\Delta_{\text{SPEC.}}$
4554.72084	0.00524	2.5×10^{-43}	0 0 0	1 2 0	11 1 10	12 1 11	0.006
4554.93436	0.00159	4.3×10^{-43}	0 0 0	1 2 0	9 2 7	10 2 8	0.010
4555.61189	0.00152	4.3×10^{-43}	0 0 0	1 2 0	9 3 7	10 3 8	-0.011
4559.07603	0.00450	4.0×10^{-43}	0 0 0	1 2 0	8 4 5	9 4 6	-0.055
4559.27739	0.00709	1.0×10^{-43}	0 0 0	1 2 0	12 1 11	13 1 12	0.025
4560.42471	0.00578	4.9×10^{-43}	0 0 0	1 2 0	8 4 4	9 4 5	-0.035
4560.73950	0.00546	1.4×10^{-43}	0 0 0	1 2 0	12 2 11	13 2 12	0.005
4562.59713	0.00157	5.0×10^{-43}	0 0 0	1 2 0	7 5 3	8 5 4	-0.084
4562.61742	0.00182	5.0×10^{-43}	0 0 0	1 2 0	7 5 2	8 5 3	-0.083
4562.66587	0.00172	3.9×10^{-43}	0 0 0	1 2 0	9 3 6	10 3 7	0.005
4563.31920	0.00257	3.1×10^{-43}	0 0 0	1 2 0	10 2 8	11 2 9	0.017
4563.53681	0.00232	3.1×10^{-43}	0 0 0	1 2 0	10 3 8	11 3 9	-0.005
4566.72730	0.01010	9.8×10^{-44}	0 0 0	1 2 0	13 1 12	14 1 13	0.000
4568.13474	0.00173	3.8×10^{-43}	0 0 0	1 2 0	9 4 6	10 4 7	-0.032
4569.92022	0.00555	3.7×10^{-43}	0 0 0	1 2 0	9 4 5	10 4 6	-0.040
4571.14325	0.00397	2.1×10^{-43}	0 0 0	1 2 0	11 3 9	12 3 10	0.000
4571.21457	0.01057	2.1×10^{-43}	0 0 0	1 2 0	11 2 9	12 2 10	0.011
4571.31450	0.00148	4.5×10^{-43}	0 0 0	1 2 0	8 5 4	9 5 5	-0.078
4571.37167	0.00239	4.5×10^{-43}	0 0 0	1 2 0	8 5 3	9 5 4	-0.080
4572.32327	0.00341	2.8×10^{-43}	0 0 0	1 2 0	10 3 7	11 3 8	0.004
4576.68002	0.00873	2.9×10^{-43}	0 0 0	1 2 0	10 4 7	11 4 8	-0.045
4578.44659	0.00536	1.4×10^{-43}	0 0 0	1 2 0	12 3 10	13 3 11	0.004
4578.84520	0.00542	1.4×10^{-43}	0 0 0	1 2 0	12 2 10	13 2 11	0.031
4579.51942	0.01344	2.7×10^{-43}	0 0 0	1 2 0	10 4 6	11 4 7	-0.010
4579.86796	0.00171	3.7×10^{-43}	0 0 0	1 2 0	9 5 5	10 5 6	-0.073
4580.01807	0.00186	3.6×10^{-43}	0 0 0	1 2 0	9 5 4	10 5 5	-0.073
4587.20862	0.00203	4.2×10^{-43}	0 0 0	1 2 0	6 0 6	7 2 5	-0.013
4589.05003	0.00296	1.8×10^{-43}	0 0 0	1 2 0	11 4 7	12 4 8	-0.006
4590.07986	0.00588	1.2×10^{-43}	0 0 0	1 2 0	12 3 9	13 3 10	0.037
4591.92873	0.00956	5.2×10^{-44}	0 0 0	1 2 0	14 3 12	15 3 13	0.004
4596.34605	0.00717	1.9×10^{-43}	0 0 0	1 2 0	11 5 7	12 5 8	-0.069
4597.93083	0.00055	1.4×10^{-42}	0 0 0	1 2 0	7 2 6	8 3 5	-0.060
4601.55652	0.00436	1.1×10^{-43}	0 0 0	1 2 0	6 6 1	7 6 2	-0.107
4601.55652	0.00446	1.1×10^{-43}	0 0 0	1 2 0	6 6 0	7 6 1	-0.107
4605.46729	0.00689	1.2×10^{-43}	0 0 0	1 2 0	12 5 7	13 5 8	-0.048
4607.32244	0.00966	7.0×10^{-44}	0 0 0	1 2 0	13 4 9	14 4 10	-0.014
4612.06658	0.00208	4.3×10^{-43}	0 0 0	1 2 0	8 3 5	9 4 6	-0.048
4627.81200	0.00800	9.5×10^{-44}	0 0 0	1 2 0	9 6 4	10 6 5	-0.068
4627.81200	0.00800	9.5×10^{-44}	0 0 0	1 2 0	9 6 3	10 6 4	-0.076

A.2.2.4 DTO $\nu_1 + \nu_3$ band

Here, the lines assigned to the $\nu_1 + \nu_3$ band of DTO obtained from the $10\,\text{GBq}$ sample are presented. These lines are published in [Her22]. For further information, see Section 5.5.2.

Table A.11: Linelist of the DTO $\nu_1 + \nu_3$ band. The columns present the assigned line position, the uncertainty on the position $\sigma_{\text{Pos.}}$, the line intensity taking natural abundance into account, lower and upper vibrational quanta, lower and upper rotational quanta and the deviation to the predictions from SPECTRA database $\Delta_{\text{SPEC.}}$.

Position	$\sigma_{\text{Pos.}}$	Intensity	$\nu_1\,\nu_2\,\nu_3$	$\nu_1'\,\nu_2'\,\nu_3'$	J K_a K_c	J' K_a' K_c'	$\Delta_{\text{SPEC.}}$
4824.47395	0.00823	1.0×10^{-43}	0 0 0	1 0 1	7 7 0	6 6 1	-0.154
4824.47395	0.00823	1.0×10^{-43}	0 0 0	1 0 1	7 7 1	6 6 0	-0.154
4833.52288	0.02267	1.1×10^{-43}	0 0 0	1 0 1	8 6 2	7 5 3	-0.126
4833.53832	0.03957	1.1×10^{-43}	0 0 0	1 0 1	8 6 3	7 5 2	-0.122
4853.90931	0.00525	1.5×10^{-43}	0 0 0	1 0 1	8 5 4	7 4 3	-0.122
4855.26923	0.00651	2.1×10^{-43}	0 0 0	1 0 1	6 6 1	5 5 0	-0.144
4855.26923	0.00651	2.1×10^{-43}	0 0 0	1 0 1	6 6 0	5 5 1	-0.144
4864.46239	0.00398	2.1×10^{-43}	0 0 0	1 0 1	7 5 2	6 4 3	-0.127
4864.57525	0.00401	2.1×10^{-43}	0 0 0	1 0 1	7 5 3	6 4 2	-0.122
4869.21541	0.00483	1.1×10^{-43}	0 0 0	1 0 1	9 4 6	8 3 5	-0.098
4871.34730	0.01071	1.6×10^{-43}	0 0 0	1 0 1	8 4 4	7 3 5	-0.111
4875.25233	0.00818	2.8×10^{-43}	0 0 0	1 0 1	6 5 2	5 4 1	-0.146
4875.26992	0.00798	2.8×10^{-43}	0 0 0	1 0 1	6 5 1	5 4 2	-0.107
4876.93906	0.00494	1.7×10^{-43}	0 0 0	1 0 1	8 4 5	7 3 4	-0.105
4883.44203	0.00334	2.4×10^{-43}	0 0 0	1 0 1	7 4 3	6 3 4	-0.109
4885.81581	0.00554	2.4×10^{-43}	0 0 0	1 0 1	7 4 4	6 3 3	-0.109
4885.89119	0.00925	3.6×10^{-43}	0 0 0	1 0 1	5 5 0	4 4 1	-0.134
4885.89623	0.00903	3.6×10^{-43}	0 0 0	1 0 1	5 5 1	4 4 0	-0.132
4888.82187	0.01287	1.0×10^{-43}	0 0 0	1 0 1	14 0 14	13 1 13	-0.086
4888.82187	0.01287	1.0×10^{-43}	0 0 0	1 0 1	14 1 14	13 0 13	-0.077
4894.38040	0.00647	1.7×10^{-43}	0 0 0	1 0 1	7 3 4	6 2 5	-0.095
4894.73628	0.00270	3.2×10^{-43}	0 0 0	1 0 1	6 4 2	5 3 3	-0.113
4895.54987	0.00352	3.2×10^{-43}	0 0 0	1 0 1	6 4 3	5 3 2	-0.116
4899.06912	0.01177	1.2×10^{-43}	0 0 0	1 0 1	11 2 9	10 2 8	-0.092
4899.06912	0.01239	1.6×10^{-43}	0 0 0	1 0 1	13 0 13	12 1 12	-0.093
4899.06912	0.01544	1.1×10^{-43}	0 0 0	1 0 1	13 0 13	12 0 12	-0.083
4899.06912	0.01113	1.1×10^{-43}	0 0 0	1 0 1	13 1 13	12 1 12	-0.086
4899.08929	0.00542	1.6×10^{-43}	0 0 0	1 0 1	13 1 13	12 0 12	-0.056
4899.11253	0.00615	1.1×10^{-43}	0 0 0	1 0 1	12 1 11	11 1 10	-0.081
4900.87516	0.00875	1.5×10^{-43}	0 0 0	1 0 1	9 3 7	8 2 6	-0.082
4905.15755	0.01172	1.0×10^{-43}	0 0 0	1 0 1	10 4 6	9 4 5	-0.100
4905.19063	0.00634	1.5×10^{-43}	0 0 0	1 0 1	10 3 7	9 3 6	-0.086

Position	$\sigma_{\text{Pos.}}$	Intensity	$\nu_1\ \nu_2\ \nu_3$	$\nu_1{}'\ \nu_2{}'\ \nu_3{}'$	J K_a K_c	J' $K_a{}'$ $K_c{}'$	$\Delta_{\text{SPEC.}}$
4905.55597	0.00223	4.1×10^{-43}	0 0 0	1 0 1	5 4 1	4 3 2	-0.119
4905.75928	0.00375	4.1×10^{-43}	0 0 0	1 0 1	5 4 2	4 3 1	-0.122
4908.11859	0.00609	1.7×10^{-43}	0 0 0	1 0 1	11 2 10	10 1 9	-0.088
4909.14333	0.01489	1.7×10^{-43}	0 0 0	1 0 1	12 1 12	11 1 11	-0.102
4909.14689	0.00960	1.7×10^{-43}	0 0 0	1 0 1	12 0 12	11 0 11	-0.090
4909.16169	0.00766	2.5×10^{-43}	0 0 0	1 0 1	12 0 12	11 1 11	-0.099
4909.38771	0.00550	1.8×10^{-43}	0 0 0	1 0 1	10 2 8	9 2 7	-0.071
4909.71010	0.00378	2.7×10^{-43}	0 0 0	1 0 1	6 3 3	5 2 4	-0.093
4910.43226	0.00515	1.7×10^{-43}	0 0 0	1 0 1	11 1 10	10 2 9	-0.084
4912.13083	0.03006	1.6×10^{-43}	0 0 0	1 0 1	10 3 8	9 3 7	-0.094
4912.61597	0.00305	2.5×10^{-43}	0 0 0	1 0 1	7 3 5	6 2 4	-0.102
4916.09437	0.00519	5.1×10^{-43}	0 0 0	1 0 1	4 4 0	3 3 1	-0.122
4916.12473	0.00241	5.1×10^{-43}	0 0 0	1 0 1	4 4 1	3 3 0	-0.121
4917.10689	0.00309	2.3×10^{-43}	0 0 0	1 0 1	10 2 9	9 1 8	-0.091
4917.46276	0.00655	1.4×10^{-43}	0 0 0	1 0 1	9 4 5	8 4 4	-0.107
4917.51167	0.00552	2.1×10^{-43}	0 0 0	1 0 1	9 3 6	8 3 5	-0.095
4918.54179	0.00616	1.4×10^{-43}	0 0 0	1 0 1	9 4 6	8 4 5	-0.110
4918.82388	0.00366	2.4×10^{-43}	0 0 0	1 0 1	10 1 9	9 1 8	-0.087
4919.02493	0.00315	4.1×10^{-43}	0 0 0	1 0 1	11 1 11	10 0 10	-0.090
4919.05551	0.01423	1.9×10^{-43}	0 0 0	1 0 1	11 0 11	10 0 10	-0.091
4919.07664	0.00979	1.9×10^{-43}	0 0 0	1 0 1	11 1 11	10 1 10	-0.093
4919.11989	0.00569	4.1×10^{-43}	0 0 0	1 0 1	11 0 11	10 1 10	-0.080
4919.50269	0.01079	3.2×10^{-43}	0 0 0	1 0 1	6 3 4	5 2 3	-0.104
4919.53074	0.01088	2.4×10^{-43}	0 0 0	1 0 1	10 2 9	9 2 8	-0.110
4920.00574	0.00389	2.7×10^{-43}	0 0 0	1 0 1	9 2 7	8 2 6	-0.083
4921.26246	0.00431	2.3×10^{-43}	0 0 0	1 0 1	10 1 9	9 2 8	-0.091
4922.88960	0.00785	2.2×10^{-43}	0 0 0	1 0 1	9 3 7	8 3 6	-0.087
4922.94581	0.00319	3.8×10^{-43}	0 0 0	1 0 1	5 3 2	4 2 3	-0.110
4925.38564	0.00300	3.0×10^{-43}	0 0 0	1 0 1	9 2 8	8 1 7	-0.091
4928.37439	0.00794	3.3×10^{-43}	0 0 0	1 0 1	9 1 8	8 1 7	-0.085
4928.74909	0.00309	4.2×10^{-43}	0 0 0	1 0 1	10 1 10	9 0 9	-0.095
4928.81590	0.00637	4.1×10^{-43}	0 0 0	1 0 1	10 0 10	9 0 9	-0.092
4928.85089	0.00673	4.1×10^{-43}	0 0 0	1 0 1	10 1 10	9 1 9	-0.091
4928.88606	0.00703	4.2×10^{-43}	0 0 0	1 0 1	10 0 10	9 1 9	-0.119
4929.33158	0.00425	1.7×10^{-43}	0 0 0	1 0 1	8 4 4	7 4 3	-0.116
4929.54971	0.00358	3.2×10^{-43}	0 0 0	1 0 1	9 2 8	8 2 7	-0.092
4929.84563	0.01670	1.7×10^{-43}	0 0 0	1 0 1	8 4 5	7 4 4	-0.107
4929.93030	0.00312	2.8×10^{-43}	0 0 0	1 0 1	8 3 5	7 3 4	-0.097
4930.99667	0.00731	3.7×10^{-43}	0 0 0	1 0 1	8 2 6	7 2 5	-0.092
4932.86375	0.00486	3.6×10^{-43}	0 0 0	1 0 1	8 2 7	7 1 6	-0.096
4933.65942	0.00308	2.9×10^{-43}	0 0 0	1 0 1	8 3 6	7 3 5	-0.102

Position	$\sigma_{\text{Pos.}}$	Intensity	$\nu_1\,\nu_2\,\nu_3$	$\nu_1'\,\nu_2'\,\nu_3'$	J K_a K_c	J' K_a' K_c'	$\Delta_{\text{SPEC.}}$
4934.73013	0.00187	4.8×10^{-43}	0 0 0	1 0 1	4 3 1	3 2 2	-0.112
4936.24023	0.00207	4.9×10^{-43}	0 0 0	1 0 1	4 3 2	3 2 1	-0.112
4938.25866	0.00432	6.2×10^{-43}	0 0 0	1 0 1	9 1 9	8 0 8	-0.095
4938.38912	0.00197	4.6×10^{-43}	0 0 0	1 0 1	9 0 9	8 0 8	-0.093
4938.46902	0.00204	4.6×10^{-43}	0 0 0	1 0 1	9 1 9	8 1 8	-0.094
4938.58320	0.00301	6.2×10^{-43}	0 0 0	1 0 1	9 0 9	8 1 8	-0.109
4939.40703	0.00099	3.5×10^{-43}	0 0 0	1 0 1	8 2 7	7 2 6	-0.120
4939.68545	0.00087	4.1×10^{-43}	0 0 0	1 0 1	7 2 6	6 1 5	-0.077
4940.80415	0.00366	2.0×10^{-43}	0 0 0	1 0 1	7 4 3	6 4 2	-0.122
4941.00723	0.00459	2.0×10^{-43}	0 0 0	1 0 1	7 4 4	6 4 3	-0.118
4942.01844	0.00897	9.4×10^{-44}	0 0 0	1 0 1	9 2 7	8 3 6	-0.090
4942.19623	0.00248	3.4×10^{-43}	0 0 0	1 0 1	7 3 4	6 3 3	-0.106
4942.32360	0.00202	4.7×10^{-43}	0 0 0	1 0 1	7 2 5	6 2 4	-0.094
4945.47304	0.00470	2.3×10^{-43}	0 0 0	1 0 1	4 2 2	3 1 3	-0.102
4945.48815	0.01053	9.9×10^{-44}	0 0 0	1 0 1	9 2 8	9 1 9	-0.097
4945.57832	0.00160	5.7×10^{-43}	0 0 0	1 0 1	3 3 0	2 2 1	-0.114
4945.87775	0.00351	5.7×10^{-43}	0 0 0	1 0 1	3 3 1	2 2 0	-0.117
4946.04218	0.00862	1.1×10^{-43}	0 0 0	1 0 1	9 4 6	9 3 7	-0.108
4946.12289	0.00254	4.5×10^{-43}	0 0 0	1 0 1	6 2 5	5 1 4	-0.100
4947.32361	0.00180	5.6×10^{-43}	0 0 0	1 0 1	7 1 6	6 1 5	-0.093
4947.50524	0.00131	7.5×10^{-43}	0 0 0	1 0 1	8 1 8	7 0 7	-0.097
4947.76246	0.00371	6.0×10^{-43}	0 0 0	1 0 1	8 0 8	7 0 7	-0.100
4947.92757	0.00160	6.0×10^{-43}	0 0 0	1 0 1	8 1 8	7 1 7	-0.095
4948.18927	0.01044	7.4×10^{-43}	0 0 0	1 0 1	8 0 8	7 1 7	-0.094
4949.05955	0.01542	1.5×10^{-43}	0 0 0	1 0 1	8 4 5	8 3 6	-0.127
4951.94292	0.00427	1.9×10^{-43}	0 0 0	1 0 1	6 4 2	5 4 1	-0.123
4952.00430	0.00420	1.9×10^{-43}	0 0 0	1 0 1	6 4 3	5 4 2	-0.125
4952.65980	0.00278	4.7×10^{-43}	0 0 0	1 0 1	5 2 4	4 1 3	-0.098
4952.81070	0.00485	1.9×10^{-43}	0 0 0	1 0 1	6 4 3	6 3 4	-0.118
4953.90551	0.00115	5.5×10^{-43}	0 0 0	1 0 1	6 2 4	5 2 3	-0.092
4954.61929	0.00592	1.5×10^{-43}	0 0 0	1 0 1	8 2 7	8 1 8	-0.094
4954.91186	0.00497	1.2×10^{-43}	0 0 0	1 0 1	4 4 0	4 3 1	-0.111
4956.43038	0.00626	8.6×10^{-43}	0 0 0	1 0 1	7 1 7	6 0 6	-0.098
4956.94388	0.00359	7.2×10^{-43}	0 0 0	1 0 1	7 0 7	6 0 6	-0.096
4957.13515	0.01114	3.3×10^{-43}	0 0 0	1 0 1	7 1 6	6 2 5	-0.107
4957.25397	0.00166	7.2×10^{-43}	0 0 0	1 0 1	7 1 7	6 1 6	-0.098
4957.37475	0.00583	1.6×10^{-43}	0 0 0	1 0 1	8 4 4	8 3 5	-0.104
4957.76414	0.00226	8.5×10^{-43}	0 0 0	1 0 1	7 0 7	6 1 6	-0.100
4957.83527	0.00679	1.9×10^{-43}	0 0 0	1 0 1	8 3 6	8 2 7	-0.103
4958.15434	0.01043	9.8×10^{-44}	0 0 0	1 0 1	8 2 6	7 3 5	-0.092
4959.46973	0.00180	5.7×10^{-43}	0 0 0	1 0 1	6 2 5	5 2 4	-0.101

Position	$\sigma_{\text{Pos.}}$	Intensity	$\nu_1\,\nu_2\,\nu_3$	$\nu_1'\,\nu_2'\,\nu_3'$	J K_a K_c	J' K_a' K_c'	$\Delta_{\text{SPEC.}}$
4959.60899	0.00217	4.9×10^{-43}	0 0 0	1 0 1	4 2 3	3 1 2	-0.104
4963.09737	0.00500	2.1×10^{-43}	0 0 0	1 0 1	7 2 6	7 1 7	-0.099
4963.13490	0.00971	1.4×10^{-43}	0 0 0	1 0 1	7 3 5	7 2 6	-0.112
4964.92830	0.00150	9.3×10^{-43}	0 0 0	1 0 1	6 1 6	5 0 5	-0.102
4965.60995	0.00158	5.7×10^{-43}	0 0 0	1 0 1	5 2 3	4 2 2	-0.103
4965.90707	0.00118	8.1×10^{-43}	0 0 0	1 0 1	6 0 6	5 0 5	-0.100
4965.93551	0.00870	3.5×10^{-43}	0 0 0	1 0 1	5 3 3	4 3 2	-0.114
4966.47098	0.00157	8.0×10^{-43}	0 0 0	1 0 1	6 1 6	5 1 5	-0.099
4967.18800	0.00204	4.9×10^{-43}	0 0 0	1 0 1	3 2 2	2 1 1	-0.108
4967.30855	0.00126	7.3×10^{-43}	0 0 0	1 0 1	5 1 4	4 1 3	-0.098
4967.44641	0.00109	9.1×10^{-43}	0 0 0	1 0 1	6 0 6	5 1 5	-0.100
4967.47790	0.00325	3.2×10^{-43}	0 0 0	1 0 1	6 3 4	6 2 5	-0.105
4969.47572	0.00167	5.9×10^{-43}	0 0 0	1 0 1	5 2 4	4 2 3	-0.106
4970.33268	0.00831	2.3×10^{-43}	0 0 0	1 0 1	7 1 6	7 0 7	-0.097
4970.47149	0.00500	3.1×10^{-43}	0 0 0	1 0 1	6 1 5	5 2 4	-0.102
4970.62320	0.00457	3.4×10^{-43}	0 0 0	1 0 1	5 3 3	5 2 4	-0.107
4970.78923	0.00737	2.8×10^{-43}	0 0 0	1 0 1	6 2 5	6 1 6	-0.098
4972.81456	0.00438	3.1×10^{-43}	0 0 0	1 0 1	4 3 2	4 2 3	-0.103
4972.91981	0.00115	9.3×10^{-43}	0 0 0	1 0 1	5 1 5	4 0 4	-0.103
4973.46752	0.00239	4.4×10^{-43}	0 0 0	1 0 1	2 2 0	1 1 1	-0.108
4974.15672	0.01492	9.5×10^{-44}	0 0 0	1 0 1	7 2 5	6 3 4	-0.104
4974.20669	0.00648	2.0×10^{-43}	0 0 0	1 0 1	3 3 1	3 2 2	-0.115
4974.70256	0.00324	8.6×10^{-43}	0 0 0	1 0 1	5 0 5	4 0 4	-0.097
4975.50279	0.00268	4.9×10^{-43}	0 0 0	1 0 1	2 2 1	1 1 0	-0.099
4977.24879	0.00164	5.2×10^{-43}	0 0 0	1 0 1	4 2 2	3 2 1	-0.108
4977.38149	0.00098	8.8×10^{-43}	0 0 0	1 0 1	5 0 5	4 1 4	-0.101
4977.79783	0.00114	7.3×10^{-43}	0 0 0	1 0 1	4 1 3	3 1 2	-0.102
4979.49508	0.00410	4.0×10^{-43}	0 0 0	1 0 1	6 3 3	6 2 4	-0.115
4979.51245	0.00268	5.2×10^{-43}	0 0 0	1 0 1	4 2 3	3 2 2	-0.100
4980.05426	0.00332	3.1×10^{-43}	0 0 0	1 0 1	8 3 5	8 2 6	-0.095
4980.44212	0.00122	8.5×10^{-43}	0 0 0	1 0 1	4 1 4	3 0 3	-0.103
4980.50418	0.00377	3.7×10^{-43}	0 0 0	1 0 1	7 3 4	7 2 5	-0.096
4980.95862	0.00721	3.3×10^{-43}	0 0 0	1 0 1	6 1 5	6 0 6	-0.108
4983.17765	0.00424	3.8×10^{-43}	0 0 0	1 0 1	4 2 3	4 1 4	-0.110
4983.45907	0.00112	8.5×10^{-43}	0 0 0	1 0 1	4 0 4	3 0 3	-0.101
4984.11487	0.00851	2.5×10^{-43}	0 0 0	1 0 1	5 1 4	4 2 3	-0.115
4984.68680	0.00147	8.0×10^{-43}	0 0 0	1 0 1	4 1 4	3 1 3	-0.104
4986.28577	0.00242	4.5×10^{-43}	0 0 0	1 0 1	7 2 5	7 1 6	-0.094
4987.67789	0.01136	3.6×10^{-43}	0 0 0	1 0 1	3 2 2	3 1 3	-0.122
4987.70395	0.00235	7.4×10^{-43}	0 0 0	1 0 1	4 0 4	3 1 3	-0.103
4987.76146	0.00203	7.2×10^{-43}	0 0 0	1 0 1	3 1 3	2 0 2	-0.105

Position	$\sigma_{\text{Pos.}}$	Intensity	$\nu_1\,\nu_2\,\nu_3$	$\nu_1'\,\nu_2'\,\nu_3'$	J K_a K_c	J' K_a' K_c'	$\Delta_{\text{SPEC.}}$
4989.53974	0.00574	3.5×10^{-43}	0 0 0	1 0 1	3 2 2	2 2 1	-0.098
4990.65319	0.00170	4.7×10^{-43}	0 0 0	1 0 1	5 1 4	5 0 5	-0.081
4991.03781	0.00452	2.6×10^{-43}	0 0 0	1 0 1	2 2 1	2 1 2	-0.107
4992.05176	0.00168	6.3×10^{-43}	0 0 0	1 0 1	6 2 4	6 1 5	-0.097
4992.42104	0.00135	7.6×10^{-43}	0 0 0	1 0 1	3 0 3	2 0 2	-0.103
4995.30643	0.00172	5.7×10^{-43}	0 0 0	1 0 1	2 1 2	1 0 1	-0.105
4995.51935	0.00194	7.4×10^{-43}	0 0 0	1 0 1	5 2 3	5 1 4	-0.099
4996.96173	0.00224	5.8×10^{-43}	0 0 0	1 0 1	3 2 1	3 1 2	-0.106
4996.98800	0.00306	7.3×10^{-43}	0 0 0	1 0 1	4 2 2	4 1 3	-0.109
4998.39750	0.00375	5.2×10^{-43}	0 0 0	1 0 1	3 0 3	2 1 2	-0.109
4998.68147	0.00199	6.4×10^{-43}	0 0 0	1 0 1	4 1 3	4 0 4	-0.110
4999.24161	0.00220	4.1×10^{-43}	0 0 0	1 0 1	2 1 1	1 1 0	-0.107
5001.73358	0.01513	5.8×10^{-43}	0 0 0	1 0 1	2 0 2	1 0 1	-0.115
5002.77076	0.00224	4.2×10^{-43}	0 0 0	1 0 1	2 1 2	1 1 1	-0.105
5003.43330	0.00336	4.0×10^{-43}	0 0 0	1 0 1	1 1 1	0 0 0	-0.105
5003.55019	0.00682	9.7×10^{-44}	0 0 0	1 0 1	8 5 3	8 5 4	-0.127
5003.63324	0.00616	9.7×10^{-44}	0 0 0	1 0 1	8 5 4	8 5 3	-0.127
5004.73736	0.00577	7.8×10^{-43}	0 0 0	1 0 1	3 1 2	3 0 3	-0.108
5004.92612	0.00910	1.6×10^{-43}	0 0 0	1 0 1	7 5 3	7 5 2	-0.149
5004.92612	0.00915	1.6×10^{-43}	0 0 0	1 0 1	7 5 2	7 5 3	-0.130
5007.14197	0.00639	4.1×10^{-43}	0 0 0	1 0 1	5 5 0	5 5 1	-0.144
5007.14197	0.00634	4.1×10^{-43}	0 0 0	1 0 1	5 5 1	5 5 0	-0.144
5008.80454	0.00130	7.8×10^{-43}	0 0 0	1 0 1	2 1 1	2 0 2	-0.105
5010.17976	0.00246	2.6×10^{-43}	0 0 0	1 0 1	6 4 3	6 4 2	-0.123
5011.07690	0.00472	4.1×10^{-43}	0 0 0	1 0 1	5 4 1	5 4 2	-0.129
5011.11613	0.00606	4.1×10^{-43}	0 0 0	1 0 1	5 4 2	5 4 1	-0.127
5011.33481	0.00612	1.9×10^{-43}	0 0 0	1 0 1	6 3 3	6 3 4	-0.118
5011.36967	0.00536	3.2×10^{-43}	0 0 0	1 0 1	1 0 1	0 0 0	-0.105
5011.94748	0.00408	6.5×10^{-43}	0 0 0	1 0 1	4 4 0	4 4 1	-0.129
5011.94748	0.00408	6.5×10^{-43}	0 0 0	1 0 1	4 4 1	4 4 0	-0.134
5013.60551	0.00327	3.2×10^{-43}	0 0 0	1 0 1	5 3 2	5 3 3	-0.118
5014.78435	0.00443	2.2×10^{-43}	0 0 0	1 0 1	2 1 1	2 1 2	-0.107
5014.96176	0.00206	5.2×10^{-43}	0 0 0	1 0 1	4 3 1	4 3 2	-0.118
5015.00572	0.00339	3.2×10^{-43}	0 0 0	1 0 1	5 3 3	5 3 2	-0.112
5015.29696	0.00518	2.0×10^{-43}	0 0 0	1 0 1	6 3 4	6 3 3	-0.114
5015.32123	0.00422	5.2×10^{-43}	0 0 0	1 0 1	4 3 2	4 3 1	-0.119
5015.79555	0.00119	8.2×10^{-43}	0 0 0	1 0 1	3 3 0	3 3 1	-0.121
5015.84844	0.00151	8.2×10^{-43}	0 0 0	1 0 1	3 3 1	3 3 0	-0.121
5016.85540	0.00219	4.5×10^{-43}	0 0 0	1 0 1	3 2 1	3 2 2	-0.112
5018.40052	0.00133	7.7×10^{-43}	0 0 0	1 0 1	2 2 0	2 2 1	-0.113
5018.66812	0.00263	4.4×10^{-43}	0 0 0	1 0 1	1 1 0	1 1 1	-0.106

Position	$\sigma_{\text{Pos.}}$	Intensity	$\nu_1\,\nu_2\,\nu_3$	$\nu_1'\,\nu_2'\,\nu_3'$	J K_a K_c	J' K_a' K_c'	$\Delta_{\text{SPEC.}}$
5018.93983	0.00294	7.7×10^{-43}	0 0 0	1 0 1	2 2 1	2 2 0	-0.114
5019.47038	0.00210	4.5×10^{-43}	0 0 0	1 0 1	3 2 2	3 2 1	-0.111
5021.16441	0.00385	2.7×10^{-43}	0 0 0	1 0 1	4 2 3	4 2 2	-0.112
5022.19332	0.00219	4.5×10^{-43}	0 0 0	1 0 1	1 1 1	1 1 0	-0.110
5024.41419	0.00682	1.7×10^{-43}	0 0 0	1 0 1	5 2 4	5 2 3	-0.101
5025.36537	0.00475	2.3×10^{-43}	0 0 0	1 0 1	2 1 2	2 1 1	-0.107
5030.13374	0.00200	6.1×10^{-43}	0 0 0	1 0 1	1 0 1	1 1 0	-0.107
5030.61869	0.00505	3.2×10^{-43}	0 0 0	1 0 1	0 0 0	1 0 1	-0.107
5031.75796	0.00497	2.4×10^{-43}	0 0 0	1 0 1	1 1 1	2 0 2	-0.107
5031.80472	0.00270	8.3×10^{-43}	0 0 0	1 0 1	2 0 2	2 1 1	-0.106
5034.73763	0.00116	8.5×10^{-43}	0 0 0	1 0 1	3 0 3	3 1 2	-0.104
5037.73717	0.00280	4.4×10^{-43}	0 0 0	1 0 1	1 1 1	2 1 2	-0.109
5038.09568	0.01039	4.1×10^{-43}	0 0 0	1 0 1	0 0 0	1 1 1	-0.095
5039.06141	0.00130	8.6×10^{-43}	0 0 0	1 0 1	5 1 4	5 2 3	-0.102
5039.22163	0.00196	7.3×10^{-43}	0 0 0	1 0 1	4 0 4	4 1 3	-0.108
5039.35779	0.00135	8.4×10^{-43}	0 0 0	1 0 1	4 1 3	4 2 2	-0.106
5039.69577	0.00267	6.1×10^{-43}	0 0 0	1 0 1	1 0 1	2 0 2	-0.106
5040.27825	0.00205	7.4×10^{-43}	0 0 0	1 0 1	6 1 5	6 2 4	-0.102
5040.75646	0.00184	6.6×10^{-43}	0 0 0	1 0 1	3 1 2	3 2 1	-0.116
5041.62301	0.00260	4.9×10^{-43}	0 0 0	1 0 1	2 1 2	3 0 3	-0.107
5043.28209	0.00313	5.6×10^{-43}	0 0 0	1 0 1	7 1 6	7 2 5	-0.085
5043.49262	0.00296	2.9×10^{-43}	0 0 0	1 0 1	9 2 7	9 3 6	-0.084
5044.68680	0.00618	1.9×10^{-43}	0 0 0	1 0 1	10 2 8	10 3 7	-0.084
5045.28115	0.00235	5.7×10^{-43}	0 0 0	1 0 1	5 0 5	5 1 4	-0.096
5045.67453	0.00193	5.8×10^{-43}	0 0 0	1 0 1	1 0 1	2 1 2	-0.109
5045.86810	0.00195	7.1×10^{-43}	0 0 0	1 0 1	2 1 2	3 1 3	-0.109
5046.42339	0.00364	4.7×10^{-43}	0 0 0	1 0 1	7 2 5	7 3 4	-0.101
5047.26491	0.00261	3.8×10^{-43}	0 0 0	1 0 1	2 2 1	3 2 2	-0.115
5048.06535	0.00833	8.2×10^{-43}	0 0 0	1 0 1	2 0 2	3 0 3	-0.103
5048.06546	0.01746	3.7×10^{-43}	0 0 0	1 0 1	8 1 7	8 2 6	-0.097
5049.69444	0.00247	5.1×10^{-43}	0 0 0	1 0 1	6 2 4	6 3 3	-0.107
5049.96278	0.00276	4.2×10^{-43}	0 0 0	1 0 1	3 1 3	3 2 2	-0.120
5050.96916	0.00462	7.0×10^{-43}	0 0 0	1 0 1	3 1 3	4 0 4	-0.106
5051.06941	0.00695	2.3×10^{-43}	0 0 0	1 0 1	4 2 3	5 1 4	-0.113
5051.11759	0.00213	6.9×10^{-43}	0 0 0	1 0 1	2 1 1	3 1 2	-0.109
5052.30701	0.00156	7.2×10^{-43}	0 0 0	1 0 1	2 0 2	3 1 3	-0.108
5052.48526	0.00485	4.2×10^{-43}	0 0 0	1 0 1	6 0 6	6 1 5	-0.102
5053.02673	0.00263	4.5×10^{-43}	0 0 0	1 0 1	4 1 4	4 2 3	-0.111
5053.24392	0.00579	4.8×10^{-43}	0 0 0	1 0 1	5 2 3	5 3 2	-0.110
5053.65001	0.00140	8.7×10^{-43}	0 0 0	1 0 1	3 1 3	4 1 4	-0.108
5054.37174	0.01056	2.4×10^{-43}	0 0 0	1 0 1	9 1 8	9 2 7	-0.095

Position	$\sigma_{\text{Pos.}}$	Intensity	$\nu_1\ \nu_2\ \nu_3$	$\nu_1{}'\ \nu_2{}'\ \nu_3{}'$	J K$_a$ K$_c$	J' K$_a{}'$ K$_c{}'$	$\Delta_{\text{SPEC.}}$
5054.43919	0.01258	2.7×10^{-43}	0 0 0	1 0 1	3 3 1	4 3 2	-0.119
5055.62648	0.00162	9.3×10^{-43}	0 0 0	1 0 1	3 0 3	4 0 4	-0.107
5056.03303	0.00190	5.9×10^{-43}	0 0 0	1 0 1	3 2 2	4 2 3	-0.113
5056.31332	0.00568	4.1×10^{-43}	0 0 0	1 0 1	4 2 2	4 3 1	-0.131
5058.30909	0.00116	8.2×10^{-43}	0 0 0	1 0 1	3 0 3	4 1 4	-0.107
5058.54461	0.00102	5.9×10^{-43}	0 0 0	1 0 1	3 2 1	4 2 2	-0.087
5059.53611	0.00143	8.2×10^{-43}	0 0 0	1 0 1	4 1 4	5 0 5	-0.106
5059.73363	0.01185	3.9×10^{-43}	0 0 0	1 0 1	4 2 3	4 3 2	-0.116
5059.73364	0.01517	2.6×10^{-43}	0 0 0	1 0 1	3 2 2	3 3 1	-0.128
5060.13308	0.00273	4.3×10^{-43}	0 0 0	1 0 1	5 2 4	5 3 3	-0.117
5060.22248	0.00459	3.0×10^{-43}	0 0 0	1 0 1	7 0 7	7 1 6	-0.094
5060.51002	0.00176	8.3×10^{-43}	0 0 0	1 0 1	3 1 2	4 1 3	-0.104
5061.07364	0.00213	9.3×10^{-43}	0 0 0	1 0 1	4 1 4	5 1 5	-0.107
5061.10981	0.00407	4.0×10^{-43}	0 0 0	1 0 1	6 2 5	6 3 4	-0.111
5061.33166	0.00350	3.5×10^{-43}	0 0 0	1 0 1	6 1 6	6 2 5	-0.105
5061.53570	0.00723	2.2×10^{-43}	0 0 0	1 0 1	8 3 5	8 4 4	-0.107
5061.58649	0.01180	1.4×10^{-43}	0 0 0	1 0 1	10 1 9	10 2 8	-0.082
5062.55329	0.00321	9.7×10^{-43}	0 0 0	1 0 1	4 0 4	5 0 5	-0.104
5062.56132	0.01206	2.8×10^{-43}	0 0 0	1 0 1	5 2 4	6 1 5	-0.106
5062.76059	0.00331	3.4×10^{-43}	0 0 0	1 0 1	7 2 6	7 3 5	-0.111
5063.47043	0.00707	4.0×10^{-43}	0 0 0	1 0 1	4 3 2	5 3 3	-0.115
5063.59911	0.00226	5.5×10^{-43}	0 0 0	1 0 1	1 1 0	2 2 1	-0.114
5064.02821	0.00353	4.0×10^{-43}	0 0 0	1 0 1	4 3 1	5 3 2	-0.120
5064.09073	0.00201	8.7×10^{-43}	0 0 0	1 0 1	4 0 4	5 1 5	-0.106
5064.41953	0.00182	6.7×10^{-43}	0 0 0	1 0 1	4 2 3	5 2 4	-0.110
5065.15695	0.00295	2.6×10^{-43}	0 0 0	1 0 1	8 2 7	8 3 6	-0.090
5065.64317	0.00396	2.6×10^{-43}	0 0 0	1 0 1	7 3 4	7 4 3	-0.105
5065.65327	0.00119	4.9×10^{-43}	0 0 0	1 0 1	1 1 1	2 2 0	-0.102
5067.33892	0.00126	8.4×10^{-43}	0 0 0	1 0 1	5 1 5	6 0 6	-0.103
5067.87124	0.00537	2.1×10^{-43}	0 0 0	1 0 1	8 0 8	8 1 7	-0.099
5068.16148	0.00187	9.1×10^{-43}	0 0 0	1 0 1	5 1 5	6 1 6	-0.104
5068.71062	0.00429	2.7×10^{-43}	0 0 0	1 0 1	6 3 3	6 4 2	-0.117
5068.74879	0.00173	6.7×10^{-43}	0 0 0	1 0 1	4 2 2	5 2 3	-0.106
5068.84395	0.00698	1.6×10^{-43}	0 0 0	1 0 1	9 3 7	9 4 6	-0.103
5069.01717	0.00941	2.1×10^{-43}	0 0 0	1 0 1	8 3 6	8 4 5	-0.103
5069.11550	0.00108	9.3×10^{-43}	0 0 0	1 0 1	5 0 5	6 0 6	-0.103
5069.16682	0.00536	2.3×10^{-43}	0 0 0	1 0 1	5 4 2	6 4 3	-0.131
5069.24551	0.01488	2.3×10^{-43}	0 0 0	1 0 1	5 4 1	6 4 2	-0.134
5069.26609	0.00141	8.5×10^{-43}	0 0 0	1 0 1	4 1 3	5 1 4	-0.103
5069.62062	0.00573	2.5×10^{-43}	0 0 0	1 0 1	7 3 5	7 4 4	-0.112
5069.93649	0.00137	8.6×10^{-43}	0 0 0	1 0 1	5 0 5	6 1 6	-0.106

Position	$\sigma_{\text{Pos.}}$	Intensity	$\nu_1\ \nu_2\ \nu_3$	$\nu_1'\ \nu_2'\ \nu_3'$	J K_a K_c	J' K_a' K_c'	$\Delta_{\text{SPEC.}}$
5071.02368	0.00183	5.4×10^{-43}	0 0 0	1 0 1	2 1 1	3 2 2	-0.103
5072.26160	0.00247	4.4×10^{-43}	0 0 0	1 0 1	5 3 3	6 3 4	-0.119
5072.38029	0.00134	6.7×10^{-43}	0 0 0	1 0 1	5 2 4	6 2 5	-0.112
5073.67945	0.00168	4.4×10^{-43}	0 0 0	1 0 1	5 3 2	6 3 3	-0.114
5074.51760	0.00155	7.7×10^{-43}	0 0 0	1 0 1	6 1 6	7 0 7	-0.106
5074.94203	0.00220	8.3×10^{-43}	0 0 0	1 0 1	6 1 6	7 1 7	-0.102
5075.49745	0.00130	8.4×10^{-43}	0 0 0	1 0 1	6 0 6	7 0 7	-0.103
5075.91597	0.00143	7.8×10^{-43}	0 0 0	1 0 1	6 0 6	7 1 7	-0.105
5077.21170	0.00287	7.9×10^{-43}	0 0 0	1 0 1	5 1 4	6 1 5	-0.103
5077.32870	0.00207	5.2×10^{-43}	0 0 0	1 0 1	3 1 2	4 2 3	-0.109
5077.42514	0.00725	1.4×10^{-43}	0 0 0	1 0 1	9 1 9	9 2 8	-0.103
5077.65628	0.00918	3.8×10^{-43}	0 0 0	1 0 1	2 1 2	3 2 1	-0.102
5077.97522	0.00369	2.5×10^{-43}	0 0 0	1 0 1	6 4 3	7 4 4	-0.125
5078.23852	0.00482	2.5×10^{-43}	0 0 0	1 0 1	6 4 2	7 4 3	-0.126
5078.67135	0.00177	6.6×10^{-43}	0 0 0	1 0 1	5 2 3	6 2 4	-0.102
5079.82552	0.00214	4.7×10^{-43}	0 0 0	1 0 1	6 2 5	7 2 6	-0.081
5079.85859	0.00900	1.2×10^{-43}	0 0 0	1 0 1	8 4 5	8 5 4	-0.125
5080.73716	0.01512	4.2×10^{-43}	0 0 0	1 0 1	6 3 4	7 3 5	-0.129
5081.24630	0.00910	6.4×10^{-43}	0 0 0	1 0 1	7 1 7	8 0 8	-0.101
5081.45328	0.00255	7.3×10^{-43}	0 0 0	1 0 1	7 1 7	8 1 8	-0.104
5081.75725	0.00175	7.3×10^{-43}	0 0 0	1 0 1	7 0 7	8 0 8	-0.102
5081.96692	0.00503	6.4×10^{-43}	0 0 0	1 0 1	7 0 7	8 1 8	-0.102
5082.61757	0.00286	4.9×10^{-43}	0 0 0	1 0 1	4 1 3	5 2 4	-0.100
5082.78130	0.00698	3.0×10^{-43}	0 0 0	1 0 1	7 2 6	8 1 7	-0.102
5083.60766	0.00262	4.2×10^{-43}	0 0 0	1 0 1	6 3 3	7 3 4	-0.109
5084.24392	0.00169	6.8×10^{-43}	0 0 0	1 0 1	6 1 5	7 1 6	-0.099
5086.94479	0.00210	5.1×10^{-43}	0 0 0	1 0 1	7 2 6	8 2 7	-0.103
5087.62148	0.00186	5.9×10^{-43}	0 0 0	1 0 1	8 1 8	9 0 9	-0.099
5087.71226	0.00188	5.1×10^{-43}	0 0 0	1 0 1	8 1 8	9 1 9	-0.106
5087.90383	0.00288	5.1×10^{-43}	0 0 0	1 0 1	8 0 8	9 0 9	-0.077
5087.98435	0.00200	5.9×10^{-43}	0 0 0	1 0 1	6 2 4	7 2 5	-0.115
5088.61220	0.01202	6.9×10^{-43}	0 0 0	1 0 1	2 2 0	3 3 1	-0.126
5088.85351	0.00380	3.6×10^{-43}	0 0 0	1 0 1	7 3 5	8 3 6	-0.113
5088.90870	0.00201	6.9×10^{-43}	0 0 0	1 0 1	2 2 1	3 3 0	-0.119
5090.43839	0.00203	5.5×10^{-43}	0 0 0	1 0 1	7 1 6	8 1 7	-0.098
5090.83193	0.00360	3.4×10^{-43}	0 0 0	1 0 1	6 1 5	7 2 6	-0.078
5093.57243	0.00224	4.0×10^{-43}	0 0 0	1 0 1	8 2 7	9 2 8	-0.105
5093.76315	0.00230	5.5×10^{-43}	0 0 0	1 0 1	9 1 9	10 1 10	-0.104
5093.84548	0.00208	5.5×10^{-43}	0 0 0	1 0 1	9 0 9	10 0 10	-0.097
5093.89542	0.00341	2.9×10^{-43}	0 0 0	1 0 1	9 0 9	10 1 10	-0.101
5096.06008	0.00732	4.2×10^{-43}	0 0 0	1 0 1	8 1 7	9 1 8	-0.110

Position	$\sigma_{\text{Pos.}}$	Intensity	$\nu_1\,\nu_2\,\nu_3$	$\nu_1'\,\nu_2'\,\nu_3'$	J K_a K_c	J' K_a' K_c'	$\Delta_{\text{SPEC.}}$
5097.08426	0.00707	5.9×10^{-43}	0 0 0	1 0 1	3 2 1	4 3 2	-0.120
5098.46320	0.00598	2.0×10^{-43}	0 0 0	1 0 1	9 2 8	10 1 9	-0.089
5098.51822	0.00560	2.8×10^{-43}	0 0 0	1 0 1	8 1 7	9 2 8	-0.095
5098.55127	0.00226	5.8×10^{-43}	0 0 0	1 0 1	3 2 2	4 3 1	-0.117
5101.43815	0.00787	3.1×10^{-43}	0 0 0	1 0 1	9 1 8	10 1 9	-0.097
5102.79633	0.00438	2.1×10^{-43}	0 0 0	1 0 1	9 1 8	10 2 9	-0.100
5103.16979	0.01062	1.4×10^{-43}	0 0 0	1 0 1	9 4 6	10 4 7	-0.109
5104.47374	0.00273	4.8×10^{-43}	0 0 0	1 0 1	4 2 2	5 3 3	-0.115
5105.24489	0.00753	1.9×10^{-43}	0 0 0	1 0 1	11 1 11	12 0 12	-0.117
5105.26991	0.00331	2.3×10^{-43}	0 0 0	1 0 1	11 1 11	12 1 12	-0.102
5105.29085	0.00469	1.9×10^{-43}	0 0 0	1 0 1	11 0 11	12 1 12	-0.112
5105.71557	0.00470	2.0×10^{-43}	0 0 0	1 0 1	10 2 9	11 2 10	-0.097
5108.80616	0.00309	4.5×10^{-43}	0 0 0	1 0 1	4 2 3	5 3 2	-0.112
5110.50768	0.00230	3.8×10^{-43}	0 0 0	1 0 1	5 2 3	6 3 4	-0.109
5111.64617	0.00164	6.6×10^{-43}	0 0 0	1 0 1	3 3 0	4 4 1	-0.131
5111.67690	0.00161	6.6×10^{-43}	0 0 0	1 0 1	3 3 1	4 4 0	-0.128
5115.14786	0.00524	2.9×10^{-43}	0 0 0	1 0 1	6 2 4	7 3 5	-0.110
5116.00434	0.01427	9.4×10^{-44}	0 0 0	1 0 1	13 1 13	14 1 14	-0.092
5116.01554	0.00870	9.4×10^{-44}	0 0 0	1 0 1	13 0 13	14 0 14	-0.086
5118.55727	0.00542	2.1×10^{-43}	0 0 0	1 0 1	7 2 5	8 3 6	-0.109
5120.20257	0.00297	3.1×10^{-43}	0 0 0	1 0 1	5 2 4	6 3 3	-0.117
5120.48280	0.00185	5.3×10^{-43}	0 0 0	1 0 1	4 3 1	5 4 2	-0.129
5120.67366	0.00210	5.3×10^{-43}	0 0 0	1 0 1	4 3 2	5 4 1	-0.129
5128.87035	0.00235	4.1×10^{-43}	0 0 0	1 0 1	5 3 2	6 4 3	-0.124
5133.19332	0.00191	5.0×10^{-43}	0 0 0	1 0 1	4 4 0	5 5 1	-0.144
5133.19333	0.00191	5.0×10^{-43}	0 0 0	1 0 1	4 4 1	5 5 0	-0.146
5136.50943	0.00453	3.0×10^{-43}	0 0 0	1 0 1	6 3 3	7 4 4	-0.116
5148.03608	0.01039	1.4×10^{-43}	0 0 0	1 0 1	8 3 5	9 4 6	-0.104
5148.32238	0.00610	2.0×10^{-43}	0 0 0	1 0 1	7 3 5	8 4 4	-0.118
5153.43894	0.00336	3.1×10^{-43}	0 0 0	1 0 1	5 5 1	6 6 0	-0.165
5153.45081	0.00874	3.1×10^{-43}	0 0 0	1 0 1	5 5 0	6 6 1	-0.153
5158.62357	0.01031	2.0×10^{-43}	0 0 0	1 0 1	7 4 3	8 5 4	-0.131
5162.06090	0.00812	2.3×10^{-43}	0 0 0	1 0 1	6 5 2	7 6 1	-0.155
5162.12432	0.00571	2.3×10^{-43}	0 0 0	1 0 1	6 5 1	7 6 2	-0.090
5167.30106	0.00740	1.3×10^{-43}	0 0 0	1 0 1	8 4 5	9 5 4	-0.131
5172.71900	0.02741	1.6×10^{-43}	0 0 0	1 0 1	6 6 0	7 7 1	-0.170
5172.71916	0.02716	1.6×10^{-43}	0 0 0	1 0 1	6 6 1	7 7 0	-0.170

A.2.2.5 DTO $2\nu_2 + \nu_3$ band

Here, the lines assigned to the $2\nu_2 + \nu_3$ band of DTO obtained from the $10\,\mathrm{GBq}$ sample are presented. These lines are published in [Her22]. For further information, see Section 5.5.2.

Table A.12: Linelist of the DTO $2\nu_2 + \nu_3$ band. The columns present the assigned line position, the uncertainty on the position $\sigma_{\mathrm{Pos.}}$, the line intensity taking natural abundance into account, lower and upper vibrational quanta, lower and upper rotational quanta and the deviation to the predictions from SPECTRA database $\Delta_{\mathrm{SPEC.}}$.

Position	$\sigma_{\mathrm{Pos.}}$	Intensity	$\nu_1\ \nu_2\ \nu_3$	$\nu_1'\ \nu_2'\ \nu_3'$	$J\ K_a\ K_c$	$J'\ K_a'\ K_c'$	$\Delta_{\mathrm{SPEC.}}$
4782.16099	0.00622	1.1×10^{-43}	0 0 0	0 2 1	11 0 11	10 0 10	0.087
4782.23826	0.00891	1.1×10^{-43}	0 0 0	0 2 1	11 1 11	10 1 10	0.104
4787.10347	0.01438	1.1×10^{-43}	0 0 0	0 2 1	10 2 8	9 2 7	0.104
4789.43759	0.00661	9.3×10^{-44}	0 0 0	0 2 1	10 3 7	9 3 6	0.108
4791.43438	0.00764	1.3×10^{-43}	0 0 0	0 2 1	10 1 9	9 1 8	0.103
4791.78151	0.00424	1.7×10^{-43}	0 0 0	0 2 1	10 0 10	9 0 9	0.095
4791.89643	0.00576	1.7×10^{-43}	0 0 0	0 2 1	10 1 10	9 1 9	0.093
4793.63660	0.00351	1.2×10^{-43}	0 0 0	0 2 1	10 2 9	9 2 8	0.094
4796.60956	0.00811	9.6×10^{-44}	0 0 0	0 2 1	10 3 8	9 3 7	0.095
4799.09061	0.00440	1.8×10^{-43}	0 0 0	0 2 1	9 1 8	8 1 7	0.095
4800.09852	0.00397	1.3×10^{-43}	0 0 0	0 2 1	9 3 6	8 3 5	0.091
4801.14481	0.00348	2.3×10^{-43}	0 0 0	0 2 1	9 0 9	8 0 8	0.092
4801.37043	0.00372	2.3×10^{-43}	0 0 0	0 2 1	9 1 9	8 1 8	0.094
4802.42753	0.01275	1.8×10^{-43}	0 0 0	0 2 1	9 2 8	8 2 7	0.094
4804.19994	0.00310	2.3×10^{-43}	0 0 0	0 2 1	8 2 6	7 2 5	0.101
4805.77934	0.00538	1.3×10^{-43}	0 0 0	0 2 1	9 3 7	8 3 6	0.093
4806.64729	0.00307	2.5×10^{-43}	0 0 0	0 2 1	8 1 7	7 1 6	0.093
4809.99252	0.00919	1.0×10^{-43}	0 0 0	0 2 1	8 1 8	7 0 7	0.101
4810.24267	0.00311	3.0×10^{-43}	0 0 0	0 2 1	8 0 8	7 0 7	0.092
4810.65726	0.00271	3.0×10^{-43}	0 0 0	0 2 1	8 1 8	7 1 7	0.089
4810.92435	0.00848	1.0×10^{-43}	0 0 0	0 2 1	8 0 8	7 1 7	0.096
4811.21708	0.00495	1.8×10^{-43}	0 0 0	0 2 1	8 3 5	7 3 4	0.088
4811.26814	0.00361	2.3×10^{-43}	0 0 0	0 2 1	8 2 7	7 2 6	0.091
4813.82627	0.00258	2.9×10^{-43}	0 0 0	0 2 1	7 2 5	6 2 4	0.094
4813.93500	0.01064	9.4×10^{-44}	0 0 0	0 2 1	9 4 6	8 4 5	0.080
4814.41854	0.00220	3.3×10^{-43}	0 0 0	0 2 1	7 1 6	6 1 5	0.093
4815.19405	0.00460	1.8×10^{-43}	0 0 0	0 2 1	8 3 6	7 3 5	0.087
4818.52496	0.00823	1.1×10^{-43}	0 0 0	0 2 1	7 1 7	6 0 6	0.080
4819.04371	0.00417	3.7×10^{-43}	0 0 0	0 2 1	7 0 7	6 0 6	0.087
4819.79008	0.00214	3.7×10^{-43}	0 0 0	0 2 1	7 1 7	6 1 6	0.086
4820.21005	0.00306	2.9×10^{-43}	0 0 0	0 2 1	7 2 6	6 2 5	0.085
4820.29970	0.00751	1.1×10^{-43}	0 0 0	0 2 1	7 0 7	6 1 6	0.083

Position	$\sigma_{\text{Pos.}}$	Intensity	$\nu_1\,\nu_2\,\nu_3$	$\nu_1{'}\,\nu_2{'}\,\nu_3{'}$	J K_a K_c	J' $\text{K}_a{'}$ $\text{K}_c{'}$	$\Delta_{\text{SPEC.}}$
4822.42498	0.00395	2.1×10^{-43}	0 0 0	0 2 1	7 3 4	6 3 3	0.085
4822.69367	0.00180	4.0×10^{-43}	0 0 0	0 2 1	6 1 5	5 1 4	0.090
4823.99028	0.00539	1.1×10^{-43}	0 0 0	0 2 1	8 4 5	7 4 4	0.045
4824.07916	0.00189	3.4×10^{-43}	0 0 0	0 2 1	6 2 4	5 2 3	0.090
4824.81110	0.00609	2.1×10^{-43}	0 0 0	0 2 1	7 3 5	6 3 4	0.079
4827.54882	0.00169	4.4×10^{-43}	0 0 0	0 2 1	6 0 6	5 0 5	0.086
4828.80633	0.00276	4.3×10^{-43}	0 0 0	0 2 1	6 1 6	5 1 5	0.085
4829.29834	0.00246	3.4×10^{-43}	0 0 0	0 2 1	6 2 5	5 2 4	0.080
4829.77771	0.00639	1.1×10^{-43}	0 0 0	0 2 1	6 0 6	5 1 5	0.079
4831.57649	0.00352	4.4×10^{-43}	0 0 0	0 2 1	5 1 4	4 1 3	0.073
4833.39849	0.00431	2.3×10^{-43}	0 0 0	0 2 1	6 3 3	5 3 2	0.077
4833.95983	0.01146	1.3×10^{-43}	0 0 0	0 2 1	7 4 4	6 4 3	0.063
4834.03829	0.01197	1.0×10^{-43}	0 0 0	0 2 1	5 1 5	4 0 4	0.080
4834.59001	0.00545	2.3×10^{-43}	0 0 0	0 2 1	6 3 4	5 3 3	0.067
4834.80417	0.00264	3.6×10^{-43}	0 0 0	0 2 1	5 2 3	4 2 2	0.081
4835.81769	0.00802	4.8×10^{-43}	0 0 0	0 2 1	5 0 5	4 0 4	0.083
4837.74820	0.00161	4.6×10^{-43}	0 0 0	0 2 1	5 1 5	4 1 4	0.083
4838.55242	0.00262	3.5×10^{-43}	0 0 0	0 2 1	5 2 4	4 2 3	0.077
4839.53123	0.00842	1.0×10^{-43}	0 0 0	0 2 1	5 0 5	4 1 4	0.089
4841.05251	0.00226	4.4×10^{-43}	0 0 0	0 2 1	4 1 3	3 1 2	0.082
4844.06501	0.00197	4.9×10^{-43}	0 0 0	0 2 1	4 0 4	3 0 3	0.082
4845.74600	0.00240	3.2×10^{-43}	0 0 0	0 2 1	4 2 2	3 2 1	0.079
4846.66264	0.00160	4.5×10^{-43}	0 0 0	0 2 1	4 1 4	3 1 3	0.081
4847.96807	0.00275	3.2×10^{-43}	0 0 0	0 2 1	4 2 3	3 2 2	0.075
4850.96483	0.00196	3.9×10^{-43}	0 0 0	0 2 1	3 1 2	2 1 1	0.081
4852.59952	0.00148	4.4×10^{-43}	0 0 0	0 2 1	3 0 3	2 0 2	0.081
4853.98585	0.02088	9.5×10^{-44}	0 0 0	0 2 1	5 4 2	4 4 1	0.046
4853.99349	0.02019	9.5×10^{-44}	0 0 0	0 2 1	5 4 1	4 4 0	0.069
4854.29241	0.00622	1.5×10^{-43}	0 0 0	0 2 1	4 3 1	3 3 0	0.073
4854.42131	0.01107	1.5×10^{-43}	0 0 0	0 2 1	4 3 2	3 3 1	0.057
4855.58225	0.00197	3.9×10^{-43}	0 0 0	0 2 1	3 1 3	2 1 2	0.078
4856.53110	0.02657	2.2×10^{-43}	0 0 0	0 2 1	3 2 1	2 2 0	0.069
4857.51319	0.00942	2.1×10^{-43}	0 0 0	0 2 1	3 2 2	2 2 1	0.059
4861.20328	0.00300	2.5×10^{-43}	0 0 0	0 2 1	2 1 1	1 1 0	0.077
4861.60962	0.00312	3.5×10^{-43}	0 0 0	0 2 1	2 0 2	1 0 1	0.066
4864.51883	0.00365	2.5×10^{-43}	0 0 0	0 2 1	2 1 2	1 1 1	0.079
4871.09716	0.00583	1.9×10^{-43}	0 0 0	0 2 1	1 0 1	0 0 0	0.080
4876.62615	0.00594	1.4×10^{-43}	0 0 0	0 2 1	2 1 1	2 1 2	0.079
4878.70450	0.00589	1.1×10^{-43}	0 0 0	0 2 1	5 2 3	5 2 4	0.090
4880.41503	0.00315	2.8×10^{-43}	0 0 0	0 2 1	1 1 0	1 1 1	0.077
4882.88862	0.00508	1.8×10^{-43}	0 0 0	0 2 1	4 2 2	4 2 3	0.074

Position	$\sigma_{\text{Pos.}}$	Intensity	$\nu_1\,\nu_2\,\nu_3$	$\nu_1\text{'}\,\nu_2\text{'}\,\nu_3\text{'}$	J K$_a$ K$_c$	J' K$_a$' K$_c$'	$\Delta_{\text{SPEC.}}$
4884.14657	0.00244	2.7×10^{-43}	0 0 0	0 2 1	1 1 1	1 1 0	0.065
4885.32525	0.00304	2.9×10^{-43}	0 0 0	0 2 1	3 2 1	3 2 2	0.077
4886.40041	0.00388	4.9×10^{-43}	0 0 0	0 2 1	2 2 0	2 2 1	0.070
4886.94666	0.00186	4.9×10^{-43}	0 0 0	0 2 1	2 2 1	2 2 0	0.072
4887.84742	0.00707	1.3×10^{-43}	0 0 0	0 2 1	2 1 2	2 1 1	0.078
4887.96643	0.00272	2.9×10^{-43}	0 0 0	0 2 1	3 2 2	3 2 1	0.075
4890.35887	0.00561	1.7×10^{-43}	0 0 0	0 2 1	4 2 3	4 2 2	0.072
4890.50192	0.00435	2.0×10^{-43}	0 0 0	0 2 1	0 0 0	1 0 1	0.082
4892.96749	0.00581	2.2×10^{-43}	0 0 0	0 2 1	5 3 2	5 3 3	0.061
4893.52043	0.00247	3.5×10^{-43}	0 0 0	0 2 1	4 3 1	4 3 2	0.068
4893.71516	0.00162	5.5×10^{-43}	0 0 0	0 2 1	3 3 0	3 3 1	0.067
4893.76316	0.00179	5.5×10^{-43}	0 0 0	0 2 1	3 3 1	3 3 0	0.065
4893.86916	0.00261	3.5×10^{-43}	0 0 0	0 2 1	4 3 2	4 3 1	0.071
4894.31983	0.00402	2.2×10^{-43}	0 0 0	0 2 1	5 3 3	5 3 2	0.072
4895.51785	0.01120	1.4×10^{-43}	0 0 0	0 2 1	6 3 4	6 3 3	0.070
4899.58251	0.00305	2.8×10^{-43}	0 0 0	0 2 1	1 1 1	2 1 2	0.080
4899.87498	0.00208	3.8×10^{-43}	0 0 0	0 2 1	1 0 1	2 0 2	0.079
4902.95796	0.00382	2.0×10^{-43}	0 0 0	0 2 1	6 4 2	6 4 3	0.067
4903.08149	0.00343	3.1×10^{-43}	0 0 0	0 2 1	5 4 1	5 4 2	0.066
4903.11843	0.00670	3.1×10^{-43}	0 0 0	0 2 1	5 4 2	5 4 1	0.068
4903.13023	0.00434	4.8×10^{-43}	0 0 0	0 2 1	4 4 0	4 4 1	0.049
4903.14331	0.02900	2.0×10^{-43}	0 0 0	0 2 1	6 4 3	6 4 2	0.082
4903.14331	0.01213	4.8×10^{-43}	0 0 0	0 2 1	4 4 1	4 4 0	0.058
4903.27444	0.00974	1.2×10^{-43}	0 0 0	0 2 1	7 4 4	7 4 3	0.062
4903.74422	0.00325	2.7×10^{-43}	0 0 0	0 2 1	1 1 0	2 1 1	0.077
4907.84377	0.00197	4.6×10^{-43}	0 0 0	0 2 1	2 1 2	3 1 3	0.077
4908.67217	0.00187	5.2×10^{-43}	0 0 0	0 2 1	2 0 2	3 0 3	0.081
4914.32048	0.02629	1.4×10^{-43}	0 0 0	0 2 1	7 5 2	7 5 3	0.042
4914.37800	0.01113	4.3×10^{-43}	0 0 0	0 2 1	2 1 1	3 1 2	0.080
4914.38154	0.01822	1.4×10^{-43}	0 0 0	0 2 1	7 5 3	7 5 2	0.086
4914.38154	0.01480	2.3×10^{-43}	0 0 0	0 2 1	6 5 1	6 5 2	0.040
4914.40756	0.00585	2.3×10^{-43}	0 0 0	0 2 1	6 5 2	6 5 1	0.063
4914.43141	0.00744	3.5×10^{-43}	0 0 0	0 2 1	5 5 1	5 5 0	0.042
4914.43141	0.00755	3.5×10^{-43}	0 0 0	0 2 1	5 5 0	5 5 1	0.043
4915.73318	0.00445	2.5×10^{-43}	0 0 0	0 2 1	2 2 1	3 2 2	0.072
4915.79557	0.00181	5.7×10^{-43}	0 0 0	0 2 1	3 1 3	4 1 4	0.078
4916.74807	0.00152	6.0×10^{-43}	0 0 0	0 2 1	3 0 3	4 0 4	0.080
4916.84675	0.00395	2.4×10^{-43}	0 0 0	0 2 1	2 2 0	3 2 1	0.079
4923.41080	0.00139	6.2×10^{-43}	0 0 0	0 2 1	4 1 4	5 1 5	0.078
4924.19405	0.00152	6.3×10^{-43}	0 0 0	0 2 1	4 0 4	5 0 5	0.081
4924.79108	0.00206	5.1×10^{-43}	0 0 0	0 2 1	3 1 2	4 1 3	0.080

Position	$\sigma_{\text{Pos.}}$	Intensity	$\nu_1\ \nu_2\ \nu_3$	$\nu_1'\ \nu_2'\ \nu_3'$	J K_a K_c	J' K_a' K_c'	$\Delta_{\text{SPEC.}}$
4925.12528	0.00262	3.8×10^{-43}	0 0 0	0 2 1	3 2 2	4 2 3	0.086
4927.07474	0.01298	2.1×10^{-43}	0 0 0	0 2 1	6 6 0	6 6 1	0.017
4927.07495	0.01188	2.1×10^{-43}	0 0 0	0 2 1	6 6 1	6 6 0	0.017
4927.71466	0.00207	3.8×10^{-43}	0 0 0	0 2 1	3 2 1	4 2 2	0.073
4930.68661	0.00399	6.1×10^{-43}	0 0 0	0 2 1	5 1 5	6 1 6	0.069
4931.21372	0.00356	6.2×10^{-43}	0 0 0	0 2 1	5 0 5	6 0 6	0.078
4932.99402	0.00456	1.8×10^{-43}	0 0 0	0 2 1	3 3 1	4 3 2	0.063
4933.14572	0.00487	1.8×10^{-43}	0 0 0	0 2 1	3 3 0	4 3 1	0.064
4934.25234	0.00741	4.5×10^{-43}	0 0 0	0 2 1	4 2 3	5 2 4	0.074
4934.82924	0.00178	5.3×10^{-43}	0 0 0	0 2 1	4 1 3	5 1 4	0.082
4937.66970	0.00213	5.7×10^{-43}	0 0 0	0 2 1	6 1 6	7 1 7	0.080
4937.97174	0.00167	5.7×10^{-43}	0 0 0	0 2 1	6 0 6	7 0 7	0.083
4943.34644	0.00496	2.8×10^{-43}	0 0 0	0 2 1	4 3 1	5 3 2	0.068
4950.17056	0.00213	4.2×10^{-43}	0 0 0	0 2 1	5 2 3	6 2 4	0.083
4950.77139	0.00289	4.0×10^{-43}	0 0 0	0 2 1	8 1 8	9 1 9	0.091
4950.83908	0.00230	4.0×10^{-43}	0 0 0	0 2 1	8 0 8	9 0 9	0.080
4952.23530	0.01261	1.2×10^{-43}	0 0 0	0 2 1	4 4 0	5 4 1	0.044
4952.24572	0.00968	1.2×10^{-43}	0 0 0	0 2 1	4 4 1	5 4 2	0.069
4952.62425	0.00672	3.1×10^{-43}	0 0 0	0 2 1	5 3 3	6 3 4	0.073
4953.08979	0.00221	4.4×10^{-43}	0 0 0	0 2 1	6 1 5	7 1 6	0.089
4953.88763	0.00397	3.0×10^{-43}	0 0 0	0 2 1	5 3 2	6 3 3	0.057
4956.91998	0.00375	3.1×10^{-43}	0 0 0	0 2 1	9 1 9	10 1 10	0.088
4956.96447	0.00414	3.1×10^{-43}	0 0 0	0 2 1	9 0 9	10 0 10	0.094
4959.81652	0.00304	3.5×10^{-43}	0 0 0	0 2 1	7 2 6	8 2 7	0.076
4961.16983	0.00317	3.6×10^{-43}	0 0 0	0 2 1	7 1 6	8 1 7	0.097
4961.20274	0.00339	3.7×10^{-43}	0 0 0	0 2 1	6 2 4	7 2 5	0.093
4962.28242	0.00257	2.9×10^{-43}	0 0 0	0 2 1	6 3 4	7 3 5	0.071
4962.80339	0.00422	2.3×10^{-43}	0 0 0	0 2 1	10 1 10	11 1 11	0.067
4962.83830	0.00424	2.3×10^{-43}	0 0 0	0 2 1	10 0 10	11 0 11	0.084
4963.76750	0.00902	1.5×10^{-43}	0 0 0	0 2 1	7 3 5	7 4 4	0.042
4967.66527	0.00336	2.8×10^{-43}	0 0 0	0 2 1	8 2 7	9 2 8	0.085
4968.49330	0.00484	1.6×10^{-43}	0 0 0	0 2 1	11 1 11	12 1 12	0.094
4968.49330	0.00480	1.6×10^{-43}	0 0 0	0 2 1	11 0 11	12 0 12	0.087
4968.68280	0.00345	2.9×10^{-43}	0 0 0	0 2 1	8 1 7	9 1 8	0.092
4971.75531	0.00369	2.5×10^{-43}	0 0 0	0 2 1	7 3 5	8 3 6	0.080
4971.82218	0.00683	3.0×10^{-43}	0 0 0	0 2 1	7 2 5	8 2 6	0.090
4972.13188	0.00567	1.4×10^{-43}	0 0 0	0 2 1	6 4 3	7 4 4	0.039
4972.26338	0.00489	1.9×10^{-43}	0 0 0	0 2 1	6 4 2	7 4 3	0.056
4973.92138	0.00772	1.1×10^{-43}	0 0 0	0 2 1	12 0 12	13 0 13	0.096
4973.92138	0.00773	1.1×10^{-43}	0 0 0	0 2 1	12 1 12	13 1 13	0.097
4975.84910	0.00506	2.1×10^{-43}	0 0 0	0 2 1	9 1 8	10 1 9	0.097

Position	$\sigma_{\text{Pos.}}$	Intensity	$\nu_1\,\nu_2\,\nu_3$	$\nu_1'\,\nu_2'\,\nu_3'$	J $K_a\,K_c$	J' $K_a'\,K_c'$	$\Delta_{\text{SPEC.}}$
4980.95862	0.01184	2.0×10^{-43}	0 0 0	0 2 1	8 3 6	9 3 7	0.050
4981.90555	0.00446	2.3×10^{-43}	0 0 0	0 2 1	8 2 6	9 2 7	0.100
4982.38679	0.00609	1.5×10^{-43}	0 0 0	0 2 1	10 2 9	11 2 10	0.092
4982.53229	0.00653	1.7×10^{-43}	0 0 0	0 2 1	7 4 3	8 4 4	0.063
4987.77792	0.00878	1.9×10^{-43}	0 0 0	0 2 1	8 3 5	9 3 6	0.088
5003.97097	0.00578	1.0×10^{-43}	0 0 0	0 2 1	9 4 5	10 4 6	0.081

A.2.3 Linelists of T$_2$O

A.2.3.1 T$_2$O $\nu_1 + \nu_3$ band from the 1 GBq sample

Here, the lines assigned to the $\nu_1 + \nu_3$ band of T$_2$O obtained from the 1 GBq sample are presented. These lines are published in [Her22]. For further information, see Section 5.5.3.

Table A.13: Linelist of the T$_2$O $\nu_1 + \nu_3$ band from the 1 GBq sample. The columns present the assigned line position, the uncertainty on the position $\sigma_{\text{Pos.}}$, the line intensity taking natural abundance into account, lower and upper vibrational quanta, lower and upper rotational quanta and the deviation to the predictions from SPECTRA database $\Delta_{\text{SPEC.}}$.

Position	$\sigma_{\text{Pos.}}$	Intensity	$\nu_1\,\nu_2\,\nu_3$	$\nu_1'\,\nu_2'\,\nu_3'$	J $K_a\,K_c$	J' $K_a'\,K_c'$	$\Delta_{\text{SPEC.}}$
4416.13094	0.00531	7.2×10^{-56}	0 0 0	1 0 1	15 1 14	14 1 13	-0.093
4416.59600	0.01938	2.5×10^{-56}	0 0 0	1 0 1	16 0 16	15 0 15	-0.094
4416.59600	0.00772	7.5×10^{-56}	0 0 0	1 0 1	16 1 16	15 1 15	-0.094
4423.98109	0.00490	1.0×10^{-55}	0 0 0	1 0 1	14 2 13	13 2 12	-0.098
4433.96900	0.00810	6.1×10^{-56}	0 0 0	1 0 1	14 0 14	13 0 13	-0.122
4433.98825	0.00192	1.8×10^{-55}	0 0 0	1 0 1	14 1 14	13 1 13	-0.094
4436.16847	0.00354	1.8×10^{-55}	0 0 0	1 0 1	12 3 10	11 3 9	-0.107
4437.30950	0.00547	1.8×10^{-55}	0 0 0	1 0 1	11 4 7	10 4 6	-0.120
4437.52110	0.00362	2.4×10^{-55}	0 0 0	1 0 1	11 3 8	10 3 7	-0.097
4442.28311	0.00248	2.8×10^{-55}	0 0 0	1 0 1	11 2 9	10 2 8	-0.100
4442.44193	0.00642	9.0×10^{-56}	0 0 0	1 0 1	13 1 13	12 1 12	-0.112
4442.47343	0.00281	2.7×10^{-55}	0 0 0	1 0 1	13 0 13	12 0 12	-0.106
4443.61097	0.00251	2.5×10^{-55}	0 0 0	1 0 1	12 2 11	11 2 10	-0.114
4448.41786	0.00367	2.2×10^{-55}	0 0 0	1 0 1	11 1 10	10 1 9	-0.110
4449.84437	0.00418	2.5×10^{-55}	0 0 0	1 0 1	10 4 7	9 4 6	-0.139
4450.67248	0.00167	3.7×10^{-55}	0 0 0	1 0 1	12 1 12	11 1 11	-0.109
4450.78759	0.00530	1.3×10^{-55}	0 0 0	1 0 1	12 0 12	11 0 11	-0.110
4451.06353	0.00513	1.3×10^{-55}	0 0 0	1 0 1	10 2 8	9 2 7	-0.106
4453.78732	0.00198	3.6×10^{-55}	0 0 0	1 0 1	10 3 8	9 3 7	-0.122
4457.81004	0.00130	4.5×10^{-55}	0 0 0	1 0 1	9 3 6	8 3 5	-0.113
4458.10094	0.00226	3.2×10^{-55}	0 0 0	1 0 1	9 4 5	8 4 4	-0.141

Position	$\sigma_{\text{Pos.}}$	Intensity	$\nu_1\,\nu_2\,\nu_3$	$\nu_1'\,\nu_2'\,\nu_3'$	J K_a K_c	J' K_a' K_c'	$\Delta_{\text{SPEC.}}$
4458.81540	0.00149	5.0×10^{-55}	0 0 0	1 0 1	11 0 11	10 0 10	-0.110
4459.95171	0.00331	4.9×10^{-55}	0 0 0	1 0 1	10 2 9	9 2 8	-0.116
4459.96779	0.00306	5.4×10^{-55}	0 0 0	1 0 1	9 2 7	8 2 6	-0.106
4465.64275	0.00313	2.2×10^{-55}	0 0 0	1 0 1	8 5 4	7 5 3	-0.164
4467.67572	0.00113	6.2×10^{-55}	0 0 0	1 0 1	9 1 8	8 1 7	-0.120
4467.71327	0.00100	6.8×10^{-55}	0 0 0	1 0 1	10 1 10	9 1 9	-0.119
4468.15360	0.00344	1.9×10^{-55}	0 0 0	1 0 1	8 3 5	7 3 4	-0.121
4468.19931	0.00226	2.1×10^{-55}	0 0 0	1 0 1	9 2 8	8 2 7	-0.121
4468.46768	0.00170	3.9×10^{-55}	0 0 0	1 0 1	8 4 5	7 4 4	-0.145
4468.81703	0.00465	1.6×10^{-55}	0 0 0	1 0 1	10 0 10	9 0 9	-0.129
4469.10271	0.00309	2.3×10^{-55}	0 0 0	1 0 1	8 2 6	7 2 5	-0.117
4471.54862*	0.00120	5.7×10^{-55}	0 0 0	1 0 1	8 3 6	7 3 5	-0.133
4474.52933	0.00280	2.2×10^{-55}	0 0 0	1 0 1	7 5 2	6 5 1	-0.163
4475.58624	0.00249	2.9×10^{-55}	0 0 0	1 0 1	9 1 9	8 1 8	-0.119
4475.69879	0.00083	8.5×10^{-55}	0 0 0	1 0 1	9 0 9	8 0 8	-0.123
4476.44857	0.00094	7.7×10^{-55}	0 0 0	1 0 1	8 2 7	7 2 6	-0.122
4477.45155	0.00185	4.2×10^{-55}	0 0 0	1 0 1	7 4 3	6 4 2	-0.150
4477.64931	0.00542	1.4×10^{-55}	0 0 0	1 0 1	7 4 4	6 4 3	-0.150
4478.40303	0.00101	6.4×10^{-55}	0 0 0	1 0 1	7 3 4	6 3 3	-0.131
4478.51362	0.00075	8.4×10^{-55}	0 0 0	1 0 1	7 2 5	6 2 4	-0.119
4482.97970	0.00075	9.6×10^{-55}	0 0 0	1 0 1	7 1 6	6 1 5	-0.119
4483.28336	0.00400	1.5×10^{-55}	0 0 0	1 0 1	6 5 2	5 5 1	-0.169
4483.37299	0.00251	3.5×10^{-55}	0 0 0	1 0 1	8 0 8	7 0 7	-0.125
4483.43015	0.00073	1.0×10^{-54}	0 0 0	1 0 1	8 1 8	7 1 7	-0.122
4484.70710	0.00237	3.0×10^{-55}	0 0 0	1 0 1	7 2 6	6 2 5	-0.127
4486.65588	0.00471	1.3×10^{-55}	0 0 0	1 0 1	6 4 2	5 4 1	-0.145
4486.71023	0.00159	3.9×10^{-55}	0 0 0	1 0 1	6 4 3	5 4 2	-0.154
4488.15433	0.00216	3.1×10^{-55}	0 0 0	1 0 1	6 2 4	5 2 3	-0.122
4488.35219	0.00284	2.2×10^{-55}	0 0 0	1 0 1	6 3 3	5 3 2	-0.138
4489.42350	0.00107	6.7×10^{-55}	0 0 0	1 0 1	6 3 4	5 3 3	-0.138
4490.98457	0.00060	1.2×10^{-54}	0 0 0	1 0 1	7 0 7	6 0 6	-0.124
4491.04423	0.00202	3.6×10^{-55}	0 0 0	1 0 1	6 1 5	5 1 4	-0.123
4491.19129	0.00170	3.9×10^{-55}	0 0 0	1 0 1	7 1 7	6 1 6	-0.126
4493.00026	0.00078	9.7×10^{-55}	0 0 0	1 0 1	6 2 5	5 2 4	-0.129
4495.62240	0.00246	2.6×10^{-55}	0 0 0	1 0 1	5 4 1	4 4 0	-0.151
4495.64147	0.00795	8.8×10^{-56}	0 0 0	1 0 1	5 4 2	4 4 1	-0.147
4497.89035	0.00120	6.0×10^{-55}	0 0 0	1 0 1	5 3 2	4 3 1	-0.140
4497.93789	0.00078	9.4×10^{-55}	0 0 0	1 0 1	5 2 3	4 2 2	-0.129
4498.32946	0.00360	2.0×10^{-55}	0 0 0	1 0 1	5 3 3	4 3 2	-0.145
4498.45376	0.00203	4.3×10^{-55}	0 0 0	1 0 1	6 0 6	5 0 5	-0.123
4498.87470	0.00057	1.3×10^{-54}	0 0 0	1 0 1	6 1 6	5 1 5	-0.128

Position	$\sigma_{\text{Pos.}}$	Intensity	$\nu_1\ \nu_2\ \nu_3$	$\nu_1'\ \nu_2'\ \nu_3'$	J K_a K_c	J' K_a' K_c'	$\Delta_{\text{SPEC.}}$
4499.47933	0.00062	1.1×10^{-54}	0 0 0	1 0 1	5 1 4	4 1 3	-0.125
4501.33566	0.00208	3.2×10^{-55}	0 0 0	1 0 1	5 2 4	4 2 3	-0.132
4505.78271	0.00050	1.3×10^{-54}	0 0 0	1 0 1	5 0 5	4 0 4	-0.127
4506.49882	0.00165	4.3×10^{-55}	0 0 0	1 0 1	5 1 5	4 1 4	-0.130
4507.03048	0.00482	1.3×10^{-55}	0 0 0	1 0 1	4 3 1	3 3 0	-0.143
4507.16609	0.00198	4.0×10^{-55}	0 0 0	1 0 1	4 3 2	3 3 1	-0.142
4507.70553	0.00236	2.7×10^{-55}	0 0 0	1 0 1	4 2 2	3 2 1	-0.135
4508.22900	0.00170	3.7×10^{-55}	0 0 0	1 0 1	4 1 3	3 1 2	-0.127
4509.70477*	0.00069	8.2×10^{-55}	0 0 0	1 0 1	4 2 3	3 2 2	-0.139
4513.08618	0.00175	4.2×10^{-55}	0 0 0	1 0 1	4 0 4	3 0 3	-0.128
4514.09331	0.00067	1.2×10^{-54}	0 0 0	1 0 1	4 1 4	3 1 3	-0.130
4516.36633	0.02203	5.7×10^{-56}	0 0 0	1 0 1	8 8 0	8 8 1	-0.226
4516.36633	0.00788	1.7×10^{-55}	0 0 0	1 0 1	8 8 1	8 8 0	-0.226
4517.18140	0.00065	9.2×10^{-55}	0 0 0	1 0 1	3 1 2	2 1 1	-0.132
4517.20921	0.00120	5.3×10^{-55}	0 0 0	1 0 1	3 2 1	2 2 0	-0.138
4520.56144	0.00108	1.1×10^{-54}	0 0 0	1 0 1	3 0 3	2 0 2	-0.131
4522.74433	0.00570	3.5×10^{-55}	0 0 0	1 0 1	7 7 0	7 7 1	-0.207
4522.74433	0.01671	1.2×10^{-55}	0 0 0	1 0 1	7 7 1	7 7 0	-0.207
4526.23026	0.00573	1.9×10^{-55}	0 0 0	1 0 1	2 1 1	1 1 0	-0.133
4528.35728	0.00336	6.1×10^{-55}	0 0 0	1 0 1	6 6 1	6 6 0	-0.189
4528.35728	0.00806	2.0×10^{-55}	0 0 0	1 0 1	6 6 0	6 6 1	-0.190
4528.36962	0.00897	2.7×10^{-55}	0 0 0	1 0 1	2 0 2	1 0 1	-0.131
4529.09487	0.00451	1.2×10^{-55}	0 0 0	1 0 1	7 6 2	7 6 1	-0.209
4529.10612*	0.00170	3.7×10^{-55}	0 0 0	1 0 1	7 6 1	7 6 2	-0.198
4529.25175	0.00086	6.0×10^{-55}	0 0 0	1 0 1	2 1 2	1 1 1	-0.132
4532.37769	0.00138	4.1×10^{-55}	0 0 0	1 0 1	7 5 2	7 5 3	-0.174
4532.84296	0.00178	6.3×10^{-55}	0 0 0	1 0 1	6 5 2	6 5 1	-0.174
4532.85234	0.00597	2.1×10^{-55}	0 0 0	1 0 1	6 5 1	6 5 2	-0.168
4533.18196	0.00525	3.1×10^{-55}	0 0 0	1 0 1	5 5 1	5 5 0	-0.180
4533.19094	0.00155	9.4×10^{-55}	0 0 0	1 0 1	5 5 0	5 5 1	-0.171
4536.21021	0.00111	5.5×10^{-55}	0 0 0	1 0 1	6 4 3	6 4 2	-0.154
4536.46709	0.00130	4.4×10^{-55}	0 0 0	1 0 1	1 0 1	0 0 0	-0.131
4536.70369	0.00081	8.3×10^{-55}	0 0 0	1 0 1	5 4 1	5 4 2	-0.156
4536.73913	0.00208	2.8×10^{-55}	0 0 0	1 0 1	5 4 2	5 4 1	-0.158
4537.21203	0.00598	4.1×10^{-55}	0 0 0	1 0 1	4 4 0	4 4 1	-0.161
4537.21768	0.00188	1.2×10^{-54}	0 0 0	1 0 1	4 4 1	4 4 0	-0.160
4538.71548	0.00112	5.8×10^{-55}	0 0 0	1 0 1	5 3 2	5 3 3	-0.142
4539.77085	0.00310	3.0×10^{-55}	0 0 0	1 0 1	4 3 1	4 3 2	-0.147
4540.03882	0.00354	1.9×10^{-55}	0 0 0	1 0 1	5 3 3	5 3 2	-0.140
4540.11403	0.00070	8.9×10^{-55}	0 0 0	1 0 1	4 3 2	4 3 1	-0.147
4540.37750	0.00048	1.4×10^{-54}	0 0 0	1 0 1	3 3 0	3 3 1	-0.149

Position	$\sigma_{\text{Pos.}}$	Intensity	$\nu_1\ \nu_2\ \nu_3$	$\nu_1'\ \nu_2'\ \nu_3'$	J K_a K_c	J' K_a' K_c'	$\Delta_{\text{SPEC.}}$
4540.42908	0.00145	4.5×10^{-55}	0 0 0	1 0 1	3 3 1	3 3 0	-0.147
4540.55944	0.00167	3.7×10^{-55}	0 0 0	1 0 1	6 3 4	6 3 3	-0.137
4541.17884	0.00098	7.0×10^{-55}	0 0 0	1 0 1	3 2 1	3 2 2	-0.138
4542.47538	0.00166	3.8×10^{-55}	0 0 0	1 0 1	2 2 0	2 2 1	-0.143
4542.62721	0.00091	6.3×10^{-55}	0 0 0	1 0 1	1 1 0	1 1 1	-0.137
4542.96679	0.00060	1.2×10^{-54}	0 0 0	1 0 1	2 2 1	2 2 0	-0.139
4543.53238	0.00280	2.3×10^{-55}	0 0 0	1 0 1	3 2 2	3 2 1	-0.141
4545.03575	0.00373	1.4×10^{-55}	0 0 0	1 0 1	8 3 6	8 3 5	-0.121
4545.16646	0.00139	4.4×10^{-55}	0 0 0	1 0 1	4 2 3	4 2 2	-0.135
4545.66063	0.00292	2.1×10^{-55}	0 0 0	1 0 1	1 1 1	1 1 0	-0.135
4548.42233	0.00212	3.3×10^{-55}	0 0 0	1 0 1	2 1 2	2 1 1	-0.134
4552.52199	0.00991	7.0×10^{-56}	0 0 0	1 0 1	3 1 3	3 1 2	-0.133
4552.54768	0.00573	1.7×10^{-55}	0 0 0	1 0 1	6 2 5	6 2 4	-0.123
4552.73584	0.00407	1.5×10^{-55}	0 0 0	1 0 1	0 0 0	1 0 1	-0.135
4557.84996	0.00449	1.5×10^{-55}	0 0 0	1 0 1	4 1 4	4 1 3	-0.129
4558.76632	0.00248	2.1×10^{-55}	0 0 0	1 0 1	1 1 1	2 1 2	-0.132
4560.41427	0.00069	8.4×10^{-55}	0 0 0	1 0 1	1 0 1	2 0 2	-0.133
4561.80183	0.00097	6.1×10^{-55}	0 0 0	1 0 1	1 1 0	2 1 1	-0.135
4565.64844	0.00056	1.0×10^{-54}	0 0 0	1 0 1	2 1 2	3 1 3	-0.135
4566.93674	0.00112	5.6×10^{-55}	0 0 0	1 0 1	2 2 1	3 2 2	-0.140
4567.48012	0.00161	3.8×10^{-55}	0 0 0	1 0 1	2 0 2	3 0 3	-0.131
4570.17890	0.00179	3.3×10^{-55}	0 0 0	1 0 1	2 1 1	3 1 2	-0.135
4572.24753	0.00435	4.2×10^{-55}	0 0 0	1 0 1	3 1 3	4 1 4	-0.129
4573.32666	0.00158	4.2×10^{-55}	0 0 0	1 0 1	3 3 0	4 3 1	-0.152
4573.86030	0.00047	1.3×10^{-54}	0 0 0	1 0 1	3 0 3	4 0 4	-0.131
4574.40286	0.00216	2.9×10^{-55}	0 0 0	1 0 1	3 2 2	4 2 3	-0.141
4576.63743	0.00073	8.7×10^{-55}	0 0 0	1 0 1	3 2 1	4 2 2	-0.137
4578.16580	0.00049	1.2×10^{-54}	0 0 0	1 0 1	3 1 2	4 1 3	-0.130
4578.30619	0.00206	2.7×10^{-55}	0 0 0	1 0 1	4 4 1	5 4 2	-0.157
4578.54031	0.00048	1.4×10^{-54}	0 0 0	1 0 1	4 1 4	5 1 5	-0.133
4579.72758	0.00141	4.7×10^{-55}	0 0 0	1 0 1	4 0 4	5 0 5	-0.129
4580.94190	0.00090	6.5×10^{-55}	0 0 0	1 0 1	4 3 2	5 3 3	-0.146
4581.47904	0.00282	2.2×10^{-55}	0 0 0	1 0 1	4 3 1	5 3 2	-0.143
4581.55763	0.00059	1.0×10^{-54}	0 0 0	1 0 1	4 2 3	5 2 4	-0.136
4582.74787	0.02873	4.9×10^{-56}	0 0 0	1 0 1	5 5 1	6 5 2	-0.184
4582.74787	0.00994	1.5×10^{-55}	0 0 0	1 0 1	5 5 0	6 5 1	-0.179
4584.56208	0.00126	4.6×10^{-55}	0 0 0	1 0 1	5 1 5	6 1 6	-0.132
4585.32841	0.00042	1.4×10^{-54}	0 0 0	1 0 1	5 0 5	6 0 6	-0.129
4585.40291	0.00159	3.4×10^{-55}	0 0 0	1 0 1	4 2 2	5 2 3	-0.130
4585.60839	0.00149	4.2×10^{-55}	0 0 0	1 0 1	4 1 3	5 1 4	-0.131
4586.20238	0.00144	4.0×10^{-55}	0 0 0	1 0 1	5 4 1	6 4 2	-0.157

Position	$\sigma_{\text{Pos.}}$	Intensity	$\nu_1\,\nu_2\,\nu_3$	$\nu_1'\,\nu_2'\,\nu_3'$	J K_a K_c	J' K_a' K_c'	$\Delta_{\text{SPEC.}}$
4589.85149	0.00086	7.3×10^{-55}	0 0 0	1 0 1	5 3 2	6 3 3	-0.141
4590.34663	0.00047	1.3×10^{-54}	0 0 0	1 0 1	6 1 6	7 1 7	-0.130
4590.69302	0.00294	2.1×10^{-55}	0 0 0	1 0 1	6 5 2	7 5 3	-0.184
4590.83029	0.00151	4.3×10^{-55}	0 0 0	1 0 1	6 0 6	7 0 7	-0.129
4592.37473*	0.00078	1.2×10^{-54}	0 0 0	1 0 1	5 1 4	6 1 5	-0.129
4593.84894*	0.00187	4.4×10^{-55}	0 0 0	1 0 1	6 4 3	7 4 4	-0.151
4593.87285*	0.00059	1.0×10^{-54}	0 0 0	1 0 1	5 2 3	6 2 4	-0.127
4594.77124	0.00066	9.9×10^{-55}	0 0 0	1 0 1	6 2 5	7 2 6	-0.132
4595.84627	0.00081	7.2×10^{-55}	0 0 0	1 0 1	6 3 4	7 3 5	-0.139
4595.94222	0.00163	3.8×10^{-55}	0 0 0	1 0 1	7 1 7	8 1 8	-0.127
4596.33776	0.00059	1.1×10^{-54}	0 0 0	1 0 1	7 0 7	8 0 8	-0.129
4598.41830	0.00263	3.5×10^{-55}	0 0 0	1 0 1	6 1 5	7 1 6	-0.129
4598.46812	0.00270	2.4×10^{-55}	0 0 0	1 0 1	6 3 3	7 3 4	-0.140
4600.82030	0.00398	2.9×10^{-55}	0 0 0	1 0 1	7 2 6	8 2 7	-0.129
4601.43770	0.00058	9.5×10^{-55}	0 0 0	1 0 1	8 1 8	9 1 9	-0.130
4601.80074	0.00208	3.2×10^{-55}	0 0 0	1 0 1	6 2 4	7 2 5	-0.121
4602.07749	0.00145	4.1×10^{-55}	0 0 0	1 0 1	7 4 3	8 4 4	-0.147
4602.68314	0.00236	2.1×10^{-55}	0 0 0	1 0 1	8 0 8	9 0 9	-0.139
4602.83548	0.00265	2.1×10^{-55}	0 0 0	1 0 1	7 3 5	8 3 6	-0.134
4603.94637	0.00069	8.6×10^{-55}	0 0 0	1 0 1	7 1 6	8 1 7	-0.126
4605.93385	0.00076	7.6×10^{-55}	0 0 0	1 0 1	9 0 9	10 0 10	-0.122
4606.24594	0.00326	1.9×10^{-55}	0 0 0	1 0 1	8 5 4	9 5 5	-0.172
4606.53412	0.00084	7.1×10^{-55}	0 0 0	1 0 1	8 2 7	9 2 8	-0.127
4607.17195	0.00085	6.4×10^{-55}	0 0 0	1 0 1	7 3 4	8 3 5	-0.127
4608.14032	0.00290	1.5×10^{-55}	0 0 0	1 0 1	9 1 9	10 1 10	-0.136
4608.80287	0.00159	3.5×10^{-55}	0 0 0	1 0 1	8 4 5	9 4 6	-0.149
4608.99222	0.00066	8.1×10^{-55}	0 0 0	1 0 1	7 2 5	8 2 6	-0.118
4609.43412	0.00103	5.3×10^{-55}	0 0 0	1 0 1	8 3 6	9 3 7	-0.132
4609.56038	0.00357	1.9×10^{-55}	0 0 0	1 0 1	8 1 7	9 1 8	-0.139
4610.20216	0.00186	3.8×10^{-55}	0 0 0	1 0 1	9 1 8	10 1 9	-0.124
4611.01785	0.00097	6.0×10^{-55}	0 0 0	1 0 1	10 1 10	11 1 11	-0.118
4611.16704	0.00319	2.0×10^{-55}	0 0 0	1 0 1	10 0 10	11 0 11	-0.119
4611.99410	0.00451	1.9×10^{-55}	0 0 0	1 0 1	9 2 8	10 2 9	-0.126
4614.29141	0.00356	1.6×10^{-55}	0 0 0	1 0 1	9 5 4	10 5 5	-0.160
4615.27978	0.00276	2.1×10^{-55}	0 0 0	1 0 1	8 2 6	9 2 7	-0.104
4616.05212	0.00659	1.5×10^{-55}	0 0 0	1 0 1	11 1 11	12 1 12	-0.125
4616.10217	0.00152	4.5×10^{-55}	0 0 0	1 0 1	11 0 11	12 0 12	-0.116
4617.41146	0.00276	4.0×10^{-55}	0 0 0	1 0 1	10 2 9	11 2 10	-0.121
4618.64559	0.00236	2.8×10^{-55}	0 0 0	1 0 1	9 4 5	10 4 6	-0.134
4620.49649	0.00124	4.7×10^{-55}	0 0 0	1 0 1	9 2 7	10 2 8	-0.109
4620.83088	0.00658	1.1×10^{-55}	0 0 0	1 0 1	12 0 12	13 0 13	-0.136

Position	$\sigma_{\text{Pos.}}$	Intensity	$\nu_1\ \nu_2\ \nu_3$	$\nu_1'\ \nu_2'\ \nu_3'$	J K_a K_c	J' K_a' K_c'	$\Delta_{\text{SPEC.}}$
4620.84284	0.00230	3.2×10^{-55}	0 0 0	1 0 1	12 1 12	13 1 13	-0.109
4620.89379	0.00196	3.0×10^{-55}	0 0 0	1 0 1	11 1 10	12 1 11	-0.111
4621.09508	0.00528	1.2×10^{-55}	0 0 0	1 0 1	10 5 6	11 5 7	-0.156
4621.37912	0.00182	3.0×10^{-55}	0 0 0	1 0 1	10 3 8	11 3 9	-0.123
4622.62417	0.00296	2.1×10^{-55}	0 0 0	1 0 1	10 4 7	11 4 8	-0.133
4623.46378	0.00735	4.1×10^{-55}	0 0 0	1 0 1	9 3 6	10 3 7	-0.116
4624.44919	0.00223	2.0×10^{-55}	0 0 0	1 0 1	12 2 11	13 2 12	-0.103
4625.42799	0.00667	7.3×10^{-56}	0 0 0	1 0 1	13 1 13	14 1 14	-0.120
4625.44235	0.00245	2.2×10^{-55}	0 0 0	1 0 1	13 0 13	14 0 14	-0.112
4628.33156	0.00275	2.2×10^{-55}	0 0 0	1 0 1	11 2 9	12 2 10	-0.102
4629.61141	0.01091	4.7×10^{-56}	0 0 0	1 0 1	13 2 12	14 2 13	-0.093
4629.72179	0.00626	8.9×10^{-56}	0 0 0	1 0 1	11 5 6	12 5 7	-0.151
4629.86623	0.02061	4.8×10^{-56}	0 0 0	1 0 1	14 0 14	15 0 15	-0.120
4629.88287	0.00584	1.4×10^{-55}	0 0 0	1 0 1	14 1 14	15 1 15	-0.102
4629.95360	0.00563	1.4×10^{-55}	0 0 0	1 0 1	13 1 12	14 1 13	-0.104
4634.07249	0.00530	9.1×10^{-56}	0 0 0	1 0 1	14 2 13	15 2 14	-0.105
4634.15538	0.00520	9.2×10^{-56}	0 0 0	1 0 1	15 0 15	16 0 16	-0.100
4634.59170	0.00584	9.2×10^{-56}	0 0 0	1 0 1	12 4 9	13 4 10	-0.118
4635.28813	0.00300	1.5×10^{-55}	0 0 0	1 0 1	11 4 7	12 4 8	-0.108
4636.48283	0.00254	2.0×10^{-55}	0 0 0	1 0 1	11 3 8	12 3 9	-0.093
4644.70670	0.00444	7.3×10^{-56}	0 0 0	1 0 1	13 3 10	14 3 11	-0.081

A.2.3.2 T_2O $\nu_1 + \nu_3$ band from the 10 GBq sample

Here, the lines assigned to the $\nu_1 + \nu_3$ band of T_2O obtained from the 10 GBq sample are presented. These lines are published in [Her23]. For further information, see Section 5.5.3.

Table A.14: Linelist of the T_2O $\nu_1 + \nu_3$ band from the 10 GBq sample. The columns present the assigned line position, the uncertainty on the position $\sigma_{\text{Pos.}}$, the line intensity taking natural abundance into account, lower and upper vibrational quanta, lower and upper rotational quanta and the deviation to the predictions from SPECTRA database $\Delta_{\text{SPEC.}}$.

Position	$\sigma_{\text{Pos.}}$	Intensity	$\nu_1\ \nu_2\ \nu_3$	$\nu_1'\ \nu_2'\ \nu_3'$	J K_a K_c	J' K_a' K_c'	$\Delta_{\text{SPEC.}}$
4379.63725	0.00275	8.3×10^{-57}	0 0 0	1 0 1	18 3 16	17 3 15	-0.049
4379.85765	0.00323	8.1×10^{-57}	0 0 0	1 0 1	19 1 18	18 1 17	-0.076
4380.23812	0.00908	8.2×10^{-57}	0 0 0	1 0 1	20 1 20	19 1 19	-0.077
4383.13025	0.00398	8.4×10^{-57}	0 0 0	1 0 1	17 3 14	16 3 13	-0.086
4383.45236	0.00954	6.2×10^{-57}	0 0 0	1 0 1	14 7 8	13 7 7	-0.131
4383.76179	0.01083	5.0×10^{-57}	0 0 0	1 0 1	16 4 12	15 4 11	-0.111
4384.87908	0.00722	3.9×10^{-57}	0 0 0	1 0 1	16 6 11	15 6 10	-0.127
4387.42105	0.01622	9.3×10^{-57}	0 0 0	1 0 1	16 5 12	15 5 11	-0.086

Position	$\sigma_{\text{Pos.}}$	Intensity	$\nu_1\ \nu_2\ \nu_3$	$\nu_1\text{'}\ \nu_2\text{'}\ \nu_3\text{'}$	J K_a K_c	J' $K_a\text{'}$ $K_c\text{'}$	$\Delta_{\text{SPEC.}}$
4388.26861	0.00696	4.7×10^{-57}	0 0 0	1 0 1	17 3 15	16 3 14	-0.064
4389.12209	0.00476	4.9×10^{-57}	0 0 0	1 0 1	18 1 17	17 1 16	-0.081
4389.12209	0.00231	1.5×10^{-56}	0 0 0	1 0 1	18 2 17	17 2 16	-0.080
4389.39941	0.00200	1.5×10^{-56}	0 0 0	1 0 1	17 2 15	16 2 14	-0.075
4389.51774	0.00168	1.5×10^{-56}	0 0 0	1 0 1	19 0 19	18 0 18	-0.080
4389.51774	0.00365	5.0×10^{-57}	0 0 0	1 0 1	19 1 19	18 1 18	-0.080
4390.04390	0.00557	4.3×10^{-57}	0 0 0	1 0 1	13 9 4	12 9 3	-0.175
4394.14959	0.00750	2.7×10^{-57}	0 0 0	1 0 1	13 8 6	12 8 5	-0.176
4394.14960	0.00904	8.0×10^{-57}	0 0 0	1 0 1	13 8 5	12 8 4	-0.174
4394.29197	0.00175	2.8×10^{-56}	0 0 0	1 0 1	15 4 11	14 4 10	-0.109
4394.61838	0.00345	2.1×10^{-56}	0 0 0	1 0 1	15 5 10	14 5 9	-0.116
4394.84081	0.00301	1.7×10^{-56}	0 0 0	1 0 1	16 3 14	15 3 13	-0.114
4395.30867	0.00311	1.0×10^{-56}	0 0 0	1 0 1	13 7 6	12 7 5	-0.157
4395.34505	0.01297	3.4×10^{-57}	0 0 0	1 0 1	13 7 7	12 7 6	-0.159
4397.85857	0.06886	1.1×10^{-56}	0 0 0	1 0 1	15 6 9	14 6 8	-0.126
4398.16160	0.00399	1.3×10^{-56}	0 0 0	1 0 1	16 4 13	15 4 12	-0.115
4398.29549	0.00214	2.6×10^{-56}	0 0 0	1 0 1	17 1 16	16 1 15	-0.081
4398.29549	0.00601	8.5×10^{-57}	0 0 0	1 0 1	17 2 16	16 2 15	-0.082
4398.36824	0.00482	6.3×10^{-57}	0 0 0	1 0 1	15 5 11	14 5 10	-0.112
4398.59901	0.00393	8.9×10^{-57}	0 0 0	1 0 1	16 2 14	15 2 13	-0.080
4398.66930	0.00350	8.9×10^{-57}	0 0 0	1 0 1	18 0 18	17 0 17	-0.086
4398.66930	0.00139	2.7×10^{-56}	0 0 0	1 0 1	18 1 18	17 1 17	-0.085
4398.78570	0.00106	3.3×10^{-56}	0 0 0	1 0 1	15 3 12	14 3 11	-0.066
4401.94033	0.00428	8.6×10^{-57}	0 0 0	1 0 1	15 4 12	14 4 11	-0.089
4401.94033	0.00562	5.9×10^{-57}	0 0 0	1 0 1	12 9 4	11 9 3	-0.210
4405.98980	0.00449	1.2×10^{-56}	0 0 0	1 0 1	12 8 5	11 8 4	-0.185
4406.00009	0.03458	3.9×10^{-57}	0 0 0	1 0 1	12 8 4	11 8 3	-0.174
4406.00009	0.01220	1.2×10^{-56}	0 0 0	1 0 1	14 5 9	13 5 8	-0.124
4406.21193	0.00298	1.2×10^{-56}	0 0 0	1 0 1	14 6 9	13 6 8	-0.148
4407.21150	0.00072	4.4×10^{-56}	0 0 0	1 0 1	16 2 15	15 2 14	-0.085
4407.23526	0.00212	1.6×10^{-56}	0 0 0	1 0 1	12 7 6	11 7 5	-0.175
4407.28822	0.00228	1.5×10^{-56}	0 0 0	1 0 1	16 1 15	15 1 14	-0.087
4407.69165	0.00131	4.6×10^{-56}	0 0 0	1 0 1	17 0 17	16 0 16	-0.090
4407.69165	0.00368	1.5×10^{-56}	0 0 0	1 0 1	17 1 17	16 1 16	-0.088
4408.05837	0.00084	4.1×10^{-56}	0 0 0	1 0 1	15 2 13	14 2 12	-0.092
4408.56086	0.00225	2.0×10^{-56}	0 0 0	1 0 1	14 3 11	13 3 10	-0.066
4408.60277	0.00122	3.3×10^{-56}	0 0 0	1 0 1	14 5 10	13 5 9	-0.122
4412.13528	0.00064	5.1×10^{-56}	0 0 0	1 0 1	14 4 11	13 4 10	-0.101
4412.50761	0.00375	1.3×10^{-56}	0 0 0	1 0 1	15 3 13	14 3 12	-0.101
4413.85114	0.01220	7.1×10^{-57}	0 0 0	1 0 1	11 9 2	10 9 1	-0.211
4415.16388	0.00177	2.2×10^{-56}	0 0 0	1 0 1	14 2 12	13 2 11	-0.087

Position	$\sigma_{\text{Pos.}}$	Intensity	$\nu_1\,\nu_2\,\nu_3$	$\nu_1'\,\nu_2'\,\nu_3'$	J K_a K_c	J' K_a' K_c'	$\Delta_{\text{SPEC.}}$
4415.64009	0.00050	8.0×10^{-56}	0 0 0	1 0 1	13 4 9	12 4 8	-0.087
4415.91635	0.00151	2.4×10^{-56}	0 0 0	1 0 1	15 2 14	14 2 13	-0.090
4416.13177	0.00046	7.2×10^{-56}	0 0 0	1 0 1	15 1 14	14 1 13	-0.092
4416.59662	0.00135	7.5×10^{-56}	0 0 0	1 0 1	16 1 16	15 1 15	-0.093
4416.59662	0.00394	2.5×10^{-56}	0 0 0	1 0 1	16 0 16	15 0 15	-0.093
4417.02131	0.00072	5.5×10^{-56}	0 0 0	1 0 1	13 5 8	12 5 7	-0.123
4417.45790	0.00077	4.8×10^{-56}	0 0 0	1 0 1	14 3 12	13 3 11	-0.108
4417.78615	0.00533	1.6×10^{-56}	0 0 0	1 0 1	11 8 3	10 8 2	-0.199
4418.09780	0.00061	9.9×10^{-56}	0 0 0	1 0 1	13 3 10	12 3 9	-0.079
4418.19546	0.00142	2.9×10^{-56}	0 0 0	1 0 1	13 6 7	12 6 6	-0.175
4418.54894	0.00326	1.8×10^{-56}	0 0 0	1 0 1	13 5 9	12 5 8	-0.131
4419.11455	0.00371	2.2×10^{-56}	0 0 0	1 0 1	11 7 4	10 7 3	-0.187
4419.12414	0.01337	7.5×10^{-57}	0 0 0	1 0 1	11 7 5	10 7 4	-0.181
4420.51182	0.01301	6.2×10^{-57}	0 0 0	1 0 1	13 6 8	12 6 7	-0.154
4421.66721	0.00166	2.8×10^{-56}	0 0 0	1 0 1	13 4 10	12 4 9	-0.110
4423.98921	0.00040	1.0×10^{-55}	0 0 0	1 0 1	14 2 13	13 2 12	-0.090
4424.56145	0.00034	1.2×10^{-55}	0 0 0	1 0 1	13 2 11	12 2 10	-0.090
4424.78756	0.00129	3.8×10^{-56}	0 0 0	1 0 1	14 1 13	13 1 12	-0.110
4425.35951	0.00475	1.2×10^{-55}	0 0 0	1 0 1	15 0 15	14 0 14	-0.098
4425.35951	0.01424	4.0×10^{-56}	0 0 0	1 0 1	15 1 15	14 1 14	-0.095
4425.72776	0.00470	6.2×10^{-57}	0 0 0	1 0 1	10 9 2	9 9 1	-0.235
4426.47596	0.00224	4.2×10^{-56}	0 0 0	1 0 1	12 4 8	11 4 7	-0.107
4427.33463	0.00100	3.9×10^{-56}	0 0 0	1 0 1	13 3 11	12 3 10	-0.105
4427.55121	0.00258	2.8×10^{-56}	0 0 0	1 0 1	12 5 7	11 5 6	-0.134
4427.71088	0.00216	5.2×10^{-56}	0 0 0	1 0 1	12 3 9	11 3 8	-0.087
4427.73390	0.00541	1.4×10^{-56}	0 0 0	1 0 1	12 6 6	11 6 5	-0.186
4428.31601	0.00088	8.3×10^{-56}	0 0 0	1 0 1	12 5 8	11 5 7	-0.135
4428.35703	0.00606	4.0×10^{-56}	0 0 0	1 0 1	12 6 7	11 6 6	-0.176
4429.53230	0.00349	1.9×10^{-56}	0 0 0	1 0 1	10 8 3	9 8 2	-0.238
4431.04096	0.00240	3.0×10^{-56}	0 0 0	1 0 1	10 7 4	9 7 3	-0.197
4431.04096	0.00635	9.9×10^{-57}	0 0 0	1 0 1	10 7 3	9 7 2	-0.197
4431.08714	0.00042	1.3×10^{-55}	0 0 0	1 0 1	12 4 9	11 4 8	-0.116
4433.24184	0.00023	1.7×10^{-55}	0 0 0	1 0 1	13 1 12	12 1 11	-0.099
4433.47598	0.00079	6.1×10^{-56}	0 0 0	1 0 1	12 2 10	11 2 9	-0.094
4433.98297	0.00167	6.1×10^{-56}	0 0 0	1 0 1	14 0 14	13 0 13	-0.108
4433.98297	0.00058	1.8×10^{-55}	0 0 0	1 0 1	14 1 14	13 1 13	-0.099
4436.16685	0.00026	1.8×10^{-55}	0 0 0	1 0 1	12 3 10	11 3 9	-0.109
4437.08169	0.00199	2.0×10^{-56}	0 0 0	1 0 1	11 6 6	10 6 5	-0.193
4437.31530	0.00020	1.8×10^{-55}	0 0 0	1 0 1	11 4 7	10 4 6	-0.114
4437.52419	0.00018	2.4×10^{-55}	0 0 0	1 0 1	11 3 8	10 3 7	-0.094
4437.62447	0.00038	1.2×10^{-55}	0 0 0	1 0 1	11 5 6	10 5 5	-0.150

Position	$\sigma_{\mathrm{Pos.}}$	Intensity	$\nu_1\,\nu_2\,\nu_3$	$\nu_1{}'\,\nu_2{}'\,\nu_3{}'$	J K_a K_c	J' $\mathrm{K}_a{}'$ $\mathrm{K}_c{}'$	$\Delta_{\mathrm{SPEC.}}$
4437.90659	0.00099	4.0×10^{-56}	0 0 0	1 0 1	11 5 7	10 5 6	-0.149
4440.47383	0.00176	6.2×10^{-56}	0 0 0	1 0 1	11 4 8	10 4 7	-0.128
4441.29906	0.00078	7.5×10^{-56}	0 0 0	1 0 1	12 1 11	11 1 10	-0.103
4441.34013	0.00443	1.6×10^{-56}	0 0 0	1 0 1	9 8 1	8 8 0	-0.224
4441.34013	0.00867	5.4×10^{-57}	0 0 0	1 0 1	9 8 2	8 8 1	-0.224
4442.28524	0.00015	2.8×10^{-55}	0 0 0	1 0 1	11 2 9	10 2 8	-0.098
4442.45120	0.00053	9.0×10^{-56}	0 0 0	1 0 1	13 1 13	12 1 12	-0.102
4442.47359	0.00015	2.7×10^{-55}	0 0 0	1 0 1	13 0 13	12 0 12	-0.105
4443.14969	0.00561	3.5×10^{-56}	0 0 0	1 0 1	9 7 2	8 7 1	-0.209
4443.14969	0.01626	1.2×10^{-56}	0 0 0	1 0 1	9 7 3	8 7 2	-0.209
4443.61371	0.00017	2.5×10^{-55}	0 0 0	1 0 1	12 2 11	11 2 10	-0.112
4444.96737	0.00096	8.7×10^{-56}	0 0 0	1 0 1	11 3 9	10 3 8	-0.114
4445.78928	0.00192	2.6×10^{-56}	0 0 0	1 0 1	10 6 4	9 6 3	-0.195
4445.82749	0.00048	7.8×10^{-56}	0 0 0	1 0 1	10 6 5	9 6 4	-0.197
4447.33146	0.00051	1.6×10^{-55}	0 0 0	1 0 1	10 5 6	9 5 5	-0.155
4447.35459	0.00121	5.1×10^{-56}	0 0 0	1 0 1	10 5 5	9 5 4	-0.154
4447.46359	0.05219	3.2×10^{-57}	0 0 0	1 0 1	6 2 4	5 0 5	-0.110
4447.56703	0.00038	1.1×10^{-55}	0 0 0	1 0 1	10 3 7	9 3 6	-0.103
4448.11402	0.00127	7.7×10^{-56}	0 0 0	1 0 1	10 4 6	9 4 5	-0.112
4448.41390	0.00024	2.2×10^{-55}	0 0 0	1 0 1	11 1 10	10 1 9	-0.114
4449.85161	0.00022	2.5×10^{-55}	0 0 0	1 0 1	10 4 7	9 4 6	-0.131
4450.67362	0.00017	3.7×10^{-55}	0 0 0	1 0 1	12 1 12	11 1 11	-0.108
4450.78929	0.00033	1.3×10^{-55}	0 0 0	1 0 1	12 0 12	11 0 11	-0.109
4451.06786	0.00036	1.3×10^{-55}	0 0 0	1 0 1	10 2 8	9 2 7	-0.102
4451.70976	0.00054	1.2×10^{-55}	0 0 0	1 0 1	11 2 10	10 2 9	-0.114
4453.79076	0.00060	3.6×10^{-55}	0 0 0	1 0 1	10 3 8	9 3 7	-0.119
4454.32059	0.00182	9.4×10^{-56}	0 0 0	1 0 1	9 6 3	8 6 2	-0.197
4454.32059	0.00519	3.1×10^{-56}	0 0 0	1 0 1	9 6 4	8 6 3	-0.206
4455.99945	0.00125	1.3×10^{-55}	0 0 0	1 0 1	9 5 4	8 5 3	-0.152
4456.12234	0.00201	3.8×10^{-56}	0 0 0	1 0 1	8 7 2	7 7 1	-0.202
4456.12298	0.00576	1.3×10^{-56}	0 0 0	1 0 1	8 7 1	7 7 0	-0.201
4456.49767	0.01183	6.2×10^{-57}	0 0 0	1 0 1	12 2 11	12 0 12	-0.109
4456.58101	0.00206	6.6×10^{-56}	0 0 0	1 0 1	9 5 5	8 5 4	-0.156
4457.80718	0.00028	4.5×10^{-55}	0 0 0	1 0 1	9 3 6	8 3 5	-0.116
4458.10663	0.00019	3.2×10^{-55}	0 0 0	1 0 1	9 4 5	8 4 4	-0.135
4458.81394	0.00010	5.0×10^{-55}	0 0 0	1 0 1	11 0 11	10 0 10	-0.112
4459.19246	0.00042	1.1×10^{-55}	0 0 0	1 0 1	9 4 6	8 4 5	-0.137
4459.95206	0.00030	4.9×10^{-55}	0 0 0	1 0 1	10 2 9	9 2 8	-0.115
4459.96810	0.00021	5.4×10^{-55}	0 0 0	1 0 1	9 2 7	8 2 6	-0.106
4460.53422	0.00035	1.4×10^{-55}	0 0 0	1 0 1	10 1 9	9 1 8	-0.126
4461.09233	0.00043	1.1×10^{-55}	0 0 0	1 0 1	11 1 11	10 1 10	-0.123

261

Position	$\sigma_{\text{Pos.}}$	Intensity	$\nu_1\ \nu_2\ \nu_3$	$\nu_1'\ \nu_2'\ \nu_3'$	J K_a K_c	J' K_a' K_c'	$\Delta_{\text{SPEC.}}$
4462.47448	0.00058	9.9×10^{-56}	0 0 0	1 0 1	8 6 3	7 6 2	-0.198
4462.47448	0.00150	3.3×10^{-56}	0 0 0	1 0 1	8 6 2	7 6 1	-0.196
4462.65107	0.00030	1.6×10^{-55}	0 0 0	1 0 1	9 3 7	8 3 6	-0.124
4464.11793	0.00925	1.5×10^{-56}	0 0 0	1 0 1	5 2 3	4 0 4	-0.120
4465.50542	0.00610	7.3×10^{-57}	0 0 0	1 0 1	11 1 10	11 1 11	-0.106
4465.57573	0.00075	7.4×10^{-56}	0 0 0	1 0 1	8 5 3	7 5 2	-0.165
4465.64141	0.00019	2.2×10^{-55}	0 0 0	1 0 1	8 5 4	7 5 3	-0.165
4467.67655	0.00011	6.2×10^{-55}	0 0 0	1 0 1	9 1 8	8 1 7	-0.119
4467.71466	0.00009	6.8×10^{-55}	0 0 0	1 0 1	10 1 10	9 1 9	-0.118
4467.96856	0.00178	1.3×10^{-55}	0 0 0	1 0 1	8 4 4	7 4 3	-0.141
4468.15239	0.00030	1.9×10^{-55}	0 0 0	1 0 1	8 3 5	7 3 4	-0.122
4468.20068	0.00024	2.1×10^{-55}	0 0 0	1 0 1	9 2 8	8 2 7	-0.120
4468.46960	0.00027	3.9×10^{-55}	0 0 0	1 0 1	8 4 5	7 4 4	-0.143
4468.81539	0.00036	1.6×10^{-55}	0 0 0	1 0 1	10 0 10	9 0 9	-0.130
4469.10740	0.00024	2.3×10^{-55}	0 0 0	1 0 1	8 2 6	7 2 5	-0.112
4470.10616	0.00296	8.1×10^{-56}	0 0 0	1 0 1	7 6 1	6 6 0	-0.185
4470.10616	0.00805	2.7×10^{-56}	0 0 0	1 0 1	7 6 2	6 6 1	-0.185
4471.55240	0.00009	5.7×10^{-55}	0 0 0	1 0 1	8 3 6	7 3 5	-0.129
4472.45898	0.01467	7.1×10^{-57}	0 0 0	1 0 1	12 2 10	12 2 11	-0.117
4474.52631	0.00108	2.2×10^{-55}	0 0 0	1 0 1	7 5 2	6 5 1	-0.166
4474.53403	0.00353	7.3×10^{-56}	0 0 0	1 0 1	7 5 3	6 5 2	-0.172
4475.22154	0.00030	2.7×10^{-55}	0 0 0	1 0 1	8 1 7	7 1 6	-0.119
4475.58485	0.00017	2.9×10^{-55}	0 0 0	1 0 1	9 1 9	8 1 8	-0.120
4475.70077	0.00008	8.5×10^{-55}	0 0 0	1 0 1	9 0 9	8 0 8	-0.121
4476.44769	0.00008	7.7×10^{-55}	0 0 0	1 0 1	8 2 7	7 2 6	-0.123
4477.45334	0.00011	4.2×10^{-55}	0 0 0	1 0 1	7 4 3	6 4 2	-0.148
4477.65157	0.00034	1.4×10^{-55}	0 0 0	1 0 1	7 4 4	6 4 3	-0.148
4478.40465	0.00013	6.4×10^{-55}	0 0 0	1 0 1	7 3 4	6 3 3	-0.130
4478.51233	0.00028	8.4×10^{-55}	0 0 0	1 0 1	7 2 5	6 2 4	-0.120
4479.95638	0.00787	6.6×10^{-57}	0 0 0	1 0 1	13 3 10	13 3 11	-0.107
4480.48801	0.00202	2.2×10^{-55}	0 0 0	1 0 1	7 3 5	6 3 4	-0.131
4481.04901	0.00283	2.3×10^{-56}	0 0 0	1 0 1	11 2 9	11 2 10	-0.114
4482.97948	0.00005	9.6×10^{-55}	0 0 0	1 0 1	7 1 6	6 1 5	-0.119
4483.28401	0.00076	1.5×10^{-55}	0 0 0	1 0 1	6 5 2	5 5 1	-0.168
4483.28402	0.00191	5.2×10^{-56}	0 0 0	1 0 1	6 5 1	5 5 0	-0.166
4483.37581	0.00021	3.5×10^{-55}	0 0 0	1 0 1	8 0 8	7 0 7	-0.122
4483.43008	0.00015	1.0×10^{-54}	0 0 0	1 0 1	8 1 8	7 1 7	-0.122
4483.98821	0.00195	3.3×10^{-56}	0 0 0	1 0 1	9 1 8	9 1 9	-0.117
4484.70745	0.00019	3.0×10^{-55}	0 0 0	1 0 1	7 2 6	6 2 5	-0.126
4486.45678	0.00401	1.5×10^{-56}	0 0 0	1 0 1	9 3 7	9 1 8	-0.134
4486.64880	0.00067	1.3×10^{-55}	0 0 0	1 0 1	6 4 2	5 4 1	-0.152

Position	$\sigma_{\text{Pos.}}$	Intensity	$\nu_1\,\nu_2\,\nu_3$	$\nu_1{}'\,\nu_2{}'\,\nu_3{}'$	J K_a K_c	J' $K_a{}'$ $K_c{}'$	$\Delta_{\text{SPEC.}}$
4486.71219	0.00013	3.9×10^{-55}	0 0 0	1 0 1	6 4 3	5 4 2	-0.152
4488.15270	0.00026	3.1×10^{-55}	0 0 0	1 0 1	6 2 4	5 2 3	-0.123
4488.35322	0.00023	2.2×10^{-55}	0 0 0	1 0 1	6 3 3	5 3 2	-0.137
4489.35787	0.00121	4.5×10^{-56}	0 0 0	1 0 1	8 2 7	8 0 8	-0.124
4489.42387	0.00008	6.7×10^{-55}	0 0 0	1 0 1	6 3 4	5 3 3	-0.138
4489.50949	0.00391	1.4×10^{-56}	0 0 0	1 0 1	3 2 1	2 0 2	-0.137
4489.92438	0.00114	4.4×10^{-56}	0 0 0	1 0 1	8 3 6	8 1 7	-0.124
4490.20607	0.00433	6.8×10^{-57}	0 0 0	1 0 1	11 11 0	11 11 1	-0.244
4490.92940	0.02676	2.9×10^{-57}	0 0 0	1 0 1	14 9 6	14 9 5	-0.164
4490.98475	0.00005	1.2×10^{-54}	0 0 0	1 0 1	7 0 7	6 0 6	-0.124
4491.04517	0.00018	3.6×10^{-55}	0 0 0	1 0 1	6 1 5	5 1 4	-0.122
4491.19186	0.00013	3.9×10^{-55}	0 0 0	1 0 1	7 1 7	6 1 6	-0.125
4491.35723	0.00636	1.1×10^{-56}	0 0 0	1 0 1	10 2 8	10 2 9	-0.114
4492.61102	0.01136	2.5×10^{-57}	0 0 0	1 0 1	12 10 2	12 10 3	-0.218
4492.61106	0.00544	7.5×10^{-57}	0 0 0	1 0 1	12 10 3	12 10 2	-0.218
4493.00070	0.00038	9.7×10^{-55}	0 0 0	1 0 1	6 2 5	5 2 4	-0.129
4493.25058	0.00165	2.9×10^{-56}	0 0 0	1 0 1	6 3 4	6 1 5	-0.128
4494.65264	0.00403	5.8×10^{-57}	0 0 0	1 0 1	13 9 4	13 9 5	-0.184
4495.61847	0.00067	2.6×10^{-55}	0 0 0	1 0 1	5 4 1	4 4 0	-0.155
4495.63410	0.00117	8.8×10^{-56}	0 0 0	1 0 1	5 4 2	4 4 1	-0.155
4496.19359	0.00255	1.7×10^{-56}	0 0 0	1 0 1	7 2 6	7 0 7	-0.123
4496.68238	0.00579	4.8×10^{-57}	0 0 0	1 0 1	11 10 2	11 10 1	-0.233
4496.68238	0.00242	1.4×10^{-56}	0 0 0	1 0 1	11 10 1	11 10 2	-0.233
4497.89018	0.00011	6.0×10^{-55}	0 0 0	1 0 1	5 3 2	4 3 1	-0.140
4497.93675	0.00007	9.4×10^{-55}	0 0 0	1 0 1	5 2 3	4 2 2	-0.130
4498.33274	0.01102	1.1×10^{-56}	0 0 0	1 0 1	12 9 4	12 9 3	-0.204
4498.33274	0.00076	2.0×10^{-55}	0 0 0	1 0 1	5 3 3	4 3 2	-0.141
4498.33274	0.01886	3.8×10^{-57}	0 0 0	1 0 1	12 9 3	12 9 4	-0.204
4498.45087	0.00016	4.3×10^{-55}	0 0 0	1 0 1	6 0 6	5 0 5	-0.126
4498.87536	0.00006	1.3×10^{-54}	0 0 0	1 0 1	6 1 6	5 1 5	-0.127
4499.47906	0.00004	1.1×10^{-54}	0 0 0	1 0 1	5 1 4	4 1 3	-0.125
4500.22486	0.01105	4.3×10^{-57}	0 0 0	1 0 1	13 7 6	13 7 7	-0.170
4500.88232	0.00446	2.8×10^{-56}	0 0 0	1 0 1	10 10 1	10 10 0	-0.280
4500.88232	0.00848	9.2×10^{-57}	0 0 0	1 0 1	10 10 0	10 10 1	-0.280
4501.33502	0.00027	3.2×10^{-55}	0 0 0	1 0 1	5 2 4	4 2 3	-0.133
4501.80208	0.00101	4.6×10^{-56}	0 0 0	1 0 1	9 2 7	9 2 8	-0.118
4501.98400	0.00144	2.2×10^{-56}	0 0 0	1 0 1	11 9 2	11 9 3	-0.213
4501.98400	0.00339	7.3×10^{-57}	0 0 0	1 0 1	11 9 3	11 9 2	-0.213
4502.24364	0.00099	5.4×10^{-56}	0 0 0	1 0 1	7 1 6	7 1 7	-0.124
4502.32264	0.00088	5.7×10^{-56}	0 0 0	1 0 1	6 2 5	6 0 6	-0.133
4502.44782	0.00525	4.4×10^{-57}	0 0 0	1 0 1	12 8 4	12 8 5	-0.180

Position	$\sigma_{\text{Pos.}}$	Intensity	$\nu_1\,\nu_2\,\nu_3$	$\nu_1{}'\,\nu_2{}'\,\nu_3{}'$	J K_a K_c	J' $\text{K}_a{}'$ $\text{K}_c{}'$	$\Delta_{\text{SPEC.}}$
4502.44782	0.00252	1.3×10^{-56}	0 0 0	1 0 1	12 8 5	12 8 4	-0.179
4503.77131	0.00374	9.3×10^{-57}	0 0 0	1 0 1	12 7 6	12 7 5	-0.166
4503.85703	0.00172	2.7×10^{-56}	0 0 0	1 0 1	11 3 8	11 3 9	-0.106
4505.59346	0.00092	4.1×10^{-56}	0 0 0	1 0 1	10 9 2	10 9 1	-0.228
4505.59346	0.00198	1.4×10^{-56}	0 0 0	1 0 1	10 9 1	10 9 2	-0.228
4505.78304	0.00014	1.3×10^{-54}	0 0 0	1 0 1	5 0 5	4 0 4	-0.127
4505.97490	0.00329	8.7×10^{-57}	0 0 0	1 0 1	11 8 4	11 8 3	-0.192
4505.97490	0.00151	2.6×10^{-56}	0 0 0	1 0 1	11 8 3	11 8 4	-0.192
4506.49968	0.00012	4.3×10^{-55}	0 0 0	1 0 1	5 1 5	4 1 4	-0.129
4507.02838	0.00041	1.3×10^{-55}	0 0 0	1 0 1	4 3 1	3 3 0	-0.145
4507.16324	0.00017	4.0×10^{-55}	0 0 0	1 0 1	4 3 2	3 3 1	-0.145
4507.29827	0.00511	6.3×10^{-57}	0 0 0	1 0 1	11 7 5	11 7 4	-0.180
4507.29827	0.00232	1.9×10^{-56}	0 0 0	1 0 1	11 7 4	11 7 5	-0.183
4507.46289	0.00227	1.9×10^{-56}	0 0 0	1 0 1	5 2 4	5 0 5	-0.124
4507.70609	0.00019	2.7×10^{-55}	0 0 0	1 0 1	4 2 2	3 2 1	-0.134
4507.85461	0.01195	3.3×10^{-57}	0 0 0	1 0 1	15 5 10	15 5 11	-0.176
4508.23312	0.00024	3.7×10^{-55}	0 0 0	1 0 1	4 1 3	3 1 2	-0.123
4509.17986	0.00046	7.5×10^{-56}	0 0 0	1 0 1	9 9 0	9 9 1	-0.243
4509.17986	0.00097	2.5×10^{-56}	0 0 0	1 0 1	9 9 1	9 9 0	-0.243
4509.45537	0.00145	1.7×10^{-56}	0 0 0	1 0 1	10 8 2	10 8 3	-0.205
4509.45537	0.00067	5.0×10^{-56}	0 0 0	1 0 1	10 8 3	10 8 2	-0.205
4509.70817	0.00012	8.2×10^{-55}	0 0 0	1 0 1	4 2 3	3 2 2	-0.136
4510.80539	0.00624	1.2×10^{-56}	0 0 0	1 0 1	10 7 3	10 7 4	-0.200
4510.80539	0.00258	3.7×10^{-56}	0 0 0	1 0 1	10 7 4	10 7 3	-0.199
4511.34174	0.00108	4.8×10^{-56}	0 0 0	1 0 1	4 2 3	4 0 4	-0.130
4511.44515	0.00230	2.4×10^{-56}	0 0 0	1 0 1	6 1 5	6 1 6	-0.125
4511.76915	0.00220	2.3×10^{-56}	0 0 0	1 0 1	8 2 6	8 2 7	-0.117
4512.90878	0.00043	9.3×10^{-56}	0 0 0	1 0 1	9 8 1	9 8 2	-0.216
4512.90878	0.00096	3.1×10^{-56}	0 0 0	1 0 1	9 8 2	9 8 1	-0.216
4513.08482	0.00012	4.2×10^{-55}	0 0 0	1 0 1	4 0 4	3 0 3	-0.129
4513.78529	0.00508	1.5×10^{-56}	0 0 0	1 0 1	10 3 7	10 3 8	-0.118
4513.89090	0.00477	9.7×10^{-57}	0 0 0	1 0 1	3 2 2	3 0 3	-0.130
4514.09215	0.00005	1.2×10^{-54}	0 0 0	1 0 1	4 1 4	3 1 3	-0.131
4514.37232	0.00321	2.4×10^{-56}	0 0 0	1 0 1	9 7 3	9 7 2	-0.202
4514.38806	0.00151	7.2×10^{-56}	0 0 0	1 0 1	9 7 2	9 7 3	-0.186
4515.84893	0.00779	7.6×10^{-57}	0 0 0	1 0 1	12 4 8	12 4 9	-0.111
4516.36651	0.00443	5.7×10^{-56}	0 0 0	1 0 1	8 8 0	8 8 1	-0.226
4516.36651	0.00153	1.7×10^{-55}	0 0 0	1 0 1	8 8 1	8 8 0	-0.226
4517.18181	0.00020	9.2×10^{-55}	0 0 0	1 0 1	3 1 2	2 1 1	-0.131
4517.20782	0.00025	5.3×10^{-55}	0 0 0	1 0 1	3 2 1	2 2 0	-0.139
4518.10570	0.00039	1.8×10^{-55}	0 0 0	1 0 1	3 2 2	2 2 1	-0.135

Position	$\sigma_{\text{Pos.}}$	Intensity	$\nu_1\,\nu_2\,\nu_3$	$\nu_1'\,\nu_2'\,\nu_3'$	J K$_a$ K$_c$	J' K$_a$' K$_c$'	$\Delta_{\text{SPEC.}}$
4518.12498	0.00122	4.7×10^{-56}	0 0 0	1 0 1	8 7 1	8 7 2	-0.212
4518.12498	0.00050	1.4×10^{-55}	0 0 0	1 0 1	8 7 2	8 7 1	-0.212
4520.17107	0.00051	9.7×10^{-56}	0 0 0	1 0 1	5 1 4	5 1 5	-0.127
4520.56253	0.00015	1.1×10^{-54}	0 0 0	1 0 1	3 0 3	2 0 2	-0.130
4520.74197	0.00041	1.1×10^{-55}	0 0 0	1 0 1	7 2 5	7 2 6	-0.123
4521.67486	0.00119	3.2×10^{-55}	0 0 0	1 0 1	3 1 3	2 1 2	-0.132
4521.67486	0.01397	1.6×10^{-56}	0 0 0	1 0 1	13 5 8	13 5 9	-0.134
4522.21236	0.00051	8.0×10^{-56}	0 0 0	1 0 1	9 3 6	9 3 7	-0.119
4522.74431	0.00122	1.2×10^{-55}	0 0 0	1 0 1	7 7 1	7 7 0	-0.207
4522.74431	0.00043	3.5×10^{-55}	0 0 0	1 0 1	7 7 0	7 7 1	-0.207
4522.89096	0.00098	4.4×10^{-56}	0 0 0	1 0 1	11 4 7	11 4 8	-0.128
4525.30150	0.00872	9.0×10^{-57}	0 0 0	1 0 1	14 6 9	14 6 8	-0.161
4525.46436	0.00342	1.1×10^{-56}	0 0 0	1 0 1	12 5 7	12 5 8	-0.142
4526.23110	0.00093	1.9×10^{-55}	0 0 0	1 0 1	2 1 1	1 1 0	-0.132
4527.38648	0.00381	3.1×10^{-56}	0 0 0	1 0 1	12 6 7	12 6 6	-0.161
4527.93617	0.00448	4.6×10^{-56}	0 0 0	1 0 1	4 1 3	4 1 4	-0.142
4528.00297	0.00495	5.7×10^{-56}	0 0 0	1 0 1	11 5 6	11 5 7	-0.149
4528.01607	0.00976	2.6×10^{-56}	0 0 0	1 0 1	10 4 6	10 4 7	-0.121
4528.35223	0.00190	2.7×10^{-55}	0 0 0	1 0 1	2 0 2	1 0 1	-0.148
4528.36002	0.00286	6.1×10^{-55}	0 0 0	1 0 1	6 6 1	6 6 0	-0.187
4528.36002	0.00830	2.0×10^{-55}	0 0 0	1 0 1	6 6 0	6 6 1	-0.187
4528.37511	0.00691	5.7×10^{-56}	0 0 0	1 0 1	6 2 4	6 2 5	-0.098
4528.62452	0.00074	5.0×10^{-56}	0 0 0	1 0 1	11 6 5	11 6 6	-0.192
4528.85274	0.00071	8.9×10^{-56}	0 0 0	1 0 1	10 6 5	10 6 4	-0.203
4528.86975	0.00128	4.6×10^{-56}	0 0 0	1 0 1	8 3 5	8 3 6	-0.128
4528.93721	0.00136	2.9×10^{-56}	0 0 0	1 0 1	10 6 4	10 6 5	-0.206
4529.10050	0.00053	3.7×10^{-55}	0 0 0	1 0 1	7 6 1	7 6 2	-0.204
4529.10050	0.00154	1.2×10^{-55}	0 0 0	1 0 1	7 6 2	7 6 1	-0.203
4529.24988	0.00012	6.0×10^{-55}	0 0 0	1 0 1	2 1 2	1 1 1	-0.134
4529.26860	0.00040	1.5×10^{-55}	0 0 0	1 0 1	9 6 3	9 6 4	-0.199
4529.34586	0.00073	2.3×10^{-55}	0 0 0	1 0 1	8 6 3	8 6 2	-0.206
4529.34586	0.00208	7.7×10^{-56}	0 0 0	1 0 1	8 6 2	8 6 3	-0.209
4529.71459	0.00113	3.3×10^{-56}	0 0 0	1 0 1	10 5 5	10 5 6	-0.157
4530.03714	0.00124	3.2×10^{-56}	0 0 0	1 0 1	12 5 8	12 5 7	-0.134
4530.18435	0.00240	1.9×10^{-56}	0 0 0	1 0 1	11 5 7	11 5 6	-0.145
4530.71198	0.00122	1.0×10^{-55}	0 0 0	1 0 1	10 5 6	10 5 5	-0.161
4530.90192	0.00024	1.6×10^{-55}	0 0 0	1 0 1	9 5 4	9 5 5	-0.163
4531.34622	0.00030	1.7×10^{-55}	0 0 0	1 0 1	8 5 4	8 5 3	-0.158
4531.42088	0.00110	5.4×10^{-56}	0 0 0	1 0 1	9 5 5	9 5 4	-0.164
4531.45750	0.00038	1.4×10^{-55}	0 0 0	1 0 1	9 4 5	9 4 6	-0.137
4531.76557	0.00087	8.8×10^{-56}	0 0 0	1 0 1	8 5 3	8 5 4	-0.156

Position	$\sigma_{\text{Pos.}}$	Intensity	$\nu_1\ \nu_2\ \nu_3$	$\nu_1'\ \nu_2'\ \nu_3'$	J K_a K_c	J' K_a' K_c'	$\Delta_{\text{SPEC.}}$
4532.36252	0.00079	1.4×10^{-55}	0 0 0	1 0 1	7 5 3	7 5 2	-0.172
4532.38112	0.00053	4.1×10^{-55}	0 0 0	1 0 1	7 5 2	7 5 3	-0.171
4532.84484	0.00897	2.1×10^{-55}	0 0 0	1 0 1	6 5 1	6 5 2	-0.175
4532.84485	0.00298	6.3×10^{-55}	0 0 0	1 0 1	6 5 2	6 5 1	-0.172
4533.18887	0.00035	9.4×10^{-55}	0 0 0	1 0 1	5 5 0	5 5 1	-0.173
4533.18887	0.00105	3.1×10^{-55}	0 0 0	1 0 1	5 5 1	5 5 0	-0.173
4533.65435	0.00226	7.6×10^{-56}	0 0 0	1 0 1	8 4 4	8 4 5	-0.163
4533.68753	0.00020	2.3×10^{-55}	0 0 0	1 0 1	7 3 4	7 3 5	-0.136
4534.32818	0.00020	2.7×10^{-55}	0 0 0	1 0 1	5 2 3	5 2 4	-0.131
4534.40853	0.00031	2.0×10^{-55}	0 0 0	1 0 1	3 1 2	3 1 3	-0.132
4535.08867	0.00150	3.6×10^{-55}	0 0 0	1 0 1	7 4 3	7 4 4	-0.148
4535.45667	0.00020	2.3×10^{-55}	0 0 0	1 0 1	8 4 5	8 4 4	-0.143
4535.72254	0.00183	1.2×10^{-55}	0 0 0	1 0 1	7 4 4	7 4 3	-0.150
4535.99068	0.00128	4.2×10^{-56}	0 0 0	1 0 1	9 4 6	9 4 5	-0.137
4536.02929	0.00026	1.8×10^{-55}	0 0 0	1 0 1	6 4 2	6 4 3	-0.153
4536.21121	0.00008	5.5×10^{-55}	0 0 0	1 0 1	6 4 3	6 4 2	-0.153
4536.46636	0.00009	4.4×10^{-55}	0 0 0	1 0 1	1 0 1	0 0 0	-0.132
4536.70274	0.00006	8.3×10^{-55}	0 0 0	1 0 1	5 4 1	5 4 2	-0.157
4536.74064	0.00017	2.8×10^{-55}	0 0 0	1 0 1	5 4 2	5 4 1	-0.156
4536.84130	0.00043	1.3×10^{-55}	0 0 0	1 0 1	6 3 3	6 3 4	-0.138
4537.04254	0.00067	7.8×10^{-56}	0 0 0	1 0 1	10 4 7	10 4 6	-0.125
4537.21701	0.00039	1.2×10^{-54}	0 0 0	1 0 1	4 4 1	4 4 0	-0.160
4537.21701	0.00117	4.1×10^{-55}	0 0 0	1 0 1	4 4 0	4 4 1	-0.156
4538.57703	0.00039	1.5×10^{-55}	0 0 0	1 0 1	4 2 2	4 2 3	-0.134
4538.71596	0.00014	5.8×10^{-55}	0 0 0	1 0 1	5 3 2	5 3 3	-0.142
4539.33217	0.00043	1.1×10^{-55}	0 0 0	1 0 1	2 1 1	2 1 2	-0.134
4539.53188	0.00337	1.4×10^{-56}	0 0 0	1 0 1	11 4 8	11 4 7	-0.117
4539.60840	0.00855	4.6×10^{-57}	0 0 0	1 0 1	5 0 5	4 2 2	-0.131
4539.77231	0.00044	3.0×10^{-55}	0 0 0	1 0 1	4 3 1	4 3 2	-0.145
4540.03682	0.00025	1.9×10^{-55}	0 0 0	1 0 1	5 3 3	5 3 2	-0.142
4540.11522	0.00005	8.9×10^{-55}	0 0 0	1 0 1	4 3 2	4 3 1	-0.145
4540.37808	0.00004	1.4×10^{-54}	0 0 0	1 0 1	3 3 0	3 3 1	-0.148
4540.42826	0.00012	4.5×10^{-55}	0 0 0	1 0 1	3 3 1	3 3 0	-0.148
4540.55927	0.00013	3.7×10^{-55}	0 0 0	1 0 1	6 3 4	6 3 3	-0.137
4541.17953	0.00031	7.0×10^{-55}	0 0 0	1 0 1	3 2 1	3 2 2	-0.138
4542.11620	0.00063	7.7×10^{-56}	0 0 0	1 0 1	7 3 5	7 3 4	-0.131
4542.47805	0.00012	3.8×10^{-55}	0 0 0	1 0 1	2 2 0	2 2 1	-0.140
4542.62912	0.00007	6.3×10^{-55}	0 0 0	1 0 1	1 1 0	1 1 1	-0.135
4542.81644	0.01057	7.7×10^{-57}	0 0 0	1 0 1	3 2 1	4 0 4	-0.129
4542.96593	0.00004	1.2×10^{-54}	0 0 0	1 0 1	2 2 1	2 2 0	-0.140
4543.47745	0.00205	2.2×10^{-56}	0 0 0	1 0 1	12 4 9	12 4 8	-0.103

Position	$\sigma_{\text{Pos.}}$	Intensity	$\nu_1\ \nu_2\ \nu_3$	ν_1' ν_2' ν_3'	J K_a K_c	J' K_a' K_c'	$\Delta_{\text{SPEC.}}$
4543.53518	0.00021	2.3×10^{-55}	0 0 0	1 0 1	3 2 2	3 2 1	-0.138
4543.64932	0.00882	4.7×10^{-57}	0 0 0	1 0 1	5 2 3	6 0 6	-0.136
4545.03359	0.00045	1.4×10^{-55}	0 0 0	1 0 1	8 3 6	8 3 5	-0.124
4545.16626	0.00011	4.4×10^{-55}	0 0 0	1 0 1	4 2 3	4 2 2	-0.135
4545.22602	0.00173	2.8×10^{-56}	0 0 0	1 0 1	9 3 6	10 1 9	-0.119
4545.66086	0.00022	2.1×10^{-55}	0 0 0	1 0 1	1 1 1	1 1 0	-0.135
4548.15936	0.00076	9.2×10^{-56}	0 0 0	1 0 1	5 2 4	5 2 3	-0.130
4548.42263	0.00014	3.3×10^{-55}	0 0 0	1 0 1	2 1 2	2 1 1	-0.134
4548.78832	0.01025	3.7×10^{-57}	0 0 0	1 0 1	13 4 10	13 4 9	-0.077
4549.39730	0.00168	2.6×10^{-56}	0 0 0	1 0 1	9 3 7	9 3 6	-0.115
4551.96598	0.00955	9.2×10^{-57}	0 0 0	1 0 1	9 4 5	10 2 8	-0.124
4552.51982	0.00068	7.0×10^{-56}	0 0 0	1 0 1	3 1 3	3 1 2	-0.135
4552.54492	0.00026	1.7×10^{-55}	0 0 0	1 0 1	6 2 5	6 2 4	-0.126
4552.73644	0.00033	1.5×10^{-55}	0 0 0	1 0 1	0 0 0	1 0 1	-0.134
4555.05002	0.00100	4.5×10^{-56}	0 0 0	1 0 1	10 3 8	10 3 7	-0.107
4555.10528	0.00924	5.4×10^{-57}	0 0 0	1 0 1	14 4 11	14 4 10	-0.082
4556.08491	0.01331	3.0×10^{-57}	0 0 0	1 0 1	10 4 6	11 2 9	-0.123
4556.69385	0.06148	6.2×10^{-57}	0 0 0	1 0 1	11 4 7	12 2 10	-0.097
4557.84938	0.00033	1.5×10^{-55}	0 0 0	1 0 1	4 1 4	4 1 3	-0.130
4558.17146	0.00618	3.7×10^{-56}	0 0 0	1 0 1	7 2 6	7 2 5	-0.111
4558.76257	0.00022	2.1×10^{-55}	0 0 0	1 0 1	1 1 1	2 1 2	-0.136
4560.41487	0.00011	8.4×10^{-55}	0 0 0	1 0 1	1 0 1	2 0 2	-0.133
4561.66911	0.00506	8.5×10^{-57}	0 0 0	1 0 1	11 3 9	11 3 8	-0.099
4561.80240	0.00007	6.1×10^{-55}	0 0 0	1 0 1	1 1 0	2 1 1	-0.134
4564.16376	0.00403	3.5×10^{-56}	0 0 0	1 0 1	5 1 5	5 1 4	-0.127
4564.69934	0.00062	7.2×10^{-56}	0 0 0	1 0 1	8 2 7	8 2 6	-0.116
4565.64887	0.00005	1.0×10^{-54}	0 0 0	1 0 1	2 1 2	3 1 3	-0.135
4566.93666	0.00011	5.6×10^{-55}	0 0 0	1 0 1	2 2 1	3 2 2	-0.140
4567.47880	0.00012	3.8×10^{-55}	0 0 0	1 0 1	2 0 2	3 0 3	-0.132
4567.91167	0.00316	1.9×10^{-55}	0 0 0	1 0 1	2 2 0	3 2 1	-0.139
4568.79765	0.00276	1.4×10^{-56}	0 0 0	1 0 1	12 3 10	12 3 9	-0.091
4570.18140	0.00039	3.3×10^{-55}	0 0 0	1 0 1	2 1 1	3 1 2	-0.133
4571.08192	0.00060	8.0×10^{-56}	0 0 0	1 0 1	6 1 6	6 1 5	-0.126
4571.70668	0.00267	1.6×10^{-56}	0 0 0	1 0 1	9 2 8	9 2 7	-0.112
4572.22403	0.00288	3.0×10^{-56}	0 0 0	1 0 1	3 0 3	3 2 2	-0.140
4572.24325	0.00012	4.2×10^{-55}	0 0 0	1 0 1	3 1 3	4 1 4	-0.134
4573.17213	0.00034	1.4×10^{-55}	0 0 0	1 0 1	3 3 1	4 3 2	-0.149
4573.33031	0.00011	4.2×10^{-55}	0 0 0	1 0 1	3 3 0	4 3 1	-0.148
4573.59997	0.00264	1.7×10^{-56}	0 0 0	1 0 1	4 0 4	4 2 3	-0.137
4573.86073	0.00003	1.3×10^{-54}	0 0 0	1 0 1	3 0 3	4 0 4	-0.131
4574.40599	0.00016	2.9×10^{-55}	0 0 0	1 0 1	3 2 2	4 2 3	-0.138

Position	$\sigma_{\text{Pos.}}$	Intensity	$\nu_1\ \nu_2\ \nu_3$	$\nu_1'\ \nu_2'\ \nu_3'$	J K_a K_c	J' K_a' K_c'	$\Delta_{\text{SPEC.}}$
4575.99823	0.00077	6.2×10^{-56}	0 0 0	1 0 1	5 0 5	5 2 4	-0.133
4576.63843	0.00009	8.7×10^{-55}	0 0 0	1 0 1	3 2 1	4 2 2	-0.136
4578.16588	0.00010	1.2×10^{-54}	0 0 0	1 0 1	3 1 2	4 1 3	-0.130
4578.16588	0.00293	2.0×10^{-56}	0 0 0	1 0 1	7 1 7	7 1 6	-0.127
4578.30313	0.00018	2.7×10^{-55}	0 0 0	1 0 1	4 4 1	5 4 2	-0.160
4578.31839	0.00055	9.1×10^{-56}	0 0 0	1 0 1	4 4 0	5 4 1	-0.163
4578.54078	0.00005	1.4×10^{-54}	0 0 0	1 0 1	4 1 4	5 1 5	-0.132
4578.64523	0.00275	3.1×10^{-56}	0 0 0	1 0 1	10 2 9	10 2 8	-0.108
4579.38922	0.00571	2.1×10^{-56}	0 0 0	1 0 1	6 0 6	6 2 5	-0.087
4579.72589	0.00010	4.7×10^{-55}	0 0 0	1 0 1	4 0 4	5 0 5	-0.131
4580.94239	0.00007	6.5×10^{-55}	0 0 0	1 0 1	4 3 2	5 3 3	-0.146
4581.47826	0.00037	2.2×10^{-55}	0 0 0	1 0 1	4 3 1	5 3 2	-0.144
4581.55723	0.00005	1.0×10^{-54}	0 0 0	1 0 1	4 2 3	5 2 4	-0.136
4582.74888	0.00099	1.5×10^{-55}	0 0 0	1 0 1	5 5 0	6 5 1	-0.178
4582.75757	0.00335	4.9×10^{-56}	0 0 0	1 0 1	5 5 1	6 5 2	-0.174
4583.42630	0.00078	5.4×10^{-56}	0 0 0	1 0 1	7 0 7	7 2 6	-0.130
4584.56276	0.00010	4.6×10^{-55}	0 0 0	1 0 1	5 1 5	6 1 6	-0.131
4584.74446	0.00061	6.5×10^{-56}	0 0 0	1 0 1	7 7 0	8 7 1	-0.220
4584.74446	0.00137	2.2×10^{-56}	0 0 0	1 0 1	7 7 1	8 7 2	-0.220
4585.12909	0.00110	4.4×10^{-56}	0 0 0	1 0 1	8 1 8	8 1 7	-0.128
4585.32799	0.00004	1.4×10^{-54}	0 0 0	1 0 1	5 0 5	6 0 6	-0.130
4585.40088	0.00058	3.4×10^{-55}	0 0 0	1 0 1	4 2 2	5 2 3	-0.132
4585.58626	0.00225	3.3×10^{-56}	0 0 0	1 0 1	7 1 6	7 3 5	-0.119
4585.61132	0.00011	4.2×10^{-55}	0 0 0	1 0 1	4 1 3	5 1 4	-0.128
4585.76692	0.00534	1.2×10^{-56}	0 0 0	1 0 1	8 1 7	8 3 6	-0.116
4586.12180	0.00039	1.3×10^{-55}	0 0 0	1 0 1	5 4 2	6 4 3	-0.157
4586.20209	0.00022	4.0×10^{-55}	0 0 0	1 0 1	5 4 1	6 4 2	-0.157
4586.60182	0.00552	8.6×10^{-57}	0 0 0	1 0 1	6 1 5	6 3 4	-0.137
4587.18726	0.00109	3.2×10^{-56}	0 0 0	1 0 1	9 1 8	9 3 7	-0.126
4587.35021	0.00457	1.5×10^{-56}	0 0 0	1 0 1	6 6 0	7 6 1	-0.209
4587.35021	0.00162	4.6×10^{-56}	0 0 0	1 0 1	6 6 1	7 6 2	-0.209
4587.93261	0.00257	2.6×10^{-56}	0 0 0	1 0 1	8 8 1	9 8 2	-0.221
4587.93261	0.00580	8.6×10^{-57}	0 0 0	1 0 1	8 8 0	9 8 1	-0.221
4588.00410	0.00269	1.5×10^{-56}	0 0 0	1 0 1	8 0 8	8 2 7	-0.126
4588.34836	0.00052	3.5×10^{-55}	0 0 0	1 0 1	5 2 4	6 2 5	-0.138
4588.52554	0.00022	2.4×10^{-55}	0 0 0	1 0 1	5 3 3	6 3 4	-0.142
4588.56877	0.00370	1.6×10^{-56}	0 0 0	1 0 1	5 1 4	5 3 3	-0.118
4589.05040	0.00345	9.3×10^{-57}	0 0 0	1 0 1	9 9 0	10 9 1	-0.231
4589.34065	0.00125	2.5×10^{-56}	0 0 0	1 0 1	8 7 1	9 7 2	-0.212
4589.34065	0.00053	7.4×10^{-56}	0 0 0	1 0 1	8 7 2	9 7 3	-0.212
4589.85187	0.00006	7.3×10^{-55}	0 0 0	1 0 1	5 3 2	6 3 3	-0.140

Position	$\sigma_{\text{Pos.}}$	Intensity	$\nu_1\ \nu_2\ \nu_3$	$\nu_1'\ \nu_2'\ \nu_3'$	J K_a K_c	J' K_a' K_c'	$\Delta_{\text{SPEC.}}$
4590.34713	0.00004	1.3×10^{-54}	0 0 0	1 0 1	6 1 6	7 1 7	-0.129
4590.67548	0.00070	6.8×10^{-56}	0 0 0	1 0 1	6 5 1	7 5 2	-0.173
4590.69978	0.00020	2.1×10^{-55}	0 0 0	1 0 1	6 5 2	7 5 3	-0.177
4590.83049	0.00010	4.3×10^{-55}	0 0 0	1 0 1	6 0 6	7 0 7	-0.129
4590.89334	0.00366	1.2×10^{-56}	0 0 0	1 0 1	12 2 11	12 2 10	-0.103
4592.14847	0.00439	9.4×10^{-57}	0 0 0	1 0 1	9 1 9	9 1 8	-0.139
4592.37733	0.00010	1.2×10^{-54}	0 0 0	1 0 1	5 1 4	6 1 5	-0.126
4592.79170	0.00385	3.2×10^{-56}	0 0 0	1 0 1	9 8 1	10 8 2	-0.223
4592.79170	0.02992	3.3×10^{-57}	0 0 0	1 0 1	11 10 1	12 10 2	-0.231
4592.81550	0.02571	1.1×10^{-56}	0 0 0	1 0 1	9 8 2	10 8 3	-0.199
4592.87978	0.00154	3.3×10^{-56}	0 0 0	1 0 1	9 0 9	9 2 8	-0.122
4592.98948	0.00235	1.8×10^{-56}	0 0 0	1 0 1	11 1 10	11 3 9	-0.118
4593.73260	0.00573	3.7×10^{-57}	0 0 0	1 0 1	10 9 1	11 9 2	-0.224
4593.73260	0.00296	1.1×10^{-56}	0 0 0	1 0 1	10 9 2	11 9 3	-0.224
4593.86284	0.00018	1.0×10^{-54}	0 0 0	1 0 1	5 2 3	6 2 4	-0.137
4593.87265	0.00042	4.4×10^{-55}	0 0 0	1 0 1	6 4 3	7 4 4	-0.128
4594.09988	0.00068	1.5×10^{-55}	0 0 0	1 0 1	6 4 2	7 4 3	-0.156
4594.13731	0.00220	6.5×10^{-56}	0 0 0	1 0 1	9 7 2	10 7 3	-0.203
4594.13731	0.00616	2.2×10^{-56}	0 0 0	1 0 1	9 7 3	10 7 4	-0.204
4594.27423	0.00540	5.2×10^{-57}	0 0 0	1 0 1	13 2 11	13 4 10	-0.113
4594.77212	0.00012	9.9×10^{-55}	0 0 0	1 0 1	6 2 5	7 2 6	-0.131
4595.84619	0.00006	7.2×10^{-55}	0 0 0	1 0 1	6 3 4	7 3 5	-0.139
4595.94177	0.00012	3.8×10^{-55}	0 0 0	1 0 1	7 1 7	8 1 8	-0.128
4595.97261	0.00080	6.4×10^{-56}	0 0 0	1 0 1	7 6 1	8 6 2	-0.211
4595.97261	0.00196	2.1×10^{-56}	0 0 0	1 0 1	7 6 2	8 6 3	-0.216
4596.33773	0.00029	1.1×10^{-54}	0 0 0	1 0 1	7 0 7	8 0 8	-0.129
4597.10572	0.00937	7.1×10^{-57}	0 0 0	1 0 1	2 0 2	3 2 1	-0.157
4597.63869	0.00102	2.8×10^{-56}	0 0 0	1 0 1	10 8 3	11 8 4	-0.204
4597.64995	0.00325	9.4×10^{-57}	0 0 0	1 0 1	10 8 2	11 8 3	-0.192
4598.08485	0.00028	1.4×10^{-55}	0 0 0	1 0 1	7 5 2	8 5 3	-0.165
4598.42199	0.00030	3.5×10^{-55}	0 0 0	1 0 1	6 1 5	7 1 6	-0.125
4598.47368	0.00020	2.4×10^{-55}	0 0 0	1 0 1	6 3 3	7 3 4	-0.134
4598.54110	0.00054	7.2×10^{-56}	0 0 0	1 0 1	7 5 3	8 5 4	-0.174
4598.99224	0.00086	5.1×10^{-56}	0 0 0	1 0 1	10 7 4	11 7 5	-0.191
4598.99224	0.00223	1.7×10^{-56}	0 0 0	1 0 1	10 7 3	11 7 4	-0.186
4599.97958	0.00511	9.9×10^{-57}	0 0 0	1 0 1	9 2 7	9 4 6	-0.130
4600.52138	0.01357	4.8×10^{-57}	0 0 0	1 0 1	11 1 11	11 1 10	-0.120
4600.82035	0.00015	2.9×10^{-55}	0 0 0	1 0 1	7 2 6	8 2 7	-0.129
4601.43864	0.00017	9.5×10^{-55}	0 0 0	1 0 1	8 1 8	9 1 9	-0.129
4601.44581	0.00132	1.4×10^{-55}	0 0 0	1 0 1	7 4 4	8 4 5	-0.134
4601.79871	0.00027	3.2×10^{-55}	0 0 0	1 0 1	6 2 4	7 2 5	-0.123

Position	$\sigma_{\text{Pos.}}$	Intensity	$\nu_1\,\nu_2\,\nu_3$	$\nu_1'\,\nu_2'\,\nu_3'$	J K_a K_c	J' K_a' K_c'	$\Delta_{\text{SPEC.}}$
4602.07612	0.00026	4.1×10^{-55}	0 0 0	1 0 1	7 4 3	8 4 4	-0.148
4602.43245	0.00429	7.3×10^{-57}	0 0 0	1 0 1	11 8 4	12 8 5	-0.188
4602.43245	0.00190	2.2×10^{-56}	0 0 0	1 0 1	11 8 3	12 8 4	-0.187
4602.68381	0.00025	2.1×10^{-55}	0 0 0	1 0 1	8 0 8	9 0 9	-0.138
4602.83441	0.00025	2.1×10^{-55}	0 0 0	1 0 1	7 3 5	8 3 6	-0.135
4602.96152	0.00355	7.4×10^{-57}	0 0 0	1 0 1	12 9 4	13 9 5	-0.193
4603.21533	0.00258	1.6×10^{-56}	0 0 0	1 0 1	11 0 11	11 2 10	-0.121
4603.83490	0.00132	3.7×10^{-56}	0 0 0	1 0 1	11 7 4	12 7 5	-0.173
4603.83491	0.00331	1.2×10^{-56}	0 0 0	1 0 1	11 7 5	12 7 6	-0.192
4603.94560	0.00005	8.6×10^{-55}	0 0 0	1 0 1	7 1 6	8 1 7	-0.127
4604.28707	0.00257	6.6×10^{-56}	0 0 0	1 0 1	8 6 3	9 6 4	-0.214
4604.28707	0.00736	2.2×10^{-56}	0 0 0	1 0 1	8 6 2	9 6 3	-0.190
4605.93439	0.00006	7.6×10^{-55}	0 0 0	1 0 1	9 0 9	10 0 10	-0.122
4606.06382	0.00370	1.0×10^{-56}	0 0 0	1 0 1	12 1 12	12 1 11	-0.111
4606.24811	0.00035	1.9×10^{-55}	0 0 0	1 0 1	8 5 4	9 5 5	-0.170
4606.53499	0.00006	7.1×10^{-55}	0 0 0	1 0 1	8 2 7	9 2 8	-0.126
4606.59871	0.00066	6.3×10^{-56}	0 0 0	1 0 1	8 5 3	9 5 4	-0.170
4607.17230	0.00025	6.4×10^{-55}	0 0 0	1 0 1	7 3 4	8 3 5	-0.127
4607.68544	0.00116	3.2×10^{-56}	0 0 0	1 0 1	3 0 3	4 2 2	-0.135
4608.14276	0.00027	1.5×10^{-55}	0 0 0	1 0 1	9 1 9	10 1 10	-0.134
4608.63885	0.00422	8.3×10^{-57}	0 0 0	1 0 1	12 7 5	13 7 6	-0.162
4608.69078	0.01275	6.0×10^{-57}	0 0 0	1 0 1	7 2 5	7 4 4	-0.115
4608.70254	0.00228	2.5×10^{-56}	0 0 0	1 0 1	12 7 6	13 7 7	-0.164
4608.80755	0.00015	3.5×10^{-55}	0 0 0	1 0 1	8 4 5	9 4 6	-0.144
4608.99230	0.00011	8.1×10^{-55}	0 0 0	1 0 1	7 2 5	8 2 6	-0.117
4609.43583	0.00008	5.3×10^{-55}	0 0 0	1 0 1	8 3 6	9 3 7	-0.130
4609.56478	0.00026	1.9×10^{-55}	0 0 0	1 0 1	8 1 7	9 1 8	-0.134
4610.20247	0.00013	3.8×10^{-55}	0 0 0	1 0 1	9 1 8	10 1 9	-0.123
4610.38428	0.02613	6.2×10^{-57}	0 0 0	1 0 1	13 0 13	13 2 12	-0.140
4610.46855	0.00181	1.1×10^{-55}	0 0 0	1 0 1	8 4 4	9 4 5	-0.147
4611.01811	0.00017	6.0×10^{-55}	0 0 0	1 0 1	10 1 10	11 1 11	-0.118
4611.16642	0.00018	2.0×10^{-55}	0 0 0	1 0 1	10 0 10	11 0 11	-0.120
4611.84167	0.00585	1.0×10^{-56}	0 0 0	1 0 1	13 8 5	14 8 6	-0.156
4611.99661	0.00023	1.9×10^{-55}	0 0 0	1 0 1	9 2 8	10 2 9	-0.123
4612.29162	0.00059	5.8×10^{-56}	0 0 0	1 0 1	9 6 3	10 6 4	-0.208
4612.39926	0.00161	1.9×10^{-56}	0 0 0	1 0 1	9 6 4	10 6 5	-0.208
4613.38106	0.00832	1.6×10^{-56}	0 0 0	1 0 1	13 7 6	14 7 7	-0.161
4613.61771	0.00584	5.2×10^{-57}	0 0 0	1 0 1	13 7 7	14 7 8	-0.155
4613.78440	0.00070	5.3×10^{-56}	0 0 0	1 0 1	9 5 5	10 5 6	-0.164
4614.28671	0.00023	1.6×10^{-55}	0 0 0	1 0 1	9 5 4	10 5 5	-0.164
4615.27277	0.00019	2.1×10^{-55}	0 0 0	1 0 1	8 2 6	9 2 7	-0.111

Position	$\sigma_{\text{Pos.}}$	Intensity	$\nu_1\,\nu_2\,\nu_3$	$\nu_1'\,\nu_2'\,\nu_3'$	J K_a K_c	J' K_a' K_c'	$\Delta_{\text{SPEC.}}$
4615.61734	0.00291	1.8×10^{-55}	0 0 0	1 0 1	8 3 5	9 3 6	-0.117
4615.90079	0.00041	9.3×10^{-56}	0 0 0	1 0 1	9 4 6	10 4 7	-0.138
4615.96144	0.00030	1.3×10^{-55}	0 0 0	1 0 1	10 1 9	11 1 10	-0.114
4616.06000	0.00029	1.5×10^{-55}	0 0 0	1 0 1	11 1 11	12 1 12	-0.117
4616.10134	0.00009	4.5×10^{-55}	0 0 0	1 0 1	11 0 11	12 0 12	-0.117
4616.44998	0.00738	6.3×10^{-57}	0 0 0	1 0 1	14 8 7	15 8 8	-0.175
4617.41052	0.00089	4.0×10^{-55}	0 0 0	1 0 1	10 2 9	11 2 10	-0.122
4618.09416	0.00958	3.2×10^{-57}	0 0 0	1 0 1	14 7 7	15 7 8	-0.129
4618.64812	0.00013	2.8×10^{-55}	0 0 0	1 0 1	9 4 5	10 4 6	-0.131
4620.07637	0.00195	1.6×10^{-56}	0 0 0	1 0 1	10 6 4	11 6 5	-0.202
4620.49723	0.00009	4.7×10^{-55}	0 0 0	1 0 1	9 2 7	10 2 8	-0.108
4620.55630	0.00280	4.5×10^{-56}	0 0 0	1 0 1	10 6 5	11 6 6	-0.200
4620.84077	0.00057	3.2×10^{-55}	0 0 0	1 0 1	12 1 12	13 1 13	-0.111
4620.84077	0.00168	1.1×10^{-55}	0 0 0	1 0 1	12 0 12	13 0 13	-0.127
4620.89306	0.00014	3.0×10^{-55}	0 0 0	1 0 1	11 1 10	12 1 11	-0.111
4621.01326	0.01052	3.7×10^{-57}	0 0 0	1 0 1	15 8 7	16 8 8	-0.118
4621.09239	0.00046	1.2×10^{-55}	0 0 0	1 0 1	10 5 6	11 5 7	-0.158
4621.38048	0.00016	3.0×10^{-55}	0 0 0	1 0 1	10 3 8	11 3 9	-0.121
4621.99226	0.00123	4.1×10^{-56}	0 0 0	1 0 1	10 5 5	11 5 6	-0.153
4622.62580	0.00018	2.1×10^{-55}	0 0 0	1 0 1	10 4 7	11 4 8	-0.132
4623.47009	0.00051	4.1×10^{-55}	0 0 0	1 0 1	9 3 6	10 3 7	-0.109
4624.07921	0.00059	6.8×10^{-56}	0 0 0	1 0 1	11 2 10	12 2 11	-0.124
4624.44830	0.00052	2.0×10^{-55}	0 0 0	1 0 1	12 2 11	13 2 12	-0.103
4624.73750	0.00445	1.1×10^{-55}	0 0 0	1 0 1	10 2 8	11 2 9	-0.108
4625.44164	0.00309	7.3×10^{-56}	0 0 0	1 0 1	13 1 13	14 1 14	-0.106
4625.44164	0.00105	2.2×10^{-55}	0 0 0	1 0 1	13 0 13	14 0 14	-0.113
4625.51783	0.00049	7.1×10^{-56}	0 0 0	1 0 1	12 1 11	13 1 12	-0.108
4626.40558	0.00424	9.1×10^{-57}	0 0 0	1 0 1	3 1 2	4 3 1	-0.146
4626.70883	0.00053	6.8×10^{-56}	0 0 0	1 0 1	11 3 9	12 3 10	-0.117
4627.06426	0.00544	7.1×10^{-56}	0 0 0	1 0 1	10 4 6	11 4 7	-0.120
4627.63685	0.00175	3.6×10^{-56}	0 0 0	1 0 1	11 6 5	12 6 6	-0.194
4628.10067	0.00185	2.8×10^{-56}	0 0 0	1 0 1	11 5 7	12 5 8	-0.150
4628.33280	0.00018	2.2×10^{-55}	0 0 0	1 0 1	11 2 9	12 2 10	-0.101
4628.89930	0.00076	4.8×10^{-56}	0 0 0	1 0 1	11 4 8	12 4 9	-0.126
4629.59535	0.00244	4.7×10^{-56}	0 0 0	1 0 1	13 2 12	14 2 13	-0.109
4629.62283	0.03045	8.3×10^{-57}	0 0 0	1 0 1	11 6 6	12 6 7	-0.174
4629.72942	0.00040	8.9×10^{-56}	0 0 0	1 0 1	11 5 6	12 5 7	-0.143
4629.87793	0.00038	1.4×10^{-55}	0 0 0	1 0 1	14 1 14	15 1 15	-0.107
4629.87793	0.00105	4.8×10^{-56}	0 0 0	1 0 1	14 0 14	15 0 15	-0.109
4629.95198	0.00023	1.4×10^{-55}	0 0 0	1 0 1	13 1 12	14 1 13	-0.105
4630.48958	0.00037	9.7×10^{-56}	0 0 0	1 0 1	10 3 7	11 3 8	-0.101

Position	$\sigma_{\text{Pos.}}$	Intensity	$\nu_1\,\nu_2\,\nu_3$	$\nu_1'\,\nu_2'\,\nu_3'$	J K_a K_c	J' K_a' K_c'	$\Delta_{\text{SPEC.}}$
4630.65390	0.00040	8.4×10^{-56}	0 0 0	1 0 1	12 3 10	13 3 11	-0.122
4631.29925	0.00101	4.5×10^{-56}	0 0 0	1 0 1	12 2 10	13 2 11	-0.098
4632.21975	0.00214	1.4×10^{-56}	0 0 0	1 0 1	12 6 7	13 6 8	-0.164
4632.67974	0.00651	5.9×10^{-57}	0 0 0	1 0 1	4 1 3	5 3 2	-0.142
4634.07654	0.00033	9.1×10^{-56}	0 0 0	1 0 1	14 2 13	15 2 14	-0.101
4634.15019	0.00242	3.1×10^{-56}	0 0 0	1 0 1	15 1 15	16 1 16	-0.103
4634.15020	0.00084	9.2×10^{-56}	0 0 0	1 0 1	15 0 15	16 0 16	-0.105
4634.22094	0.00471	3.0×10^{-56}	0 0 0	1 0 1	14 1 13	15 1 14	-0.105
4634.59259	0.00038	9.2×10^{-56}	0 0 0	1 0 1	12 4 9	13 4 10	-0.117
4634.69615	0.00063	5.6×10^{-56}	0 0 0	1 0 1	12 5 8	13 5 9	-0.140
4634.98995	0.00451	8.5×10^{-57}	0 0 0	1 0 1	12 6 6	13 6 7	-0.180
4635.01100	0.00079	4.4×10^{-56}	0 0 0	1 0 1	14 3 12	15 3 13	-0.077
4635.29105	0.00025	1.5×10^{-55}	0 0 0	1 0 1	11 4 7	12 4 8	-0.105
4635.54375	0.00175	2.3×10^{-56}	0 0 0	1 0 1	5 0 5	6 2 4	-0.129
4636.48340	0.00020	2.0×10^{-55}	0 0 0	1 0 1	11 3 8	12 3 9	-0.092
4636.65112	0.00061	8.8×10^{-56}	0 0 0	1 0 1	13 2 11	14 2 12	-0.106
4637.51705	0.00161	2.0×10^{-56}	0 0 0	1 0 1	12 5 7	13 5 8	-0.129
4638.28015	0.00143	5.6×10^{-56}	0 0 0	1 0 1	16 1 16	17 1 17	-0.101
4638.28015	0.00411	1.9×10^{-56}	0 0 0	1 0 1	16 0 16	17 0 17	-0.102
4638.30752	0.00222	1.8×10^{-56}	0 0 0	1 0 1	15 2 14	16 2 15	-0.099
4638.34591	0.00071	5.6×10^{-56}	0 0 0	1 0 1	15 1 14	16 1 15	-0.096
4638.82463	0.00787	3.3×10^{-57}	0 0 0	1 0 1	13 6 8	14 6 9	-0.164
4639.14834	0.00214	1.6×10^{-56}	0 0 0	1 0 1	13 4 10	14 4 11	-0.110
4639.25660	0.00154	2.3×10^{-56}	0 0 0	1 0 1	13 3 11	14 3 12	-0.121
4639.68528	0.00208	2.7×10^{-56}	0 0 0	1 0 1	5 1 4	6 3 3	-0.136
4639.81296	0.00174	2.0×10^{-56}	0 0 0	1 0 1	14 2 12	15 2 13	-0.094
4640.67832	0.00341	1.1×10^{-56}	0 0 0	1 0 1	13 5 9	14 5 10	-0.130
4641.27906	0.00095	4.1×10^{-56}	0 0 0	1 0 1	12 3 9	13 3 10	-0.085
4641.60698	0.00286	1.2×10^{-56}	0 0 0	1 0 1	15 3 13	16 3 14	-0.083
4642.13815	0.00177	1.7×10^{-56}	0 0 0	1 0 1	13 6 7	14 6 8	-0.171
4642.25635	0.00082	3.4×10^{-56}	0 0 0	1 0 1	16 2 15	17 2 16	-0.091
4642.25635	0.00082	3.3×10^{-56}	0 0 0	1 0 1	17 0 17	18 0 18	-0.096
4642.25635	0.00242	1.1×10^{-56}	0 0 0	1 0 1	17 1 17	18 1 18	-0.096
4642.25635	0.00241	1.1×10^{-56}	0 0 0	1 0 1	16 1 15	17 1 16	-0.111
4642.95569	0.00113	3.3×10^{-56}	0 0 0	1 0 1	12 4 8	13 4 9	-0.092
4643.37419	0.00129	3.6×10^{-56}	0 0 0	1 0 1	15 2 13	16 2 14	-0.089
4644.43791	0.00959	5.4×10^{-57}	0 0 0	1 0 1	14 6 9	15 6 10	-0.126
4644.70766	0.00051	7.3×10^{-56}	0 0 0	1 0 1	13 3 10	14 3 11	-0.080
4645.32346	0.00084	4.0×10^{-56}	0 0 0	1 0 1	13 5 8	14 5 9	-0.112
4645.52823	0.00192	1.7×10^{-56}	0 0 0	1 0 1	14 5 10	15 5 11	-0.120
4645.94500	0.00320	1.1×10^{-56}	0 0 0	1 0 1	14 3 11	15 3 12	-0.085

Position	$\sigma_{\text{Pos.}}$	Intensity	$\nu_1\ \nu_2\ \nu_3$	$\nu_1'\ \nu_2'\ \nu_3'$	J K_a K_c	J' K_a' K_c'	$\Delta_{\text{SPEC.}}$
4646.08112	0.00422	6.3×10^{-57}	0 0 0	1 0 1	18 0 18	19 0 19	-0.088
4646.08112	0.00416	6.4×10^{-57}	0 0 0	1 0 1	17 2 16	18 2 17	-0.079
4646.08112	0.00151	1.9×10^{-56}	0 0 0	1 0 1	17 1 16	18 1 17	-0.096
4646.08112	0.00154	1.9×10^{-56}	0 0 0	1 0 1	18 1 18	19 1 19	-0.088
4646.08112	0.00140	2.1×10^{-56}	0 0 0	1 0 1	16 3 14	17 3 15	-0.089
4646.90249	0.00508	6.8×10^{-57}	0 0 0	1 0 1	4 1 4	5 3 3	-0.160
4646.96089	0.00498	7.0×10^{-57}	0 0 0	1 0 1	16 2 14	17 2 15	-0.085
4648.23021	0.00328	1.0×10^{-56}	0 0 0	1 0 1	6 1 5	7 3 4	-0.137
4649.67423	0.04223	3.5×10^{-57}	0 0 0	1 0 1	19 1 19	20 1 20	-0.158
4649.67423	0.01853	1.1×10^{-56}	0 0 0	1 0 1	19 0 19	20 0 20	-0.158
4649.67423	0.04427	3.6×10^{-57}	0 0 0	1 0 1	18 1 17	19 1 18	-0.146
4649.68586	0.00526	1.1×10^{-56}	0 0 0	1 0 1	18 2 17	19 2 18	-0.125
4649.73298	0.01566	2.7×10^{-56}	0 0 0	1 0 1	14 4 11	15 4 12	-0.080
4649.73298	0.00679	6.2×10^{-56}	0 0 0	1 0 1	13 4 9	14 4 10	-0.076
4650.04323	0.00845	3.9×10^{-57}	0 0 0	1 0 1	17 3 15	18 3 16	-0.081
4650.66170	0.00318	1.1×10^{-56}	0 0 0	1 0 1	17 2 15	18 2 16	-0.042
4652.79933	0.00635	5.0×10^{-57}	0 0 0	1 0 1	6 0 6	7 2 5	-0.125
4653.26902	0.01522	5.6×10^{-57}	0 0 0	1 0 1	20 1 20	21 1 21	-0.073
4653.46376	0.00168	2.2×10^{-56}	0 0 0	1 0 1	15 3 12	16 3 13	-0.100
4653.61986	0.00824	6.3×10^{-57}	0 0 0	1 0 1	18 3 16	19 3 17	-0.087
4653.93261	0.00600	5.9×10^{-57}	0 0 0	1 0 1	15 4 12	16 4 13	-0.125
4654.83475	0.00677	4.6×10^{-57}	0 0 0	1 0 1	16 3 13	17 3 14	-0.083
4655.32664	0.00315	1.2×10^{-56}	0 0 0	1 0 1	14 4 10	15 4 11	-0.067
4655.94591	0.00541	7.0×10^{-57}	0 0 0	1 0 1	15 6 9	16 6 10	-0.137
4656.56327	0.01558	2.9×10^{-57}	0 0 0	1 0 1	20 2 19	21 2 20	-0.070
4656.61769	0.01008	2.9×10^{-57}	0 0 0	1 0 1	21 0 21	22 0 22	-0.079
4656.61769	0.01073	2.7×10^{-57}	0 0 0	1 0 1	18 4 15	19 4 16	-0.098
4657.06868	0.00406	7.5×10^{-57}	0 0 0	1 0 1	17 3 14	18 3 15	-0.064
4657.13735	0.00757	3.3×10^{-57}	0 0 0	1 0 1	19 2 17	20 2 18	-0.068
4659.05653	0.00155	2.8×10^{-56}	0 0 0	1 0 1	7 1 6	8 3 5	-0.125
4659.36145	0.00410	1.9×10^{-56}	0 0 0	1 0 1	15 4 11	16 4 12	-0.056
4660.13323	0.00240	1.5×10^{-56}	0 0 0	1 0 1	15 5 10	16 5 11	-0.073
4661.26817	0.00605	6.3×10^{-57}	0 0 0	1 0 1	16 4 13	17 4 14	-0.060
4663.58865	0.00841	5.8×10^{-57}	0 0 0	1 0 1	16 5 12	17 5 13	-0.095
4664.10886	0.00940	4.1×10^{-57}	0 0 0	1 0 1	4 2 3	5 4 2	-0.162
4666.38427	0.00541	7.2×10^{-57}	0 0 0	1 0 1	5 2 3	6 4 2	-0.153
4671.67518	0.00415	9.3×10^{-57}	0 0 0	1 0 1	7 0 7	8 2 6	-0.126
4672.49692	0.00500	6.9×10^{-57}	0 0 0	1 0 1	8 1 7	9 3 6	-0.123
4675.64856	0.00450	1.3×10^{-56}	0 0 0	1 0 1	7 2 5	8 4 4	-0.144
4682.69312	0.00574	7.3×10^{-57}	0 0 0	1 0 1	6 2 5	7 4 4	-0.151
4687.16801	0.00321	1.4×10^{-56}	0 0 0	1 0 1	9 2 7	10 4 6	-0.126

Position	$\sigma_{\text{Pos.}}$	Intensity	$\nu_1\,\nu_2\,\nu_3$	$\nu_1'\,\nu_2'\,\nu_3'$	$J\,K_a\,K_c$	$J'\,K_a'\,K_c'$	$\Delta_{\text{SPEC.}}$
4688.44558	0.00403	1.3×10^{-56}	0 0 0	1 0 1	9 1 8	10 3 7	-0.115
4694.23594	0.01037	2.7×10^{-57}	0 0 0	1 0 1	5 3 2	6 5 1	-0.165
4695.70160	0.00776	4.0×10^{-57}	0 0 0	1 0 1	10 2 8	11 4 7	-0.120

A.2.3.3 T$_2$O $2\nu_1$ band

Here, the lines assigned to the $2\nu_1$ band of T$_2$O obtained from the $10\,\text{GBq}$ sample are presented. These lines are published in [Her23]. For further information, see Section 5.5.3.

Table A.15: Linelist of the T$_2$O $2\nu_1$ band. The columns present the assigned line position, the uncertainty on the position $\sigma_{\text{Pos.}}$, the line intensity taking natural abundance into account, lower and upper vibrational quanta, lower and upper rotational quanta and the deviation to the predictions from SPECTRA database $\Delta_{\text{SPEC.}}$.

Position	$\sigma_{\text{Pos.}}$	Intensity	$\nu_1\,\nu_2\,\nu_3$	$\nu_1'\,\nu_2'\,\nu_3'$	$J\,K_a\,K_c$	$J'\,K_a'\,K_c'$	$\Delta_{\text{SPEC.}}$
4302.98473	0.00215	1.2×10^{-56}	0 0 0	2 0 0	8 5 3	7 4 4	-0.172
4303.47670	0.00084	3.7×10^{-56}	0 0 0	2 0 0	8 5 4	7 4 3	-0.175
4303.90280	0.00146	2.3×10^{-56}	0 0 0	2 0 0	9 4 5	8 3 6	-0.145
4307.62822	0.00181	1.7×10^{-56}	0 0 0	2 0 0	10 4 7	9 3 6	-0.128
4308.38326	0.00394	1.9×10^{-56}	0 0 0	2 0 0	6 6 0	5 5 1	-0.218
4308.38326	0.00136	5.7×10^{-56}	0 0 0	2 0 0	6 6 1	5 5 0	-0.218
4309.40417	0.00420	4.6×10^{-57}	0 0 0	2 0 0	16 1 16	15 0 15	-0.097
4310.22162	0.00512	4.1×10^{-57}	0 0 0	2 0 0	15 1 14	14 2 13	-0.107
4312.88067	0.00066	5.0×10^{-56}	0 0 0	2 0 0	7 5 2	6 4 3	-0.184
4313.04284	0.00182	1.7×10^{-56}	0 0 0	2 0 0	7 5 3	6 4 2	-0.182
4313.73396	0.00373	8.4×10^{-57}	0 0 0	2 0 0	9 4 6	8 3 5	-0.143
4315.97136	0.00409	1.2×10^{-56}	0 0 0	2 0 0	8 4 4	7 3 5	-0.148
4319.11167	0.00195	6.8×10^{-57}	0 0 0	2 0 0	14 2 13	13 1 12	-0.108
4320.80121	0.00087	3.6×10^{-56}	0 0 0	2 0 0	8 4 5	7 3 4	-0.153
4322.51341	0.00178	2.2×10^{-56}	0 0 0	2 0 0	6 5 1	5 4 2	-0.193
4322.55713	0.00053	6.5×10^{-56}	0 0 0	2 0 0	6 5 2	5 4 1	-0.193
4323.56406	0.00356	8.8×10^{-57}	0 0 0	2 0 0	12 3 10	11 2 9	-0.110
4323.76363	0.00509	4.9×10^{-57}	0 0 0	2 0 0	13 2 11	12 3 10	-0.112
4326.74186	0.00071	4.9×10^{-56}	0 0 0	2 0 0	7 4 3	6 3 4	-0.165
4327.53270	0.02853	4.1×10^{-57}	0 0 0	2 0 0	14 0 14	13 1 13	-0.120
4327.53270	0.01049	1.2×10^{-56}	0 0 0	2 0 0	14 1 14	13 0 13	-0.113
4327.91593	0.00673	3.6×10^{-57}	0 0 0	2 0 0	13 2 12	12 1 11	-0.118
4328.42867	0.00251	1.1×10^{-56}	0 0 0	2 0 0	13 1 12	12 2 11	-0.116
4328.77937	0.00185	1.7×10^{-56}	0 0 0	2 0 0	7 4 4	6 3 3	-0.165
4331.93200	0.00184	8.1×10^{-56}	0 0 0	2 0 0	5 5 0	4 4 1	-0.198
4331.93200	0.00541	2.7×10^{-56}	0 0 0	2 0 0	5 5 1	4 4 0	-0.206

Position	$\sigma_{\text{Pos.}}$	Intensity	$\nu_1\,\nu_2\,\nu_3$	$\nu_1{'}\,\nu_2{'}\,\nu_3{'}$	J K_a K_c	J' $K_a{'}$ $K_c{'}$	$\Delta_{\text{SPEC.}}$
4332.19646	0.00859	3.7×10^{-57}	0 0 0	2 0 0	14 2 13	14 1 14	-0.109
4334.05286	0.00484	2.0×10^{-56}	0 0 0	2 0 0	10 3 8	9 2 7	-0.125
4334.05763	0.00321	3.2×10^{-56}	0 0 0	2 0 0	7 3 4	6 2 5	-0.151
4334.34155	0.00775	5.7×10^{-57}	0 0 0	2 0 0	10 7 4	10 6 5	-0.186
4336.37418	0.00577	6.4×10^{-57}	0 0 0	2 0 0	13 1 13	12 0 12	-0.111
4336.37418	0.00211	1.9×10^{-56}	0 0 0	2 0 0	13 0 13	12 1 12	-0.125
4336.44978	0.00200	1.6×10^{-56}	0 0 0	2 0 0	12 2 11	11 1 10	-0.125
4336.61855	0.00418	6.5×10^{-57}	0 0 0	2 0 0	9 7 2	9 6 3	-0.198
4336.72482	0.00164	2.2×10^{-56}	0 0 0	2 0 0	6 4 2	5 3 3	-0.173
4337.41265	0.01009	5.1×10^{-57}	0 0 0	2 0 0	12 1 11	11 2 10	-0.132
4337.42402	0.00064	6.6×10^{-56}	0 0 0	2 0 0	6 4 3	5 3 2	-0.172
4338.86862	0.00432	6.4×10^{-57}	0 0 0	2 0 0	8 7 2	8 6 3	-0.219
4341.56570	0.00480	6.0×10^{-57}	0 0 0	2 0 0	13 1 12	13 0 13	-0.116
4341.67594	0.00546	4.7×10^{-57}	0 0 0	2 0 0	14 3 12	14 2 13	-0.108
4343.84795	0.00902	4.4×10^{-57}	0 0 0	2 0 0	6 2 4	5 1 5	-0.149
4344.28319	0.00105	3.5×10^{-56}	0 0 0	2 0 0	8 3 6	7 2 5	-0.139
4344.63293	0.00499	7.7×10^{-57}	0 0 0	2 0 0	11 2 10	10 1 9	-0.131
4345.03859	0.00132	2.9×10^{-56}	0 0 0	2 0 0	12 1 12	11 0 11	-0.128
4345.06032	0.00439	9.5×10^{-57}	0 0 0	2 0 0	12 0 12	11 1 11	-0.135
4346.22114	0.00048	8.3×10^{-56}	0 0 0	2 0 0	5 4 1	4 3 2	-0.179
4346.92579	0.02289	7.2×10^{-57}	0 0 0	2 0 0	11 2 9	10 3 8	-0.181
4347.48832	0.00211	1.6×10^{-56}	0 0 0	2 0 0	6 3 3	5 2 4	-0.160
4348.65580	0.00488	8.1×10^{-57}	0 0 0	2 0 0	11 6 5	11 5 6	-0.148
4349.71366	0.00750	4.6×10^{-57}	0 0 0	2 0 0	14 4 11	14 3 12	-0.105
4349.77428	0.00291	1.5×10^{-56}	0 0 0	2 0 0	7 3 5	6 2 4	-0.150
4350.39790	0.00316	9.3×10^{-57}	0 0 0	2 0 0	12 2 11	12 1 12	-0.129
4350.54469	0.00328	1.0×10^{-56}	0 0 0	2 0 0	10 6 5	10 5 6	-0.173
4351.94725	0.00255	1.3×10^{-56}	0 0 0	2 0 0	9 6 3	9 5 4	-0.183
4352.09002	0.01018	4.3×10^{-57}	0 0 0	2 0 0	9 6 4	9 5 5	-0.188
4352.34506	0.00112	3.2×10^{-56}	0 0 0	2 0 0	10 2 9	9 1 8	-0.134
4353.23847	0.00412	7.9×10^{-57}	0 0 0	2 0 0	13 2 11	13 1 12	-0.109
4353.55280	0.00274	1.4×10^{-56}	0 0 0	2 0 0	11 1 11	10 0 10	-0.129
4353.61163	0.00094	4.1×10^{-56}	0 0 0	2 0 0	11 0 11	10 1 10	-0.132
4353.66735	0.00608	4.9×10^{-57}	0 0 0	2 0 0	8 6 2	8 5 3	-0.195
4353.71765	0.00243	1.5×10^{-56}	0 0 0	2 0 0	8 6 3	8 5 4	-0.196
4355.33256	0.00666	1.4×10^{-56}	0 0 0	2 0 0	7 6 1	7 5 2	-0.202
4355.39909	0.00153	3.3×10^{-56}	0 0 0	2 0 0	4 4 0	3 3 1	-0.185
4355.42476	0.00040	1.0×10^{-55}	0 0 0	2 0 0	4 4 1	3 3 0	-0.185
4355.65390	0.00379	9.8×10^{-57}	0 0 0	2 0 0	10 1 9	9 2 8	-0.134
4355.90915	0.00069	5.7×10^{-56}	0 0 0	2 0 0	6 3 4	5 2 3	-0.155
4356.87817	0.00280	1.0×10^{-56}	0 0 0	2 0 0	6 6 1	6 5 2	-0.216

Position	$\sigma_{\text{Pos.}}$	Intensity	$\nu_1\,\nu_2\,\nu_3$	$\nu_1'\,\nu_2'\,\nu_3'$	J K_a K_c	J' K_a' K_c'	$\Delta_{\text{SPEC.}}$
4359.05915	0.00064	6.7×10^{-56}	0 0 0	2 0 0	5 3 2	4 2 3	-0.164
4359.23400	0.01147	4.6×10^{-57}	0 0 0	2 0 0	11 2 10	11 1 11	-0.120
4359.25538	0.01686	1.2×10^{-56}	0 0 0	2 0 0	12 3 10	12 2 11	-0.121
4359.45009	0.00432	1.4×10^{-56}	0 0 0	2 0 0	9 2 8	8 1 7	-0.141
4359.86763	0.00307	1.4×10^{-56}	0 0 0	2 0 0	11 1 10	11 0 11	-0.129
4360.11538	0.00464	7.8×10^{-57}	0 0 0	2 0 0	12 5 8	12 4 9	-0.127
4361.58417	0.00198	2.3×10^{-56}	0 0 0	2 0 0	5 2 3	4 1 4	-0.155
4361.88516	0.00079	5.6×10^{-56}	0 0 0	2 0 0	10 1 10	9 0 9	-0.137
4362.01620	0.00280	1.8×10^{-56}	0 0 0	2 0 0	10 0 10	9 1 9	-0.135
4362.83890	0.00227	2.4×10^{-56}	0 0 0	2 0 0	5 3 3	4 2 2	-0.162
4364.07423	0.00343	1.2×10^{-56}	0 0 0	2 0 0	12 4 9	12 3 10	-0.125
4365.17531	0.00134	3.6×10^{-56}	0 0 0	2 0 0	9 1 8	8 2 7	-0.140
4365.40272	0.00717	6.4×10^{-57}	0 0 0	2 0 0	9 5 5	9 4 6	-0.252
4365.89444	0.00075	5.1×10^{-56}	0 0 0	2 0 0	8 2 7	7 1 6	-0.141
4367.80244	0.00213	2.0×10^{-56}	0 0 0	2 0 0	10 2 9	10 1 10	-0.137
4368.01354	0.00206	2.5×10^{-56}	0 0 0	2 0 0	8 5 4	8 4 5	-0.168
4368.48766	0.00207	2.3×10^{-56}	0 0 0	2 0 0	9 5 4	9 4 5	-0.157
4368.63208	0.00793	1.4×10^{-56}	0 0 0	2 0 0	11 5 6	11 4 7	-0.124
4368.91596	0.00651	6.8×10^{-57}	0 0 0	2 0 0	10 1 9	10 0 10	-0.200
4369.20817	0.00456	8.8×10^{-57}	0 0 0	2 0 0	8 5 3	8 4 4	-0.162
4369.28625	0.00143	2.8×10^{-56}	0 0 0	2 0 0	4 3 1	3 2 2	-0.171
4369.66665	0.00636	6.8×10^{-57}	0 0 0	2 0 0	13 5 8	13 4 9	-0.092
4369.76899	0.01021	9.2×10^{-57}	0 0 0	2 0 0	7 5 3	7 4 4	-0.182
4369.96923	0.00936	5.9×10^{-57}	0 0 0	2 0 0	11 4 8	11 3 9	-0.129
4370.02414	0.00180	2.3×10^{-56}	0 0 0	2 0 0	9 1 9	8 0 8	-0.137
4370.21800	0.00156	2.8×10^{-56}	0 0 0	2 0 0	7 5 2	7 4 3	-0.180
4370.29339	0.00068	7.2×10^{-56}	0 0 0	2 0 0	9 0 9	8 1 8	-0.141
4370.57333	0.00062	8.6×10^{-56}	0 0 0	2 0 0	4 3 2	3 2 1	-0.168
4371.20165	0.00303	2.5×10^{-56}	0 0 0	2 0 0	6 5 2	6 4 3	-0.188
4371.34858	0.00398	8.5×10^{-57}	0 0 0	2 0 0	6 5 1	6 4 2	-0.190
4371.51695	0.00399	8.9×10^{-57}	0 0 0	2 0 0	13 3 10	13 2 11	-0.185
4371.76937	0.00214	2.0×10^{-56}	0 0 0	2 0 0	7 2 6	6 1 5	-0.149
4372.41301	0.01014	5.7×10^{-57}	0 0 0	2 0 0	5 5 1	5 4 2	-0.205
4372.46134	0.00344	1.7×10^{-56}	0 0 0	2 0 0	5 5 0	5 4 1	-0.198
4373.88848	0.00188	2.0×10^{-56}	0 0 0	2 0 0	11 2 9	11 1 10	-0.124
4374.86092	0.00165	2.8×10^{-56}	0 0 0	2 0 0	10 3 8	10 2 9	-0.127
4375.06399	0.00138	2.4×10^{-56}	0 0 0	2 0 0	10 4 7	10 3 8	-0.139
4375.22399	0.00335	1.3×10^{-56}	0 0 0	2 0 0	8 1 7	7 2 6	-0.150
4376.08020	0.00354	9.4×10^{-57}	0 0 0	2 0 0	9 2 8	9 1 9	-0.138
4376.94489	0.00308	1.3×10^{-56}	0 0 0	2 0 0	4 2 2	3 1 3	-0.170
4377.10588	0.00407	8.4×10^{-57}	0 0 0	2 0 0	9 4 6	9 3 7	-0.131

Position	$\sigma_{\text{Pos.}}$	Intensity	$\nu_1\ \nu_2\ \nu_3$	ν_1' ν_2' ν_3'	J K_a K_c	J' K_a' K_c'	$\Delta_{\text{SPEC.}}$
4377.37371	0.00081	6.6×10^{-56}	0 0 0	2 0 0	6 2 5	5 1 4	-0.150
4377.93584	0.00120	9.0×10^{-56}	0 0 0	2 0 0	8 1 8	7 0 7	-0.146
4378.15738	0.00266	2.9×10^{-56}	0 0 0	2 0 0	9 1 8	9 0 9	-0.138
4378.47844	0.00163	3.0×10^{-56}	0 0 0	2 0 0	8 0 8	7 1 7	-0.147
4378.64197	0.00047	1.0×10^{-55}	0 0 0	2 0 0	3 3 0	2 2 1	-0.173
4378.89679	0.00116	3.4×10^{-56}	0 0 0	2 0 0	3 3 1	2 2 0	-0.174
4379.40353	0.00527	4.5×10^{-57}	0 0 0	2 0 0	14 6 9	13 7 6	-0.132
4381.25230	0.00083	4.2×10^{-56}	0 0 0	2 0 0	8 4 5	8 3 6	-0.154
4381.58013	0.00744	1.3×10^{-56}	0 0 0	2 0 0	9 3 7	9 2 8	-0.138
4383.04512	0.00194	2.4×10^{-56}	0 0 0	2 0 0	5 2 4	4 1 3	-0.154
4383.71524	0.00979	1.6×10^{-56}	0 0 0	2 0 0	7 4 4	7 3 5	-0.166
4383.94999	0.00101	3.8×10^{-56}	0 0 0	2 0 0	8 2 7	8 1 8	-0.144
4384.28020	0.00435	1.0×10^{-56}	0 0 0	2 0 0	10 2 8	10 1 9	-0.132
4385.19887	0.00429	8.4×10^{-57}	0 0 0	2 0 0	13 4 9	13 3 10	-0.098
4385.49923	0.00067	4.9×10^{-56}	0 0 0	2 0 0	6 4 3	6 3 4	-0.170
4385.55926	0.00131	3.5×10^{-56}	0 0 0	2 0 0	7 1 7	6 0 6	-0.149
4385.94087	0.00100	4.1×10^{-56}	0 0 0	2 0 0	7 1 6	6 2 5	-0.150
4386.63184	0.00052	1.0×10^{-55}	0 0 0	2 0 0	7 0 7	6 1 6	-0.151
4386.81695	0.00292	1.4×10^{-56}	0 0 0	2 0 0	5 4 2	5 3 3	-0.178
4387.16569	0.00275	1.7×10^{-56}	0 0 0	2 0 0	6 4 2	6 3 3	-0.162
4387.41130	0.00257	5.1×10^{-56}	0 0 0	2 0 0	8 3 6	8 2 7	-0.157
4387.42105	0.00603	4.3×10^{-56}	0 0 0	2 0 0	5 4 1	5 3 2	-0.170
4387.42105	0.00541	4.9×10^{-56}	0 0 0	2 0 0	7 4 3	7 3 4	-0.157
4387.43513	0.00763	1.4×10^{-56}	0 0 0	2 0 0	8 1 7	8 0 8	-0.137
4387.82310	0.00172	2.8×10^{-56}	0 0 0	2 0 0	4 4 1	4 3 2	-0.181
4387.98218	0.00415	9.4×10^{-57}	0 0 0	2 0 0	4 4 0	4 3 1	-0.178
4388.22036	0.00255	1.5×10^{-56}	0 0 0	2 0 0	8 4 4	8 3 5	-0.144
4389.05126	0.00186	2.4×10^{-56}	0 0 0	2 0 0	11 4 7	11 3 8	-0.134
4389.07060	0.00062	7.5×10^{-56}	0 0 0	2 0 0	4 2 3	3 1 2	-0.151
4389.23640	0.00117	3.9×10^{-56}	0 0 0	2 0 0	9 4 5	9 3 6	-0.131
4390.00845	0.00079	5.5×10^{-56}	0 0 0	2 0 0	3 2 1	2 1 2	-0.139
4391.24773	0.00183	2.6×10^{-56}	0 0 0	2 0 0	11 3 8	11 2 9	-0.113
4391.33505	0.00483	1.6×10^{-56}	0 0 0	2 0 0	7 2 6	7 1 7	-0.110
4392.19903	0.00845	2.7×10^{-57}	0 0 0	2 0 0	16 7 10	15 8 7	-0.203
4392.30087	0.00151	2.1×10^{-56}	0 0 0	2 0 0	7 3 5	7 2 6	-0.159
4392.81236	0.00042	1.2×10^{-55}	0 0 0	2 0 0	6 1 6	5 0 5	-0.153
4394.20375	0.00171	4.8×10^{-56}	0 0 0	2 0 0	9 2 7	9 1 8	-0.128
4394.89702	0.00107	3.7×10^{-56}	0 0 0	2 0 0	6 0 6	5 1 5	-0.104
4395.60611	0.00169	2.6×10^{-56}	0 0 0	2 0 0	3 2 2	2 1 1	-0.147
4396.21266	0.00063	7.1×10^{-56}	0 0 0	2 0 0	6 3 4	6 2 5	-0.158
4396.74850	0.00447	5.3×10^{-56}	0 0 0	2 0 0	7 1 6	7 0 7	-0.149

Position	$\sigma_{\text{Pos.}}$	Intensity	$\nu_1\,\nu_2\,\nu_3$	$\nu_1'\,\nu_2'\,\nu_3'$	J K_a K_c	J' K_a' K_c'	$\Delta_{\text{SPEC.}}$
4397.25324	0.00325	1.2×10^{-56}	0 0 0	2 0 0	6 1 5	5 2 4	-0.155
4397.98271	0.00093	6.1×10^{-56}	0 0 0	2 0 0	6 2 5	6 1 6	-0.147
4399.17711	0.00270	2.4×10^{-56}	0 0 0	2 0 0	5 3 3	5 2 4	-0.160
4399.62728	0.00109	4.0×10^{-56}	0 0 0	2 0 0	5 1 5	4 0 4	-0.156
4400.31897	0.00458	8.3×10^{-57}	0 0 0	2 0 0	7 2 5	6 3 4	-0.156
4400.97345	0.00178	2.4×10^{-56}	0 0 0	2 0 0	2 2 0	1 1 1	-0.166
4401.28228	0.00087	6.3×10^{-56}	0 0 0	2 0 0	4 3 2	4 2 3	-0.171
4401.71878	0.00904	4.5×10^{-57}	0 0 0	2 0 0	15 7 8	14 8 7	-0.209
4402.47768	0.00216	6.1×10^{-56}	0 0 0	2 0 0	9 3 6	9 2 7	-0.122
4402.68631	0.00356	1.4×10^{-56}	0 0 0	2 0 0	3 3 1	3 2 2	-0.174
4402.69952	0.00081	8.0×10^{-56}	0 0 0	2 0 0	2 2 1	1 1 0	-0.165
4403.01964	0.00154	2.4×10^{-56}	0 0 0	2 0 0	8 2 6	8 1 7	-0.137
4403.17716	0.00398	1.1×10^{-56}	0 0 0	2 0 0	12 6 7	11 7 4	-0.173
4403.25450	0.00040	1.1×10^{-55}	0 0 0	2 0 0	5 0 5	4 1 4	-0.157
4403.78792	0.00111	4.1×10^{-56}	0 0 0	2 0 0	3 3 0	3 2 1	-0.171
4403.85660	0.00258	2.3×10^{-56}	0 0 0	2 0 0	5 2 4	5 1 5	-0.154
4404.27843	0.00202	2.2×10^{-56}	0 0 0	2 0 0	4 3 1	4 2 2	-0.167
4404.92481	0.00606	4.9×10^{-57}	0 0 0	2 0 0	11 5 6	10 6 5	-0.197
4405.20042	0.00054	8.2×10^{-56}	0 0 0	2 0 0	5 3 2	5 2 3	-0.160
4405.39713	0.00136	2.6×10^{-56}	0 0 0	2 0 0	8 3 5	8 2 6	-0.126
4405.81258	0.00173	2.4×10^{-56}	0 0 0	2 0 0	6 1 5	6 0 6	-0.150
4406.03993	0.00047	1.1×10^{-55}	0 0 0	2 0 0	4 1 4	3 0 3	-0.158
4406.13397	0.00153	3.0×10^{-56}	0 0 0	2 0 0	6 3 3	6 2 4	-0.152
4406.41915	0.00042	8.8×10^{-56}	0 0 0	2 0 0	7 3 4	7 2 5	-0.145
4408.81313	0.00062	7.3×10^{-56}	0 0 0	2 0 0	4 2 3	4 1 4	-0.161
4408.89408	0.00162	2.8×10^{-56}	0 0 0	2 0 0	5 1 4	4 2 3	-0.159
4409.33854	0.00292	1.0×10^{-56}	0 0 0	2 0 0	16 3 14	15 4 11	-0.195
4410.18768	0.00046	1.0×10^{-55}	0 0 0	2 0 0	7 2 5	7 1 6	-0.142
4411.65843	0.00470	7.0×10^{-57}	0 0 0	2 0 0	14 7 8	13 8 5	-0.222
4411.98084	0.00118	3.2×10^{-56}	0 0 0	2 0 0	4 0 4	3 1 3	-0.159
4412.27692	0.00113	3.4×10^{-56}	0 0 0	2 0 0	3 1 3	2 0 2	-0.160
4412.78377	0.00193	2.2×10^{-56}	0 0 0	2 0 0	3 2 2	3 1 3	-0.164
4414.10789	0.00053	9.3×10^{-56}	0 0 0	2 0 0	5 1 4	5 0 5	-0.153
4414.87741	0.00480	1.4×10^{-56}	0 0 0	2 0 0	11 6 5	10 7 4	-0.209
4415.41279	0.00568	4.3×10^{-56}	0 0 0	2 0 0	6 2 4	6 1 5	-0.144
4415.74060	0.00096	4.6×10^{-56}	0 0 0	2 0 0	2 2 1	2 1 2	-0.166
4418.69122	0.00513	8.3×10^{-56}	0 0 0	2 0 0	2 1 2	1 0 1	-0.160
4418.69925	0.00356	1.4×10^{-55}	0 0 0	2 0 0	5 2 3	5 1 4	-0.154
4419.95971	0.00260	2.0×10^{-56}	0 0 0	2 0 0	2 2 0	2 1 1	-0.171
4420.28641	0.00099	4.5×10^{-56}	0 0 0	2 0 0	4 2 2	4 1 3	-0.156
4420.51182	0.01283	6.3×10^{-57}	0 0 0	2 0 0	4 1 3	3 2 2	-0.145

Position	$\sigma_{\text{Pos.}}$	Intensity	$\nu_1\ \nu_2\ \nu_3$	$\nu_1'\ \nu_2'\ \nu_3'$	J K_a K_c	J' K_a' K_c'	$\Delta_{\text{SPEC.}}$
4420.53253	0.00055	1.1×10^{-55}	0 0 0	2 0 0	3 2 1	3 1 2	-0.162
4421.03123	0.00073	6.8×10^{-56}	0 0 0	2 0 0	3 0 3	2 1 2	-0.162
4421.05304	0.00565	1.0×10^{-56}	0 0 0	2 0 0	13 7 6	12 8 5	-0.236
4421.07541	0.00137	3.9×10^{-56}	0 0 0	2 0 0	4 1 3	4 0 4	-0.157
4421.09276	0.01976	3.5×10^{-57}	0 0 0	2 0 0	13 7 7	12 8 4	-0.233
4425.57215	0.00186	2.0×10^{-56}	0 0 0	2 0 0	1 1 1	0 0 0	-0.163
4426.35624	0.00030	1.3×10^{-55}	0 0 0	2 0 0	3 1 2	3 0 3	-0.159
4427.83485	0.01254	5.6×10^{-57}	0 0 0	2 0 0	9 5 4	8 6 3	-0.209
4428.47248	0.01044	2.7×10^{-57}	0 0 0	2 0 0	6 5 2	7 4 3	-0.250
4429.93496	0.00111	4.3×10^{-56}	0 0 0	2 0 0	2 1 1	2 0 2	-0.161
4430.23943	0.00439	1.4×10^{-56}	0 0 0	2 0 0	12 7 6	11 8 3	-0.247
4430.23943	0.01065	4.7×10^{-57}	0 0 0	2 0 0	12 7 5	11 8 4	-0.236
4431.72626	0.00533	8.8×10^{-57}	0 0 0	2 0 0	3 1 2	2 2 1	-0.162
4432.06788	0.00023	9.3×10^{-56}	0 0 0	2 0 0	1 1 0	1 0 1	-0.164
4435.48540	0.00699	5.8×10^{-57}	0 0 0	2 0 0	5 4 1	6 3 4	-0.180
4438.01012	0.01662	5.7×10^{-57}	0 0 0	2 0 0	9 6 4	8 7 1	-0.236
4438.01013	0.00571	1.7×10^{-56}	0 0 0	2 0 0	9 6 3	8 7 2	-0.223
4439.05405	0.01444	5.9×10^{-57}	0 0 0	2 0 0	11 7 5	10 8 2	-0.257
4439.05405	0.00580	1.8×10^{-56}	0 0 0	2 0 0	11 7 4	10 8 3	-0.255
4440.28675	0.00396	9.6×10^{-57}	0 0 0	2 0 0	3 2 1	4 1 4	-0.161
4445.50685	0.00335	1.2×10^{-56}	0 0 0	2 0 0	5 3 2	6 2 5	-0.160
4447.43126	0.00955	1.2×10^{-56}	0 0 0	2 0 0	4 3 2	5 2 3	-0.159
4447.46359	0.01382	1.9×10^{-56}	0 0 0	2 0 0	10 7 4	9 8 1	-0.265
4447.46359	0.03484	6.3×10^{-57}	0 0 0	2 0 0	10 7 3	9 8 2	-0.264
4447.84154	0.00057	9.0×10^{-56}	0 0 0	2 0 0	1 0 1	1 1 0	-0.165
4449.17977	0.00115	4.1×10^{-56}	0 0 0	2 0 0	2 0 2	2 1 1	-0.163
4449.36808	0.00487	1.4×10^{-56}	0 0 0	2 0 0	1 1 1	2 0 2	-0.160
4449.46974	0.00754	1.3×10^{-56}	0 0 0	2 0 0	8 6 3	7 7 0	-0.239
4449.46974	0.01945	4.2×10^{-57}	0 0 0	2 0 0	8 6 2	7 7 1	-0.238
4451.58048	0.00042	1.3×10^{-55}	0 0 0	2 0 0	3 0 3	3 1 2	-0.161
4453.64255	0.00151	3.0×10^{-56}	0 0 0	2 0 0	10 1 9	9 4 6	-0.140
4454.55302	0.00218	2.2×10^{-56}	0 0 0	2 0 0	0 0 0	1 1 1	-0.168
4455.03270	0.00048	1.3×10^{-55}	0 0 0	2 0 0	5 1 4	5 2 3	-0.157
4455.19403	0.00121	1.5×10^{-55}	0 0 0	2 0 0	11 1 10	10 4 7	-0.139
4455.30921	0.00168	3.6×10^{-56}	0 0 0	2 0 0	4 0 4	4 1 3	-0.159
4455.30921	0.00345	1.5×10^{-56}	0 0 0	2 0 0	9 7 2	8 8 1	-0.272
4455.48355	0.00122	4.1×10^{-56}	0 0 0	2 0 0	4 1 3	4 2 2	-0.161
4455.89624	0.00115	3.8×10^{-56}	0 0 0	2 0 0	6 1 5	6 2 4	-0.149
4456.54058	0.00088	6.6×10^{-56}	0 0 0	2 0 0	11 1 11	10 2 8	-0.152
4456.86570	0.00087	9.5×10^{-56}	0 0 0	2 0 0	3 1 2	3 2 1	-0.167
4457.59062	0.00093	9.4×10^{-56}	0 0 0	2 0 0	2 1 2	3 0 3	-0.168

Position	$\sigma_{\text{Pos.}}$	Intensity	$\nu_1\,\nu_2\,\nu_3$	$\nu_1{}'\,\nu_2{}'\,\nu_3{}'$	J K_a K_c	J' $K_a{}'$ $K_c{}'$	$\Delta_{\text{SPEC.}}$
4457.75671	0.00124	4.8×10^{-56}	0 0 0	2 0 0	9 2 7	9 3 6	-0.126
4458.30565	0.00056	8.6×10^{-56}	0 0 0	2 0 0	7 1 6	7 2 5	-0.141
4458.62491	0.00170	3.3×10^{-56}	0 0 0	2 0 0	9 1 8	8 4 5	-0.158
4458.65519	0.00358	2.1×10^{-56}	0 0 0	2 0 0	8 2 6	8 3 5	-0.173
4458.69057	0.00402	1.8×10^{-56}	0 0 0	2 0 0	2 1 1	2 2 0	-0.135
4460.37124	0.00056	8.3×10^{-56}	0 0 0	2 0 0	5 0 5	5 1 4	-0.154
4460.88211	0.00048	9.8×10^{-56}	0 0 0	2 0 0	1 0 1	2 1 2	-0.166
4460.99495	0.00067	7.1×10^{-56}	0 0 0	2 0 0	7 2 5	7 3 4	-0.152
4462.27306	0.00244	1.9×10^{-56}	0 0 0	2 0 0	8 1 7	8 2 6	-0.136
4462.96016	0.00160	4.0×10^{-56}	0 0 0	2 0 0	2 1 2	2 2 1	-0.172
4463.49434	0.00242	1.5×10^{-56}	0 0 0	2 0 0	9 0 9	8 3 6	-0.151
4464.18591	0.00202	2.4×10^{-56}	0 0 0	2 0 0	6 2 4	6 3 3	-0.161
4464.42474	0.00131	6.9×10^{-56}	0 0 0	2 0 0	10 0 10	9 3 7	-0.130
4464.57203	0.00729	6.9×10^{-57}	0 0 0	2 0 0	10 3 7	10 4 6	-0.136
4464.78182	0.00967	1.9×10^{-56}	0 0 0	2 0 0	3 1 3	3 2 2	-0.174
4465.37182	0.00096	4.8×10^{-56}	0 0 0	2 0 0	3 1 3	4 0 4	-0.159
4465.54387	0.00665	1.2×10^{-56}	0 0 0	2 0 0	12 1 12	11 2 9	-0.131
4465.93002	0.00129	5.1×10^{-56}	0 0 0	2 0 0	4 2 3	5 1 4	-0.157
4466.37306	0.00156	4.4×10^{-56}	0 0 0	2 0 0	2 0 2	3 1 3	-0.164
4466.41194	0.00355	2.0×10^{-56}	0 0 0	2 0 0	6 0 6	6 1 5	-0.149
4467.29127	0.00150	6.2×10^{-56}	0 0 0	2 0 0	4 1 4	4 2 3	-0.137
4467.45336	0.00152	3.3×10^{-56}	0 0 0	2 0 0	9 1 8	9 2 7	-0.128
4467.59914	0.00079	6.4×10^{-56}	0 0 0	2 0 0	5 2 3	5 3 2	-0.170
4468.57575	0.00218	2.3×10^{-56}	0 0 0	2 0 0	6 3 4	7 2 5	-0.151
4469.14087	0.00327	3.0×10^{-56}	0 0 0	2 0 0	11 0 11	10 3 8	-0.140
4469.46933	0.00182	2.5×10^{-56}	0 0 0	2 0 0	9 3 6	9 4 5	-0.148
4470.36808	0.00310	1.9×10^{-56}	0 0 0	2 0 0	5 1 5	5 2 4	-0.163
4470.58171	0.00329	1.7×10^{-56}	0 0 0	2 0 0	4 2 2	4 3 1	-0.174
4471.33206	0.00029	1.7×10^{-55}	0 0 0	2 0 0	3 0 3	4 1 4	-0.162
4472.47797	0.00031	1.8×10^{-55}	0 0 0	2 0 0	4 1 4	5 0 5	-0.158
4472.71219	0.00195	3.2×10^{-56}	0 0 0	2 0 0	3 2 1	3 3 0	-0.179
4472.87383	0.00120	4.4×10^{-56}	0 0 0	2 0 0	7 0 7	7 1 6	-0.147
4473.63713	0.00239	4.8×10^{-56}	0 0 0	2 0 0	4 2 3	4 3 2	-0.175
4473.75459	0.00671	1.8×10^{-56}	0 0 0	2 0 0	5 2 4	5 3 3	-0.177
4474.04122	0.00097	4.9×10^{-56}	0 0 0	2 0 0	6 1 6	6 2 5	-0.159
4474.30481	0.00600	9.4×10^{-57}	0 0 0	2 0 0	8 3 5	8 4 4	-0.161
4474.34900	0.00210	5.1×10^{-56}	0 0 0	2 0 0	6 2 5	6 3 4	-0.164
4475.41320	0.00216	2.3×10^{-56}	0 0 0	2 0 0	5 2 4	6 1 5	-0.157
4476.12089	0.00079	6.5×10^{-56}	0 0 0	2 0 0	4 0 4	5 1 5	-0.159
4476.33882	0.00060	8.8×10^{-56}	0 0 0	2 0 0	1 1 0	2 2 1	-0.173
4477.15163	0.00182	2.9×10^{-56}	0 0 0	2 0 0	8 2 7	8 3 6	-0.153

Position	$\sigma_{\text{Pos.}}$	Intensity	$\nu_1\ \nu_2\ \nu_3$	$\nu_1{}'\ \nu_2{}'\ \nu_3{}'$	J K_a K_c	J' $K_a{}'$ $K_c{}'$	$\Delta_{\text{SPEC.}}$
4478.47010	0.00183	3.0×10^{-56}	0 0 0	2 0 0	7 3 4	7 4 3	-0.178
4478.92975	0.00073	6.8×10^{-56}	0 0 0	2 0 0	5 1 5	6 0 6	-0.156
4479.25325	0.00743	1.0×10^{-56}	0 0 0	2 0 0	8 0 8	8 1 7	-0.147
4479.35117	0.00551	9.0×10^{-57}	0 0 0	2 0 0	7 3 5	8 2 6	-0.144
4480.87158	0.00391	1.4×10^{-56}	0 0 0	2 0 0	8 3 6	8 4 5	-0.164
4480.97488	0.00026	2.1×10^{-55}	0 0 0	2 0 0	5 0 5	6 1 6	-0.157
4481.67484	0.00540	9.7×10^{-57}	0 0 0	2 0 0	6 3 3	6 4 2	-0.186
4482.44412	0.00163	3.2×10^{-56}	0 0 0	2 0 0	2 1 1	3 2 2	-0.171
4482.62710	0.00211	2.9×10^{-56}	0 0 0	2 0 0	8 1 8	8 2 7	-0.150
4483.28401	0.00271	2.9×10^{-56}	0 0 0	2 0 0	10 2 9	10 3 8	-0.193
4483.33673	0.00243	2.4×10^{-56}	0 0 0	2 0 0	6 3 4	6 4 3	-0.140
4483.58496	0.00156	3.8×10^{-56}	0 0 0	2 0 0	10 3 8	10 4 7	-0.142
4483.79838	0.00863	1.3×10^{-56}	0 0 0	2 0 0	12 3 10	12 4 9	-0.146
4483.94682	0.00307	2.5×10^{-56}	0 0 0	2 0 0	5 3 2	5 4 1	-0.187
4484.21938	0.00063	8.5×10^{-56}	0 0 0	2 0 0	6 2 5	7 1 6	-0.149
4484.52133	0.00692	7.5×10^{-57}	0 0 0	2 0 0	5 3 3	5 4 2	-0.195
4484.85196	0.00028	2.1×10^{-55}	0 0 0	2 0 0	6 1 6	7 0 7	-0.154
4485.27711	0.00512	2.2×10^{-56}	0 0 0	2 0 0	9 0 9	9 1 8	-0.136
4485.63371	0.00415	1.5×10^{-56}	0 0 0	2 0 0	4 3 2	4 4 1	-0.200
4485.93444	0.00093	7.1×10^{-56}	0 0 0	2 0 0	6 0 6	7 1 7	-0.153
4486.47578	0.00912	5.6×10^{-57}	0 0 0	2 0 0	11 2 10	11 3 9	-0.148
4487.27110	0.00597	7.0×10^{-57}	0 0 0	2 0 0	9 1 9	9 2 8	-0.144
4487.57873	0.00051	1.0×10^{-55}	0 0 0	2 0 0	3 1 2	4 2 3	-0.166
4487.75487	0.00717	7.2×10^{-57}	0 0 0	2 0 0	9 4 5	9 5 4	-0.176
4488.10750	0.00090	6.7×10^{-56}	0 0 0	2 0 0	2 1 2	3 2 1	-0.169
4489.70177	0.00407	3.0×10^{-56}	0 0 0	2 0 0	8 3 6	9 2 7	-0.132
4490.37895	0.00205	6.4×10^{-56}	0 0 0	2 0 0	7 1 7	8 0 8	-0.146
4490.83191	0.01394	4.9×10^{-57}	0 0 0	2 0 0	10 0 10	10 1 9	-0.161
4490.92940	0.00060	2.0×10^{-55}	0 0 0	2 0 0	7 0 7	8 1 8	-0.150
4490.92940	0.02835	2.5×10^{-57}	0 0 0	2 0 0	8 4 4	8 5 3	-0.217
4491.46609	0.00822	6.3×10^{-57}	0 0 0	2 0 0	13 1 12	13 2 11	-0.116
4491.81989	0.00308	3.6×10^{-56}	0 0 0	2 0 0	4 1 3	5 2 4	-0.161
4491.82945	0.02702	8.6×10^{-57}	0 0 0	2 0 0	8 4 5	8 5 4	-0.209
4491.97158	0.00370	1.4×10^{-56}	0 0 0	2 0 0	10 1 10	10 2 9	-0.147
4492.07235	0.00173	3.0×10^{-56}	0 0 0	2 0 0	7 2 6	8 1 7	-0.147
4495.33687	0.00051	1.1×10^{-55}	0 0 0	2 0 0	5 1 4	6 2 5	-0.159
4495.60992	0.00119	1.8×10^{-55}	0 0 0	2 0 0	8 1 8	9 0 9	-0.147
4495.88267	0.00109	6.0×10^{-56}	0 0 0	2 0 0	8 0 8	9 1 9	-0.145
4496.04964	0.00511	9.7×10^{-57}	0 0 0	2 0 0	11 0 11	11 1 10	-0.137
4497.01503	0.01646	3.8×10^{-57}	0 0 0	2 0 0	5 4 1	5 5 0	-0.206
4498.20795	0.00132	3.9×10^{-56}	0 0 0	2 0 0	2 2 0	3 3 1	-0.183

Position	$\sigma_{\text{Pos.}}$	Intensity	$\nu_1\,\nu_2\,\nu_3$	$\nu_1'\,\nu_2'\,\nu_3'$	J K_a K_c	J' K_a' K_c'	$\Delta_{\text{SPEC.}}$
4498.42272	0.00181	3.7×10^{-56}	0 0 0	2 0 0	6 1 5	7 2 6	-0.158
4498.46850	0.00073	1.2×10^{-55}	0 0 0	2 0 0	2 2 1	3 3 0	-0.182
4498.93070	0.00061	8.9×10^{-56}	0 0 0	2 0 0	8 2 7	9 1 8	-0.142
4499.77874	0.00288	1.7×10^{-56}	0 0 0	2 0 0	3 1 3	4 2 2	-0.165
4500.59974	0.00095	5.1×10^{-56}	0 0 0	2 0 0	9 1 9	10 0 10	-0.143
4500.73157	0.00031	1.5×10^{-55}	0 0 0	2 0 0	9 0 9	10 1 10	-0.142
4501.44276	0.00052	1.1×10^{-55}	0 0 0	2 0 0	7 1 6	8 2 7	-0.150
4504.68066	0.00163	3.2×10^{-56}	0 0 0	2 0 0	8 1 7	9 2 8	-0.146
4504.92087	0.00183	2.6×10^{-56}	0 0 0	2 0 0	9 2 8	10 1 9	-0.139
4505.10559	0.00046	1.1×10^{-55}	0 0 0	2 0 0	3 2 1	4 3 2	-0.180
4505.38362	0.00038	1.2×10^{-55}	0 0 0	2 0 0	10 1 10	11 0 11	-0.137
4505.44752	0.00133	4.1×10^{-56}	0 0 0	2 0 0	10 0 10	11 1 11	-0.136
4506.40948	0.00134	3.7×10^{-56}	0 0 0	2 0 0	3 2 2	4 3 1	-0.180
4508.22217	0.00109	8.2×10^{-56}	0 0 0	2 0 0	9 1 8	10 2 9	-0.170
4508.77298	0.00197	2.6×10^{-56}	0 0 0	2 0 0	10 3 8	11 2 9	-0.127
4509.90970	0.00272	1.5×10^{-56}	0 0 0	2 0 0	9 6 3	9 7 2	-0.209
4509.97614	0.00322	3.2×10^{-56}	0 0 0	2 0 0	11 1 11	12 0 12	-0.132
4509.97614	0.01903	5.0×10^{-57}	0 0 0	2 0 0	9 6 4	9 7 3	-0.204
4510.00641	0.00046	9.6×10^{-56}	0 0 0	2 0 0	11 0 11	12 1 12	-0.132
4510.24282	0.00146	6.6×10^{-56}	0 0 0	2 0 0	10 2 9	11 1 10	-0.139
4510.99997	0.00152	3.5×10^{-56}	0 0 0	2 0 0	4 2 2	5 3 3	-0.175
4512.10091	0.00141	2.2×10^{-56}	0 0 0	2 0 0	10 1 9	11 2 10	-0.117
4513.04346	0.00460	8.0×10^{-57}	0 0 0	2 0 0	8 6 2	8 7 1	-0.231
4513.04346	0.00220	2.4×10^{-56}	0 0 0	2 0 0	8 6 3	8 7 2	-0.223
4513.40618	0.00156	3.5×10^{-56}	0 0 0	2 0 0	4 1 4	5 2 3	-0.158
4514.37232	0.00148	7.1×10^{-56}	0 0 0	2 0 0	12 1 12	13 0 13	-0.143
4514.37232	0.00322	2.4×10^{-56}	0 0 0	2 0 0	12 0 12	13 1 13	-0.157
4514.82845	0.00055	1.0×10^{-55}	0 0 0	2 0 0	4 2 3	5 3 2	-0.175
4515.67456	0.00062	9.4×10^{-56}	0 0 0	2 0 0	5 2 3	6 3 4	-0.168
4516.05151	0.00396	7.6×10^{-57}	0 0 0	2 0 0	11 3 9	12 2 10	-0.130
4516.07907	0.00062	5.2×10^{-56}	0 0 0	2 0 0	11 1 10	12 2 11	-0.129
4516.09787	0.00147	3.1×10^{-56}	0 0 0	2 0 0	7 6 1	7 7 0	-0.243
4518.62765	0.00413	1.7×10^{-56}	0 0 0	2 0 0	13 1 13	14 0 14	-0.116
4518.62765	0.00148	5.1×10^{-56}	0 0 0	2 0 0	13 0 13	14 1 14	-0.122
4518.85318	0.00153	1.2×10^{-55}	0 0 0	2 0 0	3 3 0	4 4 1	-0.199
4518.88064	0.00818	4.1×10^{-56}	0 0 0	2 0 0	3 3 1	4 4 0	-0.203
4519.12467	0.00202	2.7×10^{-56}	0 0 0	2 0 0	6 2 4	7 3 5	-0.160
4519.56701	0.00108	3.8×10^{-56}	0 0 0	2 0 0	12 2 11	13 1 12	-0.125
4521.44737	0.00077	6.9×10^{-56}	0 0 0	2 0 0	7 2 5	8 3 6	-0.151
4522.05720	0.00265	1.5×10^{-56}	0 0 0	2 0 0	8 2 6	9 3 7	-0.131
4522.29286	0.00264	1.8×10^{-56}	0 0 0	2 0 0	12 3 10	13 2 11	-0.121

Position	$\sigma_{\text{Pos.}}$	Intensity	$\nu_1\,\nu_2\,\nu_3$	$\nu_1{}'\,\nu_2{}'\,\nu_3{}'$	J K_a K_c	J' $K_a{}'$ $K_c{}'$	$\Delta_{\text{SPEC.}}$
4522.68281	0.00089	3.5×10^{-56}	0 0 0	2 0 0	14 1 14	15 0 15	-0.113
4523.72669	0.01007	9.0×10^{-57}	0 0 0	2 0 0	13 2 12	14 1 13	-0.164
4524.04500	0.00191	2.7×10^{-56}	0 0 0	2 0 0	13 1 12	14 2 13	-0.117
4524.19187	0.00192	2.7×10^{-56}	0 0 0	2 0 0	5 2 4	6 3 3	-0.169
4525.18958	0.00117	4.1×10^{-56}	0 0 0	2 0 0	9 2 7	10 3 8	-0.140
4525.96306	0.00142	4.0×10^{-56}	0 0 0	2 0 0	4 3 1	5 4 2	-0.197
4526.16864	0.00052	1.2×10^{-55}	0 0 0	2 0 0	4 3 2	5 4 1	-0.195
4527.08120	0.00674	5.9×10^{-57}	0 0 0	2 0 0	14 7 8	14 8 7	-0.215
4527.52851	0.00202	2.7×10^{-56}	0 0 0	2 0 0	11 2 9	12 3 10	-0.130
4527.58731	0.00553	4.4×10^{-57}	0 0 0	2 0 0	13 3 11	14 2 12	-0.129
4527.74700	0.00206	1.8×10^{-56}	0 0 0	2 0 0	14 2 13	15 1 14	-0.113
4529.51840	0.01479	6.0×10^{-57}	0 0 0	2 0 0	12 7 5	12 8 4	-0.250
4529.51840	0.00512	1.8×10^{-56}	0 0 0	2 0 0	12 7 6	12 8 5	-0.242
4530.11007	0.00353	1.2×10^{-56}	0 0 0	2 0 0	16 1 16	17 0 17	-0.165
4530.18435	0.00789	4.7×10^{-57}	0 0 0	2 0 0	16 0 16	17 1 17	-0.150
4530.27940	0.00964	2.9×10^{-56}	0 0 0	2 0 0	11 7 4	11 8 3	-0.277
4530.27940	0.00430	7.8×10^{-56}	0 0 0	2 0 0	8 7 2	8 8 1	-0.280
4530.27940	0.01025	2.6×10^{-56}	0 0 0	2 0 0	8 7 1	8 8 0	-0.280
4530.74879	0.00411	1.5×10^{-56}	0 0 0	2 0 0	10 7 3	10 8 2	-0.263
4530.74879	0.00180	4.5×10^{-56}	0 0 0	2 0 0	10 7 4	10 8 3	-0.262
4530.78752	0.00328	6.4×10^{-56}	0 0 0	2 0 0	9 7 2	9 8 1	-0.277
4530.78752	0.00931	2.1×10^{-56}	0 0 0	2 0 0	9 7 3	9 8 2	-0.277
4531.58478	0.00433	1.2×10^{-56}	0 0 0	2 0 0	15 1 14	16 2 15	-0.114
4531.85855	0.00334	1.4×10^{-56}	0 0 0	2 0 0	13 2 11	14 3 12	-0.111
4532.58622	0.00039	1.1×10^{-55}	0 0 0	2 0 0	5 3 2	6 4 3	-0.187
4533.36029	0.00120	3.7×10^{-56}	0 0 0	2 0 0	5 3 3	6 4 2	-0.189
4535.02798	0.00181	6.2×10^{-56}	0 0 0	2 0 0	6 2 5	7 3 4	-0.157
4535.94157	0.00354	1.0×10^{-56}	0 0 0	2 0 0	11 8 3	11 9 2	-0.304
4536.64029	0.00668	4.4×10^{-57}	0 0 0	2 0 0	10 8 2	10 9 1	-0.314
4536.64031	0.00287	1.3×10^{-56}	0 0 0	2 0 0	10 8 3	10 9 2	-0.314
4536.99811	0.00638	1.3×10^{-56}	0 0 0	2 0 0	9 8 1	9 9 0	-0.318
4537.17288	0.00624	5.4×10^{-57}	0 0 0	2 0 0	18 1 18	19 0 19	-0.081
4537.65666	0.00618	6.1×10^{-57}	0 0 0	2 0 0	15 2 13	16 3 14	-0.098
4538.40985	0.00139	3.3×10^{-56}	0 0 0	2 0 0	6 3 3	7 4 4	-0.176
4538.48644	0.00923	4.4×10^{-57}	0 0 0	2 0 0	17 1 16	18 2 17	-0.096
4538.60313	0.00623	3.7×10^{-56}	0 0 0	2 0 0	4 4 0	5 5 1	-0.219
4538.60604	0.00223	1.1×10^{-55}	0 0 0	2 0 0	4 4 1	5 5 0	-0.218
4539.88950	0.01193	3.7×10^{-57}	0 0 0	2 0 0	16 3 14	17 2 15	-0.165
4540.63012	0.00050	9.6×10^{-56}	0 0 0	2 0 0	6 3 4	7 4 3	-0.180
4543.01305	0.00067	8.1×10^{-56}	0 0 0	2 0 0	7 3 4	8 4 5	-0.165
4545.50312	0.00058	1.1×10^{-55}	0 0 0	2 0 0	5 4 1	6 5 2	-0.211

Position	$\sigma_{\text{Pos.}}$	Intensity	$\nu_1\ \nu_2\ \nu_3$	$\nu_1{}'\ \nu_2{}'\ \nu_3{}'$	J K_a K_c	J' $K_a{}'$ $K_c{}'$	$\Delta_{\text{SPEC.}}$
4545.51438	0.00179	3.7×10^{-56}	0 0 0	2 0 0	5 4 2	6 5 1	-0.215
4545.79138	0.00236	2.0×10^{-56}	0 0 0	2 0 0	8 3 5	9 4 6	-0.144
4545.85598	0.00505	6.5×10^{-57}	0 0 0	2 0 0	10 9 2	10 10 1	-0.299
4546.40530	0.00268	1.8×10^{-56}	0 0 0	2 0 0	6 1 6	7 2 5	-0.151
4548.26912	0.00210	2.6×10^{-56}	0 0 0	2 0 0	7 3 5	8 4 4	-0.169
4550.08161	0.00548	7.5×10^{-57}	0 0 0	2 0 0	13 3 10	14 4 11	-0.111
4551.50150	0.00238	1.6×10^{-56}	0 0 0	2 0 0	11 3 8	12 4 9	-0.130
4551.81432	0.00764	6.5×10^{-57}	0 0 0	2 0 0	10 3 7	11 4 8	-0.143
4552.00021	0.00654	1.4×10^{-56}	0 0 0	2 0 0	9 3 6	10 4 7	-0.149
4552.14014	0.00218	3.4×10^{-56}	0 0 0	2 0 0	6 4 2	7 5 3	-0.203
4552.21108	0.00087	1.0×10^{-55}	0 0 0	2 0 0	6 4 3	7 5 2	-0.203
4556.69327	0.00635	6.0×10^{-56}	0 0 0	2 0 0	8 3 6	9 4 5	-0.159
4557.35287	0.00209	3.1×10^{-56}	0 0 0	2 0 0	5 5 1	6 6 0	-0.241
4557.35287	0.00410	9.6×10^{-57}	0 0 0	2 0 0	5 0 5	6 3 4	-0.162
4557.35287	0.00081	9.3×10^{-56}	0 0 0	2 0 0	5 5 0	6 6 1	-0.241
4558.46921	0.00051	8.7×10^{-56}	0 0 0	2 0 0	7 4 3	8 5 4	-0.193
4558.71382	0.00162	3.0×10^{-56}	0 0 0	2 0 0	7 4 4	8 5 3	-0.195
4562.48400	0.00135	3.3×10^{-56}	0 0 0	2 0 0	8 2 7	9 3 6	-0.140
4563.75116	0.00035	9.9×10^{-56}	0 0 0	2 0 0	6 5 2	7 6 1	-0.230
4563.75116	0.00103	3.3×10^{-56}	0 0 0	2 0 0	6 5 1	7 6 2	-0.229
4564.40686	0.00195	2.2×10^{-56}	0 0 0	2 0 0	8 4 4	9 5 5	-0.183
4565.10591	0.00091	7.4×10^{-56}	0 0 0	2 0 0	8 4 5	9 5 4	-0.182
4566.40440	0.00300	1.5×10^{-56}	0 0 0	2 0 0	9 3 7	10 4 6	-0.146
4569.78356	0.00388	4.6×10^{-56}	0 0 0	2 0 0	9 4 5	10 5 6	-0.178
4569.92986	0.00290	9.5×10^{-56}	0 0 0	2 0 0	7 5 2	8 6 3	-0.212
4570.18140	0.02113	5.8×10^{-57}	0 0 0	2 0 0	6 0 6	7 3 5	-0.106
4571.52962	0.00249	1.9×10^{-56}	0 0 0	2 0 0	9 4 6	10 5 5	-0.168
4574.28451	0.00568	9.6×10^{-57}	0 0 0	2 0 0	10 4 6	11 5 7	-0.157
4574.34354	0.00128	2.9×10^{-56}	0 0 0	2 0 0	6 6 0	7 7 1	-0.252
4574.34354	0.00055	8.6×10^{-56}	0 0 0	2 0 0	6 6 1	7 7 0	-0.253
4575.89691	0.00218	8.3×10^{-56}	0 0 0	2 0 0	8 5 4	9 6 3	-0.207
4575.89691	0.00633	2.8×10^{-56}	0 0 0	2 0 0	8 5 3	9 6 4	-0.187
4577.85226	0.00117	3.2×10^{-56}	0 0 0	2 0 0	10 3 8	11 4 7	-0.130
4577.97149	0.00457	8.8×10^{-57}	0 0 0	2 0 0	11 4 7	12 5 8	-0.144
4579.08823	0.00421	9.2×10^{-57}	0 0 0	2 0 0	9 2 8	10 3 7	-0.133
4579.66645	0.00137	3.2×10^{-56}	0 0 0	2 0 0	7 6 2	8 7 1	-0.241
4579.66645	0.00055	9.8×10^{-56}	0 0 0	2 0 0	7 6 1	8 7 2	-0.232
4581.60615	0.00072	6.6×10^{-56}	0 0 0	2 0 0	9 5 4	10 6 5	-0.192
4581.67888	0.00192	2.2×10^{-56}	0 0 0	2 0 0	9 5 5	10 6 4	-0.188
4584.13193	0.00108	4.1×10^{-56}	0 0 0	2 0 0	7 0 7	8 3 6	-0.158
4587.08230	0.00208	1.6×10^{-56}	0 0 0	2 0 0	10 5 5	11 6 6	-0.179

Position	$\sigma_{\text{Pos.}}$	Intensity	$\nu_1\ \nu_2\ \nu_3$	$\nu_1'\ \nu_2'\ \nu_3'$	J K_a K_c	J' K_a' K_c'	$\Delta_{\text{SPEC.}}$
4587.28668	0.00075	5.0×10^{-56}	0 0 0	2 0 0	10 5 6	11 6 5	-0.176
4590.20929	0.00190	2.5×10^{-56}	0 0 0	2 0 0	9 6 4	10 7 3	-0.206
4590.26584	0.00070	7.6×10^{-56}	0 0 0	2 0 0	9 6 3	10 7 4	-0.203
4592.24944	0.00122	3.2×10^{-56}	0 0 0	2 0 0	11 5 6	12 6 7	-0.165
4592.81550	0.02337	1.2×10^{-56}	0 0 0	2 0 0	11 5 7	12 6 6	-0.131
4593.87265	0.00177	2.0×10^{-56}	0 0 0	2 0 0	12 4 9	13 5 8	-0.117
4594.89330	0.00069	6.7×10^{-56}	0 0 0	2 0 0	7 1 6	8 4 5	-0.167
4595.38393	0.00064	5.8×10^{-56}	0 0 0	2 0 0	10 6 5	11 7 4	-0.189
4595.45787	0.00192	1.9×10^{-56}	0 0 0	2 0 0	10 6 4	11 7 5	-0.191
4596.96877	0.00742	6.4×10^{-57}	0 0 0	2 0 0	12 5 7	13 6 8	-0.152
4597.04172	0.00158	3.5×10^{-56}	0 0 0	2 0 0	10 2 9	11 3 8	-0.156
4598.26787	0.00160	2.4×10^{-56}	0 0 0	2 0 0	12 5 8	13 6 7	-0.151
4598.29218	0.00037	1.1×10^{-55}	0 0 0	2 0 0	8 0 8	9 3 7	-0.139
4600.55227	0.00570	4.1×10^{-56}	0 0 0	2 0 0	11 6 5	12 7 6	-0.176
4600.71187	0.00446	1.0×10^{-56}	0 0 0	2 0 0	10 1 10	10 4 7	-0.146
4600.96887	0.00378	1.0×10^{-56}	0 0 0	2 0 0	13 5 8	14 6 9	-0.140
4602.66904	0.00105	5.7×10^{-56}	0 0 0	2 0 0	8 1 7	9 4 6	-0.152
4603.63040	0.00040	1.1×10^{-55}	0 0 0	2 0 0	9 1 9	10 2 8	-0.123
4605.40365	0.00127	2.8×10^{-56}	0 0 0	2 0 0	12 6 7	13 7 6	-0.156
4605.53371	0.00896	8.9×10^{-57}	0 0 0	2 0 0	12 6 6	13 7 7	-0.160
4610.38428	0.01007	1.6×10^{-56}	0 0 0	2 0 0	13 6 7	14 7 8	-0.149
4612.16977	0.01172	2.9×10^{-57}	0 0 0	2 0 0	8 8 1	9 9 0	-0.175
4614.07817	0.00790	5.4×10^{-57}	0 0 0	2 0 0	9 7 2	10 8 3	-0.269
4614.72651	0.00114	3.7×10^{-56}	0 0 0	2 0 0	11 2 10	12 3 9	-0.102
4614.96829	0.00342	1.0×10^{-56}	0 0 0	2 0 0	14 6 9	15 7 8	-0.127
4615.08996	0.02228	3.1×10^{-57}	0 0 0	2 0 0	14 6 8	15 7 9	-0.127
4615.08996	0.00767	9.7×10^{-57}	0 0 0	2 0 0	14 4 11	15 5 10	-0.077
4616.26121	0.00171	2.8×10^{-56}	0 0 0	2 0 0	9 0 9	10 3 8	-0.150
4616.98229	0.00051	2.0×10^{-55}	0 0 0	2 0 0	9 1 8	10 4 7	-0.149
4619.04162	0.00405	8.0×10^{-57}	0 0 0	2 0 0	14 7 8	15 8 7	-0.147
4619.54663	0.00656	4.9×10^{-57}	0 0 0	2 0 0	15 6 9	16 7 10	-0.108
4621.89460	0.00329	1.0×10^{-56}	0 0 0	2 0 0	13 3 11	14 4 10	-0.078
4622.06342	0.00749	6.7×10^{-57}	0 0 0	2 0 0	10 7 4	11 8 3	-0.196
4627.71872	0.00331	1.3×10^{-56}	0 0 0	2 0 0	10 1 9	11 4 8	-0.150
4629.62283	0.03782	6.5×10^{-57}	0 0 0	2 0 0	11 7 4	12 8 5	-0.208
4632.09804	0.01272	2.4×10^{-57}	0 0 0	2 0 0	7 2 5	8 5 4	-0.133
4638.32728	0.00510	1.1×10^{-56}	0 0 0	2 0 0	9 2 7	10 5 6	-0.149
4639.05742	0.00223	1.6×10^{-56}	0 0 0	2 0 0	12 2 11	13 3 10	-0.114
4640.63625	0.00395	9.6×10^{-57}	0 0 0	2 0 0	11 1 10	12 4 9	-0.140
4641.11748	0.00588	6.8×10^{-57}	0 0 0	2 0 0	16 4 13	17 5 12	-0.044
4643.87893	0.00716	4.1×10^{-57}	0 0 0	2 0 0	13 7 6	14 8 7	-0.228

Position	$\sigma_{\text{Pos.}}$	Intensity	$\nu_1\,\nu_2\,\nu_3$	$\nu_1'\,\nu_2'\,\nu_3'$	J K_a K_c	J' K_a' K_c'	$\Delta_{\text{SPEC.}}$
4649.56021	0.00270	1.7×10^{-56}	0 0 0	2 0 0	14 3 12	15 4 11	-0.106
4649.61099	0.00387	1.3×10^{-56}	0 0 0	2 0 0	11 2 9	12 5 8	-0.148

A.2.3.4 T$_2$O $2\nu_2 + \nu_3$ band

Here, the lines assigned to the $2\nu_2 + \nu_3$ band of T$_2$O obtained from the $10\,\text{GBq}$ sample are presented. These lines are published in [Her23]. For further information, see Section 5.5.3.

Table A.16: Linelist of the T$_2$O $2\nu_2 + \nu_3$ band. The columns present the assigned line position, the uncertainty on the position $\sigma_{\text{Pos.}}$, the line intensity taking natural abundance into account, lower and upper vibrational quanta, lower and upper rotational quanta and the deviation to the predictions from SPECTRA database $\Delta_{\text{SPEC.}}$.

Position	$\sigma_{\text{Pos.}}$	Intensity	$\nu_1\,\nu_2\,\nu_3$	$\nu_1'\,\nu_2'\,\nu_3'$	J K_a K_c	J' K_a' K_c'	$\Delta_{\text{SPEC.}}$
4300.67491	0.00059	6.6×10^{-56}	0 0 0	0 2 1	4 1 4	3 1 3	0.162
4301.11091	0.00077	4.7×10^{-56}	0 0 0	0 2 1	4 2 3	3 2 2	0.151
4304.10000	0.00056	5.2×10^{-56}	0 0 0	0 2 1	3 1 2	2 1 1	0.154
4304.27146	0.00262	1.6×10^{-56}	0 0 0	0 2 1	5 4 1	4 4 0	0.131
4304.46375	0.00335	9.5×10^{-57}	0 0 0	0 2 1	6 5 2	5 5 1	0.129
4305.55404	0.00379	7.7×10^{-57}	0 0 0	0 2 1	4 3 1	3 3 0	0.143
4305.68861	0.00160	2.3×10^{-56}	0 0 0	0 2 1	4 3 2	3 3 1	0.140
4305.77985	0.00047	6.1×10^{-56}	0 0 0	0 2 1	3 0 3	2 0 2	0.155
4305.87588	0.00365	5.8×10^{-57}	0 0 0	0 2 1	7 6 1	6 6 0	0.107
4308.13362	0.00169	1.8×10^{-56}	0 0 0	0 2 1	3 1 3	2 1 2	0.154
4308.26343	0.00100	3.0×10^{-56}	0 0 0	0 2 1	3 2 1	2 2 0	0.147
4309.15702	0.00400	1.0×10^{-56}	0 0 0	0 2 1	3 2 2	2 2 1	0.147
4312.77646	0.00379	1.1×10^{-56}	0 0 0	0 2 1	2 1 1	1 1 0	0.164
4313.35578	0.00166	1.5×10^{-56}	0 0 0	0 2 1	2 0 2	1 0 1	0.155
4314.65147	0.00629	6.4×10^{-57}	0 0 0	0 2 1	7 2 5	7 2 6	0.156
4315.63082	0.00127	3.3×10^{-56}	0 0 0	0 2 1	2 1 2	1 1 1	0.152
4320.98429	0.00251	1.2×10^{-56}	0 0 0	0 2 1	3 1 2	3 1 3	0.154
4321.33582	0.00114	2.5×10^{-56}	0 0 0	0 2 1	1 0 1	0 0 0	0.152
4325.64540	0.00617	4.7×10^{-57}	0 0 0	0 2 1	9 3 6	9 3 7	0.164
4325.78853	0.00455	6.1×10^{-57}	0 0 0	0 2 1	2 1 1	2 1 2	0.149
4326.76696	0.00297	1.6×10^{-56}	0 0 0	0 2 1	5 2 3	5 2 4	0.155
4329.01036	0.00089	3.6×10^{-56}	0 0 0	0 2 1	1 1 0	1 1 1	0.151
4330.44128	0.00457	8.3×10^{-57}	0 0 0	0 2 1	4 2 2	4 2 3	0.152
4332.19646	0.00357	1.2×10^{-56}	0 0 0	0 2 1	1 1 1	1 1 0	0.152
4332.58010	0.00251	4.0×10^{-56}	0 0 0	0 2 1	3 2 1	3 2 2	0.147
4333.53518	0.00138	2.2×10^{-56}	0 0 0	0 2 1	2 2 0	2 2 1	0.147
4334.02283	0.00059	6.6×10^{-56}	0 0 0	0 2 1	2 2 1	2 2 0	0.147

Position	$\sigma_{\text{Pos.}}$	Intensity	$\nu_1\,\nu_2\,\nu_3$	$\nu_1'\,\nu_2'\,\nu_3'$	J K$_a$ K$_c$	J' K$_a$' K$_c$'	$\Delta_{\text{SPEC.}}$
4334.87448	0.00225	1.4×10^{-56}	0 0 0	0 2 1	7 3 4	7 3 5	0.154
4334.93407	0.00259	1.3×10^{-56}	0 0 0	0 2 1	3 2 2	3 2 1	0.140
4335.33625	0.00247	1.8×10^{-56}	0 0 0	0 2 1	2 1 2	2 1 1	0.147
4337.07830	0.00145	2.5×10^{-56}	0 0 0	0 2 1	4 2 3	4 2 2	0.149
4337.14535	0.00382	7.3×10^{-57}	0 0 0	0 2 1	6 3 3	6 3 4	0.148
4337.72714	0.00367	8.4×10^{-57}	0 0 0	0 2 1	0 0 0	1 0 1	0.156
4338.29404	0.00393	3.4×10^{-56}	0 0 0	0 2 1	5 3 2	5 3 3	0.146
4338.76546	0.00193	1.7×10^{-56}	0 0 0	0 2 1	4 3 1	4 3 2	0.146
4338.90538	0.00073	7.9×10^{-56}	0 0 0	0 2 1	3 3 0	3 3 1	0.139
4338.95809	0.00143	2.6×10^{-56}	0 0 0	0 2 1	3 3 1	3 3 0	0.144
4339.08878	0.00087	5.2×10^{-56}	0 0 0	0 2 1	4 3 2	4 3 1	0.143
4339.55364	0.00289	1.1×10^{-56}	0 0 0	0 2 1	5 3 3	5 3 2	0.144
4340.71602	0.00169	2.2×10^{-56}	0 0 0	0 2 1	6 3 4	6 3 3	0.148
4340.79832	0.00604	5.2×10^{-57}	0 0 0	0 2 1	5 2 4	5 2 3	0.157
4343.03902	0.00954	4.5×10^{-57}	0 0 0	0 2 1	7 3 5	7 3 4	0.154
4344.13332	0.00440	8.3×10^{-57}	0 0 0	0 2 1	9 4 5	9 4 6	0.142
4345.22332	0.00328	1.2×10^{-56}	0 0 0	0 2 1	1 1 1	2 1 2	0.152
4345.26829	0.01160	4.6×10^{-57}	0 0 0	0 2 1	8 4 4	8 4 5	0.154
4345.63237	0.00065	4.8×10^{-56}	0 0 0	0 2 1	1 0 1	2 0 2	0.153
4345.73661	0.00147	2.2×10^{-56}	0 0 0	0 2 1	7 4 3	7 4 4	0.138
4345.86186	0.00943	2.5×10^{-56}	0 0 0	0 2 1	4 4 0	4 4 1	0.121
4345.88698	0.00196	7.4×10^{-56}	0 0 0	0 2 1	4 4 1	4 4 0	0.142
4345.90618	0.00160	5.0×10^{-56}	0 0 0	0 2 1	5 4 1	5 4 2	0.136
4345.93973	0.00264	1.7×10^{-56}	0 0 0	0 2 1	5 4 2	5 4 1	0.136
4346.05417	0.00132	3.3×10^{-56}	0 0 0	0 2 1	6 4 3	6 4 2	0.134
4346.11357	0.00476	7.7×10^{-57}	0 0 0	0 2 1	4 1 4	4 1 3	0.152
4346.18612	0.00471	9.7×10^{-57}	0 0 0	0 2 1	6 2 5	6 2 4	0.162
4346.32009	0.00495	7.2×10^{-57}	0 0 0	0 2 1	7 4 4	7 4 3	0.138
4346.91568	0.01023	1.4×10^{-56}	0 0 0	0 2 1	8 4 5	8 4 4	0.145
4348.72018	0.00095	3.4×10^{-56}	0 0 0	0 2 1	1 1 0	2 1 1	0.150
4352.22410	0.00063	5.8×10^{-56}	0 0 0	0 2 1	2 1 2	3 1 3	0.151
4353.03594	0.00166	2.2×10^{-56}	0 0 0	0 2 1	2 0 2	3 0 3	0.153
4354.35945	0.00943	2.0×10^{-56}	0 0 0	0 2 1	5 5 1	5 5 0	0.115
4354.36400	0.00305	5.9×10^{-56}	0 0 0	0 2 1	5 5 0	5 5 1	0.120
4354.55229	0.00556	1.3×10^{-56}	0 0 0	0 2 1	6 5 1	6 5 2	0.115
4354.56077	0.00170	4.0×10^{-56}	0 0 0	0 2 1	6 5 2	6 5 1	0.121
4354.62418	0.00797	3.9×10^{-57}	0 0 0	0 2 1	11 5 6	11 5 7	0.128
4354.75594	0.00111	2.6×10^{-56}	0 0 0	0 2 1	7 5 2	7 5 3	0.120
4354.77861	0.00386	8.8×10^{-57}	0 0 0	0 2 1	7 5 3	7 5 2	0.125
4354.93747	0.00452	5.7×10^{-57}	0 0 0	0 2 1	8 5 3	8 5 4	0.121
4355.01136	0.00176	1.7×10^{-56}	0 0 0	0 2 1	8 5 4	8 5 3	0.121

Position	$\sigma_{\text{Pos.}}$	Intensity	$\nu_1\ \nu_2\ \nu_3$	$\nu_1'\ \nu_2'\ \nu_3'$	J K_a K_c	J' K_a' K_c'	$\Delta_{\text{SPEC.}}$
4355.05288	0.00289	1.1×10^{-56}	0 0 0	0 2 1	9 5 4	9 5 5	0.125
4355.69785	0.00559	6.9×10^{-57}	0 0 0	0 2 1	10 5 6	10 5 5	0.127
4357.67612	0.00440	1.9×10^{-56}	0 0 0	0 2 1	2 1 1	3 1 2	0.151
4358.34002	0.00238	3.2×10^{-56}	0 0 0	0 2 1	2 2 1	3 2 2	0.148
4358.97045	0.00298	2.4×10^{-56}	0 0 0	0 2 1	3 1 3	4 1 4	0.153
4359.32117	0.00667	1.1×10^{-56}	0 0 0	0 2 1	2 2 0	3 2 1	0.149
4359.82987	0.00052	7.6×10^{-56}	0 0 0	0 2 1	3 0 3	4 0 4	0.153
4359.93531	0.01078	2.7×10^{-57}	0 0 0	0 2 1	10 3 8	10 3 7	0.168
4361.47980	0.00982	4.0×10^{-57}	0 0 0	0 2 1	6 1 6	6 1 5	0.163
4364.12730	0.00710	1.3×10^{-56}	0 0 0	0 2 1	6 6 0	6 6 1	0.104
4364.12730	0.00242	4.0×10^{-56}	0 0 0	0 2 1	6 6 1	6 6 0	0.104
4364.91281	0.00137	2.6×10^{-56}	0 0 0	0 2 1	7 6 1	7 6 2	0.092
4364.91281	0.00313	8.5×10^{-57}	0 0 0	0 2 1	7 6 2	7 6 1	0.092
4365.44369	0.00052	7.9×10^{-56}	0 0 0	0 2 1	4 1 4	5 1 5	0.152
4365.61879	0.00888	5.4×10^{-57}	0 0 0	0 2 1	8 6 2	8 6 3	0.066
4365.63967	0.00484	1.6×10^{-56}	0 0 0	0 2 1	8 6 3	8 6 2	0.085
4366.11896	0.00134	2.7×10^{-56}	0 0 0	0 2 1	4 0 4	5 0 5	0.154
4366.43163	0.00059	6.8×10^{-56}	0 0 0	0 2 1	3 1 2	4 1 3	0.153
4368.55144	0.00092	5.0×10^{-56}	0 0 0	0 2 1	3 2 1	4 2 2	0.149
4371.65193	0.00189	2.7×10^{-56}	0 0 0	0 2 1	5 1 5	6 1 6	0.148
4372.09407	0.00049	8.1×10^{-56}	0 0 0	0 2 1	5 0 5	6 0 6	0.153
4372.16230	0.00517	8.4×10^{-57}	0 0 0	0 2 1	3 3 1	4 3 2	0.140
4372.30017	0.00204	2.5×10^{-56}	0 0 0	0 2 1	3 3 0	4 3 1	0.137
4372.87831	0.00659	1.2×10^{-56}	0 0 0	0 2 1	8 7 2	8 7 1	0.054
4373.99507	0.00139	6.0×10^{-56}	0 0 0	0 2 1	4 2 3	5 2 4	0.148
4374.84337	0.00192	2.4×10^{-56}	0 0 0	0 2 1	4 1 3	5 1 4	0.153
4374.87463	0.01768	8.3×10^{-57}	0 0 0	0 2 1	7 7 1	7 7 0	0.087
4374.87463	0.00612	2.5×10^{-56}	0 0 0	0 2 1	7 7 0	7 7 1	0.087
4377.62555	0.00064	7.6×10^{-56}	0 0 0	0 2 1	6 1 6	7 1 7	0.151
4377.89738	0.00212	2.5×10^{-56}	0 0 0	0 2 1	6 0 6	7 0 7	0.161
4378.03644	0.00201	2.0×10^{-56}	0 0 0	0 2 1	4 2 2	5 2 3	0.151
4380.51958	0.00119	3.9×10^{-56}	0 0 0	0 2 1	4 3 2	5 3 3	0.141
4380.99196	0.00255	1.3×10^{-56}	0 0 0	0 2 1	4 3 1	5 3 2	0.139
4381.47525	0.00195	2.1×10^{-56}	0 0 0	0 2 1	5 2 4	6 2 5	0.149
4382.76915	0.00054	7.0×10^{-56}	0 0 0	0 2 1	5 1 4	6 1 5	0.156
4383.38776	0.00203	2.3×10^{-56}	0 0 0	0 2 1	7 1 7	8 1 8	0.160
4383.55753	0.00053	6.8×10^{-56}	0 0 0	0 2 1	7 0 7	8 0 8	0.152
4384.64060	0.00449	4.7×10^{-57}	0 0 0	0 2 1	10 8 3	10 8 2	0.063
4386.31578	0.00273	1.4×10^{-56}	0 0 0	0 2 1	8 8 1	8 8 0	0.064
4386.31578	0.00576	4.6×10^{-57}	0 0 0	0 2 1	8 8 0	8 8 1	0.064
4387.50725	0.00886	1.7×10^{-56}	0 0 0	0 2 1	4 4 1	5 4 2	0.134

Position	$\sigma_{\text{Pos.}}$	Intensity	$\nu_1\ \nu_2\ \nu_3$	$\nu_1'\ \nu_2'\ \nu_3'$	J K_a K_c	J' K_a' K_c'	$\Delta_{\text{SPEC.}}$
4387.50725	0.00256	6.0×10^{-56}	0 0 0	0 2 1	5 2 3	6 2 4	0.153
4388.68838	0.00067	5.9×10^{-56}	0 0 0	0 2 1	6 2 5	7 2 6	0.155
4388.83240	0.00375	1.5×10^{-56}	0 0 0	0 2 1	5 3 3	6 3 4	0.146
4388.94981	0.00065	5.8×10^{-56}	0 0 0	0 2 1	8 1 8	9 1 9	0.153
4389.20785	0.00299	1.9×10^{-56}	0 0 0	0 2 1	8 0 8	9 0 9	0.153
4390.11012	0.00182	2.1×10^{-56}	0 0 0	0 2 1	6 1 5	7 1 6	0.156
4393.69336	0.00087	4.4×10^{-56}	0 0 0	0 2 1	9 0 9	10 0 10	0.137
4394.43658	0.00274	1.5×10^{-56}	0 0 0	0 2 1	9 1 9	10 1 10	0.148
4396.04461	0.00292	2.6×10^{-56}	0 0 0	0 2 1	5 4 1	6 4 2	0.129
4396.74850	0.01152	1.9×10^{-56}	0 0 0	0 2 1	6 2 4	7 2 5	0.159
4396.92636	0.00097	5.3×10^{-56}	0 0 0	0 2 1	7 1 6	8 1 7	0.154
4397.02905	0.00104	4.4×10^{-56}	0 0 0	0 2 1	6 3 4	7 3 5	0.146
4398.92065	0.00098	3.5×10^{-56}	0 0 0	0 2 1	10 1 10	11 1 11	0.148
4399.39292	0.00294	1.4×10^{-56}	0 0 0	0 2 1	6 3 3	7 3 4	0.146
4402.25692	0.00239	4.4×10^{-56}	0 0 0	0 2 1	8 2 7	9 2 8	0.149
4403.48809	0.00291	1.4×10^{-56}	0 0 0	0 2 1	8 1 7	9 1 8	0.148
4404.18651	0.00631	9.2×10^{-57}	0 0 0	0 2 1	11 1 11	12 1 12	0.157
4404.22528	0.00167	2.8×10^{-56}	0 0 0	0 2 1	11 0 11	12 0 12	0.156
4404.45740	0.00390	1.0×10^{-56}	0 0 0	0 2 1	5 5 0	6 5 1	0.107
4404.48995	0.00157	2.8×10^{-56}	0 0 0	0 2 1	6 4 3	7 4 4	0.128
4404.69636	0.00545	9.5×10^{-57}	0 0 0	0 2 1	6 4 2	7 4 3	0.131
4405.06501	0.00478	1.2×10^{-56}	0 0 0	0 2 1	7 3 5	8 3 6	0.150
4405.59936	0.00087	4.8×10^{-56}	0 0 0	0 2 1	7 2 5	8 2 6	0.162
4408.66318	0.00396	1.2×10^{-56}	0 0 0	0 2 1	9 2 8	10 2 9	0.151
4409.02412	0.00555	2.0×10^{-56}	0 0 0	0 2 1	12 1 12	13 1 13	0.159
4409.02412	0.01542	6.7×10^{-57}	0 0 0	0 2 1	12 0 12	13 0 13	0.147
4409.06546	0.00121	3.9×10^{-56}	0 0 0	0 2 1	7 3 4	8 3 5	0.152
4412.86657	0.00114	3.3×10^{-56}	0 0 0	0 2 1	8 3 6	9 3 7	0.151
4413.00811	0.00442	9.0×10^{-57}	0 0 0	0 2 1	7 4 4	8 4 5	0.132
4413.07538	0.00246	1.5×10^{-56}	0 0 0	0 2 1	6 5 2	7 5 3	0.114
4413.53323	0.00176	2.7×10^{-56}	0 0 0	0 2 1	7 4 3	8 4 4	0.138
4413.64194	0.01951	1.4×10^{-56}	0 0 0	0 2 1	13 0 13	14 0 14	0.146
4413.92993	0.00954	8.1×10^{-57}	0 0 0	0 2 1	10 1 9	11 1 10	0.157
4413.92993	0.00646	1.3×10^{-56}	0 0 0	0 2 1	8 2 6	9 2 7	0.168
4414.89464	0.00179	2.6×10^{-56}	0 0 0	0 2 1	10 2 9	11 2 10	0.167
4418.07890	0.00673	9.2×10^{-57}	0 0 0	0 2 1	14 1 14	15 1 15	0.150
4418.80265	0.01211	1.1×10^{-56}	0 0 0	0 2 1	8 3 5	9 3 6	0.160
4420.12331	0.00218	1.9×10^{-56}	0 0 0	0 2 1	11 1 10	12 1 11	0.155
4420.43734	0.00529	8.7×10^{-57}	0 0 0	0 2 1	9 3 7	10 3 8	0.168
4421.09276	0.01231	6.1×10^{-57}	0 0 0	0 2 1	11 2 10	12 2 11	0.155
4421.48819	0.00488	2.3×10^{-56}	0 0 0	0 2 1	8 4 5	9 4 6	0.140

Position	$\sigma_{\text{Pos.}}$	Intensity	$\nu_1\,\nu_2\,\nu_3$	$\nu_1'\,\nu_2'\,\nu_3'$	J K_a K_c	J' K_a' K_c'	$\Delta_{\text{SPEC.}}$
4421.61643	0.00152	2.9×10^{-56}	0 0 0	0 2 1	9 2 7	10 2 8	0.167
4421.72469	0.02741	5.3×10^{-57}	0 0 0	0 2 1	7 5 3	8 5 4	0.115
4421.75119	0.00332	1.6×10^{-56}	0 0 0	0 2 1	7 5 2	8 5 3	0.115
4422.34294	0.00495	5.9×10^{-57}	0 0 0	0 2 1	15 0 15	16 0 16	0.158
4422.61420	0.00517	7.8×10^{-57}	0 0 0	0 2 1	8 4 4	9 4 5	0.143
4427.72058	0.00580	1.9×10^{-56}	0 0 0	0 2 1	10 3 8	11 3 9	0.160
4428.34285	0.00495	2.5×10^{-56}	0 0 0	0 2 1	9 3 6	10 3 7	0.153
4428.63747	0.00490	7.0×10^{-57}	0 0 0	0 2 1	10 2 8	11 2 9	0.167
4429.87416	0.00765	6.3×10^{-57}	0 0 0	0 2 1	9 4 6	10 4 7	0.149
4430.39634	0.00254	1.5×10^{-56}	0 0 0	0 2 1	8 5 4	9 5 5	0.115
4431.46897	0.01022	9.2×10^{-57}	0 0 0	0 2 1	13 1 12	14 1 13	0.175
4431.98726	0.00105	1.9×10^{-56}	0 0 0	0 2 1	9 4 5	10 4 6	0.149
4435.12837	0.00241	1.5×10^{-56}	0 0 0	0 2 1	11 2 9	12 2 10	0.169
4436.70356	0.00647	5.9×10^{-57}	0 0 0	0 2 1	14 2 13	15 2 14	0.162
4438.10471	0.00301	1.4×10^{-56}	0 0 0	0 2 1	10 4 7	11 4 8	0.152
4439.05405	0.01803	4.1×10^{-57}	0 0 0	0 2 1	9 5 5	10 5 6	0.101
4439.27229	0.00356	1.2×10^{-56}	0 0 0	0 2 1	9 5 4	10 5 5	0.123
4441.61315	0.00962	4.7×10^{-57}	0 0 0	0 2 1	10 4 6	11 4 7	0.153
4441.61315	0.00533	9.4×10^{-57}	0 0 0	0 2 1	12 3 10	13 3 11	0.160
4447.71831	0.00417	9.4×10^{-57}	0 0 0	0 2 1	10 5 6	11 5 7	0.124
4450.33456	0.00605	5.6×10^{-57}	0 0 0	0 2 1	9 6 3	10 6 4	0.076
4451.35485	0.00643	1.0×10^{-56}	0 0 0	0 2 1	11 4 7	12 4 8	0.171

A.3 Comparison of experimental data with SPECTRA database

A.3.1 Analysis on quantum number J

In this chapter the analysis on the quantum number J, more precisely $\hat{J}^2$ (cf. Section 5.8) is extended on all bands of this work. The experimental data are compared with the SPECTRA database[1] [Mik05].

---

[1]www.spectra.ru
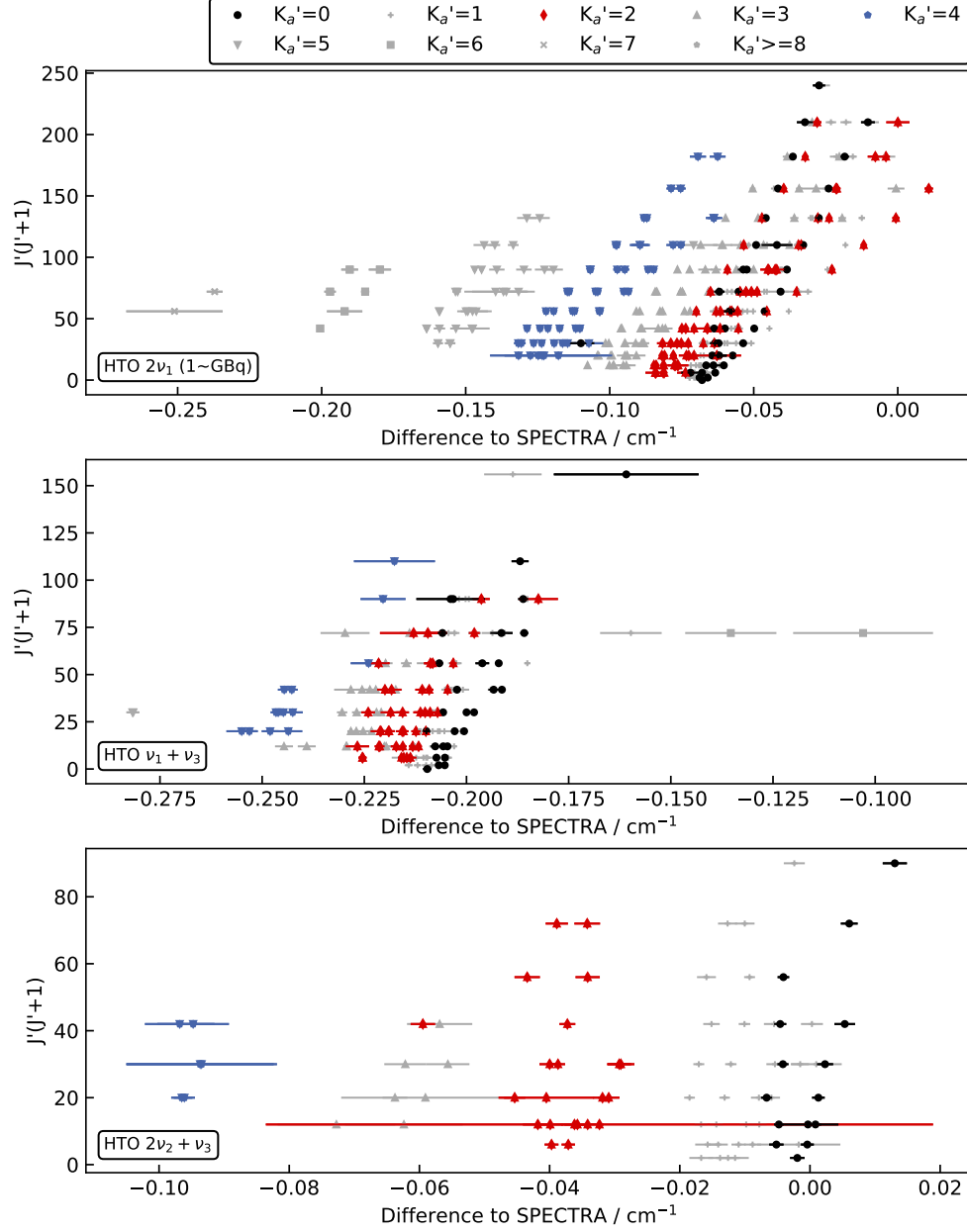
Figure A.1: Difference of the experimental data of the HTO $2\nu_1$, $\nu_1 + \nu_3$ and $2\nu_2 + \nu_3$ from the 1 GBq sample to SPECTRA database [Mik05]. The quantum number $K_a' = 3, 4$ and 5 of the individual lines are highlighted.
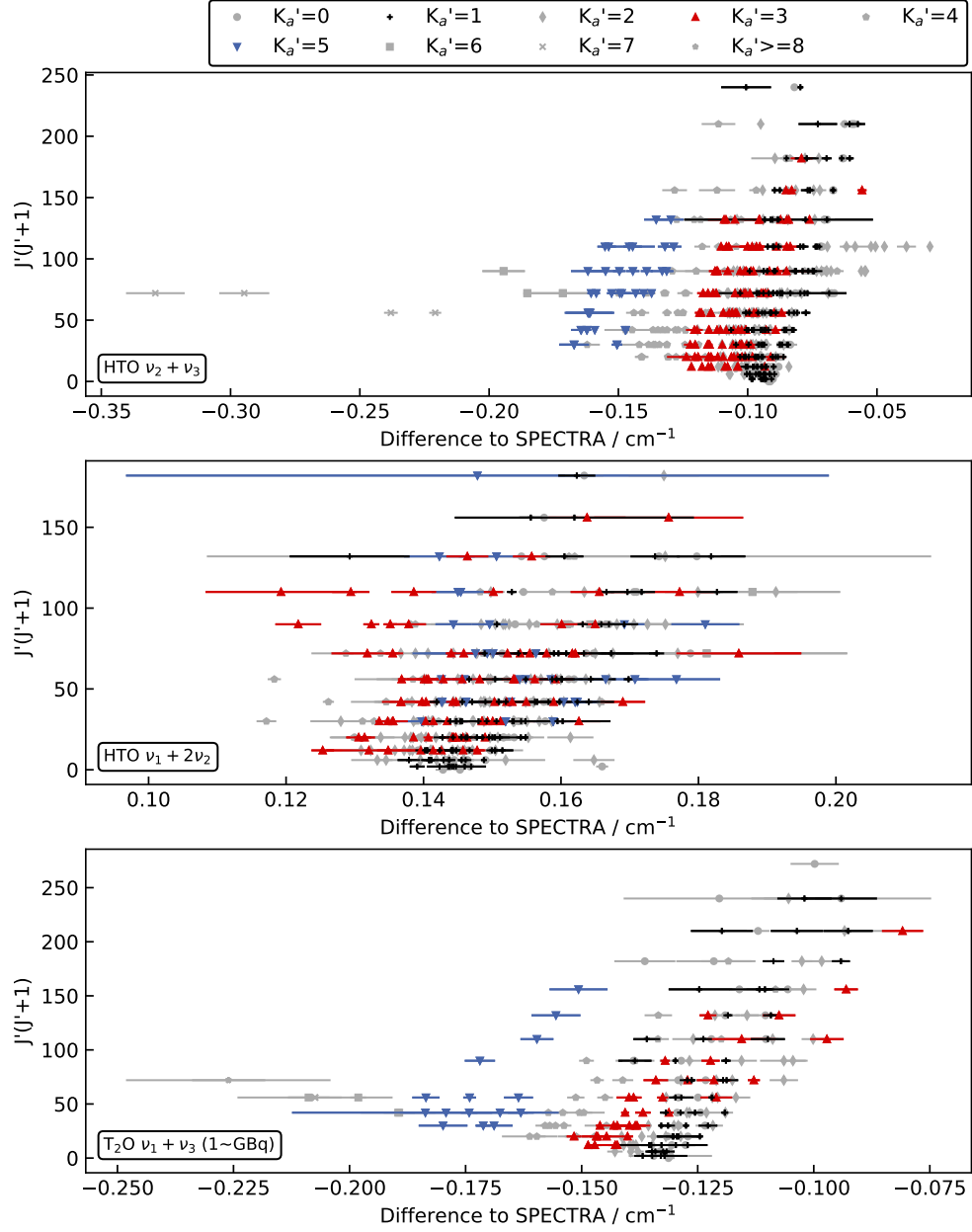
Figure A.2: Difference of the experimental data of the HTO $\nu_2 + \nu_3$, $\nu_1 + 2\nu_2$ and T$_2$O $\nu_1 + \nu_3$ from the 1 GBq sample to to SPECTRA database [Mik05]. The quantum number $K'_a = 3, 4$ and 5 of the individual lines are highlighted.
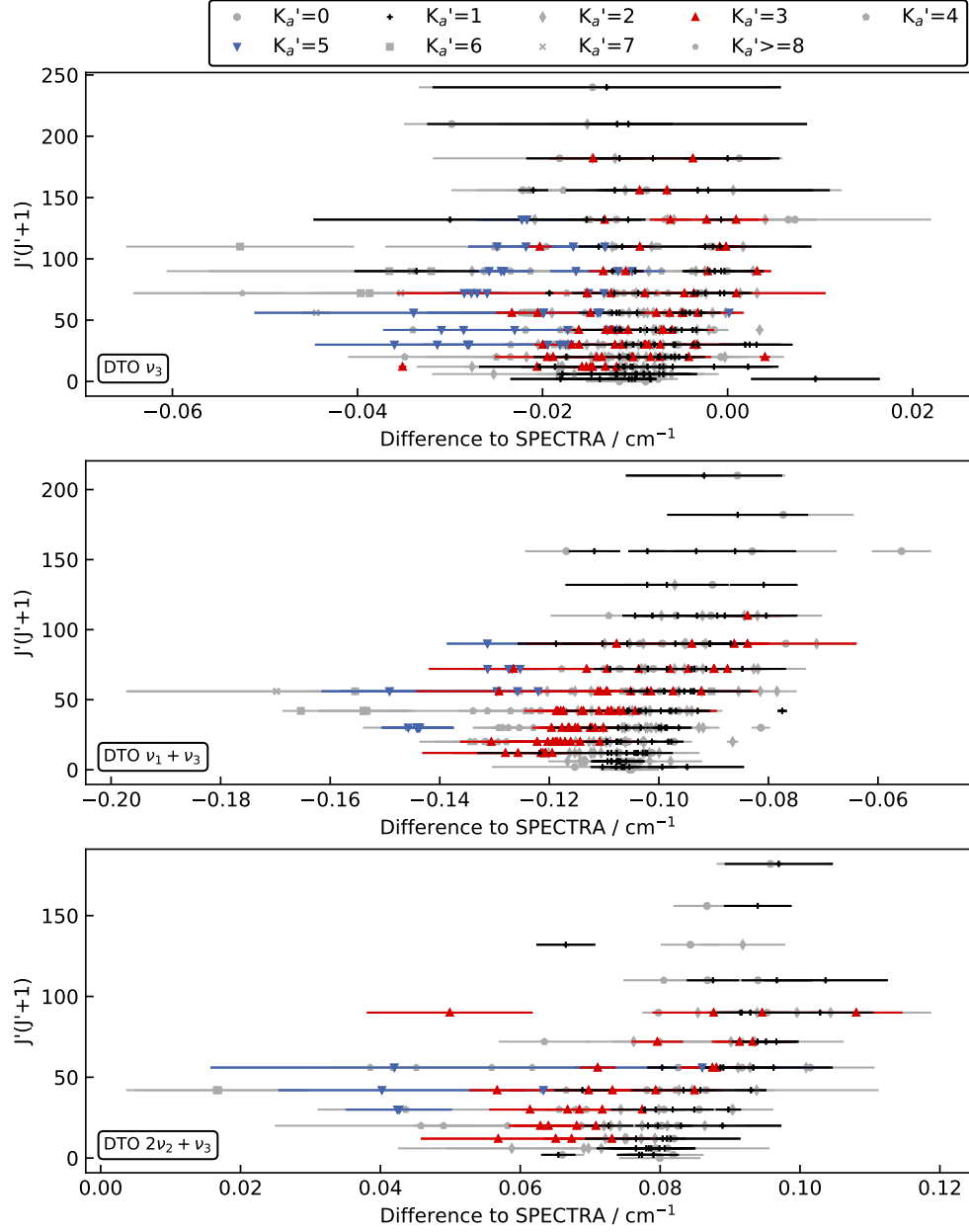
Figure A.3: Difference of the experimental data of the DTO ν_3 of the 1 GBq sample and the $\nu_1 + \nu_3$ and $2\nu_2 + \nu_3$ of the 10 GBq sample to SPECTRA database [Mik05]. The quantum number K_a' = 3, 4 and 5 of the individual lines are highlighted.
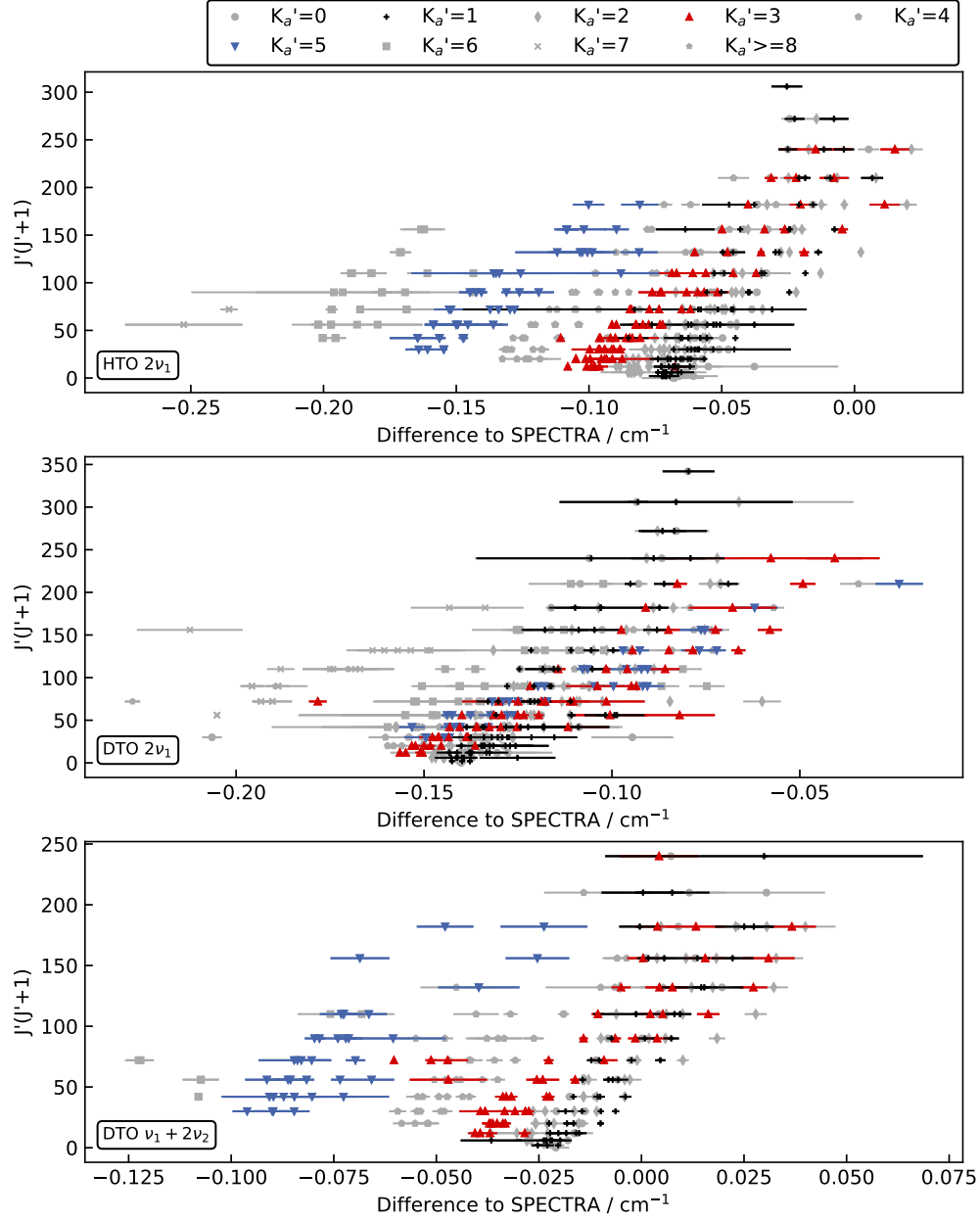
Figure A.4: Difference of the experimental data of the HTO $2\nu_1$, DTO $2\nu_1$ and $\nu_1 + 2\nu_2$ from the 10 GBq sample to SPECTRA database[Mik05]. The quantum number $K'_a = 3, 4$ and 5 of the individual lines are highlighted.
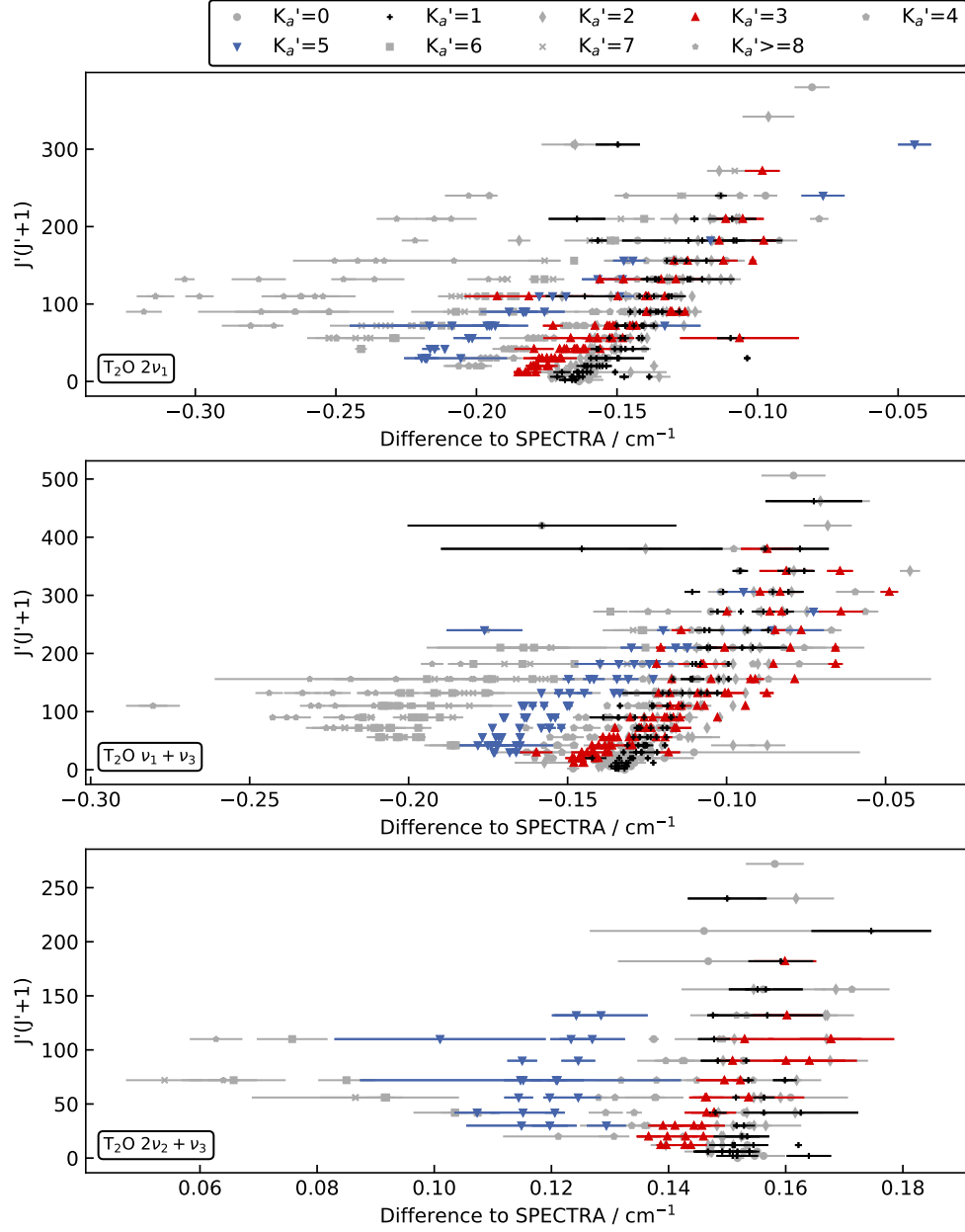
Figure A.5: Difference of the experimental data of the T_2O $2\nu_1$, $\nu_2 + \nu_3$ and $2\nu_2 + \nu_3$ from the 10 GBq sample to SPECTRA database[Mik05]. The quantum number $K'_a = 3, 4$ and 5 of the individual lines are highlighted.

A.3.2 Analysis on quantum number K_a

In this chapter the analysis on the quantum number K_a (cf. Section 5.8) is extended on all bands of this work. The experimental data are compared to the SPECTRA database[2] [Mik05].
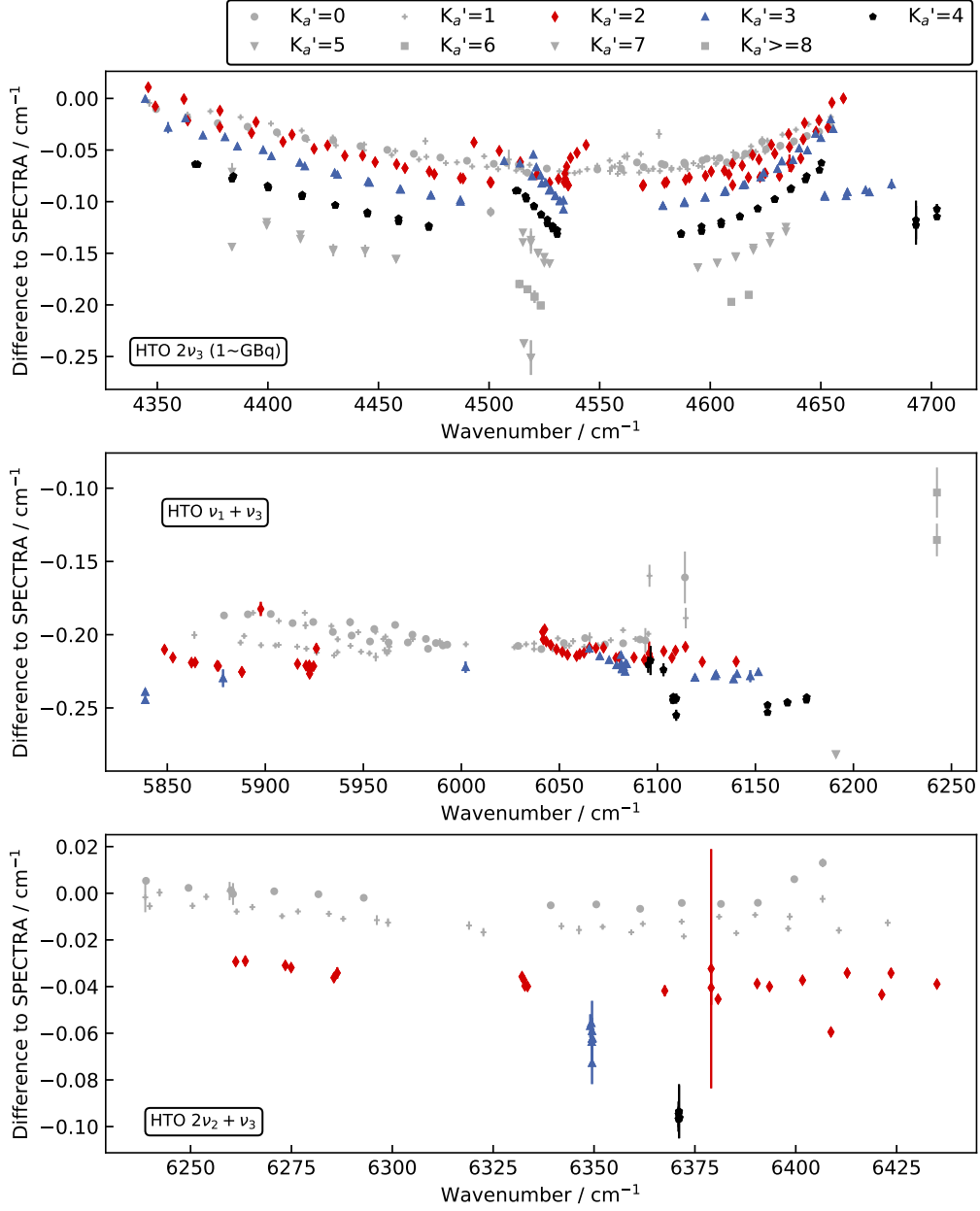
Figure A.6: Difference of the experimental data of the HTO $2\nu_1$, $\nu_1 + \nu_3$ and $2\nu_2 + \nu_3$ from the 1 GBq sample to SPECTRA database [Mik05]. The quantum number $K'_a = 3, 4$ and 5 of the individual lines are highlighted.
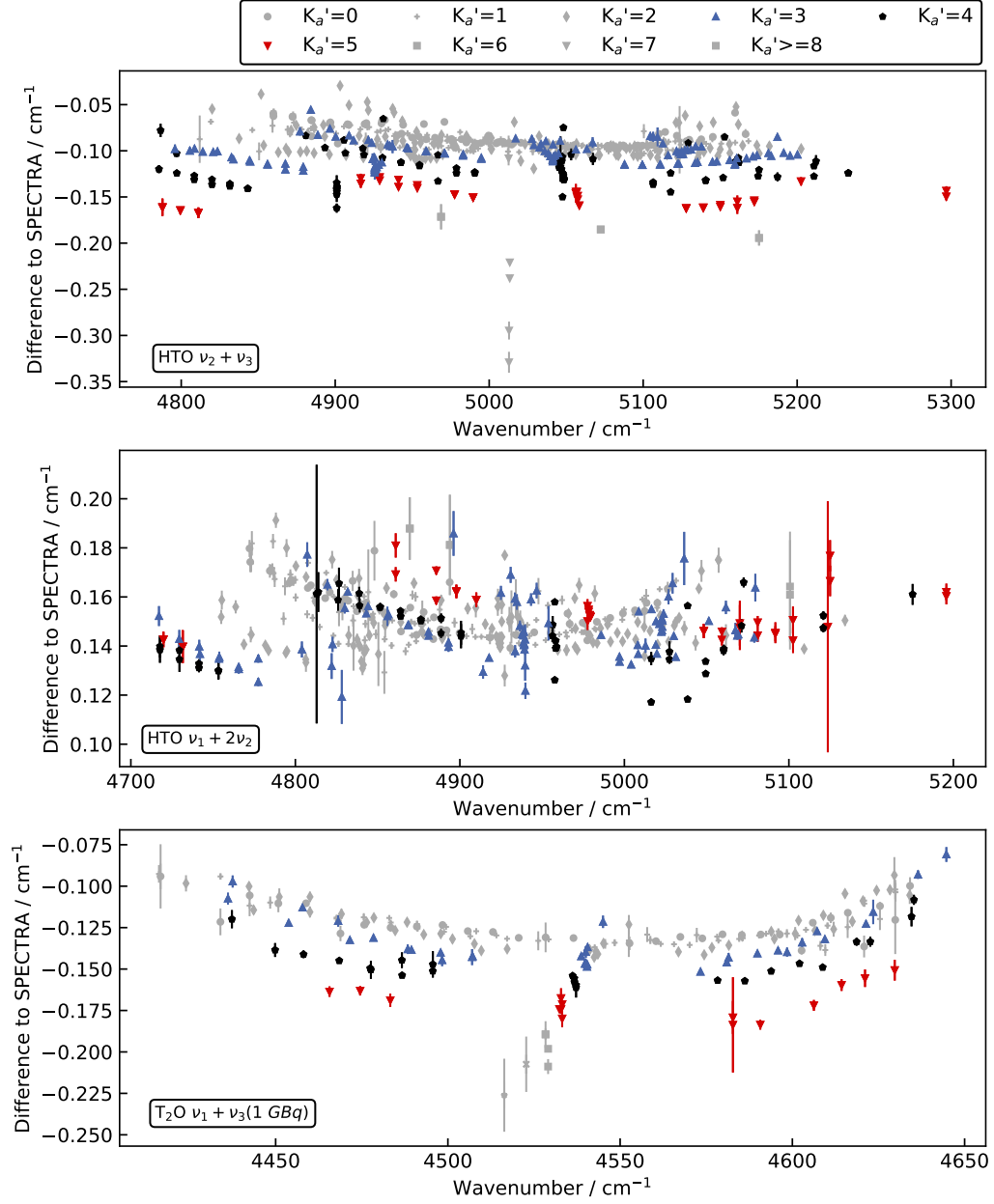
Figure A.7: Difference of the experimental data of the HTO $\nu_2 + \nu_3$, $\nu_1 + 2\nu_2$ and T$_2$O $\nu_1 + \nu_3$ from the 1 GBq sample to to SPECTRA database [Mik05]. The quantum number $K'_a = 3, 4$ and 5 of the individual lines are highlighted.
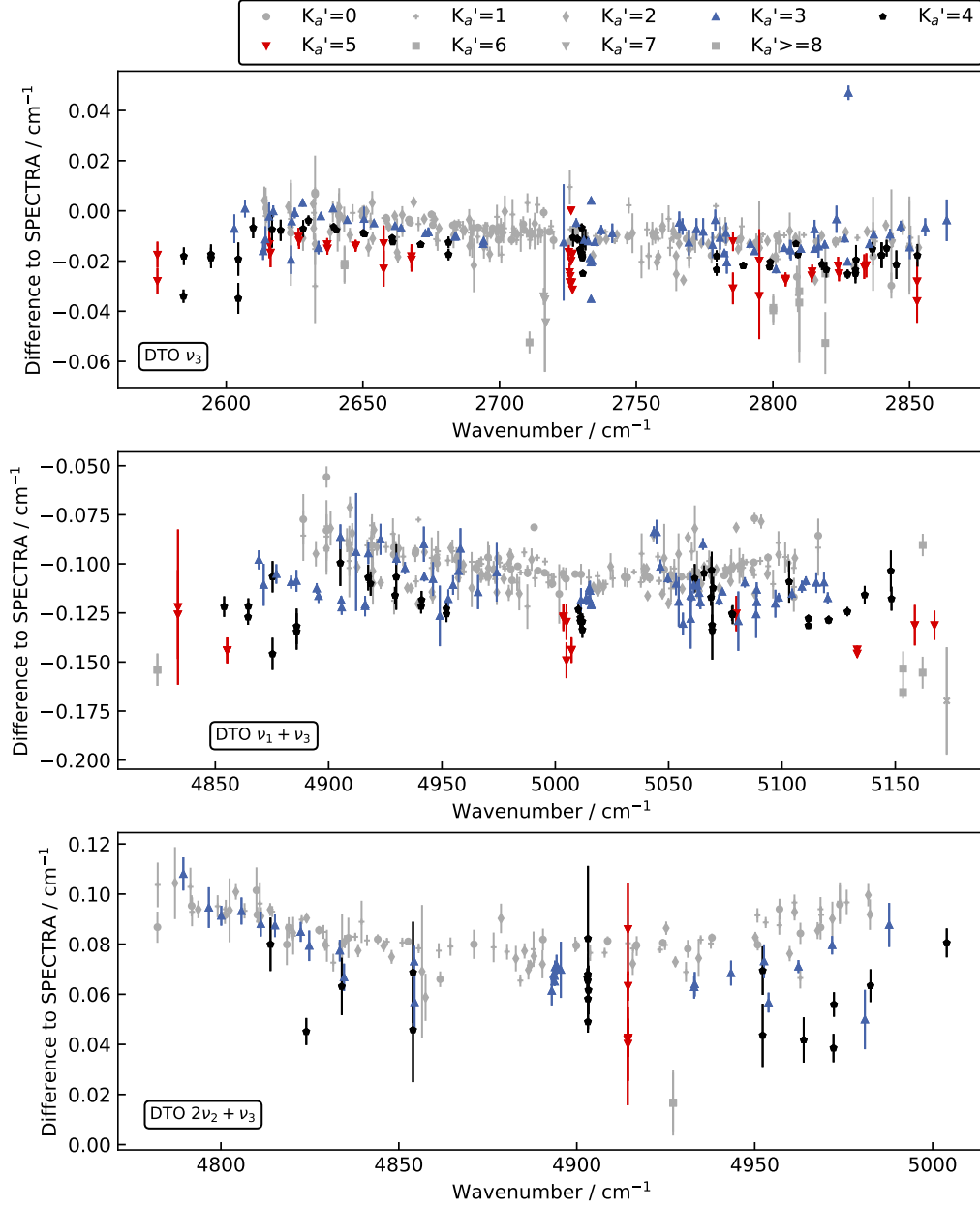
Figure A.8: Difference of the experimental data of the DTO ν_3 of the 1 GBq sample and the $\nu_1 + \nu_3$ and $2\nu_2 + \nu_3$ of the 10 GBq sample to SPECTRA database [Mik05]. The quantum number K_a' = 3, 4 and 5 of the individual lines are highlighted.
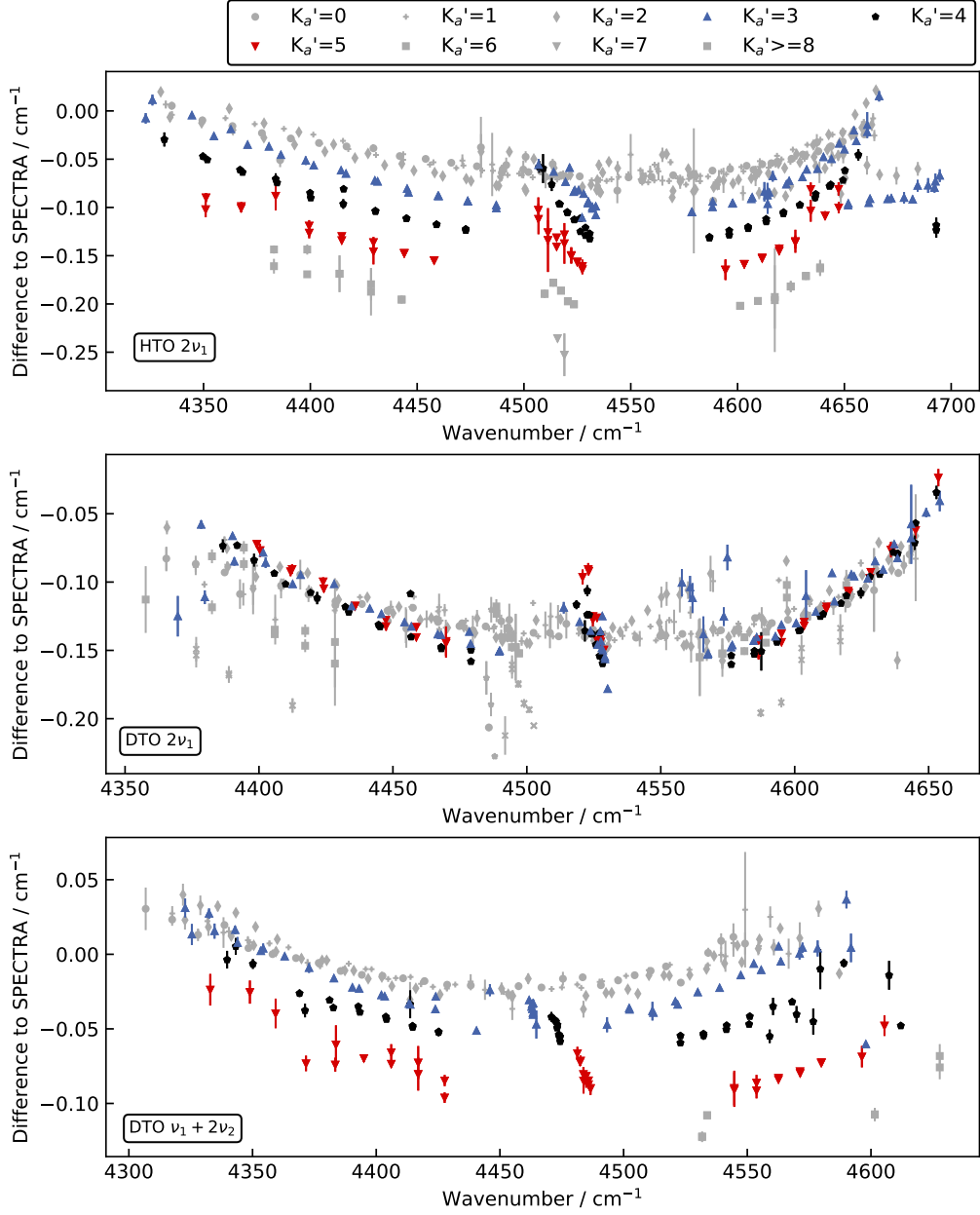
Figure A.9: Difference of the experimental data of the HTO $2\nu_1$, DTO $2\nu_1$ and $\nu_1 + 2\nu_2$ from the 10 GBq sample to SPECTRA database[Mik05]. The quantum number $K'_a = 3, 4$ and 5 of the individual lines are highlighted.
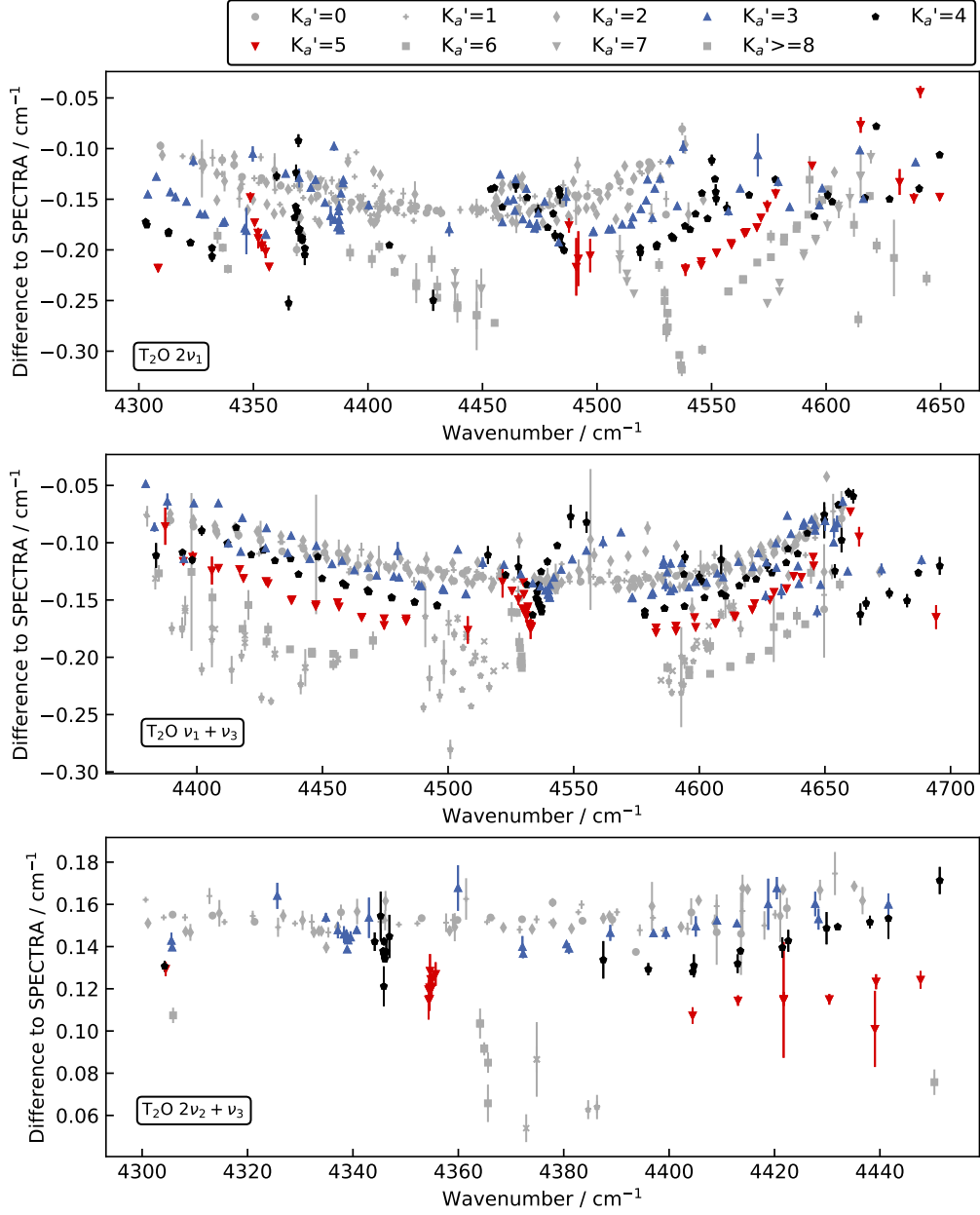
Figure A.10: Difference of the experimental data of the T_2O $2\nu_1$, $\nu_2 + \nu_3$ and $2\nu_2 + \nu_3$ from the 10 GBq sample to SPECTRA database[Mik05]. The quantum number $K'_a = 3, 4$ and 5 of the individual lines are highlighted.

Appendix B

Supplemental material to sorption study of the getter

Additional material for sorption study in Section 6.4 is provided. The material is only recommended in combination with the main work presented in Chapter 6.

B.1 Parameters of the getter sorption study

In this chapter the parameters for the functions describing the recorded data in the getter sorption study (Section 6.4 are presented.

B.1.1 Parameters of the fit function I(T)

The temperature was recorded for a serie of currents applied on the getter's heater wire using a pyrometer. The fit function is given with:

$$I = \mathrm{A} + \mathrm{B} \times (T - T_0) + \mathrm{C} \times (T - T_0)^2,$$

in units of A and °C. T_0 is $700\,°\mathrm{C}$. The obtained parameters are presented in Table B.1. Details are described in the main part.

B.1.2 Parameters of the fit function R(I)

To obtain the fit function R(I) data for voltage and current for a serie of currents applied at the getter's heater wire were taken at the *Tritium system*.

The fit function is given with

$$R = \mathrm{A} + \mathrm{B} \times (I - I_0) + \mathrm{C} \times (I - I_0)^2 + \mathrm{D} \times (I - I_0)^3,$$

where units of Ω and A are used. I_0 is $6.5\,\mathrm{A}$. The electrical resistance first need to be calculated from the current and voltage.

The parameters are presented in Table B.2. Uncertainties of the measurement devices are included in the fitting procedure.

Table B.1: Parameters of the fit function I(T) used for the calibration. Data were taken at the *Calibration setup*. The fit function is an empirical approach to describe the data.

Fit function: $I = \mathrm{A} + \mathrm{B} \times (T - T_0) + \mathrm{C} \times (T - T_0)^2$		
Parameter	Value	2σ
A	6.0686	(123)
$\mathrm{B} \times 1 \cdot 10^{-3}$	4.9202	(733)
$\mathrm{C} \times 1 \cdot 10^{-6}$	1.007	(687)
$\mathrm{Cov}_{AB} \times 1 \cdot 10^{-9}$	−1.7	
$\mathrm{Cov}_{AC} \times 1 \cdot 10^{-10}$	−1.2	
$\mathrm{Cov}_{BC} \times 1 \cdot 10^{-13}$	1.9	

B.1.3 Parameters of the fit function P(R)

The pressures of hydrogen samples H_2, D_2, T_2 and HT with (almost) equal loadings are taken for a serie of currents applied on the heater's wire. In addition, the voltage is recorded to obtain the electrical resistance of the getter.

The fit function is given with

$$P = \mathrm{A} \times \exp\left(\mathrm{B} \times (R - R_0)\right) + \mathrm{C}$$

in units of Pa and Ω. R_0 is $0.33\,\Omega$.

The parameters are presented in Table B.3. Uncertainties of measurement devices are included in the fitting procedure.

Table B.2: Parameters of the fit function R(I) used for the calibration. Data were taken at the *Tritium setup*. The fit function is an empirical approach to describe the data.

Fit function: $R = A + B \times (I - I_0) + C \times (I - I_0)^2 + D \times (I - I_0)^3$		
Parameter	Value	2σ
$A \times 1 \cdot 10^{-1}$	3.260 04	(185)
$B \times 1 \cdot 10^{-2}$	1.8193	(867)
$C \times 1 \cdot 10^{-3}$	−1.09	(317)
$D \times 1 \cdot 10^{-3}$	−1.95	(267)
$\text{Cov}_{AB} \times 1 \cdot 10^{-9}$	−1.19	
$\text{Cov}_{AC} \times 1 \cdot 10^{-8}$	−2.00	
$\text{Cov}_{AD} \times 1 \cdot 10^{-8}$	−1.774	
$\text{Cov}_{BC} \times 1 \cdot 10^{-7}$	1.294	
$\text{Cov}_{BD} \times 1 \cdot 10^{-8}$	8.27	
$\text{Cov}_{CD} \times 1 \cdot 10^{-7}$	5.08	

Table B.3: Obtained parameters for the function describing desorbed hydrogen samples of H_2, D_2, T_2 and HT with equal loadings recorded in the sorption experiment. The measured electrical resistivity has been obtained from the desorption measurement and is fitted to an empirical function. The units are Pa and Ω.

Fit function: $P = A \times \exp\left(B \times (R - R_0)\right) + C$

Gas species	H_2		D_2		T_2		HT	
Parameter	Value	2σ	Value	2σ	Value	2σ	Value	2σ
$A \times 1$	1.5933	(671)	1.6777	(601)	2.0560	(102)	1.7129	(470)
$B \times 1 \cdot 10^1$	7.303	(362)	7.231	(310)	6.808	(397)	7.340	(243)
$C \times 1 \cdot 10^{-1}$	−3.900	(576)	−3.965	(520)	−5.373	(886)	−4.073	(406)
$\text{Cov}_{AB} \times 1 \cdot 10^{-2}$	−5.80		−4.46		−9.70		−2.73	
$\text{Cov}_{AC} \times 1 \cdot 10^{-4}$	−9.55		−7.72		−22.30		−4.72	
$\text{Cov}_{BC} \times 1 \cdot 10^{-2}$	4.992		3.869		8.472		2.367	

Appendix C

List of publications obtained from this work

Here, a list of publications obtained from this work is provided, subdivided for the chapters.

Chapter 5

- Reinking, J., Hermann, V., Müller, J., Schlösser, M., Hase, F., & Orphal, J. *The fundamental ν_3 band of DTO and the $2\nu_1$ overtone band of HTO from the analysis of a high-resolution spectrum of tritiated water vapour.* Journal of Molecular Spectroscopy, 370, 111295. (2020)
- Hermann, V., Kamrad, M., Reinking, J., Schlösser, M., Hase, F., & Orphal, J. *Analysis of the $\nu_1 + 2\nu_2$, $\nu_2 + \nu_3$, $\nu_1 + \nu_3$ and the $2\nu_2 + \nu_3$ bands of $HT^{16}O$.* Journal of Quantitative Spectroscopy and Radiative Transfer, 276, 107881. (2021)
- Hermann, V., Gaisdörfer, M., Erygina, A., Lingnau, P., Schlösser, M., Hase, F., & Orphal, J. *Analysis of the $\nu_1 + \nu_3$ band of $T_2^{16}O$ and the $\nu_1 + \nu_3$ and $2\nu_2 + \nu_3$ bands of $DT^{16}O$.* Molecular Physics, 120(15-16), e2097136. (2022)
- Hermann, V., Freise, A., Schlösser, M., Hase, F., & Orphal, J. *Observation and assignment of a high-resolution FTIR-spectrum of $T_2^{16}O$, $DT^{16}O$ and $HT^{16}O$ in the range of 4300 to 4700cm^{-1}.* Journal of Molecular Spectroscopy, 398, 111859. (2023)

Chapter 6

- Cozijn, F. M. J., Diouf, M. L., Hermann, V., Salumbides, E. J., Schlösser, M., & Ubachs, W. *Rotational level spacings in HD from vibrational saturation spectroscopy.* Physical Review A, 105(6), 062823. (2022)
- Cozijn, F. M. J., Diouf, M. L., Ubachs, W., Hermann, V., & Schlösser, M. *Precision measurement of vibrational quanta in tritium hydride.* Physical Review Letters, 132(11), 113002. (2024)
- Hermann, V., Rothmund, B., Cozijn, F. M. J., Diouf, M. L., Ubachs, W., & Schlösser, M. *Pressure control of tritiated hydrogen isotopologues in hermetically sealed vessels by non-evaporable getters for sub-Doppler-resolution spectroscopy.* Vacuum, 113708. (2024)

Bibliography

[Age02]   I. A. E. Agency: 'Special issue on the global network of isotopes in precipitation'. In *Water Environment Newsletter* (2002), volume 16(5).

[Agh16]   N. Aghanim, M. Arnaud, M. Ashdown, J. Aumont, C. Baccigalupi et al.: 'Planck 2015 results-XI. CMB power spectra, likelihoods, and robustness of parameters'. In *Astronomy & Astrophysics* (2016), volume 594: A11.

[Ake22]   M. Aker et al.: 'Direct neutrino-mass measurement with sub-electronvolt sensitivity'. In *Nature Physics* (2022), volume 18(2): pages 160–166. DOI: 10.1038/s41567-021-01463-1. arXiv: 2105.08533 [hep-ex].

[Ali20]   S. Alighanbari, G. Giri, F. L. Constantin, V. Korobov and S. Schiller: 'Precise test of quantum electrodynamics and determination of fundamental constants with HD+ ions'. In *Nature* (2020), volume 581(7807): pages 152–158.

[Ali23]   S. Alighanbari, I. Kortunov, G. Giri and S. Schiller: 'Test of charged baryon interaction with high-resolution vibrational spectroscopy of molecular hydrogen ions'. In *Nature Physics* (2023), volume 19(9): pages 1263–1269.

[Ana24]   G. Ana, O. Balteanu, I. Cristescu and R. Ana: 'Concept for HCPB TER using non-evaporable getters for tritium recovery'. In *Fusion Engineering and Design* (2024), volume 201: page 114291. DOI: https://doi.org/10.1016/j.fusengdes.2024.114291.

[Ash23]   A. Ashtari Esfahani, S. Böser, N. Buzinsky, M. C. Carmona-Benitez, C. Claessens et al.: 'Tritium Beta Spectrum Measurement and Neutrino Mass Limit from Cyclotron Radiation Emission Spectroscopy'. In *Physical Review Letters* (10 2023), volume 131: page 102502. DOI: 10.1103/PhysRevLett.131.102502.

[Aus72]   J. H. Austin and T. S. Elleman: 'Tritium diffusion in 304- and 316-stainless steels in the temperature range 25 to 222 °C'. In *Journal of Nuclear Materials* (1972), volume 43: pages 119–125. DOI: 10.1016/0022-3115(72)90145-6.

[Axn14]   O. Axner, P. Ehlers, A. Foltynowicz, I. Silander and J. Wang: 'NICE-OHMS—Frequency Modulation Cavity-Enhanced Spectroscopy—Principles and Performance'. In *Cavity-Enhanced Spectroscopy and Sensing*. Edited by G. Gagliardi and H.-P. Loock. Berlin, Heidelberg: Springer Berlin Heidelberg, 2014: pages 211–251. DOI: 10.1007/978-3-642-40003-2_6.

[Bab15]   S. Babar and J. H. Weaver: 'Optical constants of Cu, Ag, and Au revisited'. In *Applied Optics* (2015), volume 54(3): pages 477–481. DOI: 10.1364/AO.54.000477.

[Bag91]   S. N. Bagayev, V. P. Chebotayev, A. K. Dimitriyev, A. E. Om, Y. V. Nekrasov et al.: 'Second-order Doppler-free spectroscopy'. In *Applied Physics B* (1991), volume 52: page 63.

[Bar79]   R. L. Barger, J. C. Bergquist, T. C. English and D. J. Glaze: 'Resolution of photon-recoil structure of the 6573-Å calcium line in an atomic beam with optical Ramsey fringes'. In *Applied Physics Letters* (1979), volume 34(12): pages 850–852. DOI: 10.1063/1.90690.

[Bel72]   J. Bellet, G. Steenbeckeliers and P. Stouffs: 'Microwave Spectrum of Radioactive isotopic Varieties HTO and T2O of Water Molecule'. In *Comptes rendus de l'Académie des sciences Série B* (1972), volume 275: pages 501–503.

[Ben62]   W. R. Bennett: 'Hole Burning Effects in a He-Ne Optical Maser'. In *Physical Review* (2 1962), volume 126: pages 580–593. DOI: 10.1103/PhysRev.126.580.

[Ber02]   P. F. Bernath: 'The spectroscopy of water vapour: Experiment, theory and applications'. In *Physical Chemistry Chemical Physics* (9 2002), volume 4: pages 1501–1509. DOI: 10.1039/B200372D.

[Bjo80]   G. C. Bjorklund: 'Frequency-modulation spectroscopy: a new method for measuring weak absorptions and dispersions'. In *Optics Letters* (1980), volume 5(1): pages 15–17.

[Bof83]   C. Boffito, B. Ferrario and D. Martelli: 'Equilibrium pressures of H2 and D2 for different getter materials and the effect of CO impurities'. In *Journal of Vacuum Science & Technology A: Vacuum, Surfaces, and Films* (1983), volume 1(2): pages 1279–1282.

[Bra15]   C. Bray, A. Pailloux and S. Plumeri: 'Tritiated water detection in the 2.17 μm spectral region by cavity ring down spectroscopy'. In *Nuclear Instruments and Methods in Physics Research Section A: Accelerators, Spectrometers, Detectors and Associated Equipment* (2015), volume 789(Supplement C): pages 43–49. DOI: https://doi.org/10.1016/j.nima.2015.03.064.

[Bro03]   J. Brown and A. Carrington: *Rotational Spectroscopy of Diatomic Molecules.* Cambridge Molecular Science. Cambridge University Press, 2003.

[Cam73]   C. Camy-Peyret, J. Flaud, G. Guelachvili and C. Amiot: 'High resolution Fourier transform spectrum of water between 2930 and 4255 cm^{-1}'. In *Molecular Physics* (1973), volume 26(4): pages 825–855. DOI: 10.1080/00268977300102131. eprint: https://doi.org/10.1080/00268977300102131.

[Car72]   R. A. Carpenter, N. M. Gailar, H. W. Morgan and P. A. Staats: 'The ν_2 fundamental vibration-rotation band of T_2O'. In *Journal of Molecular Spectroscopy* (1972), volume 44(2): pages 197–205. DOI: https://doi.org/10.1016/0022-2852(72)90099-9.

[Che18a]   J. Chen, T.-P. Hua, L.-G. Tao, Y. Sun, A.-W. Liu et al.: 'Absolute frequencies of water lines near 790 nm with 10^{-11} accuracy'. In *Journal of Quantitative Spectroscopy and Radiative Transfer* (2018), volume 205: pages 91–95. DOI: https://doi.org/10.1016/j.jqsrt.2017.10.009.

[Che18b]   C.-F. Cheng, J. Hussels, M. Niu, H. L. Bethlem, K. S. E. Eikema et al.: 'Dissociation Energy of the Hydrogen Molecule at 10^{-9} Accuracy'. In *Physical Review Letters* (2018), volume 121(1): page 013001.

[Che87]   P. P. Cherrier and J. Reid: 'High-sensitivity detection of tritiated water vapour using tunable diode lasers'. In *Nuclear Instruments and Methods in Physics Research Section A: Accelerators, Spectrometers, Detectors and Associated Equipment* (1987), volume 257(2): pages 412–416. DOI: https://doi.org/10.1016/0168-9002(87)90766-2.

[Chu87]   M.-C. Chuang and R. N. Zare: 'Rotation-vibration spectrum of HT: Line position measurements of the 1-0, 4-0, and 5-0 bands'. In *Journal of Molecular Spectroscopy* (1987), volume 121(2): pages 380–400. DOI: http://dx.doi.org/10.1016/0022-2852(87)90057-9.

[col20]   C. collaboration et al.: 'Pileup mitigation at CMS in 13 TeV data'. In *Journal of Instrumentation* (2020), volume 15(9).

[Con17]   O. Connan, D. Hébert, L. Solier, D. Maro, G. Pellerin et al.: 'Atmospheric tritium concentrations under influence of AREVA NC La Hague reprocessing plant (France) and background levels'. In *Journal of environmental radioactivity* (2017), volume 177: pages 184–193.

[Coo65]   J. W. Cooley and J. W. Tukey: 'An algorithm for the machine calculation of complex Fourier series'. In *Mathematics of computation* (1965), volume 19(90): pages 297–301.

[Cop86]   S. Cope, D. Russell, H. Fry, L. Jones and J. Barefield: 'Analysis of the fundamental asymmetric stretching mode of T_2O'. In *Journal of Molecular Spectroscopy* (1986), volume 120(2): pages 311–316. DOI: https://doi.org/10.1016/0022-2852(86)90007-X.

[Cop88]   S. Cope, D. Russell, H. Fry, L. Jones and J. Barefield: 'Analysis of the ν_1 fundamental mode of HTO'. In *Journal of Molecular Spectroscopy* (1988), volume 127(2): pages 464–471. DOI: https://doi.org/10.1016/0022-2852(88)90134-8.

[Cou12]   A. Coutens, C. Vastel, E. Caux, C. Ceccarelli, S. Bottinelli et al.: 'A study of deuterated water in the low-mass protostar IRAS 16293-2422'. In *Astronomy & Astrophysics* (2012), volume 539: A132.

[Coz18a]   F. M. J. Cozijn, P. Dupré, E. J. Salumbides, K. S. E. Eikema and W. Ubachs: 'Sub-Doppler Frequency Metrology in HD for Tests of Fundamental Physics'. In *Physical Review Letters* (15 2018), volume 120: page 153002. DOI: 10.1103/PhysRevLett.120.153002.

[Coz18b]   F. M. Cozijn, P. Dupré, E. Salumbides, K. Eikema and W. Ubachs: 'Sub-Doppler frequency metrology in HD for tests of fundamental physics'. In *Physical Review Letters* (2018), volume 120(15): page 153002.

[Coz22a]   F. Cozijn, M. Diouf, V. Hermann, E. Salumbides, M. Schlösser et al.: 'Rotational level spacings in HD from vibrational saturation spectroscopy'. In *Physical Review A* (2022), volume 105(6): page 062823.

[Coz22b]   F. Cozijn, M. Diouf and W. Ubachs: 'Saturation spectroscopy of R (0), R (2) and P (2) lines in the (2-0) band of HD'. In *The European Physical Journal D* (2022), volume 76(11): page 220.

[Coz23]   F. M. Cozijn, M. L. Diouf and W. Ubachs: 'Lamb dip of a quadrupole transition in H_2'. In *Physical Review Letters* (2023), volume 131(7): page 073001.

[Coz24a]   F. M. J. Cozijn, M. L. Diouf, W. Ubachs, V. Hermann and M. Schlösser: 'Precision Measurement of Vibrational Quanta in Tritium Hydride'. In *Physical Review Letters* (11 2024), volume 132: page 113002. DOI: 10.1103/PhysRevLett.132.113002.

[Coz24b]   F. Cozijn: 'High-Precision Rovibrational Saturation Spectroscopy of H2, HD and HT'. PhD-Thesis - Research and graduation internal. Vrije Universiteit Amsterdam, 2024. DOI: 10.5463/thesis.744.

[Cza18]   P. Czachorowski, M. Puchalski, J. Komasa and K. Pachucki: 'Nonadiabatic relativistic correction in H_2, D_2, and HD'. In *Physical Review A* (2018), volume 98(5): page 052506. DOI: 10.1103/PhysRevA.98.052506.

[Das20]   B. K. Das, R. Das, R. Verma, R. Shukla and A. Sharma: 'Improvement of deuterium emission by St 172 NEG pump in a sealed off vacuum device'. In *Vacuum* (2020), volume 181: page 109743.

[De 73]   F. C. De Lucia, P. Helminger, W. Gordy, H. W. Morgan and P. A. Staats: 'Millimeter- and Submillimeter-Wavelength Spectrum and Molecular Constants of T_2O'. In *Physical Review A* (6 1973), volume 8: pages 2785–2791. DOI: 10.1103/PhysRevA.8.2785.

[Dem08]   W. Demtröder: *Laser Spectroscopy: Vol. 1: Basic Principles*. Laser Spectroscopy. Springer Berlin Heidelberg, 2008.

[Dem10]   W. Demtröder: *Atoms, Molecules and Photons*. ‚Berlin Heidelberg: Springer, 2010. DOI: 10.1007/978-3-642-10298-1.

[DeV84]   R. DeVoe and R. Brewer: 'Laser-frequency division and stabilization'. In *Physical Review A* (1984), volume 30(5): page 2827.

[Dio19]   M. Diouf, F. Cozijn, B. Darquié, E. Salumbides and W. Ubachs: 'Lamb-dips and Lamb-peaks in the saturation spectrum of HD'. In *Optics Letters* (2019), volume 44(19): pages 4733–4736.

[Dio20]   M. Diouf, F. Cozijn, K.-F. Lai, E. Salumbides and W. Ubachs: 'Lamb-peak spectrum of the HD (2-0) P (1) line'. In *Physical Review Research* (2020), volume 2(2): page 023209.

[Dio21]   M. L. Diouf, R. Tóbiás, I. Simkó, F. M. J. Cozijn, E. J. Salumbides et al.: 'Network-Based Design of Near-Infrared Lamb-Dip Experiments and the Determination of Pure Rotational Energies of $H_2^{18}O$ at kHz Accuracy'. In *Journal of Physical and Chemical Reference Data* (2021), volume 50(2): page 023106. DOI: 10.1063/5.0052744. eprint: https://pubs.aip.org/aip/jpr/article-pdf/doi/10.1063/5.0052744/16071638/023106_1_online.pdf.

[Dio22]   M. L. Diouf, R. Tóbiás, F. M. J. Cozijn, E. J. Salumbides, C. Fábri et al.: 'Parity-pair-mixing effects in nonlinear spectroscopy of HDO'. In *Optics Express* (2022), volume 30(26): pages 46040–46059. DOI: 10.1364/OE.474525.

[Dio23]   M. Diouf: 'Saturated Ultra-Precision Spectroscopy of Water and HD with NICE-OHMS'. PhD-Thesis - Research and graduation internal. Vrije Universiteit Amsterdam, 2023. DOI: 10.5463/thesis.477.

[Dio24]   M. L. Diouf, F. M. Cozijn and W. Ubachs: 'Hyperfine structure in a vibrational quadrupole transition of ortho-H_2'. In *Molecular Physics* (2024), volume: e2304101.

[Dow13]   M. J. Down, J. Tennyson, M. Hara, Y. Hatano and K. Kobayashi: 'Analysis of a tritium enhanced water spectrum between 7200 and 7245 cm^{-1} using new variational calculations'. In *Journal of Molecular Spectroscopy* (2013), volume 289(Supplement C): pages 35–40. DOI: https://doi.org/10.1016/j.jms.2013.05.016.

[Dre83]   R. W. Drever, J. L. Hall, F. V. Kowalski, J. Hough, G. Ford et al.: 'Laser phase and frequency stabilization using an optical resonator'. In *Applied Physics B* (1983), volume 31: pages 97–105.

[Dup15]   P. Dupré: 'Birefringence-induced frequency beating in high-finesse cavities by continuous-wave cavity ring-down spectroscopy'. In *Physical Review A* (2015), volume 92(5): page 053817.

[Ery21]   A. Erygina: 'The improvement of the optical cell and the creation of a new sample for Fourier-transform infrared spectroscopy of tritiated water'. Bachelor's Thesis. Karlsruhe Institute for Techology, 2021.

[Eur14]   European Union: 'Council Directive 2013/59/Euratom of 5 December 2013 laying down basic safety standards for protection against the dangers arising from exposure to ionising radiation, and repealing Directives 89/618/Euratom, 90/641/Euratom, 96/29/Euratom, 97/43/Euratom and 2003/122/Euratom'. In *Official Journal of the European Union* (2014), volume 57.

[Fas18]   E. Fasci, A. Castrillo, H. Dinesan, S. Gravina, L. Moretti et al.: 'Precision spectroscopy of HD at 1.38 μm'. In *Physical Review A* (2018), volume 98(2): page 022516.

[Fas20]   A. Fast and S. A. Meek: 'Sub-ppb Measurement of a Fundamental Band Rovibrational Transition in HD'. In *Physical Review Letters* (2020), volume 125(2): page 023001. DOI: 10.1103/PhysRevLett.125.023001.

[Fay72]   A. Fayt and G. Steenbeckeliers: 'Determination of the ν_1 and ν_3 vibrational levels of the radioactive water molecule HTO by high resolution infrared spectroscopy and calculation of rotation constants of the fundamental state.' In *Comptes rendus de l'Académie des sciences Série B* (1972), volume 275: pages 459–460.

[Fis15]   S. Fischer, K. Schönung, B. Bornschein, R. Rolli, V. Schäfer et al.: 'Investigation of durability of optical coatings in highly purified tritium gas'. In *Fusion science and technology* (2015), volume 67(2): pages 316–319. DOI: 10.13182/FST14-T19.

[Fla72]   J. Flaud, C. Camy-Peyret and A. Valentin: 'Spectre infrarouge a haute résolution des bandes $\nu_1 + \nu_2$ et $\nu_2 + \nu_3$ de $H_2^{16}O$'. In *Journal de Physique* (1972), volume 33(8-9): pages 741–747.

[Fla73]   J. Flaud and C. Camy-Peyret: 'The $2\nu_2$, ν_1, and ν_3 bands of $H_2^{16}O$'. In *Molecular Physics* (1973), volume 26(4): pages 811–823. DOI: 10.1080/00268977300102121. eprint: https://doi.org/10.1080/00268977300102121.

[Fla75]   J. Flaud and C. Camy-Peyret: 'Vibration-rotation intensities in H_2O-type molecules application to the $2\nu_2$, ν_1, and ν_3 bands of $H_2^{16}O$'. In *Journal of Molecular Spectroscopy* (1975), volume 55(1): pages 278–310. DOI: https://doi.org/10.1016/0022-2852(75)90270-2.

[Fla76]   J. Flaud, C. Camy-Peyret and J. Maillard: 'Higher ro-vibrational levels of H_2O deduced from high resolution oxygen-hydrogen flame spectra between 2800–6200 cm^{-1}'. In *Molecular Physics* (1976), volume 32(2): pages 499–521. DOI: 10.1080/00268977600103251. eprint: https://doi.org/10.1080/00268977600103251.

[Fle23]   H. Fleurbaey, A. O. Koroleva, S. Kassi and A. Campargue: 'The high-accuracy spectroscopy of H_2 rovibrational transitions in the (2-0) band near 1.2 μm'. In *Physical Chemistry Chemical Physics* (2023), volume 25: pages 14749–14756.

[Fol08]   A. Foltynowicz, F. M. Schmidt, W. Ma and O. Axner: 'Noise-immune cavity-enhanced optical heterodyne molecular spectroscopy: Current status and future potential'. In *Applied Physics B* (2008), volume 92: pages 313–326.

[Fol09]   A. Foltynowicz: 'Fiber-laser-based Noise-Immune Cavity-Enhanced Optical Heterodyne Molecular Spectrometry'. PhD thesis. Umeå, Sweden: Umeå University, 2009.

[Fro52]   R. A. Frosch and H. Foley: 'Magnetic hyperfine structure in diatomic molecules'. In *Physical Review* (1952), volume 88(6): page 1337.

[Fry84]   H. Fry, L. Jones and J. Barefield: 'Observation and analysis of fundamental bending mode of T_2O'. In *Journal of Molecular Spectroscopy* (1984), volume 103(1): pages 41–55. DOI: https://doi.org/10.1016/0022-2852(84)90144-9.

[Fur07]   T. Furtenbacher, A. G. Császár and J. Tennyson: 'MARVEL: measured active rotational–vibrational energy levels'. In *Journal of Molecular Spectroscopy* (2007), volume 245(2): pages 115–125. DOI: https://doi.org/10.1016/j.jms.2007.07.005.

[Fur12]   T. Furtenbacher and A. G. Császár: 'MARVEL: Measured active rotational–vibrational energy levels. II. Algorithmic improvements'. In *Journal of Quantitative Spectroscopy and Radiative Transfer* (2012), volume 113(11): pages 929–935. DOI: https://doi.org/10.1016/j.jqsrt.2012.01.005.

[Gai22]   M. Gaisdörfer: 'Analysis of the $\nu_1 + \nu_3$ and $2\nu_2 + \nu_3$ transition bands of $DT^{16}O$ from a high resolution FTIR spectrum with an activity of 10^{10} GBq'. Bachelor's Thesis. Karlsruhe Institute for Techology, 2022.

[Gam19]   R. R. Gamache, B. Vispoel, C. L. Renaud, K. Cleghorn and L. Hartmann: 'Vibrational dependence, temperature dependence, and prediction of line shape parameters for the H2O-H2 collision system'. In *Icarus* (2019), volume 326: pages 186–196. DOI: https://doi.org/10.1016/j.icarus.2019.02.011.

[Gis11]   M. Gisi, F. Hase, S. Dohe and T. Blumenstock: 'Camtracker: a new camera controlled high precision solar tracker system for FTIR-spectrometers'. In *Atmospheric Measurement Techniques* (2011), volume 4(1): pages 47–54. DOI: 10.5194/amt-4-47-2011.

[Gor17]   I. E. Gordon, L. S. Rothman, C. Hill, R. V. Kochanov, Y. Tan et al.: 'The HITRAN2016 molecular spectroscopic database'. In *Journal of Quantitative Spectroscopy and Radiative Transfer* (2017), volume 203: pages 3–69.

[Gor22]   I. Gordon, L. Rothman, R. Hargreaves, R. Hashemi, E. Karlovets et al.: 'The HITRAN2020 molecular spectroscopic database'. In *Journal of Quantitative Spectroscopy and Radiative Transfer* (2022), volume 277: page 107949. DOI: https://doi.org/10.1016/j.jqsrt.2021.107949.

[Gue24]   E. R. Guest, J. Tennyson and S. N. Yurchenko: 'Predicting the rotational dependence of line broadening using machine learning'. In *Journal of Molecular Spectroscopy* (2024), volume 401: page 111901.

[Gur88]   D. F. Gurka and S. M. Pyle: 'Qualitative and quantitative environmental analysis by capillary column gas chromatography/lightpipe Fourier-transform infrared spectrometry'. In *Environmental Science & Technology* (1988), volume 22(8): pages 963–967. DOI: 10.1021/es00173a016.

[Hal76] J. L. Hall, C. J. Bordé and K. Uehara: 'Direct Optical Resolution of the Recoil Effect Using Saturated Absorption Spectroscopy'. In *Physical Review Letters* (20 1976), volume 37: pages 1339–1342.

[Haq24] J. Haqq-Misra, V. Kofman and R. K. Kopparapu: 'The Challenge of Detecting Remote Spectroscopic Signatures from Radionuclides'. In *The Astrophysical Journal* (2024), volume 973(2): page 161. DOI: 10.3847/1538-4357/ad6d5f.

[Has00] F. Hase: 'Inversion von Spurengasprofilen aus hochaufgelösten bodengebundenen FTIR-Messungen in Absorption'. PhD thesis. 2000. DOI: 10.5445/IR/2752000.

[Has12] F. Hase: 'Improved instrumental line shape monitoring for the ground-based, high-resolution FTIR spectrometers of the Network for the Detection of Atmospheric Composition Change'. In *Atmospheric Measurement Techniques* (2012), volume 5(3): pages 603–610. DOI: 10.5194/amt-5-603-2012.

[Has13] F. Hase, B. J. Drouin, C. M. Roehl, G. C. Toon, P. O. Wennberg et al.: 'Calibration of sealed HCl cells used for TCCON instrumental line shape monitoring'. In *Atmospheric Measurement Techniques* (2013), volume 6(12): pages 3527–3537. DOI: 10.5194/amt-6-3527-2013.

[Has99] F. Hase, T. Blumenstock and C. Paton-Walsh: 'Analysis of the instrumental line shape of high-resolution Fourier transform IR spectrometers with gas cell measurements and new retrieval software'. In *Applied Optics* (1999), volume 38(15): pages 3417–3422. DOI: 10.1364/AO.38.003417.

[Hel74] P. Helminger, F. C. De Lucia, W. Gordy, P. A. Staats and H. W. Morgan: 'Millimeter- and submillimeter-wavelength spectra and molecular constants of HTO and DTO'. In *Physical Review A* (4 1974), volume 10: pages 1072–1081. DOI: 10.1103/PhysRevA.10.1072.

[Her10] I. Hertel and C. Schulz: *Atome, Molekule Und Optische Physik 2 Molekule Und Photonen - Spektroskopie Und Streuphysik*. Atome, Moleküle und optische Physik. Springer Berlin Heidelberg, 2010.

[Her21] V. Hermann, M. Kamrad, J. Reinking, M. Schlösser, F. Hase et al.: 'Analysis of the $\nu_1+2\nu_2$, $\nu_2+\nu_3$, $\nu_1+\nu_3$ and the $2\nu_2+\nu_3$ bands of HT^{16}O'. In *Journal of Quantitative Spectroscopy and Radiative Transfer* (2021), volume 276: page 107881.

[Her22] V. Hermann, M. Gaisdörfer, A. Erygina, P. Lingnau, M. Schlösser et al.: 'Analysis of the $\nu_1+\nu_3$ band of T$_2^{16}$O and the $\nu_1+\nu_3$ and $2\nu_2+\nu_3$ bands of DT^{16}O'. In *Molecular Physics* (2022), volume 120(15-16): e2097136.

[Her23] V. Hermann, A. Freise, M. Schlösser, F. Hase and J. Orphal: 'Observation and assignment of a high-resolution FTIR-spectrum of T$_2^{16}$O, DT^{16}O and HT^{16}O in the range of 4300 to 4700 cm^{-1}'. In *Journal of Molecular Spectroscopy* (2023), volume 398: page 111859.

[Her24]   V. Hermann, B. Rothmund, F. M. Cozijn, M. L. Diouf, W. Ubachs et al.: 'Pressure control of tritiated hydrogen isotopologues in hermetically sealed vessels by non-evaporable getters for sub-Doppler-resolution spectroscopy'. In *Vacuum* (2024), volume: page 113708. DOI: https://doi.org/10.1016/j.vacuum.2024.113708.

[Her50]   G. Herzberg: 'Rotation-vibration spectrum of the HD molecule'. In *Nature* (1950), volume 166(4222): pages 563–563.

[Hil24]   C. Hill and IAEA. Personal communication. Aug 2024.

[Hir21]   S. Hirao and H. Kakiuchi: 'Investigation of atmospheric tritiated water vapor level around the Fukushima Daiichi nuclear power plant'. In *Fusion Engineering and Design* (2021), volume 171: page 112556.

[Höl23]   N. Hölsch, I. Doran, F. Merkt, J. Hussels, C.-F. Cheng et al.: 'Ionization and dissociation energies of HD and dipole-induced g/u-symmetry breaking'. In *Physical Review A* (2023), volume 108: page 022811. DOI: 10.1103/PhysRevA.108.022811.

[Hua20]   T.-P. Hua, Y. R. Sun and S.-M. Hu: 'Dispersion-like lineshape observed in cavity-enhanced saturation spectroscopy of HD at 1.4 μm'. In *Optics Letters* (2020), volume 45(17): pages 4863–4866. DOI: 10.1364/OL.401879.

[Hus22]   J. Hussels, N. Hölsch, C.-F. Cheng, E. J. Salumbides, H. L. Bethlem et al.: 'Improved ionization and dissociation energies of the deuterium molecule'. In *Physical Review A* (2 2022), volume 105: page 022820. DOI: 10.1103/PhysRevA.105.022820.

[Jac16]   N. Jacquinet-Husson, R. Armante, N. Scott, A. Chédin, L. Crépeau et al.: 'The 2015 edition of the GEISA spectroscopic database'. In *Journal of Molecular Spectroscopy* (2016), volume 327: pages 31–72. DOI: https://doi.org/10.1016/j.jms.2016.06.007.

[Jam18]   D. James and G. Morgan: 'Evaluation of getters for methane and ammonia decomposition'. In *Fusion Engineering and Design* (2018), volume 133: pages 1–5. DOI: 10.1016/J.FUSENGDES.2018.05.022.

[Jam75]   F. James and M. Roos: 'MINUIT: a system for function minimization and analysis of the parameter errors and corrections'. In *Computer Physics Communications* (1975), volume 10(CERN-DD-75-20): pages 343–367.

[Joh85]   J. W. C. Johns: 'High-resolution far-infrared (20-350 cm^{-1}) spectra of several isotopic species of H_2O'. In *Journal of the Optical Society of America B* (1985), volume 2(8): pages 1340–1354. DOI: 10.1364/JOSAB.2.001340.

[Joh86]   D. E. Johnson and J. G. Eden: 'High-temperature, alkali-rare-gas optical cell'. In *Review of Scientific Instruments* (1986), volume 57(12): pages 2976–2978. DOI: 10.1063/1.1139028. eprint: https://doi.org/10.1063/1.1139028.

[Jon03]   W. M. Jones: 'Vapor Pressures of Tritium Oxide and Deuterium Oxide. Interpretation of the Isotope Effects'. In *The Journal of Chemical Physics* (2003), volume 48(1): pages 207–214. DOI: 10.1063/1.1667903. eprint: https://pubs.aip.org/aip/jcp/article-pdf/48/1/207/10958405/207_1_online.pdf.

[Jon48]   W. M. Jones: 'Thermodynamic functions for tritium and tritium hydride. The equilibrium of tritium and hydrogen with tritium hydride. The dissociation of tritium and tritium hydride'. In *The Journal of Chemical Physics* (1948), volume 16(11): pages 1077–1081. DOI: 10.1063/1.1746727.

[Jóź21]   H. Jóźwiak, H. Cybulski and P. Wcisło: 'Hyperfine components of rovibrational dipole transitions in HT and DT'. In *Journal of Quantitative Spectroscopy and Radiative Transfer* (2021), volume 270: page 107662. DOI: https://doi.org/10.1016/j.jqsrt.2021.107662.

[Jóź22]   H. Jóźwiak and P. Wcisło: 'Magic wavelength for a rovibrational transition in molecular hydrogen'. In *Scientific Reports* (2022), volume 12: page 14529.

[Kal93]   M. B. Kalinowski: 'Uncertainty and range of alternatives in estimating tritium emissions from proposed fusion power reactors and their radiological impact'. In *Journal of Fusion Energy* (1993), volume 12(1): pages 157–161. DOI: 10.1007/BF01059372.

[Kam21]   M. Kamrad: 'Analysis of the $\nu_1 + 2\nu_2$ and $\nu_2 + \nu_3$ transition bands in high resolution infrared absorption spectra of HT^{16}O'. Bachelor's Thesis. Karlsruhe Institute for Techology, 2021.

[Kan84]   I. Kanesaka, M. Tsuchida, K. Kawai and T. Takeuchi: 'The IR spectrum of T$_2^{18}O$'. In *Journal of Molecular Spectroscopy* (1984), volume 104(2): pages 405–413. DOI: https://doi.org/10.1016/0022-2852(84)90134-6.

[Kas11]   S. Kassi and A. Campargue: 'Electric quadrupole and dipole transitions of the first overtone band of HD by CRDS between 1.45 and 1.33 μm'. In *Journal of Molecular Spectroscopy* (2011), volume 267(1-2): pages 36–42.

[Kas18]   S. Kassi, T. Stoltmann, M. Casado, M. Daeron and A. Campargue: 'Lamb dip CRDS of highly saturated transitions of water near 1.4 μm'. In *The Journal of Chemical Physics* (2018), volume 148(5): page 054201. DOI: 10.1063/1.5010957. eprint: https://pubs.aip.org/aip/jcp/article-pdf/doi/10.1063/1.5010957/15537807/054201_1_online.pdf.

[Kas22]   S. Kassi, C. Lauzin, J. Chaillot and A. Campargue: 'The (2-0) R(0) and R(1) transition frequencies of HD determined to a 10^{-10} relative accuracy by Doppler spectroscopy at 80 K'. In *Physical Chemistry Chemical Physics* (38 2022), volume 24: pages 23164–23172. DOI: 10.1039/D2CP02151J.

[Kaw23]   K. Kawaguchi. Personal communication. 2023.

[Kie16a]   M. Kiel, F. Hase, T. Blumenstock and O. Kirner: 'Comparison of XCO abundances from the Total Carbon Column Observing Network and the Network for the Detection of Atmospheric Composition Change measured in Karlsruhe'. In *Atmospheric Measurement Techniques* (2016), volume 9(5): pages 2223–2239. DOI: 10.5194/amt-9-2223-2016.

[Kie16b]   M. Kiel, F. Hase, T. Blumenstock and O. Kirner: 'Comparison of XCO abundances from the Total Carbon Column Observing Network and the Network for the Detection of Atmospheric Composition Change measured in Karlsruhe'. In *Atmospheric Measurement Techniques* (2016), volume 9(5): pages 2223–2239. DOI: 10.5194/amt-9-2223-2016.

[Kim03]   J. Y. Kim, J. A. Rodriguez, J. C. Hanson, A. I. Frenkel and P. L. Lee: 'Reduction of CuO and Cu_2O with H_2: H embedding and kinetic effects in the formation of suboxides'. In *Journal of the American Chemical Society* (2003), volume 125(35): pages 10684–10692.

[Kis08]   Z. Kisiel, L. Pszczółkowski, G. Cazzoli and L. Dore: 'Strong Coriolis coupling between ν5 and ν11 states of CH3CCl3 studied by millimeter-wave spectroscopy'. In *Journal of Molecular Spectroscopy* (2008), volume 251(1): pages 235–240. DOI: https://doi.org/10.1016/j.jms.2008.03.006.

[Kis09]   Z. Kisiel, E. B. Jaworska, R. A. Butler, D. T. Petkie, P. Helminger et al.: 'The rotational spectrum of chlorine nitrate (ClONO2) in the four lowest nν9 polyads'. In *Journal of Molecular Spectroscopy* (2009), volume 254(2): pages 78–86. DOI: https://doi.org/10.1016/j.jms.2009.01.005.

[Kob11]   K. Kobayashi, T. Enokida, D. Iio, Y. Yamada, M. Hara et al.: 'Near-Infrared Spectroscopy of Tritiated Water'. In *Fusion Science and Technology* (2011), volume 60(3): pages 941–943. DOI: 10.13182/FST11-A12570. eprint: https://doi.org/10.13182/FST11-A12570.

[Koc16]   R. Kochanov, I. Gordon, L. Rothman, P. Wcisło, C. Hill et al.: 'HITRAN Application Programming Interface (HAPI): A comprehensive approach to working with spectroscopic data'. In *Journal of Quantitative Spectroscopy and Radiative Transfer* (2016), volume 177: pages 15–30. DOI: https://doi.org/10.1016/j.jqsrt.2016.03.005.

[Köl11]   Z. Köllő, C. G. Alecu and H. Moosmann: 'A New Method to Measure Small Volumes in Tritium Handling Facilities, Using p-V Measurements'. In *Fusion Science and Technology* (2011), volume 60(3): pages 972–975. DOI: 10.13182/fst11-a12578.

[Kom19a]   J. Komasa, M. Puchalski, P. Czachorowski, G. Łach and K. Pachucki: 'Rovibrational energy levels of the hydrogen molecule through nonadiabatic perturbation theory'. In *Physical Review A* (3 2019), volume 100: page 032519. DOI: 10.1103/PhysRevA.100.032519.

[Kom19b]   J. Komasa, M. Puchalski, P. Czachorowski, G. Łach and K. Pachucki: 'Rovi-brational energy levels of the hydrogen molecule through nonadiabatic per-turbation theory'. In *Physical Review A* (3 2019), volume 100: page 032519. doi: 10.1103/PhysRevA.100.032519.

[Kor21]   V. I. Korobov and J.-P. Karr: 'Rovibrational spin-averaged transitions in the hydrogen molecular ions'. In *Physical Review A* (3 2021), volume 104: page 032806. doi: 10.1103/PhysRevA.104.032806.

[Kun70]   P. J. Kuntz, E. M. Nemeth, J. C. Polanyi and W. H. Wong: 'Distribution of Reaction Products. VI. Hot-Atom Reactions, T+HR'. In *The Journal of Chemical Physics* (1970), volume 52(9): pages 4654–4674. doi: 10.1063/1.1673698. eprint: https://pubs.aip.org/aip/jcp/article-pdf/52/9/4654/18868725/4654_1_online.pdf.

[Kwa04]   F. Kwabia Tchana, I. Kleiner, J. Orphal, N. Lacome and O. Bouba: 'New analysis of the Coriolis-interacting v2 and v5 bands of CH379Br and CH381Br'. In *Journal of Molecular Spectroscopy* (2004), volume 228(2): pages 441–452. doi: https://doi.org/10.1016/j.jms.2004.05.011.

[Lai19]   K.-F. Lai, P. Czachorowski, M. Schlösser, M. Puchalski, J. Komasa et al.: 'Precision tests of nonadiabatic perturbation theory with measurements on the DT molecule'. In *Physical Review Research* (3 2019), volume 1: page 033124. doi: 10.1103/PhysRevResearch.1.033124.

[Lai20]   K.-F. Lai, V. Hermann, T. M. Trivikram, M. Diouf, M. Schlösser et al.: 'Precision measurement of the fundamental vibrational frequencies of tritium-bearing hydrogen molecules: T2, DT, HT'. In *Physical Chemistry Chemical Physics* (2020), volume 22(16): pages 8973–8987. doi: https://doi.org/10.1039/D0CP00596G.

[Let77]   V. S. Letokhov and V. P. Chebotayev: *Nonlinear laser spectroscopy*. Volume 4. Springer, 1977.

[Lid04]   D. R. Lide: *CRC handbook of chemistry and physics*. Volume 85. CRC press, 2004.

[Lin21]   P. Lingnau: 'Analysis of the $\nu_1 + \nu_3$ band of $T_2^{16}O$ from a high resolution FTIR measurement'. Bachelor's Thesis. Karlsruhe Institute for Techology, 2021.

[Lok22]   A. Lokhov, S. Mertens, D. S. Parno, M. Schlösser and K. Valerius: 'Probing the Neutrino-Mass Scale with the KATRIN Experiment'. In *Annual Review of Nuclear and Particle Science* (2022), volume 72: pages 259–282. doi: 10.1146/annurev-nucl-101920-113013.

[Luc00]   L. L. Lucas and M. P. Unterweger: 'Comprehensive review and critical eval-uation of the half-life of tritium'. In *Journal of research of the National Institute of Standards and Technology* (2000), volume 105(4): page 541.

[Lv22]   Y.-N. Lv, A.-W. Liu, Y. Tan, C.-L. Hu, T.-P. Hua et al.: 'Fano-like Resonance
           due to Interference with Distant Transitions'. In *Physical Review Letters* (16
           2022), volume 129: page 163201. DOI: 10.1103/PhysRevLett.129.163201.

[Mac12]   E. Maccallini, F. Siviero, A. Bonucci, A. Conte, P. Srivastava et al.: 'Non
           evaporable getter (NEG) technology: A powerful tool for UHV-XHV systems'.
           In *AIP Conference Proceedings* (2012), volume 1451(1): pages 24–27. DOI: 10.
           1063/1.4732360. eprint: https://pubs.aip.org/aip/acp/article-pdf/1451/1/24/
           12200400/24_1_online.pdf.

[Mal83]   H. Malissa: 'On the use of capillary separation columns in GC/FTIR-spectroscopy
           and on the quantitative evaluation of the Gram-Schmidt reconstructed chroma-
           togram'. In *Fresenius' Zeitschrift für analytische Chemie* (1983), volume 316(7):
           pages 699–704. DOI: 10.1007/BF00488432.

[Mat91]   A. Mathewson, O. Gröbner, P. Strubin, P. Marin and R. Souchet: 'Compar-
           ison of synchrotron radiation induced gas desorption from Al, stainless steel
           and Cu chambers'. In *AIP Conference Proceedings*. Volume 236. 1. American
           Institute of Physics. 1991: pages 313–324.

[Mel21]   M. Melosso, M. L. Diouf, L. Bizzocchi, M. E. Harding, F. M. J. Cozijn et al.:
           'Hyperfine-Resolved Near-Infrared Spectra of $H_2^{17}O$'. In *The Journal of Physical
           Chemistry A* (2021), volume 125(36): pages 7884–7890. DOI: 10.1021/acs.jpca.
           1c05681. eprint: https://doi.org/10.1021/acs.jpca.1c05681.

[Mes84]   J. Messer, F. C. De Lucia and P. Helminger: 'Submillimeter spectroscopy of the
           major isotopes of water'. In *Journal of Molecular Spectroscopy* (1984), volume
           105(1): pages 139–155. DOI: https://doi.org/10.1016/0022-2852(84)90109-7.

[Mik05]   S. Mikhailenko, Y. L. Babikov and V. Golovko: 'Information-calculating
           system spectroscopy of atmospheric gases. The structure and main functions'.
           In *Atmospheric and Oceanic Optics* (2005), volume 18: pages 685–695.

[Mik24]   S. N. Mikhailenko, E. V. Karlovets, A. O. Koroleva and A. Campargue:
           'The far infrared absorption spectrum of $D_2^{16}O$, $D_2^{17}O$, and $D_2^{18}O$: Experimental
           line positions, empirical energy levels and recommended line lists'. In *Journal
           of Physical and Chemical Reference Data* (2024), volume 53(2): page 023102. DOI:
           10.1063/5.0202355. eprint: https://pubs.aip.org/aip/jpr/article-pdf/doi/10.1063/
           5.0202355/19868383/023102_1_5.0202355.pdf.

[Mor29]   P. M. Morse: 'Diatomic Molecules According to the Wave Mechanics. II. Vi-
           brational Levels'. In *Physical Review* (1 1929), volume 34: pages 57–64. DOI:
           10.1103/PhysRev.34.57.

[Mül18]   J. Müller: 'High-resolution spectroscopy of tritiated water and analysis of the
           $2\nu_1$ mode of HTO'. Masters's Thesis. Karlsruhe Institute for Techology, 2018.

[Mül19]   J. Müller, M. Schlösser, F. Hase, N. Ziegler, R. Grössle et al.: 'A novel custom-build light-pipe cell for high-resolution infrared absorption spectroscopy of hazardous gases'. In *Optics Express* (2019), volume.

[Nie21a]   S. Niemes: 'Calibration of a Laser-Raman-System using gas samples of all hydrogen isotopologues for KATRIN'. PhD thesis. Karlsruher Institut für Technologie (KIT), 2021. DOI: 10.5445/IR/1000128966.

[Nie21b]   S. Niemes, H. H. Telle, B. Bornschein, L. Fasselt, R. Grössle et al.: 'Accurate Reference Gas Mixtures Containing Tritiated Molecules: Their Production and Raman-Based Analysis'. In *Sensors* (2021), volume 21(18). DOI: 10.3390/s21186170.

[Oms19]   P.-E. Oms, P. Bailly du Bois, F. Dumas, P. Lazure, M. Morillon et al.: 'Inventory and distribution of tritium in the oceans in 2016'. In *Science of The Total Environment* (2019), volume 656: pages 1289–1303. DOI: https://doi.org/10.1016/j.scitotenv.2018.11.448.

[Orp94]   J. Orphal, G. Guelachvili and M. Morillonchapey: 'The ν1 and 2ν6 Bands of 35ClNO2 (Nitryl Chloride) Around 7.7 μM Studied by High-Resolution Fourier-Transform Spectroscopy'. In *Journal of Molecular Spectroscopy* (1994), volume 166(2): pages 280–286. DOI: https://doi.org/10.1006/jmsp.1994.1194.

[Pac08]   K. Pachucki and J. Komasa: 'Nonadiabatic corrections to the wave function and energy'. In *The Journal of Chemical Physics* (2008), volume 129(3): page 034102. DOI: 10.1063/1.2952517. eprint: https://pubs.aip.org/aip/jcp/article-pdf/doi/10.1063/1.2952517/15416074/034102_1_online.pdf.

[Pac22]   K. Pachucki and J. Komasa: 'Nonrelativistic energy of tritium-containing hydrogen molecule isotopologues'. In *Molecular Physics* (2022), volume 120(19-20, SI): e2040627. DOI: 10.1080/00268976.2022.2040627.

[Pap97]   D. Papousek: *Vibrational-rotational Spectroscopy And Molecular Dynamics*. Advanced Series In Physical Chemistry. World Scientific Publishing Company, 1997.

[Par97]   H. Partridge and D. W. Schwenke: 'The determination of an accurate isotope dependent potential energy surface for water from extensive ab initio calculations and experimental data'. In *Journal of Chemical Physics* (1997), volume 106(11): pages 4618–4639. DOI: 10.1063/1.473987. eprint: https://doi.org/10.1063/1.473987.

[Pen24]   R.-D. Penzhorn: *Tritium Manual*. Tritium Laboratory Karlsuhe, 2024.

[Pic05]   H. Pickett, J. Pearson and C. Miller: 'Use of Euler series to fit spectra with application to water'. In *Journal of Molecular Spectroscopy* (2005), volume 233(2): pages 174–179.

[Pic91]   H. M. PICKETT: 'The fitting and prediction of vibration-rotation spectra with spin interactions'. In *Journal of Molecular Spectroscopy* (1991), volume 148(2): pages 371–377. DOI: https://doi.org/10.1016/0022-2852(91)90393-O.

[Pol13]   O. L. POLYANSKY, R. I. OVSYANNIKOV, A. A. KYUBERIS, L. LODI, J. TENNYSON et al.: 'Calculation of Rotation–Vibration Energy Levels of the Water Molecule with Near-Experimental Accuracy Based on an ab Initio Potential Energy Surface'. In *The Journal of Physical Chemistry A* (2013), volume 117(39): pages 9633–9643. DOI: 10.1021/jp312343z. eprint: http://dx.doi.org/10.1021/jp312343z.

[Pou46]   R. V. POUND: 'Electronic frequency stabilization of microwave oscillators'. In *Review of Scientific Instruments* (1946), volume 17(11): pages 490–505.

[Puc18]   M. PUCHALSKI, J. KOMASA and K. PACHUCKI: 'Nuclear Spin-Spin Coupling in HD, HT, and DT'. In *Physical Review Letters* (2018), volume 120: page 083001. DOI: 10.1103/PhysRevLett.120.083001.

[Puc19a]   M. PUCHALSKI, J. KOMASA, P. CZACHOROWSKI and K. PACHUCKI: 'Nonadiabatic QED Correction to the Dissociation Energy of the Hydrogen Molecule'. In *Physical Review Letters* (2019), volume 122(10): page 103003. DOI: 10.1103/PhysRevLett.122.103003.

[Puc19b]   M. PUCHALSKI, J. KOMASA, A. SPYSZKIEWICZ and K. PACHUCKI: 'Dissociation energy of molecular hydrogen isotopologues'. In *Physical Review A* (2019), volume 100(2): page 020503. DOI: 10.1103/PhysRevA.100.020503.

[Rak95]   A. D. RAKIĆ: 'Algorithm for the determination of intrinsic optical constants of metal films: application to aluminum'. In *Applied Optics* (1995), volume 34(22): pages 4755–4767. DOI: 10.1364/AO.34.004755.

[Rei18]   J. REINKING: 'High resolution spectroscopy of tritiated water and analysis of the $2\nu_2$ band of HT^{16}O'. Bachelor's Thesis. Karlsruhe Institute for Techology, 2018.

[Rei19]   J. REINKING, M. SCHLÖSSER, F. HASE and J. ORPHAL: 'First high-resolution spectrum and line-by-line analysis of the $2\nu_2$ band of HTO around 3.8 microns'. In *Journal of Quantitative Spectroscopy and Radiative Transfer* (2019), volume 230: pages 61–64. DOI: https://doi.org/10.1016/j.jqsrt.2019.03.017.

[Rei20]   J. REINKING, V. HERMANN, J. MÜLLER, M. SCHLÖSSER, F. HASE et al.: 'The fundamental $\nu3$ band of DTO and the $2\nu_1$ overtone band of HTO from the analysis of a high-resolution spectrum of tritiated water vapour'. In *Journal of Molecular Spectroscopy* (2020), volume 370: page 111295.

[Rot21]   B. ROTHMUND: 'Construction and characterization of an experiment to determine the sorption behaviour of a SAES St171 getter with tritium-hydrogen mixtures'. Bachelor's Thesis. Karlsruhe Institute for Techology, 2021.

[San20]   A. Santucci, L. Farina, S. Tosti and A. Frattolillo: 'Novel Non-Evaporable Getter Materials and Their Possible Use in Fusion Application for Tritium Recovery'. In *Molecules* (2020), volume 25. DOI: 10.3390/molecules25235675.

[Sch00]   D. W. Schwenke and H. Partridge: 'Convergence testing of the analytic representation of an ab initio dipole moment function for water: Improved fitting yields improved intensities'. In *The Journal of Chemical Physics* (2000), volume 113(16): pages 6592–6597. DOI: 10.1063/1.1311392. eprint: https://pubs.aip.org/aip/jcp/article-pdf/113/16/6592/19281194/6592_1_online.pdf.

[Sch07]   F. Schwabl: *Quantenmechanik (QM I): Eine Einführung*. Springer-Lehrbuch. Springer Berlin Heidelberg, 2007.

[Sch23]   N. Schwegler, D. Holzapfel, M. Stadler, A. Mitjans, I. Sergachev et al.: 'Trapping and Ground-State Cooling of a Single H_2^+'. In *Physical Review Letters* (13 2023), volume 131: page 133003. DOI: 10.1103/PhysRevLett.131.133003.

[Sch24]   S. Schiller and S. Alighanbari. Personal communication. May 2024.

[Sch64]   F. Schmidt-Bleek and F. Rowland: 'Recoil Reactions of Tritium with Organic Compounds'. In *Angewandte Chemie International Edition in English* (1964), volume 3(12): pages 769–776.

[Sch89]   T. Schober and K. Farrell: 'Helium bubbles in α-Ti and Ti tritide arising from tritium decay: A tem study'. In *Journal of Nuclear Materials* (1989), volume 168(1): pages 171–177. DOI: https://doi.org/10.1016/0022-3115(89)90579-5.

[Sił23]   M. Siłkowski, K. Pachucki, J. Komasa and M. Puchalski: 'Leading-order QED effects in the ground electronic state of molecular hydrogen'. In *Physical Review A* (3 2023), volume 107: page 032807.

[Sim13]   B. Simmen, E. Mátyus and M. Reiher: 'Elimination of the translational kinetic energy contamination in pre-Born–Oppenheimer calculations'. In *Molecular Physics* (2013), volume 111(14-15): pages 2086–2092. DOI: 10.1080/00268976.2013.783938. eprint: https://doi.org/10.1080/00268976.2013.783938.

[Sou86]   P. C. Souers: *Hydrogen properties for fusion energy*. Univ of California Press, 1986.

[Sta56]   P. A. Staats, H. W. Morgan and J. H. Goldstein: 'Infrared Spectra of T_2O, THO, and TDO'. In *Journal of Chemical Physics* (1956), volume 24(4): pages 916–917. DOI: 10.1063/1.1742650.

[Sug85]   M. Sugisaki, H. Furuya, H. Ueki and S. Ejima: 'Surface reaction and bulk diffusion of tritium in SUS-316 stainless steel'. In *Journal of Nuclear Materials* (1985), volume 133-134: pages 280–283. DOI: https://doi.org/10.1016/0022-3115(85)90151-5.

[Tan18]   T. Tanabe: *Tritium: Fuel of Fusion Reactors*. Tokyo, Japan: Springer, 2018.

[Tan22]   M. Tanaka, C. Iwata, M. Nakada, A. Kato and N. Akata: 'Levels of atmospheric tritium in the site of fusion test facility'. In *Radiation Protection Dosimetry* (2022), volume 198(13-15): pages 1084–1089.

[Tan65]   Y.-N. Tang and F. Rowland: 'Recoil Tritium Reaction: Ring Opening and Alkyl Replacement in Substituted Cyclopropanes1'. In *The Journal of Physical Chemistry* (1965), volume 69(12): pages 4297–4304.

[Tao18]   L.-G. Tao, A.-W. Liu, K. Pachucki, J. Komasa, Y. Sun et al.: 'Toward a determination of the proton-electron mass ratio from the Lamb-dip measurement of HD'. In *Physical Review Letters* (2018), volume 120(15): page 153001.

[Tay01]   D. J. Taylor, M. Glugla and R.-D. Penzhorn: 'Enhanced Raman sensitivity using an actively stabilized external resonator'. In *Review of Scientific Instruments* (2001), volume 72(4): pages 1970–1976. DOI: https://doi.org/10.1063/1.1353190.

[Ten24]   J. Tennyson. Personal communication. Jul 2024.

[Tin12]   M. Tine, D. Kobor, I. Sakho, L. Coudert et al.: 'Determination of the vibro-rotational constants, the dipole moment's function and the intensities of the HTO's ν_1 (ν_3 by usual convention) band'. In *Journal of Modern Physics* (2012), volume 3(12): page 1945.

[Tób20]   R. Tóbiás, T. Furtenbacher, I. Simkó, A. G. Császár, M. L. Diouf et al.: 'Spectroscopic-network-assisted precision spectroscopy and its application to water'. In *Nature Communications* (2020), volume 11(1): page 1708.

[Tri16]   Tritium Laboratory Karlsruhe: *Technical terms of delivery and acceptance of TLK*. 2016.

[Tri18]   T. M. Trivikram, M. Schlösser, W. Ubachs and E. J. Salumbides: 'Relativistic and QED Effects in the Fundamental Vibration of T_2'. In *Physical Review Letters* (16 2018), volume 120: page 163002. DOI: 10.1103/PhysRevLett.120.163002.

[Uba16]   W. Ubachs, J. C. J. Koelemeij, K. S. E. Eikema and E. J. Salumbides: 'Physics beyond the Standard Model from hydrogen spectroscopy'. In *Journal of Molecular Spectroscopy* (2016), volume 320: pages 1–12.

[Ule91]   O. Ulenikov, V. Cherepanov and A. Malikova: 'On analysis of the ν_2 band of the HTO molecule'. In *Journal of Molecular Spectroscopy* (1991), volume 146(1): pages 97–103. DOI: https://doi.org/10.1016/0022-2852(91)90373-I.

[Vei87]   D. K. Veirs and G. M. Rosenblatt: 'Raman line positions in molecular hydrogen: H2, HD, HT, D2, DT, and T2'. In *Journal of Molecular Spectroscopy* (1987), volume 121(2): pages 401–419. DOI: https://doi.org/10.1016/0022-2852(87)90058-0.

[Vel08]   M. Velarde, L. Sedano and J. Perlado: 'Dosimetric impact evaluation of primary coolant chemistry of the internal tritium breeding cycle of a fusion reactor DEMO'. In *Fusion Science and Technology* (2008), volume 54(1): pages 122–126.

[Wan18]   L. M. Wang and Z.-C. Yan: 'Relativistic corrections to the ground state of H_2 calculated without using the Born-Oppenheimer approximation'. In *Physical Review A* (2018), volume 97(6): page 060501. doi: 10.1103/PhysRevA.97.060501.

[Wat06]   J. K. Watson: 'Calculated octic centrifugal distortion coefficients of non-linear molecules'. In *Journal of Molecular Structure* (2006), volume 795(1): pages 263–270. doi: https://doi.org/10.1016/j.molstruc.2006.02.038.

[Wat67]   J. K. G. Watson: 'Determination of Centrifugal Distortion Coefficients of Asymmetric-Top Molecules'. In *Journal of Chemical Physics* (1967), volume 46(5): pages 1935–1949. doi: 10.1063/1.1840957. eprint: https://doi.org/10.1063/1.1840957.

[Wat68]   J. K. Watson: 'Determination of centrifugal distortion coefficients of asymmetric-top molecules. III. Sextic coefficients'. In *The Journal of Chemical Physics* (1968), volume 48(10): pages 4517–4524.

[Wat87]   J. S. Watson, C. E. Easterly, J. B. Cannon and J. B. Talbot: 'Environmental Effects of Fusion Power Plants. Part II: Tritium Effluents'. In *Fusion Technology* (1987), volume 12(3): pages 354–363. doi: 10.13182/FST87-A25068. eprint: http://dx.doi.org/10.13182/FST87-A25068.

[Wun17]   D. Wunch, P. O. Wennberg, G. Osterman, B. Fisher, B. Naylor et al.: 'Comparisons of the Orbiting Carbon Observatory-2 (OCO-2) X_{CO_2} measurements with TCCON'. In *Atmospheric Measurement Techniques* (2017), volume 10(6): pages 2209–2238. doi: 10.5194/amt-10-2209-2017.

[Yam17]   Y. Yamamoto, H. Konda, Y. Matsuyama, H. Osawa and M. Ohnishi: 'Characteristics of Gas Mixture Supply/Pressure Control Using Non-Evaporable Getters in a Discharge-Type Fusion Neutron Source'. In *Fusion Science and Technology* (2017), volume 72: pages 773–779. doi: 10.1080/15361055.2017.1347461.

[Yan84a] P. W. J. Yang, E. L. Ethridge, J. L. Lane and P. R. Griffiths: 'Optimization of GC/FT-IR Measurements I: Construction of Light-Pipes'. In *Applied Spectroscopy* (1984), volume 38(6): pages 813–816.

[Yan84b] P. W. J. Yang and P. R. Griffiths: 'Optimization of GC/FT-IR Measurements II: Optical Design'. In *Applied Spectroscopy* (1984), volume 38(6): pages 816–821.

[Yin89]   M. Yin, B.-Z. Yu and W. N. Hansen: 'The Optical Design And Application Of Light Pipe systems In FTIR Spectrometer'. In *7th Intl Conf on Fourier Transform Spectroscopy*. Edited by D. G. Cameron. Volume 1145. International Society for Optics and Photonics. SPIE, 1989: pages 451–452. doi: 10.1117/12.969544.

[Zab20]   M. Zaborowski, M. Słowiński, K. Stankiewicz, F. Thibault, A. Cygan et al.: 'Ultrahigh finesse cavity-enhanced spectroscopy for accurate tests of quantum electrodynamics for molecules'. In *Optics Letters* (2020), volume 45(7): pages 1603–1606. DOI: 10.1364/OL.389268.

[Zob96]   N. F. Zobov, O. L. Polyansky, C. L. Sueur and J. Tennyson: 'Vibration-rotation levels of water beyond the Born-Oppenheimer approximation'. In *Chemical Physics Letters* (1996), volume 260(3): pages 381–387. DOI: https://doi.org/10.1016/0009-2614(96)00872-X.